New Main Group and Rare Earth Ring-Opening Polymerisation Catalysts

Bryony Core MChem AMRSC



Thesis submitted to the University of Oxford for the degree of Doctor of Philosophy, July 2015.

The work described in this Thesis was carried out in the Chemistry Research Laboratory, University of Oxford from October 2011 to July 2015 under the supervision of Professor Philip Mountford. All work is my own unless stated to the contrary, and has not previously been submitted for any degree at this or any other university.

Bryony Core

July 2015

Abstract

Bryony Core July 2015
Trinity College D. Phil Thesis

This Thesis describes the synthesis and characterisation of new Group 2, Group 3 and lanthanide amide, alkyl, halide, borohydride and alkoxide complexes, and their uses as catalysts for the living ROP and immortal ring-opening polymerisation (*i*ROP) of *rac*-, *L*, *D*- and *meso*-lactide.

Chapter One introduces cyclic esters and possible mechanistic pathways leading to polyesters by ROP. Living and immortal ROP, including their kinetic characteristics are discussed. An overview of ROP from an industrial perspective and a literature review are also given.

Chapter Two describes the synthesis and characterisation of a new series of magnesium and zinc amide, alkyl, halide, borohydride and alkoxide complexes supported by a carbazole-bis(dimethyloxazoline) ligand. Their activities towards the ROP of *rac*-, *L*- and *meso*-lactide are presented. Detailed mechanistic studies using spectroscopic techniques are discussed and a new mechanism is proposed.

Chapter Three describes the synthesis and characterisation of a new series of calcium, strontium, yttrium, lanthanum and samarium amide, alkyl, halide, borohydride and alkoxide complexes supported by a carbazole-bis(dimethyloxazoline) ligand. Their activities towards the ROP of *rac*-, *L*- and *meso*-lactide are presented. Detailed mechanistic studies using spectroscopic techniques are discussed.

Chapter Four describes the synthesis and characterisation of a new series of magnesium, calcium, strontium, yttrium, lanthanum and samarium amide, halide and borohydride complexes supported by a chiral carbazole-bis(isopropyloxazoline) ligand. Their activities towards the ROP of *rac*-, *L*-, *D*- and *meso*-lactide are presented.

Chapter Five contains experimental details and characterising data for the new complexes reported in this Thesis.

CD Appendix contains .CIF files for all the new crystallographically-characterised complexes.

Contents

	Declaration	i
	Abstract	ii
	Contents	iii
	Acknowledgements	vii
	Abbreviations	viii
	Notes	xi
Chapter One – Introduction		1
1.1	Overview	2
1.2	General introduction	2
1.3	Introduction to biodegradable and biorenewable polyesters	3
1.4	Polymer molecular weight: definitions	4
1.5	Polymer Analysis	6
1.5.1	Nuclear Magnetic Resonance Spectroscopy (NMR)	6
1.5.2	Gel Permeation Chromatography (GPC)	7
1.5.3	Matrix-Assisted Laser Desorption/Ionisation Time of Flight Mass Spectrometry (MALDI-ToF MS)	8
1.6	Stereocontrol and tacticity of PLA	8
1.6.1	Characterisation of polymer chain sequences by NMR spectroscopy	10
1.7	Ionic and metal free ROP	13
1.7.1	Anionic ROP	13
1.7.2	Cationic ROP	14
1.7.3	Organocatalysts	15
1.8	Metal-mediated ROP	16
1.8.1	Coordination-insertion polymerisation	16
1.8.2	Activated-monomer ROP	19
1.9	ROP: thermodynamic and kinetic considerations	19
1.9.1	Living polymerisation	22
1.9.2	Immortal ring-opening polymerisation	23
1.10	Literature review	26
1.10.1	Industrial ROP catalysts	26
1.10.2	Initiators for the formation of isotactic/stereoblock PLA from *rac*-LA	27
1.10.3	Initiators for the formation of heretotactic PLA from *rac*-LA	30

1.10.4 Initiators for the stereocontrolled ROP of *meso*-LA 33
1.11 Oxazoline ligands in the ROP of cyclic esters 35
1.12 Aims and outlook 39
1.13 References for Chapter One 39

Chapter Two – $CzOx^{Me_2}$-supported magnesium and zinc complexes for the ROP of *rac*-, *L*- and *meso*-LA and their mechanistic studies 54

2.1 Overview 55
2.2 Introduction 55
2.2.1 Alkaline earth complexes as ROP catalysts 55
2.2.2 Early work alkaline earth and lanthanide borohydride initiators in ROP 59
2.2.2.1 Lanthanide borohydride initiators in ROP 59
2.2.2.2 Alkaline earth borohydride initiators in ROP 61
2.2.3 Coordination modes of the borohydride ligand 64
2.2.4 Mechanistic considerations 66
2.2.5 Borate esters as chain transfer agents in immortal ROP 67
2.3 Synthesis and characterisation of $CzOx^{Me_2}$-supported magnesium and zinc complexes 68
2.3.1 Synthesis of protioligand $HCzOx^{Me_2}$ (**1.45**) 68
2.3.2 Synthesis and characterisation of $CzOx^{Me_2}$-supported magnesium and zinc alkyl, amide and alkoxide complexes 69
2.3.3 Synthesis and characterisation of $CzOx^{Me_2}$-supported magnesium borohydride and halide complexes 76
2.4 *In situ* generation of trialkyl borate esters as chain transfer agents 82
2.5 Polymerisation studies: ROP of *L*- and *rac*-LA 87
2.6 Polymerisation studies: ROP of *meso*-LA 114
2.7 Summary and conclusions 117
2.8 References for Chapter Two 119

Chapter Three – CzOx^{Me_2}-supported calcium, strontium, yttrium, lanthanum and samarium complexes for the ROP of *rac*-, *L*- and *meso*-LA and their mechanistic studies 127

3.1 Overview 128
3.2 Synthesis and characterisation of CzOx^{Me_2}-supported calcium and strontium complexes 128
3.2.1 Synthesis and characterisation of CzOx^{Me_2}-supported calcium amide, alkoxide and homoleptic complexes 128
3.2.2 Diffusion measurement by NMR Spectroscopy 134
3.2.3 Synthesis and characterisation of CzOx^{Me_2}-supported calcium and strontium halide, borohydride and homoleptic complexes 136
3.3 Synthesis and characterisation CzOx^{Me_2}-supported yttrium, lanthanum and samarium borohydride complexes 143
3.4 *In situ* generation of trialkyl borate esters as chain transfer agents 148
3.5 Polymerisation studies: ROP of *rac*-, *L*- and *meso*-LA 154
3.5.1 Polymerisation studies: ROP of *rac*- and *meso*-LA with Group 2 complexes 155
3.5.2 Polymerisation studies: ROP of *rac*- and *meso*-LA with Group 3 and lanthanide complexes 171
3.6 Summary and conclusions 180
3.7 References for Chapter Three 183

Chapter Four – CzOx^{iPr}-supported alkaline earth and rare earth complexes for the ROP of *rac*-, *D*-, *L*- and *meso*-LA 186

4.1 Overview 187
4.2 Introduction 187
4.2.1 Chiral initiators for the stereoselective ROP of lactide 187
4.3 Synthesis and characterisation of CzOx^{iPr}-supported Group 2 complexes 197
4.3.1 Synthesis of protioligand (*S*,*S*)- and (*R*,*R*)-HCzOx^{iPr} (**(*S*,*S*)-** and **(*R*,*R*)-1.46**) and (*S*,*S*)-Li(CzOx^{iPr}) (**(*S*,*S*)-33**) 197

4.3.2	Synthesis and characterisation of CzOx$^{i\text{Pr}}$-supported potassium, magnesium and calcium borohydride and amide complexes	200
4.4	Synthesis and characterisation of CzOx$^{i\text{Pr}}$-supported Group 3 and lanthanide complexes	205
4.5	*In situ* generation of trialkyl borate esters as chain transfer agents	207
4.6	Polymerisation studies: ROP of *rac*-, *L*-, *D*- and *meso*-LA	209
4.6.1	Polymerisation studies: ROP of *rac*-, *L*-, *D*- and *meso*-LA with Group 2 catalysts	210
4.6.2	Polymerisation studies: ROP of *rac*-, *L*-, *D*- and *meso*-LA with Group 3 and lanthanide catalysts	228
4.7	Summary and conclusions	236
4.8	References for Chapter Four	239
Chapter Five – Experimental details and characterising data		243
5.1	General methods and instrumentation	244
5.2	Literature preparations and reagent purification	245
5.3	Ligand numbering system	246
5.4	Experimental details and characterising data for Chapter Two	246
5.5	Experimental details and characterising data for Chapter Three	251
5.6	Experimental details and characterising data for Chapter Four	258
5.7	Polymerisation procedures	268
5.8	X-ray data collection and processing parameters	269
5.9	References for Chapter Five	269
Appendix		xiii
CD appendix		

Acknowledgements

First and foremost, I would like to thank my supervisor, Prof. Philip Mountford, for his assistance, support and advice throughout the course of my DPhil. This has deepened my knowledge of chemistry and self-awareness. I am grateful for all the opportunities that were given which I may build on for my future career.

I would like to express my sincere thanks to members of the Mountford group, past and present, who brought the lab to life and made it so enjoyable to be a part of. I would like to thank Dr. Matthew Blake for supervising me in my first year and providing ongoing advice since, Dr. Junjuda Unruangsri as my compatriot in the many trials and tribulations of ROP, Dr. Insun Yu whose insight proved invaluable in the final months of my DPhil, Dr. Andrew Schwarz for his wisdom within (and without) the lab and Lucy Budden whose singular determination throughout her Part II is a quality I continue to admire. A special mention must go to Dr. Laura Groom, Dr. Adam Russell, Richard Collins and Laura Stevenson. I owe them endless thanks for being great friends and providing support when times got tough. I truly enjoyed our shared experiences throughout these years. Additionally, I would like to thank Dr. Minggang Hu who left an indelible mark on the lab during his stay. I cannot finish without acknowledging Matt, Insun and Laura Stevenson for their help to proofread my chapters.

Additionally, I must express my gratitude to Dr. Ben Ward of the University of Cardiff with whom I collaborated in the early years of my DPhil. I would like to thank Dr. Nick Rees, Collin Sparrow and Dr. Amber Thompson for their great help with NMR spectroscopy, mass spectrometry and X-Ray crystallography. Without them, I would not be able to put all my work together.

Lastly, I reserve the greatest thanks for my parents, grandparents, parents-in-law and my brother, who have always been behind my success during my DPhil, as with other areas of my life. I would like to extend my deepest gratitude to my husband, Mike Brant, whose love and support are essential to my success, as well as picking me up on several occasions at 5 am after particularly arduous polymerisations. Without the people mentioned above, it would have been impossible to get this Thesis done.

Abbreviations

General

Å	Ångstrom
av.	average
ca.	*circa*, about
calcd	calculated
cal	calories
CTA	chain-transfer agent(s)
cf.	*confer*, compare
d	day(s)
^{o}	degrees
^{o}C	degrees Celsius
DFT	Density Functional Theory
equiv(s).	equivalent(s)
g	gram(s)
GPC	gel permeation chromatography
h	hour(s)
*i*ROP	immortal ring-opening polymerisation
η	intrinsic viscosity
J	Joule(s)
k	kilo
K	Kelvin
k_{obs}	observed rate constant
k_{i}	rate constant of initiation
k_{p}	rate constant of propagation
k_{tr}	rate constant of chain-transfer reaction
L	litre(s)
mg	milligram(s)
min	minute(s)
mL	millilitre(s)
μL	microliter(s)
ROP	ring-opening polymerisation
RT	room temperature
s	second(s)

SEC	Size Exclusion Chromatography
T	temperature
T_g	glass transition temperature
T_m	melting temperature

Chemical

Ar	aryl group
Bn	benzyl
BnOH	benzyl alcohol
Cp	C_5H_5
Cp*	C_5Me_5
$CzOx^{Me_2}$	2,2'-(3,6-di-*tert*-butyl-9λ^2-carbazole-1,8-diyl)bis(4,4-dimethyl-4,5-dihydrooxazole)
$CzOx^{iPr}$	2,2'-(3,6-di-*tert*-butyl-9λ^2-carbazole-1,8-diyl)bis(4-isopropyl-4,5-dihydrooxazole)
Cy	cyclohexyl
D-lactide	(*R*,*R*)-cis-3,6-dimethyl-1,4-dioxane-2,5-dione
DMAP	4-dimethylaminopyridine
^{n}Bu	*n*-butyl
^{t}Bu	*tert*-butyl
^{i}Pr	*iso*-propyl
^{i}PrOH	isopropyl alcohol
L	a supporting ligand (set)
LA	lactide
L-lactide	(*S*,*S*)-cis-3,6-dimethyl-1,4-dioxane-2,5-dione
Me	methyl
Meso-lactide	(*R*,*S*)-cis-3,6-dimethyl-1,4-dioxane-2,5-dione
M_n	number average molecular weight
M_p	peak molecular weight
M-OR	metal alkoxide
M_w	weight average molecular weight
PDI	poly dispersity index
Ph	phenyl
PhCHO	benzaldehyde
P_m	probability of *meso*- linkages
PLA	poly(lactic acid)

P_r	probability of racemic linkages
py	pyridine
R	generic aryl or alkyl
rac-lactide	a racemic mixture of *D*- and *L*-lactide
ROP	ring opening polymerisation
$Sn(Oct)_2$	tin octanoate
THF	tetrahydrofuran

Mass Spectrometry

EI	electron impact
FI	field ionisation
m/z	mass to charge ratio
MS	mass spectrometry
MALDI-ToF MS	matrix-assisted laser desorption/ionization - time of flight mass spectrometry

Nuclear Magnetic Resonance Spectroscopy

^{11}B-{^{1}H}	proton-decoupled ^{11}B
^{13}C-{^{1}H}	proton-decoupled ^{13}C
app.	apparent
br	broad
COSY	correlation spectroscopy
d	doublet
dq	doublet of quartets
HETCOR	heteronuclear correlation
HMBC	heteronuclear multiple bond correlation
HMQC	heteronuclear single quantum correlation
i	*ipso*
J	coupling constant
m	*meta*
m	multiplet
NMR	nuclear magnetic resonance
nOe	nuclear Overhauser effect
o	*ortho*
p	*para*

ppm	parts per million
q	quartet
ROESY	rotating-frame nuclear Overhauser Effect spectroscopy
s	singlet
sept	septet
t	triplet
VT	variable temperature
δ	chemical shift in ppm

Infrared Spectroscopy

br	broad
FT-IR	fourier transform infrared red
IR	infrared red
m	medium
s	strong
w	weak
ν	frequency

Note about numbering of compounds described in this Thesis

Literature compounds described in this Thesis are numbered **1.x**, **2.x**, **3.x**, **4.x**, according to the Chapter in which they first occur. The new compounds described in this Thesis are numbered **1** - **58**. MALDI-ToF mass spectroscopy was performed by Colin Sparrow, and elemental analysis were performed by Stephen Boyer at London Metropolitan University and Elemental Microanalysis Ltd at Devon.

Chapter One

Introduction

1.1 Overview

This Chapter provides an introduction to the metal catalysed ring opening polymerisation (ROP) of cyclic esters wherein desirable polymer properties and analytical tools used for characterisation are discussed. An account of the main mechanistic pathways, including living and immortal ROP, will be provided. A general literature review is provided, with emphasis given to catalysts which effect a high degree of stereocontrol. Moreover, oxazoline-based ancillary ligands are discussed, which are the focus of this work.

1.2 General introduction

In 1909 Leo Baekeland created the first synthetic polymer, Bakelite: a resin synthesised from phenol and formaldehyde.[1] Due to its electrical and thermal insulating properties, along with resistance to chemical degradation, Bakelite soon found application in the non-conducting components of electrical devices such as radio casings. Bakelite paved the way for the vast multitudes of synthetic polymers which were synthesised on an industrial scale after the First and Second World Wars; poly(ethylene), a polymer first produced in the 1930s, now enjoys an annual worldwide production of approximately 80 million tonnes.[2] Synthesised through the catalytic polymerisation of gaseous ethene, poly(ethylene) is highly prized for its properties such as malleability and thermal resistance which can be tuned with the judicious selection of reaction conditions. Following its discovery in 1954, Ziegler and Natta were awarded the Nobel Prize for Chemistry for their discovery and development of the production of poly(propylene): a polymer with extremely high durability and chemical resistance.[1] Because of their hard-wearing properties, both poly(ethylene) and poly(propylene) have become ubiquitous in daily life and have numerous applications, such as packaging, textiles and machinery components. Synthetic polymers are not restricted to hydrocarbon monomers, and indeed the choice of monomer has a profound effect on the macroscopic properties of the final polymer. Poly(lactide) (PLA) and other polyesters were first reported by Carothers in 1932, in which the polymer was synthesised through condensation polymerisation at elevated temperatures.[3] Further development in the area led DuPont to patent high molecular weight PLA in 1954.[4] In 2010, bioplastics comprised 300,000 tons of the

global plastic market, with several companies now actively pursuing their development, including NatureWorks LLC: the market leader in PLA technology.[5, 6]

Petroleum-derived polymers such as poly(ethylene) still play an indispensible role in modern life today; however, the same properties that render them so attractive, such as long term chemical stability, also pose significant environmental challenges. These polymers are not readily biodegradable and also rely on non-renewable feedstocks for production. It is for these reasons, combined with the volatile price of oil, that in recent years considerable attention has been paid to the development of biodegradable polymers.[7]

1.3 Introduction to biodegradable and biorenewable polyesters

In response to the growing demands placed upon plastics from non-renewable resources, a significant new class of biodegradable polyesters from renewable resources has emerged in recent years, typically incorporating a linear, aliphatic polymer chain. Of considerable importance are the polymers PLA and poly(caprolactone) (PCL).[5, 8-15] Such polymers are of particular interest due to their unique properties, with PLA finding application as a direct substitute for oil-derived polymers in packaging materials.[16, 17] Furthermore, their biocompatibility allows them to be used *in vivo* as drug delivery systems or as tissue scaffolding.[18-22]

Traditional synthetic routes rely on polycondensation methodologies achieved through the step polymerisation of the corresponding α-hydroxy acid. In order to produce polymers of high M_n, it is necessary to apply high temperatures in conjunction with the constant removal of water and the addition of a catalyst, both of which add to the overall cost of synthesis.[7]

The most efficient method for the preparation of PLA and PCL is ring-opening polymerisation (ROP) of the corresponding cyclic ester (Figure 1.1) allowing for a greater degree of control of molecular weight and molecular weight distribution (M_n/M_w) when compared to condensation polymerisation.[23, 24]

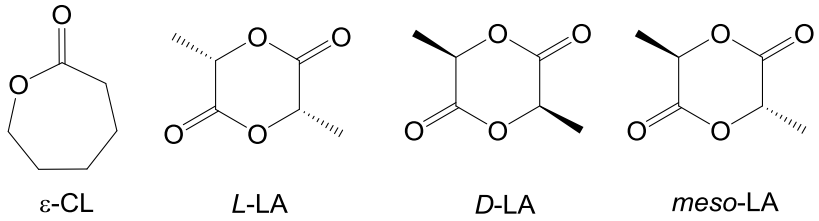
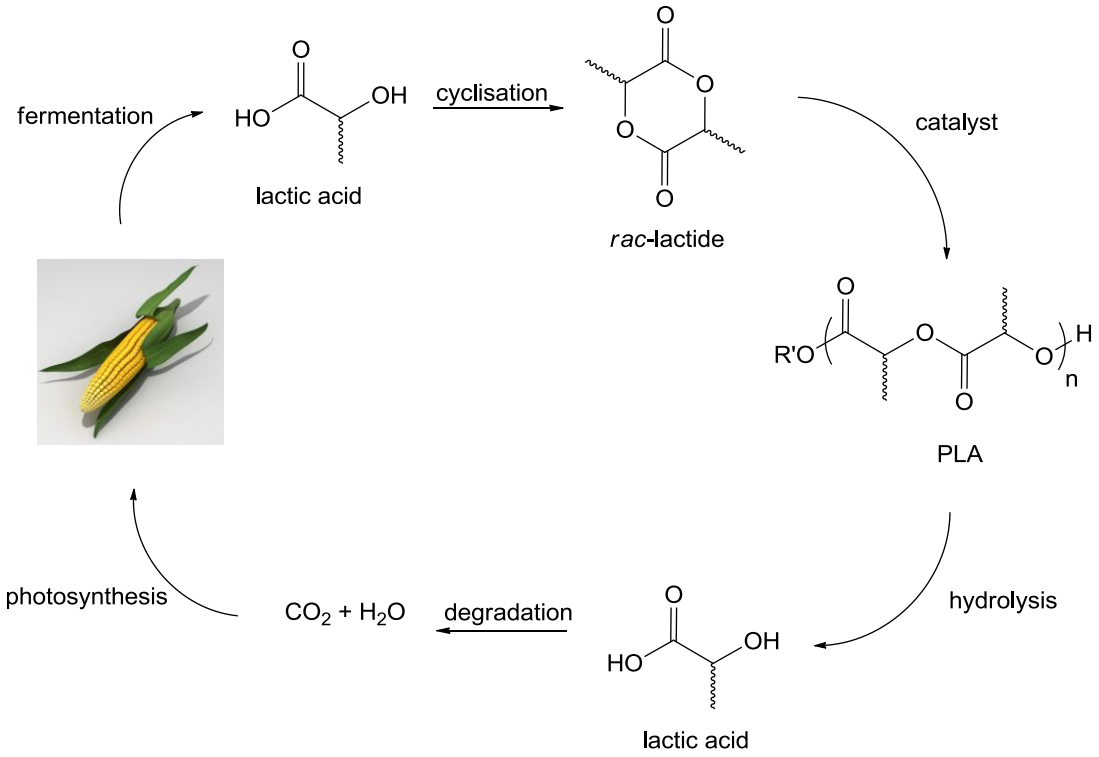


Figure 1.1. PCL and PLA monomers.

Despite sharing the biocompatible properties of PLA, PCL is synthesised from the ROP of ε-caprolactone which is produced industrially through the Baeyer-Villager oxidation of cyclohexanone with peroxyacetic acid.[25] However, as lactide can be obtained through renewable resources such as corn and sugar beet, PLA is particularly attractive as a biocompatible polyester. Once synthesised, PLA undergoes hydrolysis to form lactic acid (Scheme 1.1): a non-toxic metabolite utilised in the Krebs Cycle.[7, 21]



Scheme 1.1. The lifecycle of PLA.

1.4 Polymer molecular weight: definitions

Polymers exist as a non-uniform set of polymer chains of varying degree of polymerisation and molecular weight, which are distributed according to a Gaussian

distribution around an average value. The molecular weight distribution can be defined by the relationship between the number of moles of each polymer species (N_i) and the molar mass of that species (M_i).[1] The number average molecular weight, M_n, is given in Equation 1.1.

$$M_n = \frac{\sum M_i N_i}{\sum N_i}$$

Equation 1.1

The weight average molecular weight, M_w, is given in Equation 1.2 where W_i is the total mass of the polymer having molar mass M_i.

$$M_w = \frac{\sum W_i M_i}{\sum W_i}$$

Equation 1.2

The polydispersity index, or PDI, is a measure of the distribution of molar mass of polymer chains in a sample and is defined as the weight average molecular weight divided by the number average molecular weight (M_w/M_n) (Equation 1.3).

$$PDI = \frac{M_w}{M_n}$$

Equation 1.3

The weight average molecular weight, M_w, is biased towards polymer chains of higher molecular weights and as such is greater than M_n resulting in the PDI typically being greater than unity. During an ideal living polymerisation, only initiation and propagation occur, allowing polymer chains of predictable molecular weight to be obtained based on the initial monomer loading. Theoretically, polymers produced in this manner would have chains of uniform length and therefore a PDI of 1.0; however, in practice, even highly controlled polymerisation reactions do not result in a PDI of 1.0. Side reactions such as deleterious transesterification, slow initiation and termination reactions produce polymer chains whose molecular weights vary significantly from the ideal value distorting M_w and M_n. The degree to which these side reactions occur dictates the extent to which the PDI deviates from unity. In ROP,

polymers with a PDI of 1.0-1.2 are considered to have a narrow distribution, from 1.2-1.8 moderate and 1.8 and above, broad.

The performance of the catalyst is also assessed by the agreement of experimentally obtained M_n with the theoretically derived M_n, calculated from the % conversion of monomer which is generally monitored throughout the course of the polymerisation reaction. A well-controlled system would therefore be expected to produce polymers with a narrow PDI of 1.0-1.2 along with close agreement between experimental and calculated M_n. These criteria are used to assess catalyst performance throughout this Thesis.

1.5 Polymer analysis

Polymers such as PLA are characterised through a variety of analytical techniques. These include ^{1}H and $^{13}C\{^{1}H\}$ NMR spectroscopy, Gel Permeation Chromatography (GPC) and Matrix-Assisted Laser Desorption/Ionisation Time of Flight Mass Spectrometry (MALDI-ToF MS).

1.5.1 Nuclear Magnetic Resonance Spectroscopy (NMR)

^{1}H NMR spectroscopy is used to reveal structural information about the polymer such as polymer end-groups and M_n for polymers up to 2,000 g mol^{-1}; however, information obtained in this way may be unreliable due to the high proportion of polymer backbone proton resonances compared to those for the end-group, rendering the end-groups unobservable.[26] Additional structural information such as the degree of transesterification or the presence of cyclic polymers may not be determined as these resonances typically overlap with those of the linear polymer chain. ^{1}H NMR spectroscopy is used to determine the % monomer conversion during a polymerisation reaction by comparative integration of the polymer backbone resonances with those of the unreacted monomer at a particular time. This permits the construction of kinetic profiles allowing insight into the polymerisation mechanism to be obtained. During a living polymerisation, plots of molecular weight versus % conversion are used to inspect how closely the polymer chains produced adhere to their theoretical value and allow for the monitoring of any unwanted side reactions such as transesterification. Finally, in the case of PLA, $^{1}H\{^{1}H\}$ NMR spectroscopy can also be used to analyse the degree of tacticity of the polymer produced, which is detailed in Section 1.6.1.

1.5.2 Gel Permeation Chromatography (GPC)

Gel Permeation Chromatography (GPC) is a type of size exclusion chromatography (SEC) which is commonly used to determine the molecular weight and polydispersity index of a polymer sample based on their hydrodynamic volume: a measure of the dynamic volume of a polymer based on its interaction with solvent molecules.[27] An organic solvent, such as THF, is used to dissolve the polymeric sample which is eluted through a stationary phase such as a column packed with porous beads of styrene divinyl benzene copolymer. These porous beads allow for the diffusion of both solvent and solute molecules which are thus separated according to size. Small polymer molecules are retained within the pores for a longer duration in comparison to larger molecules and as such have a greater retention time.[28] Detected using refractive index (RI) methods, polymer properties such as M_n and M_w, along with PDI may be accurately measured by comparison to external standards such as poly(styrene) with known M_w, M_n and M_p (distribution maximum point).[29]

For polymers of identical molecular weight, polyesters such as PLA and PCL have very different hydrodynamic radii to their poly(styrene) counterparts, and as such would experience different retention times. It is necessary to account for the different hydrodynamic radii of PLA and PCL to poly(styrene) to obtain their absolute values. The hydrodynamic volume of a polymer in a given solution is equal to [η]M, where [η] is the intrinsic viscosity, and M the molecular weight, and can be related through the Mark-Houwink relationship (Equation 1.4).[1, 27, 30]

$$[\eta] = KM^{\alpha}$$

Equation 1.4

The values α and K are determined experimentally for each individual polymer type by plotting log[η] against log(M) over a range of molecular weights. They are unique to each individual polymer-solvent system and are temperature-dependent. Values of α range from 0-2 and relate to the nature of the polymer in solution: 0 indicative of a hard sphere, 1 coils or helical structures and 2 a rigid rod. The M_n, M_w and PDI values reported in this Thesis are obtained at 30 °C and using THF as the eluent to which the Mark-Houwink corrections are applied after calibration with appropriate poly(styrene) standards.[31] Unfortunately cyclic polymers may not be accurately measured using RI,

thus cyclic products formed by transesterification are taken into account by approximation.

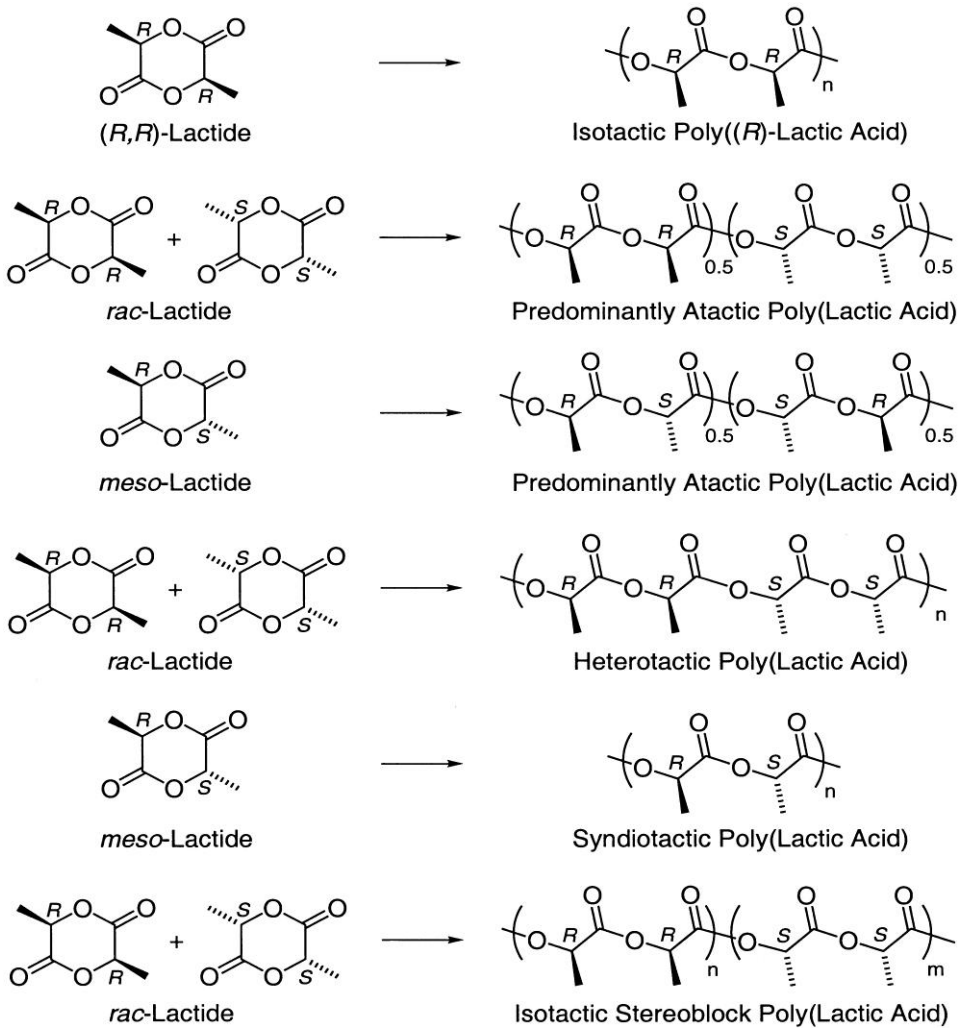
1.5.3 Matrix-Assisted Laser Desorption/Ionisation Time of Flight Mass Spectrometry (MALDI-ToF MS)

MALDI-ToF MS is used in the field of ROP to determine structural characteristics of the polymer which may not be accurately determined through other analytical techniques such as ^{1}H NMR spectroscopy, including the determination of the polymer end-group, the presence of cyclic structures and transesterification. MALDI-ToF MS is a soft ionisation technique which allows for the structural analysis of large organic molecules such as polymers which would otherwise be fragmented by traditional mass spectrometry techniques such as vaporisation. Polymer chains are embedded in a matrix comprising organic molecules which absorb readily in the UV to IR range such as *trans*-2-[3-(4-*tert*-butylphenyl)-2-methyl-2-propenylidene]malononitrile or 4-hydroxy-3-methoxy-cinnamic acid, which is subsequently irradiated with a UV laser beam, triggering the desorption of the top layer of the matrix material into a stream containing a mixture of neutral and ionised matrix molecules.[32] A cationic dopant such as sodium or potassium ions binds to the polymer molecules which are passed through a time-of-flight mass spectrometer, separating the ion particles according to their mass-to-charge (*m*/*z*) ratio. The MALDI-ToF mass spectrometer and techniques employed are outlined in detail in Section 5.1.

1.6 Stereocontrol and tacticity of PLA

The microstructure of PLA plays a large role in determining the macroscopic properties of the polymer such as its physical and mechanical properties alongside chemical properties such as rate of degradation.[17, 33] The resultant stereochemistry is dependent on both the stereochemistry of monomer employed during the polymerisation process and the initiator used. Lactide has two stereocentres and as such exists as three stereoisomers: *L*-LA containing two *S* stereocentres, *D*-LA containing two *R* stereocentres and *meso*-LA containing one *R* and one *S* stereocentre. *Rac*-LA is the racemic mixture of *L*- and *D*-LA. Both *rac*-LA and enantiopure *L*-LA are commercially available and are therefore the most widely studied in ROP; however both *D*- and *meso*-LA are available through industrial sources. As LA has two stereocentres, PLA can have a number of microstructures: isotactic, syndiotactic,

heterotactic and atactic (Scheme 1.2) determined by the type of monomer and the initiator.



Scheme 1.2. Lactide monomers and PLA microstructures.[33]

Random enchainment of *D*- and *L*-LA produces atactic PLA which is amorphous with a glass transition temperature of T_g = 55-60 °C, experiencing a low tensile strength and rapid degradation.[22, 34] Pure isotactic poly(*L*-lactide) (PLLA) or poly(*D*-lactide) (PDLA) is semi-crystalline with a melting temperature of $T_m \approx 180$ °C and has a high tensile strength and slow degradation.[34-37] High T_m values are not restricted to enantiopure PLLA or PDLA, and can be exceeded with stereocomplex PLA synthesised by post-polymerisation blending of homopolymers PLLA and PDLA in 50:50 ratio (T_m = 230 °C)[38] and stereoblock PLA (T_m = 205 °C).[39]

The utilisation of *rac*-LA as a monomer has extended the range of PLA microstructures. It is possible to synthesise heterotactic PLA from the alternating

enchainment of *D*- and *L*-LA,[40-64] isotactic stereoblock or stereogradient PLA,[33, 65-78] or heterotactic-isotactic stereoblock PLA.[79, 80] As heterotactic PLA is amorphous, it is difficult to determine its melting point; however, $T_m \approx 130$ °C and $T_g > 45$ °C have been reported.[81-83] Regarding *meso*-LA, it is possible to synthesise either syndiotactic PLA, a crystalline material with $T_m = 152$ °C,[84] if catalysts show a preference for either the *R*- or *S*-stereocentre, or heterotactic PLA if the preference alternates between the *R*- and *S*-stereocentre,[33, 41, 58, 85-93] in which case *RSSRRS* stereosequences are produced.[33, 94-97]

Efficient stereocontrol during polymerisation is exerted through two possible mechanisms during the ROP of *rac*- and *meso*-LA: chain end control and enantiomorphic site control. For an achiral catalyst, stereoenrichment is achieved through chain end control and is the process by which the last unit in the growing chain preferentially selects the stereoisomer to be inserted into the chain. In this case, high stereoselectivities are dependent on steric crowding at the metal centre Alternatively, in enantiomorphic site control, the chirality of the catalyst influences which stereoisomer is inserted into the polymer chain. In chiral complexes, it is likely that both site control and chain end control interact either constructively or destructively to polymerise LA with stereoselectivity.[98]

1.6.1 Characterisation of polymer chain sequences by NMR spectroscopy

According to Bernoullian statistical models, *vide infra*, PLA derived from either *rac*- or *meso*-LA have five tetrad sequences in relative ratios which are determined by the catalyst's ability to enchain monomers in either a *racemic* (*r*) or *meso* (*m*) dyad (2 stereocentres, 1 LA unit). The notation employed by Bovey to describe dyad enchainment is *r* and *m*, where *r* refers to a *racemic* dyad (*RS* or *SR*) and *m* refers to a *meso* dyad (*SS* or *RR*),[99] although it should be noted that PLA literature often contains the notation *i*/*s*, wherein *i* denotes isotactic enchainment (*SS* or *RR*) and *s* denotes syndiotactic enchainment (*RS* or *SR*).

The tacticity of the resultant PLA can be determined from analysis of tetrad resonances (4 stereocentres, 2 LA units) in the $^{13}C\{^1H\}$ and $^1H\{^1H\}$ NMR and the stereosequence is derived from assignments corresponding to the methine region in $^1H\{^1H\}$ NMR and the methine or carbonyl region in $^{13}C\{^1H\}$ NMR. These

assignments are based on those made by Lillie and Schulz,[100] and later Schindler and Harper.[101] The assignment of the NMR resonances to the specific PLA stereosequences were confirmed with HETCOR NMR techniques such as HMQC and HMBC and further analysis of the PLA backbone at the hexad level was conducted using high resolution techniques.[102-109] Figure 1.2 details the currently accepted assignments.[102]

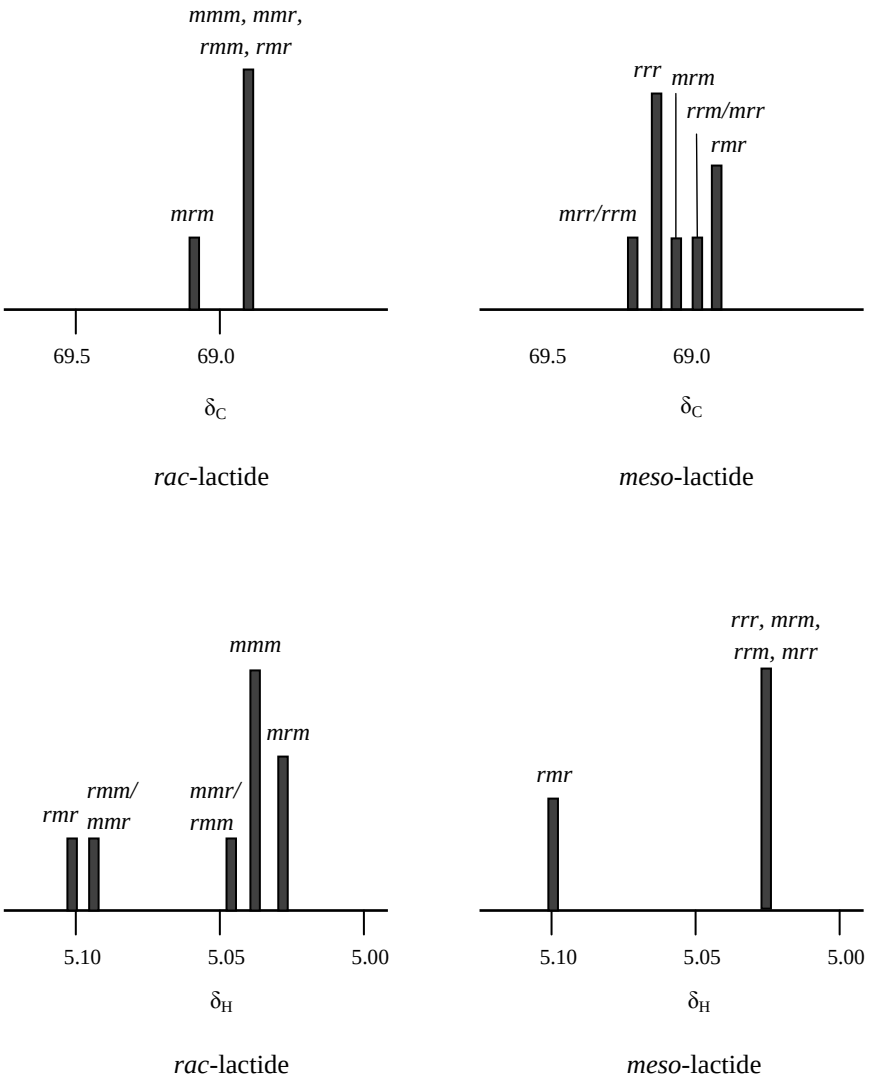


Figure 1.2. Schematic representation of the assignment of PLA tetrads in $^{13}C\{^{1}H\}$ and $^{1}H\{^{1}H\}$ NMR.[102]

The probability of the occurrence of a particular dyad depending on the monomer employed can be calculated using Bernoullian statistics, and equations detailing these probabilities are outlined in Table 1.1.[58]

Table 1.1. Tetrad probabilities based on Bernoullian statistics.[58]

Tetrad	Probability	
	***rac*-LA**	***meso-LA***
[*mmm*]	$P_m^2 + \frac{P_r P_m}{2}$	0
[*mmr*]	$\frac{P_r P_m}{2}$	0
[*rmm*]	$\frac{P_r P_m}{2}$	0
[*rmr*]	$\frac{P_r^2}{2}$	$\frac{P_m^2 + P_r P_m}{2}$
[*rrr*]	0	$P_r^2 + \frac{P_r P_m}{2}$
[*rrm*]	0	$\frac{P_r P_m}{2}$
[*mrr*]	0	$\frac{P_r P_m}{2}$
[*mrm*]	$\frac{P_r^2 + P_r P_m}{2}$	$\frac{P_m^2}{2}$

Starting with *rac*-LA, it is possible to obtain either isotactic or heterotactic PLA, determined by the relative rate constants of *racemic* enchainment ($k_{R/SS}$) and *meso* enchainment ($k_{S/SS}$). Where the two are roughly equal, atactic polymer will result. The degree of heterotactic bias can be expressed as a probability, P_r (or P_m), in which there is a higher probability of forming an *r*-dyad through the insertion of an *L*-LA monomer following a *D*-LA monomer, or vice versa, occurring because the rate constant of *racemic* enchainment is larger than the rate constant of *meso* enchainment (i.e. $k_{R/SS} > k_{R/RR}$). In addition, P_r may be described in terms of rate constants of enchainment: $P_r = k_{R/SS}/(k_{R/SS} + k_{R/RR}) = k_{S/RR}/(k_{S/RR} + k_{S/SS})$. The probability of forming isotactic polymer increases if the rate of *meso* enchainment is larger than that of *racemic* enchainment. Both isotactic and heterotactic PLA formed from *rac*-LA can be expressed in terms of P_r on a scale from 0-1: $P_r > 0.5$ indicates heterotactic PLA whereas $P_r < 0.5$ indicates isotactic PLA. The degree of heterotactic bias can be calculated from application of the above Bernoullian statistics to the resonances in the methine region in the $^1H\{^1H\}$ NMR spectrum. In heterotactic PLA the dominant tetrads will be *rmr* and *mrm* peaks corresponding to *RSSR* and *SSRR* stereosequences

respectively, whilst the *rmm* and *mmr* peaks arise from atactic PLA. P_r can be calculated from the integration of these peaks against the total peak area; however, it is possible to derive P_r by integration of the *rmr* tetrad against the *rmm* tetrad.[33, 58]

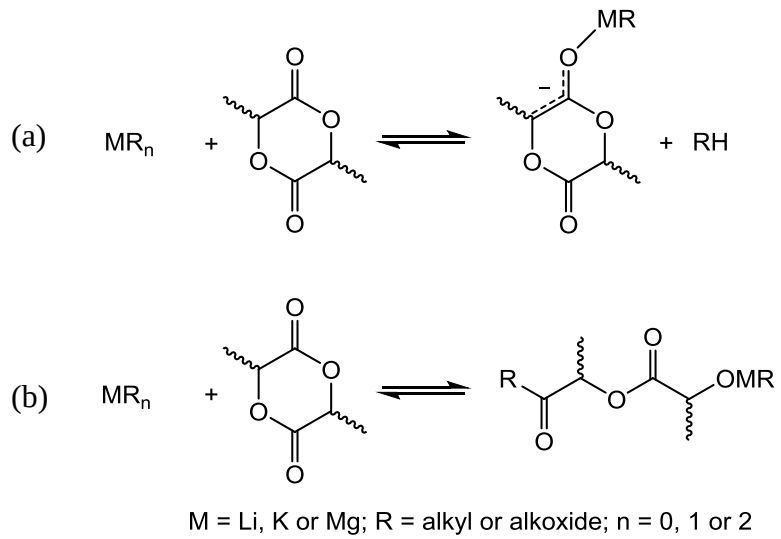
For *meso*-LA, the possible PLA microstructures are syndiotactic or heterotactic and are likewise determined by the relative rate constants of enchainment. In this case, syndiotactic PLA is produced when *racemic* enchainment is favoured ($k_{R/RS} > k_{R/SR}$), therefore $P_r > 0.5$, whereas heterotactic PLA is produced when meso enchainment is favoured ($k_{R/SR} > k_{R/RS}$), $P_r < 0.5$.

1.7 Ionic and metal free ROP

There are many suitable mechanisms through which ROP can occur facilitated by reactive nucleophiles and electrophiles or metal-based initiators.[110] Cationic and anionic pathways have been studied, as well as metal-free systems typically employing organocatalysts or enzymes.[111-113] This section discusses these processes in more detail.

1.7.1 Anionic ROP

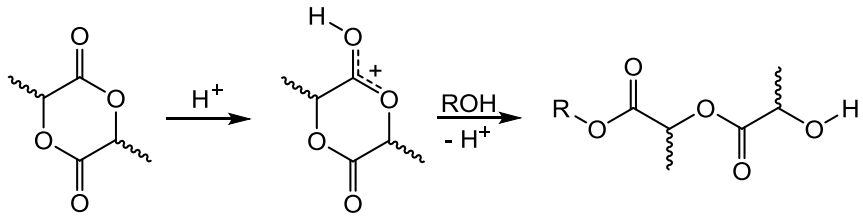
The anionic ROP of lactide has been much less investigated than the coordination-insertion mechanism (Section 1.8.1). This is because whilst higher activities are anticipated when using strong nucleophilic or basic initiators, deleterious side reactions such as transesterification, *vide infra*, become increasingly significant. Investigation into the mechanism of anionic ROP have shown it occurs through acyl bond cleavage with the initiation step being either deprotonation of the monomer, or ring-opening through nucleophilic attack (Scheme 1.3).[21] The two pathways can be differentiated through end-group analysis as the end-group of the polymer produced from nucleophilic attack typically results in ester end-group formation, whereas the deprotonation route does not show any such initiator fragments.[114]



Scheme 1.3. Two mechanistic pathways for the initiation of anionic ROP of LA; (a) deprotonation, (b) nucleophilic attack.[21]

1.7.2 Cationic ROP

The first report of successful cationic ROP of lactide came in the late 1980s by Kricheldorf *et al*, who demonstrated that ROP can occur using trifluoromethanesulfonic acid (HOTf) and methyl trifluoromethanesulfonic acid (MeOTf) as cationic initiators.[115, 116] Analysis of the end-groups by ^{1}H NMR revealed that polymers obtained from MeOTf had a methyl ester end-group, suggesting that the initiation proceeds *via* alkyl-oxygen bond cleavage, as opposed to acyl-oxygen bond cleavage (Scheme 1.4).



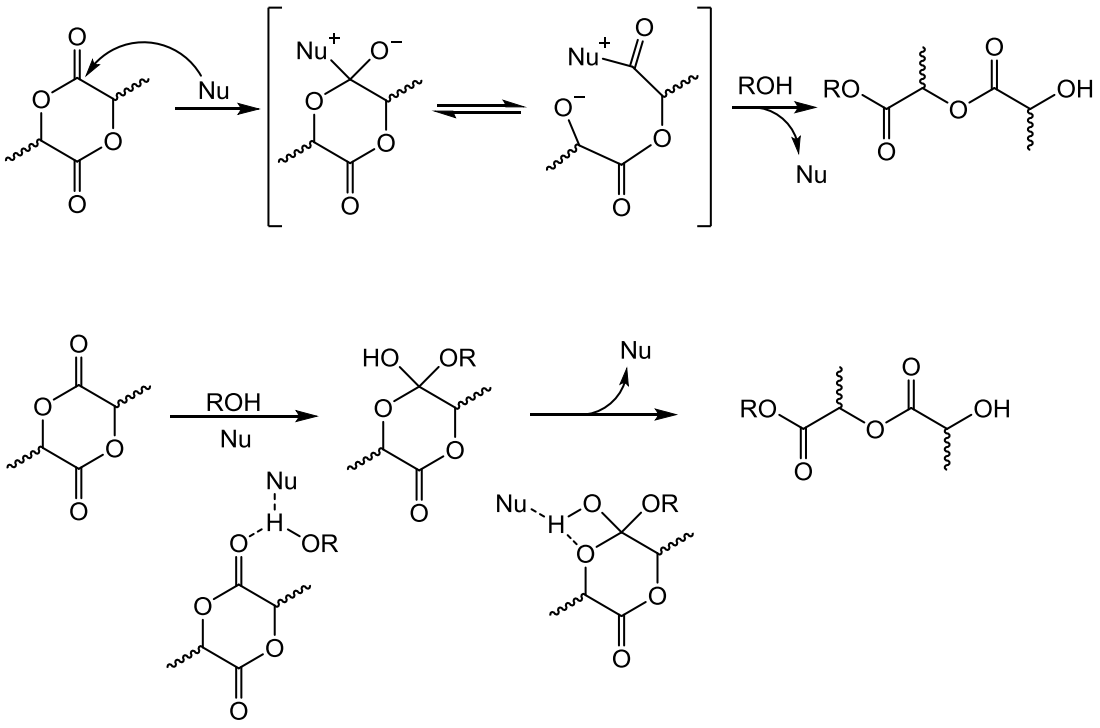
Scheme 1.4. Cationic polymerisation.

This work was expanded upon by Bourissou *et al.* who incorporated a primary or secondary alcohol, such as isopropanol, along with HOTf during polymerisation.[117] The polymerisation exhibited controlled behaviour in which the external alcohol was consumed quantitatively; there was minimal transesterification and no epimerisation of the stereogenic centres of the polymer backbone occurred. In these circumstances,

the end-group was an isopropyl ester group, indicative of acyl-oxygen bond cleavage, contrary to the findings above. Kinetic analysis supported a first-order dependence on [LA], with $k_{obs} = 6.8 \times 10^{-3}$ min^{-1}. On the basis of these findings, Bourissou postulated that the polymerisation proceeded *via* an activated-monomer cationic polymerisation.

1.7.3 Organocatalysts

Organocatalysts are attractive alternatives to metal-based initiators for the ROP of LA as they can be simple, readily available organic molecules which are air and moisture stable, and may be easily removed from the polymer post-polymerisation by washing or trapping with resin beads.[111] Pyridines, *N*-heterocyclic carbenes and phosphazenes are efficient catalysts for the ROP of LA.[112, 118-121] In the presence of a protic initiator such as an alcohol, the organocatalysts most likely polymerise lactide *via* nucleophilic activation of the monomer or base-catalysed transesterification (Scheme 1.5).



Scheme 1.5. Organocatalytic ROP proceeding through nucleophilic (top) or basic (bottom) pathways, where Nu = amine, NHC, phosphazene; ROH = initiating protic agent or growing polymer chain.[110]

The first breakthrough nucleophilic organocatalyst to be used for ROP was 4-dimethylaminopyridine, DMAP, reported in 2001 by Hedrick and coworkers.[118] Using an alcohol as an initiator, the amines were found to be effective initiators for

the ROP of LA at 35 °C in CH_2Cl_2 with reaction times ranging from 20-96 h. Following these results, investigations into NHCs as initiators for ROP were undertaken, and the imidazol-2-ylidene, IMes, carbene shown to be a highly active and well-controlled catalyst.[119, 122, 123]

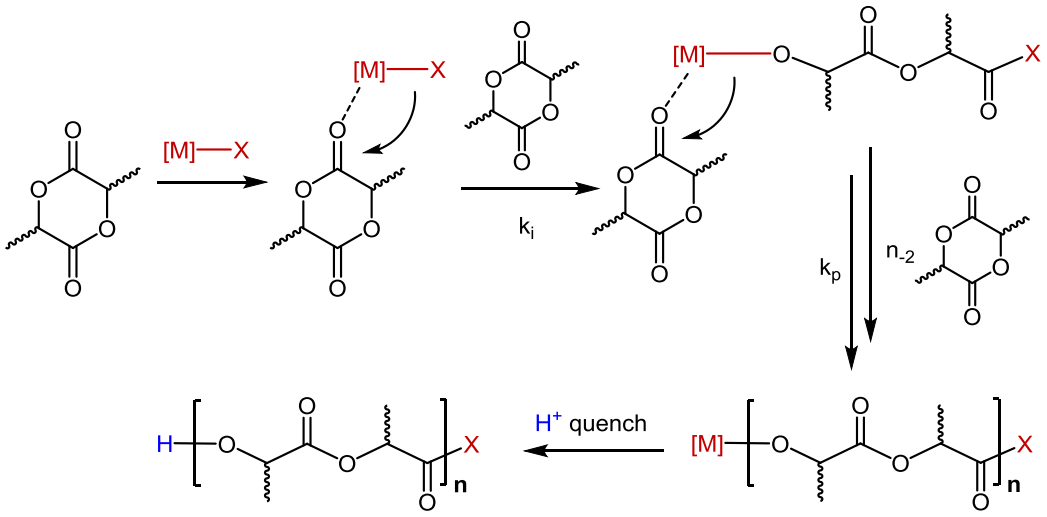
1.8 Metal-mediated ROP

The metal-mediated ROP of cyclic esters typically employs a Lewis acidic metal centre supported by a polydentate ancillary ligand and at least one nucleophilic group, such as an alkoxide, amide or borohydride. A wide range of metals have been studied in this regard including alkali metals,[124-130] alkaline earth metals,[50, 58, 131-135] yttrium,[40, 43, 67, 136] lanthanides,[137-140] Group 4 metals,[141-149] zinc,[58, 150-152] tin,[153-158] aluminium[33, 74, 143, 159-164] and indium.[76, 77, 165] These metals typically follow either activated-monomer or coordination-insertion mechanisms, both of which are discussed in more detail below.

1.8.1 Coordination-insertion polymerisation

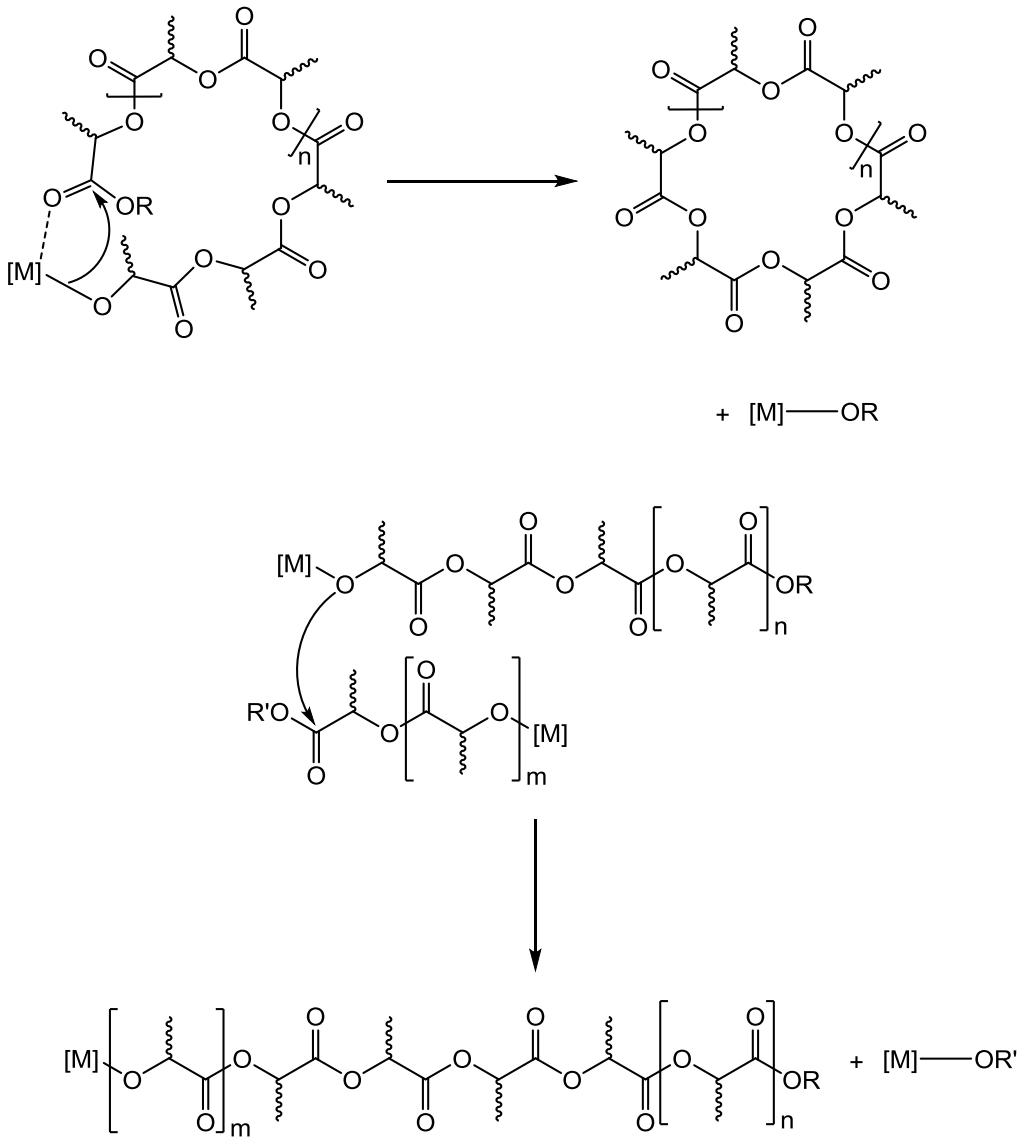
The coordination-insertion mechanism is the most extensively used method to synthesise PLA industrially and in academia. Coordination of the acyl-oxygen to the Lewis acidic metal centre activates it towards attack from initiating group, X, cleaving the acyl-oxygen bond to ring-open the monomer (Scheme 1.6).[7, 21, 110] Insertion of a subsequent lactide monomer allows propagation to continue until full consumption of the monomer. The polymer is liberated through hydrolytic quenching.

In coordination-insertion, propagation is limited by $[catalyst]_0$ and $[monomer]_0$. As a result, obtaining polymers with a molecular weight in close agreement to theoretical values, initiation must be fast compared to propagation ($k_i > k_p$). If initiation is competitive with propagation, insertion of a monomer into the metal-initiator bond of the precatalyst may be favoured kinetically over insertion into a growing polymer chain, causing incomplete initiation, greater than expected polymer weights and broad molecular weight distributions as a result of a large variation in the polymer chain lengths. This is a common occurrence when inefficient initiating groups such as amides are employed.[52, 55, 166-169]



Scheme 1.6. Coordination-insertion mechanism for the ROP of LA. X = initiating group and k_i and k_p are the rate constants of initiation and propagation, respectively.[7, 21, 110]

Polyesters generated through coordination-insertion mechanisms are subject to deleterious side reactions which compete with monomer insertion to alter the structure of the growing polymer chain. These include slow initiation, termination and intermolecular and intramolecular transesterification (Scheme 1.7).[21] As the polyester chain contains multiple ester functional groups, it is possible that one of the acyl-oxygens from the chain competitively coordinate to the metal centre in a similar fashion to monomer insertion, giving rise to branched or cyclic polymers. Intramolecular transesterification, or "back-biting", is the coordination of a terminal acyl-oxygen to the metal centre, followed by intramolecular nucleophilic attack from the metal alkoxide to produce a macrocyclic polymer.[170] Intermolecular transesterification is the redistribution of polymer chains on active propagating species following nucleophilic attack from the active metal alkoxide on an ester linkage on an adjacent polymer.[170, 171] Both processes can be identified using MALDI-ToF MS. Cyclic esters can be identified from their lack of an end-group, and the presence of peak envelopes of Δ m/z = 72.0 g mol^{-1}, corresponding to half a lactide unit, is indicative of transesterification.[170, 172]

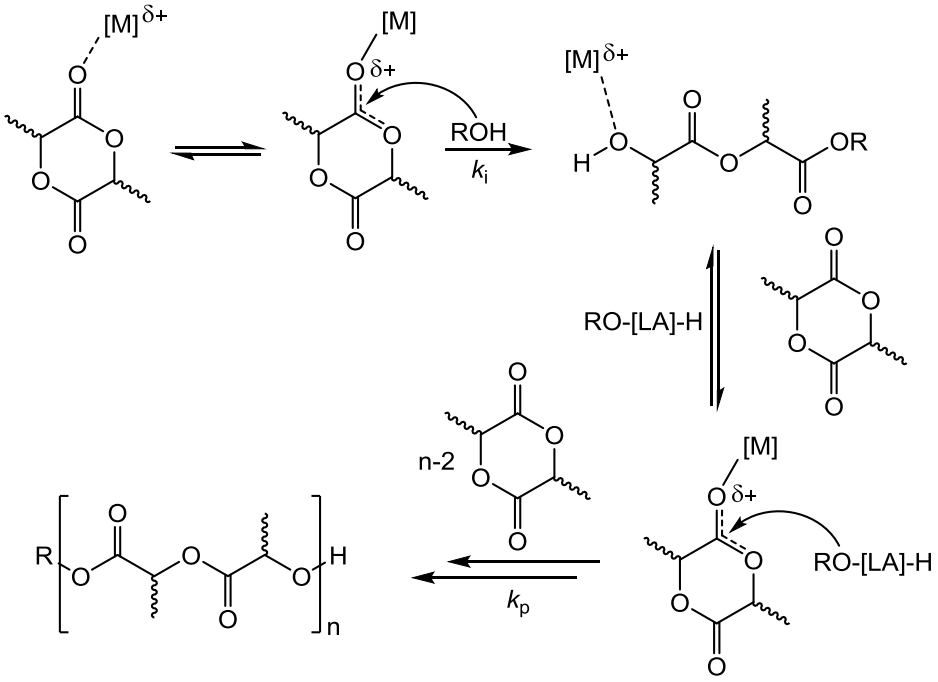


Scheme 1.7. Intramolecular (top) and intermolecular (bottom) transesterification processes in ROP. [M] = metal initiator and R and R' = alkyl groups on the PLA chain.[21, 170-172]

Post-polymerisation transesterification contributes to a decreasing M_n alongside increasing PDI at high monomer conversions.[166] Poor agreement between experimental and calculated M_n, non-linear growth of M_n versus % conversion, broad PDIs and analysis with MALDI-ToF MS can all indicate the degree to which transesterification occurs during a polymerisation reaction. Transesterification may be reduced through optimisation of reaction conditions, including prompt isolation of the polymer upon reaction completion.

1.8.2 Activated-monomer ROP

The activated-monomer mechanism is an alternative pathway for the ROP of LA to the more common coordination-insertion pathway, and frequently employs a simple Lewis acidic metal salt, such as a triflate, which coordinates to the acyl-oxygen of the LA monomer, activating it towards nucleophilic attack from an incoming exogenous alcohol, such as isopropanol or benzyl alcohol (Scheme 1.8).[173, 174] If initiation is efficient, all of the alcohol will be consumed prior to propagation, allowing for one polymer chain to grow per alcohol molecule as opposed to metal centre, and as such the polymer molecular weight is dependent on the $[monomer]_0$:$[alcohol]_0$ ratio.[49, 175, 176] This concept is known as immortal polymerisation and is further discussed in Section 1.9.2.



Scheme 1.8. Mechanism for activated-monomer facilitated ROP of LA. k_i and k_p are the rate constants of initiation and propagation, respectively.[173, 174, 176]

1.9 ROP: thermodynamic and kinetic considerations

The polymerisation of cyclic monomers differs significantly from the polymerisation of unsaturated monomers because it reaches an equilibrium with a relatively high concentration of unreacted monomer. This permits the monomer thermodynamic polymerisability to be inferred from the value of the equilibrium monomer

concentration ($[M]_{eq}$).[177] However, the formal thermodynamic criteria for monomer polymerisability is given by its Gibbs free energy, and similarly for all chemical processes, polymerisation is only possible when $\Delta G_p(xy) < 0$, where x and y denote monomer and polymer states, respectively.

The principal driving force in the ring-opening polymerisation of cyclic monomers is the relief of ring strain which is caused by deviation from non-distorted bond angles, bond distortion, eclipsed hydrogen atoms and nonbonding interactions between substituents.[110] As the polymerisation of most cyclic esters is accompanied with a decrease in entropy due to the loss of translational degrees of freedom, polymerisation is only possible when $|\Delta H_p| > -T\Delta S_p$. Systems in which any monomer-polymer-solvent nonbonding interactions can be disregarded allows the enthalpy of polymerisation to be considered mostly a result of ring strain: a higher ring strain results in a lower equilibrium monomer concentration.

Most six-membered rings cannot be polymerised due to their low ring strain; however, lactide is readily polymerised. In 1990, Duda and Penczek determined the thermodynamic parameters for the polymerisation of *L*-lactide under melt conditions at a temperature range of 80-133 °C. The standard thermodynamic parameters were subsequently found to be $\Delta H°_p$ = -22.9 kJ mol^{-1} and $\Delta S°_p$ = -41.1 J K^{-1} mol^{-1}.[178] In contrast with cyclohexane which occupies a chair conformation, the ester group of δ-valerolactone forces the molecule to adopt a planar conformation introducing ring strain in the form of eclipsed C–H bonds. This increased ring strain can be quantified when comparing their relative thermodynamic parameters: for cyclohexane $\Delta H°_p$ = 2.9 kJ mol^{-1} and $\Delta S°_p$ = -10.5 J K^{-1} mol^{-1} whereas for δ-valerolactone $\Delta H°_p$ = -27.4 kJ mol^{-1} and $\Delta S°_p$ = -65.0 J K^{-1} mol^{-1}.[177, 179] Due to the presence of two ester groups, crystallographically characterised *D*-LA assumes a skew boat conformation in which the ester groups are planar.[180] As *L*-LA should adopt the same conformation, its high degree of ring strain can therefore be attributed to bond opposition and bond angle distortion.

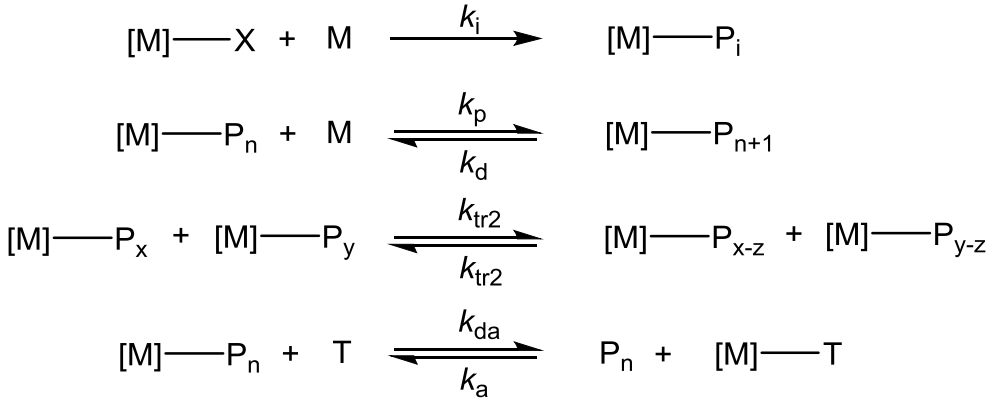
Whilst the above thermodynamic parameters hold true for the ROP of *D*-, *L*- and *rac*-LA, they are not valid for *meso*-LA, which has to be considered separately. As shown in Figure 1.1, *D*- and *L*-LA have two identical stereocentres within the ring, either *R*,*R* or *S*,*S* respectively, resulting in the two methyl groups lying *cis* to each other on the

six-membered ring. *Meso*-LA has two opposite stereocentres, *R,S*, resulting in a *trans* configuration of the methyl groups relative to each other on the ring. In 1992, Kricheldorf investigated the polymerisation of both *rac*- and *meso*-LA using several organotin initiators and found that the polymerisation of *meso*-LA gave lower polymer yields over the same time period when compared to *rac*-LA.[181] For instance, after 2 h at 120 °C, tributyltin methoxide gave a total PLA yield of 91% for *rac*-LA compared to 27% for *meso*-LA. This was hypothesised to be a result of the *trans* conformation of the Me groups which would confer additional thermodynamic stability to the *meso*-LA monomer compared to the less stable *cis* configuration of *rac*-LA. Kricheldorf obtained similar findings with trialkyl aluminium catalysts in the presence of alcohol coinitiators.[182] Contrary to these results, in 2000 Chisholm discovered preferential polymerisation of a 1:1 mixture of *meso*-LA and *rac*-LA in CD_2Cl_2 at 22 °C producing atactic PLA in the presence of trispyrazolyl- and trisindazolylborate supported magnesium and zinc alkoxide initiators.[51] To explain these findings, the solid state structure of *meso*-LA was obtained and found to be between a twist boat and planar conformation. PC MODEL calculations using the coordinate data of the solid state structures of *meso*-LA and *rac*-LA were performed finding the relative minimised energies (MMX) of *meso*-LA in the planar conformation and *rac*-LA to be 0.24 kcal mol^{-1} and 0.14 kcal mol^{-1}, respectively. In addition, consistent valence force field (CVFF) calculations showed that *rac*-LA is 0.4 kcal mol^{-1} more stable than *meso*-LA, further supporting the experimental findings of Chisholm *et al*. More recent work by Okuda using indium, alkaline earth and Group 3 initiators support the hypothesis that the polymerisation of *meso*-LA is faster than *rac*-LA attributed to the lower stability of the monomer.[85, 86, 89, 93, 95, 183]

The thermodynamic parameters of polymerisation are not the sole measure of a monomer's reactivity, and it is necessary to consider the kinetics of the polymerisation process. As the polymerisation of cyclic esters is in equilibrium, depropagation, k_d, as well as propagation, k_p, may occur. In addition, consideration of the polymerisation kinetics allows for valuable insight to be obtained into the activity of initiators.

1.9.1 Living polymerisation

A polymerisation reaction in which there are no termination or transesterification pathways and in which the activation is sufficiently rapid such that $k_i \geq k_p$ is considered to be a living polymerisation.[184, 185] In such a system, the reaction proceeds with a linear increase in polymer molecular weight versus monomer conversion and little chain transfer, with 1 polymer chain growing per metal initiator, resulting in predictable molecular weights and a narrow molecular weight distribution.[58, 186, 187] Scheme 1.9 details elementary kinetic models for a living polymerisation where M is the monomer, [M]–P is the propagating polymer chain, T is a deactivating agent, k_i is the rate constant of initiation, k_p is the rate constant of propagation, k_d is the rate constant of depropagation, k_{tr2} is the rate constant of bimolecular transfer to a polymer with chain rupture (transesterification), and k_{da} and k_a are the rate constants of temporary deactivation and activation, respectively.[110, 171]



Scheme 1.9. Kinetic scheme of a living polymerisation.

The rate law for a living polymerisation may be considered in terms of k_p, where both k_i and k_{tr2} are omitted as they do not impact the rate.[7] Additionally, k_p may be reported as k_{obs} or k_{app}: the pseudo first-order rate constant, which details the apparent rate constant under certain reaction conditions and is derived experimentally by monitoring the consumption of LA monomer against time. Living polymerisations typically show a first-order dependence in $[LA]_0$ (Equation 1.5).

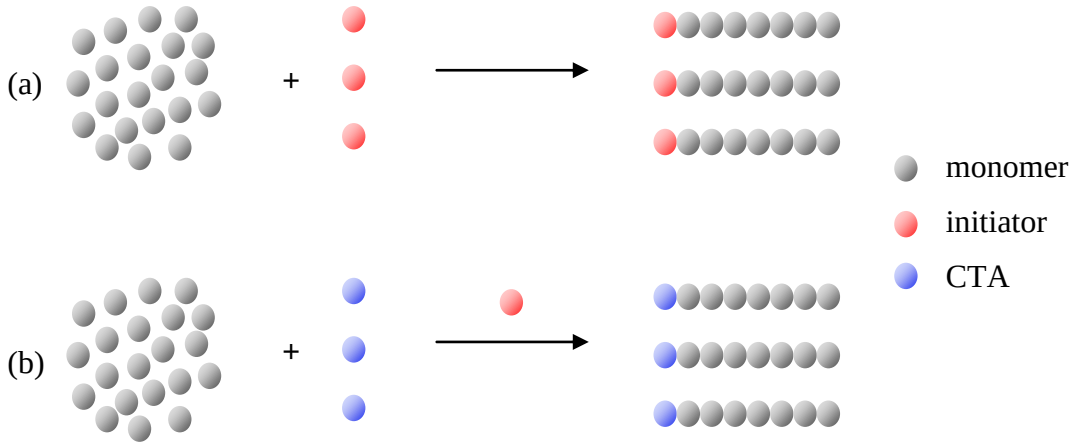
$$-\frac{d[LA]}{dt} = k_p[LA]_0[I]_0^n$$

Equation 1.5

An ideal living polymerisation in which there is an absence of chain transfer or termination reactions should reveal a linear relationship between $[LA]_0$ and time upon construction of a semilogarithmic kinetic plot. Whilst it has been suggested that comprehensive treatment of kinetic data should incorporate the equilibrium monomer concentration into the first-order rate equation, the elementary Equation 1.5 is satisfactory for relative comparisons.[110, 188] In addition to termination which results in rate decrease as the reaction proceeds, deviations from linearity also occur when there is slow initiation resulting in rate increase.[110] So-called "induction periods" in which there is a latency period prior to a linear dependency have been reported in the literature and may be the result of formation of initiator aggregates or where there exists another impediment to the metal-initiator bond such as ligand rearrangement.[26, 189-193] Whilst living polymerisations are typically first-order in $[LA]_0$, second-order polymerisations have been reported previously in the literature.[194-197] Previous reports have indicated that a second-order dependence on $[LA]_0$ may be the result of two lactide monomers entering the transition state cooperatively or non-innocent ligands.[165, 194, 198]

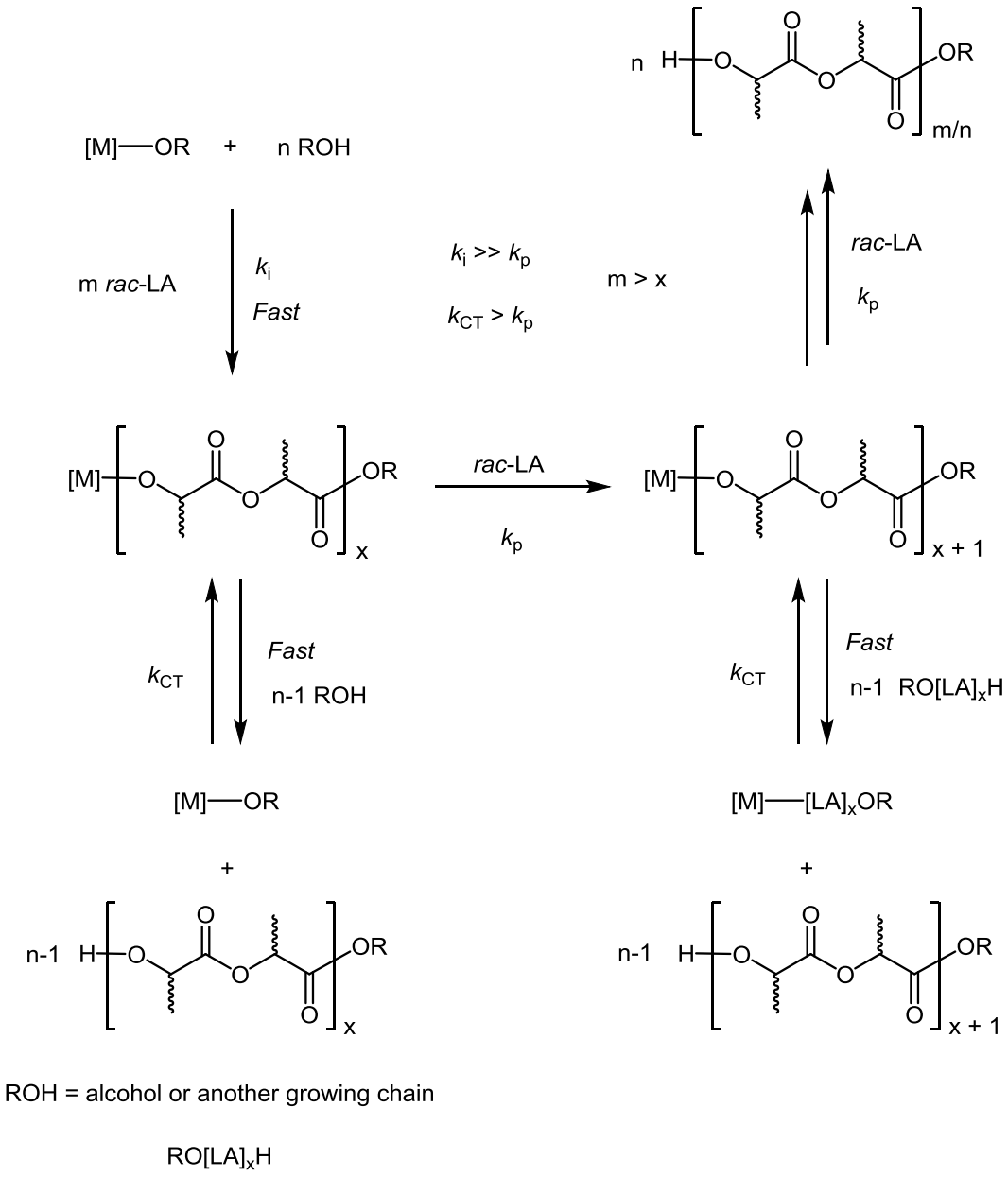
1.9.2 Immortal ring-opening polymerisation

In the late 1980s, Inoue pioneered the first "immortal polymerisation" system in which the polymerisation of an epoxide was catalysed by a porphyrin-supported aluminium alkoxide[199-201] which was expanded to include the immortal ring-opening polymerisation (*i*ROP) of cyclic esters.[202-204] This process has been further developed using Al precatalysts,[205-207] and has extended to other metals such as alkali metals,[208] Mg,[176, 209, 210] Ca,[26, 176, 211] Zn,[128] In,[165, 212] Sn[213] and Y.[42, 49, 167, 214-216] Unlike living polymerisation in which the initiator can be killed by protic contaminants leading to premature termination of polymerisation, in *i*ROP the protic species react with the growing chain to produce polymers of narrow molecular weight distribution where the number of polymer molecules corresponds to the number of molecules of protic species, or chain transfer agents (CTA), added.[217] A graphical representation of the concepts of living and immortal polymerisation is presented in Scheme 1.10.



Scheme 1.10. Representation of living polymerisation (a) and *i*ROP (b).[173, 217]

As with living ROP, *i*ROP requires a higher rate of initiation versus propagation ($k_i > k_p$) to allow for controlled polymer growth. In addition the rate of chain transfer must also be greater than propagation ($k_{CT} > k_p$) to produce polymers of narrow molecular weight distribution.[217] The alcohol initiators, or alcohol-terminated polymer chains, are so-called "chain transfer agents" (CTA) as they are labile on the metal centre, allowing for rapid exchange between the growing polymer chains. Metal catalyst-mediated immortal ROP can occur through two mechanisms: coordination-insertion and activated-monomer. In systems of the type [M]–X, where X is a nucleophilic initiating group, treatment with a protic CTA generates a new active species *in situ* through protonolysis of the [M]–X bond. During initiation, the incoming monomer coordinates to the catalyst, activating the carbonyl bond to nucleophilic attack from the alkoxide initiator and forming the propagating species [M]–$[LA]_n$–OR. The growing polymer then undergoes rapid exchange with other protic species, such as additional equivalents of alcohol, allowing for rapid and reversible interchange between active and dormant chains. Scheme 1.11 illustrates the mechanism through which *i*ROP occurs.



Scheme 1.11. *i*ROP of *rac*-LA using alcohol chain transfer agents.[42, 216, 217]

*i*ROP has many advantages over classical living ROP: it requires lower quantities of precatalyst therefore offering enhanced productivity and lowering the cost of reaction. In addition to these economic reasons, polymers produced in this manner typically have a narrower molecular weight distribution than those produced according to living ROP as there is little opportunity for deleterious transesterification reactions to occur as the polymer predominantly exists as a dormant chain during polymerisation. Provided that $k_{CT} > k_p$, the molecular weight of the polymer should be in close agreement with the expected values where M_n is determined by the [*rac*-LA]$_0$:[coinitiator]$_0$ ratio, allowing for well-controlled polymer synthesis. If the rate of

chain transfer is slow relative to propagation, this can lead to an increase in the molecular weight distribution as the active chain is bound to the metal centre for a comparatively long period, and may result in higher than anticipated molecular weights due to inefficient chain transfer. Furthermore, the end-groups may be easily functionalised, as the end-group is determined by the CTA employed.[218] Research in the Mountford group has previously demonstrated the ability of BnOH and $BnNH_2$ to act as CTA in the ROP of *rac*-LA producing BnO- and BnNH-capped polymers.[49, 128, 165, 219, 220]

1.10 Literature review

1.10.1 Industrial ROP catalysts

The most widely used catalyst in the industrial ROP of lactide is tin (II) octanoate, $Sn(Oct)_2$, selected for its ease of handling, versatility, solubility and its FDA approval as a food additive (Figure 1.3).[17, 22] It is proposed that $Sn(Oct)_2$ operates through an activated-monomer mechanism through which a monomer coordinated to the metal catalyst is ring-opened by an alcohol co-initiator, followed by propagation *via* a coordination-insertion mechanism.[221, 222] Although $Sn(Oct)_2$ is approved for use as a food additive, it remains restricted for biomedical applications due to its toxicity.[222] As such, alternative less toxic initiators based on aluminium and zinc have been developed.[223-226] Despite their less toxic nature, both aluminium and zinc initiators are far less active than their tin counterparts.

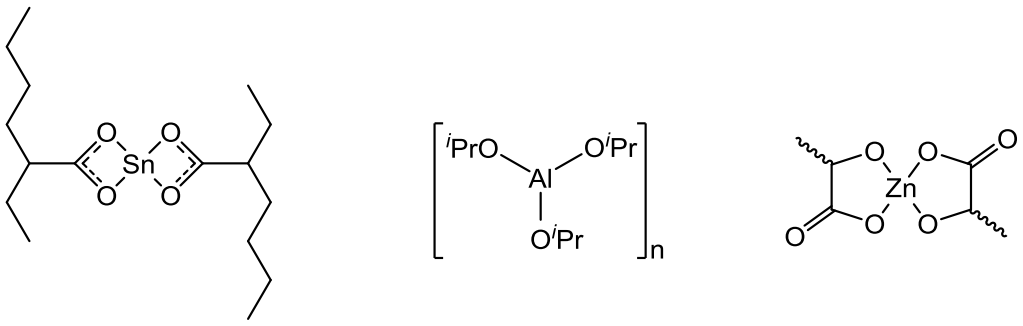


Figure 1.3. Structures of industrially-employed ROP catalysts, $Sn(Oct)_2$, aluminium isopropoxide and zinc lactate.[110]

As the macroscopic properties of PLA depend greatly on stereotacticity, considerable efforts have been made to develop well-defined single site catalysts capable of exerting stereocontrol during polymerisation. A selection of the most prominent examples is discussed in Sections 1.10.2-1.10.4.

1.10.2 Initiators for the formation of isotactic/stereoblock PLA from *rac*-LA

A major breakthrough in the field of stereoselective ROP of LA came from Spassky and coworkers in 1996.[227] They discovered that the chiral initiator, the (*R*)-enantiomer of bis(naphthyl) aluminium salen complex **1.1** (Figure 1.4) preferentially polymerising *D*-LA over *L*-LA by a ratio of 20:1, resulting in the formation of tapered stereoblock PLA from *rac*-LA. At conversions less than 50%, the PLA was predominantly isotactic PDLA, but at conversions higher than 60% only *L*-LA remained in solution, forming predominantly PLLA. Full conversion of 75 equivalents of *rac*-LA was only achieved after 113 h due to the low rate of propagation of *L*-LA compared to *D*-LA. The resultant PLA had a T_m = 187 °C, higher than that of enantiopure isotactic PLA with T_m = 170-180 °C. Coates and Ovitt prepared the analogous complex, **1.2**, with an isopropoxide initiating group to prevent formation of a bimetallic side product when using **1.1**, and polymerised *rac*-LA under identical conditions to Spassky.[33, 228] Through analysis of stereoerrors present in the methine region of the $^1H\{^1H\}$ NMR spectrum, they reported the microstructure of the material produced to be a stereoblock copolymer of PLLA and PDLA with T_m = 179 °C, and not enantiomerically pure PLA, as suggested by Baker and Smith.[229]

Feijen used the Jacobsen ligand to prepare enantiomerically pure (*R*,*R*)-**1.3** and *rac*-**1.3**.[74, 75] It was shown that (*R*,*R*)-**1.3** had a moderate activity in the polymerisation of *rac*-LA, and was shown to have a strong preference for the polymerisation of *L*-LA compared to *D*-LA, whereby *L*-LA was preferentially polymerised 14 times faster than *D*-LA. *Rac*-**1.3** was shown to form stereoblock PLA from *rac*-LA in toluene at 70 °C (P_m = 0.93 at 85% conversion) and also under melt conditions at 130 °C (P_m = 0.88). Examination by Chisholm revealed that the stereoselectivity arising from the ROP of *rac*-LA using (*R*,*R*)-**1.3** was the result of a combination of the chirality of the complex, the initiating group and solvent, rendering it difficult to definitively ascribe the selectivity to either chain end or enantiomorphic site control.[98, 230]

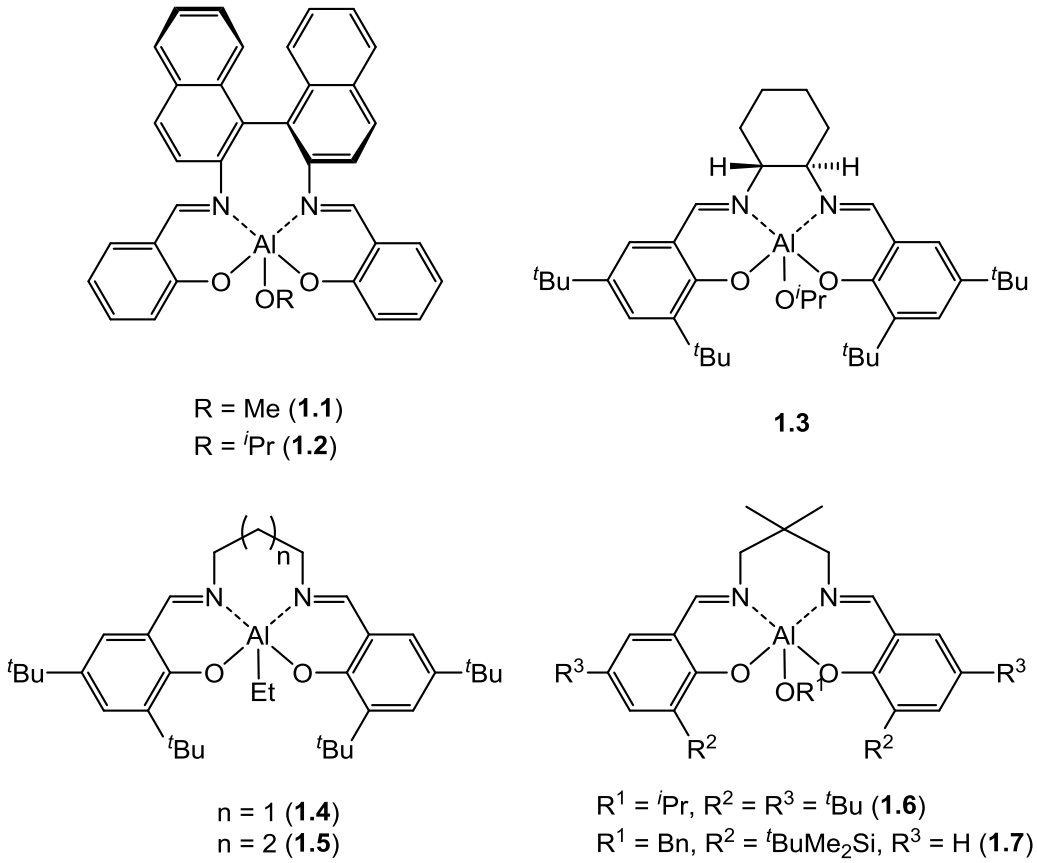
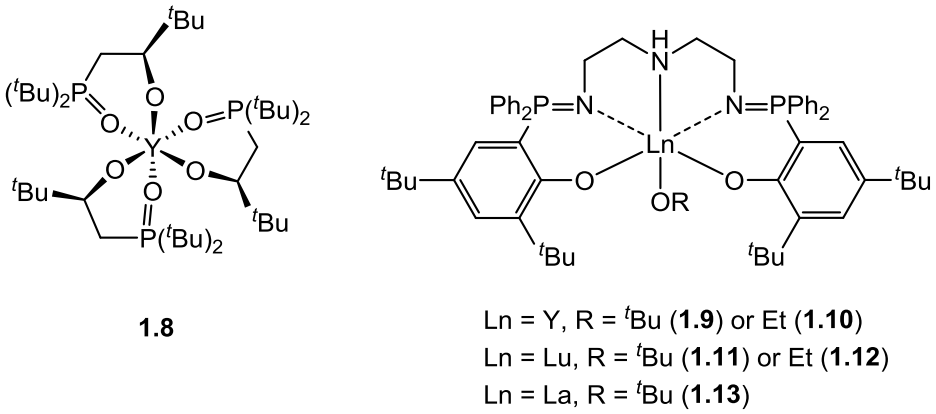


Figure 1.4. Salen-supported aluminium alkoxide initiators.[33, 65, 69, 74, 75, 98, 164, 227-232]

Achiral salen ligands have also proved to be efficient initiators for the stereocontrolled ROP of *rac*-LA arising in stereoblock PLA. Nomura *et al*. reported the isoselective polymerisation of *rac*-LA from the *in situ* generated aluminium alkoxide initiators **1.4** and **1.5** in the presence of an exogenous alcohol coinitiator.[231] Using benzyl alcohol and proceeding *via* a chain end control mechanism, complex **1.5** with an isopropylene bridge produced isotactically enriched PLA with a higher P_m = 0.91 compared to that produced by **1.4**. It was postulated that the higher degree of enrichment was due to increased flexibility arising from the isopropylene bridge. In 2003, Chen and coworkers reported complex **1.6** generating stereoblock PLA from *rac*-LA with a P_m of 0.90 and a T_m of 201 °C.[65, 69] Further work conducted by Nomura *et al*. proved **1.6** maintained its high isoselectivity under bulk melt conditions (P_m = 0.84 and T_m = 169 °C).[232] In 2007, Nomura *et al.* synthesised the analogous complex **1.7** featuring a bulky ^{t}BuMe$_2$Si substituent in the *ortho* position on the phenol groups. This catalyst formed the highest stereoblock PLA prepared to date using an achiral catalyst with *rac*-LA (P_m = 0.98 and T_m = 210 °C).[164]



1.8

Ln = Y, R = ^{t}Bu (**1.9**) or Et (**1.10**)
Ln = Lu, R = ^{t}Bu (**1.11**) or Et (**1.12**)
Ln = La, R = ^{t}Bu (**1.13**)

Figure 1.5. Rare earth initiators for isoselective ROP of *rac*-LA.[62, 63, 66, 67, 233]

Initiators which produce isotactically enriched PLA are not limited to salen-supported aluminium alkoxide complexes. In 2008, Arnold *et al*. showed that the racemic C_3-symmetric yttrium alkoxide complex **1.8** (Figure 1.5) produced isotactically enriched PLA even at -18 °C, offering good control over molecular weights and narrow PDIs.[233] The polymer had a P_m of up to 0.83, and the chains were found to be terminated by a ligand molecule, suggesting in the absence of an alcohol the alkoxide ligand acts as the initiating group. Analysis of the stereoerrors present in the methine region of the ^{1}H{^{1}H} NMR spectrum revealed the polymer to be stereocomplex PLA. The resonances belonging to the *mmr*:*mrm*:*rmr*:*mrr* tetrads in the ratio 1:2:1:1 are indicative of a single insertion defect, producing a polymer chain with a stereocomplex backbone (i.e. –*RRRRRRSSRRRRRR*–) as opposed to a stereoblock backbone (i.e. –*RRRRRRSSSSSSRRRR*–).

Recently Williams *et al*. introduced a series of well-controlled heteroselective phosphasalen-supported yttrium alkoxide complexes with featuring alkyl diimine linker groups.[62, 63] However, the introduction of an diethylamine linker between the diimine to generate the hexacoordinate yttrium complexes **1.9** and **1.10** allowed for the controlled production of moderately isotactically enriched PLA (P_m = 0.72-0.84) under a temperature range of 258-298 K.[67] Determination of the polymer structure revealed it to be stereoblock isotactic PLA produced *via* a chain end control mechanism, and the observed stereocontrol was attributed to increased steric hindrance at the site of insertion. Further investigation by Williams into metal-size dependency of these complexes showed that the analogous lutetium complex **1.11** had a slightly higher degree of isoselectivity than **1.9** and **1.10** (P_m = 0.81-0.84 at 298 K)

whereas the lanthanum analogue **1.13** produced moderately heterotactic PLA (P_r = 0.72).[66] Whilst the isotactic enrichment of the aluminium salen complexes was found to be higher, complexes **1.9-1.11** offer higher activities and greater tolerance to high monomer loading, increasing their applicability.

1.10.3 Initiators for the formation of heterotactic PLA from *rac*-LA

The chain end controlled ROP of *rac*-LA is more frequently found to furnish heterotactically enriched PLA and herein the most prominent examples of initiators affording highly heterotactically enriched PLA are discussed. A common occurrence when employing oxygen based ligands is the tendency for complexes to exist as dimers or higher aggregates in the solid state.[124, 125, 195, 234-236] This problem may be circumvented through the employment of nitrogen containing ancillary ligands: the additional substituent on the nitrogen atom is expected to provide greater steric hindrance prevent aggregation.[110]

Amino-bis(phenolate) ligands are tetradentate [ONNO]-based ligands featuring a donor group on a pendant arm and have been coordinated to a number of Group 3 metals and lanthanides for investigations into the ROP of LA.[40-42] Several prominent examples are noted in Figure 1.6. These ligands are particularly versatile as, in addition to metal and initiating group variation, there is scope to tune the ligand through variation of the substituents on the phenolate rings from ^{t}Bu groups and also the donor functionality of the pendant arm. As a general trend, complexes employing such ligands are typically highly active for the ROP of LA, reaching completion after a few minutes at room temperature in toluene or THF, and are very well-controlled.[41]

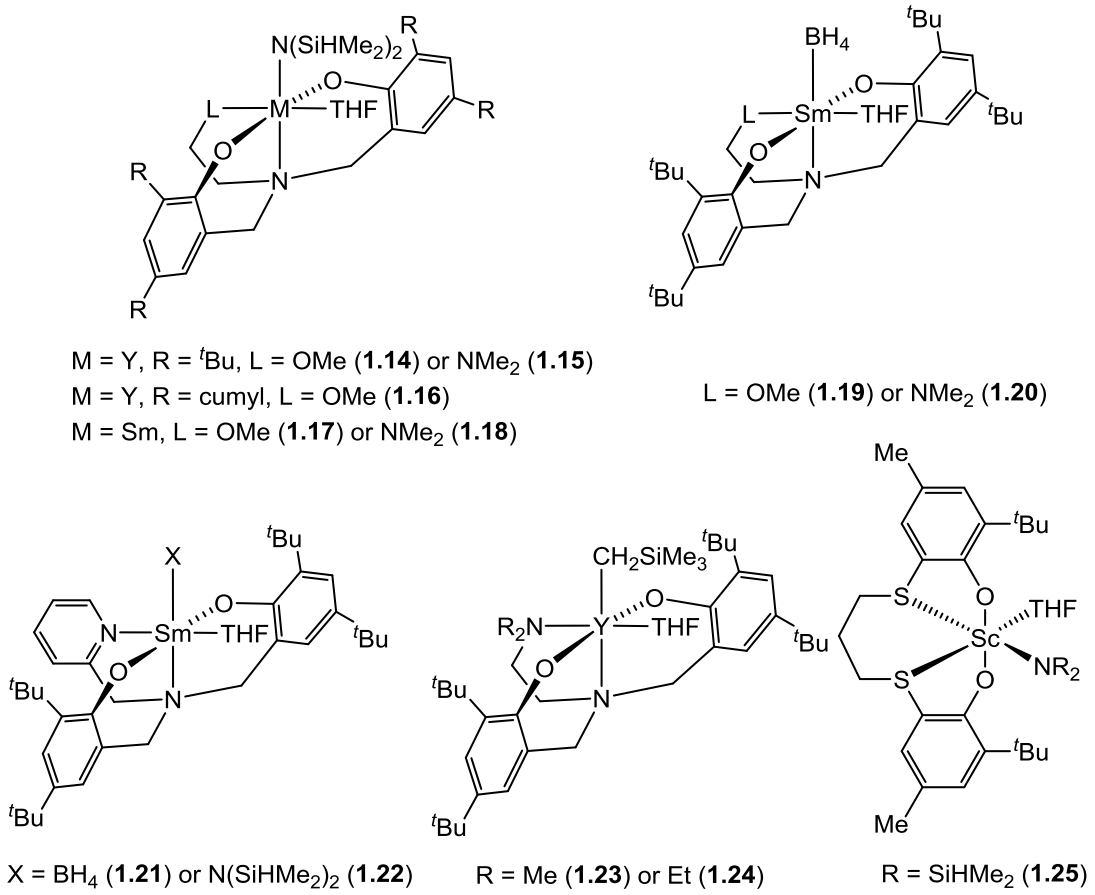


Figure 1.6. Examples of amino-bis(phenolate) and 1,ω–dithiaalkanediyl-bridged bis(phenolate) rare earth complexes.[41, 46, 90, 166, 194, 237]

Carpentier reported the amino-bis(phenolate) supported yttrium complexes **1.14**-**1.16**, synthesised from the treatment of 1 equivalent of the protioligand with $Y\{N(SiHMe_2)_3\}THF_2$.[41, 237] The influence of the pendant donor group was examined through the comparison of **1.14** and **1.15**: when treated with 100 equivalents of *rac*–LA in THF at room temperature, both reached completion after 5 minutes (M_n(calc) = 14,400 g mol^{-1}); however, **1.14** showed slightly improved molecular weight control (M_n(obs) = 15,500 g mol^{-1} for **1.14** *cf.* M_n(obs) = 20,900 g mol^{-1} for **1.15**) and a much greater heteroselectivity (P_r = 0.80 for **1.14** *cf.* P_r = 0.60 for **1.15**). Upon substitution of the ^{t}Bu groups on the phenolate rings in **1.14** to more bulky cumyl substituents, **1.16**, the heterotactic bias was further improved (P_r = 0.90) and was attributed to increased steric bulk in the *ortho* positions on the rings. Despite this, **1.16** showed poorer molecular weight control (M_n(obs) = 26,300 g mol^{-1}) and was 4 times slower to reach full conversion than **1.14**.

Samarium analogues of **1.14** and **1.15**, **1.17** and **1.18**, were synthesised by Dr. Hellen E. Dyer, along with borohydride and amide complexes **1.19**-**1.22**.[166, 194] The borohydride complexes, $Sm(O_2N^L)(BH_4)(THF)$ (where L = OMe (**1.19**), NMe_2 (**1.20**) or pyr (**1.21**)) were found to exist as monomeric THF adducts; however, upon sustained exposure to reduced pressure, the THF ligand dissociated and the complex adopted a dimeric structure, bridging through the phenolate rings of the ligand. Their potential as catalysts for the ROP of *rac*-LA was evaluated: each complex was treated with 200 equivalents of *rac*-LA in THF at room temperature and their activity and molecular weight control monitored. All complexes were highly active; the highest activity was recorded with **1.20**, which reached 80% conversion after 5 minutes and 92% conversion after 30 minutes. The molecular weights were consistently lower than expected, for instance, with **1.19** after 5 min M_n(obs) = 11,600 g mol^{-1} (M_n(calc) = 18,160 g mol^{-1}) and after 30 min M_n(obs) = 13,800 g mol^{-1} (M_n(calc) = 23,348 g mol^{-1}), and molecular weight distributions were moderate to broad (PDI = 1.41-1.79). Analysis of the polymer using MALDI-ToF MS revealed the presence of cyclic structures. All complexes had a strong heterotactic bias (P_r = 0.78-0.84), similar to those observed by Carpentier; however, a decline in heterotactic enrichment of 0.01-0.06 was observed for all complexes between 5 and 30 minutes. These findings are consistent with transesterification side reactions in which scrambling of the heterotactic tetrads occur.

Under similar conditions, selected reactions were conducted with the samarium amide complexes, $Sm(O_2N^L)\{N(SiHMe_2)_2\}(THF)$ (where L = OMe (**1.17**), NMe_2 (**1.18**) or pyr (**1.22**)). These complexes were found to be considerably more active for the ROP of *rac*-LA, for example **1.17** reached 95% monomer conversion after 5 minutes; however, molecular weight control was significantly poorer with higher than anticipated molecular weights obtained after 5 minutes of reaction (M_n(obs) = 58,200 g mol^{-1} *cf.* M_n(calc) = 27,512 g mol^{-1}) which subsequently decreased after 30 minutes (M_n(obs) = 33,800 g mol^{-1} *cf.* M_n(calc) = 28,088 g mol^{-1}) with concurrent broadening of PDI (1.43 to 1.94). The MALDI-ToF MS spectra were dominated by cyclic polymers, which provide further evidence of post-polymerisation transesterification reactions producing polymer chains of greatly varying length and cyclic entities. A similar degree of heterotactic enrichment to that reported by Carpentier was also observed with these complexes (P_r = 0.76-0.81).

Cui *et al*. reported two achiral yttrium alkyl complexes $Y(O_2N^L)(CH_2SiMe_3)(THF)$ (where L = Me (**1.23**) or Et (**1.24**)), which had comparatively lower activities than the amides reported by Carpentier but had significantly higher heteroselectivity with P_r values of 0.95-0.99.[46] Analysis of the propagating species with ^{1}H NMR was conducted and revealed that the ligand retained its geometry during polymerisation, with the pendant arm remaining coordinated to the metal centre favouring insertion of the alternating enantiomeric forms of the monomer.

Okuda *et al*. synthesised a range of Group 3 and lanthanide complexes supported by 1,ω-dithiaalkanediyl-bridged bis(phenolate) ligands.[60, 61] Notably, scandium complex **1.25** showed excellent heteroselectivity (P_r = 0.96) when polymerising 300 equivalents of *rac*-LA in the presence of 1 equivalent ^{i}PrOH in THF at room temperature, reaching 63% conversion after 8 h. A derivative of this complex was synthesised through treatment of **1.25** with (*R*)-*tert*-butyl lactate and used as a model complex to understand the mechanism of propagation leading to the high stereocontrol. The complex was structurally characterised using X-ray crystallography and found to be dimeric in the solid state. Analysis of the complex by ^{1}H NMR spectroscopy in C_6D_6 revealed the complex retained its dimeric structure in solution, existing as a single diastereomer with a *Λ,Λ* configuration induced by the *R* configuration of the lactate ester. Ligand interaction with incoming monomers favoured the insertion of alternating enantiomeric forms of the monomer, emphasising the role ligand recognition plays in stereocontrol.[61, 90]

1.10.4 Initiators for the stereocontrolled polymerisation of *meso*-LA

Meso-LA is a obtained as a byproduct of the purification of *L*-LA; however, despite being known for over 25 years,[238] there is a relative paucity of stereoselective single site initiators for the ROP of *meso*-LA when compared to the number documented for the ROP of *L*- or *rac*-LA. A few selected examples are given in Figure 1.8. As highly syndiotactic PLA has a T_m range of 119-150 °C, indicative of partial crystallinity,[90] the efficient stereocontrolled polymerisation of *meso*-LA is of considerable interest in order to further reduce cost of production and waste in pursuit of biorenewable PLA. As [ONNO]-tetradentate ligands such as salen and amino-bis(phenolates) have shown a great capacity for effecting highly stereoregular PLA from *rac*-LA, it is unsurprising

that they have been successfully applied to the ROP of *meso*-LA affording highly syndiotactic and heterotactic PLA.[41, 58, 90]

Following the work of Spassky and coworkers on the isoselective polymerisation of *rac*-LA,[227] Ovitt and Coates probed the stereoselectivity of both the (*R*,*R*)-enantiomer and a racemic mixture of the salen-supported aluminium isopropoxide complex **1.2** in the ROP of *meso*-LA.[33, 87] When treated with 100 equivalents of *meso*-LA at 70 °C in toluene, enantiopure **(*R*,*R*)-1.2** reached 94% conversion after 40 h. The polymerisation was well-controlled producing polymer of M_n(obs) = 12,030 g mol^{-1} *cf.* M_n(calc) = 13,540 g mol^{-1}) with a molecular weight distribution of 1.05. Its high degree of syndiotacticity (P_r = 0.96) resulted in the polymer exhibiting crystallinity, with a T_m = 152 °C. Interestingly, when ***rac*-1.2** was employed, the polymer produced was amorphous (M_n(obs) = 13,600 g mol^{-1} *cf.* M_n(calc) = 13,600 g mol^{-1}; PDI = 1.07); however, structural analysis revealed the polymer to have a high degree of heterotactic enrichment (P_m = 0.80).

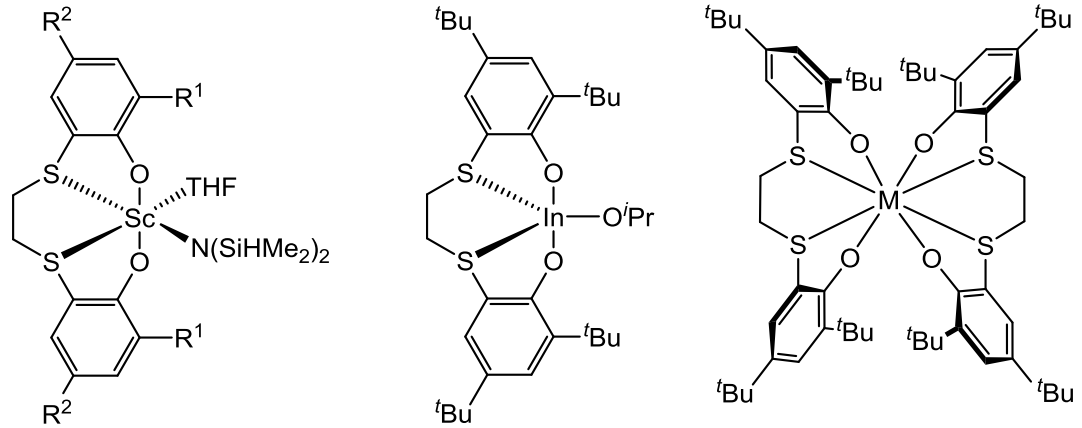


Figure 1.7. Examples of initiators for the stereocontrolled ROP of *meso*-LA.[90, 94, 239]

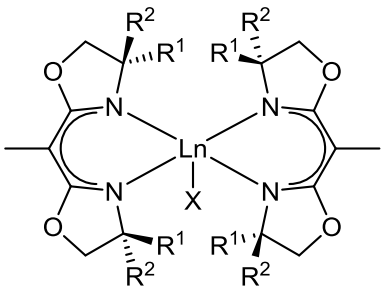
In 2010, Okuda *et al*. reported a series of heteroselective rare earth initiators for the ROP of *meso*-LA employing a 1,ω-dithia-alkanediyl-bridged bis(phenolate), or [OSSO], supporting ligand (Figure 1.7).[90] In the presence of 100 equivalents of *meso*-LA in toluene at 25 °C, both complexes were found to be moderately active: following 30 min, complex **1.26** achieved >99% conversion, whereas complex **1.27** achieved 88% conversion. Significantly, both complexes were highly syndioselective: **1.27** afforded a slightly higher degree of syndiotactic enrichment than complex **1.26**,

which was attributed to the greater steric bulk of the cumyl substituents (P_r = 0.92 *cf.* 0.88). However, complex **1.27** exhibited poorer molecular weight control with considerably broader polydispersities than **1.26**. An analogous indium complex (**1.28**), previously employed for the ROP of *L*-LA,[239] was found to be less active than the scandium congeners, but offered comparable selectivity: when treated with 100 equivalents of *meso*-LA in toluene at 25 °C, **1.28** achieved >99% conversion following 16 h, affording highly syndiotactically enriched PLA (P_r = 0.93) Moreover, **1.28** offered narrower polydispersities than either **1.26** or **1.27** (PDI = 1.09).

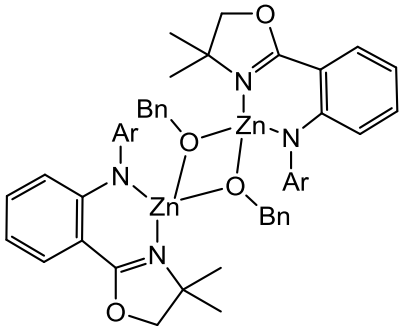
Further work by Okuda *et al*. showed the potential for Group 4 complexes featuring [OSSO]-type supporting ligands to afford heterotactic (P_m > 0.70) PLA from *meso*-LA.[94] Although complexes **1.29** and **1.30** exhibited modest activities for the ROP of *meso*-LA, achieving 79% and 81% monomer conversion, respectively, after 48 h at a 1 mol % catalyst loading in toluene at 100 °C, both complexes were highly heteroselective (P_m *ca*. 0.75-0.80). Variation of the substituents on **1.29** to the more bulky –C(CH_3)$_2$Ph allowed for slightly higher heteroselectivities to be accessed (P_m = 0.90).

1.11 Oxazoline ligands in ROP of cyclic esters

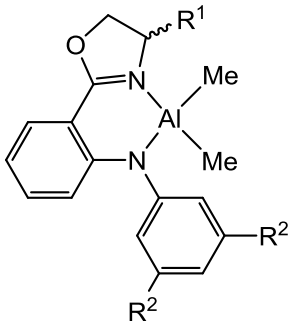
During development of chiral metal complexes for catalysis, oxazoline ligands have become increasingly prevalent and have found numerous applications in catalysis; for further information the reader is directed to several recent reviews on the subject.[240-244] Oxazoline ligands offer several key advantages when compared to other ligand types: they are derived from α-amino acids which provide numerous possible chiral building blocks for ligand design and synthesis. Further, they can be synthesised easily from carboxylic acid or nitrile functional groups, allowing for a wide range of ligand architectures to be accessed. Finally, the position of the chiral centre on the oxazoline ring close to the ligating nitrogen atom places the chiral centre in close proximity to the metal centre, allowing for a greater degree of stereocontrol to be exerted on the active site during catalysis.



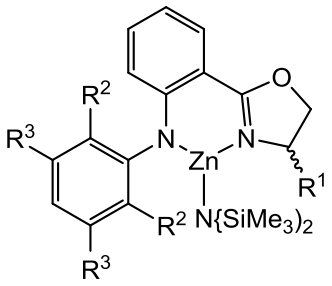
Ln = Y, R^1 = R^2 = Me (**1.31**)
Ln = La, R^1 = R^2 = Me (**1.32**)
Ln = Y, R^1 = ^{i}Pr, R^2 = H (**1.33**)
X = N{$SiMe_3$}$_2$



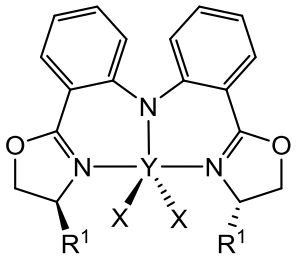
Ar = 2,4,6-trimethylphenyl (**1.34**)
Ar = 2-methoxyphenyl (**1.35**)



R^1 = (*S*)-^{i}Pr, R^2 = H (**1.36**)
R^1 = (*R*)-^{t}Bu, R^2 = H (**1.37**)
R^1 = (*R*)-Ph, R^2 = H (**1.38**)
R^1 = (*S*)-^{i}Pr, R^2 = CF_3 (**1.39**)



R^1 = (*S*)-^{i}Pr, R^2 = Me, R^3 = H (**1.40**)
R^1 = (*R*)-Ph, R^2 = H, R^3 = CF_3 (**1.41**)



R^1 = ^{i}Pr, R^2 = H (**1.42**)
R^1 = Bn, R^2 = H (**1.43**)
R^1 = H, R^2 = Ph (**1.44**)
X = N{$SiMe_3$}$_2$

Figure 1.8 Examples of initiators employing supporting ligands with oxazoline-moieties for the ROP of LA.[245-252]

Although oxazoline-based ligands have been used extensively in catalysis in general, to date their use in the ROP of cyclic esters is limited to a handful of examples (Figure 1.8). Despite mono- and bis[bis(oxazolinato)] Group 3 complexes being known since 1999, their application was restricted to hydroamination;[253, 254] however, in 2006, Carpentier *et al.* evaluated chiral and achiral yttrium and lanthanum bis[bis(oxazolinato)] complexes for the polymerisation of *rac*-LA and *rac*-BBL.[245] Complexes **1.31-1.33** were found to be highly active: reaching >98% conversion after 5-10 min. Although narrow to moderate polydispersities of 1.07 to 1.44 were obtained, the molecular weights were higher than anticipated, for example in the presence of 100 equivalents of *rac*-LA in THF, **1.33** produced PLA with M_n(obs) = 36,400 g mol^{-1} *cf.* M_n(calc) = 14,400 g mol^{-1}. In addition, no stereoselectivity was observed with either achiral or chiral catalysts.

Chen *et al*. reported a series of amido-oxazolinate and anilido-oxazolinate complexes of zinc and main group metals.[246-249] Dimeric complexes **1.34** and **1.35** were found to be active for the ROP of *L*-LA in toluene at 50 °C, employing exogenous benzyl alcohol as a chain transfer agent. In the absence of benzyl alcohol, **1.35** polymerised 100 equivalents of *L*-LA reaching 97% conversation after 40 minutes, with M_n(obs) = 24,900 g mol^{-1} *cf.* M_n(calc) = 14,000 g mol^{-1}), whereas under the same conditions and in the presence of 1 equivalent of benzyl alcohol, **1.35** reached 96% conversion after 20 minutes, with M_n(obs) = 12,900 g mol^{-1} (M_n(calc) = 6,900 g mol^{-1}). As these complexes were not tested with *rac*-LA, it is not possible to evaluate their ability to exert any stereocontrol during polymerisation.

More recently, there have been a number of notable advances in the successful application of supporting ligands featuring an oxazolinate moiety in the stereocontrolled ROP of *rac*-LA, obtaining either hetereotactically or isotactically enriched PLA. In 2014, Du *et al.* reported several aluminium chiral anilido-oxazolinate complexes capable of generating either heterotactic or isotactic PLA, depending on the steric and electronic nature of the substituents employed.[250] Complexes **1.36-1.39** were treated with 50 equivalents of *rac*-LA and 1 equivalent of BnOH in toluene at 80 °C. All showed moderate activities reaching >95% conversion after 24 h, with good agreement between observed and expected molecular weights and moderate polydispersities of 1.20 to 1.64. Of the series, complexes **1.36** and **1.37** showed the highest heteroselectivity, with P_r = 0.69 and 0.74, respectively. However, when the oxazoline moiety contained a sterically bulky substituent such as a phenyl group, as in complex **1.38**, moderately isotactically enriched PLA was obtained (P_m = 0.60). Complex **1.39** also exhibited a slight isotactic bias (P_m = 0.57), which was attributed to the presence of electron-withdrawing substituents at the R^2 position. In tandem with these results, Du *et al.* reported similar zinc chiral anilido-oxazolinate complexes which generated highly isotactically enriched PLA.[251] Complexes **1.40** and **1.41** were treated with 100 equivalents of *rac*-LA, producing isotactic stereoblock PLA with P_m = 0.90 and 0.91, respectively. The thermal properties of the resultant polymers were examined: the PLA obtained from both complexes was 212-214 °C, representing some of the highest T_m values recorded for PLA derived directly from *rac*-LA.

In 2014, Ward *et al*. reported a series of yttrium and lanthanide complexes supported by the bis(oxazolinylphenyl)amide (BOPA) ligand and tested their activity for the ROP of *rac*-LA.[252] Yttrium complexes **1.42-1.44** were found to be moderately active for the polymerisation of *rac*-LA; however, as with other metal amide systems, the experimentally obtained molecular weights were considerably higher than the theoretical values. For instance, in the presence of 100 equivalents of *rac*-LA in THF at 25 °C, **1.43** reached 98% conversion after 120 minutes, with M_n(obs) = 22,290 g mol^{-1} *cf*. M_n(calc) = 14,286 g mol^{-1}) and had a moderate polydispersity of 1.44. All complexes showed a preference for the formation of heterotactically enriched PLA, with P_r values lying in the range of *ca*. 0.7-0.8. Complex **1.43,** supported by Bn-BOPA, had a higher P_r of 0.81 in comparison to its less sterically encumbered counterparts, indicating increasing steric bulk of the substituents on the oxazoline rings leads to an increase in stereocontrol during polymerisation.

In 2011, Berg *et al*. developed an achiral carbazole-bis(oxazoline) ligand, HCzOx^{Me_2} (**1.45**) (Figure 1.9) as a monoanionic tridentate support for five- and six-coordinate lanthanide dialkyl and dihalide complexes.[255] As potential precatalysts for ethylene polymerisation, these complexes proved to have low catalytic activities; however, they were found to be remarkably thermally stable, chemically inert and resistant to ligand redistribution due to steric saturation around the metal. A chiral variant, (*S*,*S*)-HCzOx$^{i_{Pr}}$ (**(*S*,*S*)-1.46**) (Figure 1.9) synthesised by Connell *et al.* for reaction with $CrCl_3$ in the enantioselective synthesis of butadien-2-ylcarbinols, affording chiral alcohols in good yields and enantioselectivities.[256]

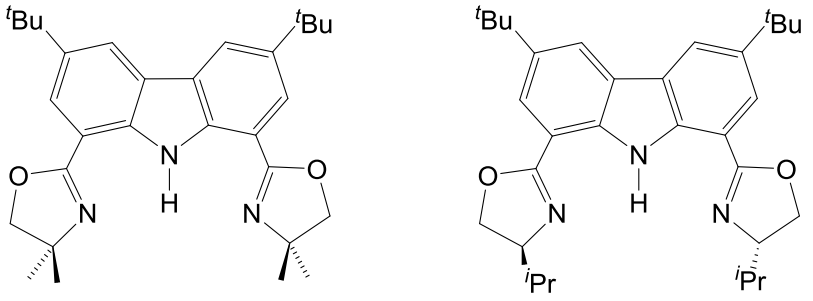


Figure 1.9. Carbazole-bis(oxazoline) ligands HCzOx^{Me_2} and (*S*,*S*)-HCzOx$^{i_{Pr}}$ used in this Thesis.[255, 256]

Due to its chemical stability and resistance to redistribution, this ligand framework is used extensively throughout this Thesis as a supporting ligand for alkaline earth and lanthanide complexes for the ROP of cyclic esters. In comparison to the similar BOPA ligand used in complexes **1.42-1.44**, it is hoped that the introduction of a tethered backbone confers additional stability to the complexes. Furthermore, the bis(oxazonlinato) offers the opportunity to compare the performance of achiral and chiral catalysts.

1.12 Aims and outlook

Motivated by a surge in the industrial production of biodegradable polymers in recent decades, many studies have attempted to design well-defined single site catalysts aimed at enhancing polymer properties and reducing undesirable side effects, of the type (L)M-X (where L is the ancillary ligand, M is a Lewis acidic metal and X is an initiating group). The works described in this Thesis describe the development of alkaline earth and lanthanide borohydride complexes supported by bis(oxazolinate) ligands as controlled initiators for the ROP of *rac*-, *L*-, *D*- and *meso*-LA. Furthermore, the employment of borate esters as chain transfer agents in immortal ROP is presented.

1.13 References for Chapter One

1. D. Walton and P. Lorimer, *Polymers, Oxford Chemistry Primers*, Oxford University Press, 2000.
2. A. L. Baner and O. G. Piringer, *Plastic Packaging: Interactions with Food and Pharmaceuticals*, 2nd edn., Wiley, 2008.
3. W. H. Carothers, G. L. Dorough and F. J. van Natta, *J. Am. Chem. Soc.*, 1932, **54**, 761-772.
4. C. E. Lowe, *Google Patents*, 1954.
5. A. P. Gupta and V. Kumar, *Eur. Polym. J.*, 2007, **43**, 4053-4074.
6. K. Madhavan Nampoothiri, N. R. Nair and R. P. John, *Bioresource Technol.*, 2010, **101**, 8493-8501.
7. R. H. Platel, L. M. Hodgson and C. K. Williams, *Polym. Rev.*, 2008, **48**, 11-63.
8. B. J. O'Keefe, M. A. Hillmyer and W. B. Tolman, *Dalton Trans.*, 2001, 2215-2224.

9. C. K. Williams and M. A. Hillmyer, *Polym. Rev.*, 2008, **48**, 1-10.
10. C. A. Wheaton, P. G. Hayes and B. J. Ireland, *Dalton Trans.*, 2009, 4832-4846.
11. E. Chiellini and R. Solaro, *Adv. Mater.*, 1996, **8**, 305-313.
12. S. Mecking, *Angew. Chem. Int. Ed.*, 2004, **43**, 1078-1085.
13. M. Labet and W. Thielemans, *Chem. Soc. Rev.*, 2009, **38**, 3484-3504.
14. M. A. Woodruff and D. W. Hutmacher, *Prog. Polym. Sci.*, 2010, **35**, 1217-1256.
15. M. J. Stanford and A. P. Dove, *Chem. Soc. Rev.*, 2010, **39**, 486-494.
16. R. Auras, B. Harte and S. Selke, *Macromolecular Bioscience*, 2004, **4**, 835-864.
17. R. E. Drumright, P. R. Gruber and D. E. Henton, *Adv. Mater.*, 2000, **12**, 1841-1846.
18. Y. Ikada and H. Tsuji, *Macromol. Rapid Commun.*, 2000, **21**, 117-132.
19. H. Tamber, P. Johansen, H. P. Merkle and B. Gander, *Adv. Drug Deliv. Rev.*, 2005, **57**, 357-376.
20. H. R. Kricheldorf, *Chemosphere*, 2001, **43**, 49-54.
21. O. Dechy-Cabaret, B. Martin-Vaca and D. Bourissou, *Chem. Rev.*, 2004, **104**, 6147-6176.
22. A.-C. Albertsson and I. K. Varma, *Biomacromolecules*, 2003, **4**, 1466-1486.
23. D. K. Gilding and A. M. Reed, *Polymer*, 1979, **20**, 1459-1464.
24. M. Okada, *Prog. Polym. Sci.*, 2002, **27**, 87-133.
25. R. Raja and J. Meurig Thomas, *Z. Anorg. Allg. Chem.*, 2005, **631**, 2942-2946.
26. Z. Zhong, P. J. Dijkastra, C. Birg, M. Westerhausen and J. Feijen, *Macromolecules*, 2001, **34**, 3863-3868.
27. A. Rudin and H. L. W. Hoegy, *J. Polym. Sci. A: Polym. Chem.*, 1972, **10**, 217-235.
28. D. A. Skoog, *Principle of Instrumental Analysis*, 6th edn., Thompson Brooks/Cole: Belmont, California, 2006.
29. B. Trathnigg, *Prog. Polym. Sci.*, 1995, **20**, 615-650.
30. P. C. Hiemenz and T. P. Lodge, *Polymer Chemistry*, 2nd edn., CRC Press, New York, USA, 2007.

31. J. R. Dorgan, J. Janzen, D. M. Knauss, S. B. Hait, B. R. Limoges and M. H. Hutchinson, *J. Polym. Sci. B: Polym. Phys.*, 2005, **43**, 3100-3111.
32. R. C. Beavis, B. T. Chait and K. G. Standing, *Rapid Commun. Mass Sp.*, 1989, **3**, 436-439.
33. T. M. Ovitt and G. W. Coates, *J. Am. Chem. Soc.*, 2002, **124**, 1316-1326.
34. A. Södergård and M. Stolt, *Prog. Polym. Sci.*, 2002, **27**, 1123-1163.
35. W. Amass, A. Amass and B. Tighe, *Polym. Int.*, 1998, **47**, 89-144.
36. J. Lunt, *Polym. Degrad. Stab.*, 1998, **59**, 145-152.
37. N. Nomura, J. Hasegawa and R. Ishii, *Macromolecules*, 2009, **42**, 4907-4909.
38. Y. Ikada, K. Jamshidi, H. Tsuji and S. H. Hyon, *Macromolecules*, 1987, **20**, 904-906.
39. N. Yui, P. J. Dijkstra and J. Feijen, *Die Makromolekulare Chemie*, 1990, **191**, 481-488.
40. C.-X. Cai, A. Amgoune, C. W. Lehmann and J.-F. Carpentier, *Chem. Commun.*, 2004, 330-331.
41. A. Amgoune, C. M. Thomas, T. Roisnel and J.-F. Carpentier, *Chem. Eur. J.*, 2006, **12**, 169-179.
42. A. Amgoune, C. M. Thomas and J.-F. Carpentier, *Macromol. Rapid Commun.*, 2007, **28**, 693-697.
43. J. S. Klitzke, T. Roisnel, E. Kirillov, O. de Lázerro Casagrande and J.-F. Carpentier, *Organometallics*, 2014, **33**, 309-321.
44. E. Grunova, E. Kirillov, T. Roisnel and J.-F. Carpentier, *Dalton Trans.*, 2010, **39**, 6739-6752.
45. M. Bouyahyi, N. Ajellal, E. Kirillov, C. M. Thomas and J.-F. Carpentier, *Chem. Eur. J.*, 2011, **17**, 1872-1883.
46. X. Liu, X. Shang, T. Tang, N. Hu, F. Pei, D. Cui, X. Chen and X. Jing, *Organometallics*, 2007, **26**, 2747-2757.
47. Z. Mou, B. Liu, X. Liu, H. Xie, W. Rong, L. Li, S. Li and D. Cui, *Macromolecules*, 2014, **47**, 2233-2241.
48. H. Xie, Z. Mou, B. Liu, P. Li, W. Rong, S. Li and D. Cui, *Organometallics*, 2014, **33**, 722-730.
49. L. Clark, M. G. Cushion, H. D. Dyer, A. D. Schwarz, R. Duchateau and P. Mountford, *Chem. Commun.*, 2010, **46**, 273-275.

50. M. G. Cushion and P. Mountford, *Chem. Commun.*, 2011, **47**, 2276–2278.
51. M. H. Chisholm, N. W. Eilerts, J. C. Huffman, S. S. Iyer, M. Pacold and K. Phomphrai, *J. Am. Chem. Soc.*, 2000, **122**, 11845-11854.
52. M. H. Chisholm, J. Gallucci and K. Phomphrai, *Inorg. Chem.*, 2002, **41**, 2785-2794.
53. M. H. Chisholm, J. Gallucci and K. Phomphrai, *Chem. Commun.*, 2003, 48-49.
54. M. H. Chisholm, J. C. Gallucci and K. Phomphrai, *Inorg. Chem.*, 2004, **43**, 6717-6725.
55. M. H. Chisholm, J. C. Gallucci and K. Phomphrai, *Inorg. Chem.*, 2005, **44**, 8004-8010.
56. V. Balasanthiran, M. H. Chisholm, C. B. Durr and J. C. Gallucci, *Dalton Trans.*, 2013, **42**, 11234-11241.
57. M. Cheng, A. B. Attygalle, E. Lobkovsky and G. W. Coates, *J. Am. Chem. Soc.*, 1999, **121**, 11583-11584.
58. B. M. Chamberlain, M. Cheng, D. R. Moore, T. M. Ovitt, E. Lobkovsky and G. W. Coates, *J. Am. Chem. Soc.*, 2001, **123**, 3229-3238.
59. A. Stopper, K. Press, J. Okuda, I. Goldberg and M. Kol, *Inorg. Chem.*, 2014, **53**, 9140-9150.
60. H. Ma, T. P. Spaniol and J. Okuda, *Angew. Chem. Int. Ed.*, 2006, **45**, 7818-7821.
61. H. Ma, T. P. Spaniol and J. Okuda, *Inorg. Chem.*, 2008, **47**, 3328-3339.
62. T. P. A. Cao, A. Buchard, X. F. Le Goff, A. Auffrant and C. K. Williams, *Inorg. Chem.*, 2012, **51**, 2157-2175.
63. C. Bakewell, T.-P.-A. Cao, X. F. Le Goff, N. J. Long, A. Auffrant and C. K. Williams, *Organometallics*, 2013, **32**, 1475-1483.
64. L. M. Hodgson, R. H. Platel, A. J. P. White and C. K. Williams, *Macromolecules*, 2008, **41**, 8603-8607.
65. Z. Tang, X. Chen, X. Pang, Y. Yang, X. Zhang and X. Jing, *Biomacromolecules*, 2004, **5**, 965-970.
66. C. Bakewell, A. J. P. White, N. J. Long and C. K. Williams, *Angew. Chem. Int. Ed.*, 2014, 9226-9230.

67. C. Bakewell, T. P. A. Cao, N. Long, X. F. Le Goff, A. Auffrant and C. K. Williams, *J. Am. Chem. Soc.*, 2012, **134**, 20577-20580.
68. C. Bakewell, R. H. Platel, S. K. Cary, S. M. Hubbard, J. M. Roaf, A. C. Levine, A. J. P. White, N. J. Long, M. Haaf and C. K. Williams, *Organometallics*, 2012, **31**, 4729-4736.
69. Z. Tang, X. Chen, Y. Yang, X. Pang, J. Sun, X. Zhang and X. Jing, *J. Polym. Sci. A: Polym. Chem.*, 2004, **42**, 5974-5982.
70. Z. Tang, Y. Yang, X. Pang, J. Hu, X. Chen, N. Hu and X. Jing, *J. Appl. Polym. Sci.*, 2005, **98**, 102-108.
71. M. Wisniewski, A. L. Borgne and N. Spassky, *Macromol. Chem. Phys.*, 1997, **198**, 1227-1238.
72. A. Bhaw-Luximon, D. Jhurry and N. Spassky, *Polym. Bull.*, 2000, **44**, 31-38.
73. D. Jhurry, A. Bhaw-Luximon and N. Spassky, *Macromol. Symp.*, 2001, **175**, 67-80.
74. Z. Zhong, P. J. Dijkstra and J. Feijen, *Angew. Chem. Int. Ed.*, 2002, **41**, 4510-4513.
75. Z. Zhong, P. J. Dijkstra and J. Feijen, *J. Am. Chem. Soc.*, 2003, **125**, 11291-11298.
76. I. Yu, A. Acosta-Ramírez and P. Mehrkhodavandi, *J. Am. Chem. Soc.*, 2012, **134**, 12758-12773.
77. D. C. Aluthge, B. O. Patrick and P. Mehrkhodavandi, *Chem. Commun.*, 2013, **49**, 4295-4297.
78. J. Fang, I. Yu, P. Mehrkhodavandi and L. Maron, *Organometallics*, 2013, **32**, 6950-6956.
79. W. Zhao, Y. Wang, X. Liu, X. Chen and D. Cui, *Chem. Asian J.*, 2012, **7**, 2403-2410.
80. W. Zhao, Y. Wang, X. Liu, X. Chen, D. Cui and E. Y. X. Chen, *Chem. Commun.*, 2012, **48**, 6375-6377.
81. C. Romain, B. Heinrich, S. B. Laponnaz and S. Dagorne, *Chem. Commun.*, 2012, **48**, 2213-2215.
82. A. P. Dove, *Chem. Commun.*, 2008, 6446-6470.
83. J. M. Becker, R. J. Pounder and A. P. Dove, *Macromol. Rapid Commun.*, 2010, **31**, 1923-1937.

84. J.-C. Buffet and J. Okuda, *Polym. Chem.*, 2011, **2**, 2758-2763.
85. J.-C. Buffet, J. P. Davin, T. P. Spaniol and J. Okuda, *New J. Chem.*, 2011, **35**, 2253-2257.
86. A. Kapelski and J. Okuda, *J. Polym. Sci. A: Polym. Chem.*, 2013, **51**, 4983-4991.
87. T. M. Ovitt and G. W. Coates, *J. Am. Chem. Soc.*, 1999, **121**, 4072-4073.
88. A. Sauer, J.-C. Buffet, T. P. Spaniol, H. Nagae, K. Mashima and J. Okuda, *ChemCatChem*, 2013, **5**, 1088-1091.
89. J.-C. Buffet and J. Okuda, *Chem. Commun.*, 2011, **47**, 4796-4798.
90. J.-C. Buffet, A. Kapelski and J. Okuda, *Macromolecules*, 2010, **43**, 10201-10203.
91. H. Du, A. H. Velders, P. J. Dijkstra, J. Sun, Z. Zhong, X. Chen and J. Feijen, *Chem. Eur. J.*, 2009, **15**, 9836-9845.
92. J.-C. Buffet and J. Okuda, *Dalton Trans.*, 2011, **40**, 7748-7754.
93. A. Kapelski, J.-C. Buffet, T. P. Spaniol and J. Okuda, *Chem. Asian J.*, 2012, **7**, 1320-1330.
94. A. Sauer, J.-C. Buffet, T. P. Spaniol, H. Nagae, K. Mashima and J. Okuda, *Inorg. Chem.*, 2012, **51**, 5764-5770.
95. J.-C. Buffet, A. N. Martin, M. Kol and J. Okuda, *Polym. Chem.*, 2011, **2**, 2378-2384.
96. A. Pietrangelo, M. A. Hillmyer and W. B. Tolman, *Chem. Commun.*, 2009, 2736-2737.
97. A. Pietrangelo, S. C. Knight, A. K. Gupta, L. J. Yao, M. A. Hillmyer and W. B. Tolman, *J. Am. Chem. Soc.*, 2010, **132**, 11649-11657.
98. M. H. Chisholm, N. J. Patmore and Z. Zhou, *Chem. Commun.*, 2005, 127-129.
99. F. A. Bovey and P. A. Mirau, *NMR of Polymers*, Academic Press, San Diego, 1996.
100. E. Lillie and R. C. Schulz, *Makromol. Chem.*, 1975, **176**, 1901-1906.
101. A. Schindler and D. Harper, *J. Polym. Sci. C: Polym. Lett.*, 1976, **14**, 729-734.
102. M. T. Zell, B. E. Padden, A. J. Paterick, K. A. M. Thakur, R. T. Kean, M. A. Hillmyer and E. J. Munson, *Macromolecules*, 2002, **35**, 7700-7707.

103. M. Bero, J. Kasperczyk and Z. J. Jedlinski, *Die Makromolekulare Chemie*, 1990, **191**, 2287-2296.
104. J. E. Kasperczyk, *Macromolecules*, 1995, **28**, 3937-3939.
105. J. E. Kasperczyk, *Polymer*, 1999, **40**, 5455-5458.
106. K. A. M. Thakur, R. T. Kean, K. A. M. Thakur, M. T. Zell, B. E. Padden and E. J. Munson, *Chem. Commun.*, 1998, 1913-1914.
107. K. A. M. Thakur, R. T. Kean, E. S. Hall, J. J. Kolstad, T. A. Lindgren, M. A. Doscotch, J. I. Siepmann and E. J. Munson, *Macromolecules*, 1997, **30**, 2422-2428.
108. I. Rashkov, J. L. Espartero, N. Manolova and M. Vert, *Macromolecules*, 1996, **29**, 57-62.
109. M. H. Chisholm, S. S. Iyer, M. E. Matison, D. G. McCollum and M. Pagel, *Chem. Commun.*, 1997, 1999-2000.
110. P. Dubois, O. Coulembier and J.-M. Raquez, *Handbook of Ring-Opening Polymerization*, Wiley-VCH, 2009.
111. A. P. Dove, *ACS Macro Lett.*, 2012, **1**, 1409-1412.
112. N. E. Kamber, W. Jeong, R. M. Waymouth, R. C. Pratt, B. G. G. Lohmeijer and J. L. Hedrick, *Chem. Rev.*, 2007, **107**, 5813-5840.
113. M. K. Kiesewetter, E. J. Shin, J. L. Hedrick and R. M. Waymouth, *Macromolecules*, 2010, **43**, 2093-2107.
114. A. Bhaw-Luximon, D. Jhurry, N. Spassky, S. Pensec and J. Belleney, *Polymer*, 2001, **42**, 9651-9656.
115. H. R. Kricheldorf and R. Dunsing, *Die Makromolekulare Chemie*, 1986, **187**, 1611-1625.
116. H. R. Kricheldorf and I. Kreiser, *Die Makromolekulare Chemie*, 1987, **188**, 1861-1873.
117. D. Bourissou, B. Martin-Vaca, A. Dumitrescu, M. Graullier and F. Lacombe, *Macromolecules*, 2005, **38**, 9993-9998.
118. F. Nederberg, E. F. Connor, M. Möller, T. Glauser and J. L. Hedrick, *Angew. Chem. Int. Ed.*, 2001, **40**, 2712-2715.
119. A. P. Dove, R. C. Pratt, B. G. G. Lohmeijer, D. A. Culkin, E. C. Hagberg, G. W. Nyce, R. M. Waymouth and J. L. Hedrick, *Polymer*, 2006, **47**, 4018-4025.

120. L. Zhang, F. Nederberg, R. C. Pratt, R. M. Waymouth, J. L. Hedrick and C. G. Wade, *Macromolecules*, 2007, **40**, 4154-4158.

121. M. Myers, E. F. Connor, T. Glauser, A. Möck, G. Nyce and J. L. Hedrick, *J. Polym. Sci. A: Polym. Chem.*, 2002, **40**, 844-851.

122. E. F. Connor, G. W. Nyce, M. Myers, A. Möck and J. L. Hedrick, *J. Am. Chem. Soc.*, 2002, **124**, 914-915.

123. G. W. Nyce, T. Glauser, E. F. Connor, A. Möck, R. M. Waymouth and J. L. Hedrick, *J. Am. Chem. Soc.*, 2003, **125**, 3046-3056.

124. M. H. Chisholm, C.-C. Lin, J. C. Gallucci and B.-T. Ko, *Dalton Trans.*, 2003, 406-412.

125. B.-T. Ko and C.-C. Lin, *J. Am. Chem. Soc.*, 2001, **123**, 7973-7977.

126. A. K. Sutar, T. Maharana, S. Dutta, C.-T. Chen and C.-C. Lin, *Chem. Soc. Rev.*, 2010, **39**, 1724-1746.

127. W.-Y. Lu, M.-W. Hsiao, S. C. N. Hsu, W.-T. Peng, Y.-J. Chang, Y.-C. Tsou, T.-Y. Wu, Y.-C. Lai, Y. Chen and H.-Y. Chen, *Dalton Trans.*, 2012, **41**, 3659-3667.

128. Y. Huang, W. Wang, C.-C. Lin, M. P. Blake, L. Clark, A. D. Schwarz and P. Mountford, *Dalton Trans.*, 2013, **42**, 9313-9324.

129. S.-C. Rosca, D.-A. Rosca, V. Dorcet, C. M. Kozak, F. M. Kerton, J.-F. Carpentier and Y. Sarazin, *Dalton Trans.*, 2013, **42**, 9361-9375.

130. J. Zhang, C. Jian, Y. Gao, L. Wang, N. Tang and J. Wu, *Inorg. Chem.*, 2012, **51**, 13380-13389.

131. M. H. Chisholm and N. W. Eilerts, *Chem. Commun.*, 1996, 853-854.

132. V. Poirier, T. Roisnel, J.-F. Carpentier and Y. Sarazin, *Dalton Trans.*, 2009, 9820-9827.

133. B. J. Ireland, C. A. Wheaton and P. G. Hayes, *Organometallics*, 2010, **29**, 1079-1084.

134. R. A. Collins, J. Unruangsri and P. Mountford, *Dalton Trans.*, 2013, **42**, 759–769.

135. T. J. J. Whitehorne, B. Vabre and F. Schaper, *Dalton Trans.*, 2014, **43**, 6339-6352.

136. B. M. Chamberlain, Y. Sun, J. R. Hagadorn, E. W. Hemmesch, V. G. Young, M. Pink, M. A. Hillmyer and W. B. Tolman, *Macromolecules*, 1999, **32**, 2400-2402.

137. M. Visseaux and F. Bonnet, *Coord. Chem. Rev.*, 2011, **255**, 374-420.

138. A. Otero, J. Fernández-Baeza, A. Lara-Sánchez, C. Alonso-Moreno, I. Márquez-Segovia, L. F. Sánchez-Barba and A. M. Rodríguez, *Angew. Chem. Int. Ed.*, 2009, **48**, 2176-2179.

139. A. Buchard, R. H. Platel, A. Auffrant, X. F. Le Goff, P. Le Floch and C. K. Williams, *Organometallics*, 2010, **29**, 2892-2900.

140. J. Kratsch, M. Kuzdrowska, M. Schmid, N. Kazeminejad, C. Kaub, P. Oña-Burgos, S. M. Guillaume and P. W. Roesky, *Organometallics*, 2013, **32**, 1230-1238.

141. M. D. Jones, S. L. Hancock, P. McKeown, P. M. Schafer, A. Buchard, L. H. Thomas, M. F. Mahon and J. P. Lowe, *Chem. Commun.*, 2014, **50**, 15967-15970.

142. T. R. Forder, M. F. Mahon, M. G. Davidson, T. Woodman and M. D. Jones, *Dalton Transactions*, 2014, **43**, 12095-12099.

143. S. L. Hancock, M. F. Mahon and M. D. Jones, *New J. Chem.*, 2013, **37**, 1996-2001.

144. Z. R. Turner, J.-C. Buffet and D. O'Hare, *Organometallics*, 2014, **33**, 3891-3903.

145. A. D. Schwarz, A. L. Thompson and P. Mountford, *Inorg. Chem.*, 2009, **48**, 10442-10454.

146. A. D. Schwarz, K. R. Herbert, C. Paniagua and P. Mountford, *Organometallics*, 2010, **29**, 4171-4188.

147. R. L. Webster, N. Noroozi, S. G. Hatzikiriakos, J. A. Thomson and L. L. Schafer, *Chem. Commun.*, 2013, **49**, 57-59.

148. A. Sauer, A. Kapelski, C. Fliedel, S. Dagorne, M. Kol and J. Okuda, *Dalton Trans.*, 2013, **42**, 9007–9023.

149. M. Jeong Go, J. Min Lee, K. Mun Lee, C. Hwa Oh, K. H. Park, S. H. Kim, M. Kim, H.-R. Park, M. H. Park, Y. Kim and J. Lee, *Polyhedron*, 2014, **67**, 286-294.

150. C. A. Wheaton, B. J. Ireland and P. G. Hayes, *Organometallics*, 2009, **28**, 1282-1285.

151. H. Sun, J. S. Ritch and P. G. Hayes, *Inorg. Chem.*, 2011, **50**, 8063-8072.

152. Z. Liu, W. Gao, J. Zhang, D. Cui, Q. Wu and Y. Mu, *Organometallics*, 2010, **29**, 5783-5790.

153. H. R. Kricheldorf, K. Bornhorst and H. Hachmann-Thiessen, *Macromolecules*, 2005, **38**, 5017-5024.

154. N. Nimitsiriwat, V. C. Gibson, E. L. Marshall and M. R. J. Elsegood, *Dalton Trans.*, 2009, 3710-3715.

155. A. P. Dove, V. C. Gibson, E. L. Marshall, H. S. Rzepa, A. J. P. White and D. J. Williams, *J. Am. Chem. Soc.*, 2006, **128**, 9834-9843.

156. A. Kowalski, J. Libiszowski, T. Biela, M. Cypryk, A. Duda and S. Penczek, *Macromolecules*, 2005, **38**, 8170-8176.

157. N. Nimitsiriwat, E. L. Marshall, V. C. Gibson, M. R. J. Elsegood and S. H. Dale, *J. Am. Chem. Soc.*, 2004, **126**, 13598-13599.

158. M. Lahcini, P. M. Castro, M. Kalmi, M. Leskelä and T. Repo, *Organometallics*, 2004, **23**, 4547-4549.

159. S. L. Hancock, M. F. Mahon and M. D. Jones, *Dalton Trans.*, 2013, **42**, 9279-9285.

160. T. R. Forder and M. D. Jones, *New J. Chem.*, 2015, **39**, 1974-1978.

161. I. dos Santos Vieira, E. L. Whitelaw, M. D. Jones and S. Herres-Pawlis, *Chem. Eur. J.*, 2013, **19**, 4712-4716.

162. W. Zhang, Y. Wang, L. Wang, C. Redshaw and W.-H. Sun, *J. Organomet. Chem.*, 2014, **750**, 65-73.

163. Z. Tang and V. C. Gibson, *Eur. Polym. J.*, 2007, **43**, 150-155.

164. N. Nomura, R. Ishii, Y. Yamamoto and T. Kondo, *Chem. Eur. J.*, 2007, **13**, 4433-4451.

165. M. P. Blake, A. D. Schwarz and P. Mountford, *Organometallics*, 2011, **30**, 1202-1214.

166. H. D. Dyer, S. Huijser, N. Susperregui, F. Bonnet, A. D. Schwarz, R. Duchateau, L. Maron and P. Mountford, *Organometallics*, 2010, **29**, 3602-3621.

167. H. Ma and J. Okuda, *Macromolecules*, 2005, **38**, 2665-2673.

168. A. P. Dove, V. C. Gibson, E. L. Marshall, A. J. P. White and D. J. Williams, *Dalton Trans.*, 2004, 570-578.

169. M. S. Hill and P. B. Hitchcock, *Dalton Trans.*, 2002, 4694-4702.

170. N. Spassky, V. Simic, M. S. Montaudo and L. G. Hubert-Pfalzgraf, *Macromol. Chem. Phys.*, 2000, **201**, 2432-2440.

171. J. Baran, A. Duda, A. Kowalski, R. Szymanski and S. Penczek, *Macromol. Rapid Commun.*, 1997, **18**, 325-333.

172. H. R. Kricheldorf, M. Berl and N. Scharnagl, *Macromolecules*, 1988, **21**, 286-293.

173. N. Nomura, A. Taira, T. Tomioka and M. Okada, *Macromolecules*, 2000, **33**, 1497-1499.

174. N. Nomura, A. Taira, A. Nakase, T. Tomioka and M. Okada, *Tetrahedron*, 2007, **63**, 8478-8484.

175. W. Zhao, D. Cui, X. Liu and X. Chen, *Macromolecules*, 2010, **43**, 6678-6684.

176. Y. Sarazin, B. Liu, T. Roisnel, L. Maron and J.-F. Carpentier, *J. Am. Chem. Soc.*, 2011, **133**, 9069-9087.

177. F. S. Dainton and K. J. Ivin, *Q. Rev. Chem. Soc.*, 1958, **12**, 61-92.

178. A. Duda and S. Penczek, *Macromolecules*, 1990, **23**, 1636-1639.

179. A. A. Evstropov, B. V. Lebedev, T. G. Kulagina and N. K. Lebedev, *Vysokomol. Soedin. Ser. A*, 1982, **24**, 568.

180. G. J. van Hummel, S. Harkema, F. E. Kohn and J. Feijen, *Acta Crystallogr. B*, 1982, **38**, 1679-1681.

181. H. R. Kricheldorf, C. Boettcher and K. U. Toennes, *Polymer*, 1992, **33**, 2817-2824.

182. H. R. Kricheldorf and C. Boettcher, *Die Makromolekulare Chemie*, 1993, **194**, 1653-1664.

183. J. P. Davin, J.-C. Buffet, T. P. Spaniol and J. Okuda, *Dalton Trans.*, 2012, **41**, 12612-12618.

184. M. Szwarc, *Nature*, 1956, **178**, 1168-1169.

185. M. Szwarc, *J. Polym. Sci. A: Polym. Chem.*, 1998, **36**, IX-XV.

186. T. Aida, *Prog. Polym. Sci.*, 1994, **19**, 469-528.

187. R. P. Quirk and B. Lee, *Polym. Int.*, 1992, **27**, 359-367.

188. M. Save, M. Schappacher and A. Soum, *Macromol. Chem. Phys.*, 2002, **203**, 889-899.

189. T. Ouhadi, A. Hamitou, R. Jerome and P. Teyssie, *Macromolecules*, 1976, **9**, 927-931.

190. C. K. Williams, L. E. Breyfogle, S. K. Choi, W. Nam, V. G. Young, M. A. Hillmyer and W. B. Tolman, *J. Am. Chem. Soc.*, 2003, **125**, 11350-11359.

191. A. Kowalski, J. Libiszowski, A. Duda and S. Penczek, *Macromolecules*, 2000, **33**, 1964-1971.

192. Z. Zhong, S. Schneiderbauer, P. J. Dijkstra, M. Westerhausen and J. Feijen, *J. Polym. Environ.*, 2002, **9**, 31-38.

193. A. J. Chmura, M. G. Davidson, M. D. Jones, M. D. Lunn and M. F. Mahon, *Dalton Trans.*, 2006, 887-889.

194. F. Bonnet, A. R. Cowley and P. Mountford, *Inorg. Chem.*, 2005, **44**, 9046-9055.

195. M.-L. Hsueh, B.-H. Huang, J. Wu and C.-C. Lin, *Macromolecules*, 2005, **38**, 9482-9487.

196. Y. Gao, Z. Dai, J. Zhang, X. Ma, N. Tang and J. Wu, *Inorg. Chem.*, 2014, **53**, 716-726.

197. J.-C. Wu, B.-H. Huang, M.-L. Hsueh, S.-L. Lai and C.-C. Lin, *Polymer*, 2005, **46**, 9784-9792.

198. P. I. Binda and E. E. Delbridge, *Dalton Trans.*, 2007, 4685-4692.

199. S. Asano, T. Aida and S. Inoue, *J. Chem. Soc., Chem. Commun.*, 1985, 1148-1149.

200. S. Inoue and T. Aida, *Makromol. Chem. M. Symp.*, 1986, **6**, 217-224.

201. S. Inoue, *Makromol. Chem. M. Symp.*, 1986, **3**, 295-300.

202. M. Endo, T. Aida and S. Inoue, *Macromolecules*, 1987, **20**, 2982-2988.

203. S. Inoue, *J. Macromol. Sci. Chem.*, 1988, **25**, 571-582.

204. T. Aida, Y. Maekawa, S. Asano and S. Inoue, *Macromolecules*, 1988, **21**, 1195-1202.

205. I. D'Auria, M. Lamberti, M. Mazzeo, S. Milione and C. Pellecchia, *J. Polym. Sci. A: Polym. Chem.*, 2014, **52**, 49-60.

206. B.-T. Ko and C.-C. Lin, *Macromolecules*, 1999, **32**, 8296-8300.

207. M.-L. Hsueh, B.-H. Huang and C.-C. Lin, *Macromolecules*, 2002, **35**, 5763-5768.

208. J. Zhang, J. Xiong, Y. Sun, N. Tang and J. Wu, *Macromolecules*, 2014, **47**, 7789-7796.

209. M. J. Walton, S. J. Lancaster and C. Redshaw, *ChemCatChem*, 2014, **6**, 1892-1898.

210. Y. Wang, W. Zhao, X. Liu, D. Cui and E. Y. X. Chen, *Macromolecules*, 2012, **45**, 6957-6965.

211. Y. Sarazin, V. Poirier, T. Roisnel and J.-F. Carpentier, *Eur. J. Inorg. Chem.*, 2010, 3423-3428.

212. C. Xu, I. Yu and P. Mehrkhodavandi, *Chem. Commun.*, 2012, **48**, 6806-6808.

213. L. Wang, V. Poirier, F. Ghiotto, M. Bochmann, R. D. Cannon, J.-F. Carpentier and Y. Sarazin, *Macromolecules*, 2014, **47**, 2574-2584.

214. E. Martin, P. Dubois and R. Jérôme, *Macromolecules*, 2000, **33**, 1530-1535.

215. M. T. Gamer, P. T. Roesky, I. Palard, M. Le Hellaye and S. M. Guillaume, *Organometallics*, 2007, **26**, 651-657.

216. A. Amgoune, C. M. Thomas and J.-F. Carpentier, *Pure Appl. Chem.*, 2007, **79**, 2013-2030.

217. N. Ajellal, J.-F. Carpentier, C. Guillaume, S. M. Guillaume, M. Helou, V. Poirier, Y. Sarazin and A. A. Trifonov, *Dalton Trans.*, 2010, **39**, 8363-8378.

218. I. Barakat, P. Dubois, R. Jérôme and P. Teyssié, *J. Polym. Sci. A: Polym. Chem.*, 1993, **31**, 505-514.

219. L. Clark, G. B. Deacon, C. M. Forsyth, P. C. Junk, P. Mountford, J. P. Townley and J. Wang, *Dalton Trans.*, 2013, **42**, 9294-9312.

220. L. Clark, G. B. Deacon, C. M. Forsyth, P. C. Junk, P. Mountford and J. P. Townley, *Dalton Trans.*, 2010, **39**, 6693-6704.

221. M. Ryner, K. Stridsberg, A.-C. Albertsson, H. von Schenck and M. Svensson, *Macromolecules*, 2001, **34**, 3877-3881.

222. G. Schwach, J. Coudane, R. Engel and M. Vert, *Polym. Bull.*, 1996, **37**, 771-776.

223. P. Vanhoorne, P. Dubois, R. Jerome and P. Teyssie, *Macromolecules*, 1992, **25**, 37-44.

224. G. Schwach, J. Coudane, R. Engel and M. Vert, *Polym. Bull.*, 1994, **32**, 617-623.

225. G. Schwach, J. Coudane, R. Engel and M. Vert, *Polym. Int.*, 1998, **46**, 177-182.

226. G. Schwach and M. Vert, *Int. J. Biol. Macromol.*, 1999, **25**, 283-291.

227. N. Spassky, M. Wisniewski, C. Pluta and A. Le Borgne, *Macromol. Chem. Phys.*, 1996, **197**, 2627-2637.

228. T. M. Ovitt and G. W. Coates, *J. Polym. Sci., Part A: Polym. Chem.*, 2000, **38**, 4686-4692.

229. C. P. Radano, G. L. Baker and M. R. Smith, *J. Am. Chem. Soc.*, 2000, **122**, 1552-1553.

230. M. H. Chisholm, J. C. Gallucci, K. T. Quisenberry and Z. Zhou, *Inorg. Chem.*, 2008, **47**, 2613-2624.

231. N. Nomura, R. Ishii, M. Akakura and K. Aoi, *J. Am. Chem. Soc.*, 2002, **124**, 5938-5939.

232. R. Ishii, N. Nomura and T. Kondo, *Polym. J.*, 2004, **36**, 261-264.

233. P. L. Arnold, J.-C. Buffet, R. P. Blaudeck, S. Sujecki, A. J. Blake and C. Wilson, *Angew. Chem. Int. Ed.*, 2008, **120**, 6122-6125.

234. B.-T. Ko, C.-C. Wu and C.-C. Lin, *Organometallics*, 2000, **19**, 1864-1869.

235. Y.-C. Liu, B.-T. Ko and C.-C. Lin, *Macromolecules*, 2001, **34**, 6196-6201.

236. M. H. Chisholm, D. Navarro-Llobet and W. J. Simonsick, *Macromolecules*, 2001, **34**, 8851-8857.

237. C.-X. Cai, L. Toupet, C. W. Lehmann and J.-F. Carpentier, *J. Organomet. Chem.*, 2003, **683**, 131-136.

238. G. Entenmann and D. Bendix, Boehringer Ingelheim KG, 1988, vol. DE 3820299.

239. I. Peckermann, A. Kapelski, T. P. Spaniol and J. Okuda, *Inorg. Chem.*, 2009, **48**, 5526-5534.

240. H. A. McManus and P. J. Guiry, *Chem. Rev.*, 2004, **104**, 4151-4202.

241. G. Desimoni, G. Faita and K. A. Jørgensen, *Chem. Rev.*, 2006, **106**, 3561-3651.

242. A. I. Meyers, *J. Org. Chem.*, 2005, **70**, 6137-6151.

243. G. C. Hargaden and P. J. Guiry, *Chem. Rev.*, 2009, **109**, 2505-2550.

244. A. K. Ghosh, P. Mathivanan and J. Cappiello, *Tetrahedron: Asymmetry*, 1998, **9**, 1-45.

245. A. Alaaeddine, A. Amgoune, S. Bellemin-Laponnaz, J.-F. Carpentier, S. Dagorne and C. M. Thomas, *Eur. J. Inorg. Chem.*, 2006, 3652-3658.

246. C.-T. Chen, C.-Y. Chan, C.-A. Huang, M.-T. Chen and K.-F. Peng, *Dalton Trans.*, 2007, 4073–4078.

247. C.-T. Chen, M.-T. Chen, H.-J. Weng, C.-A. Huang and K.-F. Peng, *Eur. J. Inorg. Chem.*, 2009, 2129–2135.

248. M.-T. Chen, P.-J. Chang, C.-A. Huang, K.-F. Peng and C.-T. Chen, *Dalton Trans.*, 2009, 9068–9074.

249. M.-T. Chen and C.-T. Chen, *Dalton Trans.*, 2011, 12886–12894.

250. S. Bian, S. Abbina, Z. Lu, E. Kolodka and G. Du, *Organometallics*, 2014, **33**, 2489-2495.

251. S. Abbina and G. Du, *ACS Macro Lett.*, 2014, **3**, 689-692.

252. S. D. Bennett, B. A. Core, M. P. Blake, S. J. A. Pope, P. Mountford and B. D. Ward, *Dalton Trans.*, 2014, **43**, 5871-5885.

253. H. W. Gorlitzer, M. Spiegler and R. Anwander, *J. Chem. Soc., Dalton Trans.*, 1999, 4287-4288.

254. S. Hong, S. Tian, M. V. Metz and T. J. Marks, *J. Am. Chem. Soc.*, 2003, **125**, 14768-14783.

255. J. Zou, D. J. Berg, D. Stuart, R. McDonald and B. Twamley, *Organometallics*, 2011, **30**, 4958-4967.

256. M. Durán-Galván, S. A. Worlikar and B. T. Connell, *Tetrahedron*, 2010, **66**, 7707-7719.

Chapter Two

$CzOx^{Me2}$-supported magnesium and zinc complexes for the ROP of *rac*-, *L*- and *meso*-LA and their mechanistic studies

2.1 Overview

This Chapter will describe detailed investigations into the living and immortal ROP of *rac*-, *L*- and *meso*-LA using magnesium and zinc catalysts supported by the carbazole-bis(oxazoline) ligand, $CzOx^{Me_2}$. A summary and discussion of the results will be presented, as well as in-depth mechanistic studies conducted with deuterium labelling experiments and spectroscopic analyses. Ten new complexes will be presented, two of which are *in situ* generated, along with three X-ray crystallographic structures.

2.2 Introduction

2.2.1 Alkaline earth complexes as ROP catalysts

The chemistry of transition metals is central to catalysis: their readily available d-orbitals play a pivotal role in the fast and reversible adoption of different oxidation states. Until recently, the potential of main group organometallic complexes within catalysis has been comparatively underdeveloped and underexploited. The past decade has witnessed a surge in interest in the application of organoalkaline earth complexes in a number of catalytic transformations, including asymmetric catalysis[1-6] and polymerisation.[1, 7-12] For a comprehensive discussion of alkaline earth complexes as catalysts for the ROP of cyclic esters, the reader is directed to recent relevant reviews.[13-21]

Complexes featuring alkaline earth metals are particularly attractive as potential catalysts: they are among the most abundant elements in the Earth's crust, rendering them considerably cheaper and more accessible than transition metals and lanthanides.[22] Their location within the Periodic Table affords them very unique and interesting chemistry as they combine the nucleophilicity of Group 1 metals with the Lewis acidity of Group 3 metals, which is of particular importance for monomer binding and activation. Furthermore, their low toxicity and biocompatibility is advantageous from a ROP perspective, reducing the need to remove catalyst residues from the polymer and permitting their use in biomedical applications. A few examples of prominent alkaline earth complexes as initiators for the polymerisation of cyclic esters are given in Figure 2.1.

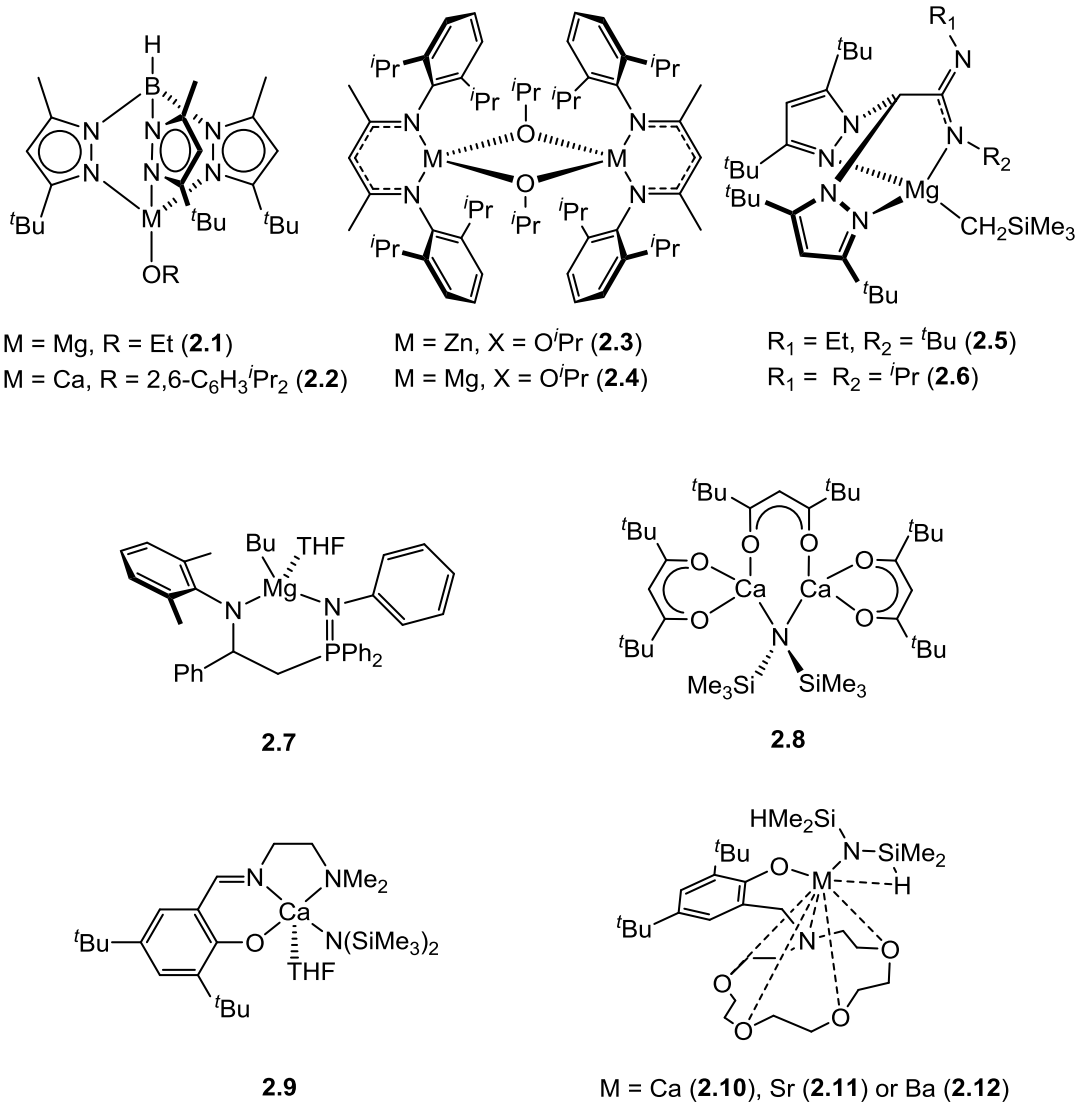


Figure 2.1. Examples of alkaline earth complexes for ROP of lactide.[11, 12, 23-32]

The initial breakthrough came from Chisholm *et al.* who, in a study into well-defined initiators for the ROP of lactide, reported a series of tris(pyrazolyl) (Tp) and tris(indazolyl)borate magnesium complexes, including the magnesium alkoxide complex {HB(3-^{t}Bupz)$_3$}Mg(OEt) (**2.1**) (HB(3-^{t}Bupz)$_3$ = tris(3-*tert*-butylpyrazolyl)borate).[11, 12] **2.1** was found to be highly active for the ROP of lactide, converting 500 equivalents of *L*-LA to 90% conversion in CH_2Cl_2 at RT in 1 h. A linear relationship between molecular weight and % conversion was observed, with narrow molecular weight distributions (PDI = 1.1-1.25). Around the time of publication, this represented one of the most active initiators for ROP. In the years that followed, the calcium analogue was reported. The complex HB(3-^{t}Bupz)$_3$Ca(O-2,6-C$_6$H$_3$^{i}Pr$_2$) (**2.2**) was shown to be a highly efficient initiator for the ROP of *rac*-LA,

reaching 90% conversion within 1 min and affording highly heterotactic PLA, with P_r = 0.90: the first calcium-based initiator capable of stereocontrolled ROP of *rac*-LA.[23,24]

The β-diketiminate ligand, also known as ^{Dipp}NacNac (^{Dipp}NacNac = CH(C(Me)(2,6-$NC_6H_3{}^iPr_2$))$_2$), was employed by both the groups of Chisholm and Coates to generate a new series of low coordinate alkaline earth complexes. In 2000, Coates and Ovitt reported the synthesis and characterisation of dimeric zinc and magnesium alkoxide complexes **2.3** and **2.4**.[25] Complex **2.4** was found to be highly active, but poorly controlled, polymerising 200 equivalents of *rac*-LA in CH_2Cl_2 to full conversion after 20 min to yield atactic PLA with PDI = 1.59. The addition of 1 equivalent of ^{i}PrOH led to the formation of narrow molecular distributions (PDI ≈ 1.20-1.35), which was ascribed to the interaction of ^{i}PrOH with **2.4**, modifying its reactivity. In contrast, **2.3** was considerably less active; however, upon examination, the PLA microstructure was revealed to be highly heterotactic (P_r = 0.90), produced *via* a chain end control mechanism. Similarly, Chisholm *et al.* noted the similar monomeric complex (^{Dipp}NacNac)Mg(O^{t}Bu) afforded atactic PLA in CH_2Cl_2 and benzene; however, in THF it had a similar heterotactic enrichment to its zinc counterpart (^{Dipp}NacNac)Zn(O^{t}Bu), indicating a strong solvent dependency on the observed stereocontrol.[33, 34]

The hetereoscorpionate ligands employing acetamidinate groups were first introduced as useful ancillary ligands for the synthesis of Mg complexes by Sánchez-Barba *et al.* in 2007.[35] Initial results with the sterically unencumbered {tbpamd}MgR and {pbpamd}MgR (R = C_3H_5, ^{t}Bu or CH_2SiMe_3) complexes in which the chelating pyrazolyl rings contained Me substituents proved disappointing: treatment with 100 equivalents of *L*- or *rac*-LA required an elevated temperature of 70 °C and prolonged reaction times to achieve only partial conversion. In 2011, Sánchez-Barba *et al.* reported similar complexes {tbp*amd}Mg(CH_2SiMe_3) (**2.5**) and {pbp*amd}Mg(CH_2SiMe_3) (**2.6**) in which the Me substituents were replaced with ^{t}Bu groups, which outperformed their less bulky counterparts.[32] Complexes **2.5** and **2.6** proved to be highly effective initiators, fully converting 100-200 equivalents of either *L*- or *rac*-LA at RT in <5 min. Furthermore, the polymerisation was very well-controlled, with good agreement between the expected and observed molecular

weights and narrow PDIs. Heterotactically-enriched PLA was obtained, with P_r = 0.70-0.79.

Reported by Cui *et al*. in 2014, the phosphinamino-amine supported magnesium complex {(2,6-$C_6H_3Me_2$)NC(Ph)CHP(Ph_2)NPh}Mg(Bu)(THF) (**2.7**) was synthesised and shown to be highly active and well-controlled during the ROP of 200 equivalents of *rac*-LA, reaching 94% conversion after 10 min in THF at 25 °C.[31] The complex was tested at 0 °C with 50-1000 equivalents of *rac*-LA, and was found to be highly heteroselective (P_r = 0.98, 0 °C). This is the highest heterotacticity achieved to date when employing a magnesium catalyst.

In 2003, Westerhausen, Feijen and coworkers synthesised {(TMHD)Ca(THF)}$_2${μ-N($SiMe_3$)$_2$}(μ-TMHD) (**2.8**) from the protonolysis reaction between 3 equivalents of H-TMHD (2,2,6,6,-tetramethylheptane-3,5,-dione) and 2 equivalents of Ca{N($SiMe_3$)$_2$}$_2$(THF)$_2$.[28] As expected for a complex with an amide initiating group, **2.8** was found to be highly active for the ROP of lactide; however, it offered poor control over molecular weight with broad PDIs. When treated with propan-2-ol, the living polymerisation became more controlled with better agreement between observed and expected M_n and a moderate PDI of 1.26.[29] In 2008, Darensbourg *et al.* reported that the Schiff base calcium complex **2.9** was active for the ROP of lactide after 30 min when treated with up to 700 equivalents of *L*-LA at room temperature. The polymer produced had higher than expected molecular weights, despite having very narrow PDIs, and was found to be atactic.[30]

The synthesis of well-defined heteroleptic alkaline earth complexes becomes increasingly challenging on descent of the group to the heavier metals Ca, Sr and Ba, due to the Schlenk equilibrium facilitating redistribution to undesirable homoleptic complexes. Recent developments by Carpentier *et al*. have shown the potential for heteroleptic complexes featuring heavier alkaline earth metals to be isolated and applied to ROP.[26] A series of alkaline earth bis(trimethylsilyl)amide complexes supported by an amino-ether phenolate ligand 2-{(1,4,7,10-tetraoxa-13-azacyclopentadecan-13-yl)methyl}-4,6-di-*tert*-butylphenolate (LO^3) were isolated, M = Ca (**2.10**), Sr (**2.11**) and Ba (**2.12**); these complexes were stable in solution because of an internal β-agostic Ae···H–Si interaction. Although only treated with *L*-LA, preventing exploration of their stereocontrol, they were found to be competent

catalysts for immortal ROP (*i*ROP) in the presence of 10 to 100 equivalents of exogenous alcohol such as propan-2-ol, benzyl alcohol or propargyl alcohol, reaching high conversion in both toluene and THF within 1 h.[27] The complexes were found to be reactive in the order Ca (**2.10**) < Sr (**2.11**) < Ba (**2.12**): attributed to the anticipated increase in nucleophilic reactivity of the active species as a result of the increasing electropositivity of the metal on descent of the group.

2.2.2 Early alkaline earth and lanthanide borohydride initiators in ROP

2.2.2.1 Lanthanide borohydride initiators in ROP

Over the past 15 years, lanthanide borohydride complexes have received considerable attention as efficient initiators for the polymerisation of a range of cyclic esters as either "ligand-free" $Ln(BH_4)_3(THF)_x$ (Ln = Pr, x = 2; Ln = Y, x = 2.5; Ln = La, Nd, Sm or Yb, x = 3;),[36-43] or heteroleptic $(L)Ln(BH_4)$ complexes.[44-54] $(L)Ln(BH_4)$ systems have been shown to outperform their amide counterparts, $(L)Ln(NR_2)$, in terms of molecular weight control and initiating efficiency, and are comparable to alkoxides.[55] A few selected examples are given in Figure 2.2.

The first report of rare earth borohydride complex to be utilised in the polymerisation of cyclic esters came from Guillaume *et al*. in 2003, in which the polymerisation of ε-CL using "ligand-free" $Nd(BH_4)_3(THF)_3$ successfully resulted in the formation of α,ω-hydroxytelechelic PCL.[36] Following this, Mountford and coworkers reported a series of dimeric diamino-bis(phenolate)-supported complexes of the type $[Ln(O_2NN')(BH_4)(THF)]_2$ (Ln = Y (**2.13**) Nd (**2.14**) or Sm (**1.21**)) which were active for the ROP of cyclic esters in 2005.[44] These complexes were synthesised *via* a salt metathesis reaction between Na_2O_2NN' and the corresponding $Ln(BH_4)_3(THF)_3$ in THF, and their activity towards the ROP of *rac*-LA probed. The complexes were found to exert reasonable control over molecular weight obtaining moderate to broad polydispersities of 1.34 to 1.97. Significantly, they demonstrated the potential of rare earth borohydride complexes to exert a good degree of stereocontrol, with the yttrium analogue producing PLA with P_r = 0.83-0.87. Further studies were undertaken in 2010 with samarium analogues, which showed the highest degree of molecular control;[45] a detailed discussion of these complexes with comparison to their amide counterparts is given in Chapter 1.

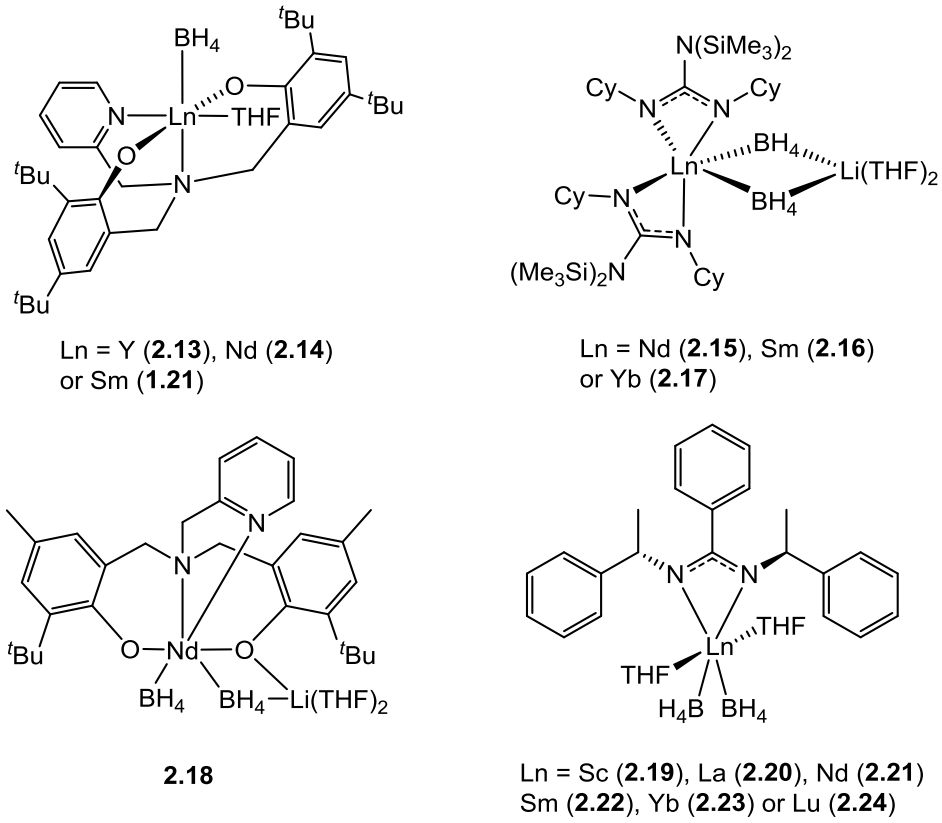


Figure 2.2. Examples of supported lanthanide borohydride complexes for the ROP of lactide.[44-48]

In 2007, Trifonov *et al*. synthesised a series of heteroleptic lanthanide bis(borohydride) complexes supported by bulky guanidinate ligands *via* salt metathesis of 2 equivalents of $Li[(Me_3Si)_2NC(NCy)_2]$ with the corresponding $Ln(BH_4)_3(THF)_2$ (M = Nd, Sm or Yb) in toluene at 65 °C to obtain complexes **2.15**-**2.17**.[46] Despite all complexes producing atactic PLA, the neodymium complex **2.15** was found to be highly active and exerted good control over molecular weight. A neodymium borohydride complex supported by a diamino-bis(phenolate) ligand (**2.18**) was subsequently synthesised and its activity towards the ROP of *rac*-LA and *rac*-BBL tested.[47] Complex **2.18** was moderately active when treated with 50-500 equivalents of *rac*-LA in THF at 20 °C with reasonable control over molecular weights and moderate polydispersities, showing a marked decrease in activity when the solvent employed during polymerisation was changed from THF to toluene.

More recently, Roesky *et al.* synthesised the first examples of enantiomerically pure chiral rare earth borohydride complexes supported by amidinate ligands.[48] Complexes

2.19-**2.24** were accessed through salt metathesis reactions between (*S*)-KPEBA and $Ln(BH_4)_3(THF)_3$ (Ln = Sc, La, Nd, Sm, Yb or Lu). The complexes were tested for their polymerisation activity in THF with 50-500 equivalents of *rac*-LA. Generally, all complexes showed narrow polydispersities, lying in the range of *ca*. 1.10-1.30; however, the experimentally obtained molecular weights were lower than those calculated. For example, after 3 h in the presence of 150 equivalents *rac*-LA in THF at 23 °C **2.22** reached 40% conversion, with M_n(obs) = 5,700 g mol^{-1} *cf.* M_n(calc) = 8,650 g mol^{-1}, attributed to a significant degree of transesterification reactions during polymerisation. Unfortunately, the chiral environment surrounding the active site imparted no stereocontrol during polymerisation, producing atactic PLA in all cases.

2.2.2.2 Alkaline earth borohydride initiators in ROP

In recent years, lanthanide borohydride complexes have emerged as a new class of efficient initiators for the polymerisation of cyclic esters. The potential similarities between complexes of the heavier alkaline earth metals and the lanthanides,[22, 56, 57] particularly with regard to ionic radii and chemical behaviour, have prompted recent investigation into alkaline earth borohydride complexes as ROP catalysts. Several examples are given in Figure 2.3.

In 2011, Mountford *et al.* reported the first cationic calcium borohydride complexes and a charge neutral calcium borohydride complex for the ROP of *rac*-LA.[58] Employing a similar methodology used to access mono- and dicationic lanthanide analogues,[59-63] $[Ca(BH_4)(THF)_5][BPh_4]$ (**2.25**) was synthesised by treatment of commercially available $Ca(BH_4)_2(THF)_2$ with 1 equivalent of $[Et_3NH][BPh_4]$ in THF at -78 °C. Reaction with $HC(3,5\text{-}Me_2pz_3)_3$ (Tpm) in CH_2Cl_2 afforded $[(Tpm)Ca(BH_4)(THF)_2][BPh_4]$ (**2.26**) in 74% yield. Both **2.25** and **2.26** were crystallographically and spectroscopically characterised and found to possess a κ^3-bound BH_4 ligand. Polymerisation of *rac*-LA in THF with **2.25** was slow even at the elevated temperature of 70 °C: treatment with varying equivalents of *rac*-LA between 50-200 required reaction times of 3-5 h. Nevertheless, monomer consumption was found to follow first-order kinetics and M_n increased linearly with conversion, with excellent agreement between experimentally observed and calculated molecular weights. The slow reaction time of **2.25** was improved upon by the Tpm-supported complex **2.26** was employed: attributed to the ability of the ligand to discourage

binuclear complex formation or excessive chelation from the growing PLA chain. Up to 250 equivalents of *rac*-LA could be converted in THF at room temperature, showing good agreement between M_n(obs) and M_n(calc) and narrow PDIs. However; neither complex was able to exert any stereocontrol during polymerisation producing only atactic polymer. An analogous charge neutral complex ($Tp^{tBu,Me}$)Ca(BH_4)(THF) (**2.28**) was synthesised *via* a salt metathesis reaction of Ca(BH_4)$_2$(THF)$_2$ and K$Tp^{tBu,Me}$ in THF. Complex **2.28** proved to be highly active for ROP: when treated with 200 equivalents of *rac*-LA in THF at RT, >90% conversion was achieved after 5 min. In addition, the polymerisation was well-controlled with excellent agreement between M_n(obs) and M_n(calc). Tetrad analysis of the polymer backbone with $^1H\{^1H\}$ NMR revealed heterotactically-enriched PLA with P_r = 0.88-0.90.

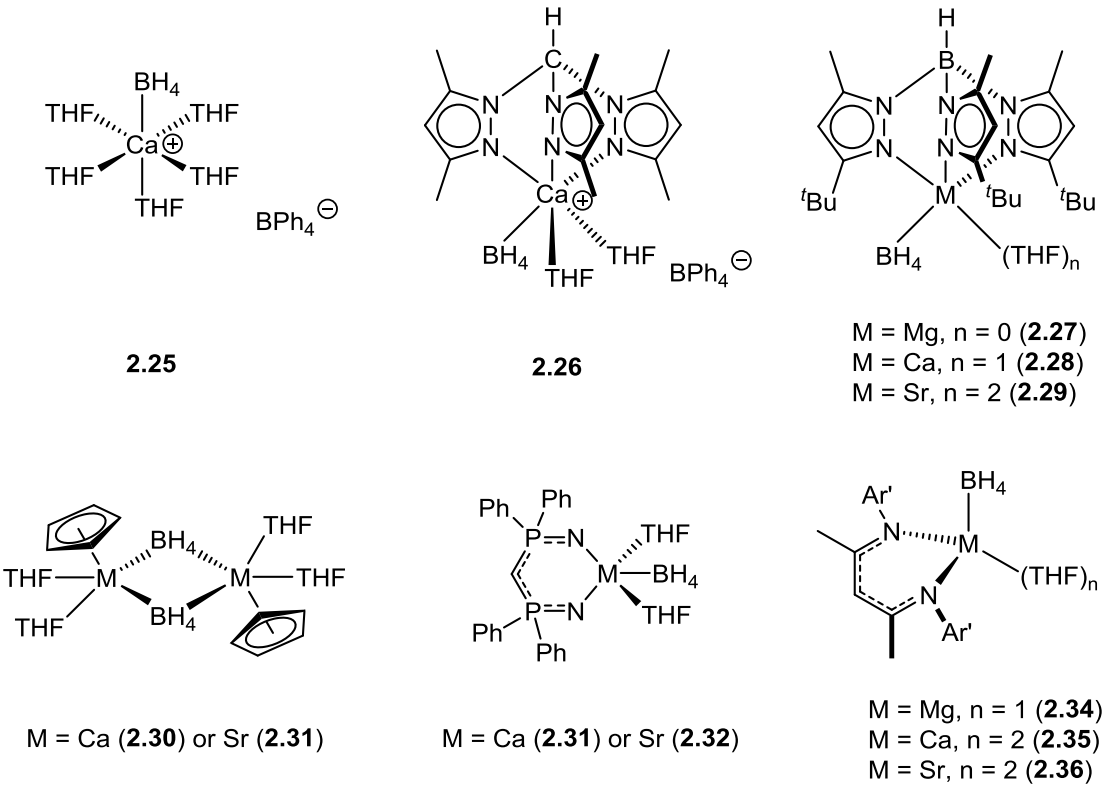


Figure 2.3. Examples of alkaline earth borohydride initiators for ROP of lactide (Ar' = 2,6-$C_6H_3{}^iPr_2$).[58, 64-67]

Further investigations to expand the family of charge neutral ($Tp^{tBu,Me}$)-supported alkaline earth borohydride complexes first reported by Mountford *et al.* in 2011, led to the synthesis of analogous complexes ($Tp^{tBu,Me}$)Mg(BH_4) (**2.27**) and ($Tp^{tBu,Me}$)Sr(BH_4)(THF)$_2$ (**2.29**).[67] Unexpectedly, **2.27** was found to be inactive

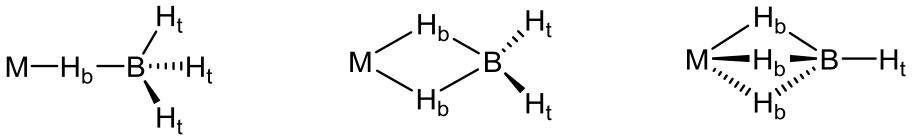
towards the ROP of *rac*-LA when treated with 100 equivalents in THF at room temperature. An increased temperature of 70 °C was required for polymerisation, but the polymer was revealed to have lower than expected molecular weights with no stereoselectivity observed. Extensive mechanistic studies were undertaken in order to deduce the causes of this poor performance, discussed in detail in Section 2.5. In contrast, **2.29** was found to be an efficient initiator for polymerisation, achieving over 95% conversion when treated with 100 equivalents of *rac*-LA in THF at room temperature. The activity was too high to allow for full kinetic analysis; however, the observed M_n was consistently higher than expected, indicative of partial catalyst activation or a greater rate of propagation to initiation. The polymer was found to be moderately heterotactically enriched (P_r = 0.60-0.70).

Following the initial pioneering work conducted by Mountford *et al*. in 2011, Roesky, Guillaume, Maron and coworkers reported a series of calcium and strontium borohydride complexes with various supporting ligands.[64, 65] Half-sandwich complexes **2.30** and **2.31** were obtained following treatment of the corresponding $M(BH_4)_2(THF)_2$ (M = Ca (**2.30**) or Sr (**2.31**)) with KCp* in THF, along with bis(phosphinimino)methanide $\{Me_3SiNPPh_2)_2CH\}M(BH_4)(THF)_2$ (M = Ca (**2.32**) or Sr (**2.33**)) complexes. Complex **2.30** was characterised crystallographically and the BH_4 ligands were determined to be bridging between the two strontium atoms, giving rise to a dimeric structure. Although it was not possible to structurally authenticate **2.30** using X-ray crystallography, a similar dimeric structure featuring bridging BH_4 groups was postulated on the basis of the appearance of a molecular ion peak consistent with a dimer present in the EI-MS and the X-ray crystallographically characterised structure of **2.30**. When treated with 100-500 equivalents of *L*-LA, **2.30** and **2.31** were found to be reasonably active towards polymerisation, producing PLA with good control over molecular weights and narrow polydispersities. Surprisingly, **2.31** had lower activities in the ROP of *L*-LA when compared to **2.30**: this was postulated by DFT to be a result of lower energetic parameters for B–H activation for the calcium complex. Substantially decreased activities were observed in the case of **2.33** and **2.33**, both requiring prolonged reaction times, especially when treated with high monomer loadings. In all cases, α,ω-dihydroxytelechelic PLA was produced.

In 2013, Mountford *et al.* published a family of ^{Dipp}NacNac supported alkaline earth borohydride complexes, ^{Dipp}NacNacMg(BH_4)(THF) (**2.34**) and ^{Dipp}NacNacM(BH_4)$(THF)_2$ (M = Ca (**2.35**) or Sr (**2.36**)), synthesised *via* a salt metathesis reaction between ^{Dipp}NacNacK and the corresponding metal bis(borohydride) starting material in THF.[66] **2.34** was found to be highly active when treated with 20-300 equivalents of *rac*-LA, reaching *ca*. 85-90% conversion within 5 min, with moderate levels of heteroselectivity (P_r = 0.74-0.86). Loading experiments were conducted to observe the agreement of M_n with calculated values at high monomer loadings: good agreement was observed until *ca*. 175 equivalents *rac*-LA, after which apparent transesterification reactions lead to lower than anticipated results. Analysis of the polymer with MALDI-ToF MS revealed a mixture of α,ω-dihydroxytelechelic PLA and apparent HOCH(Me)-/aldehyde (-CH(Me)CHO) end-groups. Initial assessment of **2.35** and **2.36** showed both to be considerably less active than **2.34**, attributed to the formation of bi- or poly-metallic species during reaction. In addition, in both cases the growth of M_n *vs*. % conversion was found to be non-linear, which was initially ascribed to deleterious transesterification reactions, supported by MALDI-ToF MS analysis which confirmed the presence of macrocyclic polymer, in addition to the presence of -CH_2OH and apparent -CHO termini, based on *m*/*z* values.

2.2.3 Coordination modes of the borohydride ligand

The structural and chemical properties of covalent borohydride complexes of the rare earths have been reviewed in the literature extensively.[42, 68, 69] The BH_4 group offers several advantages as a ligand, a consequence of its chemical reactivity and structural versatility. Borohydrides can adopt several hapticities when bound to the metal centre to satisfy the coordination sphere, adopting terminal (κ^1, κ^2 and κ^3) and bridging geometries (Figure 2.4). From a reactivity perspective, borohydrides can be considered *pseudo*-halides, insofar as they are monoanionic and easily substituted; moreover, they can also be considered as extended hydrides because of their ability to undergo reductive polymerisation.[36, 70]



κ^1 κ^2 κ^3

Figure 2.4. Possible coordination modes of the borohydride ligand.

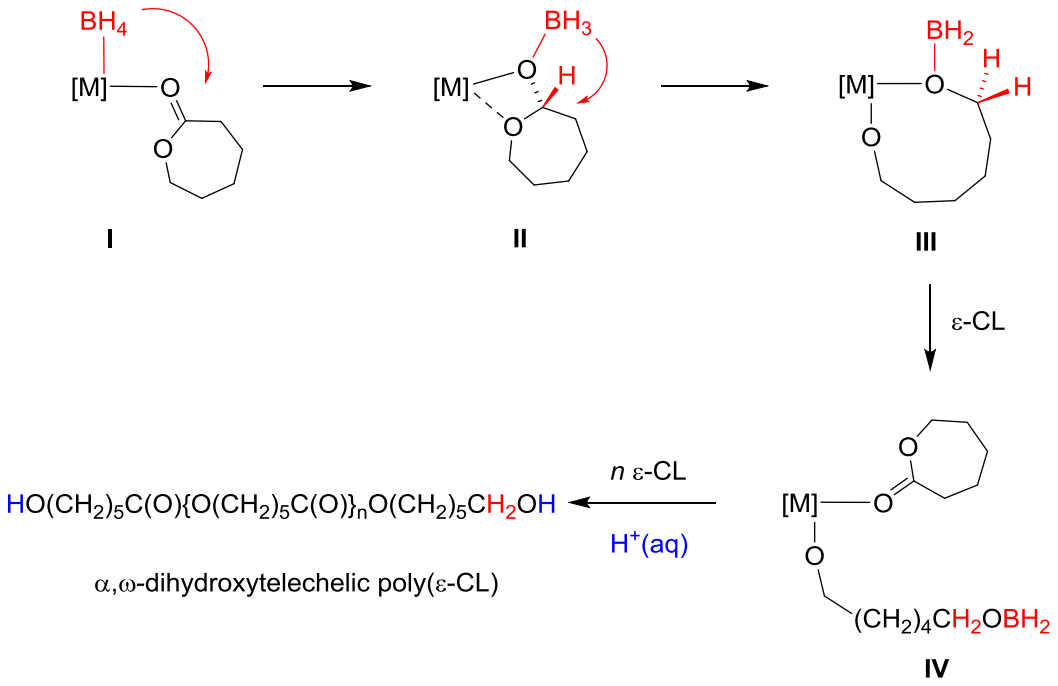
Techniques available for the structural characterisation of a borohydride complex are X-ray diffraction, neutron diffraction, IR and NMR spectroscopy. Along with X-ray diffraction, IR spectroscopy is routinely employed to deduce the hapticity of the borohydride ligand, both in the solid state and solution, enabled by analysis of diagnostic bands appearing between 2500-1000 cm^{-1}. The position and appearance of these bands can be assigned to B–H stretches corresponding to the appropriate structural configuration, allowing the κ^1, κ^2 and κ^3 coordination modes to be distinguished (Table 2.1).[68]

Table 2.1. IR active functional vibrational transitions commonly observed for mononuclear MBH_4 configurations.[68]

Structure	Freq. (cm^{-1})	Normal mode	Symmetry	Comments
Monodentate	2450-2300	$B–H_t$	A_1, E	Strong doublet
	~2000	$B–H_b$ stretching	A_1	Strong
	~2000-1700	$M–H_b$ stretching	A_1	Often broad
	1150-1000	BH_3 deformation	A_1, E	Strong band
Bidentate	2600-2400	$B–H_t$ stretching	A_1, B_1	Strong doublet (50-80 cm^{-1})
	2150-1650	$B–H_b$ stretching	A_1, B_2	Strong band, possible shoulder
	1500-1300	$M–H_b$ stretching	A_1	Strong band
	1200-1100	BH_2 deformation	B_2	Strong
Tridentate	2600-2450	$B–H_t$ stretching	A_1	Strong singlet
	2200-2100	$B–H_b$ stretching	A_1, E	Doublet (50-80 cm^{-1})
	1250-1150	Bridge deformation	E	Strong
Ionic	2300-2200	$B–H_t$ stretching	T_2	Strong broad
	1100-1050	BH_2 deformation	T_2	Strong broad

2.2.4 Mechanistic considerations

Following the establishment of lanthanide borohydride systems as efficient initiators for the ROP of cyclic esters, detailed experimental studies and DFT calculations were undertaken by Guillaume, Maron, Roesky and Mountford in order to understand the precise nature of the mechanism by which polymerisation occurs.[36, 37, 55, 71-73] A proposed mechanism is outlined in Scheme 2.1.[72]



Scheme 2.1. Mechanism for the borohydride-initiated ROP of ε-CL producing α,ω-dihydroxytelechelic PCL.[72]

In the first step, the monomer coordinates to the metal centre of [M]–BH_4 to form an adduct (**I**), followed by hydride transfer to the acyl carbon and BH_3 transfer to the anionic oxygen (**II**). A second hydride transfer to generate a fully reduced carbonyl group promotes the ring-opening of ε-CL (**III**) and propagation occurs with subsequent monomer insertion (**IV**). A hydrolytic work up post-polymerisation allows for the isolation of α,ω-dihydroxytelechelic PCL.

Whilst this mechanism is consistent with end-group analysis of the polymer produced from ε-CL, the ROP of other cyclic esters, such as *rac*-LA, with [M]–BH_4 does not necessarily lead to exclusively α,ω-dihydroxytelechelic polymer. Guillaume showed that the poly(TMC) formed with $Sm(BH_4)_3(THF)_3$ contains a mixture of -CH_2OH and

-CHO polymer end-groups.[39] Following experimental results obtained by Mountford *et al*. which suggested that the polymerisation of *rac*-LA with complexes **1.19-1.21** led to a mixture of -CH_2OH and -CHO terminated PLA, DFT calculations were undertaken to gain further insight into their origin.[45] The necessity of two hydride transfers for the production of α,ω-dihydroxytelechelic PLA was confirmed; however, it was postulated that the -CHO terminus arose following BH_3 elimination and subsequent ring-opening of the monomer: a process not observed during the ring-opening of ε-CL. Despite these findings, Trifonov *et al.* were not able to unambiguously determine the precise nature of all PLA termini produced with lanthanide borohydride systems **2.15-2.17**.[46, 49]

2.2.5 Borate esters as chain transfer agents in immortal ROP

To date, boron-containing compounds have found a wide variety of uses in a number of organic syntheses and organometallic transformations.[74-76] In 1991, Ewen and Marks independently showed that tris(pentafluorylphenyl)borane, $B(C_6F_5)_3$, was a highly effective cocatalyst when used in conjunction with Group 4 metallocene alkyls for the polymerisation of olefins through alkyl abstraction.[77, 78] Further work by Aoshima *et al.* demonstrated the ability of $B(C_6F_5)_3$ to act as a catalyst for copolymerisation of alkyl vinyl ethers and isobutylene oxide through cationic vinyl addition and ring opening.[79]

Borane derivatives have also found application as chain transfer agents in metallocene-mediated olefin polymerisation. The B–H or B–R bond in organoborane hydrides such as 9-borabicyclo[3.3.1]nonane (9-BBN), dimesitylborane and di(2,4,6-triisopropylphenyl)borane coordinated to the metal centre in a four-membered transistion state, permitting the exchange between the growing polymer chain and the alkyl substituents.[80-87] The resultant molecular weight of the borane-terminated polyolefin was dependent on the ratio of $[monomer]_0$:$[CTA]_0$.

Until very recently, the use of boron derivatives as CTAs was limited solely to the field of olefin polymerisation; however, unpublished results in the Mountford group have demonstrated the ability of trialkyl borate esters to act as highly effective CTAs in the ROP of cyclic esters including *rac*-LA.[67] In 2008, Sun *et al*. reported the reaction between lanthanide borohydrides and aldehyde and ketone derivatives to generate *in situ* lanthanide alkoxide complexes which proved to be highly efficient

initiators for the ROP of ε-CL.[88] In light of Sun's work, the reaction of ($Tp^{tBu,Me}$)M(BH_4) (M = Mg, Ca or Sr) with 4.5 equivalents of benzaldehyde produced the corresponding alkoxide complex and 1 equivalent of $B(OBn)_3$. It was subsequently demonstrated that $B(OBn)_3$ and other trialkyl borate esters were capable of acting as effective CTA, sometimes offering excellent degrees of molecular weight control in the ROP of ε-CL and *rac*-LA.[89]

2.3 Synthesis and characterisation of $CzOx^{Me2}$-supported magnesium and zinc complexes

2.3.1 Synthesis of protioligand $HCzOx^{Me2}$ (1.45)

The known protioligand $HCzOx^{Me2}$ was synthesised in high yield over several steps according to modified literature procedures.[90-92] Literature procedures allow for an overall yield following a four step synthesis of 30%; however, modifying the procedures by refluxing the precursor 3,6-di-*tert*-butyl-9*H*-carbazole-1,8-dicarbonitrile in chlorobenzene in the presence of 2.5 equivalents of zinc chloride and 3 equivalents of 2-amino-2-methylpropan-1-ol for 168 hours instead of 72 hours allowed for an improved overall yield of 40%. **1.45** was characterised with X-ray crystallography (Figure 2.5). Selected bond lengths and angles are given in Table 2.2.

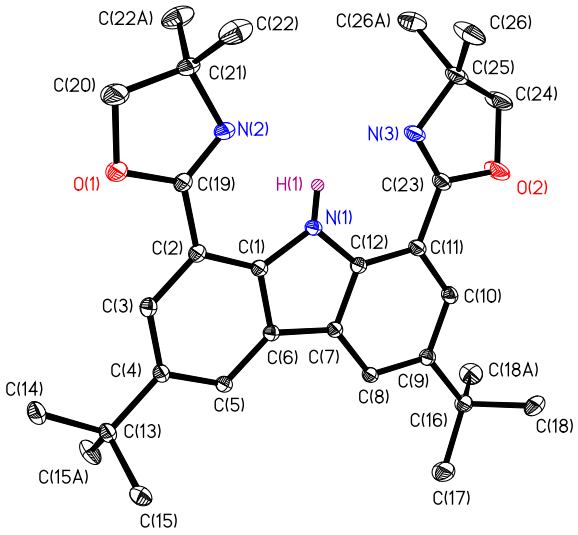


Figure 2.5. Displacement ellipsoid plot of $HCzOx^{Me2}$ (**1.45**) (20% probability level). C-bound H-atoms, THF of crystallisation and minor disorder components omitted for clarity. H(1) is drawn as a sphere of arbitrary radius. Atoms carrying the suffix 'A' are related to their counterparts by the symmetry operator (x, ½-y, z).

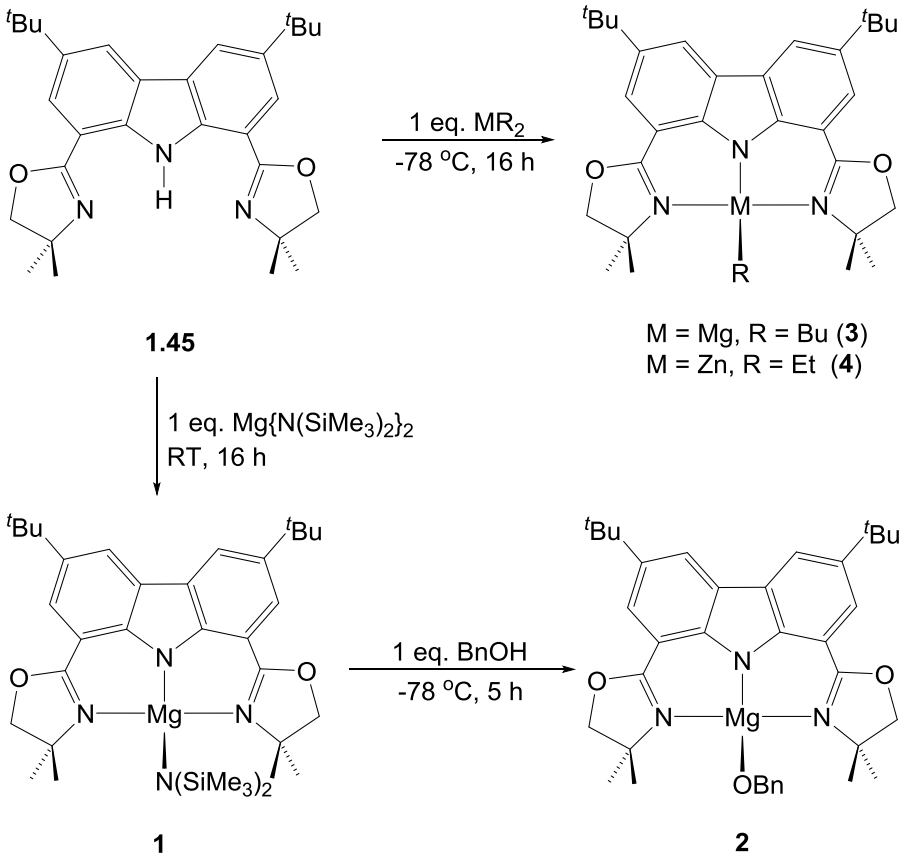
Table 2.2. Selected bond distances (Å) and angles (°) for $HCzOx^{Me_2}$ (**1.45**).

N(1)-H(1)	0.87(3)	N(2)-C(21)	1.480(3)
N(1)- C(1)	1.380(3)	O(1)-C(19)	1.364(3)
N(2)-C(19)	1.268(3)	O(1)-C(20)	1.449(3)
C(1)-N(1)-C(12)	108.5(2)	C(19)-N(2)-C(21)	107.3(2)
C(1)-N(1)-H(1)	126(2)	C(19)-O(1)-C(20)	104.7(2)
N(1)-C(1)-C(2)	130.4(2)	O(1)-C(19)-N(2)	118.6(2)
C(1)-C(2)-C(19)	120.5(2)	C(2)-C(19)-N(2)	125.8(2)

The solid state structure of compound **1.45** was determined for comparison with its metal complexes. The N(1)-H(1) bond length of 0.87(3) Å lies within the expected range of 0.82-0.94 Å.[93] The C(1)-C(2)-C(19) and C(2)-C(19)-N(2) bond angles are 120.5(2)° and 125.8(2)° which are anticipated to contribute to the determination the bite angle (β) of the ligand when coordinated to a metal centre. Notably, the core of the molecule is completely planar, with a dihedral angle of 0.0° for C(1)-C(2)-C(19)-N(2) and C(12)-C(11)-C(23)-N(3).

2.3.2 Synthesis and characterisation of $CzOx^{Me_2}$-supported magnesium and zinc alkyl, amide and alkoxide complexes

In order to generate the new complexes $Mg(CzOx^{Me_2})\{N(SiMe_3)_2\}$ (**1**), $Mg(CzOx^{Me_2})(OBn)$ (**2**), $Mg(CzOx^{Me_2})(Bu)$ (**3**) and $Zn(CzOx^{Me_2})(Et)$ (**4**), direct metallation with **1.45** was attempted. Scheme 2.2 details the synthesis of new compounds **1**-**4**, synthesised *via* protonolysis reactions with the appropriate metal precursor.



Scheme 2.2. Synthesis of magnesium and zinc complexes **1**-**4** *via* protonolysis reactions.

The protonolysis reaction of **1.45** with 1 equivalent of $Mg\{N(SiMe_3)_2\}_2$ at room temperature resulted in the formation of $Mg(CzOx^{Me2})\{N(SiMe_3)_2\}$ (**1**) in 73% yield after a cold pentane wash to remove side products. The introduction of the bulky $N(SiMe_3)_2$ ligand removes the mirror symmetry observed in the protioligand, thus creating a diastereotopic environment for the methylene protons and methyl substituents on the oxazoline ring. This diastereopicity can be detected by ^{1}H NMR spectroscopy: in C_6D_6 at 25 °C these protons are chemically inequivalent and appear as two doublets with geminal coupling of ^2J = 8.0 Hz, corresponding to the orientation of these protons towards and away from the $N(SiMe_3)_2$ group. The steric bulk of the $N(SiMe_3)_2$ group results in slow exchange between the two distinct environments, which allows the observation of the distinct methyl group and methylene proton environments at room temperature. The ^{1}H NMR spectrum of **1** at 95 °C in toluene-d_8 confirms a broadening of the peaks; unfortunately fast exchange limit could not be reached due to the limitation of the solvent boiling point (Figure

2.6). Assuming a coalescence point of 89 °C (362 K), Equation 2.1 can be used in order to derive ΔG, where T_c = temperature of coalescence in degrees Kelvin and Δv = difference in frequency of the two resonances at 298 K. At a coalescence point of 89 °C (362 K), ΔG_{362} = 71.5±0.4 kJ mol^{-1}.

$$\Delta G = 4.575 \times T_c \left(9.972 + log\left(\frac{T_c}{\Delta v}\right)\right)$$

Equation 2.1

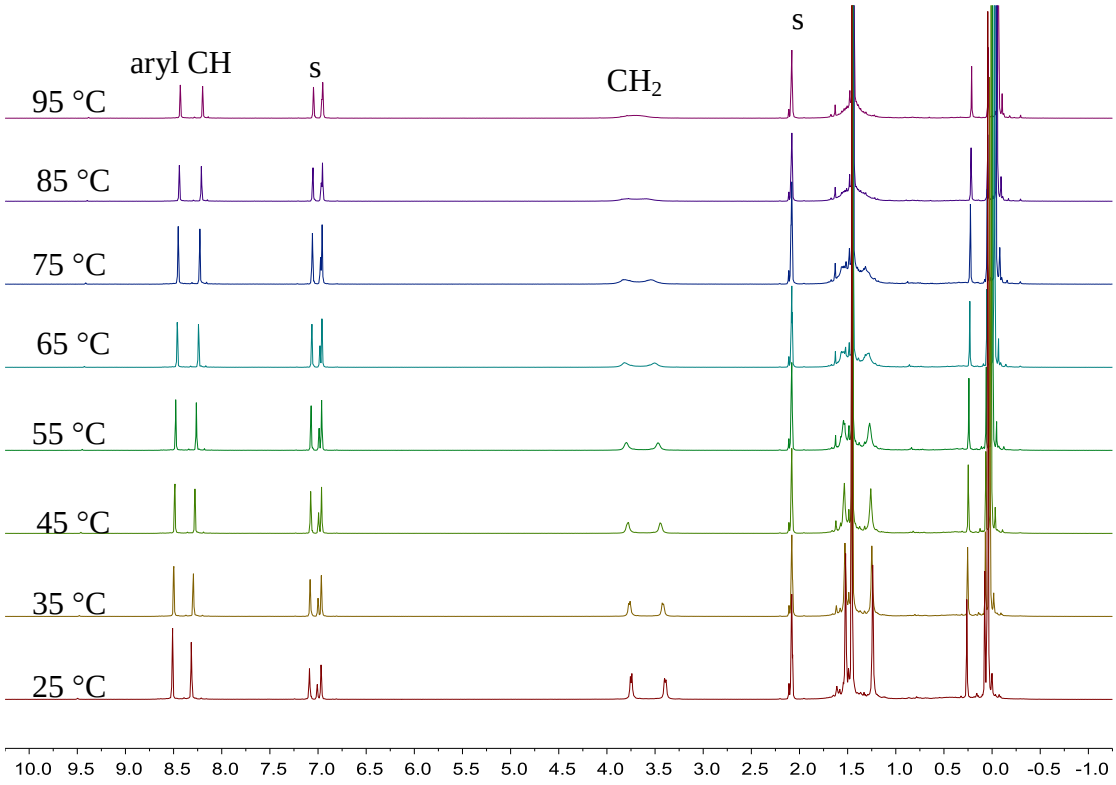


Figure 2.6. Variable temperature ^{1}H NMR (toluene-d_8, 500.3 MHz) of **1** from 25 to 95 °C. "s" denotes residual protio solvent.

A ROESY NMR was performed in an attempt to assign the inequivalent doublets. An nOe (Nuclear Overhauser Effect) was observed between the methylene proton environments oriented towards and away from the $N(SiMe_3)_2$ group, as well as the methyl groups on the oxazoline rings; however, no nOe between the $N(SiMe_3)_2$ group and either methyl group or methylene proton environments was observed. This confirms that there is a degree of fluxionality allowing the $N(SiMe_3)_2$ group to invert to either side of the ligand. **1** was crystallographically characterised (Figure 2.7) and its structure supports that depicted in Scheme 2.2.

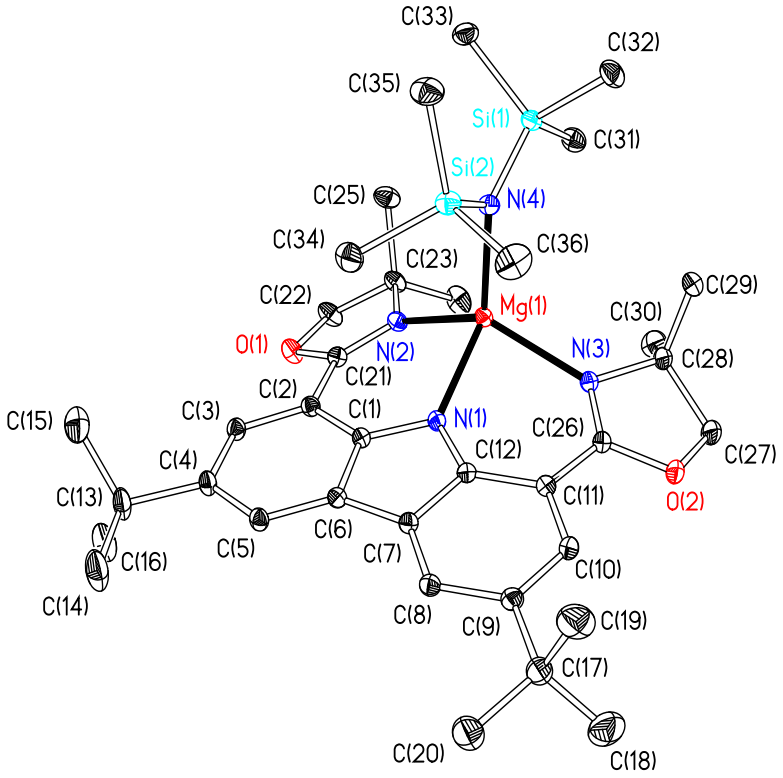


Figure 2.7. Displacement ellipsoid plot of Mg(CzOx^{Me2}){N(SiMe$_3$)$_2$} (**1**) (20% probability level). H atoms, minor disorder and toluene of crystallisation omitted for clarity.

Table 2.3. Selected bond distances (Å) and angles (°) for Mg(CzOx^{Me2}){N(SiMe$_3$)$_2$} (**1**).

Mg(1)-N(1)	2.0301(16)	Mg(1)-N(2)	2.1843(17)
Mg(1)-N(3)	2.1843(17)	Mg(1)-N(4)	2.0261(17)
N(1)-Mg(1)-N(2)	85.04(6)	N(1)-Mg(1)-N(3)	83.80(6)
N(1)-Mg(1)-N(4)	128.45(7)	N(2)-Mg(1)-N(4)	128.45(7)
N(2)-Mg(1)-N(3)	135.46(7)	N(3)-Mg(1)-N(4)	110.19(7)
Mg(1)-N(4)-Si(1)	129.56(9)	N(4)-Mg(1)-Si(2)	110.57(8)
C(1)-C(2)-C(21)	119.69(16)	C(2)-C(21)-N(2)	128.39(17)
C(11)-C(26)-N(3)	127.61(18)		

Mg(CzOx^{Me2}){N(SiMe$_3$)$_2$} (**1**) is four coordinate in which the Mg coordinates to the three N donors of the CzOx^{Me2} ligand and the N donor of a N(SiMe$_3$)$_2$ ligand, adopting a distorted tetrahedral geometry. The bond length of the Mg to the

silylamido N atom (Mg(1)-N(4)) is 2.0261(17) Å and falls within a normal range for a Mg-N=C bond length of 1.99-2.27 Å.[93] Bonds Mg(1)-N(2) and Mg(1)-N(3) are identical (2.1843(17) Å) and are significantly longer than bonds Mg(1)-N(1) (2.0301(16) Å) and Mg(1)-N(4) (2.0261(17) Å) due to the rigidity of the carbazole fragment of the $CzOx^{Me2}$ ligand. The C(1)-C(2)-C(21) bond angle is 119.69(16)°, which is very similar to the corresponding bond angle in **1.45** (120.5(2)°). The slight elongation of the C(2)-C(21)-N(2) from the corresponding bond angle in **1.45** (125.8(2)°) to 128.39(17)° is a result of the ligand backbone accommodating the magnesium centre; however, distortion is relatively restricted due to the rigidity of the carbazole backbone. This accounts for the comparatively long Mg(1)-N(2) and Mg(1)-N(3) bonds. The narrower angle between Mg(1)-N(4)-Si(2) of 110.57(8)° compared to Mg(1)-N(4)-Si(1) (129.56(9)°) is perhaps a result of steric repulsion from the methyl substituents on the oxazoline rings causing the $N(SiMe_3)_2$ group to distort to minimise the steric interaction. This distortion places a hydrogen located on C(34) in close proximity to the metal centre, with a Mg···H distance of 3.03 Å; however, whilst close, this is outside the sum of the van der Waals radii of 2.79 Å.[94, 95] Therefore there is no evidence to support the existence of a γ-agostic interaction. Both Mg(1)-N(4)-Si(1) and Mg(1)-N(4)-Si(2) angles fall within a normal range of 105-135°.[93] The atoms N(2) and N(3) of the $CzOx^{Me2}$ ligand deviate from the planarity seen in **1.45** whereby the oxazoline rings are rotated out of the plane so as to facilitate the adoption of a distorted tetrahedral geometry around the Mg atom. The dihedral angle for C(1)-C(2)-C(21)-N(2) is -17.2° and for C(12)-C(11)-C(26)-N(3) is 14.1°.

As Ae complexes are prone to redistribution to homoleptic species,[22] attempts were made to synthesise the corresponding $Mg(CzOx^{Me2})_2$ complex through the addition of 2 equivalents of **1.45** to $Mg\{N(SiMe_3)_2\}_2$ to evaluate the propensity for the formation of such complexes. The reaction mixture was heated at 90 °C in toluene for 72 h; however, after this time the resultant products were the heteroleptic complex **1** and 1 equivalent of protioligand. In view of the difficulty of formation the homoleptic species under forcing conditions, no further attempts were made to synthesise this compound.

As reported in the literature, amides are poorly controlled initiators for the ROP of lactide, experiencing much greater rates of propagation to initiation resulting in much higher than anticipated molecular weights, in addition to forming cyclic polymers with no observable end-groups.[34, 96, 97] Attention was subsequently moved to the formation of target magnesium alkoxide complexes, which are typically more controlled due to their faster rate of initiation relative to propagation. The synthesis of Mg(CzOx^{Me2})(OBn) (**2**) proved to be non-facile: the treatment of complex **1** with 1 equivalent of benzyl alcohol at room temperature in C_6D_6 or toluene resulted in protonolysis of the starting complex to produce **1.45** and $Mg(OBn)_2$. It was possible to synthesise Mg(CzOx^{Me2})(OBn) (**2**) through kinetic control, in which a toluene solution of benzyl alcohol, cooled to -10 °C, was added dropwise over one hour to a dilute toluene solution of **1** at -78 °C (Scheme 2.2). The solution was gradually warmed to room temperature to afford complex **2** in 48% yield. This reaction was low yielding due to competing protonolysis of **1**, the products of which had to be removed *via* a cold pentane wash post-reaction. Despite repeated attempts, diffraction-quality crystals of **2** suitable for X-ray crystallography could not be obtained.

The reaction of 1 equivalent of protioligand **1.45** with 1 equivalent of $MgBu_2$ in a 1M solution in heptanes at -78 °C resulted in the formation of Mg(CzOx^{Me2})(Bu) (**3**). The product was isolated following a cold pentane wash as an orange-yellow powder in 52% yield, and fully characterised by ^{1}H and ^{13}C{^{1}H} NMR spectroscopy, IR spectroscopy, mass spectrometry and elemental analysis. Analysis of **3** by ^{1}H NMR revealed the hydrogen atoms of the closest CH_2 group to the magnesium centre (α-CH_2) to be significantly downfield shifted at 0.06-0.01 ppm, and having a complex coupling pattern consistent with an AA'XX' system. The appearance of AA'XX' spectra has been previously documented by Whitesides *et al.* in the Grignard reagent $PhCH_2CH_2MgCl$, and more recently by Chisholm *et al*. who observed its appearance in a number of supported magnesium alkyl complexes.[98, 99] Where R is sufficiently small, for example R = H, a M–CH_2CH_2R fragment will exist in equilibrium as a statistical distribution in which approximately 67% adopts a gauche conformation, resulting in the appearance of a simple triplet or quartet in the ^{1}H NMR spectrum. However, an increase in the steric bulk of R results in the anti-isomer becoming more favourable, resulting in the more complex coupling pattern observed. Diffraction-quality crystals of **3** were grown from a saturated pentane solution (Figure 2.8).

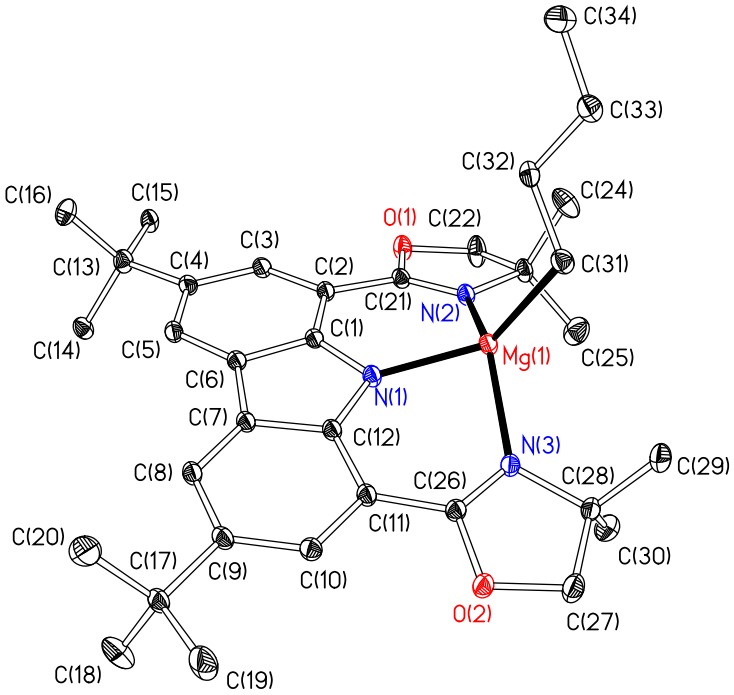


Figure 2.8. Displacement ellipsoid plot of Mg(CzOx^{Me2})(Bu) (**3**) (20% probability level). H atoms and minor disorder omitted for clarity.

Table 2.3. Selected bond distances (Å) and angles (°) for Mg(CzOx^{Me2})(Bu) (**3**).

Mg(1)-N(1)	2.0183(19)	Mg(1)-N(2)	2.1837(19)
Mg(1)-N(3)	2.1785(19)	Mg(1)-C(31)	2.133(2)
N(1)-Mg(1)-N(2)	85.02(7)	N(2)-Mg(1)-N(3)	135.97(8)
N(1)-Mg(1)-N(3)	85.33(7)	N(2)-Mg(1)-C(31)	108.55(9)
N(1)-Mg(1)-C(31)	136.45(10)	N(3)-Mg(1)-C(31)	107.89(8)
C(1)-C(2)-C(21)	120.27(18)	C(2)-C(21)-N(2)	127.89(19)
C(11)-C(26)-N(3)	128.12(19)		

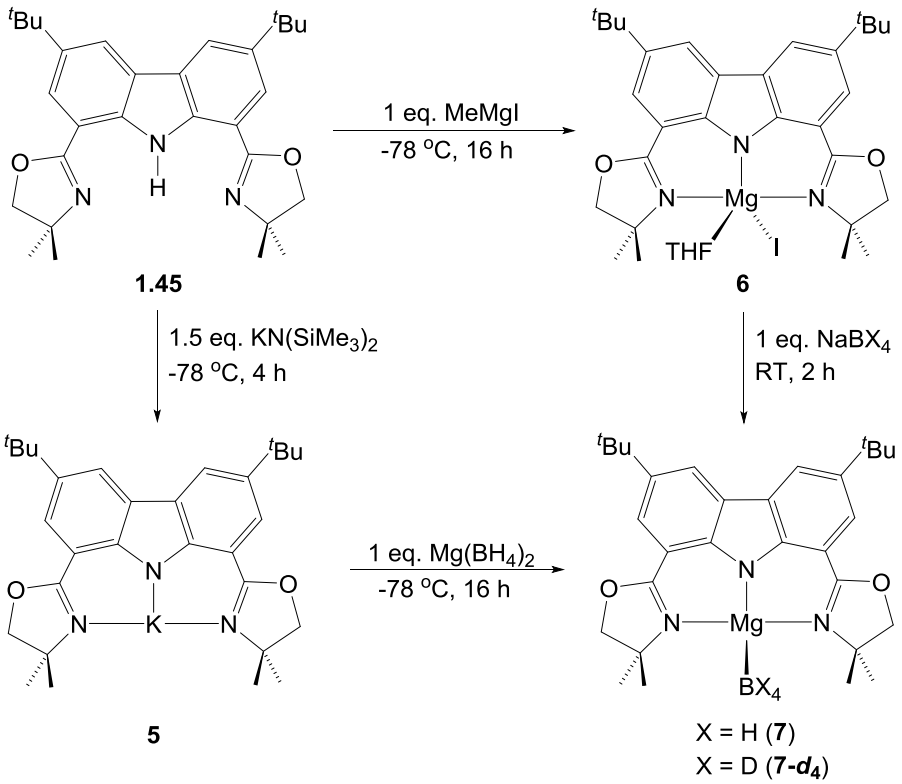
Mg(CzOx^{Me2})(Bu) (**3**) is a four coordinate complex, in which the Mg centre adopts a distorted tetrahedral geometry and is coordinated to the three N donors of the CzOx^{Me2} ligand and C(31) of the Bu ligand. In **3**, unlike **1**, none of the Mg-N bonds are equal, with Mg(1)-N(1) significantly shorter than the others by *ca*. 0.16 Å (2.0183(19) Å *cf*. 2.1837(19) and 2.1785(19) Å); however, all Mg(1)-N bond lengths fall within the expected Mg-N=C bond length range of 1.99-2.27 Å.[93] The C(1)-C(2)-C(21) bond angle of 120.27(18)° is identical within error to the corresponding bond

angle in **1.45**, and the C(2)-C(21)-N(2) bond angle of 127.89(19)° is very similar to that of **1**, serving to confirm the conformational rigidity of the $CzOx^{Me_2}$ ligand when coordinated to the metal centre. The ligand deviates from its planar structure in **1.45** to accommodate the metal centre, with dihedral angles of -11.1° for C(1)-C(2)-C(21)-N(2) and 8.6° for C(12)-C(11)-C(26)-N(3).

As previously discussed, it is desirable to design active initiators for the ROP of lactide using biologically benign metals, as catalyst residues are incorporated into the polymer structure without removal post-polymerisation. Both magnesium and zinc are biocompatible; whilst they have several similar properties, such as ionic radii,[100] their chemical reactivity can be quite different.[25, 34, 96] For comparative purposes, the analogous zinc complex $Zn(CzOx^{Me_2})(Et)$ (**4**) was synthesised from the reaction of **1.45** with 1 equivalent of $ZnEt_2$ in a 1.1M toluene solution to yield the final product as a yellow powder in 48% yield. Complex **4** was fully characterised by ^{1}H and $^{13}C\{^{1}H\}$ NMR spectroscopy, IR spectroscopy and mass spectrometry and elemental analysis. As the alkyl fragment is $M–CH_2CH_3$, the complex coupling pattern is present in the ^{1}H NMR of **3** is not observed.

2.3.3 Synthesis and characterisation of $CzOx^{Me_2}$-supported magnesium borohydride and halide complexes

For the reaction of the protioligand (**1.45**) with metal precursors *via* salt metathesis, **1.45** was deprotonated by reaction with an excess of $KN(SiMe_3)_2$ to afford the potassiated salt $K(CzOx^{Me_2})$ (**5**) following a toluene and pentane wash as a sparingly soluble yellow solid in 74% yield. Although it was characterised with ^{1}H NMR, IR spectroscopy and mass spectrometry and elemental analysis, due to its extremely low solubility, a satisfactory $^{13}C\{^{1}H\}$ NMR spectrum for **5** could not be obtained, nor a crystal structure. Scheme 2.3 details the synthesis of complex **5** and the synthesis of the new magnesium complexes $Mg(CzOx^{Me_2})I(THF)$ (**6**) and $Mg(CzOx^{Me_2})(BH_4)$ (**7**), synthesised *via* protonolysis from the corresponding Grignard reagant, MeMgI, or *via* salt metathesis with $Mg(BH_4)_2$, respectively.



Scheme 2.3. Synthesis of K(CzOx^{Me2}) (**5**) and magnesium complexes Mg(CzOx^{Me2})I(THF) (**6**), Mg(CzOx^{Me2})(BH$_4$) (**7**) and Mg(CzOx^{Me2})(BD$_4$) (**7-*d*$_4$**) *via* protonolysis and salt metathesis reactions.

An alternative synthetic pathway to obtaining Mg(CzOx^{Me2})(OBn) (**2**) is the salt metathesis of Mg(CzOx^{Me2})X(THF) (X = Cl, Br or I) with 1 equivalent of NaOBn or KOBn, potentially offering improved yields compared to the existing synthetic method. Therefore, attempts to synthesise Mg(CzOx^{Me2})I(THF) (**6**) were undertaken. Reaction of MeMgI in Et$_2$O with **1.45** allowed **6** to be obtained after dissolving in THF in 84% yield. Owing to poor solubility in benzene, the complex was fully characterised by ^{1}H and ^{13}C{^{1}H} NMR spectroscopy in THF-*d*$_8$; however, it was possible to dissolve a sufficient amount of **6** in C$_6$D$_6$ order to obtain a ^{1}H NMR spectrum which revealed there to be 1 coordinated THF molecule.

NaOBn and KOBn were synthesised *via* the reaction of benzyl alcohol with excess NaN(SiMe$_3$)$_2$ or KN(SiMe$_3$)$_2$ in THF, producing an insoluble white powder which was purified by washing several times with pentane to remove the excess base and any unreacted benzyl alcohol. Treatment of **6** with 1 equivalent of NaOBn or KOBn resulted in the successful formation of target complex **2**; however, there was

concurrent protonolysis of the complex to form protioligand and a mixture of side-products which could not be removed to isolate the desired complex in high purity. It is anticipated that this decomposition is a result of the presence of residual BnOH, which remains coordinated to the cationic alkali metal following deprotonation of the alcohol with a base, despite employment of a large excess of base. Therefore, clean reaction with **6** with an alkali metal benzyl oxide to yield target complex **2** was not possible, instead resulting in degradation of the starting material.

Following the successful synthesis of several alkaline earth borohydride initiators,[58, 64-67] attempts were made to synthesise the target complex Mg(CzOx^{Me_2})(BH_4) (**7**). Commercially available $Mg(BH_4)_2$ was treated with complex **5** at -78 °C in THF to form **7** *via* salt metathesis in 69% yield after extraction into toluene followed by removal of the volatiles *in vacuo*. Alternatively, **7** may be synthesised through the addition of 1 equivalent of $NaBH_4$ to **6** in THF at 25 °C. Employing this procedure, **7** is obtained in the slightly lower yield of 59%, following extraction into toluene and removal of the volatiles. Analysis of the powder by ^{1}H NMR spectroscopy in pyridine-d_5 and C_6D_6 revealed there to be no coordinated THF in the final product. **7** was fully characterised by ^{1}H, ^{13}C{^{1}H} and ^{11}B NMR spectroscopy, solid state, THF and benzene solution IR spectroscopy, mass spectrometry and elemental analysis. Whilst the ^{11}B NMR spectrum confirmed the presence of the BH_4 group, resonances corresponding to the hydrogen atoms in the borohydride group were only observable as a very broad singlet in the ^{1}H NMR spectrum of **7**, instead of a quartet with $^1J_{^{11}B\text{-}H}$ of 80-90 Hz.[68] Previously, the "washing out" of the B–H coupling into a singlet has been attributed to rapid exchange between the terminal and bridging hydride environments; however, this is not correct.[101, 102] Rather, it is due to spin-lattice relaxation of the quadrupolar ^{11}B and ^{10}B nuclei, in which the quadrupole moment at the nucleus interacts with the electric field gradient at the nuclei, the direction of which fluctuates due to molecular reorientation.[101, 103, 104] When the rate of exchange between spin states becomes sufficiently rapid, the coupled protons are no longer able to distinguish the spin states, and thus the coupling is unobserved.

As discussed in Section 2.2.3, a useful technique to gain insight into the coordination mode of a borohydride complex is IR specroscopy. As a Nujol mull, **7** cannot be easily assigned as either bidentate or tridentate: only a broad band at 2250 cm^{-1} is

present which may imply either a polymeric {Mg(μ-BH_4)Mg} structure, or the presence of more than one coordination mode present in the solid state.[68] To observe whether the hapticity of the borohydride group is identical in the solid state and in the presence of a donor solvent, solution IR spectroscopy can be conducted using THF as a solvent. Following coordination of a THF molecule once the complex is dissolved in THF, **7** can be assigned as tridentate by the presence of a strong B–H_t stretching absorption at 2407 cm^{-1} and a B–H_b–Mg stretching absorption with 58 cm^{-1} splitting at 2184 and 2126 cm^{-1} (Figure 2.9). Furthermore, the lack of a doublet between 2600-2400 cm^{-1} with 50-80 cm^{-1} splitting confirms the absence of a bidentate coordination mode.

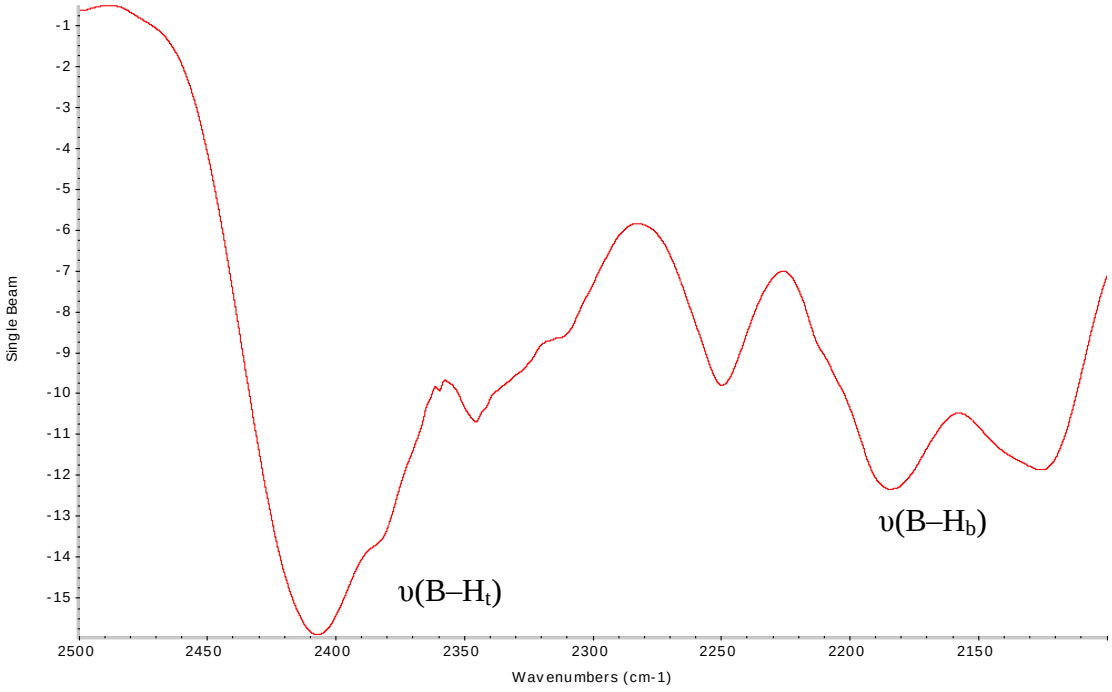


Figure 2.9. THF solution IR spectrum of Mg($CzOx^{Me2}$)(BH_4) (**7**) (background has been subtracted).

A series of CpLn(BH_4) (Ln = Er, Yb) were prepared by Marks and Grynkewich whose IR spectra revealed only a single sharp peak at 2280 cm^{-1}.[105] This was attributed to the adoption of a polymeric structure, instead of an ionic conformation, in which the borohydride ligands bridged the metal centres. To observe whether **7** was dimeric when dissolved in a non-donor solvent, the complex was dissolved in benzene and an IR spectrum was taken of the resultant solution. Gratifyingly, a similar spectrum to that of the THF solution was obtained, showing a B–H_t stretch at 2412

cm^{-1} and a $B–H_b$ doublet with 58 cm^{-1} splitting at 2163 and 2105 cm^{-1}. Therefore it can be concluded that **7** does not adopt a dimeric configuration in either benzene or THF solution. It is postulated that in the solid state **7** may adopt a polymeric structure, or multiple bonding modes may be present, resulting in an ambiguous IR spectrum, but it is not possible at this stage to be certain of its structure in the solid state.

Diffraction-quality crystals were grown from slow diffusion of pentane into a dilute THF solution and structurally authenticated as the THF-adduct $Mg(CzOx^{Me2})(BH_4)(THF)$ (**7-THF**) (Figure 2.10). The lack of THF in the final product may be explained by the extended exposure to reduced pressures causing the ligated THF to be removed, following extraction into a non-donor solvent and removal of solvent *in vacuo*.

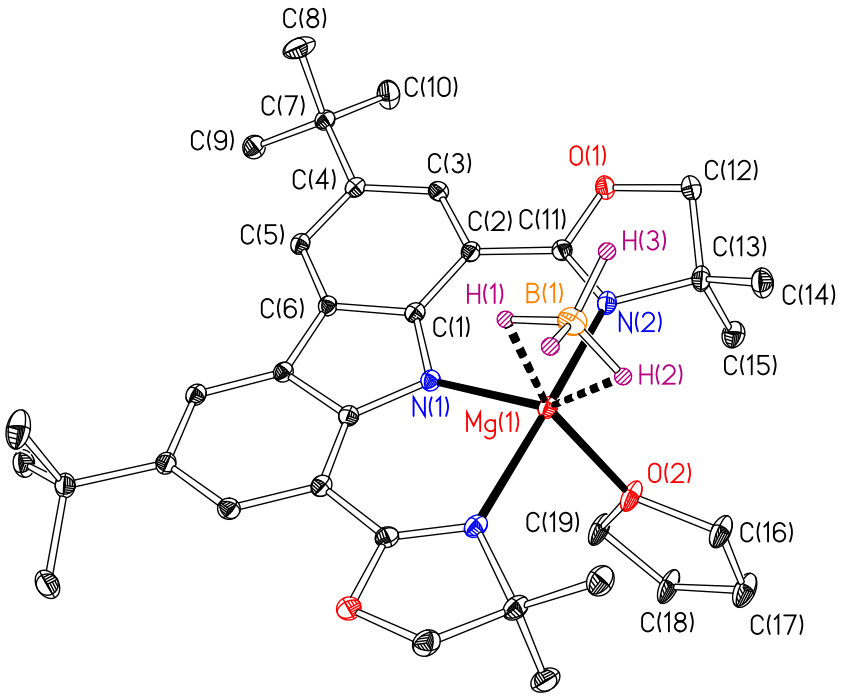


Figure 2.10. Displacement ellipsoid plot of $Mg(CzOx^{Me2})(BH_4)(THF)$ (**7-THF**) (20% probability level). C-bound H atoms and minor disorder omitted. Atoms are related to their counterparts by the symmetry operator (x, -y+3/2, z).

Table 2.4. Selected bond distances (Å) and angles (°) for Mg(CzOx^{Me_2})(BH_4)(THF) (**7-THF**).

Mg(1)-N(1)	2.043(3)	Mg(1)-H(2)	1.94(4)
Mg(1)-N(2)	2.2526(19)	B(1)-H(1)	1.18(4)
Mg(1)-O(2)	2.083(2)	B(1)-H(2)	1.18(4)
Mg(1)···B(1)	2.445(4)	B(1)-H(3)	1.10(3)
Mg(1)-H(1)	1.97(4)		
N(1)-Mg(1)-N(2)	87.36(5)	N(2)-Mg(1)-O(2)	88.59(5)
N(2)-Mg(1)···B(1)	93.76(5)	N(2)-Mg(1)-N(2A)	172.08(10)
N(1)-Mg(1)-O(2)	117.32(10)	N(1)-Mg(1)···B(1)	113.62(12)
O(2)-Mg(1)···B(1)	129.05(12)		

THF-adduct Mg(CzOx^{Me_2})(BH_4)(THF) (**7-THF**) is *pseudo*-five coordinate in which the Mg is coordinated to the three N donors of the CzOx^{Me_2} ligand, a κ^2-bound BH_4 ligand and the O donor of a molecule of THF. The geometry of **7-THF** is best described as *pseudo*-trigonal bipraymidal, in which N(1), the BH_4 ligand and the THF molecule occupying distorted equatorial positions, and N(2) and N(3) occupying the axial positions. The N(2)-Mg(1)-N(3) bond angle shows a slight deviation from linearity (172.08°). In contrast to previous complexes in this series, **1** and **3**, the dihedral angle is C(1)-C(2)-C(11)-N(2) is 2.0°, showing little deviation from the planarity of protioligand **1.45**, as a result of the adoption of the *pseudo* trigonal bipraymidal geometry. The Mg(1)-N(1) bond length of 2.043(3) Å is similar to those found in complexes **1** (*ca*. 2.03 Å) and **3** (*ca*. 2.02 Å). Due to the adoption of a distorted trigonal bipyramidal geometry in which the magnesium centre sits in the plane of the ligand, reducing the rotation around the C(2)-C(11) bond, the Mg(1)-N(2) bond is slightly elongated in comparison (2.2526(19) Å) to *ca*. 2.18 Å in complexes **1** and **3**, but all fall within the normal range for Mg-N=C bonds of 1.99-2.27 Å.[93]

Complex **7-THF** possesses a κ^2-bound BH_4 ligand in the solid state as a THF adduct, which represents a shift from the κ^3-bound BH_4 ligand in THF solution, observed in the IR spectrum. The hydrogen atoms of the BH_4 ligand were located in a Fourier difference map and positionally and isotropically refined and the Mg-H distances are within the usual range of 1.90-2.32 Å.[93] The Mg···B distance of 2.445(4) Å is within

the range anticipated for a κ^2-bound BH_4 ligand (2.39-2.57 Å) and is longer than the range of a κ^3-bound BH_4 ligand (2.22-2.34 Å), supporting the adoption of a bidentate coordination mode.[93] There is precedent for the adoption of κ^2-bound BH_4 ligands in magnesium complexes within the literature: *pseudo* four-coordinate $Mg(BH_4)_2(NH_3)_2$ contains one κ^2- and κ^3-bound BH_4 ligand whereas *pseudo* six-coordinate $Mg(BH_4)_2(py)_4$ has two κ^2-bound BH_4 ligands.[106, 107] The characterisation of (^{Dipp}NacNac)Mg(BH_4)(THF) (**2.32**) by THF solution IR spectroscopy also revealed a κ^2-bound BH_4 ligand.[66] Furthermore, complexes (PhO)Mg(BH_4)$(THF)_2$, found to be dimeric, and O(2,6-$C_6H_3{}^tBu_2$)Mg(BH_4)(THF)(DME) possessed bidentate κ^2-bound BH_4 ligands in the solid state. IR characterisation confirmed the bidentate nature of the borohydride group for the diglyme adduct in a Nujol mull; however, the resolution was not sufficiently clear to identify the bonding mode of the dinuclear compound.[108]

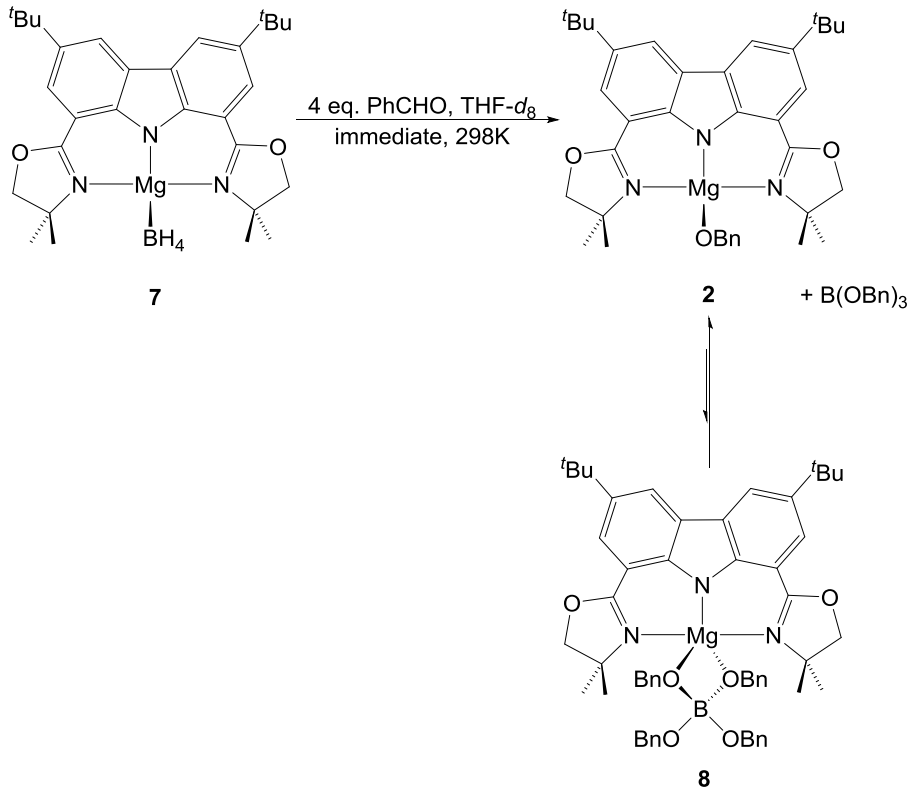
Although the mechanism for the ROP of ε-CL with lanthanide and alkaline earth borohydride complexes is well-established, there remains a degree of uncertainty surrounding the mechanism for the ROP of lactide with these complexes, *vide supra*. In order to gain insight into the polymerisation mechanism, deuterium labelled Mg($CzOx^{Me_2}$)(BD_4) (**7-*d*$_4$**) was synthesised. Complex **7-*d*$_4$** was synthesised *via* the salt metathesis reaction of Mg($CzOx^{Me_2}$)I(THF) (**6**) and 1 equivalent of $NaBD_4$ in THF at room temperature, in an analogous fashion to previous literature reports.[109] The product was isolated as a yellow powder in 62% yield and fully characterised with ^{1}H, ^{2}H, ^{13}C{^{1}H} and ^{11}B NMR spectroscopy, solid state and THF solution IR spectroscopy, and mass spectrometry. The ^{2}H NMR spectrum showed a broad singlet at 0.6 ppm, and the ^{11}B NMR spectrum revealed a singlet at -35.3 ppm; both corresponding to the BD_4 ligand. IR spectroscopic analysis of a THF solution of **7-*d*$_4$** in a THF solution revealed the borohydride group to occupy a κ^3 bonding mode, with expected isotropically shifted stretching frequencies of 1884 cm^{-1} (B–D_t, ν_D/ν_H = 0.79), 1636 and 1597 cm^{-1} (B–D_b, ν_D/ν_H = 0.76): a doublet with 39 cm^{-1} splitting.

2.4 *In situ* generation of trialkyl borate esters as chain transfer agents

Immortal ROP (*i*ROP) offers several advantages over living ROP, outlined in Section 1.9.2. The most common class of molecules used as chain transfer agents (CTAs) are

protic species such as alcohols. However, the addition of such species can potentially lead to the decomposition of the catalyst, for instance protonolysis of the supporting ligand. An investigation into the stability of several complexes in the presence of an exogenous alcohol, such as benzyl alcohol, was undertaken to probe their resilience to any undesirable side reactions. 1 equivalent of BnOH was added to a C_6D_6 solution of Mg(CzOx^{Me_2}){N(SiMe$_3$)$_2$} (**1**) and Mg(CzOx^{Me_2})(Bu) (**3**) at room temperature, leading to the desired formation of Mg(CzOx^{Me_2})(OBn) (**2**); however, the major product observed was protioligand **1.45**. Whilst it is possible to obtain **2** from protonolysis of **1** with BnOH in high purity without unwanted side products, it requires the use of low temperatures. The addition of alcohols as chain transfer agents for *i*ROP is therefore not appropriate in this instance due to the propensity for these complexes to decompose in the presence of protic species.

In a preliminary experiment, 4.5 equivalents of benzaldehyde were added to a 0.01M solution of **7** in THF-d_8 on an NMR tube scale in order to replicate polymerisation conditions and monitor the reaction over time. Both the ^{1}H and ^{11}B NMR spectra showed there to be an immediate transformation from **7** to Mg(CzOx^{Me_2})(OBn) (**2**) and tribenzyl borate ester, B(OBn)$_3$, which existed in an equilibrium between two discrete species and a tetracoordinated adduct Mg(CzOx^{Me_2}){B(OBn)$_4$} (**8**) (Scheme 2.4). *In situ* generated **8** was analysed by ^{1}H and ^{13}C{^{1}H} NMR spectroscopy; however, the resultant spectra were highly complex due to the number of species in solution. ^{11}B NMR analysis showed both **2** and **8** were present in solution at this concentration with resonances at 3.8 and 18.7 ppm corresponding to Mg(CzOx^{Me_2}){$\underline{B}$(OBn)$_4$} and $\underline{B}$(OBn)$_3$, respectively. The resonance at 3.8 ppm corresponding to the proposed tetracoordinated {B(OBn)$_4$}$^-$ moiety is consistent with a range of other such tetracoordinated borate esters.[67] Gratifyingly, treatment of **7** with 4.5 equivalents of benzaldehyde did not result in the formation of decomposition products, such as the protioligand observed when complexes **1** and **3** were treated with benzyl alcohol. Thus, the addition of an aldehyde to a BH_4-containing complex to generate a complex containing an alkoxide initiator, with the concurrent evolution of a trialkyl borate ester is an elegant method through which CTAs can be introduced to a polymerisation whilst circumventing possible catalyst decomposition.



Scheme 2.4. Transformation of **7** to **2**, $B(OBn)_3$ and **8** through the addition of 4.5 equivalents of benzaldehyde.

The solution containing **2** and **8** was found to be stable at room temperature in a THF-d_8 solution for several days with no apparent decomposition to the protioligand or redistribution to the homoleptic species $Mg(CzOx^{Me_2})_2$. A similar reaction was conducted in C_6D_6, immediately resulting in a similar ^{11}B NMR spectrum, showing there to be no significant solvent dependence for this reaction; however, the position of the equilibrium was found to be concentration and temperature dependent. In a 0.01M THF-d_8 solution, the equilibrium favours the formation of **2** and $B(OBn)_3$; however, as expected, an increase in concentration led to a shift in the equilibrium such that a greater amount of **8** was produced. 1 equivalent of $B(OBn)_3$ was added to a solution of **2** in THF-d_8 order to independently verify the reaction between 4.5 equivalents of benzaldehyde and **7**. The addition of 1 equivalent of $B(OBn)_3$ to externally synthesised **2** results in almost identical ^1H and ^{11}B NMR spectra to that for *in situ* generated **2** and **8**, with the ^{11}B NMR spectrum showing resonances at 3.7 and 18.8 ppm. As an alternative synthetic route to $Mg(CzOx^{Me_2})(OBn)$ (**2**), **7** was treated with 4.5 equivalents of benzaldehyde in THF at room temperature followed by

removal of the volatiles under reduced pressure in an attempt to isolate **2** from $B(OBn)_3$. However, attempts to completely remove the $B(OBn)_3$ under reduced pressure and *via* sublimation failed, preventing the isolation of **2** *via* this route.

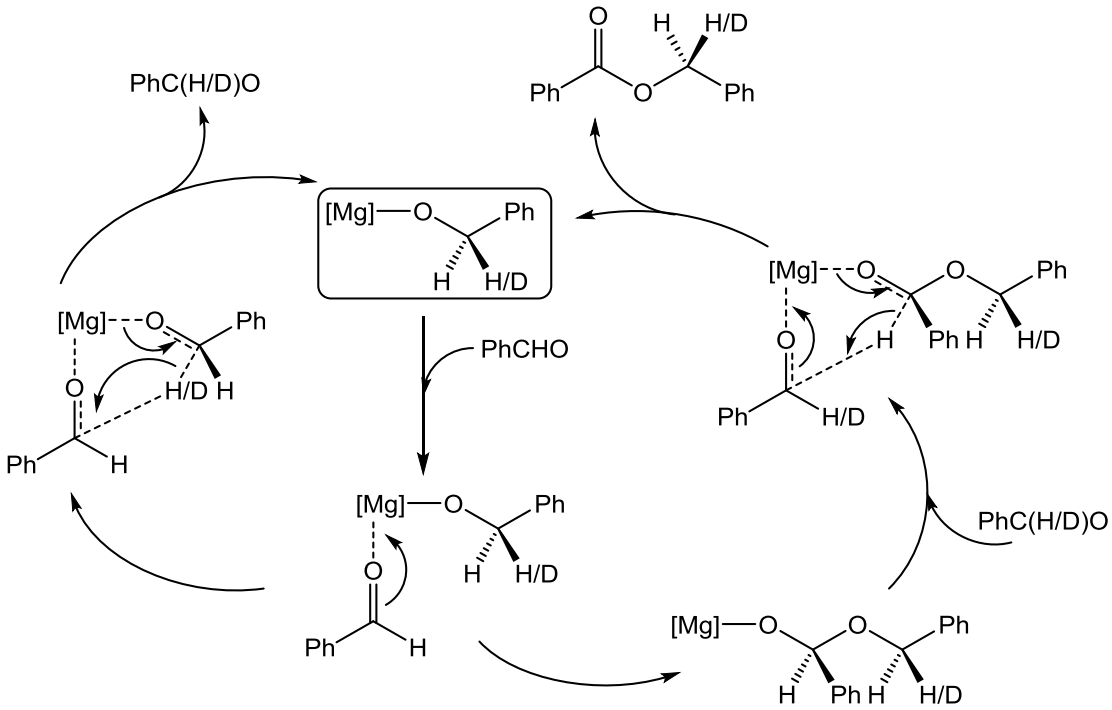
An excess of 0.5 equivalents of benzaldehyde was employed to ensure full consumption of **7**; however, the effect of a slight excess of benzaldehyde in the presence of *in situ* generated **2** and **8** required investigation, as alkaline earth amide and aryloxide complexes have been employed as competent catalysts for the Tishcenko reaction: a disproportionation reaction in which two molecules of an aldehyde dimerise to form the corresponding ester. In 2001, Roesky *et al.* successfully employed homoleptic lanthanide amide complexes of the type $Ln\{N(SiMe_3)_2\}_3$ (Ln = Y, La or Sm) to promote the Tishchenko reaction of benzaldehyde to generate benzyl benzoate.[110] Following this result, Procopiou and coworkers demonstrated the capability of similar heavier alkaline earth homoleptic complexes ($M\{N(SiMe_3)_2\}_2(THF)_2$; M = Ca, Sr or Ba) to generate benzyl benzoate from benzaldehyde with a 1 mol % catalyst loading.[111] Furthermore, in 2012 Coles *et al*. showed that guanidinate-supported magnesium aryloxide and amide complexes were able to promote the Tishchenko reaction of benzaldehyde.[112]

2, $B(OBn)_3$ and **8** were generated *in situ* following the addition of 4 equivalents of benzaldehyde to **7** in C_6D_6. A further 6 equivalents of benzaldehyde were added to the solution; the mixture was monitored by ^{1}H NMR spectroscopy and found to be active for the Tishchenko reaction, resulting in 100% conversion of benzaldehyde to benzyl benzoate after 3 days. As a comparison, 2 equivalents of benzaldehyde were added to a C_6D_6 solution of **1** which showed 58% conversion to benzyl benzoate after 1 week with no signs of catalyst decomposition. Since it is clear that the Tishchenko reaction is comparatively slow to the ROP process, *vide infra*, this side reaction could be considered non-competitive having no impact on polymerisation.

The *in situ* conversion of $Mg(CzOx^{Me2})(BH_4)$ (**7**) to $Mg(CzOx^{Me2})(OBn)$ (**2**) and $B(OBn)_3$ was replicated with the deuterium analogue $Mg(CzOx^{Me2})(BD_4)$ (**7-*d*$_4$**). Thus 4.5 equivalents of benzaldehyde were added to **7-*d*$_4$** to immediately generate $Mg(CzOx^{Me2})(OCHDPh)$ (**2-*d***) and $B(OCHDPh)_3$ in THF-d_8 at room temperature. The ^{1}H NMR spectrum of **2-*d***, $B(OCHDPh)_3$ and **8-*d*$_4$** is identical to the protio-analogues; however, integration of the total resonances corresponding to –OCHDPh is

half that of the protio- compounds, *i.e*. 4H instead of 8H. Unsurprisingly, the ^{11}B NMR spectrum was identical to that obtained from reaction of **7** with 4.5 equivalents of benzaldehyde, with resonances at 3.8 and 18.7 ppm corresponding to Mg(CzOx^{Me2}){B(OCHDPh)$_4$} (**8-*d*$_4$**) and B(OCHDPh)$_3$, respectively. Of particular interest was the ^{2}H NMR spectrum: as anticipated, a broad singlet at 4.6 ppm and a sharp singlet at 5.0 ppm were observed, corresponding to the 3 possible -OCHDPh in environments in **2-*d*** and **8-*d*$_4$**, and free B(OCHDPh)$_3$, respectively. However, a resonance at 10.0 ppm was also observed, indicative of the presence of PhCDO.

A ^{1}H NMR experiment was therefore conducted in which 4 equivalents of benzaldehyde were added to **7-*d*$_4$** in THF-d_8 to generate quantitatively **2-*d***, B(OCHDPh)$_3$, and **8-*d*$_4$**, followed by a further 5 equivalents of benzaldehyde. Since the Tishchenko reaction is slow, the reaction was followed by ^{1}H NMR spectroscopy at regular intervals to observe the consumption of benzaldehyde to form PhCDO by monitoring the decrease in intensity of the resonance at 9.98 ppm corresponding to PhCHO, relative to those at 7.87, 7.62 and 7.53 ppm, corresponding to the protons on the phenyl ring. The possibility that the exchange of benzaldehyde to PhCDO could occur because of direct reaction with the BD$_4$ group was considered: if exchange occurred in this manner, some Mg(CzOx^{Me2})(BH$_x$D$_{4-x}$) would be produced, alongside generation of PhCDO; however, **7-*d*$_4$** was completely consumed prior to the appearance of PhCDO. Subsequently, it was considered that the signal at 9.98 ppm was decreasing in intensity due to formation of the Tishchenko product, benzyl benzoate. However, integration of the benzaldehyde environment relative to the proton environments on the phenyl ring of benzaldehyde showed a decrease in relative intensity over time from 87% after 7.5 min to 74% after 12 h. A signal at 5.34 ppm in the ^{1}H NMR spectrum corresponding to the Tishchenko product benzyl benzoate-*d* (PhCO$_2$CHDPh) was present after 12 h. Similarly, analysis of the ^{2}H NMR spectrum in THF after 12 h revealed resonances at 10.0 and 5.3 ppm, confirming the presence of PhCDO and PhCO$_2$CHDPh. Considering these observations, a proposed mechanism for this exchange process is given in Scheme 2.5.



Scheme 2.5. Proposed mechanism for the scrambling of PhCHO to PhCDO and Tishchenko reaction.

The incoming aldehyde undergoes β-hydride or β-deuteride abstraction from the proximal alkoxide ligand, eliminating a new aldehyde molecule and generating a metal-alkoxide complex. The β-hydride elimination of but-1-ene from the reaction of selected aldehydes and ketones, such as benzaldehyde, with the complex ^{Dipp}NacNacMgBu has been previously documented by Chisholm *et al.*[98] It is postulated that the β-hydride transfer occurs *via* a 6-membered transition state in a chair conformation (Figure 2.12).

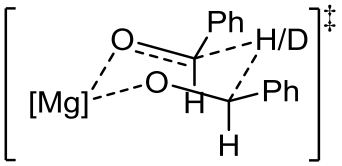


Figure 2.12. 6-membered transition state formed during β-hydride transfer.[98]

2.5 Polymerisation studies: ROP of *L*- and *rac*-LA

A primary aim of this work is to evaluate the potential of the complexes Mg(CzOx^{Me2}){N(SiMe$_3$)$_2$} (**1**), Mg(CzOx^{Me2})(OBn) (**2**), Mg(CzOx^{Me2})(Bu) (**3**), Zn(CzOx^{Me2})(Et) (**4**) and Mg(CzOx^{Me2})(BH$_4$) (**7**) as catalysts for the ROP of lactide.

They were tested initially in the absence of any additives. Further to these preliminary results, additional studies were undertaken in which trialkyl borate esters of the type $B(OR)_3$ were used alongside several precatalysts either externally added or generated *in situ* in order to facilitate the *i*ROP of LA. The *in situ* generated Mg(CzOx^{Me2})(OBn) (**2**) and $B(OBn)_3$ were synthesised by addition of 4.5 equivalents of benzaldehyde to a THF solution of Mg(CzOx^{Me2})(BH_4) (**7**) and stirred for 5 min prior to addition of LA to ensure complete conversion from a borohydride to alkoxide initiator. Polymerisation experiments were conducted in THF at room temperature, and under these conditions all complexes were found to be active. The polymerisation was followed by collection of aliquots at regular time intervals, and the polymer samples were characterised by ^{1}H NMR spectroscopy, Gel Permeation Chromatography and MALDI-ToF mass spectrometry. Following a preliminary investigation into the activity of Mg(CzOx^{Me2})(OBn) (**2**) with *L*-LA, further studies into the activity of catalysts **1**-**4**, **7** and **7**-$\boldsymbol{d_4}$ with *rac*-LA were undertaken. The results are summarised in Tables 2.5-2.7.

Table 2.5. Selected data for the polymerisation of *L*-LA using Mg(CzOx^{Me2})(OBn) (**2**) in THF.[a]

Entry	Monomer	Additive (eq.)	Conv.[b] %	Time (min)	M_n(obs)[c] (g mol^{-1})	M_n(calc)[d] (g mol^{-1})	M_w/M_n[c]
1	*L*	-	95	60	14,080	13,798	1.20
2	*L*	$B(OBn)_3$ (1)	94	60	5,190	3,494	1.13

[a] Conditions: [*L*-LA]$_0$:[**2**]$_0$ = 100:1, 4 mL THF at 23 °C. [*L*-LA]$_0$ = 1.0 M. [b] Measured by ^{1}H NMR ($CDCl_3$) analyses, to nearest integer. [c] Molecular weights (g mol^{-1}) determined from GPC using appropriate Mark-Houwink corrections. [d] Expected average M_n (g mol^{-1}) for stated number of chains per metal and stated % conversion: M_n (calc for entry 1) = (conversion (%) × 100 × 144.1) + 108.1; (calc for entry 2) = ¼(conversion (%) × 100 × 144.1) + 108.1.

Mg(CzOx^{Me2})(OBn) (**2**) was moderately active for the ROP of *L*-LA (Table 2.5, entry 1): 95% monomer conversion was achieved following 60 min, and kinetic analysis revealed the polymerisation to observe a first-order in [LA], with k_{obs} = 2.91(9) h^{-1}, R^2 = 0.993 (Figure 2.13). First-order dependencies on monomer concentration are commonly encountered in the ROP of both *rac*- and *L*-LA with a variety of different catalytic systems.[25, 113-115]

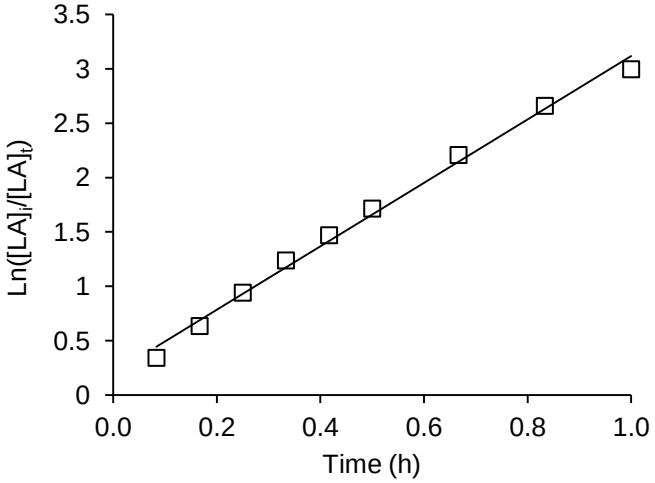


Figure 2.13. Data for the ROP of *L*-LA using Mg(CzOx^{Me2})(OBn) (**2**). Semilogarithmic first-order plot of ln([LA]$_i$/[LA]$_t$) *vs*. time (k_{obs} = 2.92(9) h^{-1}, R^2 = 0.993); vertical-axis intercept = 0.20(5) (expected value = ln([LA]$_i$/[LA]$_0$) = 0). Conditions: 4 mL THF, 23 °C, [*L*-LA]$_0$:[**2**]$_0$ = 100:1, [*L*-LA]$_0$ = 1.0 M.

A high degree of molecular weight control throughout polymerisation was observed: a plot of M_n *vs*. % conversion showed linear growth with a gradient of 123(3) g mol^{-1} (% conversion)$^{-1}$ (R^2 = 0.996), resulting in good agreement between the observed and expected molecular weights, in addition to narrow PDIs of 1.07 at 29% conversion, increasing to 1.20 at 95% conversion. MALDI-ToF MS analysis revealed the resultant polymer chains to have the anticipated -OBn terminus with an absence of transesterification side-reactions.

The addition of 1 equivalent of B(OBn)$_3$ resulted in a similar monomer conversion of 94 % being reached after 60 min (Table 2.5, entry 2); however, the reaction was found to be second-order in [LA] (k_{obs} = 16.0(6) M^{-1} h^{-1}, R^2 = 0.991) (Figure 2.14). Second-order dependencies in [LA] are unusual, but not unprecedented in ROP: previous reports have alluded to either non-innocence of the supporting ligands during propagation, or, in the formation of heterotactic PLA, a cooperative transition state in which two lactide units of opposite chirality come together in the rate-limiting step.[44, 116, 117] In this instance, a marked shift between the order of reaction with respect to lactide occurs on the addition of the borate CTA from first- to second-order. Although the precise role of B(OBn)$_3$ in effecting this alteration is not understood at this stage, it is postulated to be a product of complex associative and dissociative preequilibria prior to and following the lactide ring-opening event, resulting in an apparent second-

order dependency. Consideration of the resultant molecular weights confirmed the occurrence of chain transfer mediated by $B(OBn)_3$. However, the molecular weights were slightly higher than expected, which is interpreted as being caused by inefficient chain transfer caused by higher k_p *vs.* k_{CT}. Again, this reaction was marked by an absence of transesterification, apparent in the MALDI-ToF MS.

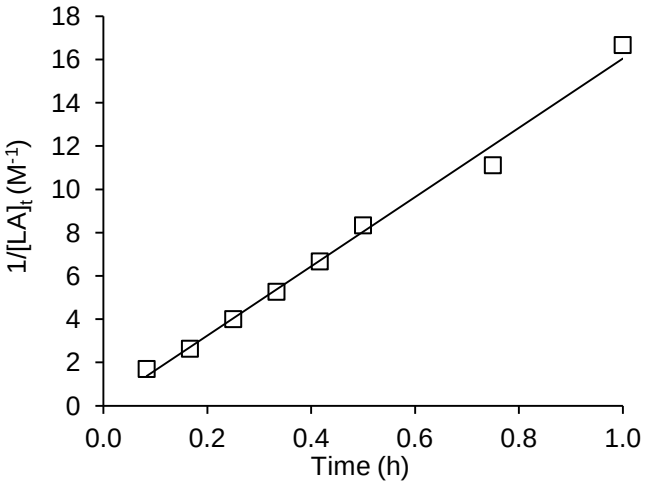


Figure 2.14. Data for the ROP of *L*-LA using Mg(CzOx^{Me_2})(OBn) (**2**). Second-order plot of $1/[LA]_t$ *vs.* time (k_{obs} = 16.4(6) M^{-1} h^{-1}, R^2 = 0.992); vertical-axis intercept = 0.0(3) M^{-1} (expected value = $1/[L\text{-LA}]_0$ = 1 M^{-1}). Conditions: 4 mL THF, 23 °C, $[L\text{-LA}]_0$:$[\mathbf{2}]_0$ = 100:1, $[L\text{-LA}]_0$ = 1.0 M.

The findings of the ROP of *rac*-LA with complexes **1**-**4**, **7** and **7**-$\boldsymbol{d_4}$ in the presence of various additives are summarised in Table 2.6. Mg(CzOx^{Me_2}){N(SiMe$_3$)$_2$} (**1**) was found to be very active for the ROP of 100 equivalents of *rac*-LA in THF at room temperature (Table 2.6, entry 1). Complex **1** reached 93% monomer conversion after 60 min with $[rac\text{-LA}]_0$:$[\mathbf{1}]_0$ = 100:1. After kinetic analysis the reaction was found to be first-order in monomer concentration, with k_{obs} = 3.67(8) h^{-1} (R^2 = 0.997), following an induction period, which may reflect slow initiation compared to propagation (Figure 2.15).

Table 2.6. Selected data for the polymerisation of *rac*-LA using Mg(CzOx^{Me2}){N(SiMe$_3$)$_2$} (**1**), Mg(CzOx^{Me2})(OBn) (**2**), Mg(CzOx^{Me2})(Bu) (**3**), Zn(CzOx^{Me2})(Et) (**4**), Mg(CzOx^{Me2})(BH$_4$) (**7**) and Mg(CzOx^{Me2})(BD$_4$) (**7-d$_4$**) in THF.[a]

Entry	Catalyst	Additive (eq.)	Conv.[b] %	Time (min)	M_n(obs)[c] (g mol^{-1})	M_n(calc)[d] (g mol^{-1})	M_w/M_n[c]	P_r[b]
1	Mg(CzOx^{Me2}){N(SiMe$_3$)$_2$} (**1**)	-	93	60	24,620	13,563	1.45	0.78-0.81
2	Mg(CzOx^{Me2}){N(SiMe$_3$)$_2$} (**1**)	B(OBn)$_3$ (1)	93	50	4,870	3,508	1.57	0.80-0.82
3	Mg(CzOx^{Me2})(OBn) (**2**)	-	93	30	12,330	13,509	1.11	0.77-0.80
4	Mg(CzOx^{Me2})(OBn) (**2**)	B(OBn)$_3$ (1)	92	30	3,660	3,422	1.10	0.76-0.77
5	Mg(CzOx^{Me2})(OBn) (**2**)	B(OBn)$_3$ (3)	93	90	2,150	1,448	1.17	0.69-0.70
6	Mg(CzOx^{Me2})(Bu) (**3**)	-	93	30	12,600	13,459	1.21	0.74-0.75
7	Zn(CzOx^{Me2})(Et) (**4**)	-	90	1,560	163,840	12,999	1.38	0.59-0.61
8	Mg(CzOx^{Me2})(BH$_4$) (**7**)	-	88	120	12,510	12,685	1.14	0.82-0.84
9	Mg(CzOx^{Me2})(BD$_4$) (**7-*d*$_4$**)[e]	-	88	2,880	5,580	12,687	1.30	0.72-0.79
10	Mg(CzOx^{Me2})(BH$_4$) (**7**)	B(OMe)$_3$ (1)	92	180	3,300	3,339	1.13	0.79-0.82
11	Mg(CzOx^{Me2})(BH$_4$) (**7**)	B(OBn)$_3$ (1)	92	240	3,480	3,396	1.18	0.73-0.76
12	Mg(CzOx^{Me2})(BH$_4$) (**7**)	PhCHO (4.5)	90	30	5,340	3,350	1.09	0.77-0.79

[a] Conditions: [*rac*-LA]$_0$:[initiator]$_0$ = 100:1, 4 mL THF at 23 °C. [*rac*-LA]$_0$ = 1.0 M. [b] Measured by ^{1}H NMR (CDCl$_3$) analyses. [c] Molecular weights (g mol^{-1}) determined from GPC using appropriate Mark-Houwink corrections. [d] Expected average M_n (g mol^{-1}) for stated number of chains per metal and stated % conversion: M_n (calc for entry 1) = (conversion (%) × 100 × 144.1) + 161.4; (calc for entry 2) = ¼((conversion (%) × 100 × 144.1)/4 + 161.4) + ¾((conversion (%) × 100 × 144.1)/4 + 108.1); (calc for entry 3) = (conversion (%) × 100 × 144.1) + 108.1; (calc for entries 4 and 12) = ¼ (conversion (%) × 100 × 144.1) + 108.1; (calc for entry 5) = 1/10 (conversion (%) × 100 × 144.1) + 108.1; (calc for entry 6) = (conversion (%) × 100 × 144.1) + 58.1; (calc for entry 7) = (conversion (%) × 100 × 144.1) + 30.1; (calc for entry 8) = (conversion (%) × 100 × 144.1) + 4.0; (calc for entry 9) = (conversion (%) × 100 × 144.1) + 6,0; (calc for entry 10) = ¼((conversion (%) × 100 × 144.1)/4 + 4.0) + ¾((conversion (%) × 100 × 144.1)/4 + 32.0); (calc for entry 11) = ¼((conversion (%) × 100 × 144.1)/4 + 4.0) + ¾((conversion (%) × 100 × 144.1)/4 + 108.1);. [e] Conditions: [*rac*-LA]$_0$:[initiator]$_0$ = 100:1, 4 mL THF at 60 °C. [*rac*-LA]$_0$ = 1.0 M.

As discussed in Chapter 1, the molecular weight control typically offered with amide initiators is poor, due to this higher rate of propagation *vs*. initiation. In this instance, the molecular weight did not grow linearly with % conversion: after 60 min the observed molecular weight was 24,620 g mol^{-1} as opposed to the expected value of 13,563 g mol^{-1} with a rather moderate PDI of 1.45.

Analysis with MALDI-ToF MS confirmed the dominance of macrocyclic polymer structures; polymers containing the -N(SiMe$_3$)$_2$ end-group were not observed. Peak envelopes of Δ*m/z* 72 g mol^{-1} further confirmed the prevalence transesterification during the reaction.

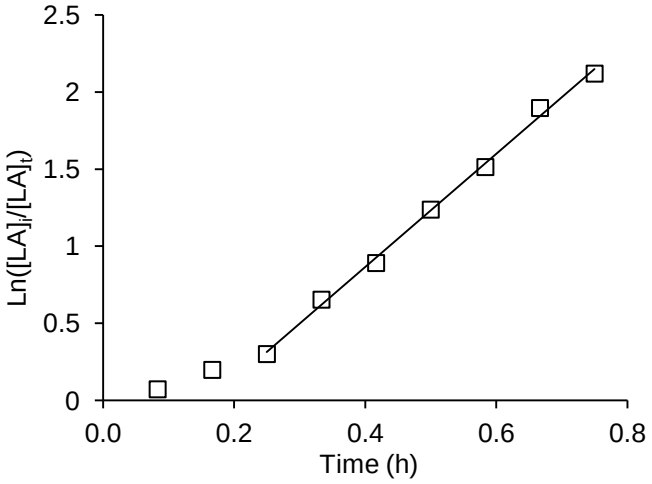


Figure 2.15. Data for the ROP of *rac*-LA using Mg(CzOx^{Me2}){N(SiMe$_3$)$_2$} (**1**). Semilogarithmic first-order plot of ln([LA]$_i$/[LA]$_t$) *vs*. time (k_{obs} = 3.67(8) h^{-1}, R^2 = 0.997). Conditions: 4 mL THF, 23 °C, [*rac*-LA]$_0$:[**1**]$_0$ = 100:1, [*rac*-LA]$_0$ = 1.0 M.

As trialkyl borate esters have been shown to be effective chain transfer agents in the ROP of lactide, 1 equivalent of B(OBn)$_3$ was added to a THF solution of **1** prior to polymerisation, to observe if the reaction became more controlled during *i*ROP (Table 2.6, entry 2). Analysis of the molecular weight throughout polymerisation confirmed the occurrence of chain transfer, as the observed molecular weights were in moderate agreement with the calculated values, although the growth was again non-linear, reaching a maximum of 5,560 g mol^{-1} at 73% conversion, which decreased towards the end of the reaction, again evidence of transesterification. The observed molecular weights were higher than anticipated: a result of a higher rate of propagation (k_{prop}) versus (k_{CT}), resulting in ineffective chain transfer. MALDI-ToF MS analysis

confirmed the occurrence of chain transfer as the major distribution comprising polymer chains with OBn end-groups was observed in conjunction with a minor distribution of cyclic polymers. In order to verify the nature of the complex following the addition of $B(OBn)_3$ to **1**, 1 equivalent of $B(OBn)_3$ was added to **1** in THF-d_8. The ^1H and ^{11}B NMR spectra revealed there to be no reaction between **1** and $B(OBn)_3$, indicating that the borate ester acts solely as a chain transfer agent, and does not undergo an exchange reaction to produce $Mg(CzOx^{Me_2})(OBn)$ (**2**) and $B(OBn)_2\{N(SiMe_3)_2\}$ prior to the addition of *rac*-LA. In order to determine the order in lactide concentration, plots of $\ln[LA]_t/[LA]_i$ *vs*. time and $1/[LA]_i$ *vs*. time were constructed; however, the reaction did not clearly show either a first- or second-order dependency on monomer concentration, rather appearing to observe an intermediary non-integer order between 1 and 2. For instance, the apparent first-order rate constant was determined to be with k_{obs} = 18.5(9) h^{-1} (R^2 = 0.985), whereas the second-order rate constant was with k_{obs} = 2.9(2) M^{-1} h^{-1} (R^2 = 0.961). Although the polymerisation of 100 equivalents of *L*-LA with $Mg(CzOx^{Me_2})(OBn)$ (**2**) showed a clear shift from a first- to second-order dependency on lactide concentration following the addition of $B(OBn)_3$, in this instance the change is not as delineated. This may be attributed to the complex preequilibra surrounding the association and dissociation of the trialkkyl borate ester surrounding the ring-opening event to result in a non-integer apparent kinetic regime.

$Mg(CzOx^{Me_2})(Bu)$ (**3**) was found to be very active when treated with 100 equivalents of *rac*-LA, achieving 93% conversion after 30 min (Table 2.6, entry 6). A kinetic analysis was undertaken and the ROP found to be first-order in lactide concentration (k_{obs} = 7.5(4) h^{-1}, R^2 = 0.985). Gratifyingly, **3** exerted excellent control over molecular weight which grew linearly with % conversion and was in close agreement with the theoretically calculated values (Figure 2.16).

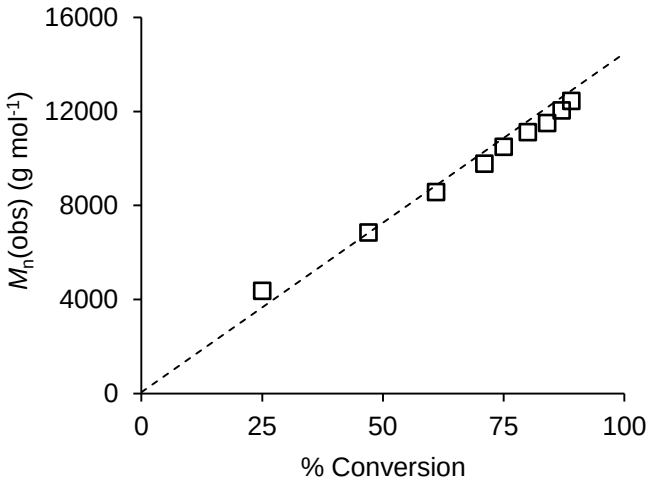


Figure 2.16. M_n(obs) *vs.* % conversion plot for ROP of *rac*-LA using Mg(CzOx^{Me2})(Bu) (**3**). The dashed line represents M_n calculated for one chain PLA per metal centre. Conditions: 4 mL THF, 23 °C, [*rac*-LA]$_0$:[**3**]$_0$ = 100:1, [*rac*-LA]$_0$ = 1.0 M. PDI = 1.16-1.27.

Structural analysis of polymer samples with MALDI-ToF MS revealed the non-hydroxy end-group to be the Bu initiating group, with peak envelopes of Δ*m/z* 144 g mol^{-1}, indicating an absence of transesterification reactions, further confirming the initiating efficiency of **3**. In some instances the efficacy of metal alkyl initiators is comparable to that of the corresponding metal amide initiators;[118] however, reports have emerged demonstrating their capacity to act as well-controlled catalysts exerting excellent molecular weight control.[32, 35, 119-123] Both **1** and **3** showed a preference for the formation of heterotactically-enriched PLA, producing comparable heterotacticities of P_r = 0.78-0.82 for **1** and P_r = 0.74-0.75 for **3**.

As several reports have indicated the superiority of zinc catalysts using identical ancillary ligands to their magnesium analogues to furnish heterotactically enriched PLA, albeit with lower activities,[25, 33] the ROP capability of Zn(CzOx^{Me2})(Et) (**4**) was probed. As expected, **4** was considerably slower than **3**, due to the decreased polarity in the zinc-ethyl bond compared to the magnesium-butyl bond in addition to magnesium's higher oxophilicty,[34] reaching 90% conversion after 26 h (Table 2.6, entry 7). Surprisingly, the molecular weight control was extremely poor (at 90% conversion, M_n(obs) = 163,840 g mol^{-1} *cf.* M_n(calc) = 12,999 g mol^{-1}; PDI = 1.38); furthermore, the moderate heteroselectivity previously observed with **3** was markedly decreased (P_r = 0.59-0.61). Of particular interest was the analysis with MALDI-ToF

MS which showed that the initiating group for the polymerisation was in fact not the Et group as expected, but the $CzOx^{Me2}$ ligand, which imparted a yellow colour to the polymer samples. Due to the extremely poor performance of $Zn(CzOx^{Me2})(Et)$ (**4**), no further investigations using this catalyst or any derivatives thereof were pursued.

$Mg(CzOx^{Me2})(OBn)$ (**2**) was treated with 100 equivalents of *rac*-LA with a varying number of equivalents of the chain transfer agent $B(OBn)_3$ (Table 2.6, entries 3-5). In the absence of a chain transfer agent, **2** was found to be similarly active as the previously studied magnesium initiators, especially **3**, and converted 100 equivalents of *rac*-LA to 93% conversion after 30 min. As observed with **3**, complex **2** offered excellent molecular weight control with concurrent narrow PDIs of 1.06-1.11; the gradient of a linear plot of M_n(obs) (g mol^{-1}) *cf.* % conversion was 136(3) g mol^{-1} (% conversion)$^{-1}$ (R^2 = 0.996), in very close agreement with the expected value of 144.1 g mol^{-1} (Figure 2.17). Kinetic analysis revealed the reaction to be first-order in [LA] consumption with k_{obs} = 6.8(1) h^{-1}, R^2 = 0.991. Notably, the polymerisation of 100 equivalents of *L*-LA in THF with **2** (Table 2.5, entry 1) was slower when compared to the equivalent polymerisation with *rac*-LA (Table 2.6, entry 3). This comparative rate decrease can be attributed to the preference for the catalyst to form *racemic* dyads (*RS* or *SR*) as opposed to *meso* dyads (*RR* or *SS*) (i.e. $k_{R/SS} > k_{R/RR}$) during monomer insertion and enchainment, resulting in heterotactically enriched PLA when using *rac*-LA as a feedstock. Employing *L*-LA as a feedstock forces the catalyst to enchain monomers *via* unfavourable *meso* dyads to afford in isotactic PLLA, resulting in a slower observed rate of polymerisation.

1 equivalent of $B(OBn)_3$ was added to a THF solution of **2** prior to polymerisation, with no appreciable decrease in activity observed, reaching 92% conversion after 30 min. Chain transfer was found to be highly efficient: the gradient of a linear plot of M_n(obs) (g mol^{-1}) *vs.* % conversion was 38.0(5) g mol^{-1} (% conversion)$^{-1}$ (R^2 = 0.999), in good agreement with an anticipated growth of 4 chains of PLA per metal centre (Figure 2.17). This is indicative of a higher k_{CT} relative to k_{prop}, such that chain transfer between active and dormant chains takes place sufficiently rapidly so as not to impact on molecular weight. Again, narrow polydispersities of 1.10-1.14 were observed. Kinetic analysis revealed the reaction to follow neither a first- nor second-order dependence on lactide concentration, instead following an apparently non-

integer order between 1 and 2, in a comparable fashion to the ROP of *rac*-LA with **1** in the presence of 1 equivalent of $B(OBn)_3$. This is similarly attributed to complex preequilibria surrounding lactide insertion giving rise to an intermediate kinetic regime.

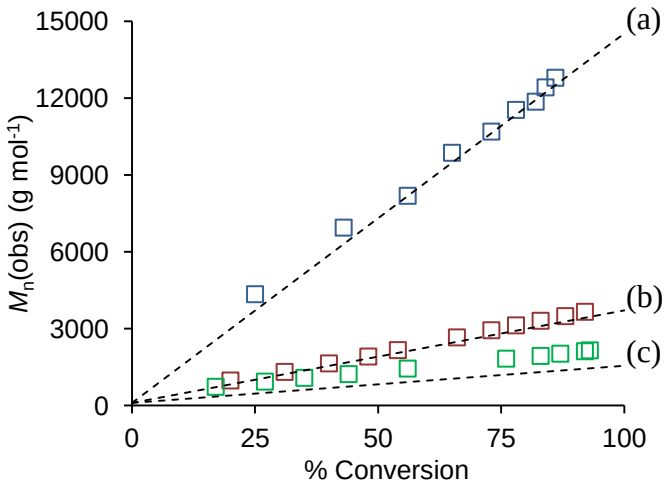


Figure 2.17. M_n(obs) (g mol^{-1}) *vs*. % conversion plot for the ROP of *rac*-LA using $Mg(CzOx^{Me_2})(OBn)$ (**2**); the dashed lines are the M_n(calc) in each case. Conditions: 4 mL THF, 23 °C, $[rac\text{-LA}]_0$:$[\mathbf{2}]_0$ = 100:1, $[rac\text{-LA}]_0$ = 1.0 M: (a) with no $B(OBn)_3$, expecting 1 chain PLA per metal centre (blue squares); (b) with 1 eq. $B(OBn)_3$, expecting 4 chains PLA per metal centre (red squares); (c) with 3 eq. $B(OBn)_3$, expecting 10 chains PLA per metal centre (green squares).

Addition of 3 equivalents of $B(OBn)_3$ to THF solution of **2** prior to polymerisation appears to have a greater impact on the subsequent polymerisation. The rate of polymerisation was substantially slower: 93% conversion was attained after 90 min when treated with 100 eq. *rac*-LA. As demonstrated in the NMR studies in which $Mg(CzOx^{Me_2})(OBn)$ (**2**) and $B(OBn)_3$ are generated *in situ* from $Mg(CzOx^{Me_2})BH_4$ (**7**) and 4.5 equivalents of benzaldehyde, the alkoxide complex and trialkyl borate ester can exist in equilibrium between the two discrete species and as a single tetracoordinated borate adduct. It is anticipated that during polymerisation, a similar equilibrium between the catalyst and borate chain transfer agent may occur. If this adduct is not the active species during polymerisation, the addition of further equivalents of $B(OBn)_3$ would drive the equilibrium to generate more inactive adduct, reducing the concentration of active species in solution and decreasing the rate of polymerisation, as observed. Unlike polymerisation in the absence of $B(OBn)_3$, the

reaction was determined to be second-order with respect to the concentration of lactide, (k_{obs} = 9.2(3) M^{-1} h^{-1}, R^2 = 0.991). The addition of further equivalents of the borate ester results in a clear second-order dependence in [LA], which further suggests that the trialkyl borate ester species impacts upon the overall kinetic regime, although its exact role remains unknown. The catalyst continued to exert good molecular weight control over the polymer produced, although the control was slightly less effective with increasing equivalents of $B(OBn)_3$. Narrow PDIs of 1.02-1.17 were observed.

In all cases, the expected polymer end-group (OBn) was observed in the MALDI-ToF MS analysis, along with two molecular weight distributions, confirming the occurrence of intramolecular and intermolecular transesterification (Figure 2.18; top). The $PhCH_2O$- and HOC(H)Me termini were clearly observed in the ^1H NMR spectrum in $CDCl_3$ of a polymer sample following quenching with wet THF (M_n(obs) = 2,150 g mol^{-1}) (Figure 2.18; bottom). The internal PLA resonances were visible as overlapping methyl doublets at ca. 1.5 ppm and overlapping methine quartets at ca. 5.2 ppm. Moreover, the terminating HOC(H)Me proton was visible at 4.35 ppm, and the $PhCH_2O$- phenyl proton resonances as a multiplet at 7.38-7.29 ppm. The HOC(H)Me proton was visible as a broad multiplet at 2.80-2.70 ppm. Unfortunately, the $PhCH_2O$- protons were obscured by the internal methine resonances of the PLA chain. Although all runs showed a preference for the formation of heterotactically-enriched PLA (P_r = 0.69-0.80), the degree of enrichment decreased slightly with increased number of equivalents of $B(OBn)_3$ added.

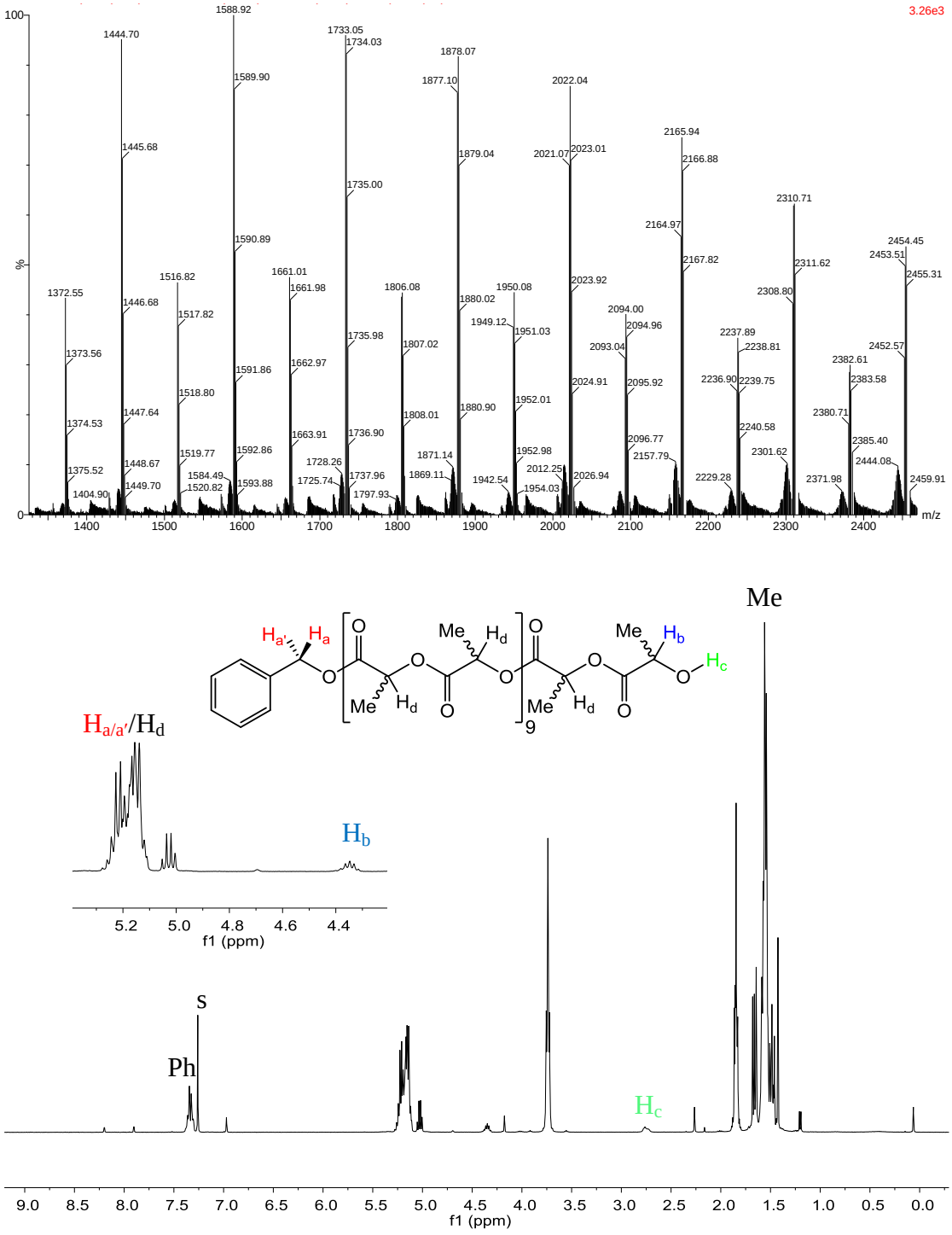


Figure 2.18. Top: MALDI-ToF MS of PLA synthesised from Mg(CzOx^{Me2})(OBn) (**2**) and 3 eq. B(OBn)$_3$. M_n by GPC analysis was 2,030 g mol^{-1}. Bottom: ^{1}H NMR ($CDCl_3$, 400.1 MHz, 298 K) spectrum of PLA synthesised from Mg(CzOx^{Me2})(OBn) (**2**) and 3 eq. B(OBn)$_3$. "s" denotes residual solvent signals. M_n by GPC analysis was 2,150 g mol^{-1}.

Following the pioneering work in the Mountford group using alkaline earth borohydride complexes for initiators for ROP,[58, 66] catalyst Mg(CzOx^{Me2})(BH$_4$) (**7**) was screened with 100 equivalents of *rac*-LA (Table 2.6, entry 8). The complex was found to be moderately active, with a lower activity than other magnesium catalysts in this series: 88% monomer conversion was achieved after 120 min and the polymerisation was found to be second-order in lactide concentration with k_{obs} = 3.91(8) M^{-1} h^{-1}, R^2 = 0.997. **7** showed a high degree of molecular weight control (M_n(obs) = 12,510 g mol^{-1} *vs*. M_n(calc) = 12,685 g mol^{-1}; PDI = 1.14) (Figure 2.19) and afforded PLA with the highest degree of heterotactic enrichment observed thus far with catalysts in this series, P_r = 0.82-0.84.

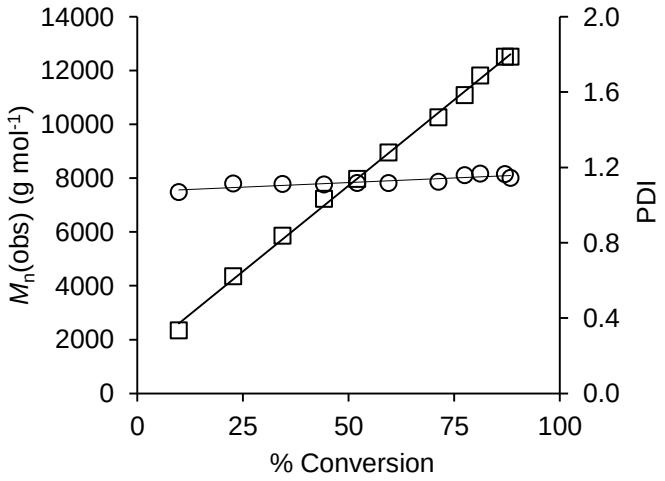


Figure 2.19. M_n(obs) (g mol)$^{-1}$ *vs*. % conversion plot (squares) and PDI *vs*. % conversion plot (circles) for the ROP of *rac*-LA using Mg(CzOx^{Me2})(BH$_4$) (**7**).

Crucially, analysis with MALDI-ToF MS showed two peaks for PLA chains comprising 10 LA units: a peak at 1483 g mol^{-1} corresponding to [H-[LA]$_9$-OC(H)MeCO$_2$C(H)CH$_2$OH + K]$^+$ in addition to a peak at 1481 g mol^{-1}, which has previously been attributed to an aldehyde terminated polymer chain (i.e. [H-[LA]$_9$-OC(H)MeCO$_2$C(H)C(H)O + K]$^+$).[45, 66] However, Trifonov *et al*. were unable to determine the precise nature of the end-group for these polymer chains by ^{1}H NMR,[47] and studies undertaken within the Mountford group have demonstrated the possibility for the polymer chain to be terminated with a ring-closed lactide unit, herein denoted as LA-H.[67] In order to definitively assign the end-groups, **7** was treated with 15 equivalents of *rac*-LA in 4 mL THF at room temperature to isolate and characterise the resultant PLA. The catalyst achieved 82% conversion after 4 days at room

temperature (M_n(obs) = 2,830 g mol^{-1}, PDI = 1.34). Subsequently, the polymerisation was quenched with dry HCl in diethyl ether, the resultant product extracted into CH_2Cl_2 and the volatiles removed *in vacuo* to isolate the PLA. The polymer was characterised by ^{1}H and ^{13}C{^{1}H} NMR in $CDCl_3$ and THF-d_8, GPC and MALDI-ToF MS. Analysis with MALDI-ToF MS showed peaks at 1481 and 1483 g mol^{-1} corresponding to either an apparent aldehyde polymer end-group (1481 g mol^{-1}) or an alcohol end-group (1483 g mol^{-1}) (Figure 2.20).

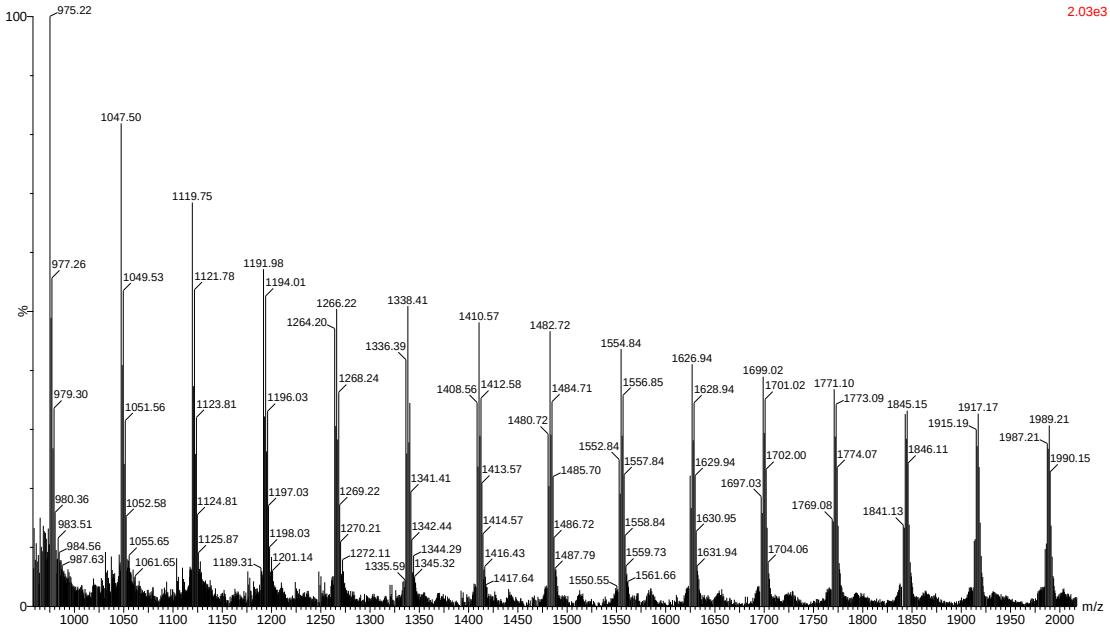


Figure 2.20. MALDI-ToF MS of PLA synthesised from Mg(CzOx^{Me_2})(BH$_4$) (**7**). M_n by GPC analysis was 2,460 g mol^{-1}.

Complete analysis of the ^{1}H NMR spectrum was hampered by broadening in the diagnostic region of 4.0-5.5 ppm. Tentative assignments were based on the characterisation of (Tp^{tBu,Me})Mg(LA-H) by J. Unruangsri.[89] However, several peaks were apparent in the region of 5.45-5.70 ppm, corresponding to LA-H, suggestive of the presence of polymer chains terminated by a ring-closed lactide unit (Figure 2.21). It was not immediately apparent why several peaks were present in this region, as there would be only a total of two diastereotopic forms of LA-H. Whilst the polymer end-groups could not be unambiguously assigned, crucially there appeared no resonance corresponding to an aldehyde terminus at 9.0-12.0 ppm. Further to these preliminary results, a comprehensive study into the precise nature of the PLA end-groups was undertaken.

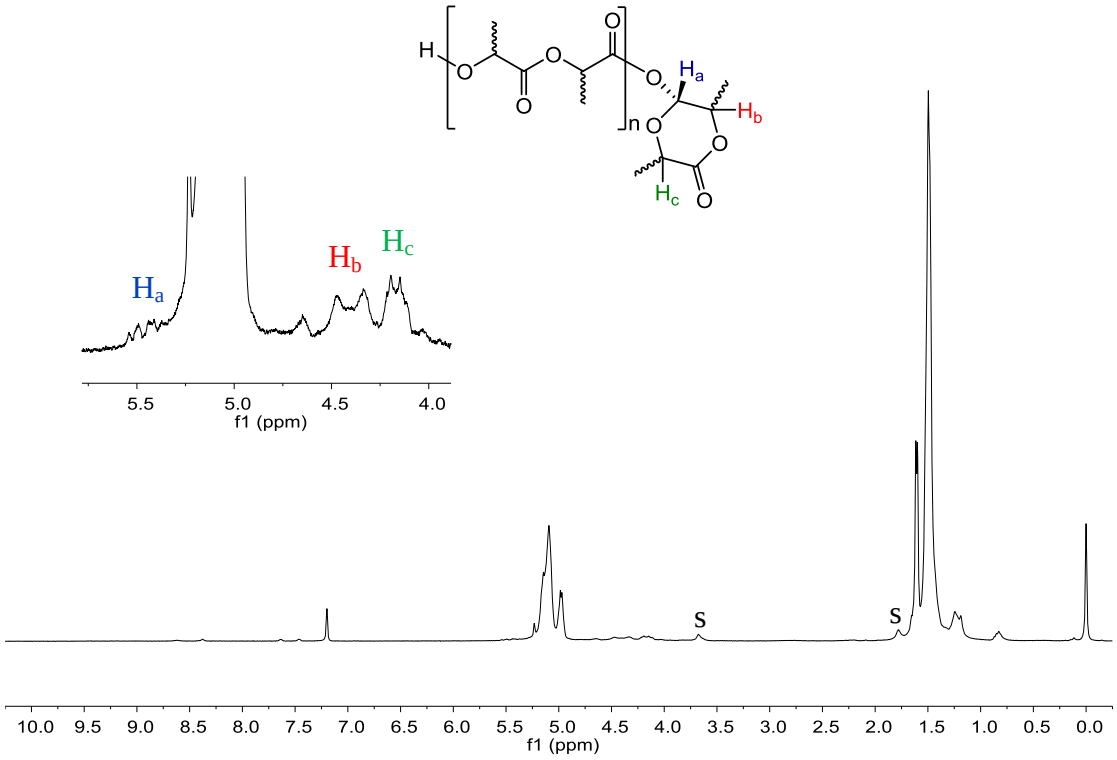


Figure 2.21. ^{1}H NMR (THF-d_8, 400.1 MHz, 298 K) spectrum of PLA synthesised from Mg(CzOx^{Me_2})(BH$_4$) (**7**). "s" denotes residual solvent signals.

An identical bulk polymerisation was conducted with Mg(CzOx^{Me_2})(BD$_4$) (**7-*d*$_4$**); however, treatment with 15 equivalents of *rac*-LA in 4 mL THF at 23 °C failed to produce any PLA after 24 h. The temperature was increased to 60 °C, and the volume of THF decreased to 1 mL. Under these conditions, the catalyst was found to be active, achieving 85% conversion after 30 h (M_n(obs) = 2,340 g mol^{-1}, PDI = 1.23). The polymerisation was quenched with dry HCl in diethyl ether, the PLA extracted into CH_2Cl_2 and characterised by ^{1}H, ^{2}H and ^{13}C{^{1}H} NMR spectroscopy, GPC and MALDI-ToF MS. Disappointingly, the ^{1}H NMR spectrum was similarly broad in the diagnostic region of 4.0-6.0 ppm; however, the resonances between 5.40-5.70 ppm previously observed in the PLA isolated from Mg(CzOx^{Me_2})(BH$_4$) (**7**) were no longer present, further suggesting their correspondence to LA-D environments.

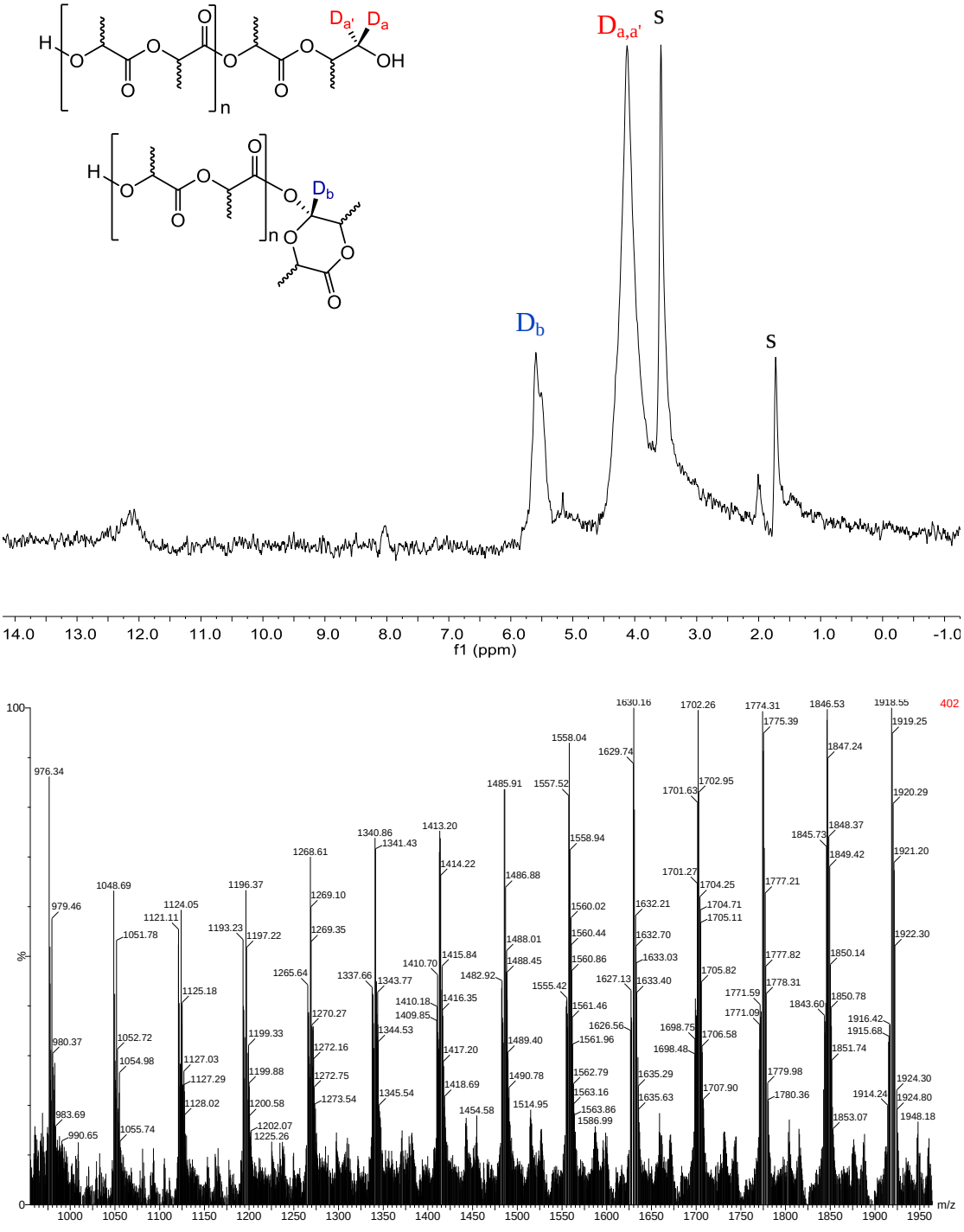


Figure 2.22. Top: ^{2}H NMR spectrum (THF, 76.7 MHz, 298 K) of PLA synthesised from Mg(CzOx^{Me2})(BD$_4$) (**7-*d*$_4$**); "s" denotes residual solvent signals. Bottom: MALDI-ToF MS of PLA synthesised from Mg(CzOx^{Me2})(BD$_4$) (**7-*d*$_4$**). M_n by GPC analysis was 2,340 g mol^{-1}.

The ^{2}H NMR spectrum revealed two major broad resonances at 4.1 and 5.6 ppm (Figure 2.22; top). These peaks are consistent with CH(Me)C$\underline{D}_2$OH and LA-$\underline{D}$ termini, respectively. These findings further serve to confirm the existence of a non-ring opened LA terminus obtained from the employment of borohydride catalysts in the ROP of lactide, which would be indistinguishable from an aldehyde end-group using MALDI-ToF MS. The minor broad peak at 12.1 ppm corresponds to partially N-deuterated HCzOx^{Me2} (**1.45-*d***) which would be expected to be formed during hydrolytic work up of the reaction mixture and exchange between the N-H and a deuterium-containing species. The MALDI-ToF MS revealed two peaks at 1483 and 1486 g mol^{-1}, which are in agreement with the calculated values for the polymer chains [H-[LA]$_9$-[LA-D] + K]$^+$ (1483 g mol^{-1}) and [H-[LA]$_9$-OC(H)MeCO$_2$C(H)CD$_2$OH + K]$^+$ (1486 g mol^{-1}), (Figure 2.22; bottom).

Peculiarly, the polymerisation of 15 equivalents of *rac*-LA with Mg(CzOx^{Me2})(BD$_4$) (**7-*d*$_4$**) required a longer reaction time, higher temperature and greater lactide concentration than with Mg(CzOx^{Me2})(BH$_4$) (**7**). An equivalent reaction was conducted under identical conditions with **7**: the polymerisation of 15 equivalents of *rac*-LA in 1 mL THF at 60 °C achieved 91% conversion after 5 h reaction time (M_n(obs) = 2,460 g mol^{-1}, PDI = 1.31), considerably faster than **7-*d*$_4$**. It was postulated that this may be a kinetic isotope effect which impacts the rates of hydride transfer to the LA moiety. To investigate the origin of this rate decrease, **7-*d*$_4$** was treated with 100 equivalents of *rac*-LA in 4 mL THF at room temperature. However, after 24 h no polymer had been produced. The reaction was repeated at an elevated temperature of 60 °C, and the catalyst achieved 88% conversion after 48 h (Table 2.6, entry 9). As for the ROP of *rac*-LA with **7** at 23 °C, kinetic analysis revealed there to be no observed induction period with a second-order dependence on [LA] (k_{obs} of 0.179(6) M^{-1} h^{-1}, R^2 = 0.993), attributed to the evolution of a trialkyl borate ester following the addition of *rac*-LA (Figure 2.23).

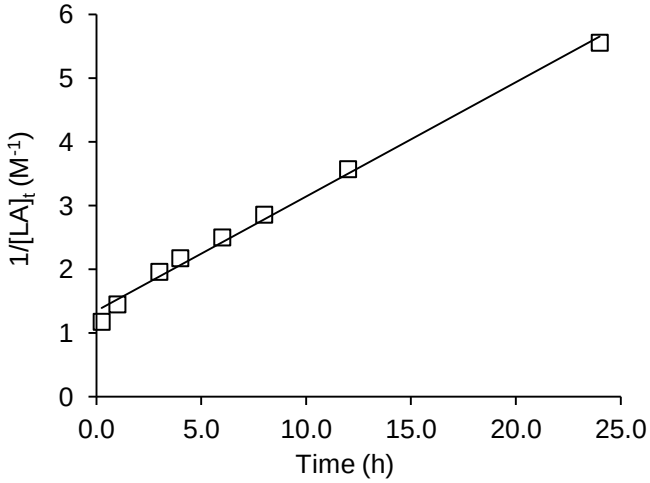


Figure 2.23. Data for the ROP of *rac*-LA using Mg(CzOx^{Me2})(BD$_4$) (**7-*d*$_4$**). Second-order plot of 1/[LA]$_t$ *vs*. time (k_{obs} = 0.179(6) M^{-1} h^{-1}, R^2 = 0.993); vertical-axis intercept = 1.35(6) M^{-1} (expected value = 1/[LA]$_0$ = 1 M^{-1}). Conditions: 4 mL THF, 60 °C, [*rac*-LA]$_0$:[**7-*d*$_4$**]$_0$ = 100:1. [*rac*-LA]$_0$ = 1.0 M.

In comparison to **7**, the molecular weight control was found to be poorer, with a broader PDI of 1.30 and considerably lower than expected molecular weights (M_n(obs) = 5,580 g mol^{-1} *cf.* M_n(calc) = 12,711 g mol^{-1}), which may be a result of the elevated temperatures employed. Structural analysis with MALDI-ToF MS revealed two distributions with peak envelopes of $\Delta m/z$ 72 g mol^{-1}, confirming the occurrence of intermolecular transesterification. The major distribution revealed two peaks at 1482 and 1485 g mol^{-1} corresponding to LA-D (calculated value = 1483 g mol^{-1}) and CH(Me)CD$_2$OH (calculated value = 1486 g mol^{-1}) termini, respectively.

In order to understand the origin of the rate decrease in the k_{obs} of **7** compared to other catalysts in this series, especially Mg(CzOx^{Me2})(OBn) (**2**) and Mg(CzOx^{Me2})(Bu) (**3**), and the further rate decrease with **7-*d*$_4$**, detailed ^{1}H and ^{11}B NMR studies were undertaken. To gain insight into the mechanism of initiation with **7**, 10 equivalents of *rac*-LA were added to a THF-d_8 solution at room temperature. Unfortunately, analysis of the ^{1}H NMR was again restricted by broadening in the region of interest between 4.0-6.0 ppm. Nonetheless, three doublets were observed at 5.53, 5.62 and 5.65 ppm, which were unchanged after several hours in solution. As a comparison, a similar investigation was conducted into the reactivity between Mg(CzOx^{Me2})(OBn) (**2**) and 10 equivalents of *rac*-LA; Figure 2.24 shows an overlay of the ^{1}H NMR spectra of this experiment with that of the reaction between **7** and 10 equivalents of *rac*-LA for

comparison. The reaction proceeded cleanly to generate OBn-terminated PLA. The HOC(H)Me proton could be identified at 4.39 ppm, which is similar to its assignment in $CDCl_3$, *vide supra*. The phenyl ring protons were observed as a multiplet at 7.36 to 7.26 ppm, and the $PhCH_2O$ protons were observed at 5.01 ppm. In this instance, a resonance corresponding to HOC(H)Me was unobserved. This reaction highlights the difference in reactivity between the two complexes on exposure to *rac*-LA: **2** reacts to form one clearly identifiable PLA product, whereas **7** appears to generate multiple different species. Although full characterisation of the products observed in the ^1H NMR spectrum after the reaction between **7** and *rac*-LA remains elusive, it is postulated that they correspond to a mixture of the diastereomeric forms of Mg(CzOx^{Me2})(LA-H), and other products of the reaction between **7** and *rac*-LA, which may not be catalytically active, leading to a decrease in rate of polymerisation relative to other magnesium complexes in this series featuring different initiating groups.

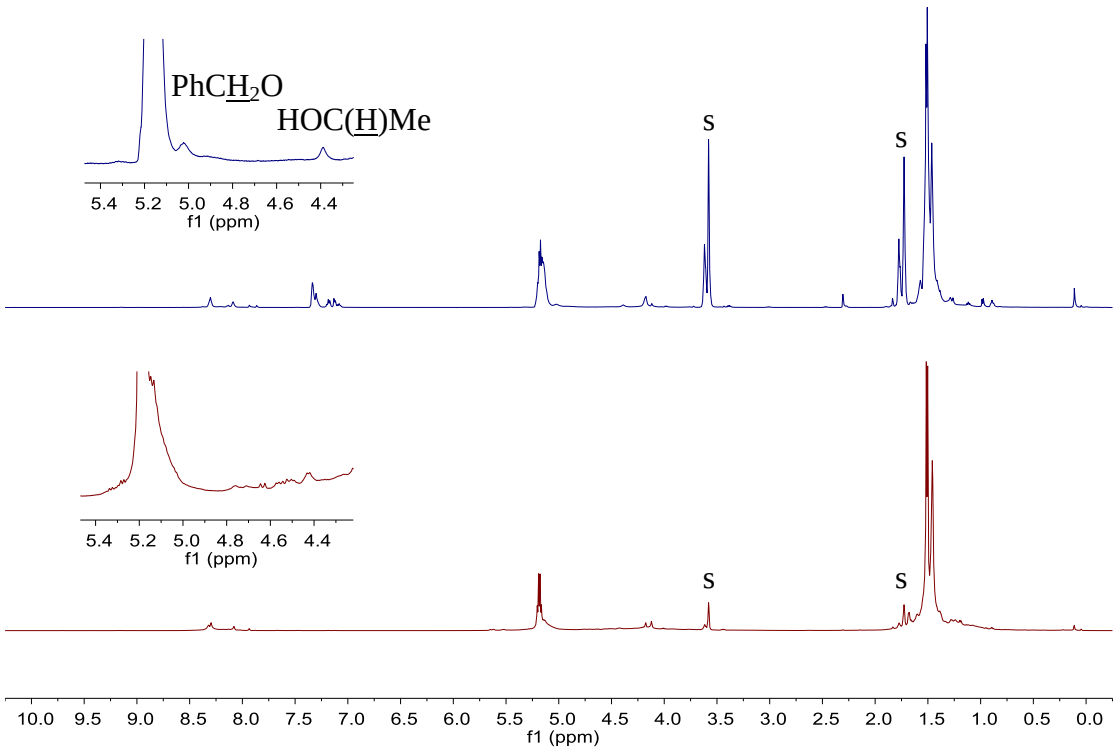


Figure 2.24. ^1H NMR spectra (THF-d_8, 500.3 MHz, 298 K) of Mg(CzOx^{Me2})(BH_4) (**7**) and 10 eq. *rac*-LA (red) and Mg(CzOx^{Me2})(OBn) (**2**) and 10 eq. *rac*-LA (blue). "s" denotes residual solvent signals.

Examination of the ^{11}B NMR spectrum following addition of 10 equivalents of *rac*-LA revealed the immediate consumption of the borohydride, and the emergence of major singlets at 8.0 and 22.9 ppm, with minor resonances at 2.2 and 10.5 ppm (Figure 2.25). Based on the literature reported ^{11}B NMR spectrum of $B(OMe)_3$ and previous work conducted by the Mountford group, it is postulated that the resonance at 22.9 ppm corresponds to $\underline{B}(LA\text{-}H)_3$, or another $B(OR)_3$ species.[89, 124, 125] The evolution of a borate ester following the addition of lactide to **7** may account for the observed second-order dependency on [LA] when treated with 100 equivalents of *rac*-LA in 4 mL THF.

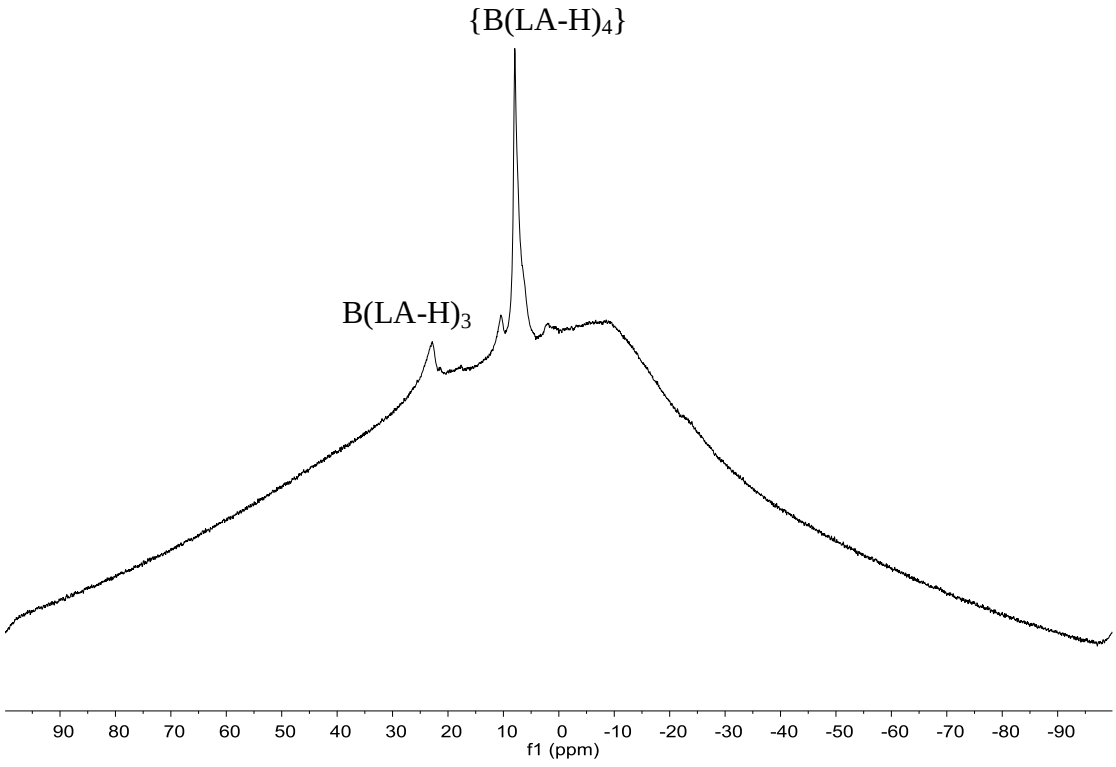


Figure 2.25. ^{11}B NMR spectrum (THF-d_8, 160.4 MHz, 298 K) of $Mg(CzOx^{Me2})(BH_4)$ (**7**) and 10 eq. *rac*-LA.

Following the first hydride transfer from the borohydride ligand to a LA monomer, the newly formed BH_3 can remain coordinated to the LA-H monomer, or can dissociate to react with THF to form BH_3(THF). Subsequently, BH_3(THF) reacts with LA molecules present in solution to form $BH_{3-x}(LA\text{-}H)_x$ *via* an exchange mechanism with the magnesium complex, eventually forming $B(LA\text{-}H)_3$. Investigations undertaken by J. Unruangsri also demonstrate the ability of a magnesium alkoxide complex to undergo scrambling in the presence of stoichiometric amounts of

BH_3(THF) to produce the corresponding borohydride complex: the reaction between 3 equivalents of ($Tp^{tBu,Me}$)Mg(OBn) and 4 equivalents of BH_3(THF) showed instantaneous formation of ($Tp^{tBu,Me}$)Mg(BH_4) and $B(OBn)_3$ in the ^{11}B NMR spectrum.[89] Prior attempts to independently synthesise B(LA-H)$_3$ to verify the assignment of the resonance observed at 22.9 ppm were unsuccessful; however, a preliminary investigation in which treatment of 3 equivalents of *rac*-LA with a four-fold excess of 1 M BH_3(THF) in THF at room temperature immediately resulted in a broad resonance at 22.9 ppm in the ^{11}B NMR spectrum, confirming the hypothesis that the resonance at 22.9 ppm is ultimately a product of the reaction between BH_3(THF) and *rac*-LA, although its precise structure remains unclear. Upon addition of lactide to **7**, a quartet at -1.1 ppm corresponding to BH_3(THF) was not observed in the ^{11}B NMR spectrum, which may be due to its short lifespan in solution following rapid onwards reaction with lactide. Nonetheless, the resultant products strongly agree with the previously proposed mechanism. Based on previous literature observations, the resonance at 8.0 ppm may correlate to a tetracoordinated $\{B(OR)_4\}^-$ anionic species.[124] It is postulated that the $BH_{3-x}(LA\text{-}H)_x$ species form tetracoordinated borate ester adducts with Mg($CzOx^{Me2}$)(LA-H) to generate Mg($CzOx^{Me2}$)$\{BH_{4-x}(LA\text{-}H)_x\}$, in an analogous fashion to the coordination of $B(OBn)_3$ to Mg($CzOx^{Me2}$)(OBn) (**2**) to generate Mg($CzOx^{Me2}$)$\{B(OBn)_4\}$ (**8**).

As **7-*d*$_4$** has a substantially lower rate of reaction in comparison to **7**, a similar ^{11}B NMR study was undertaken in which **7-*d*$_4$** was treated with 10 equivalents of *rac*-LA (Figure 2.26). The ^{11}B NMR spectrum shows full consumption of **7-*d*$_4$** within 5 min, indicating that the first deuteride transfer to a LA monomer occurs rapidly and is therefore not rate-limiting. Following addition, the ^{11}B NMR spectrum revealed several major resonances at 6.5, 8.1 and 23.2 ppm, with minor resonances observed at 2.2, 10.6, 21.8 ppm. It is likely that the three peaks at between 6-11 ppm correlate to a tetracoordinated $\{BD_{4-x}(LA\text{-}D)_x\}^-$ species, whilst the peak at 23.2 ppm correlates to $BD_{3-x}(LA\text{-}D)_3$. After 1 h, the peaks at 6.5, 8.1 and 10.6 ppm were observed to merge into one broad environment, and after 12 h, had become a broad singlet at 7.2 ppm.

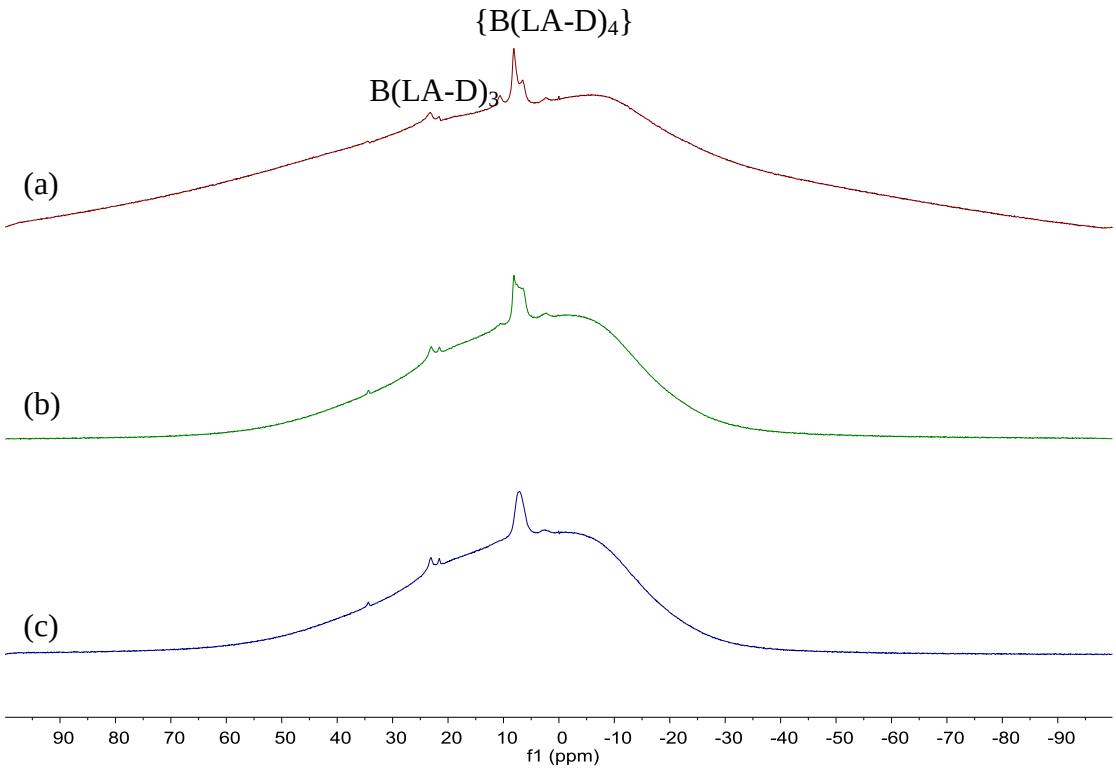
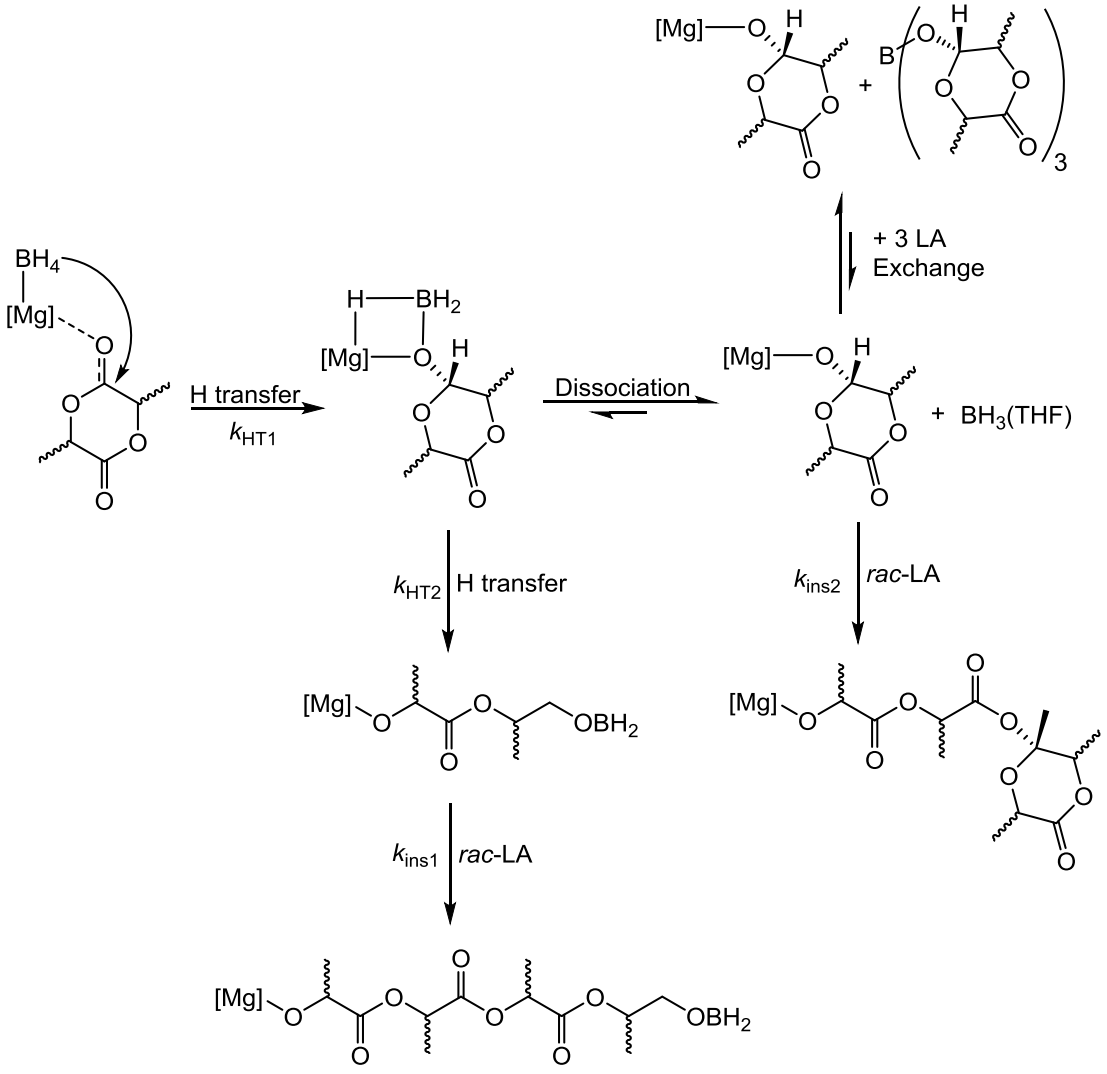


Figure 2.26. ^{11}B NMR spectrum (THF-d_8, 160.4 MHz, 298 K) of Mg(CzOx^{Me2})(BD$_4$) (**7-*d*$_4$**) and 10 eq. *rac*-LA. (a) Products formed immediately at 298 K. (b) Products formed after 5 min at 298 K. (c) Products formed after 1 h at 298 K.

The ^{1}H and ^{11}B NMR studies, in conjunction with the deuterium labelling investigations, indicate that throughout the polymerisation run only partial activation of the initiator to a productive species occurs, resulting in a decrease in k_{obs}. Based on these findings, a proposed mechanism for the formation of these species is depicted in Scheme 2.6, in which k_{HT1} = rate constant of first hydride transfer, k_{HT2} = rate constant of second hydride transfer, k_{ins1} = rate constant of insertion into metal-polymeryl chain and k_{ins2} = rate constant of insertion into metal-LA-H bond.

Following the rapid first hydride transfer from the precatalyst to the lactide monomer, the intermediate Mg(CzOx^{Me2})(LA-H) is formed, whose initiating capability remains unknown, and which may not rapidly undergo either a second hydride transfer or insertion into the Mg-LA-H alkoxide bond. As multiple reaction pathways are available to **7** on the addition of lactide, as evidenced by the multiple products observed in the ^{1}H NMR spectrum following addition of 10 equivalents of *rac*-LA to the complex, it is postulated that not all of the starting complex becomes a productive species, but may react to form a catalytically inactive species. At this stage, the

precise nature of these catalytically inactive species remain ambiguous; however, this would lead to a lower catalyst loading and concentration than expected and result in a decrease in rate of polymerisation. Crucially, this partial precatalyst activation is obscured: typically this effect would result in higher than anticipated molecular weights, but the concurrent generation of a $B(OR)_3$ species, such as $B(LA\text{-}H)_3$, results in chain transfer, thus lowering the molecular weights and masking the detection of incomplete catalyst activation. However, as $B(LA\text{-}H)_3$ is more sterically encumbered than other primary trialkyl borate esters, such as $B(OBn)_3$, which have been investigated as CTAs in *i*ROP, its efficacy as a CTA is unknown, and may result in a reduced capacity to effect chain transfer.



Scheme 2.6. Proposed mechanism for the productive part of the process of lactide initiation and insertion mediated by hydride transfer with catalyst $Mg(CzOx^{Me_2})(BH_4)$ (**7**).

Further experiments were conducted in which 1 equivalent of a trialkyl borate ester, such as $B(OBn)_3$ or $B(OMe)_3$ was added to **7** to investigate whether the presence of external chain transfer agents results in an increase in k_{obs}, which has shown previously to be slower with borohydride initiating groups in comparison to other classical initiators. Unfortunately, the presence of either CTA did not result in an observed rate increase (Table 2.6, entries 8 and 9). In the presence of the sterically encumbered $B(OBn)_3$, **7** reached 92% conversion after 240 min; the reaction was found to be second-order in [LA] (k_{obs} = 2.24(3) M^{-1} h^{-1}, R^2 = 0.998). Using the less bulky CTA $B(OMe)_3$ resulted in an increased rate of polymerisation, achieving 92% conversion after 180 min (k_{obs} = 4.0(1) M^{-1} h^{-1}, R^2 = 0.996); which is identical within error to the k_{obs} for the ROP of *rac*-LA with **7** in the absence of any CTA (k_{obs} = 3.91(8) M^{-1} h^{-1}, R^2 = 0.997) (Figure 2.27).

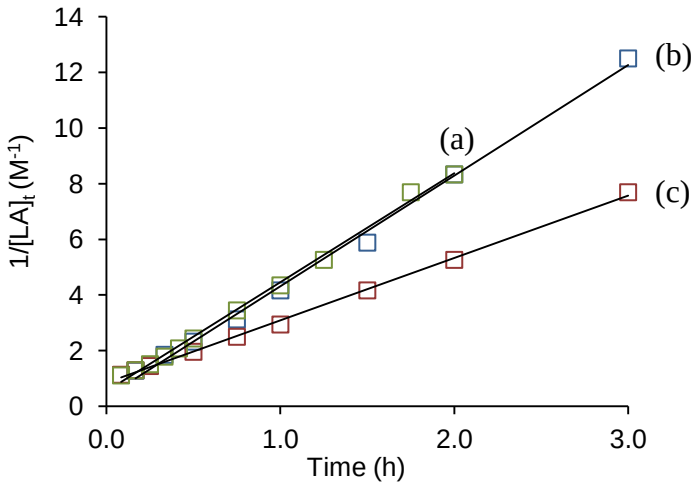


Figure 2.27. Data for ROP of *rac*-LA using $Mg(CzOx^{Me_2})(BH_4)$ (**7**) with $B(OBn)_3$ and $B(OMe)_3$. Top: Second-order plot of $1/[LA]_t$ *vs*. time (a) $Mg(CzOx^{Me_2})(BH_4)$ (**7**) k_{obs} = 3.91(8) M^{-1} h^{-1}, R^2 = 0.997; vertical-axis intercept = 0.55(7) M^{-1} (expected value = $1/[LA]_0$ = 1 M^{-1}) (green squares), (b) $Mg(CzOx^{Me_2})(BH_4)$ (**7**) and 1 eq. $B(OMe)_3$: k_{obs} = 4.0(1) M^{-1} h^{-1}, R^2 = 0.996; vertical-axis intercept = 0.3(1) M^{-1} (expected value = $1/[LA]_0$ = 1 M^{-1}) (blue squares) and (c) $Mg(CzOx^{Me_2})(BH_4)$ (**7**) and 1 eq. $B(OBn)_3$: k_{obs} = 2.24(3) M^{-1} h^{-1}, R^2 = 0.998; vertical-axis intercept = 0.86(5) M^{-1} (expected value = $1/[LA]_0$ = 1 M^{-1}) (red squares).

Notably, the molecular weight control in both cases was excellent: the molecular weight grew linearly throughout the polymerisation and was found to agree closely with the theoretical values, confirming that trialkyl borate esters are highly effective

CTAs (Figure 2.28). Analysis using MALDI-ToF MS revealed the presence of two polymer distributions: the major distribution corresponded to chains terminated with the appropriate –OR group for the CTA agent employed, whereas the minor distribution corresponded to end-groups observed when employing borohydride initiating groups, namely $CH(Me)CH_2OH$ and LA-H. The employment of either CTA resulted in moderately heterotactically enriched PLA (Table 2.6, entry 8, P_r =0.79-0.82; Table 2.6, entry 9, P_r = 0.73-0.76), within the range previously observed with these systems.

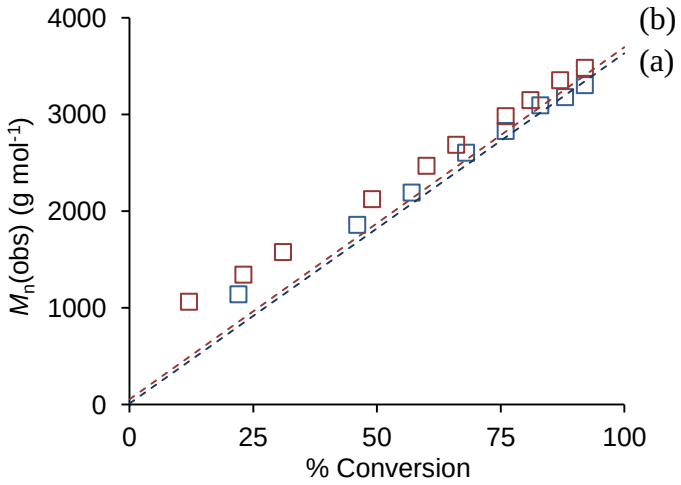


Figure 2.28. M_n(obs) *vs.* % conversion plot for (a) Mg(CzOx^{Me_2})(BH_4) (**7**) and 1 eq. $B(OMe)_3$ (blue squares) and (b) Mg(CzOx^{Me_2})(BH_4) (**7**) and 1 eq. $B(OBn)_3$ (red squares). The dashed line represents M_n calculated for four chains PLA per metal centre in each case. (a) Mg(CzOx^{Me_2})(BH_4) (**7**) and 1 eq. $B(OMe)_3$ (blue squares) and (b) Mg(CzOx^{Me_2})(BH_4) (**7**) and 1 eq. $B(OBn)_3$ (red squares). Conditions: 4 mL THF, 23 °C, [*rac*-LA]$_0$:[**7**]$_0$:[$B(OR)_3$]$_0$ = 100:1:1, [*rac*-LA]$_0$ = 1.0 M.

Several reports in the literature have illustrated the potential solvent dependency on the type of stereocontrol observed during the ROP of *rac*-LA, with donor solvents affording heterotactically enriched PLA, whilst non-donor solvents such as toluene or CD_2Cl_2 affording atactic or isotactic PLA.[126-128] Several NMR scale experiments were undertaken in order to screen the effect of solvent on observed stereocontrol using **7**. A 1M stock solution of 20 equivalents of *rac*-LA in toluene was added to a 0.01M stock solution of catalyst in toluene at room temperature, and the reaction monitored by ^{1}H NMR spectroscopy. Unfortunately, the catalyst and monomer were poorly soluble in toluene, and required an extended reaction time of 4 h to reach 83%

conversion. The polymer was subsequently isolated and analysed by $^{1}H\{^{1}H\}$ NMR in $CDCl_3$. The resultant PLA was found to have a moderate degree of heteroenrichment (P_r = 0.74), with M_n(obs) = 2,820 g mol^{-1} (M_n(calc) = 2,396 g mol^{-1}) and a narrow PDI of 1.19 at 83% monomer conversion. A similar experiment was repeated in CD_2Cl_2: in this instance rapid polymerisation to 90% conversion was achieved after 1 h. Despite this, a similar degree of heteroenrichment was also observed (P_r = 0.72), with M_n(obs) = 2,950 g mol^{-1} (M_n(calc) = 2,598 g mol^{-1}) and a similarly narrow PDI of 1.17 at 90% monomer conversion. As the PLA produced in both instances had similar degrees of heterotacticity to that obtained in THF, no further investigations were undertaken in non-donor solvents.

Following the successful *in situ* transformation of **7** to Mg(CzOx^{Me2})(OBn) (**2**), $B(OBn)_3$ and Mg(CzOx^{Me2}){$B(OBn)_4$} (**8**), the activity of this system for the ROP of *rac*-LA was investigated and compared to the activity of externally synthesised Mg(CzOx^{Me2})(OBn) (**2**) in the presence of 1 equivalent of $B(OBn)_3$. In the presence of 4.5 equivalents of benzaldehyde, **7** was found to reach 92% conversion after 30 min (Table 2.6, entry 12), compared to 120 min to reach 88% conversion in the absence of benzaldehyde, indicating that using a borohydride initiating group is considerably slower than that employing an alkoxide initiator. Molecular weight control was reasonable: a plot of the growth of M_n *vs*. % conversion was found to give a gradient of 58(1) g mol^{-1} (% conversion)$^{-1}$ (R^2 = 0.998), which is slightly higher than the expected 36 g mol^{-1} (corresponding to 4 chains per metal centre), attributed to ineffective chain transfer (Figure 2.29). Analysis by MALDI-ToF MS revealed the PLA end-group to be -OBn, as expected, confirming that the borohydride is fully converted to an alkoxide and 1 equivalent of $B(OBn)_3$ prior to initiation. Analysis of a semilogarthmic plot of $\ln[LA]_i/[LA]_t$ *vs*. time and $1/[LA]_t$ *vs*. time revealed the reaction followed an intermediate non-integer kinetic order, analogously to externally synthesised Mg(CzOx^{Me2})(OBn) (**2**) and 1 equivalent of $B(OBn)_3$.

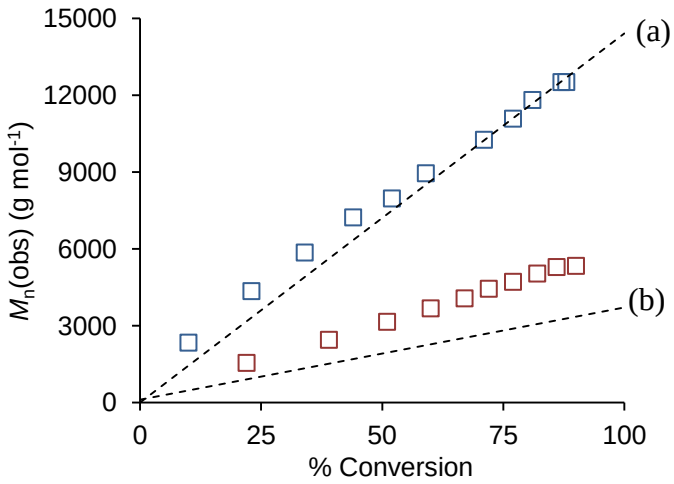


Figure 2.29. M_n(obs) (g mol^{-1}) *vs*. % conversion plot for the ROP of *rac*-LA using (a) Mg(CzOx^{Me2})(BH$_4$) (**7**), [*rac*-LA]$_0$:[**7**]$_0$ = 100:1, [*rac*-LA]$_0$ = 1.0 M, expecting 1 chain PLA per metal centre (blue squares); and (b) Mg(CzOx^{Me2})(BH$_4$) (**7**) + 4.5 eq. PhCHO, [*rac*-LA]$_0$:[PhCHO]$_0$:[**7**]$_0$= 100:4.5:1, [*rac*-LA]$_0$ = 1.0 M, expecting 4 chains PLA per metal centre (red squares); the dashed lines are the M_n calc in each case. Conditions: 4 mL THF, 23 °C.

In light of the previous findings in which it was confirmed that in the presence of Mg(CzOx^{Me2})(OCHDPh) and B(OCHDPh)$_3$, excess PhCHO undergoes scrambling to form PhCDO, control experiments were conducted to observe the effect of excess benzaldehyde on the polymerisation.

Table 2.7. Selected data for the polymerisation of *rac*-LA using Mg(CzOx^{Me2})(OBn) (**2**) and Mg(CzOx^{Me2})(BH$_4$) (**7**) in THF.[a]

Entry	Catalyst	Additive (eq.)	Conv.[b] %	Time (min)	M_n(obs)[c] (g mol^{-1})	M_n(calc)[d] (g mol^{-1})	M_w/M_n[c]
1	**7**	PhCHO (8)	90	45	5,370	3,350	1.07
2	**2**	B(OBn)$_3$ (1) + PhCHO (0.5)	91	30	5,160	3,386	1.10

[a] Conditions: [*rac*-LA]$_0$:[**7**]$_0$ = 100:1, 4 mL THF at 23 °C. [*rac*-LA]$_0$ = 1.0 M. [b] Measured by ^{1}H NMR (CDCl$_3$) analyses. [c] Molecular weights (g mol^{-1}) determined from GPC using appropriate Mark-Houwink corrections. [d] Expected average M_n (g mol^{-1}) for stated number of chains per metal and stated % conversion: M_n (calc for entries 1-2) = ¼ (conversion (%) × 100 × 144.1) + 108.1.

In the first instance, a large excess of 8 equivalents of benzaldehyde was added to Mg(CzOx^{Me2})(BH$_4$) (**7**) prior to the ROP of 100 equivalents of *rac*-LA (Table 2.7,

entry 1). 90% monomer conversion was achieved after 45 min; the polymerisation was found to be second-order in [LA] with k_{obs} = 11.8(3) M^{-1} h^{-1} (R^2 = 0.996). The observed growth of molecular weight did not appear to be impacted by the addition of excess equivalents of benzaldehyde (M_n(obs) = 5,610 g mol^{-1}, M_n(calc) = 3,386 g mol^{-1}, PDI = 1.07), nor did the heterotactic enrichment (P_r = 0.77-0.78). A further experiment was conducted in which 0.5 equivalents of benzaldehyde was added to a THF solution containing independently synthesised Mg($CzOx^{Me_2}$)(OBn) (**2**) and 1 equivalent of $B(OBn)_3$ prior to the addition of 100 equivalents of *rac*-LA (Table 2.7, entry 2). The reaction reached 91% monomer conversion after 30 min with a second-order dependence in [LA] (k_{obs} = 21.7(4) M^{-1} h^{-1}, R^2 = 0.997). Further analysis into the molecular weight revealed higher than anticipated molecular weights, with a gradient from the plot of M_n *vs.* % conversion to be 56(1) g mol^{-1} (R^2 = 0.998), which is a product of slightly inefficient chain transfer. The addition of excess benzaldehyde to previously studied systems confirms its innocence during polymerisation: the rate of reaction did not appear to be rapidly slowed by the addition of excess benzaldehyde, nor was there any appreciable impact on the observed molecular weights.

2.6 Polymerisation studies: ROP of *meso*-LA

Catalysts which are able to furnish highly stereoenriched PLA from *meso*-LA are comparatively underdeveloped to those available for the stereocontrolled ROP of *rac*-LA. Complex **7** was tested for its activity towards the ROP of *meso*-LA, both in the absence and presence of 4.5 equivalents of benzaldehyde (Table 2.8, entries 1 and 2, respectively). An increase in the rate of polymerisation of *meso*-LA in comparison to *rac*-LA was anticipated, as the relative stability of *meso*-LA is lower than that of *L*-LA, as detailed in Chapter 1, and under both reaction conditions, **7** was found to polymerise *meso*-LA faster than *rac*-LA.

Table 2.8. Selected data for the polymerisation of *meso*-LA using Mg(CzOx^{Me_2})(BH_4) (**7**) in THF.[a]

Entry	Additive (eq.)	Conv.[b] %	Time (min)	M_n(obs)[c] (g mol^{-1})	M_n(calc)[d] (g mol^{-1})	M_w/M_n[c]	P_r
1	-	93	40	9,420	13,405	1.17	0.70
2	PhCHO (4.5)	92	10	6,820	3,422	1.21	0.63-0.66

[a] Conditions: [*meso*-LA]$_0$:[**7**]$_0$ = 100:1, 4 mL THF at 23 °C. [*meso*-LA]$_0$ = 1.0 M. [b] Measured by ^{1}H NMR ($CDCl_3$) analyses. [c] Molecular weights (g mol^{-1}) determined from GPC using appropriate Mark-Houwink corrections. [d] Expected average M_n (g mol^{-1}) for stated number of chains per metal and stated % conversion: M_n (calc for entry 1) = (conversion (%) × 100 × 144.1) + 4.0; (calc for entry 2) = ¼(conversion (%) × 100 × 144.1) + 108.1.

In the absence of any additives, **7** achieved 93% conversion after 40 min (k_{obs} = 4.2(2) h^{-1}, R^2 = 0.992), and the addition of 4.5 equivalents of benzaldehyde further increased the rate, achieving 92% conversion after 10 min. Kinetic analysis showed the reaction did not clearly observe either a first- or second-order dependence in [LA], instead observing a non-integer intermediate value which is indicative of complex preequilibria associated with the coordination of the trialkyl borate ester to the metal centre prior to and following the ring-opening of a lactide monomer. In the absence of benzaldehyde, molecular weights obtained by **7** were found to be lower than anticipated, a result of the presence of a trialkyl borate ester such as B(LA-H)$_3$ acting as a CTA and consistent with previous observations (Figure 2.30). Upon generation of **2** and B(OBn)$_3$ through the addition of 4.5 equivalents of benzaldehyde to **7**, the molecular weights confirmed the immortal nature of the polymerisation; however, they are higher than expected. The inefficiency of chain transfer with B(OBn)$_3$ may be further compounded by the increased rate of propagation of *meso*-LA compared to the rate of propagation of *rac*-LA, as a result to the relative instability of the monomer. Of particular interest was the degree of either heterotactic or syndiotactic enrichment of the polymer backbone.

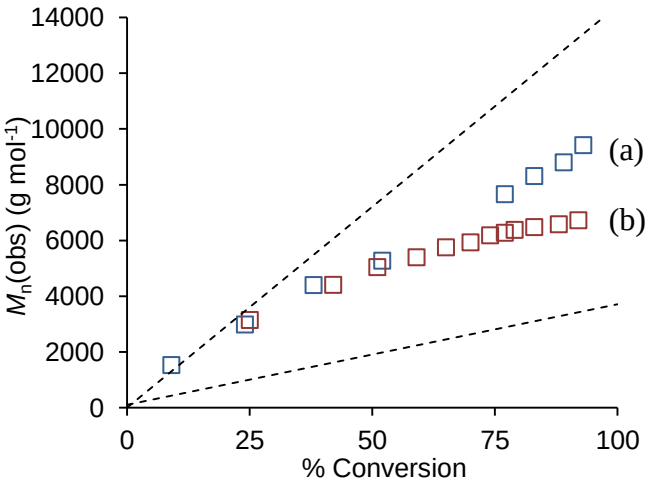


Figure 2.30. M_n(obs) (g mol^{-1}) *vs*. % conversion plot for the ROP of *meso*-LA using (a) Mg(CzOx^{Me_2})(BH$_4$) (**7**), [*meso*-LA]$_0$:[**7**]$_0$ = 100:1, [*meso*-LA]$_0$ = 1.0 M, expecting 1 chain PLA per metal centre (blue squares); and (b) Mg(CzOx^{Me_2})(BH$_4$) (**7**) + 4.5 eq. PhCHO, [*meso*-LA]$_0$:[PhCHO]$_0$:[**7**]$_0$= 100:4.5:1, [*rac*-LA]$_0$ = 1.0 M, expecting 4 chains PLA per metal centre (red squares); the dashed lines are the M_n calc in each case. Conditions: 4 mL THF, 23 °C.

Analysis by ^{1}H{^{1}H} NMR spectroscopy showed the PLA to be slightly syndiotactically enriched, (Figure 2.31). After application of the appropriate Bernoullian statistics, the P_r values were calculated to be 0.70 for the ROP of *meso*-LA using **7** in the absence of benzaldehyde and 0.63-0.66 for the ROP of *meso*-LA using **7** in the presence of benzaldehyde. As the ROP of *rac*-LA using **7** affords highly heterotactically-enriched PLA (P_r > 0.5) it is unsurprising that the ROP of *meso*-LA results in the formation of syndiotactically-enriched PLA (P_r > 0.5), as enchainment *via racemic* dyads (*RS* or *SR*) occurs preferentially to enchainment *via meso* dyads (*SS* or *RR*) resulting in a syndiotactic bias. A review of selected complexes which are capable of the stereoselective ROP of *meso*-LA is provided in Chapter 1.

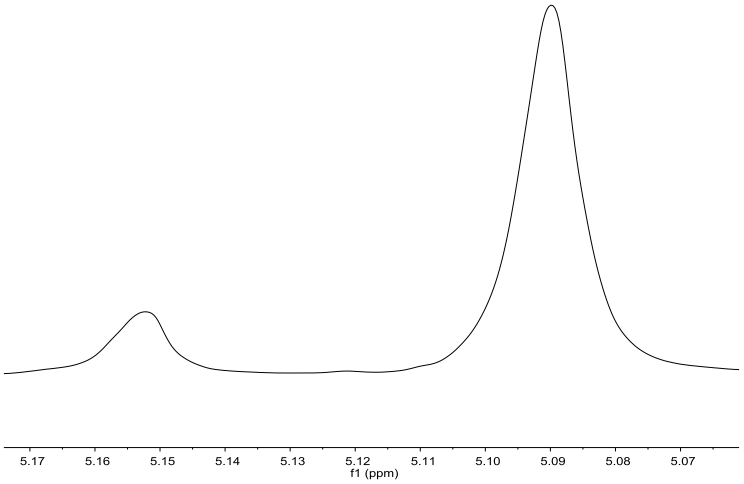


Figure 2.31. $^{1}H\{^{1}H\}$ NMR ($CDCl_3$, 400.1 MHz, 298 K) of PLA synthesised from $Mg(CzOx^{Me2})(BH_4)$ (**7**) and *meso*-LA.

2.7 Summary and conclusions

This Chapter has described the synthesis and characterisation of a series of $CzOx^{Me2}$-supported magnesium and zinc complexes, complexes **1**-**4**, **6**, **7** and **7-*d*$_4$** and their application as initiators for the ROP of *rac*-, *L*- and *meso*-lactide. Complexes **1**, **3**, **4** and **6** were prepared in good yields through protonolysis reactions between $HCzOx^{Me2}$ (**1.45**) and the corresponding metal precursor in toluene. Complex **2** was prepared through the controlled protonolysis of complex **1** with benzyl alcohol in toluene. Complex **7** was prepared in good yield through the salt metathesis of $K(CzOx^{Me2})$ (**5**) with $Mg(BH_4)_2$; however, both complexes **7** and **7-*d*$_4$** could be prepared through the salt metathesis reaction of **6** with sodium borohydride or borodeuteride. Complex **7** exhibited unusual borohydride bonding modes in the solid state, indicating a polymeric structure or a mixture of κ^2- and κ^2-BH_4 modes. All complexes were found to be stable with regards to Schlenk redistribution.

In situ generation of magnesium alkoxide initiators concurrently with trialkyl borate esters was achieved through the reaction of a magnesium borohydride complex with four equivalents of aldehyde. The reaction between **7** and 4 equivalents of benzaldehyde afforded **2** and $B(OBn)_3$, which could exist in equilibrium between discrete species or as a tetracoordinated adduct. Complex **7-*d*$_4$** underwent a similar reaction with 4 equivalents of benzaldehyde to yield **2-*d*** and $B(OCHDPh)_3$. The

addition of excess benzaldehyde to **2-*d*** and $B(OCHDPh)_3$ indicated the possibility of deuterium exchange *via* β-hydride transfer to yield PhCDO.

Complex **2** was probed for its activity towards the ROP of *L*-LA in the presence of various additives. The activity of **2** towards the polymerisation of *L*-LA was substantially slower than for *rac*-LA; as enchainment occurs preferentially through a *racemic* dyad in *rac*-LA to produce heterotactically enriched PLA, enchainment *via* the comparatively less favourable *meso* dyad results in a slower rate of reaction. In the absence of any additives, first-order-like kinetic behaviour was observed; however on the addition of $B(OBn)_3$ a second-order dependency on monomer concentration was observed, which is attributed to preequilibria caused by association and dissociation of the borate ester resulting in an apparent second-order kinetic regime being observed.

Complexes **1**-**4** and **7** were active towards the ROP of *rac*-lactide at room temperature in THF. Although highly active, **1** offered poor molecular weight control resulting in the formation of cyclic polymers, but its performance was ameliorated through the addition of $B(OBn)_3$ which acted as a chain transfer agent. Surprisingly, **3** was active and well-controlled, producing polymer chains with butyl end-groups; however, the zinc analogue (**4**) was considerably less active. In this instance, the $CzOx^{Me2}$ was found to be the initiating group. Highly active and controlled catalyst **2** was tested with a varying number of equivalents of $B(OBn)_3$, which showed the increasing addition of borate ester resulted in a decrease in activity, due to the formation of more inactive tetracoordinated adduct. In the presence of benzaldehyde, the polymerisation behaviour of **7** was found to be in good agreement with externally derived **2** and $B(OBn)_3$; the obtained molecular weights indicated a degree of chain transfer, confirming the immortal nature of the polymerisation. However, without benzaldehyde, **7** exhibited a substantially decreased rate compared to other catalysts in this series. Complexes **1**-**3** and **7** produced heterotactically enriched PLA, with moderate to high P_r values. The polymer obtained from **4** was found to be atactic. Complex **7** was found to be highly active towards the ROP of *meso*-LA producing moderately syndiotactically enriched PLA.

NMR tube scale experiments with **7** and 10 equivalents of *rac*-LA revealed the formation of a ring-closed $Mg(CzOx^{Me2})(LA\text{-}H)$ intermediate, whose existence was

further confirmed through the analysis of the polymer produced with **7-*d*$_4$**, showing (LA-H)-capped polymer chains as well as α,ω-dihydroxytelechelic PLA. A new mechanism was proposed to explain the reactivity between **7** and lactide. Further ^{1}H and ^{11}B NMR investigations suggest partial activation of **7** to form catalytically active species. Although all the products formed from the reaction of **7** with lactide are unknown, the existence of catalytically inactive species is strongly suggested due to the low rate of polymerisation observed with **7**, in comparison to other magnesium catalysts with different initiating groups. The addition of borate esters to **7** prior to polymerisation did not result in an increased rate, supporting the presence of unknown catalytically inactive species which are the result of the reaction between **7** and lactide.

Control experiments were conducted in order to probe the innocence of the addition of excess equivalents of benzaldehyde in which it was added in excess to two known polymerisations. No deleterious effects were observed during the polymerisation, confirming the innocence of benzaldehyde during ROP.

2.8 References for Chapter Two

1. S. Harder, *Alkaline-Earth Metal Compounds: Oddities and Applications*, 1st edn., Springer, 2013.
2. Y. M. A. Yamada and M. Shibasaki, *Tet. Lett.*, 1998, **39**, 5561-5564.
3. T. Poisson, T. Tsubogo, Y. Yamashita and S. Kobayashi, *J. Org. Chem.*, 2010, **75**, 963-965.
4. S. Saito, T. Tsubogo and S. Kobayashi, *J. Am. Chem. Soc.*, 2007, **129**, 5364-5365.
5. T. Tsubogo, S. Saito, K. Seki, Y. Yamashita and S. Kobayashi, *J. Am. Chem. Soc.*, 2008, **130**, 13321-13332.
6. S. Kobayashi, T. Tsubogo, S. Saito and Y. Yamashita, *Org. Lett.*, 2008, **10**, 807-809.
7. R. Kempe, *Chem. Eur. J.*, 2007, **13**, 2764-2773.
8. L. R. Sita, *Angew. Chem. Int. Ed.*, 2009, **48**, 2464-2472.
9. S. Harder, F. Feil and A. Weeber, *Organometallics*, 2001, **20**, 1044-1046.
10. W. E. Lindsell, F. C. Robertson and I. Soutar, *Eur. Polym. J.*, 1983, **19**, 115-120.

11. M. H. Chisholm and N. W. Eilerts, *Chem. Commun.*, 1996, 853-854.
12. M. H. Chisholm, N. W. Eilerts, J. C. Huffman, S. S. Iyer, M. Pacold and K. Phomphrai, *J. Am. Chem. Soc.*, 2000, **122**, 11845-11854.
13. M. J. Stanford and A. P. Dove, *Chem. Soc. Rev.*, 2010, **39**, 486-494.
14. B. J. O'Keefe, M. A. Hillmyer and W. B. Tolman, *Dalton Trans.*, 2001, 2215-2224.
15. M. Okada, *Prog. Polym. Sci.*, 2002, **27**, 87-133.
16. O. Dechy-Cabaret, B. Martin-Vaca and D. Bourissou, *Chem. Rev.*, 2004, **104**, 6147-6176.
17. C. A. Wheaton, P. G. Hayes and B. J. Ireland, *Dalton Trans.*, 2009, 4832-4846.
18. C. M. Thomas, *Chem. Soc. Rev.*, 2010, **39**, 165-173.
19. A. K. Sutar, T. Maharana, S. Dutta, C.-T. Chen and C.-C. Lin, *Chem. Soc. Rev.*, 2010, **39**, 1724-1746.
20. N. Ajellal, J.-F. Carpentier, C. Guillaume, S. M. Guillaume, M. Helou, V. Poirier, Y. Sarazin and A. A. Trifonov, *Dalton Trans.*, 2010, **39**, 8363-8378.
21. J.-F. Carpentier, *Macromol. Rapid Commun.*, 2010, **31**, 1696-1705.
22. S. Harder, *Chem. Rev.*, 2010, **110**, 3852-3876.
23. M. H. Chisholm, J. Gallucci and K. Phomphrai, *Chem. Commun.*, 2003, 48-49.
24. M. H. Chisholm, J. C. Gallucci and K. Phomphrai, *Inorg. Chem.*, 2004, **43**, 6717-6725.
25. B. M. Chamberlain, M. Cheng, D. R. Moore, T. M. Ovitt, E. Lobkovsky and G. W. Coates, *J. Am. Chem. Soc.*, 2001, **123**, 3229-3238.
26. Y. Sarazin, D. Rosca, V. Poirier, T. Roisnel, A. Silvestru, L. Maron and J.-F. Carpentier, *Organometallics*, 2010, **29**, 6569-6577.
27. B. Liu, T. Roisnel, J. P. Guegan, J.-F. Carpentier and Y. Sarazin, *Chem. Eur. J.*, 2012, **18**, 6289-6301.
28. M. Westerhausen, S. Schneiderbauer, A. N. Kneifel, Y. Söltl, P. Mayer, H. Nöth, Z. Zhong, P. J. Dijkastra and J. Feijen, *Eur. J. Inorg. Chem.*, 2003, 3432-3439.
29. Z. Zhong, S. Schneiderbauer, P. J. Dijkastra, M. Westerhausen and J. Feijen, *Polym. Bull.*, 2003, **51**, 175-182.

30. D. J. Darensbourg, W. Choi, O. Karroonnirun and N. Bhuvanesh, *Macromolecules*, 2008, **41**, 3493-3502.
31. H. Xie, Z. Mou, B. Liu, P. Li, W. Rong, S. Li and D. Cui, *Organometallics*, 2014, **33**, 722-730.
32. L. F. Sánchez-Barba, A. Garcés, J. Fernández-Baeza, A. Otero, C. Alonso-Moreno, A. Lara-Sánchez and A. M. Rodríguez, *Organometallics*, 2011, **30**, 2775-2789.
33. M. H. Chisholm, J. C. Huffman and K. Phomphrai, *Dalton Trans.*, 2001, 222-224.
34. M. H. Chisholm, J. Gallucci and K. Phomphrai, *Inorg. Chem.*, 2002, **41**, 2785-2794.
35. L. F. Sánchez-Barba, A. Garcés, M. Fajardo, C. Alonso-Moreno, J. Fernández-Baeza, A. Otero, A. Antiñolo, J. Tejeda, A. Lara-Sánchez and M. I. López-Solera, *Organometallics*, 2007, **26**, 6403-6411.
36. S. M. Guillaume, M. Schappacher and A. Soum, *Macromolecules*, 2003, **36**, 54-60.
37. I. Palard, A. Soum and S. M. Guillaume, *Macromolecules*, 2005, **38**, 6888-6894.
38. I. Palard, M. Schappacher, A. Soum and S. M. Guillaume, *Polym. Int.*, 2006, **55**, 1132-1137.
39. I. Palard, M. Schappacher, B. Belloncle, A. Soum and S. M. Guillaume, *Chem. Eur. J.*, 2007, **13**, 1511-1521.
40. Y. Nakayama, S. Okuda, H. Yasuda and T. Shiono, *React. Func. Polym.*, 2007, **67**, 798-806.
41. Y. Nakayama, K. Sasaki, N. Watanabe, Z. Cai and T. Shiono, *Polymer*, 2009, **50**, 4788-4793.
42. M. Visseaux and F. Bonnet, *Coord. Chem. Rev.*, 2011, **255**, 374-420.
43. F. Bonnet, F. Stoffelbach, G. Fontaine and S. Bourbigot, *RSC Advances*, 2015, **5**, 31303-31310.
44. F. Bonnet, A. R. Cowley and P. Mountford, *Inorg. Chem.*, 2005, **44**, 9046-9055.
45. H. D. Dyer, S. Huijser, N. Susperregui, F. Bonnet, A. D. Schwarz, R. Duchateau, L. Maron and P. Mountford, *Organometallics*, 2010, **29**, 3602-3621.

46. G. G. Skvortsov, M. V. Yakovenko, P. M. Castro, G. K. Fukin, A. V. Cherkasov, J.-F. Carpentier and A. A. Trifonov, *Eur. J. Inorg. Chem.*, 2007, 3260-3267.
47. M. A. Sinenkov, G. K. Fukin, A. V. Cherkasov, N. Ajellal, T. Roisnel, F. M. Kerton, J.-F. Carpentier and A. A. Trifonov, *New J. Chem.*, 2011, **35**, 204-212.
48. J. Kratsch, M. Kuzdrowska, M. Schmid, N. Kazeminejad, C. Kaub, P. Oña-Burgos, S. M. Guillaume and P. W. Roesky, *Organometallics*, 2013, **32**, 1230-1238.
49. T. V. Mahrova, G. K. Fukin, A. V. Cherkasov, A. A. Trifonov, N. Ajellal and J.-F. Carpentier, *Inorg. Chem.*, 2009, **48**, 4258-4266.
50. X. Zhang, C. Wang, M. Xue, Y. Zhang, Y. Yao and Q. Shen, *J. Organomet. Chem.*, 2012, **713**, 182-188.
51. W. Li, M. Xue, J. Tu, Y. Zhang and Q. Shen, *Dalton Trans.*, 2012, **41**, 7258-7265.
52. X. Shen, M. Xue, R. Jiao, Y. Ma, Y. Zhang and Q. Shen, *Organometallics*, 2012, **31**, 6222-6230.
53. M. V. Yakovenko, A. A. Trifonov, E. Kirillov, T. Roisnel and J.-F. Carpentier, *Inorg. Chim. Acta*, 2012, **383**, 137-142.
54. Y.-H. Wang, D. Xiang, R. Ren, J. Luo, W.-L. Sun and Z.-Q. Shen, *Chinese J. Polym. Sci.*, 2014, **32**, 1500-1506.
55. I. Palard, M. Schappacher, A. Soum and S. M. Guillaume, *Polym. Int.*, 2006, **55**, 1132-1137.
56. K. Izod, W. Clegg and S. T. Liddle, *Organometallics*, 2000, **19**, 3640-3643.
57. S. Harder, *Angew. Chem. Int. Ed.*, 2004, **43**, 2714-2718.
58. M. G. Cushion and P. Mountford, *Chem. Commun.*, 2011, **47**, 2276–2278.
59. Y. Sarazin, V. Poirier, T. Roisnel and J.-F. Carpentier, *Eur. J. Inorg. Chem.*, 2010, 3423-3428.
60. L. Clark, M. G. Cushion, H. D. Dyer, A. D. Schwarz, R. Duchateau and P. Mountford, *Chem. Commun.*, 2010, **46**, 273-275.
61. D. Robert, M. Kondracka and J. Okuda, *Dalton Trans.*, 2008, 2667–2669.
62. T. Arliguie, L. Belkhiri, S.-E. Bouaoud, P. Thuéry, C. Villiers, A. Boucekkine and M. Ephritikhine, *Inorg. Chem.*, 2009, **48**, 221-230.
63. M. Visseaux, M. Mainil, M. Terrier, A. Mortreux, P. Roussel, T. Mathivet and M. Destarac, *Dalton Trans.*, 2008, 4558-4561.

64. S. Marks, M. Kuzdrowska, P. W. Roesky, L. Annunziata, S. M. Guillaume and L. Maron, *ChemPlusChem*, 2012, **77**, 350 - 353.
65. M. Kuzdrowska, L. Annunziata, S. Marks, M. Schmid, C. G. Jaffredo, P. W. Roesky, S. M. Guillaume and L. Maron, *Dalton Trans.*, 2013, **42**, 9352-9360.
66. R. A. Collins, J. Unruangsri and P. Mountford, *Dalton Trans.*, 2013, **42**, 759–769.
67. J. Unruangsri, D. Phil Thesis, University of Oxford, 2014.
68. T. J. Marks and J. R. Kolb, *Chem. Rev.*, 1977, **77**, 263.
69. M. Ephritikhine, *Chem. Rev.*, 1997, **97**, 2193-2242.
70. F. Jaroschik, F. Bonnet, X.-F. Le Goff, L. Ricard, F. Nief and M. Visseaux, *Dalton Trans.*, 2010, 6761–6766.
71. J. Jenter, P. W. Roesky, N. Ajellal, S. M. Guillaume, N. Susperregui and L. Maron, *Chem. Eur. J.*, 2010, **16**, 4629-4638.
72. N. Barros, P. Mountford, S. M. Guillaume and L. Maron, *Chem. Eur. J.*, 2008, **14**, 5507-5518.
73. I. Palard, A. Soum and S. M. Guillaume, *Chem. Eur. J.*, 2004, **10**, 4054-4062.
74. N. Miyaura and A. Suzuki, *Chem. Rev.*, 1995, **95**, 2457-2483.
75. N. Miyaura, Y. Yamamoto, R. H. Crabtree and D. M. P. Mingos, Elsevier, Oxford, 2007, pp. 145-244.
76. S. Darses and J.-P. Genet, *Chem. Rev.*, 2008, **108**, 288-325.
77. J. A. Ewen and M. J. Elder, Fina Technology, Inc., EP 426637, USA, 1991.
78. X. Yang, C. L. Stern and T. J. Marks, *J. Am. Chem. Soc.*, 1991, **113**, 3623-3625.
79. A. Kanazawa, S. Kanaoka and S. Aoshima, *J. Am. Chem. Soc.*, 2013, **135**, 9330-9333.
80. G. Xu and T. C. Chung, *Macromolecules*, 1999, **32**, 8689-8692.
81. G. Xu and T. C. Chung, *J. Am. Chem. Soc.*, 1999, **121**, 6763-6764.
82. T. C. Chung, G. Xu, Y. Lu and Y. Hu, *Macromolecules*, 2001, **34**, 8040-8050.
83. T. C. Chung, *Prog. Polym. Sci.*, 2002, **27**, 39-85.
84. W. Lin, J. Dong and T. C. M. Chung, *Macromolecules*, 2008, **41**, 8452-8457.
85. W. Lin, H. Niu, T. C. M. Chung and J.-Y. Dong, *J. Polym. Sci. A: Polym. Chem.*, 2010, **48**, 3534-3541.
86. T. C. M. Chung, *Macromolecules*, 2013, **46**, 6671-6698.
87. S. B. Amin and T. J. Marks, *Angew. Chem. Int. Ed.*, 2008, **47**, 2006-2025.

88. G. Wu, W. Sun and Z. Shen, *React. Func. Polyms.*, 2008, **68**, 822-830.
89. J. Unruangsri, *D. Phil Thesis*, *University of Oxford*, 2014.
90. Y. Liu, M. Nishiura, Y. Wang and Z. Hou, *J. Am. Chem. Soc.*, 2006, **128**, 5592-5593.
91. V. C. Gibson, S. K. Spitzmesser, A. J. P. White and D. J. Williams, *Dalton Trans.*, 2003, 2718-2727.
92. J. Zou, D. J. Berg, D. Stuart, R. McDonald and B. Twamley, *Organometallics*, 2011, **30**, 4958-4967.
93. D. A. Fletcher, R. F. McMeeking and D. Parkin, *J. Chem. Inf. Comput. Sci.*, 1996, **36**, 746.
94. A. Bondi, *J. Phys. Chem.*, 1964, **68**, 441-451.
95. M. Mantina, A. C. Chamberlin, R. Valero, C. J. Cramer and D. G. Truhlar, *J. Phys. Chem. A.*, 2009, **113**, 5806-5812.
96. M. H. Chisholm, J. C. Gallucci and K. Phomphrai, *Inorg. Chem.*, 2005, **44**, 8004-8010.
97. H. Ma and J. Okuda, *Macromolecules*, 2005, **38**, 2665-2673.
98. M. H. Chisholm, K. Choojun, J. C. Gallucci and P. M. Wambua, *Chem. Sci.*, 2012, **3**, 3445-3457.
99. G. M. Whitesides and J. D. Roberts, *J. Am. Chem. Soc.*, 1965, **87**, 4878-4888.
100. F. A. Cotton and G. Wilkinson, *Advanced Inorganic Chemistry*, 5th edn., John Wiley & Sons, Inc., 1988.
101. T. J. Marks and L. A. Shimp, *J. Am. Chem. Soc.*, 1972, **94**, 1542-1550.
102. H. Beall and C. H. Bushweller, *Chem. Rev.*, 1973, **73**, 465-486.
103. J. A. Pople, *Mol. Phys.*, 1958, **1**, 168-174.
104. H. G. Hertz, *Prog. Nuc. Mag. Res. Sp.*, 1967, **3**, 159-230.
105. T. J. Marks and G. W. Grynkewich, *Inorg. Chem.*, 1976, **15**, 1302.
106. M. Bremer, H. Nöth and M. Warchhold, *Eur. J. Inorg. Chem.*, 2003, **2003**, 111-119.
107. G. Soloveichik, J.-H. Her, P. W. Stephens, Y. Gao, J. Rijssenbeek, M. Andrus and J. C. Zhao, *Inorg. Chem.*, 2008, **47**, 4290-4298.
108. M. Bremer, G. Linti, H. Nöth, M. Thomann-Albach and G. E. W. J. Wagner, *Z. Anorg. Allg. Chem.*, 2005, **631**, 683-697.
109. K. O. Saliu, G. H. Maunder, M. J. Ferguson, A. Sella and J. Takats, *Inorg. Chim. Acta*, 2009, **362**, 4616-4622.

110. M. R. Bürgstein, H. Berberich and P. W. Roesky, *Chem. Eur. J.*, 2001, **7**, 3078-3085.

111. M. R. Crimmin, A. G. M. Barrett, M. S. Hill and P. A. Procopiou, *Org. Lett.*, 2007, **9**, 331-333.

112. B. M. Day, W. Knowelden and M. P. Coles, *Dalton Trans.*, 2012, **41**, 10930-10933.

113. Y. Huang, W.-C. Hung, M.-Y. Liao, T.-E. Tsai, Y.-L. Peng and C.-C. Lin, *J. Polym. Sci. A: Polym. Chem.*, 2009, **47**, 2318-2329.

114. F. Drouin, P. O. Oguadinma, T. J. J. Whitehorne, R. E. Prud'homme and F. Schaper, *Organometallics*, 2010, **29**, 2139-2147.

115. Z. Zhong, P. J. Dijkstra and J. Feijen, *J. Am. Chem. Soc.*, 2003, **125**, 11291-11298.

116. M. P. Blake, A. D. Schwarz and P. Mountford, *Organometallics*, 2011, **30**, 1202-1214.

117. P. I. Binda and E. E. Delbridge, *Dalton Trans.*, 2007, 4685-4692.

118. S. D. Bennett, B. A. Core, M. P. Blake, S. J. A. Pope, P. Mountford and B. D. Ward, *Dalton Trans.*, 2014, **43**, 5871-5885.

119. Z. Mou, B. Liu, X. Liu, H. Xie, W. Rong, L. Li, S. Li and D. Cui, *Macromolecules*, 2014, **47**, 2233-2241.

120. M. Honrado, A. Otero, J. Fernández-Baeza, L. F. Sánchez-Barba, A. Garcés, A. Lara-Sánchez and A. M. Rodríguez, *Organometallics*, 2014, **33**, 1859-1866.

121. M. Honrado, A. Otero, J. Fernández-Baeza, L. F. Sánchez-Barba, A. Lara-Sánchez, J. Tejeda, M. P. Carrión, J. Martínez-Ferrer, A. Garcés and A. M. Rodríguez, *Organometallics*, 2013, **32**, 3437-3440.

122. A. Otero, J. Fernández-Baeza, L. F. Sánchez-Barba, J. Tejeda, M. Honrado, A. Garcés, A. Lara-Sánchez and A. M. Rodríguez, *Organometallics*, 2012, **31**, 4191-4202.

123. C. Alonso-Moreno, A. Garcés, L. F. Sánchez-Barba, M. Fajardo, J. Fernández-Baeza, A. Otero, A. Lara-Sánchez, A. Antiñolo, L. Broomfield, M. I. López-Solera and A. M. Rodríguez, *Organometallics*, 2008, **27**, 1310-1321.

124. H. Nöth and H. Vahrenkamp, *Chem. Ber.*, 1966, **99**, 1049-1067.

125. C. D. Good and D. M. Ritter, *J. Am. Chem. Soc.*, 1962, **84**, 1162-1166.

126. H.-J. Chuang, H.-L. Chen, J.-L. Ye, Z.-Y. Chen, P.-L. Huang, T.-T. Liao, T.-E. Tsai and C.-C. Lin, *J. Polym. Sci. A: Polym. Chem.*, 2013, **51**, 696-707.
127. A. Garcés, L. F. Sánchez-Barba, J. Fernández-Baeza, A. Otero, M. Honrado, A. Lara-Sánchez and A. M. Rodríguez, *Inorg. Chem.*, 2013, **52**, 12691-12701.
128. W. Yi and H. Ma, *Inorg. Chem.*, 2013, **52**, 11821-11835.

Chapter Three

$CzOx^{Me2}$-supported calcium, strontium, yttrium, lanthanum and samarium complexes for the ROP of *rac*-, *L*- and *meso*-LA and their mechanistic studies

3.1 Overview

This Chapter will describe detailed investigations into the living and immortal ROP of *rac*-, *L*- and *meso*-LA using calcium, strontium, yttrium, lanthanum and samarium catalysts supported by the carbazole-bis(oxazoline) ligand, $CzOx^{Me_2}$. A comparative overview of the polymerisation results of the yttrium complex $Y(CzOx^{Me_2})(BH_4)_2(THF)$ (**16**) synthesised by L. Budden, a Part II student in the Mountford Group, will be provided. A summary and discussion of the results will be presented, alongside mechanistic studies conducted with deuterium labelling experiments. Twenty new complexes will be presented, eight of which are *in situ* generated, along with four X-ray crystallographic structures.

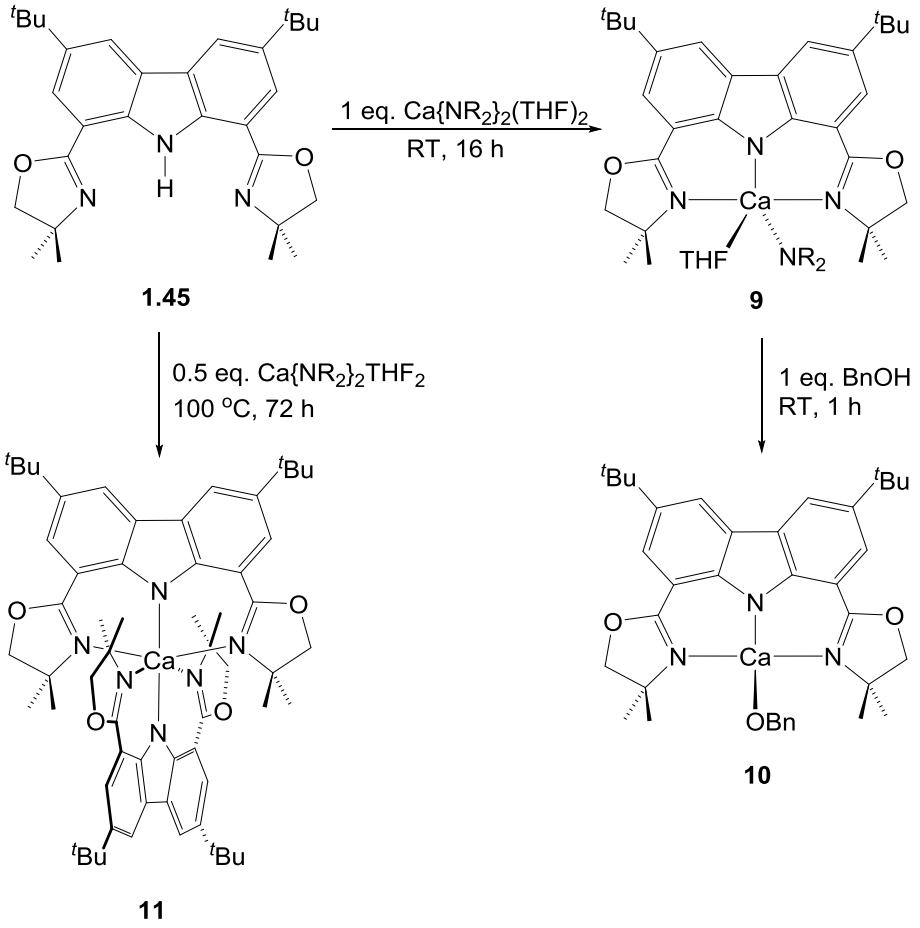
3.2 Synthesis and characterisation of $CzOx^{Me_2}$-supported calcium and strontium complexes

3.2.1 Synthesis and characterisation of $CzOx^{Me_2}$-supported calcium amide, alkoxide and homoleptic complexes

Following the successful results obtained with magnesium complexes **1**-**3**, **6** and **7**, in Chapter 2, heavier alkaline earth analogues using calcium and strontium were synthesised to investigate the behaviour of the catalysts on descending Group 2. Due to increased reactivity, a common problem encountered when using heavier alkaline earth metals to generate heteroleptic species is their redistribution *via* the Schlenk equilibrium to homoleptic species,[1] therefore particular attention was focussed on monitoring the propensity for the complexes synthesised to undergo this reaction. Scheme 3.1 details the synthesis of new complexes **9**-**11**, synthesised *via* protonolysis reactions with the appropriate metal precursor.

The protonolysis reaction of 1 equivalent of **1.45** with 1 equivalent of $Ca\{N(SiMe_3)_2\}_2(THF)_2$ in toluene at room temperature afforded $Ca(CzOx^{Me_2})\{N(SiMe_3)_2\}(THF)$ (**9**) as a yellow powder in 68% yield following a cold pentane wash to remove liberated $HN(SiMe_3)_2$, which was not readily removed under reduced pressure. Unlike the magnesium analogue, $Mg(CzOx^{Me_2})\{N(SiMe_3)_2\}$ (**1**), resonances corresponding to the methyl substituents and methylene protons on the oxazoline rings of the ligand appeared as sharp singlets in the ^1H NMR spectrum at

1.51 and 3.69 ppm, respectively. Complex **9** was characterised fully with ^{1}H NMR, ^{13}C{^{1}H} NMR and IR spectroscopy, mass spectrometry and elemental analysis. Diffraction-quality crystals were grown from a saturated THF solution at room temperature, and the complex was structurally authenticated with X-ray crystallography (Figure 3.1). Selected bond lengths and angles are given in Table 3.1.



Scheme 3.1. Synthesis of calcium complexes **9-11** *via* protonolysis reactions (R = $SiMe_3$).

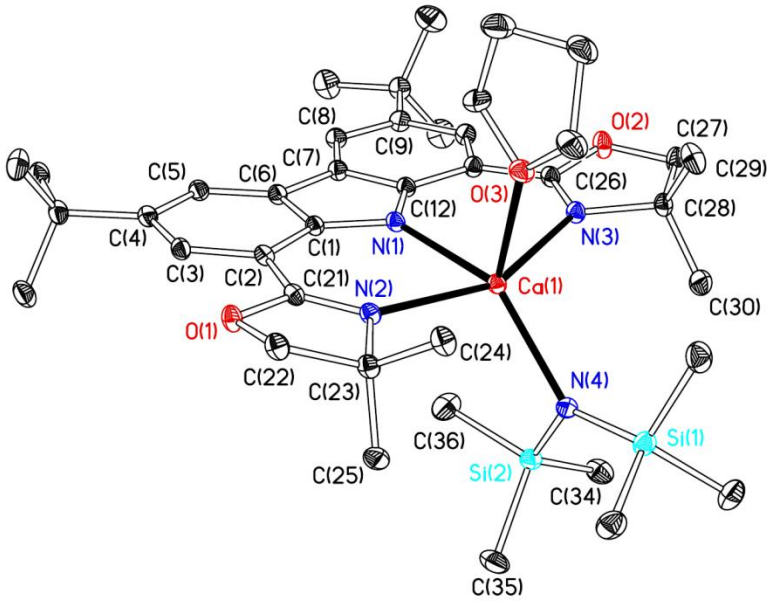


Figure 3.1. Displacement ellipsoid plot of Ca(CzOx^{Me_2}){N(SiMe$_3$)$_2$}(THF) (**9**) (20% probability level). H atoms and a THF molecule of crystallisation omitted for clarity.

Table 3.1. Selected bond distances (Å) and angles (°) for Ca(CzOx^{Me_2}){N(SiMe$_3$)$_2$}(THF) (**9**).

Ca(1)-N(1)	2.400(2)	Ca(1)-N(2)	2.4716(19)
Ca(1)-N(3)	2.506(2)	Ca(1)-N(4)	2.371(2)
Ca(1)-O(3)	2.4028(18)	N(4)-Si(1)	1.695(2)
Ca(1)···H(361)	2.76(5)	Ca(1)···H(362)	2.78(5)
Si(1)-C(31)	1.887(3)	Si(1)-C(32)	1.876(3)
Si(1)-C(33)	1.886(3)	Si(2)-C(34)	1.884(3)
Si(2)-C(35)	1.886(3)	Si(2)-C(36)	1.877(3)
N(1)-Ca(1)-N(2)	78.39(6)	N(1)-Ca(1)-N(3)	78.80(7)
N(1)-Ca(1)-N(4)	141.59(7)	N(1)-Ca(1)-O(3)	96.37(7)
N(2)-Ca(1)-N(3)	155.47(7)	N(2)-Ca(1)-N(4)	100.10(7)
N(2)-Ca(1)-O(3)	85.99(7)	N(3)-Ca(1)-N(4)	103.36(7)
N(3)-Ca(1)-O(3)	87.67(7)	N(4)-Ca(1)-O(3)	121.94(7)
Ca(1)-N(4)-Si(1)	130.80(12)	Ca(1)-N(4)-Si(2)	105.96(10)
Ca(1)···H(361)-C(36)	92(3)	Ca(1)···H(362)-C(36)	94(3)

Ca(CzOx^{Me2}){N(SiMe$_3$)$_2$}(THF) (**9**) is five-coordinate in which the Ca coordinates to three N donors of the CzOx^{Me2} ligand, the N donor of the N(SiMe$_3$)$_2$ ligand and the O donor of a THF ligand. The coordination geometry of **9** lies between a distorted trigonal bipyramidal in which N(2) and N(3) occupy the axial positions, and a distorted square pyramidal, in which O(2) occupies the axial position. In an ideal square pyramid, the bond angles of N(2)-Ca(1)-N(3) and N(1)-Ca(1)-N(4) would be 180°; however, they are considerably distorted from linearity (155.47(7)° and 141.59(7)°, respectively) due to the fixed ligand. Furthermore, consideration of the structure as trigonal bipyramidal reveals appreciable distortion in the bond angles of the equatorial substituents from the ideal. This deviation from either structure can be attributed to the steric bulk of the N(SiMe$_3$)$_2$ group and the rigidity of the ligand. An index of the degree of trigonality in a five coordinate system has been defined by Addison and coworkers as $\tau = (\beta-\alpha)/60$, in which β represents the largest angle within the coordination sphere and α the second largest.[2] The apical donor for a square pyramidal geometry is selected on the basis that it does not define either α or β, in this case O(3). In an ideal tetragonal, i.e. square pyramidal structure, $\alpha = \beta = 180°$, therefore τ is equal to zero, whereas in a trigonal bipyramidal conformation, $\alpha = 120°$, thus τ becomes unity. For Ca(CzOx^{Me2}){N(SiMe$_3$)$_2$}(THF) (**9**), $\tau = 0.23$, indicating the complex tends towards a square pyramidal structure. Unlike the magnesium complexes Mg(CzOx^{Me2}){N(SiMe$_3$)$_2$} (**1**) and Mg(CzOx^{Me2})(Bu) (**3**) in which the metal is considerably displaced, the Ca is situated closer to the plane of the ligand, in which the dihedral angles of C(1)-C(2)-C(21)-N(2) and C(12)-C(11)-C(26)-N(3) are -6.04° and 8.24°, respectively. All Ca-N=C bond lengths were found to lie within the expected range of 2.28-2.78 Å.[3]

The decreased bond angle between Ca(1)-N(4)-Si(2) (105.96(10)°) compared to Ca(1)-N(4)-Si(1) (130.80(12)°) place H(361) and H(362) in close proximity to the Ca centre, which may be a caused by a displacement of the N(SiMe$_3$)$_2$ group to accommodate the THF molecule, resulting in a distortion of the bond angles. The Ca(1)···H(361) and Ca(1)···H(362) bond lengths of 2.76(5) Å and 2.78(5) Å, respectively, are found to be shorter than the sum of the van der Waals radii of 3.41 Å.[4, 5] This may indicate the presence of a γ-agostic C-H or a β-Si-C interaction,[6, 7] or may be attributed to the steric hindrance between the N(SiMe$_3$)$_2$ group and the THF

molecule. Although rare, γ-agostic C-H interactions have been observed previously in rare earth complexes including $Cp^*_2Y\{N(SiMe_3)_2\}$, $Cp^*_2Y\{CH(SiMe_3)_2\}$ and $U\{CH(SiMe_3)_2\}_3$,[8, 9] and in Group 4 metallocenium cationic complexes, such as $[Cp_2TiCH_2CHMe(SiMe_3)]^+$ and [*rac*-Me_2Si(1-Ind)$_2ZrCH_2SiMe_3$]$^+$;[10, 11] however, in this instance the Ca(1)···H bond lengths (*ca*. 2.77 Å) are comparatively longer than the complexes in which γ-agostic C-H interactions have been confirmed (*ca*. 2.42-2.62 Å).

The successful synthesis of $Ca(CzOx^{Me_2})\{N(SiMe_3)_2\}(THF)$ (**9**) provided an intermediate for the synthesis of the desired target complex $Ca(CzOx^{Me_2})(OBn)$ (**10**). Synthesis of **10** was considerably more straightforward than the synthesis of the magnesium analogue $Mg(CzOx^{Me_2})(OBn)$ (**2**): treatment of **9** in toluene with benzyl alcohol at room temperature afforded $Ca(CzOx^{Me_2})(OBn)$ (**10**) as a yellow powder in 38% yield, following a pentane wash to remove side-products including liberated $HN(SiMe_3)_2$ and protioligand formed from the protonolyis of **9** to liberate **1.45** and $Ca(OBn)_2$. Unlike **9**, **10** was not sufficiently soluble in C_6D_6 to allow characterisation by $^{13}C\{^1H\}$ NMR spectroscopy; however it was sufficiently soluble to obtain a ^1H NMR spectrum in C_6D_6, which confirmed the lack of THF molecules present in the final compound. Full ^1H and $^{13}C\{^1H\}$ NMR characterisation was conducted in THF-d_8. In light of the unexpectedly low coordination number of the calcium centre in **10**, NMR investigations were undertaken in order to determine the precise bonding mode of the species in solution, *vide infra*. Despite repeated attempts, it was not possible to obtain crystals of **10** for X-ray crystallography.

Although complexes **9** and **10** remained stable in solution at room temperature for several days without evidence of redistribution to form the homoleptic species $Ca(CzOx^{Me_2})_2$ (**11**), efforts were undertaken to independently synthesise **11** in order to verify its possible synthesis and allow future synthetic routes using calcium precursors to be monitored for the presence of the homoleptic species. Complex **11** was synthesised through the addition of 1 equivalent of $Ca\{N(SiMe_3)_2\}_2(THF)_2$ to 2 equivalents of **1.45** in toluene; however, after reaction at room temperature only the heteroleptic complex **9** was obtained alongside 1 equivalent of unreacted protioligand. The reaction mixture was heated to 100 °C for 3 days and subsequent purification to isolate the desired product from the heteroleptic complex **9** afforded **11** as an air- and

moisture-stable yellow-green powder in 28% yield. Complex **11** was found to be insoluble in benzene, THF and pyridine, but was sparingly soluble in CH_2Cl_2, and was fully characterised by ^{1}H and $^{13}C\{^{1}H\}$ NMR spectrsocopy, IR spectroscopy, mass spectrometry and elemental analysis. The slow evaporation of a saturated CH_2Cl_2 solution afforded **11** as single crystals which were characterised using X-ray crystallography (Figure 3.2). Selected bond lengths and angles are given in Table 3.2.

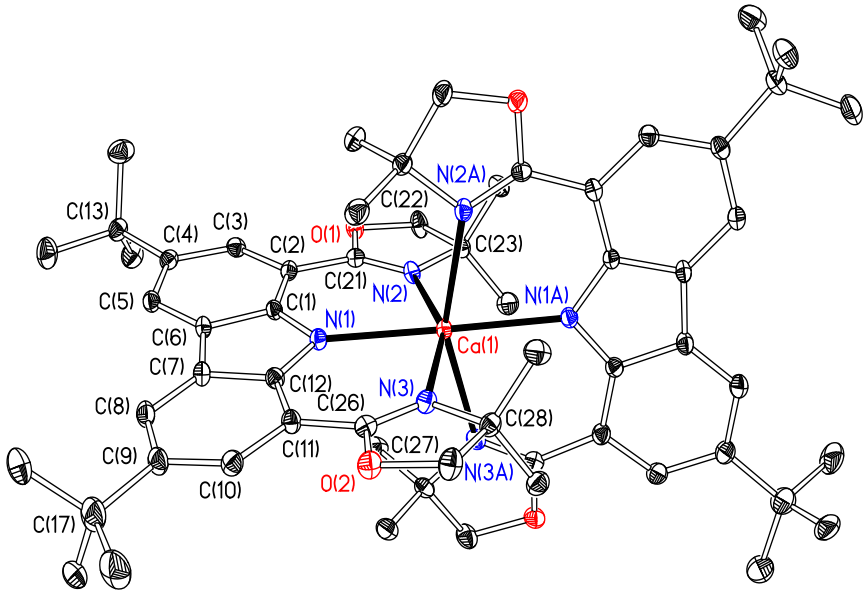


Figure 3.2. Displacement ellipsoid plot of $Ca(CzOx^{Me2})_2$ (**11**) (20% probability level). H atoms, minor disorder, and a CH_2Cl_2 molecule of crystallisation omitted. Atoms carrying the suffix 'A' are related to their counterparts by the symmetry operator 1-*x*, 2-*y*, *z*.

Table 3.2. Selected bond distances (Å) and angles (°) for $Ca(CzOx^{Me2})_2$ (**11**).

Ca(1)-N(1)	2.411(2)	Ca(1)-N(2)	2.484(2)
Ca(1)-N(3)	2.475(3)		
N(1)-Ca(1)-N(2)	78.53(8)	N(1)-Ca(1)-N(3)	78.64(8)
N(1)-Ca(1)-N(1A)	179.09(12)	N(1)-Ca(1)-N(2A)	100.85(8)
N(1)-Ca(1)-N(3A)	102.00(8)	N(2)-Ca(1)-N(3)	157.06(8)
N(2)-Ca(1)-N(1A)	100.85(8)	N(2)-Ca(1)-N(2A)	96.34(11)
N(2)-Ca(1)-N(3A)	90.12(8)	N(3)-Ca(1)-N(1A)	102.00(8)
N(3)-Ca(1)-N(2A)	90.12(8)	N(3)-Ca(1)-N(3A)	92.41(12)

$Ca(CzOx^{Me_2})_2$ (**11**) is six coordinate in which the Ca centre coordinates to the three N donors on each $CzOx^{Me_2}$ ligand, adopting a distorted octahedral geometry in which the ligands occupy a *mer* configuration. The Ca(1)-N(1) bond length of 2.411(2) Å is considerably shorter than either Ca(1)-N(2) or Ca(1)-N(3) (2.484(2) and 2.475(3) Å), which is likely a product of the rigidity of the carbazole backbone of the ligand positioning the N donors on the oxazoline rings at a greater distance from the calcium centre, although all Ca-N=C bond lengths fall within the expected range of 2.28-2.78 Å.[3] The N(1) and N(1A) atoms occupy axial positions in the octahedral geometry, with an almost linear N(1)-Ca(1)-N(1A) bond angle of 179.09(12)°. The equatorial positions are occupied by N(2), N(2A), N(3) and N(3A), which are again distorted from ideal 90° bond angles by the inflexibility of the oxazoline rings connected to the carbazole backbone. The dihedral angles C(1)-C(2)-C(21)-N(2) and C(12)-C(11)-C(26)-N(3) are -5.02° and -9.47°, respectively, confirming the planarity of the ligand. The effective encompassing of the reactive calcium centre by the two $CzOx^{Me_2}$ ligands accounts for the air- and moisture-stability of this complex.

3.2.2 Diffusion measurement by NMR Spectroscopy

In collaboration with Dr. Nick Rees at the University of Oxford Chemistry Department, research was undertaken investigating the diffusion coefficient, *D*, of several complexes in solution using a technique known as Diffusion Ordered Spectroscopy (DOSY) or Pulsed Gradient Spin Echo (PGSE) NMR spectroscopy. For a detailed discussion of DOSY and the determination of the diffusion coefficient, *D*, the reader is directed to the relevant literature.[12-14] Assuming a spherical shape of the molecule in solution, *D* is related to the inverse cube root of the volume using the Stokes-Einstein equation (Equation 3.1), where *D* = diffusion coefficient, k_B = Boltzmann's constant, *T* = temperature, η = solvent viscosity, r_H = hydrodynamic radius of molecule and *V* = molecular volume.

$$D = \frac{k_B T}{6\pi\eta r_H} = \frac{k_B T}{6\pi\eta\left(\frac{3V}{4\pi}\right)^{1/3}}$$

Equation 3.1

DOSY NMR has been successfully employed to determine the molecular volume of several metal alkoxide complexes and distinguish between monomeric and dimeric structures.[15, 16] Complexes featuring alkoxide ligands may exist as dimeric species in solution, affecting their behaviour during polymerisation,[17] thus the conformation of Mg(CzOx^{Me_2})(OBn) (**2**) and Ca(CzOx^{Me_2})(OBn) (**10**) in THF were confirmed through the determination of their diffusion coefficients using DOSY NMR spectrsocopy. Samples were prepared as 0.01M THF-d_8 solutions containing HCzOx^{Me_2} (**1.45**) as an internal standard. The diffusion coefficient of Mg(CzOx^{Me_2})(Bu) (**3**) was determined as it is known to be monomeric in the solid state and likely in solution. For comparison, molecular volumes based on crystal structures where available were determined using Accelrys Discovery Studio Visualiser 4.0 based on a solvent accessible surface area using a 1.4 Å probe. These data, along with the diffusion coefficients for compounds **1.45**, **2**, **3** and **10** are summarised in Table 3.3.

Table 3.3. Summary of diffusion coefficients, NMR volumes and X-ray crystallographically determined volumes for HCzOx^{Me_2} (**1.45**) and complexes Mg(CzOx^{Me_2})(OBn) (**2**), Mg(CzOx^{Me_2})(Bu) (**3**) and Ca(CzOx^{Me_2})(OBn) (**10**).

Complex	X-ray volume (Å^3)[a]	NMR Volume (Å^3)[b]	*D* (compound) $\times 10^{-10}$ (m^2 s^{-1})[c]	*D* (**1.45**) $\times 10^{-10}$ (m^2 s^{-1})[c]
1.45	908	706	8.73	-
2	-	1,012	7.69	8.67
3	975	885	8.04	8.73
10	-	1,065	7.56	8.73

[a] Calculated from crystal structure using Accelrys Discovery Studio and 1.4 Å probe. [b] Molecular volume calculated from DOSY NMR. [c] Diffusion constant.

The diffusion coefficient of a molecule is dependent on its size and shape; once determined from the Stokes-Einstein equation, the hydrodynamic radius (r_H) may be determined. Through the comparison of known monomeric compounds to species of unknown aggregation, the ratio of the diffusion coefficients, and thus hydrodynamic

radii, may be determined. In 1965, Tanner and coworkers indicated that a dimer should have a diffusion coefficient of 72-75% of that of the corresponding monomer.[13] **3** was assumed to have a similar diffusion coefficient to the monomeric forms of **2** and **10**. The ratios of diffusion coefficients for **2**:**3** and **10**:**3** are 0.87 and 0.83, respectively, indicating that both **2** and **10** are monomeric in a 0.01 M THF solution.

The error associated with *D* is usually lower than 5%,[18] therefore once the three other parameters, *T*, η and *c*, are determined, an accurate value of *r* may be obtained. Accurate values for both *T* and η can be measured; however, for small molecules whose radius (r_H) approaches that of the solvent in which *D* is calculated (r_{solv}), *c* differs significantly between 4 (slip-boundary conditions) and 6 (stick-boundary conditions).[19] An expression of c as a function of r_{solv}/r_H was derived by Wirtz,[20, 21] who posited that a value of 6 is valid once r_H is greater than 40 Å, and subsequently improved upon by Chen,[22] who predicted that *c* is equal to 6 when $r_H \approx 15$ Å. Considering the van der Waals radius of THF is 2.596 Å,[23] the classical Stokes-Einstein equation is only accurate for molecules with a radius which is approximately five times larger than that of the solvent. Macchioni and coworkers estimated the error on the derived r_H values arising from the classical Stokes-Einstein equation to be between 9 and 32%.[18] Furthermore, another correction factor (f_s) must be considered for molecules which are either prolate or oblate ellipsoids.[24] A modified Stokes-Einstein equation which takes the relative radii of the solute to the solvent and molecular shape was proposed by Macchioni *et al*. in 2008 (Equation 3.2).[25]

$$D = \frac{k_B T}{c(r_{solv}, r_H) f_s(a, b) \pi \eta r_H}$$

Equation 3.2

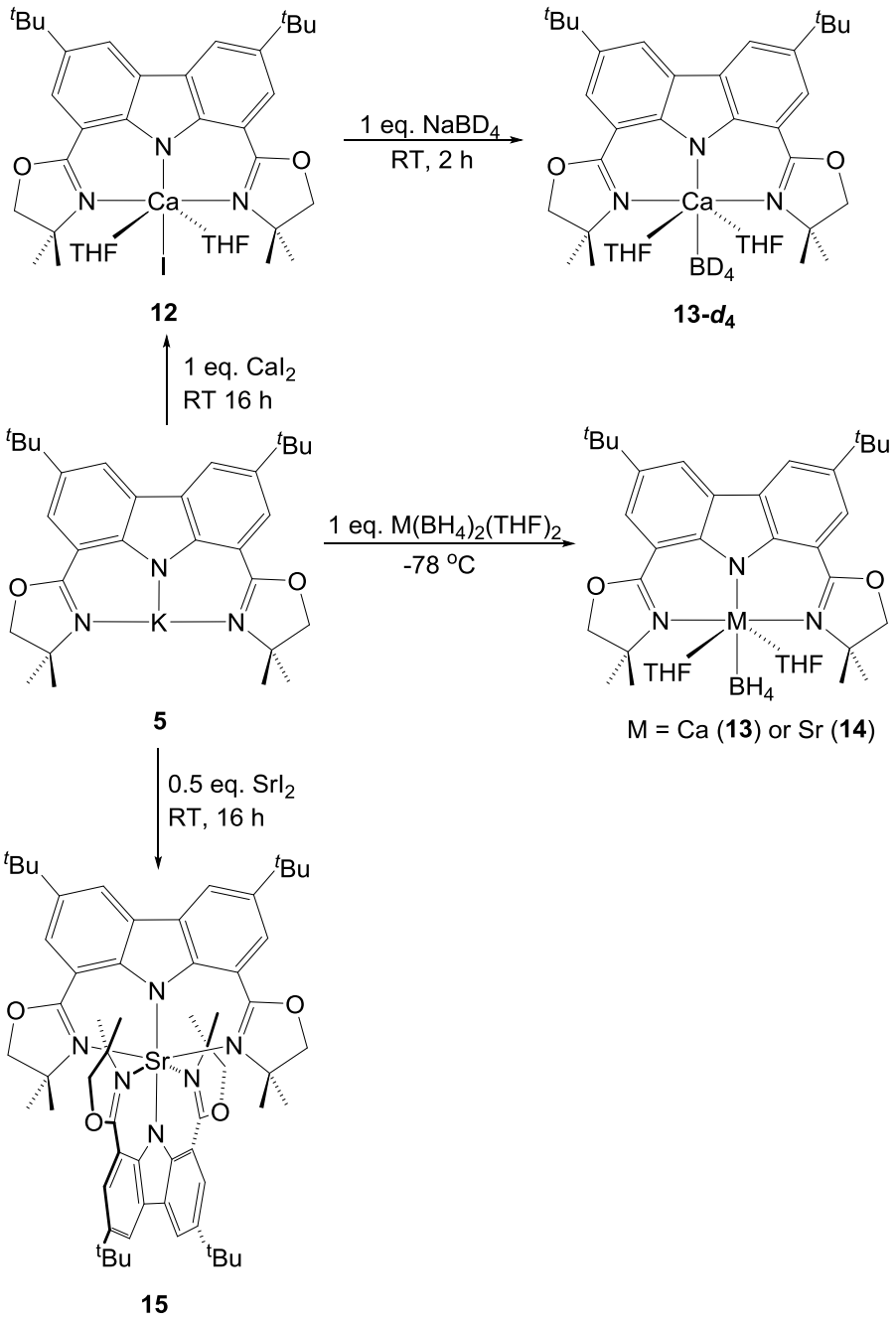
3.2.3 Synthesis and characterisation of $CzOx^{Me_2}$-supported calcium and strontium halide, borohydride and homoleptic complexes

In a similar fashion to the preparation of the magnesium analogues, calcium and strontium complexes **12-15** were accessed *via* a salt metathesis reaction between $K(CzOx^{Me_2})$ (**5**) and 1 equivalent of the appropriate metal precursor (Scheme 3.2). In lieu of protonolysis with a corresponding Grignard reagent, the reaction of 1

equivalent of **5** with 1 equivalent of CaI_2 previously stirred in THF for 16 h to aid reactivity, afforded $Ca(CzOx^{Me2})I(THF)_2$ (**12**) as a yellow powder in 69% yield. As with **10**, complex **12** was similarly insoluble in benzene, resulting in full NMR characterisation in THF-d_8; however, a ^{1}H NMR spectrum in pyridine-d_5 showed there were 2 molecules of coordinated THF in **12**.

Single crystals of **12** were grown from a saturated THF solution; however, the diffraction quality was not sufficient to allow for complete data to be obtained. Although direct comparison of bond lengths or angles with other complexes within the series was not possible, nonetheless, the monomeric conformation of **12** and the coordination of 2 molecules of THF through the O donor could be confirmed. As an alternative route to the synthesis of **10**, **12** was treated with 1 equivalent of NaOBn or KOBn, resulting in formation of **10** alongside decomposition products including $HCzOx^{Me2}$ (**1.45**). Unfortunately, attempts to purify the target complex were unsuccessful.

The analogous treatment of 1 equivalent of SrI_2 with **5** in THF at -78 °C followed by immediate removal of the solvent resulted in the rapid formation of the desired complex $Sr(CzOx^{Me2})I(THF)_2$. However, a secondary species was concurrently produced, postulated to be $Sr(CzOx^{Me2})_2$ (**15**) which may be formed following the redistribution of 2 equivalents of $Sr(CzOx^{Me2})I(THF)_2$ to **15** and SrI_2. To independently verify the nature of secondary species, **15** was synthesised *via* the salt metathesis reaction of 1 equivalent of **5** with 0.5 equivalents of SrI_2 in THF at room temperature, to afford a yellow powder in 41% yield. The product was fully characterised and the resonances observed in the ^{1}H NMR spectrum in CD_2Cl_2 were found to correlate with the unknown species formed during the attempted synthesis of $Sr(CzOx^{Me2})I(THF)_2$. In view of the instability of the heteroleptic complex $Sr(CzOx^{Me2})I(THF)_2$, no further attempts were made to isolate it.



Scheme 3.2. Synthesis of calcium and strontium complexes **12-15** *via* salt metathesis reactions.

Borohydride complexes $Ca(CzOx^{Me_2})(BH_4)(THF)_2$ (**13**) and $Sr(CzOx^{Me_2})(BH_4)(THF)_2$ (**14**) were synthesised following reaction with either commercially available $Ca(BH_4)_2(THF)_2$ or $Sr(BH_4)_2(THF)_2$, synthesised from the reaction of $Sr(O^iPr)_2$ and $BH_3(THF)$. Following reaction in THF at room temperature

for 16 hours and purification, complex **13** was obtained as an orange-yellow powder in 61% yield. Analysis of the ^{1}H NMR spectrum of **13** in C_6D_6 revealed the complex to have 0 or 2 coordinated THF molecules, depending on the duration of exposure of **13** to reduced pressure during purification. Several drops of THF-d_8 were added to a C_6D_6 solution of THF-free Ca(CzOx^{Me_2})(BH_4), resulting in the formation of an identical ^{1}H NMR spectrum to Ca(CzOx^{Me_2})(BH_4)(THF)$_2$ (**13**) in C_6D_6. The lack of coordinated THF molecules suggests that Ca(CzOx^{Me_2})(BH_4) may form a dimeric or polymeric structure in order to satisfy the coordination sphere of the metal, in which the borohydride ligands bridge between metal centres. Insight into the specific bonding mode of **13** was provided with IR spectroscopy, *vide infra*.

The synthesis of Sr(CzOx^{Me_2})(BH_4)(THF)$_2$ (**14**) was problematic due to the relative instability of the complex to the calcium congener: following a salt metathesis reaction between Sr(BH_4)$_2$(THF)$_2$ and **5** in THF at -78 °C, the product was extracted into toluene, whereupon the ^{1}H NMR spectrum revealed decomposition to the homoleptic complex **15** and protioligand **1.45**, amongst other unidentified species. The complex was successfully synthesised through extraction of the product in THF at -78 °C and subsequent rapid removal of the solvent under reduced pressure. Complex **14** was fully characterised by ^{1}H, ^{13}C{^{1}H} and ^{11}B NMR spectroscopy, solid state and THF solution IR spectroscopy and mass spectrometry. The bulk purity of the complex was verified through elemental analysis. In order to ascertain the number of THF molecules coordinated to the strontium centre, a ^{1}H NMR spectrum was obtained in C_6D_6, confirming the presence of two coordinated THF molecules. The complex was found to be unstable after being dissolved in a non-donor solvent, and rapidly underwent redistribution to **15**. Whilst its resistance towards redistribution was improved upon by employing a donor solvent such as THF, formation of the homoleptic complex was observed after several hours at room temperature. The marked predilection for redistribution to homoleptic species for Sr^{2+}, compared to Mg^{2+} and Ca^{2+} confirms the increasing reactivity of the metal centre on descent of the group. Unfortunately, single crystals of **14** could not be obtained for X-ray crystallography, due to its short lifespan in solution.

In order to gain a deeper insight into the bonding mode of the borohydride ligands in Ca(CzOx^{Me_2})(BH_4)(THF)$_2$ (**13**) and Sr(CzOx^{Me_2})(BH_4)(THF)$_2$ (**14**), their IR spectra in

the solid state and in THF solution were obtained. The solid state IR spectrum of **13** revealed a single broad absorption centred around 2281 cm^{-1}, whereas **15** showed a comparatively sharp singlet at 2292 cm^{-1} which correlate to either a polymeric structure (Chapter 2, Table 2.1),[26] or indicate multiple coordination geometries for the BH_4 ligand are present in the solid state. A comparison of these spectra to that of $Mg(CzOx^{Me_2})(BH_4)$ (**7**) as a Nujol mull is given in Figure 3.3. It is interesting to note the increase in wavenumber for the ν(B–H) bands with increasing metal size, in addition to a concurrent sharpening of the T_2 band from a broad absorption to a singlet. This can be attributed to the increased ionicity of the M-BH_4 bond, resulting in an increasingly symmetrical boron environment. The presence of coordinated THF molecules in both **13** and **14** suggests that the formation of a dimeric and polymeric structure in the solid state is unlikely given the saturation of the coordination sphere. Unfortunately, distinguishing between polymeric borohydride bonding modes, or the occupation of multiple coordination modes in the solid state with IR spectroscopy remains elusive.

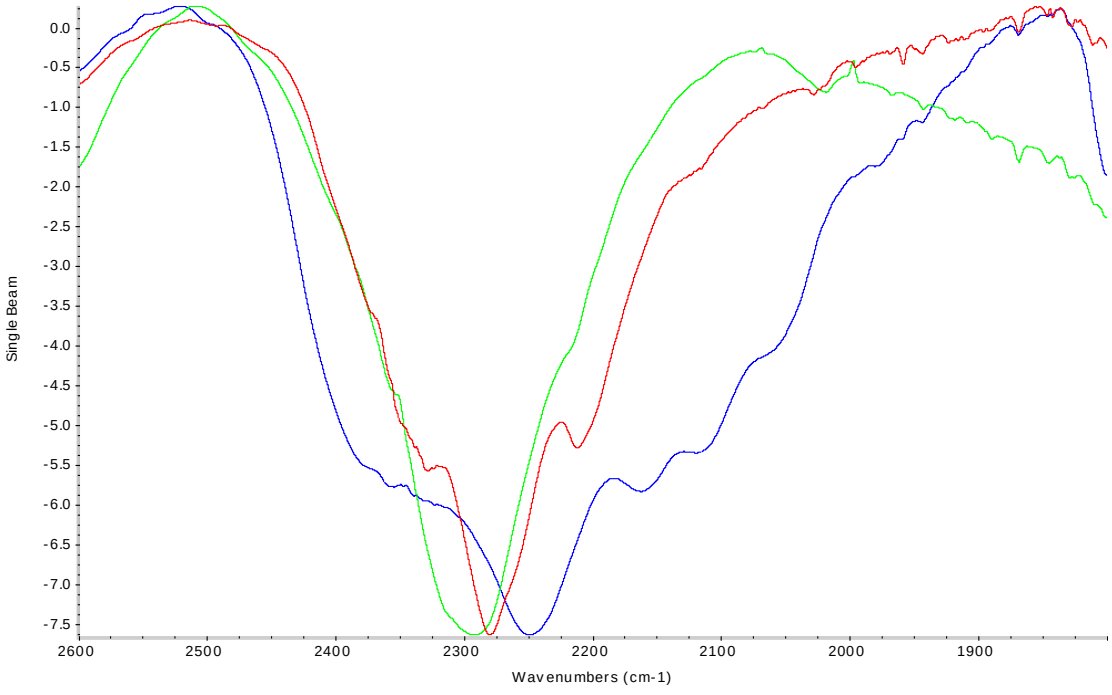


Figure 3.3. Solid IR spectra (Nujol mull) of $Mg(CzOx^{Me_2})(BH_4)$ (**7**) (blue), $Ca(CzOx^{Me_2})(BH_4)(THF)_2$ (**13**) (red) and $Sr(CzOx^{Me_2})(BH_4)(THF)_2$ (**14**) (green).

Analysis of the THF solution IR spectra revealed the borohydride ligands in both Ca(CzOx^{Me2})(BH$_4$)(THF)$_2$ (**13**) and Sr(CzOx^{Me2})(BH$_4$)(THF)$_2$ (**14**) to be tridentate with bands at 2381 cm^{-1} (B–H$_t$), 2258 and 2175 cm^{-1} (B–H$_b$ doublet with 83 cm^{-1} splitting) and 2381 cm^{-1}, (B–H$_t$), 2249 and 2168 cm^{-1} (B–H$_b$ doublet with 81 cm^{-1} splitting). The decrease in frequencies of the ν(B–H$_t$) band with increased frequencies of the ν(B–H$_b$) bands in both **13** and **14** relative to the magnesium analogue **7** can be attributed to the increase in ionicity of the M-BH$_4$ bond with increased metal size, in which the A_1 and E band frequencies converge on the T_2 band found in ionic borohydrides. It is interesting to note the similarity in frequencies observed for complexes **13** and **14** both in the solid state and in THF solution compared to **7**, suggesting there is a larger decrease in covalency between the Mg-BH$_4$ and Ca-BH$_4$ bonds, than between the Ca-BH$_4$ and Sr-BH$_4$ bonds.

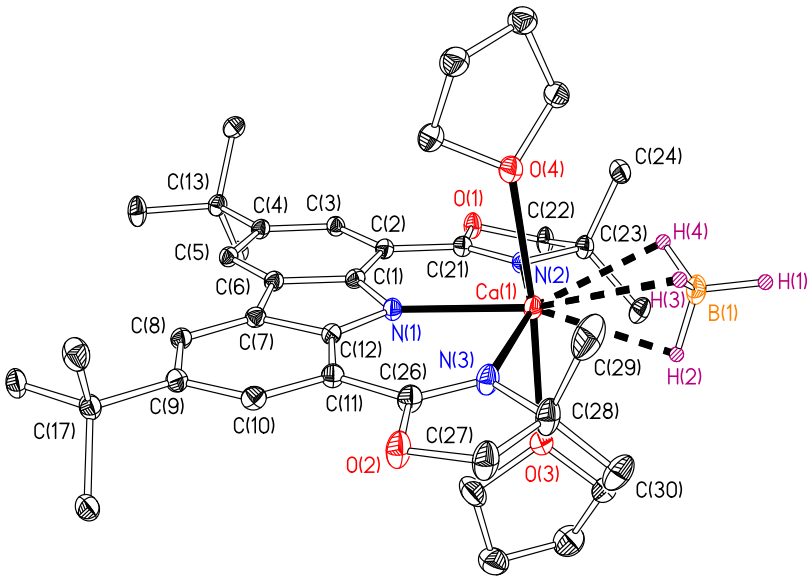


Figure 3.4. Displacement ellipsoid plot of Ca(CzOx^{Me2})(BH$_4$)(THF)$_2$ (**13**) (20% probability level). C-bound H-atoms and THF of crystallisation omitted for clarity.

Table 3.4. Selected bond distances (Å) and angles (°) for $Ca(CzOx^{Me_2})(BH_4)(THF)_2$ (**13**).

Ca(1)-N(1)	2.399(2)	Ca(1)-N(2)	2.522(3)
Ca(1)-N(3)	2.510(4)	Ca(1)-O(3)	2.413(3)
Ca(1)-O(4)	2.417(3)	Ca(1)-H(2)	2.52(5)
Ca(1)-H(3)	2.78(5)	Ca(1)-H(4)	2.46(5)
Ca(1)···B(1)	2.729(5)		
N(1)-Ca(1)-N(2)	79.05(10)	N(1)-Ca(1)-N(3)	79.18(11)
N(1)-Ca(1)-O(3)	90.52(11)	N(1)-Ca(1)-O(4)	84.66(10)
N(1)-Ca(1)···B(1)	174.47(14)	N(2)-Ca(1)-N(3)	156.93(11)
N(2)-Ca(1)-O(3)	88.55(11)	N(2)-Ca(1)-O(4)	91.43(12)
N(2)-Ca(1)···B(1)	100.09(13)	N(3)-Ca(1)-O(3)	84.08(12)
N(3)-Ca(1)-O(4)	91.43(12)	N(3)-Ca(1)···B(1)	102.30(14)
O(3)-Ca(1)-O(4)	173.96(10)	O(3)-Ca(1)···B(1)	94.93(14)
O(4)-Ca(1)···B(1)	89.97(14)	C(1)-C(2)-C(21)	124.3(3)
C(12)-C(11)-C(26)	124.6(3)		

Diffraction-quality crystals of $Ca(CzOx^{Me_2})(BH_4)(THF)_2$ (**13**) were grown from a saturated THF solution and the complex was structurally authenticated with X-ray crystallography (Figure 3.4). **13** is pseudo-six coordinate in which the Ca is coordinated to the three N donors of the $CzOx^{Me_2}$ ligand, a κ^3-bound BH_4 ligand and the O donor of two molecules of THF. The geometry of **13** may be described as octahedral in which bond angles N(1)-Ca(1)···B(1) and O(3)-Ca(1)-O(4) are almost linear (174.47(17)° and 173.96(10)°, respectively), whereas the bond angle N(2)-Ca(1)-N(3) shows the greatest degree of distortion at 156.93(11)° caused by the fixed ligand. Bond lengths Ca(1)-N(1), Ca(1)-N(2) and Ca(1)-N(3) are found to fall within a normal Ca-N=C bond length range of 2.28-2.78 Å.[3]

Compound **13** possesses a κ^3-bound borohydride ligand in the solid state, which is in agreement with the tridentate configuration observed in THF solution *via* IR spectroscopy. The hydrogen atoms were located in the Fourier difference map and refined positionally and isotropically. Other supported calcium complexes featuring a κ^3-bound borohydride ligand in the literature include the $(^{Dipp}NacNac)Ca(BH_4)(THF)_2$

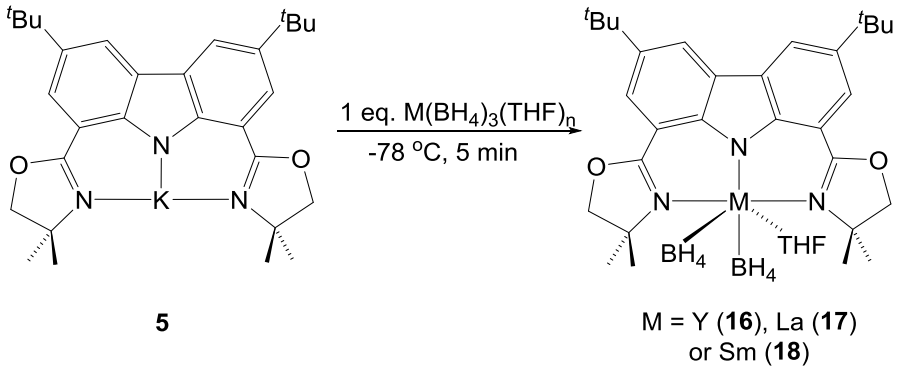
and ($Tp^{tBu,Me}$)Ca(BH_4)(THF) complexes previously synthesised by Mountford *et al.*[27, 28]

In order to verify the mechanism proposed for the ROP of lactide with a calcium borohydride complex was similar to that of magnesium borohydride complex **7**, a deuterium labelled analogue of **13** was synthesised *via* the salt metathesis reaction of 1 equivalent of $NaBD_4$ with **12**. Ca($CzOx^{Me_2}$)(BD_4)$(THF)_2$ (**13-*d*$_4$**) was isolated as a yellow powder and fully characterised. Analysis with ^{2}H NMR spectroscopy in THF confirmed the presence of a broad singlet at 0.2 ppm and with ^{11}B NMR a singlet at -36.5 ppm, both corresponding to the BD_4 group. The THF solution IR spectrum showed a κ^3-bound borodeuteride ligand, with isotropically shifted stretching frequencies of a singlet at 1791 cm^{-1} (B–D_t, ν_D/ν_H = 0.75) and a doublet with 1635 and 1600 (B–D_t, ν_D/ν_H = 0.72 and 0.74, respectively, 35 cm^{-1} splitting).

3.3 Synthesis and characterisation $CzOx^{Me_2}$-supported yttrium, lanthanum and samarium borohydride complexes

The series of catalysts was expanded to include $CzOx^{Me_2}$-supported Group 3 and lanthanide bis(borohydride) complexes. Under direct supervision by the author, complex Y($CzOx^{Me_2}$)$(BH_4)_2$(THF) (**16**) was synthesised by L. Budden, a Part II student in the Mountford Group. $Y(BH_4)_3(THF)_2$ was synthesised *via* an adapted literature procedure.[29] Onwards reaction with 1 equivalent of K($CzOx^{Me_2}$) (**5**) in THF at -78 °C afforded the Y($CzOx^{Me_2}$)$(BH_4)_2$(THF) (**16**) as a yellow powder in a moderate yield of 58%, which was fully characterised by ^{1}H, ^{11}B and ^{13}C{^{1}H} NMR, solid state and THF solution IR spectroscopy, mass spectrometry and elemental analysis. Following this preliminary result, the samarium and lanthanum analogues, La($CzOx^{Me_2}$)$(BH_4)_2$(THF) (**17**) and Sm($CzOx^{Me_2}$)$(BH_4)_2$(THF) (**18**), were also synthesised *via* a similar method of the reaction of **5** with the appropriate metal tris(borohydride) precursor (Scheme 3.3). As with previous borohydride complexes in this series, a broad singlet corresponding to the hydrogen atoms of the borohydride ligands was observed in the ^{1}H NMR, instead of the expected quartet. This is attributed to "washing out" of the $^1J_{B\text{-}H}$ coupling, similarly observed with Mg($CzOx^{Me_2}$)BH_4 (**7**).[26] Single crystals of complex **18** were grown from a 1:3 THF:pentane solution at -30 °C and the complex was structurally authenticated by

X-ray crystallography (Figure 3.5). Selected bond lengths and angles are given in Table 3.5.



Scheme 3.3. Synthesis of yttrium, lanthanum and samarium complexes **16**-**18** *via* salt metathesis reactions (M = Y, n = 2; M = Sm or La, n = 3).

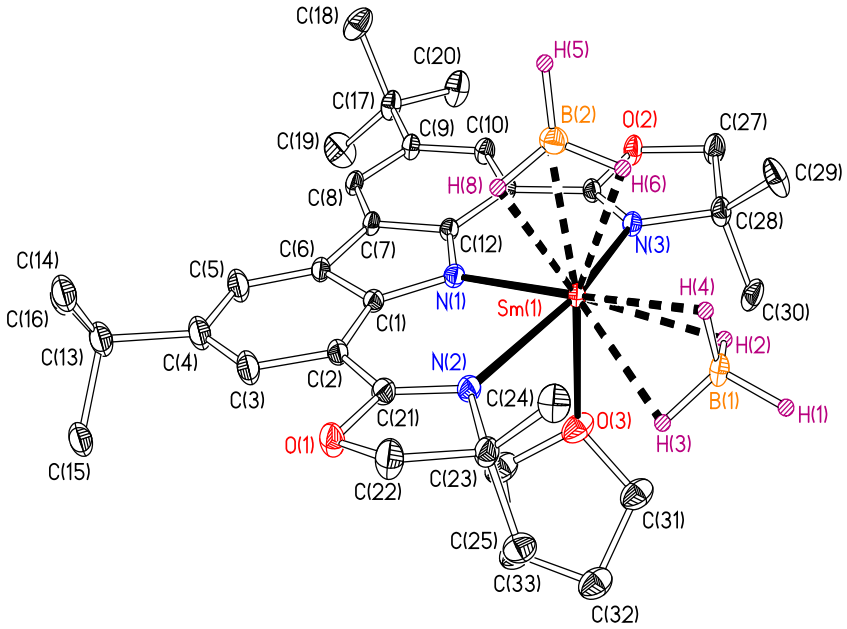


Figure 3.5. Displacement ellipsoid plot of Sm(CzOx^{Me2})(BH$_4$)$_2$(THF) (**18**) (20% probability level). C-bound H-atoms omitted for clarity.

Table 3.5. Selected bond distances (Å) and angles (°) for $Sm(CzOx^{Me_2})(BH_4)_2(THF)$ (**18**).

Sm(1)-N(1)	2.389(6)	Sm(1)-N(2)	2.486(6)
Sm(1)-N(3)	2.515(6)	Sm(1)-O(3)	2.513(6)
Sm(1)-H(2)	2.401	Sm(1)-H(3)	2.418
Sm(1)-H(4)	2.510	Sm(1)···B(1)	2.574(8)
Sm(1)-H(6)	2.508	Sm(1)-H(7)	2.508
Sm(1)-H(8)	2.587	Sm(1)···B(2)	2.600(10)
N(1)-Sm(1)-N(2)	79.53(18)	N(1)-Sm(1)-N(3)	78.85(18)
N(1)-Sm(1)-O(3)	78.1(2)	N(1)-Sm(1)···B(1)	160.1(3)
N(1)-Sm(1)···B(2)	93.3(3)	N(2)-Sm(1)-N(3)	156.54(19)
N(2)-Sm(1)-O(3)	83.5(2)	N(2)-Sm(1)···B(1)	97.8(2)
N(2)-Sm(1)···B(2)	95.3(3)	N(3)-Sm(1)-O(3)	83.2(2)
N(3)-Sm(1)···B(1)	99.5(2)	N(3)-Sm(1)···B(2)	95.0(3)
O(3)-Sm(1)···B(1)	82.1(3)	O(3)-Sm(1)···B(2)	171.4(3)

$Sm(CzOx^{Me_2})(BH_4)_2(THF)$ (**18**) is *pseudo*-six coordinate in which the Sm is coordinated to the three N donors of the $CzOx^{Me_2}$ ligand, two κ^3-bound BH_4 ligands and the O donor of a molecule of THF, assuming a *pseudo*-octahedral geometry. The BH_4 ligands are positioned *cis* relative to each other, and the rigid $CzOx^{Me_2}$ ligand adopts a *mer* configuration, similarly to other octahedral complexes employing this ligand (**11** and **15**). Bond angles N(1)-Sm(1)···B(1) and N(2)-Sm(1)-N(3) show the greatest deviation from linearity (160.1(3) and 156.54(19)°, respectively), whereas the O(3)-Sm(1)···B(2) bond angle is 171.4(3)°: a product of the conformational lock of the $CzOx^{Me_2}$ ligand enforced by the carbazole backbone. The Sm occupies a position close to the plane of the carbazole backbone, evidenced by the relatively planar dihedral angles C(1)-C(2)-C(21)-N(2) (-4.2°) and C(11)-C(12)-C(26)-N(3) (-2.6°). All Sm-N=C bond lengths were within the expected range of 2.35-2.79 Å.[3] The Sm(1)···B(1) and Sm(1)···B(2) bond lengths of (2.574(8) and 2.600(10)Å) are consistent with tridentate samarium-bound borohydride groups.[3]

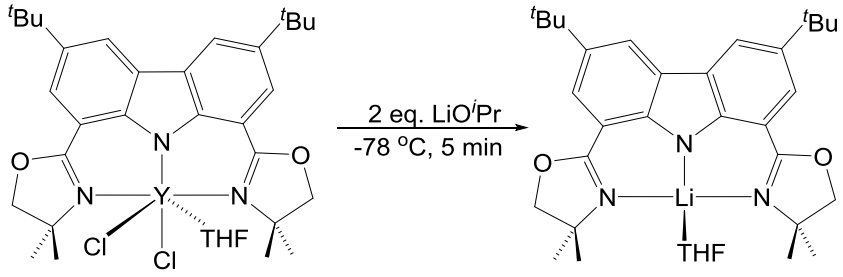
Table 3.6. Solid state (Nujol mull) and solution (THF) ν(B–H) stretching frequencies (cm^{-1}) for complexes $M(CzOx^{Me_2})(BH_4)_2(THF)$ (M = Y (**16**), La (**17**) or Sm(**18**)).

	16	**17**	**18**
Solid state			
$\nu(B–H_t)$	2466	2427	2444
$\nu(B–H_b)$	2215, 2160	2220, 2174	2215, 2182
Solution			
$\nu(B–H_t)$	2451	2434	2444
$\nu(B–H_b)$	2238, 2180	2223, 2171	2230, 2184

Complexes **16-18** were examined by solid state and THF solution IR spectroscopy in order to gain insight into the bonding mode of the borohydride ligands. A summary of the stretching frequencies observed is detailed in Table 3.6. All complexes possess κ^3-borohydride ligands both in the solid state and in a THF solution. As the degree of covalency of the metal-borohydride bond decreases, there is a concurrent decrease in the frequency at which the $\nu(B–H_t)$ band appear in both the solid state and THF solution IR spectra, with increasing metal size such that Y > Sm > La.

Efforts to synthesise yttrium amide complexes $Y(CzOx^{Me_2})\{N(SiHMe_2)_2\}_2$ and $Y(CzOx^{Me_2})\{N(SiMe_3)_2\}_2$ as intermediates for the onwards reaction to obtain the corresponding yttrium alkoxides through the protonolysis reaction of **1.45** with 1 equivalent of $Y\{N(SiHMe_2)_2\}_3(THF)_2$ and $Y\{N(SiMe_3)_2\}_3$ in toluene were met with little success: no reaction was observed at room temperature, and upon heating to 90 °C unidentified multiple species were formed which did not correspond to the products, nor could they be isolated. Therefore, an alternative methodology was employed by L. Budden under the author's direct supervision, in which the literature compound $Y(CzOx^{Me_2})Cl_2(THF)$ (**3.1**) was synthesised and treated with 2 equivalents of a commercially available 1.0 M lithium isopropoxide in hexanes solution in THF at -78 °C. However, the target complex $Y(CzOx^{Me_2})(O^iPr)_2(THF)$ was not obtained, instead affording $Li(CzOx^{Me_2})$ (**19**) *via* transmetallation (Scheme 3.4). To confirm, **19** was independently synthesised *via* the deprotonation of **1.45** with 1 equivalent of a 2.5 M hexanes solution of ^{n}BuLi. Analysis with ^{7}Li NMR revealed a singlet at 3.6

ppm, which independently authenticated the production of **19** in the reaction of **3.1** with lithium isopropoxide, instead of the desired product. No further attempts to synthesise yttrium alkoxide complexes of the type $Y(CzOx^{Me_2})(OR)_2$ were undertaken.



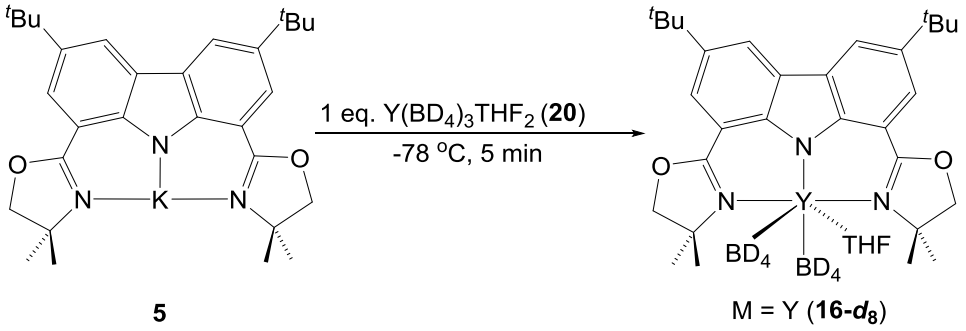
3.1 **19**

Scheme 3.4. Synthesis of $Li(CzOx^{Me_2})$ (**19**) *via* transmetallation.

To complement the deuterium labelling experiments employed to investigate the mechanism of ROP of *rac*-LA with alkaline earth borohydride complexes, the deuterium analogue of **16** was synthesised. In a similar fashion to the synthesis of $Mg(CzOx^{Me_2})(BD_4)$ (**7-*d*$_4$**) and $Ca(CzOx^{Me_2})(BD_4)(THF)_2$ (**13-*d*$_4$**), **3.1** was treated with 2 equivalents of $NaBD_4$ at -78 °C in THF. Surprisingly, there appeared to be no reaction: analysis of the ^{11}B NMR spectrum of the product following extraction and purification confirmed there to be no boron species in the final product, and the ^{1}H NMR spectrum was identical to that of the starting material. Therefore, an alternative approach was sought, based on the successful reaction of $Y(BH_4)_3(THF)_2$ with $K(CzOx^{Me_2})$ (**5**) to obtain $Y(CzOx^{Me_2})(BH_4)_2(THF)$ (**16**).

$Y(BD_4)_3(THF)_2$ (**20**) was synthesised *via* an adapted literature procedure via the salt metathesis reaction of commercially available YCl_3 and 3.5 equivalents of $NaBD_4$ in THF and fully characterised; the number of coordinated THF molecules was determined through elemental analysis.[29] Base-free $Y(BD_4)_3$ was synthesised in 2012 by Grochala *et al.* through a mechanochemical reaction between YCl_3 and $LiBD_4$ after the reaction using $NaBD_4$ failed; however, no solution characterisation was undertaken.[30] Analysis of the ^{2}H NMR spectrum of **20** revealed an apparent doublet at 1.13 ppm, corresponding to B<u>D</u>$_4$, with a $^{2}J_{YD}$ coupling of 15.5 Hz. The onwards reaction with 1 equivalent of $K(CzOx^{Me_2})$ (**5**) afforded $Y(CzOx^{Me_2})(BD_4)_2(THF)$ (**16-*d*$_8$**) as a yellow powder in 50% yield (Scheme 3.5). Analysis of **16-*d*$_8$** with ^{2}H NMR

spectroscopy revealed an apparent singlet at 1.6 ppm. The appearance of an apparent doublet for **20** and an apparent singlet for **16-*d*$_8$** in the ^{2}H NMR spectrum is again attributed to rapid relaxation of the quadrupolar nuclei resulting in the washing out of the $^2J_{YD}$ coupling. THF solution IR spectroscopy confirmed isotropically shifted B-D$_t$ and B-D$_b$ bands at 1842 (ν_D/ν_H = 0.75) and 1668 and 1587 (ν_D/ν_H = 0.75 and 0.73, respectively, 81 cm^{-1} splitting).

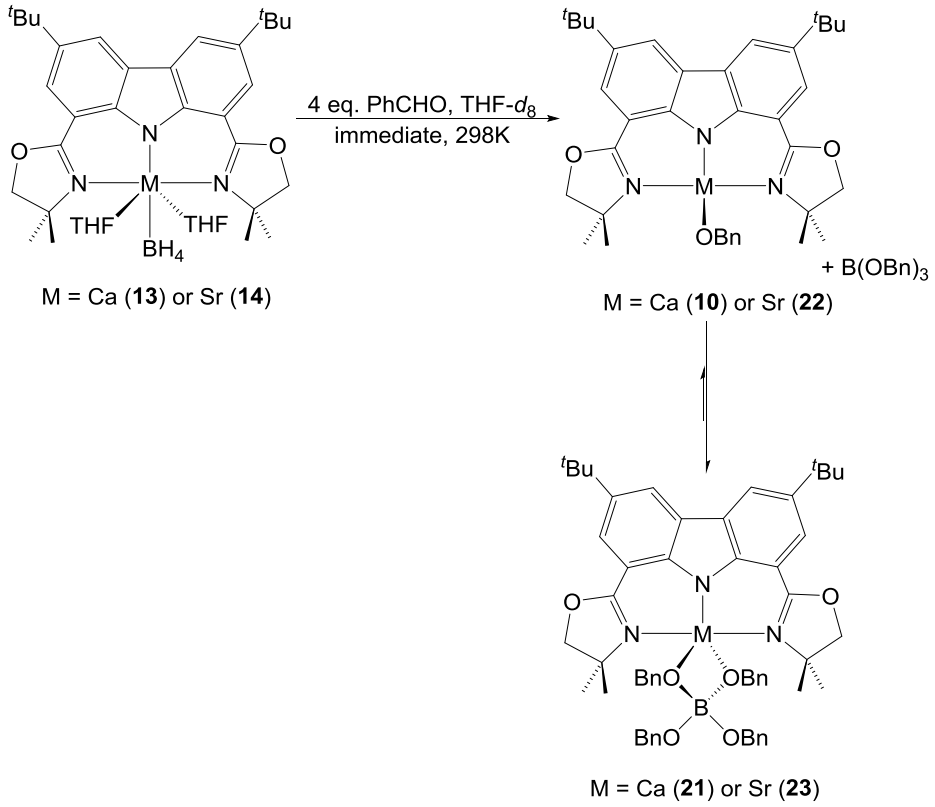


Scheme 3.5. Synthesis of Y(CzOx^{Me2})(BD$_4$)$_2$(THF) (**16-*d*$_8$**) *via* a salt metathesis reaction with Y(BD$_4$)$_3$(THF)$_2$ (**20**).

3.4 *In situ* generation of trialkyl borate esters as chain transfer agents

Chapter 2 describes the successful *in situ* generation of Mg(CzOx^{Me2})(OBn) (**2**) and B(OBn)$_3$ through the treatment of Mg(CzOx^{Me2})(BH$_4$) (**7**) with 4.5 equivalents of benzaldehyde for the *i*ROP of lactide. In a similar manner, the treatment of Ca(CzOx^{Me2})(BH$_4$)(THF)$_2$ (**13**) and Sr(CzOx^{Me2})(BH$_4$)(THF)$_2$ (**14**) with 4.5 equivalents of benzaldehyde in 0.01 M THF-*d*$_8$ solution at room temperature led to the immediate formation of the corresponding alkoxides, Ca(CzOx^{Me2})(OBn) (**10**) and Sr(CzOx^{Me2})(OBn) (**22**), with concurrent evolution of B(OBn)$_3$ which was monitored with ^{1}H and ^{11}B NMR spectroscopy. The discrete species existed in equilibrium with the tetracoordinated adduct, either Ca(CzOx^{Me2}){B(OBn)$_4$} (**21**) or Sr(CzOx^{Me2}){B(OBn)$_4$} (**23**) (Scheme 3.6). On descent of the group, the equilibrium favoured the formation of the tetracoordinated adduct over free B(OBn)$_3$, M(CzOx^{Me2}){B(OBn)$_4$} (M = Mg (**8**), Ca (**21**) or Sr (**23**)): attributed to the increased metal size and therefore decreased steric hindrance when forming the adduct. However, the position of the equilibrium was found to be both concentration and temperature dependent, with an increase in solution concentration promoting the formation of the adducts. Identical reactions in C$_6$D$_6$ also resulted in the immediate

generation of the metal alkoxides and borate esters, showing the reaction to be solvent independent. 1 equivalent of $B(OBn)_3$ was added to a THF-d_8 solution of independently synthesised **10** to verify the reaction between **13** and 4.5 equivalents of benzaldehyde. The resultant ^1H and ^{11}B NMR spectra were identical to those obtained from the *in situ* generation of **10** and **21**, with the ^{11}B NMR spectrum confirming the appearance of resonances at 3.9 and 18.8 ppm, corresponding to $\{\underline{B}(OBn)_4\}$ and $\underline{B}(OBn)_3$, respectively.



Scheme 3.6. Transformation of complexes **13** to **10**, $B(OBn)_3$ and **21**, and **14** to **22**, $B(OBn)_3$ and **23** through the addition of 4.5 eq. PhCHO.

Detailed studies into the equilibrium constant, K_{eq}, for the dissociation process of **21** to **10** and $B(OBn)_3$ were conducted. 4.5 equivalents of benzaldehyde were added to a 0.01 M THF-d_8 solution of **13** and the ^1H NMR spectra were recorded between -25 and 35 °C (Figure 3.6).

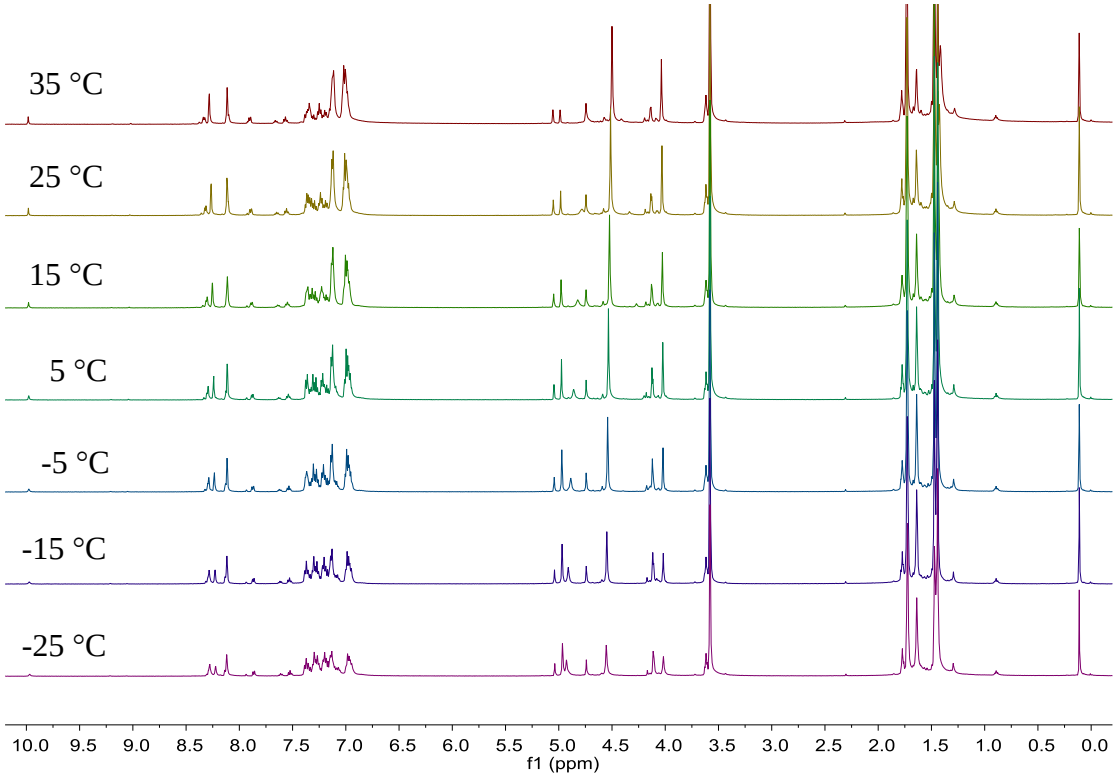


Figure 3.6. Variable temperature ^{1}H NMR spectra (THF-d_8, 500.3 MHz) of Ca(CzOx^{Me_2})(OBn) (**10**) and B(OBn)$_3$, and **21** between -25 and 35 °C.

The absolute integrals of the resonances corresponding to the methylene protons on the oxazoline rings in the adduct **21** and the methylene protons of the benzyl groups in free B(OBn)$_3$ were measured at 10 °C intervals between -25 and 35 °C. The integrals were normalised, and the fraction of the adduct in solution was obtained from the sum of the integrals. In turn, the equilibrium constant of the dissociation of **21** to **10** and B(OBn)$_3$ was derived from the Van't Hoff plot of ln K_{eq} *vs*. 1/T (K^{-1}) (Figure 3.7). The enthalpy and entropy of dissociation were determined to be ΔH = 31.2(7) kJ mol^{-1} and ΔS = 63(2) J mol^{-1}, respectively. ΔG_{298} = 12.3(9) kJ mol^{-1} and ΔG_{255} = 15.1(8) kJ mol^{-1}, which, in conjunction with the positive value obtained for ΔS, show dissociation is favoured at increasing temperatures, and that under polymerisation conditions, complexation of B(OBn)$_3$ to form the adduct **21** is favoured. Analysis of the ^{11}B NMR spectra at -25 °C revealed a dominant peak at 3.8 ppm corresponding to the {B(OBn$_4$}$^-$ group in complex **21**. Upon heating to 35 °C, the major species formed remained the tetracoordinated borate ester adduct; however, a minor peak at 18.8 ppm corresponding to B(OBn)$_3$ increased in intensity relative to the spectra at -

25 °C, indicating that increasing the temperature results in dissociation becoming more favourable.

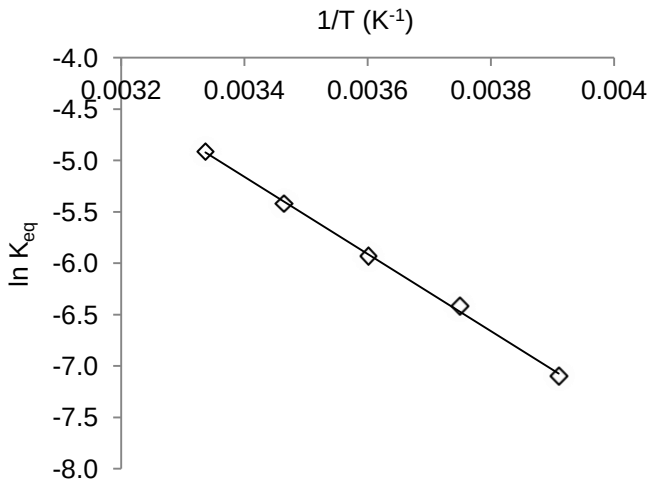
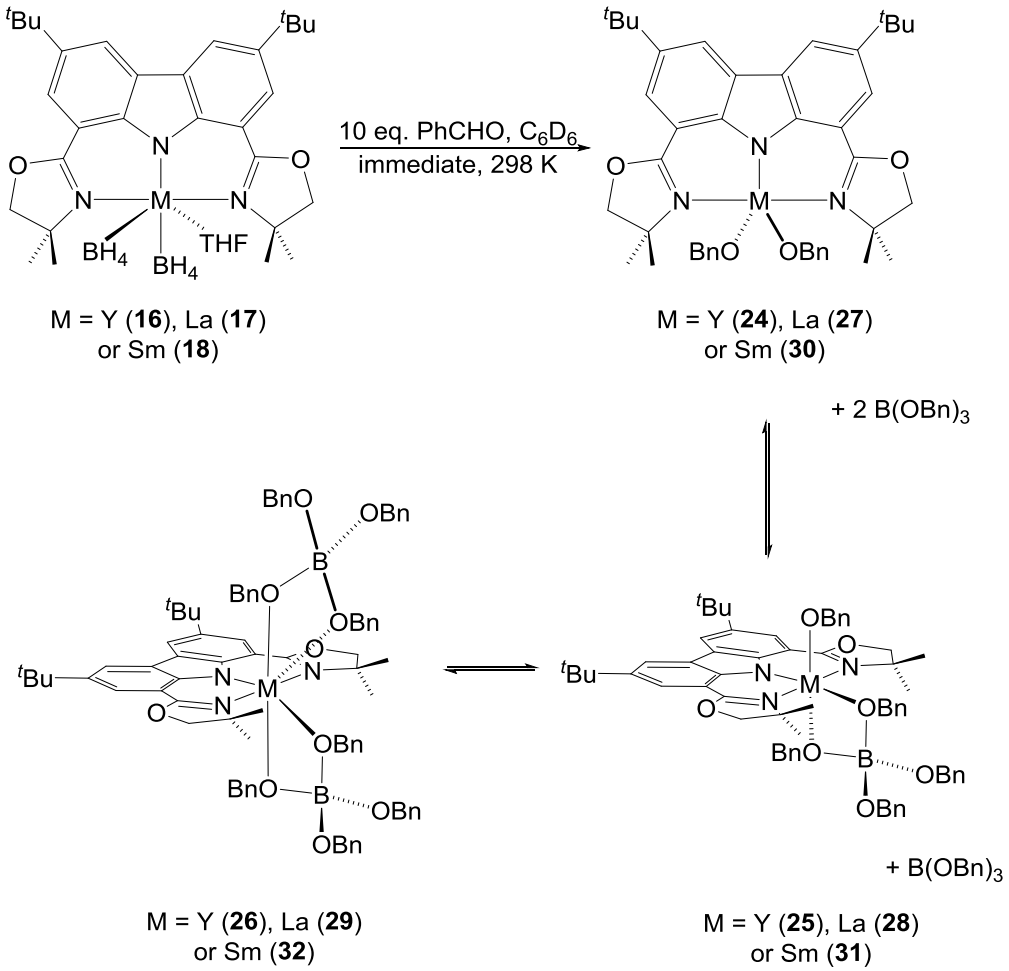


Figure 3.7. Van't Hoff Plot of ln K_{eq} *vs*. 1/T (K^{-1}) (R^2 = 0.999) for *in situ* generated Ca($CzOx^{Me2}$)(OBn) (**10**) and $B(OBn)_3$: ΔH = 31.2(7) kJ mol^{-1}, ΔS = 63(2) J K^{-1} mol^{-1} and ΔG = 12.3(9) kJ mol^{-1}. The gradient of the linear fit corresponds to $-\Delta H/R$, and the intercept to $\Delta S/R$.

A complementary investigation into the *in situ* generation of rare earth bis(alkoxide) species from the starting bis(borohydride) complexes synthesised independently was undertaken. Preliminary results obtained by L. Budden revealed the addition of 10 equivalents of benzaldehyde successfully resulted in the full consumption of starting complex Y($CzOx^{Me2}$)(BH_4)$_2$(THF) (**16**), generating Y($CzOx^{Me2}$)$(OBn)_2$ (**24**) and 2 equivalents of $B(OBn)_3$ at room temperature in C_6D_6 (Scheme 3.7). 10 equivalents of benzaldehyde were employed in order to ensure complete conversion of the starting borohydride complex to the corresponding alkoxide. Analysis of the ^{1}H NMR and ^{11}B NMR spectra confirmed the presence of multiple species in solution: although complex, the resultant ^{1}H NMR spectrum confirmed the evolution of free $B(OBn)_3$. The ^{11}B NMR spectrum was more insightful: the quintet corresponding to **16** at -23.4 ppm disappeared, producing two singlets at 3.9 and 18.8 ppm, which, based on previous findings, were attributed to Y($CzOx^{Me2}$)(OBn){$\underline{B}(OBn)_4$} (**25**) and dissociated $\underline{B}(OBn)_3$, respectively.



Scheme 3.7. Transformation of complexes **16** to **24**, $B(OBn)_3$, **25** and **26**, **17** to **27**, $B(OBn)_3$, **28** and **29** and **18** to **30**, $B(OBn)_3$, **31** and **32** through the addition of 10 eq. PhCHO.

The treatment of rare earth complexes La(CzOx^{Me2})$(BH_4)_2$(THF) (**17**) and Sm(CzOx^{Me2})$(BH_4)_2$(THF) (**18**) with 10 equivalents of benzaldehyde at room temperature in C_6D_6 resulted in the comparable *in situ* generation of La(CzOx^{Me2})$(OBn)_2$ (**27**) and Sm(CzOx^{Me2})$(OBn)_2$ (**30**) with 2 equivalents of $B(OBn)_3$. These discrete species also existed in equilibrium forming mono(tetracoordinated) adducts, La(CzOx^{Me2})(OBn){$B(OBn)_4$} (**28**) and Sm(CzOx^{Me2})(OBn){$B(OBn)_4$} (**31**), confirmed by ^{11}B NMR spectroscopy.

An important distinction between the observations obtained from the *in situ* transformation of borohydride to alkoxide initiators using supported alkaline earth mono(borohydride) complexes, such as **7**, **13** and **14**, is the potential for the

coordination of two borate esters to the metal centre. The larger ionic radii of the rare earths permits for the adoption of high coordination numbers,[31, 32] which may allow for the formation of a bis(tetracoordinated) adduct M(CzOx^{Me2}){B(OBn)$_4$}$_2$ (M = Y (**26**), La (**29**) or Sm (**32**)) with a seven coordinate metal centre; however, such a species would probably experience a large degree of steric hindrance. Indeed, the room temperature ^{11}B NMR spectrum of Y(CzOx^{Me2})(OBn)$_2$ (**24**) and 2 equivalents of B(OBn)$_3$ shows the major product to be the free B(OBn)$_3$, with a secondary peak corresponding to the mono(tetracoordinated) adduct **25** at 3.9 ppm. However, a minor resonance at 8.7 ppm may correspond to the bis(tetracoordinated) adduct **26**.

In the absence of excess B(OBn)$_3$, the ^{11}B NMR spectrum of *in situ* generated Sm(CzOx^{Me2})(OBn)$_2$ (**30**) and 2 equivalents of B(OBn)$_3$ in THF-d_8 at 25 °C reveals resonances at 18.9 and 2.3 ppm. The major singlet at 18.9 ppm corresponds to free B(OBn)$_3$, indicating that equilibrium favours the fully dissociated species, whilst the minor singlet at 2.3 ppm corresponds to the one of the tetracoordinated adducts. To identify whether this resonance was either the mono- or bis(tetracoordinated) adduct, 3 further equivalents of B(OBn)$_3$ were added to the solution and the ^{1}H and ^{11}B NMR spectra were recorded at regular intervals between -65 and 25 °C (Figure 3.8). At 25 °C, three resonances may be observed in the ^{11}B NMR spectrum: the major singlet at 18.9 ppm, and two minor singlets at 7.4 and 2.3 ppm, the bis(tetracoordinated) (**32**) and mono(tetracoordinated) adducts (**31**), respectively. On descent to -65 °C, these resonances become more prominent, indicating that the associative process becomes more favourable at lower temperatures. Owing to the complexity of the associative and dissociative processes occurring between M(CzOx^{Me2})(OBn)$_2$ (M = Y (**24**), La (**27**) or Sm (**30**)) and 2 equivalents of B(OBn)$_3$ attempts to derive the activation parameters for dissociation of the borate ester from the tetracoordinated adducts were not successful.

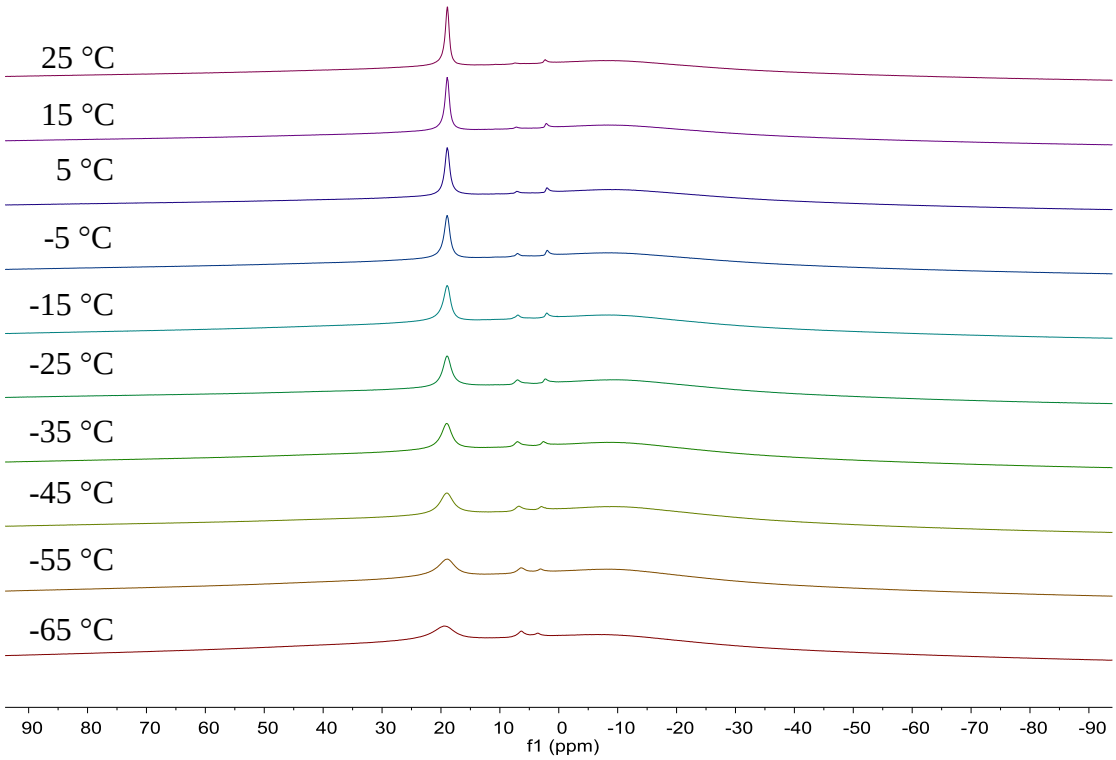


Figure 3.8. Variable temperature ^{11}B NMR spectra (THF-d_8, 160 MHz) of *in situ* generated Sm(CzOx^{Me2})(OBn)$_2$ (**30**) and 2 eq. of B(OBn)$_3$ in the presence of 3 additional eq. of B(OBn)$_3$ between -65-25 °C.

3.5 Polymerisation studies: ROP of *rac*-, *L*- and *meso*-LA

Complexes Ca(CzOx^{Me2}){N(SiMe$_3$)$_2$}(THF) (**9**), Ca(CzOx^{Me2})(OBn) (**10**), Ca(CzOx^{Me2})(BH$_4$)(THF)$_2$ (**13**), Sr(CzOx^{Me2})(BH$_4$)(THF)$_2$ (**14**), Y(CzOx^{Me2})(BH$_4$)$_2$(THF) (**16**), La(CzOx^{Me2})(BH$_4$)$_2$(THF) (**17**) and Sm(CzOx^{Me2})(BH$_4$)$_2$(THF) (**18**) were evaluated as catalysts for the ROP of lactide. These complexes were tested initially in the absence of any additives, and further studies were conducted to investigate their performance in the presence of B(OBn)$_3$, either externally added or generated *in situ*. *In situ* generated complexes were synthesised following the addition of the appropriate number of equivalents of benzaldehyde to a THF solution of the corresponding supported metal borohydride complex, and stirred for 5 min prior to the addition of lactide ensuring complete consumption of the starting complex. Polymerisation experiments were conducted in THF at room temperature, and under these conditions all complexes were found to be active. The polymerisation was followed by the collection of aliquots at regular time

intervals, and the polymer samples were characterised by ^{1}H NMR spectroscopy, Gel Permeation Chromatography and MALDI-ToF MS. The results are summarised in Tables 3.7 and 3.8.

3.5.1 Polymerisation studies: ROP of *rac*- and *meso*-LA with Group 2 complexes

Ca(CzOx^{Me_2}){N(SiMe$_3$)$_2$}(THF) (**9**) was found to be highly active for ROP, reaching 91% conversion of 100 equivalents of *rac*-LA after 15 min (Table 3.7, entry 1). The catalyst offered very poor molecular weight control (at 91% conversion, M_n(obs) = 41,940 g mol^{-1} *cf.* M_n(calc) = 13,275 g mol^{-1}, PDI = 2.25). The poor molecular weight control is typical of catalysts employing amide initiators, and is a consequence of poor agreement between the rate of initiation and the rate of propagation. Moreover, the broad molecular weight distribution can be attributed to a high incidence of transesterification, confirmed through the analysis of the MALDI-ToF MS in which peak envelopes of $\Delta m/z$ 72 g mol^{-1} and the absence of an observable N(SiMe$_3$)$_2$ end-group resulting in cyclic structures are indicative of transesterification.

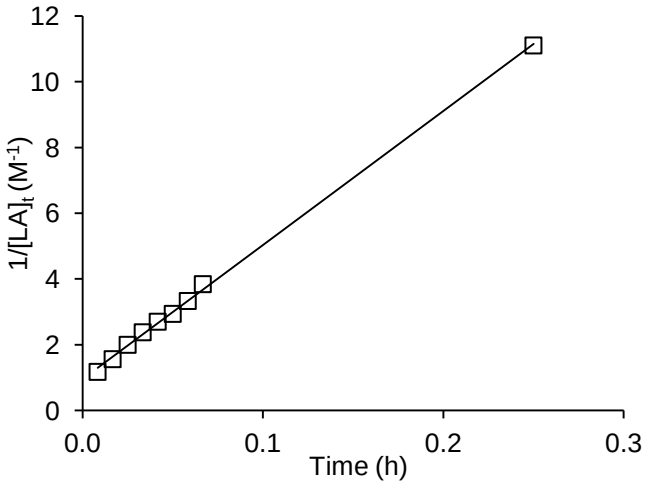


Figure 3.9. Data for the ROP of *rac*-LA using Ca(CzOx^{Me_2}){N(SiMe$_3$)$_2$}(THF) (**9**). Second-order plot of 1/[LA]$_t$ *vs*. time (k_{obs} = 40.8(4) M^{-1} h^{-1}, R^2 = 0.999); vertical-axis intercept = 0.96(4) M^{-1} (expected value = 1/[LA]$_0$ = 1 M^{-1}).

Table 3.7. Selected data for the polymerisation of *rac*-, *L*- and *meso*-LA using complexes Ca(CzOx^{Me_2}){N(SiMe$_3$)$_2$}(THF) (**9**), Ca(CzOx^{Me_2})(OBn) (**10**), Ca(CzOx^{Me_2})$_2$ (**11**), Ca(CzOx^{Me_2})(BH$_4$)(THF)$_2$ (**13**) and Sr(CzOx^{Me_2})(BH$_4$)(THF)$_2$ (**14**) in THF.[a]

Entry	Catalyst	Monomer	Additive (eq.)	Conv.[b] %	Time (min)	M_n(obs)[c] (g mol^{-1})	M_n(calc)[d] (g mol^{-1})	M_w/M_n[c]	P_r[b]
1	Ca(CzOx^{Me_2}){N(SiMe$_3$)$_2$}(THF) (**9**)	*rac*	-	91	15	24,080	13,275	2.13	0.63-0.70
2	Ca(CzOx^{Me_2})(OBn) (**10**)	*rac*	-	93	3.5	15,950	13,509	1.31	0.63-0.70
3	Ca(CzOx^{Me_2})(OBn) (**10**)	*rac*	B(OBn)$_3$ (1)	90	50	4,700	3,350	1.76	0.59-0.64
4	Ca(CzOx^{Me_2})(BH$_4$)(THF)$_2$ (**13**)	*rac*	-	88	180	9,780	12,685	1.48	0.60-0.67
5	Ca(CzOx^{Me_2})(BH$_4$)(THF)$_2$ (**13**)	*rac*	B(OBn)$_3$ (1)	90	1,440	3,600	3,324	1.63	0.52-0.56
6	Ca(CzOx^{Me_2})(BH$_4$)(THF)$_2$ (**13**)	*rac*	PhCHO (4.5)	93	360	4,280	3,458	1.75	0.50-0.53
7	Ca(CzOx^{Me_2})(BH$_4$)(THF)$_2$ (**13**)	*rac*	PhCHO (8)	88	360	3,340	3,530	1.53	0.51-0.55
8	Ca(CzOx^{Me_2})(BH$_4$)(THF)$_2$ (**13**)	*L*	-	88	240	12,780	12,685	1.81	-
9	Ca(CzOx^{Me_2})(BH$_4$)(THF)$_2$ (**13**)	*L*	PhCHO (4.5)	95	420	4,800	3,530	1.28	-
10	Ca(CzOx^{Me_2})(BH$_4$)(THF)$_2$ (**13**)	*meso*	-	97	5	13,540	12,829	1.58	0.66-0.69
11	Ca(CzOx^{Me_2})(BH$_4$)(THF)$_2$ (**13**)	*meso*	PhCHO (4.5)	89	5	6,740	3,314	1.23	0.60-0.66
12	Sr(CzOx^{Me_2})(BH$_4$)(THF)$_2$ (**14**)	*rac*	-	91	2	15,540	13,117	1.70	0.60-0.65
13	Sr(CzOx^{Me_2})(BH$_4$)(THF)$_2$ (**14**)	*rac*	PhCHO (4.5)	92	300	5,540	3,422	1.89	0.49-0.53

[a] Conditions: $[LA]_0$:$[initiator]_0$ = 100:1, 4 mL THF at 23 °C. $[LA]_0$ = 1.0 M. [b] Measured by ^{1}H NMR ($CDCl_3$) analyses. [c] Molecular weights (g mol^{-1}) determined from GPC using appropriate Mark-Houwink corrections. [d] Expected average M_n (g mol^{-1}) for stated number of chains per metal and stated % conversion: M_n (calc for entry 1) = (conversion (%) × 100 × 144.1) + 161.4; (calc for entry 2) = (conversion (%) × 100 × 144.1) + 108.1; (calc for entries 3, 6, 7, 9, 11 and 13) = ¼(conversion (%) × 100 × 144.1) + 108.1; (calc for entries 4, 8, 10 and 12) = (conversion (%) × 100 × 144.1) + 4.0; (calc for entry 5) = ¼((conversion (%) × 100 × 144.1) + 4.0) + ¾((conversion (%) × 100 × 144.1) + 108.1).

The reaction observed a second-order dependence on [LA], with k_{obs} = 40.8(4) M^{-1} h^{-1} (R^2 = 0.999), (Figure 3.9). The origin of the kinetic regime is not readily apparent, as a trialkyl borate ester is not present in this instance. Instead, it is may be a product of either two lactide units of opposing chirality coming together during the transition state, non-innocence of the ligand, which have been alluded to previously in the literature.[33-35] In comparison to the magnesium analogue, Mg(CzOx^{Me_2}){N(SiMe$_3$)$_2$} (**1**), the degree of heteroselectivity was reduced, affording PLA with a moderate degree of enrichment (P_r = 0.63-0.70).

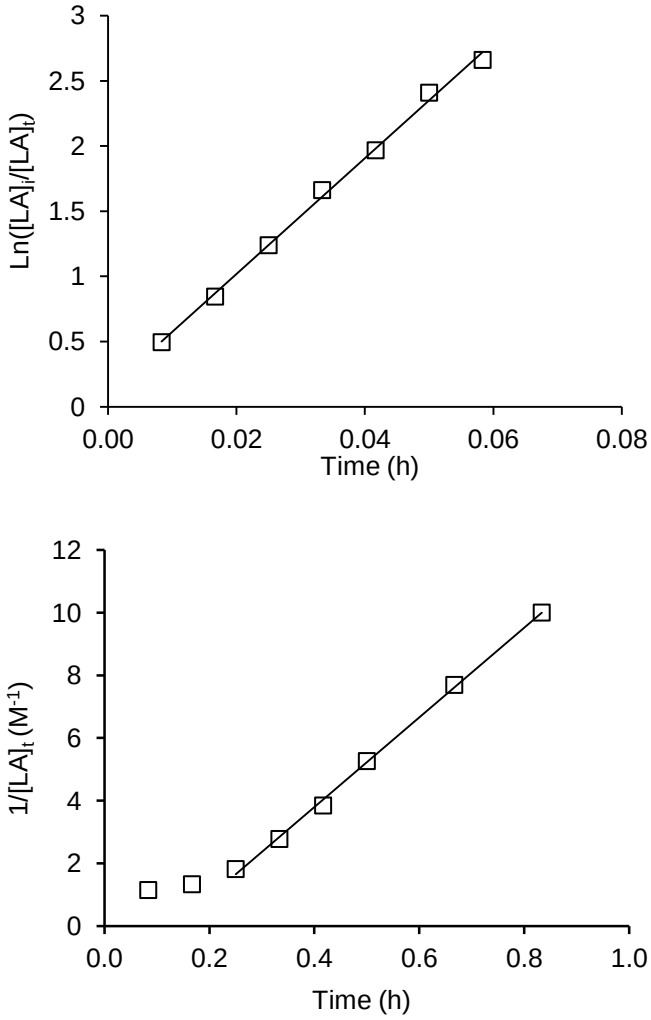


Figure 3.10. Data for the ROP of *rac*-LA using Ca(CzOx^{Me_2})(OBn) (**10**). Top: with no additives; first-order plot of ln$[LA]_i/[LA]_t$ *vs.* time (k_{obs} = 44(1) h^{-1}, R^2 = 0.997); vertical-axis intercept = 0.13(4) (expected value = ln$[LA]_i/[LA]_0$ = 0). Bottom: with 1 eq. B(OBn)$_3$; second-order plot of $1/[LA]_t$ *vs.* time (k_{obs} = 14.3(3) M^{-1} h^{-1}, R^2 = 0.998).

The activity of Ca(CzOx^{Me2})(OBn) (**10**) towards the ROP of *rac*-LA was examined both in the absence and presence of B(OBn)$_3$ as a chain transfer agent (Table 3.7, entries 2 and 3). In the absence of any additives, **10** was extremely active, achieving 93% conversion in 3.5 min. On the addition of 1 equivalent of B(OBn)$_3$, the reaction slowed considerably, achieving 90% conversion after 50 min, after a slight induction period. Notably, the kinetic regime demonstrated a clear shift from a first- to second-order dependency on [LA] following the addition of the borate ester, which mirrors previous experiments conducted in Chapter 2 (Figure 3.10). The induction period and subsequent decreased rate of reaction may be attributed to complexation of the catalyst in the presence of B(OBn)$_3$ to form an inactive tetracoordinated borate ester adduct, which must dissociate in order to allow polymerisation. Furthermore, the shift in k_{obs} from first- to second-order can be similarly attributed to the presence of preequilibria involving a borate ester species, resulting in a second-order dependence.

Ca(CzOx^{Me2})(OBn) (**10**) offered a moderate degree of molecular weight control: in the absence of any additives, the obtained molecular weight was in reasonably close agreement with those anticipated. Nonetheless, they are consistently higher throughout the course of the polymerisation (Figure 3.11), which may be indicative of poor agreement between the rates of initiation and propagation, observed with amide initiators. The molecular weights confirm the immortal nature of the polymerisation on the addition of 1 equivalent of B(OBn)$_3$, which correspond to the growth of between 3 and 4 chains per metal centre. Of interest are the considerably narrower molecular weight dispersities observed in the absence of a chain transfer agent, compared to in its presence. Chain transfer agents typically result in narrower PDIs as a consequence of reduced opportunity for the occurrence of transesterification.[36] In this instance it appears that the prolonged reaction time may have a deleterious effect which negates the additional benefits conferred by the addition of B(OBn)$_3$. In both cases, the degree of heterotactic enrichment was modest; however, in the absence of B(OBn)$_3$, **10** afforded a slightly higher degree of enrichment (P_r = 0.63-0.70 *cf.* 0.59-0.64).

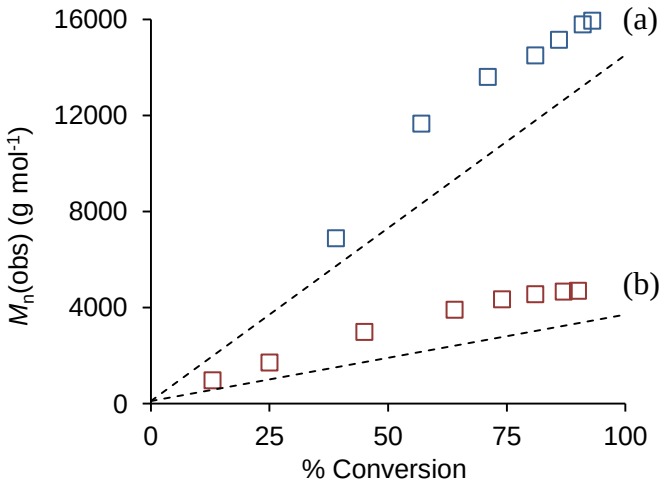


Figure 3.11. M_n(obs) (g mol^{-1}) *vs*. % conversion plot for the ROP of *rac*-LA using Ca(CzOx^{Me_2})(OBn) (**10**); the dashed lines are the M_n(calc) in each case. Conditions: 4 mL THF, 23 °C, [*rac*-LA]$_0$:[**10**]$_0$ = 100:1 [*rac*-LA]$_0$ = 1.0 M: (a) with no B(OBn)$_3$, expecting 1 chain per metal centre (blue squares); (b) with 1 eq. B(OBn)$_3$, expecting 4 chains per metal centre (red squares).

Ca(CzOx^{Me_2})(BH$_4$)(THF)$_2$ (**13**) proved to be substantially less active than **10** for the ROP of *rac*-LA, reaching 88% conversion after 180 min (Table 3.7, entry 4). Based on the analogous observation with Mg(CzOx^{Me_2})(BH$_4$) (**7**), this may be attributed to incomplete precatalyst activation to form a productive species immediately following the reduction of LA with the borohydride ligand, resulting in a much lower than expected rate of reaction. Most unusually, the reaction appeared to follow a third-order dependence in monomer concentration (Figure 3.12; top). This is the first instance of a third-order dependence on lactide concentration observed in the ROP of *rac*-LA. At this stage, the precise mechanism of the rate-determining step is unknown; however, it is unlikely that this is due to the involvement of three lactide units at the transition state. Again, it is postulated to be a result of complex preequilibria caused by the presence of a B(OR)$_3$ species, such as B(LA-H)$_3$, produced by the reaction between BH$_3$(THF) and *rac*-LA, which may associate to the metal centre giving rise to an apparent third-order dependency on [LA].

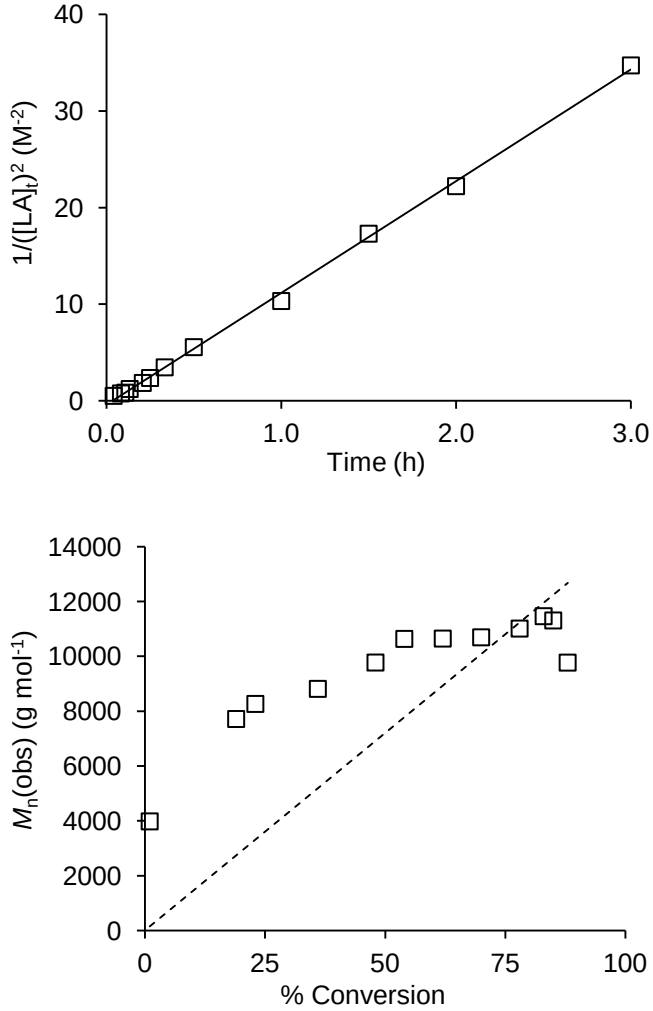


Figure 3.12. Data for the ROP of *rac*-LA using Ca(CzOx^{Me_2})(BH$_4$)(THF)$_2$ (**13**). Top: third-order plot of $1/([LA]_t)^2$ *vs.* time (k_{obs} = 11.6(1) M^{-2} h^{-1}, R^2 = 0.999). Bottom: M_n(obs) (g mol^{-1}) *vs.* % conversion plot for the ROP of *rac*-LA using Ca(CzOx^{Me_2})(BH$_4$)(THF)$_2$ (**13**); the dashed line is the M_n(calc), expecting 1 chain per metal centre. Conditions: 4 mL THF, 23 °C, [*rac*-LA]$_0$:[**13**]$_0$ = 100:1 [*rac*-LA]$_0$ = 1.0 M.

Complex **13** offered poor molecular weight control with non-linear growth in M_n *vs.* % conversion with no induction period: during the first half life, the molecular weights were considerably higher than expected, a result of incomplete precatalyst to catalyst activation. However; M_n growth after ~50% conversion was hampered by a combination of transesterification and immortal ROP caused by the presence of a trialkyl borate ester species such as B(LA-H)$_3$, resulting in a final M_n(obs) = 9,780 g mol^{-1} at 88% completion (Figure 3.12; bottom). The deleterious effects of

transesterification can also confirmed by the moderately broad PDIs observed which increased throughout the reaction to 1.48. Analysis with MALDI-ToF MS revealed the presence of multiple distributions confirming the polymer chain end-groups to be a mixture of OBn and borohydride-derived termini, in addition to minor distributions with peak envelopes of $\Delta m/z$ 72 g mol^{-1}, confirming the presence of transesterification during polymerisation.

Addition of 1 equivalent of $B(OBn)_3$ to the complex prior to polymerisation resulted in much improved behaviour, albeit with a concurrent decrease in rate, reaching 90% conversion after 24 h (Table 3.7, entry 5). In this instance, the kinetics appeared to follow a non-integer order between 1 and 2, and could not be definitively assigned as either first- or second-order. The decrease in rate on addition of a borate ester may be caused by a preference for the formation of an inactive tetracoordinated adduct. Gratifyingly, the poor molecular weight control observed with **13** was substantially improved upon following addition of $B(OBn)_3$: a plot of M_n(obs) growth *vs*. % conversion resulted in a linear growth of molecular weight, with a gradient of 31.8(6) g mol^{-1} (% conversion)$^{-1}$ (R^2 = 0.998), corresponding to approximately 4 chains per metal centre following an initial jump in molecular weight to 1,090 g mol^{-1} at 11% monomer conversion (M_n(calc) = 478 g mol^{-1}). The improvement in chain transfer may be attributed to a decrease in the rate of propagation resulting in more efficient chain transfer. The PDI remained moderate at 1.63 at the end of the reaction. Both in the absence and presence of $B(OBn)_3$, **13** produced polymers with a modest heterotactic bias, with P_r in the range of ~0.55-0.65.

To further examine the mechanism of initiation with **13**, deuterium labelling studies were conducted with $Ca(CzOx^{Me2})(BD_4)(THF)_2$ (**13-*d*$_4$**) in the presence of 15 equivalents of *rac*-LA, achieving 55% conversion after 24 h, and 85% conversion following 96 h of reaction. A comparable experiment was conducted with **13**, which achieved 85% conversion following a reaction time of 24 h, indicating the presence of a considerable kinetic isotope effect. The bulk PLA obtained from both **13** and **13-*d*$_4$** were quenched with dry HCl in diethyl ether, extracted into CH_2Cl_2, and analysed with ^{1}H NMR, ^{13}C{^{1}H} NMR, GPC and MALDI-ToF MS. The ^{1}H NMR spectrum of the PLA obtained from **13** was broad in the diagnostic region between 4.0-5.0 ppm;

however, two doublets were observed at 5.62 and 5.65 ppm, which have been previously assigned as LA-H.

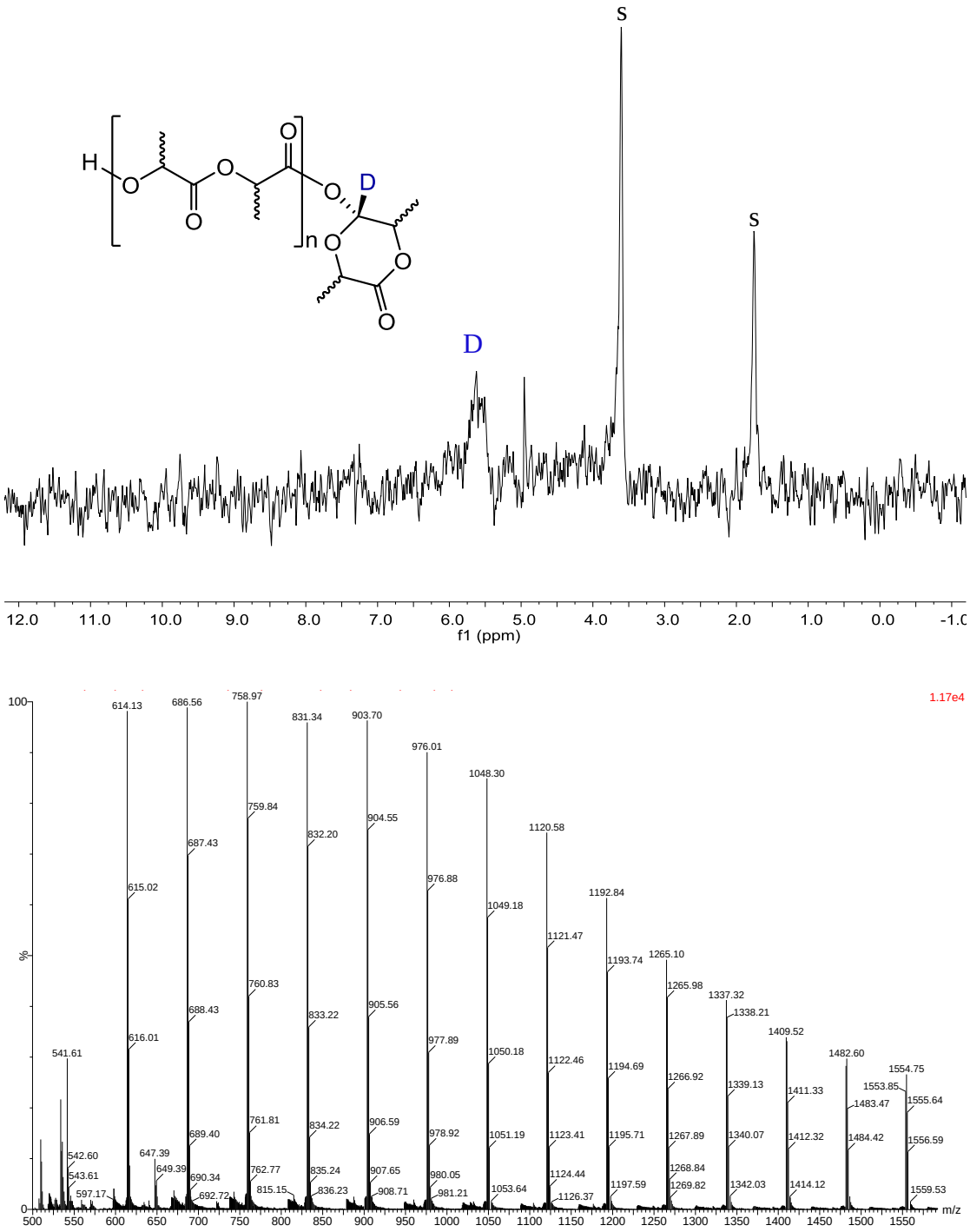


Figure 3.13. Top: ^{2}H NMR spectrum (THF, 76.7 MHz, 298 K) of PLA obtained from Ca(CzOx^{Me2})(BD$_4$)(THF)$_2$ (**13-*d*$_4$**); "s" denotes residual solvent signals. Bottom: MALDI-ToF MS of PLA synthesised from Ca(CzOx^{Me2})(BD$_4$)(THF)$_2$ (**13-*d*$_4$**). M_n by GPC analysis = 2,260 g mol^{-1}.

Concomitant analysis of the ^{1}H NMR spectrum of the PLA obtained from **13-*d*$_4$** confirmed their disappearance. Curiously, the ^{2}H NMR spectrum revealed only one deuterium environment: a broad peak at 5.5 ppm, corresponding to a LA-D end-group; no α,ω-dihydroxytelechelic PLA was observed (Figure 3.13; top). Similarly, the MALDI-ToF MS only confirmed a peak at 1482 g mol^{-1} corresponding to the LA-D terminus (expected value 1483 g mol^{-1}) (Figure 3.13; bottom). It can be concluded that the second deuteride transfer is considerably less favourable than insertion into the Ca-alkoxy bond of intermediate Ca(CzOx^{Me_2})(LA-D). However, analysis of the MALDI-ToF MS of the PLA obtained from **13** reveal the presence of both LA-H and CH(Me)CH$_2$OH end-groups, indicating that the second hydride transfer occurs competitively with insertion into the Ca(CzOx^{Me_2})(LA-H) intermediate. These findings support the hypothesis that **13** undergoes a similar mechanism of initiation to that proposed in Chapter 2 in which full catalyst activation is not achieved during polymerisation due to the formation of catalytically inactive species which are a product of the multiple reaction pathways undergone by the starting borohydride complex on exposure to lactide. However, as yet the precise nature of these species is not fully understood.

4.5 equivalents of benzaldehyde were added to Ca(CzOx^{Me_2})(BH$_4$)(THF)$_2$ (**13**) in to evaluate the performance of the *in situ* generated alkoxide Ca(CzOx^{Me_2})(OBn) (**10**) and B(OBn)$_3$ in the ROP of *rac*-LA (Table 3.7, entry 6). The rate of reaction decreased with respect to the rate of **13** with no additives, achieving 93% conversion after 360 min, which may be attributed to the presence of a trialkyl borate ester species which forms a tetracoordinated adduct with the metal centre of the complex, reducing the concentration of uncoordinated **10** in solution and thus decreasing the rate of reaction. Close examination of the kinetic regime revealed an almost zero-order dependence on [LA], with a k_{obs} = -0.142(6) M h^{-1} (R^2 = 0.990), indicating that lactide is not involved in the rate-determining step (Figure 3.14).

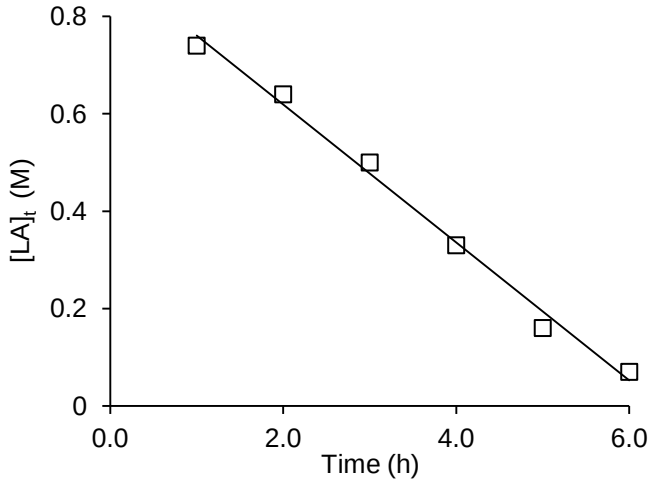


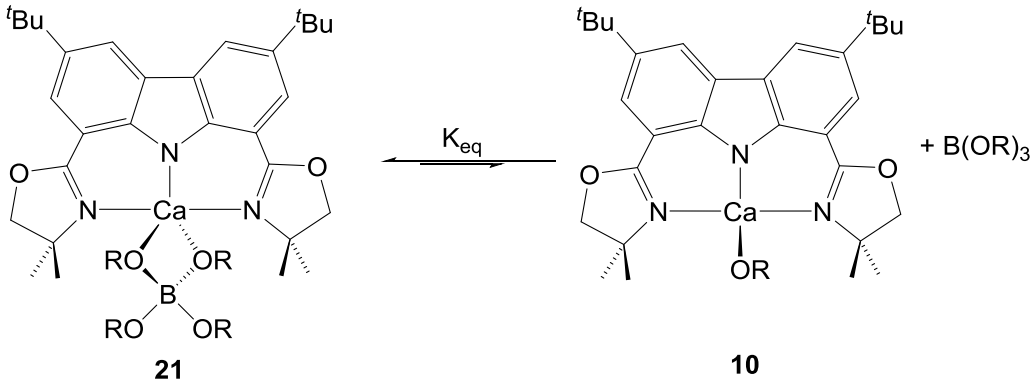
Figure 3.14. Data for the ROP of *rac*-LA with Ca(CzOx^{Me_2})(BH$_4$)(THF)$_2$ (**13**) with 4.5 eq. PhCHO; zero-order plot of [LA]$_t$ *vs*. time (k_{obs} = -0.142(6) M h^{-1}, R^2 = 0.992); vertical-axis intercept = 0.90(2) M (expected value = [LA]$_0$ = 1 M).

An apparent zero-order dependence on monomer concentration is relatively unusual, and there have been only a handful of recent examples which confirm a zero-order dependence on ε-caprolactone and *rac*-LA.[37-39] Scheme 3.8 details the mechanism through which **10** is stabilised by coordination of free B(OBn)$_3$ to form the tetracoordinated adduct **21**. A lactide molecule coordinates to the catalytically active species **10** (k_1) to form **10-LA**, and can subsequently either dissociate (k_{-1}) or undergo nucleophilic attack at the carbonyl by the OBn initiating group of **10-LA** (k_2). The amount of **10** available to undergo reaction with an incoming monomer is determined by the position of the preequilibrium between **10** and B(OBn)$_3$ (Equation 3.3).

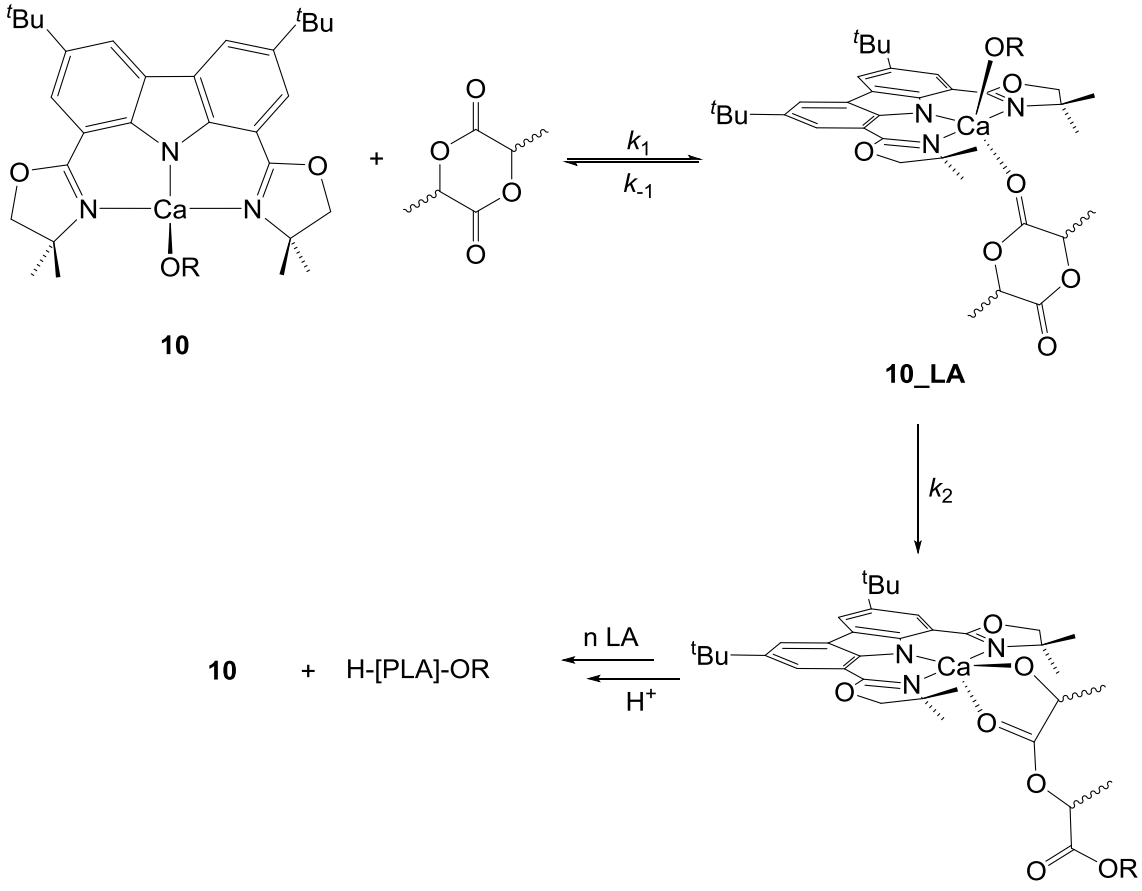
$$[\mathbf{10}] = K_{eq}\frac{[\mathbf{21}]}{[B(OBn)_3]}$$

Equation 3.3

(a) Tetracoordinated borate adduct preequilibrium



(b) Ring-opening *via* non-adduct **10**



Scheme 3.8. Proposed mechanism for the ROP of *rac*-LA catalysed by $Ca(CzOx^{Me_2})(BH_4)(THF)_2$ (**13**) with 4.5 eq. PhCHO.[38]

This mechanism may be represented by the Michaelis-Menten model (Equation 3.4), which accounts for reversible binding of the cyclic ester to the metal centre. If the Michaelis constant (K_m, Equation 3.5) is less than the concentration of lactide

monomer (K_m << [LA]), saturation kinetics can occur, leading to an apparent zero-order dependency on [LA] (Equation 3.6).

$$-\frac{d[LA]}{dt} = \frac{k_2[\mathbf{10}][LA]}{K_M + [LA]}$$

Equation 3.4

$$K_M = \frac{k_{-1} + k_2}{k_1}$$

Equation 3.5

$$-\frac{d[LA]}{dt} = k_2[\mathbf{10}]$$

Equation 3.6

Molecular weight analysis confirmed the immortal nature of the polymerisation: a plot of M_n(obs) *vs*. % conversion showed a linear growth of molecular weight, with a gradient of 34(1) g mol^{-1} (% conversion)$^{-1}$ (R^2 = 0.993), corresponding to 4 chains per metal centre. However, the obtained molecular weights were higher than expected (at 93%, M_n(obs) = 4,280 g mol^{-1} *cf*. M_n(calc) = 3,458 g mol^{-1}) caused by an initial increase in the molecular weight growth (Figure 3.15). Analysis of the MALDI-ToF MS confirmed the presence of PLA chains terminated with an OBn end-group at the non-hydroxy end, and peak envelopes between the major and minor distributions of $\Delta m/z$ 72 g mol^{-1} indicated the occurrence of transesterification during the polymerisation. The resultant polymer was predominantly atactic.

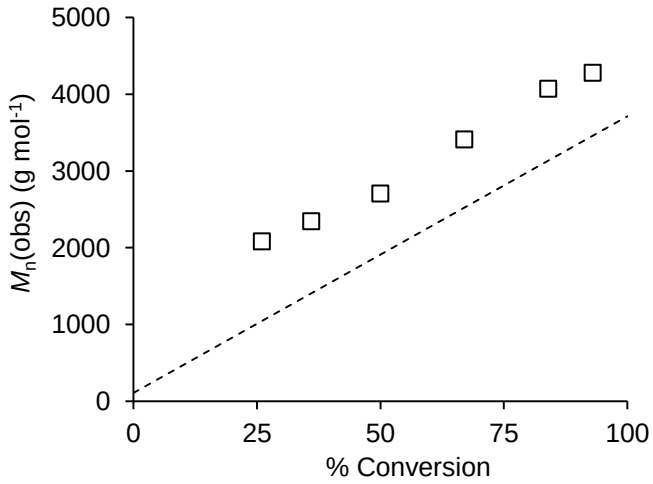


Figure 3.15. M_n(obs) (g mol^{-1}) *vs*. % conversion plot for the ROP of *rac*-LA using Ca(CzOx^{Me_2})(BH$_4$)(THF)$_2$ (**13**) and 4.5 eq. PhCHO; the dashed line is the M_n(calc), expecting 4 chains per metal centre. Conditions: 4 mL THF, 23 °C, [*rac*-LA]$_0$:[**13**]$_0$: [PhCHO]$_0$= 100:1:4.5, [*rac*-LA]$_0$ = 1.0 M.

Unusually, the rate of polymerisation was considerably slower than analogous polymerisation with Ca(CzOx^{Me_2})(OBn) (**10**) and 1 equivalent of B(OBn)$_3$ (Table 3.7, entry 3) which could be considered an identical system. This cannot be attributed to incomplete conversion of **13** to **10** and 1 equivalent of B(OBn)$_3$ on addition of 4.5 equivalents of benzaldehyde, as monitoring the reaction between the starting borohydride complex and benzaldehyde by ^{1}H and ^{11}B NMR confirms its immediate formation. Furthermore, the solution containing complex **13** and 4.5 equivalents of benzaldehyde is stirred for 5 min prior to the addition of *rac*-LA.

To investigate the impact of excess benzaldehyde on the ROP of *rac*-LA with the *in situ* generated complex **10** and 1 equivalent of B(OBn)$_3$, a four-fold excess of benzaldehyde was added to **13** prior to polymerisation (Table 3.7, entry 7). In the presence of 8 equivalents of benzaldehyde, 88% conversion was reached after 360 min, and the dependence on lactide was determined to be zero-order (k_{obs} = -0.115(3) M h^{-1}, R^2 = 0.996). The presence of a further excess of benzaldehyde did not appear to impact upon the rate of reaction, and thus it may be concluded that its role in polymerisation is innocent. The origin of the discrepancy in rate of reaction and kinetic regime between the externally synthesised and *in situ* generated Ca(CzOx^{Me_2})(OBn) (**10**) and B(OBn)$_3$ not readily apparent at this stage.

The behaviour of Ca(CzOx^{Me_2})(BH$_4$)(THF)$_2$ (**13**) when polymerising *L*-LA was examined in order to investigate the unusual kinetic regimes observed both in the absence and presence of benzaldehyde (Table 3.7, entries 8 and 9). In the absence of benzaldehyde, **13** achieved 88% conversion after 240 min following a third-order dependence on *L*-LA (k_{obs} = 8.8(1) M^{-2} h^{-1}, R^2 = 0.998). The reduction in k_{obs} is consistent with the preference of **13** to enchain lactide *via racemic* dyads, resulting in a slower reaction when enchaining solely *via meso* dyads. At 20% conversion, M_n(obs) was significantly higher than M_n(calc) (9,160 g mol^{-1} *cf.* 2,886 g mol^{-1}), consistent with partial catalyst activation, after which the growth in molecular weight corresponds to approximately 3 to 4 chains per metal centre, resulting in a final M_n(obs) which agreed well with the expected values (12,780 g mol^{-1} *cf.* 12,685 g mol^{-1}). This may be attributed to the occurrence of back-biting, suggested by moderate PDIs of 1.48-1.81, and immortal polymerisation, with a trialkyl borate ester species such as B(LA-H)$_3$ acting as a chain transfer agent.

The addition of 4.5 equivalents of benzaldehyde to **13** resulted in comparable behaviour to the polymerisation of *rac*-LA: after 240 min 88% conversion was reached, most closely following a zero-order dependency on lactide concentration (k_{obs} = -0.134(6) M h^{-1}, R^2 = 0.990), which is identical within error to the k_{obs} for *rac*-LA. As the polymerisation of *rac*-LA exhibited no stereocontrol, producing atactic PLA, it is unsurprising that the k_{obs} for the ROP of *L*-LA is identical within error to that for the ROP of *rac*-LA as, in order to produce atactic PLA, $k_{R/SS} \approx k_{R/RR}$. Following an initial increase to 1,960 g mol^{-1} at 20% conversion (M_n(calc) = 829 g mol^{-1}), the molecular weight grew linearly with conversion, with a gradient of M_n(obs) *vs*. % conversion resulting a gradient of 42(2) g mol^{-1} (% conversion)$^{-1}$ (R^2 = 0.988).

The polymerisation of 100 equivalents of *meso*-LA with Ca(CzOx^{Me_2})(BH$_4$)(THF)$_2$ (**13**) (Table 3.7, entry 10) is marked by a comparatively long induction period of ~2 min before which the catalyst reaches 89% conversion after 5 min (Figure 3.16). The induction period can be ascribed to partial activation of the catalyst immediately following initiation, which is observed with *meso*-LA due to its comparatively higher rate of reaction than *rac*-LA. Gratifyingly, the growth in molecular weight is linear throughout the polymerisation in close agreement with M_n(calc) (at 89%, M_n(obs) =

13,540 g mol^{-1} *cf.* M_n(calc) = 12,829 g mol^{-1}), despite broadening PDIs of 1.07-1.58. In addition, analysis with ^{1}H{^{1}H} NMR spectroscopy revealed the PLA backbone to be moderately syndiotactically enriched, with P_r = 0.66-0.69, comparable to the degree of enrichment observed with Mg(CzOx^{Me_2})BH$_4$ (**7**). Following the induction period, kinetic analysis revealed the reaction to follow a first-order dependence on lactide (k_{obs} = 50(2) h^{-1}, R^2 = 0.996); this deviation from the third-order kinetics observed with *rac*- and *L*-LA may be attributed to the different activation parameters associated with the ring-opening of a *meso*-LA molecule (Chapter 1, Section 1.9). The rate of polymerisation is considerably faster with *meso*-LA due to the decreased stability of the monomer, which may affect the relative rates of preequilibria, resulting in the observation of a different kinetic regime.

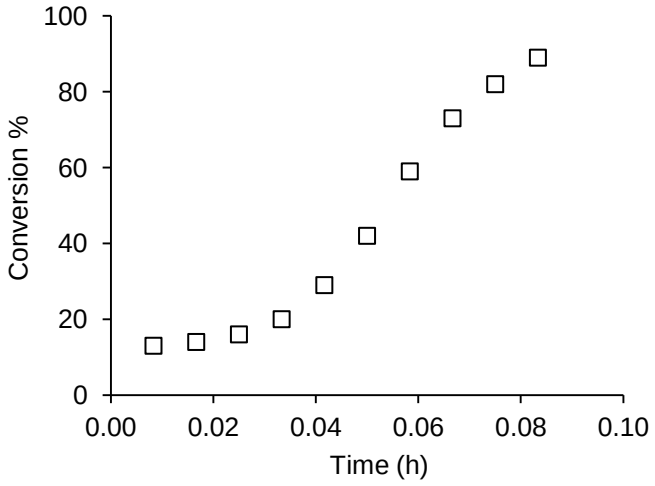


Figure 3.16. Plot of % conversion *vs*. time for the ROP of *meso*-LA with Ca(CzOx^{Me_2})(BH$_4$)(THF)$_2$ (**13**).

The addition of 4.5 equivalents of benzaldehyde to Ca(CzOx^{Me_2})(BH$_4$)(THF)$_2$ (**13**) to generate *in situ* Ca(CzOx^{Me_2})(OBn) (**10**) and B(OBn)$_3$ results in considerably altered behaviour when treated with 100 equivalents of *meso*-LA: notably the reaction no longer proceeds following an induction period and observes a second-order dependence on monomer concentration (k_{obs} = 86(2) M^{-1} h^{-1}, R^2 = 0.995). 89% monomer conversion is achieved after 5 min, which is comparable to the rate of reaction without any additives present. Although it is expected that the addition of benzaldehyde to generate an alkoxide initiator will result in an accelerated rate of reaction, the formation of B(OBn)$_3$ which can coordinate to the metal may slow the

relative rate. Whilst the molecular weights support the immortal nature of the polymerisation, their growth against conversion corresponds to approximately 2 chains growing per metal centre, instead of 4: indicative of inefficient chain transfer in which the rate of propagation exceeds the rate of chain transfer. The molecular weight distribution is remains reasonably narrow throughout the polymerisation (PDI = 1.16-1.23), although the MALDI-ToF MS reveals there to be two molecular weight distributions, showing the presence of intermolecular transesterification. The degree of syndiotactic enrichment is comparable to the other systems previously examined (P_r = 0.60-0.66).

$Sr(CzOx^{Me2})(BH_4)(THF)_2$ (**14**) was found to be highly active for the ROP of *rac*-LA, polymerising 100 equivalents to 91% conversion after 2 minutes (Table 3.7, entry 12); the rate of polymerisation was too rapid to permit a comprehensive kinetic analysis. Whilst **14** was extremely active, it was poorly controlled: the molecular weights obtained were found to be slightly higher than expected (M_n(obs) = 15,540 g mol^{-1} *cf.* M_n(calc) = 13,117 g mol^{-1}) indicating that **14** follows a similar initiation mechanism to the magnesium and calcium congeners **7** and **13**, respectively, in which partial catalyst activation results in poorly controlled molecular weights. In comparison to its lighter counterparts, **14** resulted in PLA with a very broad molecular weight distribution (PDI = 1.48-1.80). Analysis with MALDI-ToF MS revealed the polymer produced to be cyclic with no observable end-group, with peak envelopes of $\Delta m/z$ 72 g mol^{-1}, indicative of a high degree of transesterification, The addition of 4.5 equivalents of benzaldehyde to **14** to generate $Sr(CzOx^{Me2})(OBn)$ (**22**) and $B(OBn)_3$ resulted in a significantly longer rate of reaction: 92% monomer conversion was achieved after 300 min (Table 3.7, entry 13). Unlike $Ca(CzOx^{Me2})(BH_4)(THF)_2$ (**13**), the reaction observed a first-order dependency in lactide concentration (k_{obs} = 0.58(2) h^{-1}, R^2 = 0.996) (Figure 3.17) indicating that the Michaelis-Menten model is no longer applicable, as K_M is no longer sufficiently less than the rate of ring-opening (k_2) to result in a zero-order dependency on [LA]. As for the lighter congeners, $Sr(CzOx^{Me2})(OBn)$ (**22**) and $B(OBn)_3$ enacted a moderate degree of chain transfer, with the growth in polymer molecular weight during the polymerisation consistent with the propagation of approximately three chains per metal centre. Unlike **14**, the OBn termini were observed in the PLA obtained from the *in situ* generated alkoxide; however, peak envelopes of $\Delta m/z$ 72 g mol^{-1} confirmed the presence of

transesterification, mirrored in the broad polydispersities obtained (PDI = 1.24-1.89). For both systems, no stereocontrol was observed, resulting in atactic polymer.

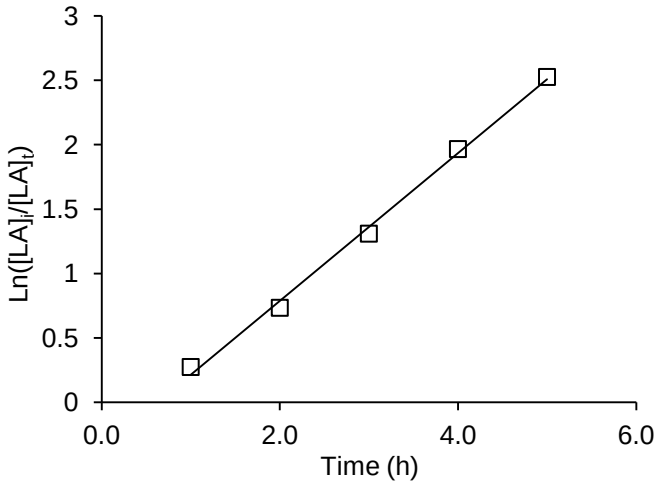


Figure 3.17. Data for the ROP of *rac*-LA with Sr(CzOx^{Me_2})(BH$_4$)(THF)$_2$ (**14**) and 4.5 eq. PhCHO; first-order plot of ln[LA]$_i$/[LA]$_t$ *vs*. time (k_{obs} = 0.57(2) h^{-1}, R^2 = 0.997).

3.5.2 Polymerisation studies: ROP of *rac*- and *meso*-LA with Group 3 and lanthanide complexes

Y(CzOx^{Me_2})(BH$_4$)$_2$(THF) (**16**), tested by L. Budden under direct supervision of the author, proved to be an active and well-controlled catalyst for the ROP of *rac*-LA (Table 3.8, entry 1). Following a short initial induction period of ~5 min, the catalyst reached 91% conversion after 50 min with a clear first-order dependency on lactide concentration (k_{obs} = 3.6(2) h^{-1}, R^2 = 0.991). Of considerable interest was whether the two borohydride initiators participated in the polymerisation to result in the growth of two polymer chains per metal centre. The observed molecular weights appear to support the propagation of approximately three chains per metal centre following an initial jump (Figure 3.18).

Table 3.8. Selected data for the polymerisation of *rac*- and *meso*-LA using complexes Y(CzOx^{Me_2})(BH$_4$)$_2$(THF) (**16**), La(CzOx^{Me_2})(BH$_4$)$_2$(THF) (**17**), and Sm(CzOx^{Me_2})(BH$_4$)$_2$(THF) (**18**) in THF.[a]

Entry	Catalyst	Monomer	Additive (eq.)	Conv.[b] %	Time (min)	M_n(obs)[c] (g mol^{-1})	M_n(calc)[d] (g mol^{-1})	M_w/M_n[c]	P_r[b]
1[e]	Y(CzOx^{Me_2})(BH$_4$)$_2$(THF) (**16**)	*rac*	-	94	50	6,690	6,561	1.35	0.84-0.87
2[e]	Y(CzOx^{Me_2})(BH$_4$)$_2$(THF) (**16**)	*rac*	B(OBn)$_3$ (2)	93	45	2,620	1,757	1.34	0.81-0.83
3[e]	Y(CzOx^{Me_2})(BH$_4$)$_2$(THF) (**16**)	*rac*	B(OMe)$_3$ (2)	91	45	2,240	1,664	1.29	0.80-0.83
4[e]	Y(CzOx^{Me_2})(BH$_4$)$_2$(THF) (**16**)	*rac*	PhCHO (10)	90	3	2,810	1,729	1.21	0.79-0.83
5[e]	Y(CzOx^{Me_2})(BH$_4$)$_2$(THF) (**16**)	*meso*	-	92	10	5,460	6,633	1.21	0.54-0.58
6[e]	Y(CzOx^{Me_2})(BH$_4$)$_2$(THF) (**16**)	*meso*	PhCHO (10)	93	1	2,770	1,783	1.20	0.52-0.54
7	La(CzOx^{Me_2})(BH$_4$)$_2$(THF) (**17**)	*rac*	-	98	1.5	7,280	7,065	1.64	0.52-0.61
8	La(CzOx^{Me_2})(BH$_4$)$_2$(THF) (**17**)	*rac*	PhCHO (10)	96	1.5	5,300	1,837	1.42	0.47-0.52
9	Sm(CzOx^{Me_2})(BH$_4$)$_2$(THF) (**18**)	*rac*	-	93	3.5	6,340	6,705	1.58	0.84-0.87
10	Sm(CzOx^{Me_2})(BH$_4$)$_2$(THF) (**18**)	*rac*	PhCHO (10)	96	0.5	3,870	1,855	1.21	0.80

[a] Conditions: [LA]$_0$:[initiator]$_0$ = 100:1, 4 mL THF at 23 °C. [LA]$_0$ = 1.0 M. [b] Measured by ^{1}H NMR (CDCl$_3$) analyses. [c] Molecular weights (g mol^{-1}) determined from GPC using appropriate Mark-Houwink corrections. [d] Expected average M_n (g mol^{-1}) for stated number of chains per metal and stated % conversion: M_n (calc for entries 1, 5, 7 and 9) = ½ (conversion (%) × 100 × 144.1) + 4.0; (calc for entries 4, 6, 8 and 10) = 1/8 (conversion (%) × 100 × 144.1) + 108.1; (calc for entry 2) = ¼((conversion (%) × 100 × 144.1) + 4) + ¾((conversion (%)× 100 × 144.1) + 108.1); (calc for entry 3) = ¼((conversion (%) × 100 × 144.1) + 4.0) + ¾((conversion (%)× 100 × 144.1) + 32.0). [e] Performed by L. Budden.

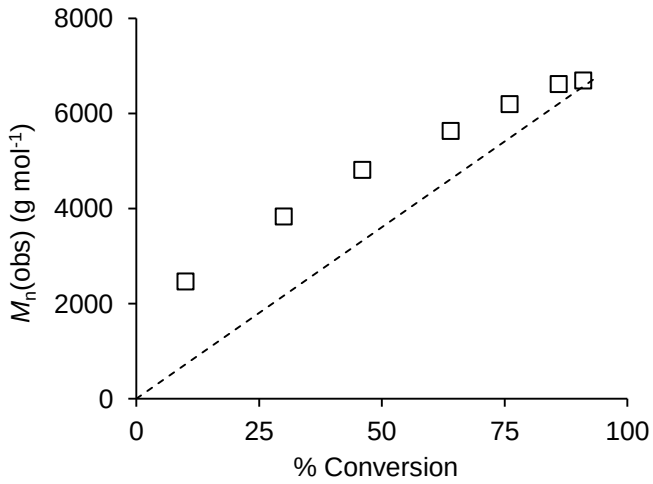


Figure 3.18. M_n(obs) (g mol^{-1}) *vs*. % conversion plot for the ROP of *rac*-LA using Y(CzOx^{Me_2})(BH$_4$)$_2$(THF) (**16**); the dashed line corresponds to M_n(calc). Conditions: 4 mL THF, 23 °C, [*rac*-LA]$_0$:[**16**]$_0$ = 100:1 [*rac*-LA]$_0$ = 1.0 M.

Following these unexpected observations, ^{1}H and ^{11}B NMR studies were undertaken in order to understand the mechanism of initiation and propagation for **16**. Following treatment of **16** with 20 equivalents of *rac*-LA, the ^{11}B NMR spectrum revealed the consumption of the starting borohydride and the evolution of two resonances at 8.5 and 23.1 ppm, which have been tentatively assigned as corresponding to {B(LA-H)$_4$}$^-$ and B(LA-H)$_3$, respectively. B(LA-H)$_3$ may act as a chain transfer agent, accounting for the growth of approximately three chains of polymer per metal centre, as opposed to the two anticipated. Although it is possible for B(LA-H)$_3$ to act as a CTA, the presence of secondary alkoxide substituents may reduce its efficiency, leading to the growth of fewer chains per metal centre.

As established for the magnesium and calcium borohydride systems previously investigated, a deuterium labelling study was undertaken in order to establish the mechanism of initiation for **16**. Complex **16** was treated with 15 equivalents of *rac*-LA in 4 mL THF at 23 °C, achieving 90% monomer conversion after 6 h. The reaction was quenched with dry HCl in diethyl ether, the polymer extracted into CH_2Cl_2 and fully characterised with ^{1}H NMR spectroscopy, ^{13}C{^{1}H} NMR spectroscopy, GPC and MALDI-ToF MS. Analysis of the PLA end-groups by ^{1}H NMR was limited due to broadening. Nonetheless multiple doublets of doublets were observed in the region of 5.4-5.7 ppm, which may correspond to several LA-H

environments, in agreement with previous observations (Chapter 2). There were no resonances in the range 9.0-12.0 ppm which would correlate to an aldehyde terminus. GPC analysis revealed the polymer obtained to have an observed molecular weight of 1,360 g mol^{-1} *cf.* M_n(calc) = 977 g mol^{-1} (PDI = 1.23). A further experiment was conducted in which **16-*d*$_8$** was treated with 15 equivalents of *rac*-LA in 4 mL THF at 23 °C, and under these conditions the catalyst was active, reaching 95% monomer conversion in 6 h. In this instance, the rate deceleration caused by a kinetic isotope effect observed in **7-*d*$_4$** and **13-*d*$_4$** was not observed for **16-*d*$_8$**. The reaction was quenched with dry HCl in diethyl ether, the polymer extracted into CH_2Cl_2 and fully characterised. As anticipated, the ^{1}H NMR spectrum of the PLA in THF-d_8 revealed the absence of the doublets of doublets observed for **16**, indicative that they correspond to a borohydride-derived polymer end-group. Analysis of the ^{2}H NMR spectrum obtained in THF revealed very similar resonances to that of the PLA obtained from **7-*d*$_4$**: two broad resonances were observed at 4.2 and 5.5 ppm, corresponding to -C(H)MeC$\underline{D}_2$OH and -LA-$\underline{D}$, respectively (Figure 3.19). Furthermore, the MALDI-ToF MS confirm peaks at 1482 and 1485 g mol^{-1}, which are in close agreement with the calculated values for the PLA chains [H-[LA]$_9$-[LA-D]-K]$^+$ (1483 g mol^{-1}) and [H-[LA]$_9$-[C(H)MeCO$_2$C(H)MeCD$_2$OH]-K]$^+$ (1486 g mol^{-1}).

These findings confirm the mechanism proposed in Chapter 2, in which complex **16** undergoes one hydride transfer to form Y(CzOx^{Me2})(LA-H)$_2$. The rate increase during the ROP of *rac*-LA when treating **16** with 10 equivalents of benzaldehyde to generate the bis(alkoxide) complex *in situ* suggests that only partial activation of the starting complex to form an active catalytic species is achieved; however, this effect is concealed by the concurrent evolution of a trialkyl borate ester species such as B(LA-H)$_3$, resulting in the occurrence of chain transfer and a reduction in molecular weights. The lack of difference in rate observed for **16** and **16-*d*$_8$** suggests that the second hydride transfer does not experience the same kinetic isotope effect slowing the rate of the second hydride transfer observed for **7-*d*$_4$** and **13-*d*$_4$**.

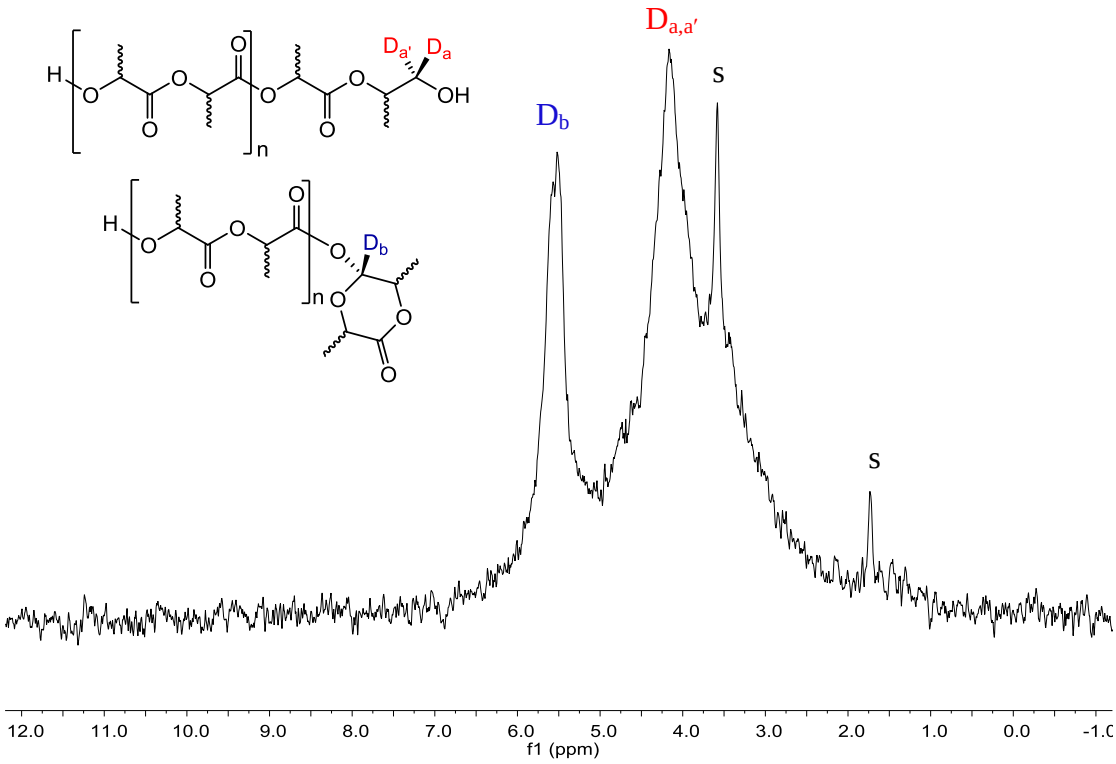


Figure 3.19. ^{2}H NMR spectrum (THF, 76.7 MHz, 298 K) of PLA synthesised from Y(CzOx^{Me2})(BD$_4$)$_2$ (**16-*d*$_8$**); "s" denotes residual solvent signals.

2 equivalents of a trialkyl borate ester such as B(OBn)$_3$ and B(OMe)$_3$ were introduced prior to polymerisation to investigate the efficacy of externally added chain transfer agents on the ROP of *rac*-LA with **16** (Table 3.8, entries 2 and 3, respectively). Their addition did not prevent the borohydride initiation mechanism, resulting in similar rates of reaction observed for **16** in the absence of any additives (Figure 3.20). All reactions observed a first-order dependence in lactide concentration; however, unusually, the addition of either CTA resulted only in a slight rate increase. For B(OMe)$_3$, k_{obs} = 5.7(1) h^{-1} (R^2 = 0.997) following a similar induction period of ~5 min. Notably, the addition of B(OBn)$_3$ resulted in a slightly shorter induction period of ~3 min, followed by a further increase in the observed rate constant (k_{obs} = 6.4(2) h^{-1}, R^2 = 0.996). ^{1}H and ^{11}B NMR studies were conducted to probe further the reactivity of **16** in the presence of B(OBn)$_3$ or B(OMe)$_3$. On the addition of 2 equivalents of either trialkyl borate ester to a THF-d_8 solution of **16**, no exchange resulting in the consumption of the borohydride groups and the formation of Y(CzOx^{Me2})(OR)$_2$ (R = Me or Bn) and B(OR)$_{3-x}$(H)$_x$ was observed. The increase in

rate is tentatively ascribed to mass transport limitation, in which the polymer produced with **16** in the absence of any CTAs results in a comparatively more viscous solution to that obtained during the polymerisation with **16** in conjunction with either $B(OBn)_3$ or $B(OMe)_3$, which form shorter polymer chains and thus a less viscous solution. The more viscous solution caused by the longer polymer chains obtained with **16** without additives may inhibit the diffusion of the monomer within the solution to the metal centre, resulting in a decreased rate of polymerisation.

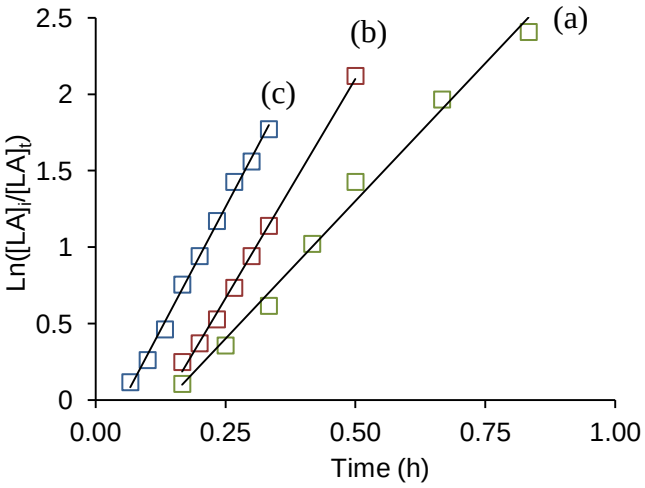


Figure 3.20. Data for the ROP of *rac*-LA with $Y(CzOx^{Me_2})(BH_4)_2(THF)$ (**16**) in the presence of various additives. Semi-logarithmic plot of $\ln[LA]_i/[LA]_t$ *vs*. time. (a) **16** with no additives: k_{obs} = 3.6(2) h^{-1}, R^2 = 0.991 (green squares). (b) **16** with 2 eq. $B(OMe)_3$: k_{obs} = 5.7(1) h^{-1}, R^2 = 0.997 (red squares). (c) **16** with 2 eq. $B(OBn)_3$: k_{obs} = 6.4(2) h^{-1}, R^2 = 0.996 (blue squares).

Molecular weight analysis of the resultant polymer revealed $B(OMe)_3$ to be the superior CTA, producing polymer which is in closer agreement to the calculated molecular weights, attributed to the reduced steric hindrance of the -OMe substituents in comparison to the -OBn substituents. Following an initial increase a plot of M_n(obs) *vs*. conversion for the employment of $B(OMe)_3$ as a CTA resulted in a linear increase with a gradient of 20.7(4) g mol^{-1} (% conversion)$^{-1}$ (R^2 = 0.998): in close agreement with the expected value of 18 g mol^{-1} (% conversion)$^{-1}$ for 8 polymer chains per metal centre. Analysis with MALDI-ToF MS confirmed the presence of two polymer distributions: in each case the major distribution corresponded to chains terminated with the appropriate -OR end-group, and a minor distribution corresponding to the -$CH(Me)CH_2OH$ and -(LA-H) end-groups of the borohydride initiator. Analysis of the

polymer backbone by $^{1}H\{^{1}H\}$ NMR spectroscopy revealed both CTAs to result in moderately high heterotacticities ($P_r \approx 0.80$-0.83); however they were slightly lower than the degree of enrichment observed for **16** in the absence of any additives (P_r = 0.84-0.87).

The addition of 10 equivalents of benzaldehyde to **16** resulted in a considerably increased rate of reaction: 90% monomer conversion was achieved after 3 min, with no observable induction period. Plots of $\ln[LA]_i/[LA]_t$ *vs*. time and $1/[LA]_t$ *vs*. time were constructed in order to derive the order in lactide consumption; however, the reaction conformed to neither first- nor second-order, with a non-integer intermediate value between 1 and 2 being observed instead. As for previous systems studied in Chapter 2, this is indicative of preequilibria associated with the presence of a triakyl borate ester throughout polymerisation, impacting on the apparent order in [LA]. Nevertheless, the overall rate acceleration further confirms the proposed mechanism for the initiation of lactide with **16** in the absence of any additives: the conversion of the borohydride groups to alkoxide initiators results in a more efficient initiation process which does not result in the formation of catalytically inactive species reducing the overall rate of polymerisation. The molecular weight appeared to increase linearly with conversion. Even so, the molecular weights were higher than expected, indicative of slightly inefficient chain transfer with $B(OBn)_3$ (M_n(obs) = 2,810 g mol^{-1} *cf.* M_n(calc) = 1,729 g mol^{-1}). The presence of OBn end-groups was confirmed by MALDI-ToF MS which revealed a peak at 1587 g mol^{-1}, corresponding to 10 lactide units. The degree of heterotactic enrichment appeared to be slightly reduced compared to **16** in the absence of benzaldehyde, with P_r = 0.79-0.83.

Following the high degrees of heterotactic enrichment observed with the polymerisation of *rac*-LA, **16** was treated with 100 equivalents of *meso*-LA in order to investigate its potential to exert stereocontrol during the polymerisation. In the absence of benzaldehyde, **16** achieved 92% monomer conversion after 10 min, following a short induction period of ~2 min. Kinetic analysis revealed the reaction to follow a first-order dependence on lactide concentration, with k_{obs} = 25.4(8) h^{-1} (R^2 = 0.996) (Figure 3.21; top). The molecular weight was found to agree closely with that expected for 2 polymer chains growing per metal centre. However, after ~50% conversion, they were found to be lower than anticipated, which may be attributed to

deleterious transesterification reactions becoming increasingly prevalent towards the end of the reaction (Figure 3.21; bottom).

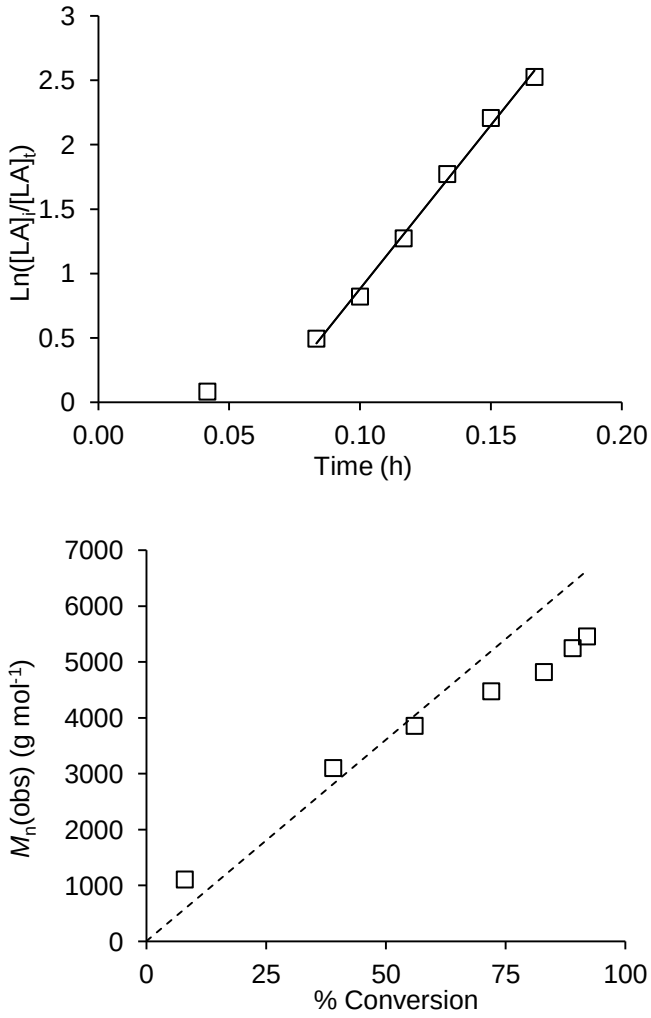


Figure 3.21. Data for the ROP of *meso*-LA using Y(CzOx^{Me_2})(BH$_4$)$_2$(THF) (**16**). Top: Semi-logarithmic plot of ln[LA]$_i$/[LA]$_t$ *vs*. time (k_{obs} = 25.4(8) h^{-1}, R^2 = 0.996). Bottom: M_n(obs) (g mol^{-1}) *vs*. % conversion plot; the dashed lines correspond to M_n(calc). Conditions: 4 mL THF, 23 °C, [*rac*-LA]$_0$:[**16**]$_0$ = 100:1 [*rac*-LA]$_0$ = 1.0 M.

The addition of 10 equivalents of benzaldehyde in order to generate *in situ* complex Y(CzOx^{Me_2})(OBn)$_2$ (**24**) and 2 equivalents of B(OBn)$_3$ resulted in a large rate increase, resulting in the catalyst reaching 93% conversion after 1 min. Unfortunately, a kinetic analysis was not possible due to the extremely high rate of reaction. The observed molecular weights were considerably higher than those calculated (at 93% conversion, M_n(obs) = 2,770 g mol^{-1} *cf.* M_n(calc) = 1,783 g mol^{-1}): the inefficiency of chain transfer observed during the polymerisation of *rac*-LA may be more

pronounced when polymerising *meso*-LA, due to the comparatively faster rate of propagation associated with *meso*-LA. Disappointingly, both in the presence and absence of benzaldehyde, **16** offered little stereocontrol, producing slightly syndiotactically enriched PLA ($P_r \approx 0.55$-0.60).

Following the successful results obtained by L. Budden, attention was focussed on the performance of La(CzOx^{Me_2})(BH$_4$)$_2$(THF) (**17**) and Sm(CzOx^{Me_2})(BH$_4$)$_2$(THF) (**18**) for the ROP of *rac*-LA (Table 3.8, entries 8 and 10). Both **17** and **18** were highly active for the ROP of *rac*-LA, reaching completion within <5 min. Due to its larger size, **17** was faster than **18**, achieving 98% conversion after 1.5 min; however, due to its high activity, kinetic analysis was not possible to determine the order in lactide consumption. Following an induction period of ~0.5 min, **18** achieved 93% conversion after 3.5 min, and observed a first-order dependence in [LA] (k_{obs} = 60(3) h^{-1}, R^2 = 0.991). The presence of an induction period mirrors the behaviour observed with **16**, which may be attributed to incomplete catalyst activation following the immediate introduction of lactide to the precatalyst. Both **17** and **18** produced polymer whose molecular weights were observed to be in close agreement to those expected; however, in the case of **18**, it is apparent that this is a result of transesterification resulting in a decrease in M_n(obs) with a concurrent broadening of PDI. At 9% conversion, M_n(obs) was found to be 1,780 g mol^{-1} (M_n(calc) = 652 g mol^{-1}), whilst at 93% M_n(obs) agreed well with M_n(calc) (6,340 and 6,705 g mol^{-1}, respectively). The observed increase in PDI from 1.28 to 1.58 over the course of the reaction supports the hypothesis that transesterification is the cause of the apparently good molecular weight agreement observed in this instance. Gratifyingly, **18** offered good stereocontrol, resulting in highly heterotactically-enriched PLA (P_r = 0.84-0.87); in contrast, **17** resulted in predominantly atactic polymer (P_r = 0.52-0.61). This reduction in heteroselectivity may be attributed to the increasing ionic radius of the metal resulting in a larger coordination sphere and a subsequent loss of stereocontrol.[40-42] Analysis with MALDI-ToF MS confirmed that both **17** and **18** afforded α,ω-dihydroxytelechelic and (LA-H)-terminated PLA chains.

The activity of complexes **17** and **18** as also examined in the presence of 10 equivalents of benzaldehyde resulting in the *in situ* generation of the corresponding alkoxides La(CzOx^{Me_2})(OBn)$_2$ (**27**) and Sm(CzOx^{Me_2})(OBn)$_2$ (**30**), with concurrent

evolution of 2 equivalents of $B(OBn)_3$. Both **27** and **30** were extremely active initiators for the ROP of *rac*-LA in the presence of $B(OBn)_3$. In comparison to **17**, **27** with 2 equivalents of $B(OBn)_3$ was marginally more active, reaching 70% conversion after 0.5 min (*cf*. 51% conversion after 0.5 min); however, 96% conversion was achieved after the same reaction time of 1.5 min. Unfortunately, the molecular weight control was poor (M_n(obs) = 5,300 g mol^{-1} *cf*. M_n(calc) = 1,837g mol^{-1}), which may be due to an extremely high rate of propagation compared to the rate of chain transfer, resulting in relatively little chain transfer throughout the polymerisation. Nonetheless, **27** with 2 equivalents of $B(OBn)_3$ afforded a lower molecular weight distribution, which may be accounted for by the presence of the CTA which reduces the incidence of deleterious transesterification reactions. Similarly, **30** with 2 equivalents of $B(OBn)_3$ was found to be more active than its bis(borohydride) counterpart, reaching 96% conversion after 0.5 min. Chain transfer was more pronounced in this instance, with an observed molecular weight closer to the expected value, although chain transfer was still not completely efficient (M_n(obs) = 3,870 g mol^{-1} *cf*. M_n(calc) = 1,837 g mol^{-1}). Gratifyingly, **30** with 2 equivalents of $B(OBn)_3$ resulted in a narrower PDI of 1.21 and also exhibited a moderately high degree of stereocontrol producing heterotactically-enriched PLA (P_r = 0.80). In both instances, the MALDI-ToF MS revealed peaks at 1587 g mol^{-1}, corresponding to a polymer chain of 10 lactide units, confirming the presence of OBn termini. The presence of two distributions with peak envelopes of $\Delta m/z$ 72 g mol^{-1} indicated the occurrence of transesterification during polymerisation.

As expected, the activities observed for complexes **16**-**18** and **24**, **27** and **30** generally increase with increasing metal size, such that Y < Sm < La. Moreover, whilst both **16**, **24**, **18** and **30** offered high degrees of stereoenrichment, **17** and **27** produced atactic polymer, which may be a product of the rapid rate of reaction and subsequent loss of stereocontrol associated with a larger coordination sphere due to the increased size of the metal.[40-42]

3.6 Summary and conclusions

This Chapter has described the synthesis and characterisation of a series of $CzOx^{Me_2}$-supported calcium, strontium, yttrium, lanthanum and samarium complexes, complexes **9**-**18**, **13**-$\boldsymbol{d_4}$ and **16**-$\boldsymbol{d_8}$ and their application as catalysts for the ROP of *rac*-

LA, *L*- and *meso*-lactide. Complexes **9** and **11** were prepared through protonolysis reactions between $HCzOx^{Me2}$ (**1.45**) and $Ca\{N(SiMe_3)_2\}_2(THF)_2$ in toluene; however **11** required the application of forcing conditions and was obtained in a low yield. The controlled reaction of **10** with benzyl alcohol in toluene afforded complex **10** in a moderate yield. DOSY NMR spectroscopy was utilised to determine the THF solution conformation of complexes **2** and **10** though the determination of their diffusion coefficients and the onwards comparison to the diffusion coefficient of monomeric **3**. All complexes were determined to be monomeric in THF.

Complexes **12**-**15** were prepared in good yields through the salt metathesis of $K(CzOx^{Me2})$ (**5**) with the appropriate metal precursor; however, complex **13**-$\boldsymbol{d_4}$ was obtained through the salt metathesis reaction of **12** with sodium borodeuteride. Heteroleptic strontium complexes were found to undergo redistribution according to the Schlenk equilibrium readily at room temperature in both donor and non-donor solvents. Group 3 and lanthanide complexes **16**-**18** were prepared through the salt metathesis of **5** with the appropriate metal tris(borohydride) starting material in moderate yields. Attempts to independently synthesise complexes of the sort $Y(CzOx^{Me2})(OBn)_2$ were unsuccessful: the reaction of LiO^iPr with the known complex $Y(CzOx^{Me2})(Cl)_2(THF)$ instead resulted in the formation of **19** *via* transmetallation. **16**-$\boldsymbol{d_8}$ could not be obtained using an analogous method employed to synthesise **7**-$\boldsymbol{d_4}$ and **13**-$\boldsymbol{d_4}$, but was obtained from the direct reaction of **5** with $Y(BD_4)_3(THF)_2$ (**20**).

Analysis of the IR spectra of complexes **13** and **14** in the solid state revealed unusual borohydride bonding, in which the borohydride group appeared to be either polymeric or ionic. However, on dissolution into THF, both complexes were readily assigned as tridentate: comparison of the υ(B–H) bands for **7**, **13** and **14** confirmed a decrease in covalency of the M-BH_4 bond on descent of the group. The bonding mode of the borohydride groups in **16**-**18** were clearly tridentate in both the solid state and in THF solution.

The addition of benzaldehyde to complexes **13**, **14** and **16**-**18** resulted in the *in situ* transformation from the borohydride to the corresponding alkoxide with concurrent evolution of $B(OBn)_3$. The equilibrium constant for the dissociation of $B(OBn)_3$ from

10 were determined from a Van't Hoff plot of ln K_{eq} *vs*. 1/T. The generation of **24**, **27** and **30** with 2 equivalents of $B(OBn)_3$ allowed for the coordination of either one or two molecules of $B(OBn)_3$ to form mono- and bis(tetracoordinated) adducts.

Whilst complex **9** was determined to be a poorly controlled initiator for the ROP of *rac*-LA, **10** offered good molecular weight control and moderate heterotactic enrichment in the absence of $B(OBn)_3$; however the catalyst's performance was not enhanced through its addition. Deuterium labelling experiments with **13-*d*$_4$** confirmed that **13** undergoes a similar initiation mechanism to that depicted in Chapter 2 for **7**, accounting for the relative decrease in rate observed with **13**. Kinetic analysis of the behaviour of **13** revealed an apparent third-order dependence on lactide concentration, the origin of which has not yet been determined. On the addition of benzaldehyde, *in situ* generated **10** and $B(OBn)_3$ were comparatively slower than **13** and observed a zero-order dependence on lactide concentration: attributed to saturation kinetics in accordance with the Michaelis-Menton model. The ROP of *meso*-LA with **13** in the absence and presence of benzaldehyde resulted in comparatively rapid rate of reaction, attributed to the decreased stability of the monomer, forming PLA with a moderate degree of syndiotacticity. Employment of **14** resulted in an increased rate of reaction with *rac*-LA with a concurrent loss of molecular weight control, due to the increased reactivity of strontium compared to calcium. Addition of benzaldehyde to generate **23** and $B(OBn)_3$ again resulted in a decreased rate of reaction due to the propensity of the discrete species to form a tetracoordinated borate adduct.

Using similar deuterium labelling experiments, **16** was found to polymerise *rac*-LA *via* a similar mechanism as **7** and **13**, suggesting that both Group 2 and 3 catalysts with borohydride initiators form La-H terminated polymer chains, which are generated from a M($CzOx^{Me_2}$)(LA-H) intermediate produced during the initiation process. The decreased rate observed for borohydride complexes **13** and **16** observed in comparison to catalysts with different initiating groups, may be ascribed to the formation of catalytically inactive species produced on exposure of the borohydride complexes to lactide; however, the exact nature of these species remains elusive at this stage. **16** was moderately active for the ROP of *rac*-LA producing highly heterotactically-enriched PLA. Both **17** and **18** were found to be extremely active for the ROP of *rac*-LA but only **18** exhibited stereocontrol during the polymerisation. On

the addition of benzaldehyde, the relative rates of the *in situ* generated bis(alkoxide) complexes to the borohydride initiators increased as expected, additionally resulting in narrower PDIs and comparable degrees of heterotacticity. Whilst the ROP of *meso*-LA with **16** both in the absence and presence of any additives proceeded rapidly, little stereocontrol was observed.

3.7 References for Chapter Three

1. S. Harder, *Chem. Rev.*, 2010, **110**, 3852-3876.
2. A. W. Addison, T. N. Rao, J. Reedijk, J. van Rijn and G. C. Verschoor, *J. Chem. Soc., Dalton Trans.*, 1984, 1349-1356.
3. D. A. Fletcher, R. F. McMeeking and D. Parkin, *J. Chem. Inf. Comput. Sci.*, 1996, **36**, 746.
4. A. Bondi, *J. Phys. Chem.*, 1964, **68**, 441-451.
5. M. Mantina, A. C. Chamberlin, R. Valero, C. J. Cramer and D. G. Truhlar, *J. Phys. Chem. A.*, 2009, **113**, 5806-5812.
6. W. T. Klooster, L. Brammer, C. J. Schaverien and P. H. M. Budzelaar, *J. Am. Chem. Soc.*, 1999, **121**, 1381-1382.
7. L. Perrin, L. Maron, O. Eisenstein and M. F. Lappert, *New J. Chem.*, 2003, **27**, 121-127.
8. K. H. Den Haan, J. L. De Boer, J. H. Teuben, A. L. Spek, B. Kojic-Prodic, G. R. Hays and R. Huis, *Organometallics*, 1986, **5**, 1726-1733.
9. W. G. Van der Sluys, C. J. Burns and A. P. Sattelberger, *Organometallics*, 1989, **8**, 855-857.
10. A. F. Dunlop-Brière, M. C. Baird and P. H. M. Budzelaar, *J. Am. Chem. Soc.*, 2013, **135**, 17514-17527.
11. J.-M. Ducéré and L. Cavallo, *Organometallics*, 2006, **25**, 1431-1433.
12. C. S. Johnson Jr, *Prog. NMR. Spectrosc.*, 1999, **34**, 203-256.
13. E. O. Stejskal and J. E. Tanner, *J. Chem. Phys.*, 1965, **42**, 288-292.
14. H. Barjat, G. A. Morris, S. Smart, A. G. Swanson and S. C. R. Williams, *J. Magn. Reson. Ser. B*, 1995, **108**, 170-172.
15. I. Yu, A. Acosta-Ramirez and P. Mehrkhodavandi, *J. Am. Chem. Soc.*, 2012, **134**, 12758-12773.

16. C. Fliedel, V. Rosa, F. M. Alves, A. M. Martins, T. Aviles and S. Dagorne, *Dalton Trans.*, 2015.
17. I. Yu, A. Acosta-Ramírez and P. Mehrkhodavandi, *J. Am. Chem. Soc.*, 2012, **134**, 12758-12773.
18. D. Zuccaccia and A. Macchioni, *Organometallics*, 2005, **24**, 3476-3486.
19. J. T. Edward, *J. Chem. Ed.*, 1970, **47**, 261.
20. A. Spernol and K. Z. Wirtz, *Z. Naturforsch. A.: Astrophys., Phys., Phys. Chem.*, 1953, **8**, 522.
21. A. Gierer and K. Z. Wirtz, *Z. Naturforsch. A.: Astrophys., Phys., Phys. Chem.*, 1953, **8**, 532.
22. H. C. Chen and S. H. Chen, *J. Phys. Chem.*, 1984, **88**, 5118-5121.
23. B. M. Schulze, D. L. Watkins, J. Zhang, I. Ghiviriga and R. K. Castellano, *Org. Biomol. Chem.*, 2014, **12**, 7932-7936.
24. F. Perrin, *J. Phys. Radium.*, 1936, **7**, 1.
25. A. Macchioni, G. Ciancaleoni, C. Zuccaccia and D. Zuccaccia, *Chem. Soc. Rev.*, 2008, **37**, 479-489.
26. T. J. Marks and J. R. Kolb, *Chem. Rev.*, 1977, **77**, 263.
27. R. A. Collins, J. Unruangsri and P. Mountford, *Dalton Trans.*, 2013, **42**, 759–769.
28. M. G. Cushion and P. Mountford, *Chem. Commun.*, 2011, **47**, 2276–2278.
29. S. M. Cendrowski-Guillaume, G. Le Gland, M. Nierlich and M. Ephritikhine, *Organometallics*, 2000, **19**, 5654-5660.
30. T. Jaroń and W. Grochala, *J. Nucl. Mater.*, 2012, **420**, 307-313.
31. K. Dehnicke and A. Greiner, *Angew. Chem. Int. Ed.*, 2003, **42**, 1340-1354.
32. F. A. Cotton and G. Wilkinson, in *Advanced Inorganic Chemistry*, John Wiley & Sons, 5th edn., 1988, pp. 955-979.
33. F. Bonnet, A. R. Cowley and P. Mountford, *Inorg. Chem.*, 2005, **44**, 9046-9055.
34. M. P. Blake, A. D. Schwarz and P. Mountford, *Organometallics*, 2011, **30**, 1202-1214.
35. P. I. Binda and E. E. Delbridge, *Dalton Trans.*, 2007, 4685-4692.
36. N. Ajellal, J.-F. Carpentier, C. Guillaume, S. M. Guillaume, M. Helou, V. Poirier, Y. Sarazin and A. A. Trifonov, *Dalton Trans.*, 2010, **39**, 8363-8378.

37. K. Ding, M. O. Miranda, B. Moscato-Goodpaster, N. Ajellal, L. E. Breyfogle, E. D. Hermes, C. P. Schaller, S. E. Roe, C. J. Cramer, M. A. Hillmyer and W. B. Tolman, *Macromolecules*, 2012, **45**, 5387−5396.
38. Y. Huang, W. Wang, C.-C. Lin, M. P. Blake, L. Clark, A. D. Schwarz and P. Mountford, *Dalton Trans.*, 2013, **42**, 9313-9324.
39. M. Normand, V. Dorcet, E. Kirillov and J.-F. Carpentier, *Organometallics*, 2013, **32**, 1694-1709.
40. A. Amgoune, C. M. Thomas, T. Roisnel and J.-F. Carpentier, *Chem. Eur. J.*, 2006, **12**, 169-179.
41. C.-X. Cai, A. Amgoune, C. W. Lehmann and J.-F. Carpentier, *Chem. Commun.*, 2004, 330-331.
42. S. D. Bennett, B. A. Core, M. P. Blake, S. J. A. Pope, P. Mountford and B. D. Ward, *Dalton Trans.*, 2014, **43**, 5871-5885.

Chapter Four

CzOx^{iPr}-supported alkaline earth and rare earth complexes for the ROP of *rac*-, *D*-, *L*- and *meso*-LA

4.1 Overview

This Chapter will describe detailed investigations into the living and immortal ROP of *rac*-, *L*-, *D*- and *meso*-LA using magnesium, calcium, strontium, yttrium, lanthanum and samarium catalysts supported by the carbazole-bis(oxazoline) ligands, (*S*,*S*)- and (*R*,*R*)-HCzOx$^{i\text{Pr}}$; a summary and discussion of the polymerisation results will be presented. Twenty-nine new complexes will be presented, thirteen of which are *in situ* generated, along with two X-ray crystallographic structures.

4.2 Introduction

Given the dependence of the macroscopic properties of PLA on the polymer microstructure, considerable attention has been focussed on developing catalysts which can exert a high degree of stereocontrol during polymerisation to afford isotactically enriched PLA with a high T_m.[1-18] In particular, aluminium catalysts supported by chiral salen-type ligands have shown potential as isoselective catalysts; however, they can exhibit low activities at high catalyst loading, requiring prolonged reaction times to achieve high monomer conversion.[1, 4-6] A detailed discussion of complexes of this type is provided in Chapter 1. Accordingly, substantial efforts have been undertaken to develop highly active complexes with chiral ancillary ligands which yield isotactic PLA *via* an enantiomorphic site control mechanism.

4.2.1 Chiral initiators for the stereoselective ROP of lactide

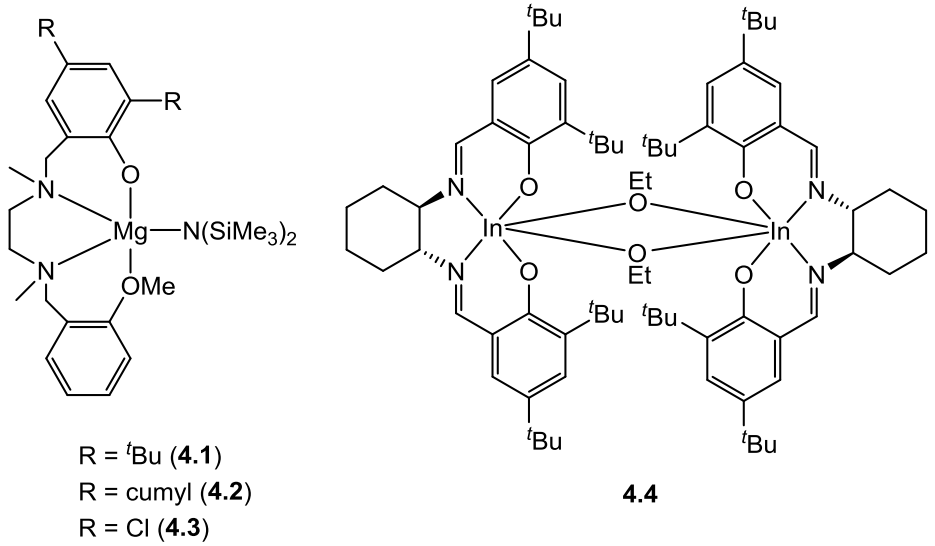


Figure 4.1. Examples of chiral complexes with salan and salen ancillary ligands for ROP of *rac*-LA.[19, 20]

A handful of chiral salan- or salen-supported metal complexes employing Group 2 and heavier Group 13 metals have been reported for the stereocontrolled ROP of *rac*-LA. Following a report by Wu *et al*. in 2005 in which a dinuclear magnesium alkoxide initiator supported with a chiral salen ligand afforded slightly isotactically enriched PLA,[21] Ma *et al*. synthesised a series of chiral magnesium complexes featuring an unsymmetrical salan-like ligand, and investigated their behaviour during the ROP of *rac*-LA (Figure 4.1).[19] The protonolysis of $Mg\{N(SiMe_3)_2\}_2$ with the protioligands L^1H (2-{*N*-[2-(*N*′-(2-methoxybenzyl)-*N*′-methylamino)ethyl]-*N*-methylamino}methyl-4,6-di-*tert*-butylphenol), L^2H (2-{*N*-[2-(*N*′-(2-methoxybenzyl)-*N*′-methylamino)ethyl]-*N*-methylamino}methyl-4,6-bis(2-phenylpropan-2-yl)phenol) or L^3H (2-{*N*-[2-(*N*′-(2-methoxybenzyl)-*N*′-methylamino)ethyl]-*N*-methylamino}methyl-4,6-dichlorophenol), in toluene afforded complexes **4.1**-**4.3** in moderate yields. Complexes **4.1**-**4.3** were found to be active when treated with 200 equivalents of *rac*-LA in toluene or THF at 25 °C, achieving high monomer to polymer conversion after 90 min. In the absence of any coinitiators, the molecular weights were higher than anticipated, and the PDIs broad (1.28-2.21). On the addition of 1 equivalent of propan-2-ol, the molecular weight control improved such that the observed molecular weights were in reasonable agreement with those calculated, with a concurrent reduction of PDI. Notably, all complexes furnished isotactically enriched PLA (P_m = 0.60-0.70) when toluene was used as a polymerisation solvent. In contrast the use of THF as a solvent resulted in a decrease in isoselectivity, and afforded atactic or slightly heterotactic PLA (P_r = 0.50-0.62). The ligand substituents were found to impart little effect on the degree of selectivity observed under the various reaction conditions.

A dinuclear indium ethoxide complex supported by a chiral salen ligand was reported by Mehrkhodavandi *et al*. in 2013.[20] Deprotonation of either the racemic or enantiopure protioligand, *N*,*N*′-bis(3,5-di-*tert*-butylsalicylidene)-1,2-cyclohexanediamine (*rac*- or (*R*,*R*)-H_2(ONNO)) followed by addition of $InCl_3$ and treatment with sodium ethoxide afforded the racemic or enantiopure dinuclear complex $[(ONNO)In(\mu\text{-}OEt)]_2$ (**4.4**) with bridging ethoxide groups. ***Rac*-4.4** proved to be active for the ROP of *rac*-LA, achieving 97% monomer conversion in 30 min in CH_2Cl_2 at room temperature. The molecular weights observed in the polymerisation of varying equivalents of lactide agreed closely with the expected values and also

resulted in moderate molecular weight distributions. Both ***rac*-** and **(*R*,*R*)-4.4** afforded isotactically enriched PLA (P_m = 0.74 and 0.77, respectively), whilst circumventing the low rates of polymerisation typically observed with aluminium salen complexes. The origin of the observed selectivity with **(*R*,*R*)-4.4** was investigated through the polymerisation of both *L*- and *D*-LA, which revealed there to be a strong monomer preference: k_{obs} for the polymerisation of *L*-LA was 22(5) × 10^{-4} s^{-1}; whereas k_{obs} for the polymerisation of *D*-LA was 4.3(9) × 10^{-4} s^{-1}, similar to the rate observed for the ROP of *rac*-LA (k_{obs} = 4.6(9) × 10^{-4} s^{-1}). The polymer was determined to be stereoblock, as the P_m was highest at <20 % and >95% monomer conversion, and lowest at ~50% conversion, indicative of an *L*-enriched stereoblock at low conversions as the favoured monomer is consumed, followed by a *D*-enriched stereoblock at high conversions as the disfavoured monomer is consumed. The mechanism of insertion affording the isoselectivity observed was attributed to enantiomorphic site control for both ***rac*-** and **(*R*,*R*)-4.4**.

Chiral aminophenolate supporting ligands have emerged as a new class of ligands capable of affording stereoregular PLA from *rac*-LA. Several examples are shown in Figure 4.2. In 2008, Mehrkhodavandi and coworkers reported a dinuclear chiral indium catalyst supported by a diaminophenolate ligand, obtained from a "one-pot" reaction between a racemic mixture of the protioligand ±H_2NNO^tBu (±H_2NNO^tBu = 2,4-di-*tert*-butyl-6-(((2-(dimethylamino)cyclohexyl)amino)methyl)phenol) with 2 equivalents of KCH_2Ph and $InCl_3$ to form [$((NNO^tBu)InCl)_2(\mu\text{-}OEt)(\mu\text{-}Cl)$] (**4.5**).[22] Complex **4.5** retained its dinuclear conformation in solution and it was anticipated that both the **(*S*,*S*/*S*,*S*)-** and **(*R*,*R*/*R*,*R*)-4.5** enantiomers were present in solution; however, only one enantiomer was present the solid state (**(*R*,*R*/*R*,*R*)-4.5**). When treated with 200 equivalents of *rac*-LA in CH_2Cl_2 at room temperature, a racemic mixture of complex **4.5** achieved 90% monomer conversion after 30 min. Analysis of the polymer microstructure revealed a modest degree of isotactic enrichment (P_i = 0.53-0.62). A further investigation into the selectivity of enantiopure **(*S*,*S*/*S*,*S*)-** and **(*R*,*R*/*R*,*R*)-4.5** in the presence of *rac*-, *L*- and *D*-LA was performed in 2012.[23] Comparison of the rates of ROP of *L*- and *D*-LA with **(*R*,*R*/*R*,*R*)-4.5** revealed a k_L/k_D value of ≈ 14; a similar value was obtained for k_D/k_L with **(*S*,*S*/*S*,*S*)-4.5**. Although the enantiopure catalysts showed a high degree of monomer preference with regards to the relative rates of ROP or either *L*- or *D*-LA, the ROP of *rac*-LA with either

enantiopure catalyst resulted in atactic PLA. Theoretical investigations into the mechanism of lactide polymerisation with **(*R,R*/*R,R*)-4.5** at the DFT level by computing the first and second insertions supported the observed selectivity for both enantiopure and racemic **4.5**.[24] The polymerisation followed two kinetic regimes: until 64% monomer conversion, k_{obs} was 0.62×10^{-3} s^{-1}, whereas from 73% to 90% conversion $k_{obs} = 0.21 \times 10^{-3}$ s^{-1}, which was attributed to the polymerisation of the favoured monomer followed by the disfavoured monomer. A similar complex, $[((NNO_{Me})InI)(\mu\text{-}OEt)]_2$ (**4.6**) was evaluated as a catalyst for the stereoselective ROP of *rac*-LA. Unlike the monoethoxy-bridged complex, **(*S,S*/*S,S*)-4.6** does not show any site selectivity: the k_D/k_L value for the ROP of *L*- and *D*-LA is ~2, with a similar k_L/k_D value when using **(*R,R*/*R,R*)-4.6**. However, the ROP of *rac*-LA with either enantiopure catalyst resulted in slight isotactic enrichment ($P_m = 0.65$). The difference in selectivities observed was attributed to the equal rates of coordination of a *D*-LA monomer to **(*R,R*/*R,R*)-4.6** as the rate of propagation of an *L*-LA monomer, resulting in the formation of atactic polymer; however, in **±-4.6** and all isomers of **4.5**, chain end control dominates to afford similar P_m values of ~0.6.

In 2009, an analogous zinc complex was reported by Mehrkhodavandi and coworkers. $(NN^{Me}O^{tBu})Zn(OPh)$ (**4.7**) was synthesised following the reaction of ±- or (*R,R*)-$H_2NN^{Me}O^{tBu}$ ($H_2NN^{Me}O^{tBu}$ = 2-(*tert*-butyl)-6-(((dimethylamino)cyclohexyl)(methyl)amino)methyl)-4-methylphenol) with diethyl zinc, followed by protonolysis with phenol.[25] Both ±- or **(*R,R*)-4.7** were treated with 2000 equivalents of *rac*-LA in CH_2Cl_2 at room temperature; however, both exhibited low activities, achieving 100% monomer conversion following 40 h, with poor agreement between observed and calculated molecular weights and high molecular weight distributions. Analysis of the polymer microstructure revealed the polymer to be atactic.

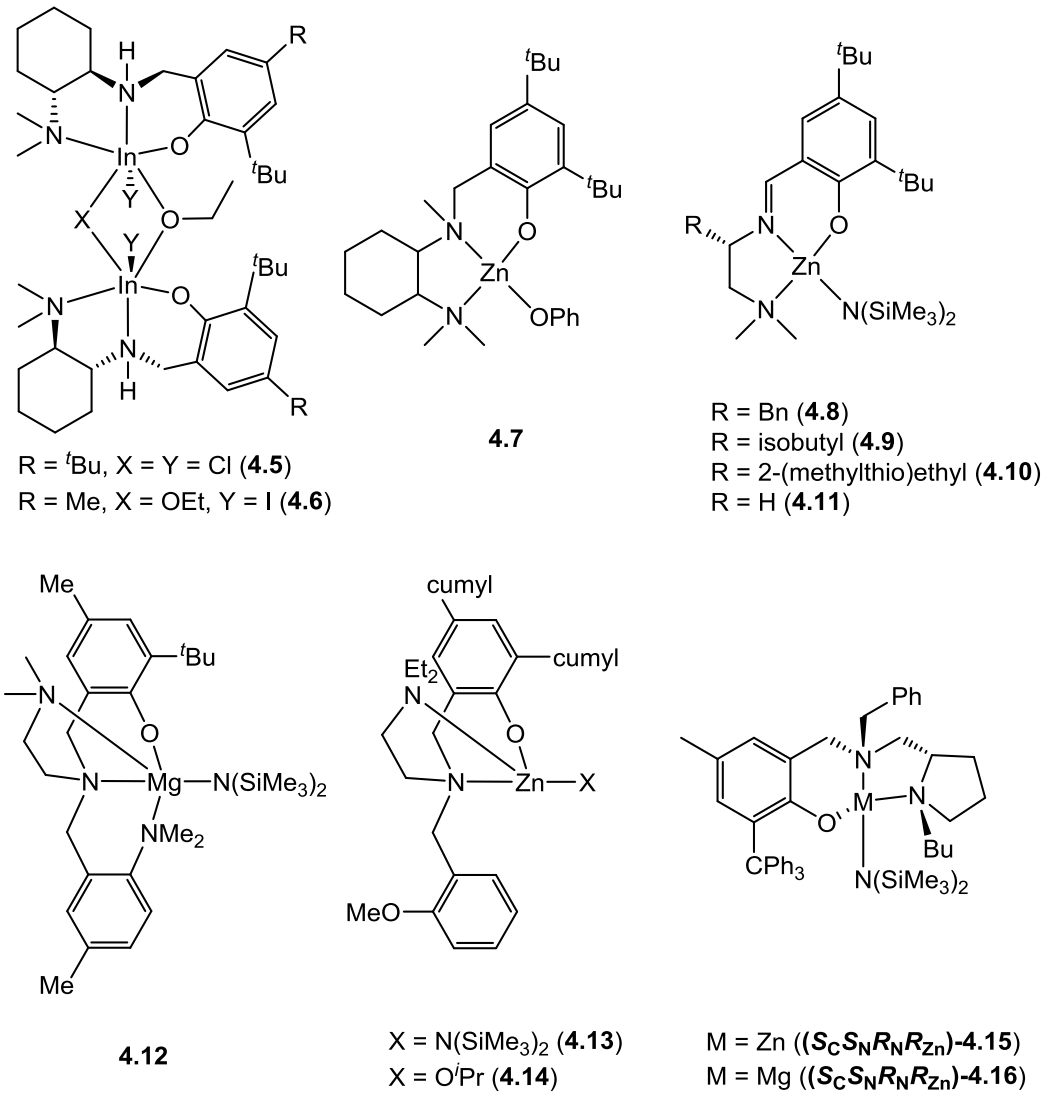


Figure 4.2. Examples of chiral complexes with aminophenolate ancillary ligands for ROP of *rac*-LA.[22, 23, 25-29]

In 2010, Darensbourg *et al*. employed a series of chiral NNO-tridentate ancillary ligands derived from chiral amino acids, for the synthesis of supported zinc complexes (**4.8**-**4.11**) whose performance as initiators for the ROP of *rac*-LA was subsequently evaluated.[26] Their performance in the ROP of either *L*- or *D*-LA was initially investigated and it was found that the value of k_D/k_L was close to unity for chiral complexes **4.8**-**4.10**, indicating an absence of monomer preference. Unsurprisingly, the more sterically encumbered complexes **4.9** and **4.11** polymerised *L*-LA at a higher rate than **4.8**; however, k_{obs} for **4.10** was found to be the lowest of all the complexes studied, which was attributed to presence of a sulfur donor which chelates to the metal centre resulting in a decrease in rate. When treated with 50

equivalents of *rac*-LA in $CHCl_3$ at room temperature, complexes **4.8** and **4.9** were moderately active, achieving 97 and 98% monomer conversion following 2 h, respectively. Complexes **4.10** and **4.11** were considerably less active, achieving similar % conversions after 24 h. In all cases, molecular weights grew linearly with time, and the polydispersities were narrow to moderate (PDI ≈ 1.05-1.30), indicative of the catalysts' living character. All catalysts exhibited a heterotactic bias during polymerisation, resulting in the formation of heterotactic PLA ($P_r \approx 0.70$-0.85), which was attributed to the dominance of a chain end control mechanism throughout polymerisation.

Ma and coworkers reported a series of magnesium and zinc complexes supported by unsymmetrical aminophenolate ancillary ligands, which exhibited a degree of stereocontrol during the ROP of *rac*-LA.[27, 28] In 2010, the complex (L^1)Mg{N($SiMe_3$)$_2$} (**4.12**) (L^1 = 6-*tert*-butyl-2-{*N*-(2-(*N*,*N*-dimethlyamino)-5-methylbenzyl)-*N*-[2-(*N*,*N*-dimethyl)aminoethyl]aminomethyl}-4-methylphenolate) was synthesised *via* a protonolysis reaction between L^1H and Mg{N($SiMe_3$)$_2$}$_2$ in toluene, and was tolerant to high loadings of *rac*-LA, both in the absence and presence of propan-2-ol as a coinitiator. When treated with 10,000 equivalents of *rac*-LA in toluene at room temperature in the absence of any additives, **4.12** achieved 91% monomer conversion following 15 min. Although, the molecular weights were lower than expected, the molecular weight dispersities were moderate, and the catalyst demonstrated a slight isotactic bias during polymerisation, producing polymer with $P_m = 0.59$. The addition of 1 or 2 equivalents of propan-2-ol to act as a chain transfer agent did not impact the observed isoselectivity. Subsequently, a zinc silylamido initiator featuring an unsymmetrical aminophenolate ligand was reported in 2012. (L^2)Zn{N($SiMe_3$)$_2$} (**4.13**) (L^2 = 4,6-dicumyl-2-{*N*-(2-methoxybenzyl)-*N*-[2-(*N*′,*N*′-diethyl amino)ethyl]aminomethyl}-phenolate) was synthesised *via* the protonolysis reaction between L^2H and Zn{N($SiMe_3$)$_2$}$_2$ in toluene to afford complex **4.13**. When treated with 200 equivalents of *rac*-LA in toluene or THF at ambient temperatures, **4.13** was moderately active, achieving 95% monomer conversion after 3 h in toluene, and 89% monomer conversion after 2 h in THF. In both instances, isotactically enriched PLA was obtained, with $P_m = 0.65$. Further investigations were conducted following addition of 1 equivalent of propan-2-ol to **4.13** to generate *in situ* the corresponding alkoxide complex, (L^2)Zn(O^iPr) (**4.14**). The addition of propan-2-ol to

generate **4.14** *in situ* resulted in increased rates of polymerisation; however, the degree of isotactic enrichment remained unchanged.

In 2014, Ma and coworkers reported a series of zinc and magnesium initiators bearing the chiral aminophenolate supporting ligand, (*S*)- or (*R*)-2-{*N*-benzyl-*N*-[(1-n-butyl-2-pyrrolidinyl)methyl]}aminomethyl-4-methyl-6-tritylphenolate ((*S*)- or (*R*)-L^3).[29] Complexes **($S_C S_N R_N R_{Zn}$)-4.15** and **($S_C S_N R_N R_{Mg}$)-4.16** were synthesised following reaction of (*S*)-L^3H with 1 equivalent of the appropriate metal precursor via a protonolysis reaction, and their catalytic activity towards *rac*-, *L*- and *D*-LA were examined, and compared to the opposite enantiomeric form of the complexes. When treated with 200 equivalents of *rac*-LA in toluene at room temperature, **($S_C S_N R_N R_{Zn}$)-4.15** achieved 84% conversion following 180 min. Analysis of the polymer microstructure revealed the polymer to be isotactically enriched (P_m = 0.80); the degree of enrichment was found to be solvent-independent. Curiously, the equivalent reactions undertaken with **($S_C S_N R_N R_{Mg}$)-4.16** resulted in very different behaviour: in toluene at room temperature **($S_C S_N R_N R_{Mg}$)-4.16** achieved 90% conversion after 25 min, but produced heterotactically enriched polymer (P_r = 0.81). The degree of enrichment was found to be solvent dependent: when conducted in donor solvents such as THF or pyridine the ROP of *rac*-LA with **($S_C S_N R_N R_{Mg}$)-4.16** resulted in a decrease in heterotactic bias (P_r = 0.70 and 0.59, respectively). The respective enantiomers of both **($S_C S_N R_N R_{Zn}$)-4.15** and **($S_C S_N R_N R_{Mg}$)-4.16** were in agreement with the degrees of enrichment observed when polymerising *rac*-LA. The mechanism of isoselectivity observed with **($S_C S_N R_N R_{Zn}$)-4.15** was probed through the polymerisation of *D*- or *L*-LA, which revealed nearly a four-fold rate preference for the ROP of *D*-LA relative to *L*-LA. Employing a model complex in which the silylamine initiator was replaced by (*S*)-methyl lactate or (*R*)-*tert*-butyl lactate, a mechanism through which this monomer preference results in the formation of isotactic PLA was postulated, in which both enantiomorphic site control and chain end control were present, with the former being dominant. The origin of the heteroselectivity observed with **($S_C S_N R_N R_{Mg}$)-4.16** was first investigated with the polymerisation of *D*- and *L*-LA; however, the values of k_L/k_D for both enantiomers were found to be close to unity, indicating very little monomer preference. The dominance of a chain end control mechanism resulting in heterotactically enriched PLA was attributed to the larger coordination sphere of magnesium in comparison to

zinc. It is hypothesised that two lactide molecules may coordinate to the metal centre and the last inserted lactate terminus selects a monomer of opposing chirality to insert, resulting in the formation of heterotactic PLA. This hypothesis is supported by the reduction in chirality observed when employing a donor solvent during polymerisation, as the solvent molecule may block a vacant site resulting in diminished selectivity.

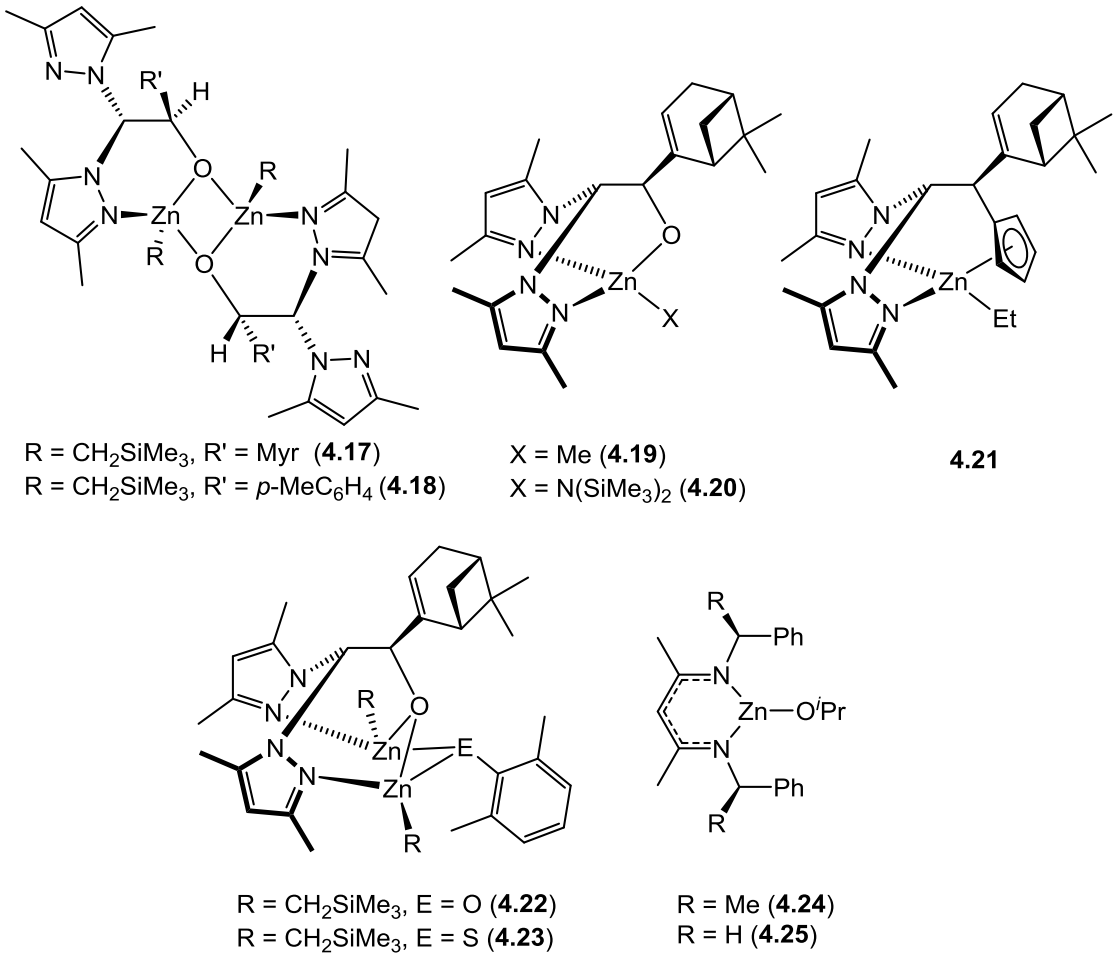


Figure 4.3. Examples of chiral complexes with heteroscorpionate and diketiminate ancillary ligands for ROP of *rac*-LA (Myr = (*R*)-1-[(1*R*)-6,6-dimethylbicyclo[3.1.1]hept-2-en-2-yl]).[30-34]

The first report of complexes supported by enantiopure chiral NNO-scorpionate ligands came from Rodriguez *et al*. in 2012 (Figure 4.3).[30] Treatment of the enantiopure protioligand (*R*,*R*)-bpzmmH ((*R*,*R*)-bpzmm = (1*R*)-1-[(1*R*)-6,6-dimethylbicyclo[3.1.1]-2-hepten-2-yl]-2,2-bis(3,5-dimethylpyrazol-1-yl)ethoxide}
with dimethyl zinc resulted in the formation of the mononuclear Zn(Me)((*R*,*R*)-

bpzmm) (**4.19**); however, employment of a bulkier zinc alkyl such as $Zn(CH_2SiMe_3)_2$ resulted in the formation of dinuclear complex $\{Zn(CH_2SiMe_3)((R,R)\text{-bpzmm})\}_2$ (**4.17**): both **4.17** and **4.19** were enantiopure. Treatment of a racemic mixture of a protioligand such as bptzteH (bpzte = 2,2-bis(3,5-dimethylpyrazol-1-yl)-1-*para*-tolylethoxide) with $Zn(CH_2SiMe_3)_2$ afforded a racemic mixture of the dinuclear complex $\{Zn(CH_2SiMe_3)(bptzte)\}_2$ (**4.18**). In 10 mL THF, complexes **4.17** and **4.18** were treated with 100 equivalents of *L*-LA, and both were found to be active. At 50 °C, **4.18** achieved 97% monomer conversion in 4.5 h, whereas **4.17** achieved 60% monomer conversion in 3.5 h. Ensuing investigations employing *rac*-LA as the monomer revealed complex **4.17** produced slightly more heterotactically enriched PLA than **4.18** (P_r = 0.77 *cf.* 0.72). Rodriguez *et al*. subsequently reported a series of enantiopure heteroscorpionate-supported zinc complexes featuring an amide initiating group.[31] The enantiomerically pure complex $Zn\{N(SiMe_3)_2\}((R,R)\text{-bpzmm})$ (**4.20**) was synthesised following the protonolysis reaction of (*R*,*R*)-bpzmmH with 1 equivalent of $Zn\{N(SiMe_3)_2\}_2$ in toluene in an excellent yield of 87%. Treatment of **4.20** with 100 equivalents of *rac*-LA in either 40 mL of toluene or 10 mL THF at 50 °C resulted in the formation of heterotactically enriched PLA ($P_r \approx 0.75\text{-}0.80$). In all instances, complexes **4.17**-**4.20** exerted good molecular weight control during polymerisation, resulting in good agreement between observed and calculated molecular weights with narrow polydispersities (PDI ≈ 1.10). Furthermore, analysis with MALDI-ToF MS revealed the initiation process to occur *via* transfer of the amide or alkyl initiating group to the monomer followed by ring-opening and subsequent propagation.

In 2013, Rodrigues *et al.* introduced an enantiopure heteroscorpionate-cyclopentadienyl hybrid ligand, $ZnEt(\kappa^2\text{-}\eta^1\text{-}R,S\text{-bpmycp})$ (**4.21**).[32] **4.21** was synthesised *via* the deprotonation of the cyclopentadienyl group of the enantiomerically pure regioisomers (*R*,*R*)-bpmycpH ((*R*,*R*)-bpmycpH = 1-{2.2-bis(3.5-dimethyl-1*H*-pyrazol-1-yl)-1-(2*R*)-2-[(1*R*)-6,6-[3.1.1]-2-hepten-2-yl]ethyl} cyclopentadiene) and (*R*,*R*)-bpmycp′H ((*R*,*R*)-bpmycp′H = 2-{2,2-bis(3,5-dimethyl-1*H*-pyrazol-1-yl)-1-(2*R*)-2-[(1*R*)-6,6-[3.1.1]-2-hepten-2-yl]ethyl}cyclopentadiene) with diethyl zinc in toluene at reflux to afford the product in an excellent yield of 90%. The catalytic performance of **4.21** was evaluated with *L*-LA: following treatment with 100 equivalents of *L*-LA in 25 mL toluene at room temperature, 57%

monomer conversion was achieved following 12 h. Elevation of the reaction temperature to 50 °C resulted in an increase in activity: in toluene 62% monomer conversion was reached following 1.5 h, whereas in 10 mL THF, 25% monomer conversion was reached after 3 h. Further to these preliminary investigations, **4.21** was treated with 100 equivalents of *rac*-LA in toluene both at 20 and 50 °C. As expected, higher activities were observed at the elevated temperature (47% monomer conversion was achieved after 4 h); however, both experiments resulted in the formation of isotactically enriched PLA, with P_m = 0.77 (20 °C) and 0.73 (50 °C), with enchainment dominated by an enantiomorphic site control mechanism.

The enantiopure dinuclear complexes **4.22** and **4.23** were synthesised following the protonolysis reaction of (*R*,*R*)-bpzmmH with 1 equivalent of $Zn(CH_2SiMe_3)_2$ in toluene, followed by treatment with 2,6-$C_6H_3Me_2OH$ to afford **4.22** in 83% yield, or 2,6-$C_6H_3Me_2SH$ to afford **4.23** in 85% yield.[33] When treated with 100 equivalents of *rac*-LA in toluene at 50 °C, both **4.22** and **4.23** were found to be active. After 4 h, **4.22** achieved 48% monomer conversion with excellent molecular weight control (M_n(obs) = 6,900 g mol^{-1} *cf.* M_n(calc) = 6,800 g mol^{-1}; PDI = 1.05). Complex **4.23** was less active, achieving 25% monomer conversion within the same time period; however, the molecular weight control was also found to be excellent (M_n(obs) = 3,600 g mol^{-1} *cf.* M_n(calc) = 3,800 g mol^{-1}; PDI = 1.15). Both complexes afforded isotactically enriched PLA (P_m = 0.71-0.73), with polymer T_m of 161-164 °C. Analysis of the PLA backbone tetrads with $^1H\{^1H\}$ NMR spectroscopy revealed an enantiomorphic site control mechanism to be dominant.

A series of aliphatic diketiminate-supported zinc complexes were synthesised by Schaper and coworkers in 2010 featuring either inherent chirality or formed chiral rotamers.[34] The target complexes {(*S*,*S*)-$^{CH(Me)Ph}$nacnac}Zn(O^{i}Pr) (**4.24**) and {^{Bn}nacnac}Zn(O^{i}Pr) (**4.25**) were synthesised from the treatment of either (*S*,*S*)-{$^{CH(Me)Ph}$nacnac}Zn{N(SiMe$_3$)$_2$} or {^{Bn}nacnac}Zn{N(SiMe$_3$)$_2$} with 1 equivalent of propan-2-ol. Only one environment was observed for the NC$\underline{H}_2$Ph hydrogen atoms in the ^1H NMR spectrum, suggestive of C_{2v} symmetry. Both complexes **4.24** and **4.25** were found to be active for the ROP of *rac*-LA when treated with 300 equivalents of monomer in CH_2Cl_2 at room temperature, achieving >95% monomer conversion after 3 and 1.5 h, respectively. Although the polymer molecular weights were higher than expected, attributed to catalyst decomposition, the narrow polydispersities observed

(PDI = 1.1) were consistent with a living polymerisation. Furthermore, analysis of the polymer microstructure revealed a strong preference for the alternating insertion of (*R*,*R*)- and (*S*,*S*)-enantiomers, leading to the formation of heterotactically enriched PLA (P_r = 0.84-0.87 and 0.65-0.71 for **4.24** and **4.25**, respectively).

4.3 Synthesis and characterisation of CzOx$^{i\mathrm{Pr}}$-supported Group 1 and 2 complexes

4.3.1 Synthesis of protioligand (*S*,*S*)- and (*R*,*R*)-HCzOx$^{i\mathrm{Pr}}$ ((*S*,*S*)- and (*R*,*R*)-1.46) and (*S*,*S*)-Li(CzOx$^{i\mathrm{Pr}}$) ((*S*,*S*)-33)

The protioligand (*S*,*S*)-HCzOx$^{i\mathrm{Pr}}$ (**(*S*,*S*)-1.46**) was synthesised according to modified literature procedures in a five stage synthesis in 31 % overall yield, analogously to HCzOx$^{\mathrm{Me2}}$ (**1.45**).[35-39] Employment of either *D*- or *L*-valinol during the synthesis allowed either enantiomeric form of **1.46** to be accessed, and (*R*,*R*)-HCzOx$^{i\mathrm{Pr}}$ (**(*R*,*R*)-1.46**) was isolated in 22% overall yield; however, the addition of an excess of *rac*-valinol during synthesis resulted in the formation of a statistical distribution of products including **(*S*,*S*)-, (*R*,*R*)-** and ***meso*-1.46**. Both **(*S*,*S*)-** and **(*R*,*R*)-1.46** were characterised by X-ray diffraction: the molecular structure of **(*S*,*S*)-1.46** is given in Figure 4.4 and selected bond lengths and angles are given in Table 4.1.

Based on the success obtained by Ward *et al.* in the synthesis of rare earth complexes employing chiral bis(oxazolinylphenyl)amide (BOPA) supporting ligands featuring different substituents on the oxazoline rings,[40] further variation of the substituents of the oxazoline rings was attempted: 3,6-di-*tert*-butyl-9*H*-carbazole-1,8-dicarbonitrile was refluxed for 7 days in chorobenzene with an excess of *L*-phenylalaninol or *D*-phenylglycinol in the presence of anhydrous zinc chloride. Whilst the desired products (*S*,*S*)-HCzOx$^{\mathrm{Ph}}$ and (*S*,*S*)-HCzOx$^{\mathrm{Bn}}$ were successfully synthesised, the major product obtained was proposed to be (*S*,*S*)-Zn(CzOx$^{\mathrm{Ph}}$)$_2$ and (*S*,*S*)-Zn(CzOx$^{\mathrm{Bn}}$)$_2$, respectively. Attempts to liberate the protioligand through protonation with dilute and concentrated aqueous HCl were unsuccessful, instead resulting in decomposition of the ligand. No further attempts were made to synthesise any additional chiral carbazole-bis(oxazoline) ligands.

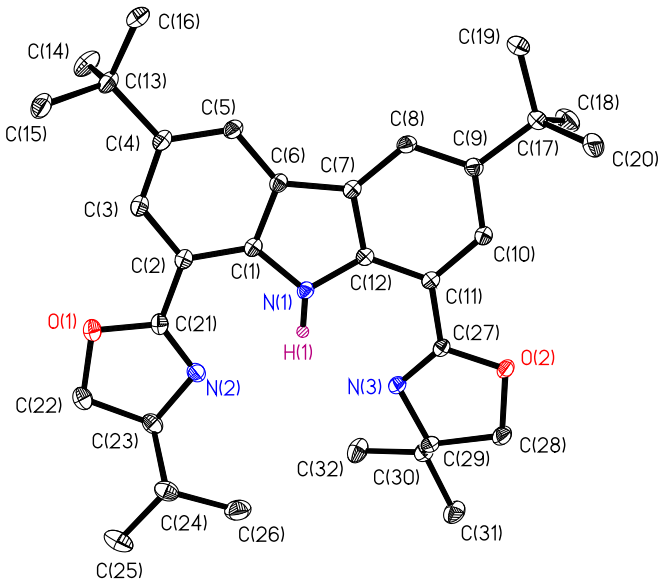


Figure 4.4. Displacement ellipsoid plot of (*S*,*S*)-HCzOx$^{i\text{Pr}}$ (**(*S*,*S*)-1.46**) (20% probability level). C-bound H atoms omitted for clarity. H(1) repositioned geometrically.

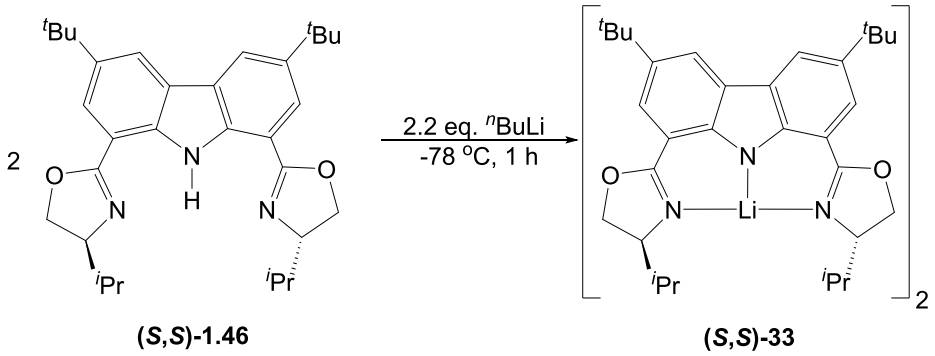
Table 4.1. Selected bond distances (Å) and angles (°) for (*S*,*S*)-HCzOx$^{i\text{Pr}}$ (**(*S*,*S*)-1.46**).

N(1)-H(1)	0.89	N(1)-C(1)	1.3756(12)
N(2)-C(23)	1.4797(13)	N(2)-C(21)	1.2703(14)
O(1)-C(21)	1.3632(12)	O(1)-C(22)	1.4478(14)
N(1)-C(1)-C(2)	129.19(9)	C(1)-C(2)-C(21)	120.49(9)
C(2)-C(21)-N(2)	125.03(9)	C(12)-C(11)-C(27)	119.95(8)

The solid state structure of **(*S*,*S*)-1.46** was determined for comparison with its metal complexes. The N(1)-H(1) bond length of 0.89 Å lies within the expected range of 0.82-0.94 Å.[41] The core of the molecule is planar, with dihedral angles of 0.2° for C(1)-C(2)-C(21)-N(2) and 10.1° C(12)-C(11)-C(27)-N(3).

(*S*,*S*)-1.46 was deprotonated in the presence of 1.1 equivalents of *n*-butyllithium (^{n}BuLi) solution in hexanes to afford the lithium salt, (*S*,*S*)-Li(CzOx$^{i\text{Pr}}$) (**(*S*,*S*)-33**) (Scheme 4.1). **(*S*,*S*)-33** was isolated as a yellow powder following a cold pentane wash to remove the excess ^{n}BuLi in 69% yield. Unlike previously synthesised K(CzOx$^{\text{Me2}}$) (**5**), **(*S*,*S*)-33** was soluble in a range of solvents including pentane, from

which diffraction-quality crystals were obtained. The molecular structure of **(*S*,*S*)-33** is given in Figure 4.5, and selected bond lengths and angles are given in Table 4.2.



(*S*,*S*)-1.46 **(*S*,*S*)-33**

Scheme 4.1. Synthesis of (*S*,*S*)-Li(CzOx^{iPr}) (**(*S*,*S*)-33**) *via* a protonolysis reaction.

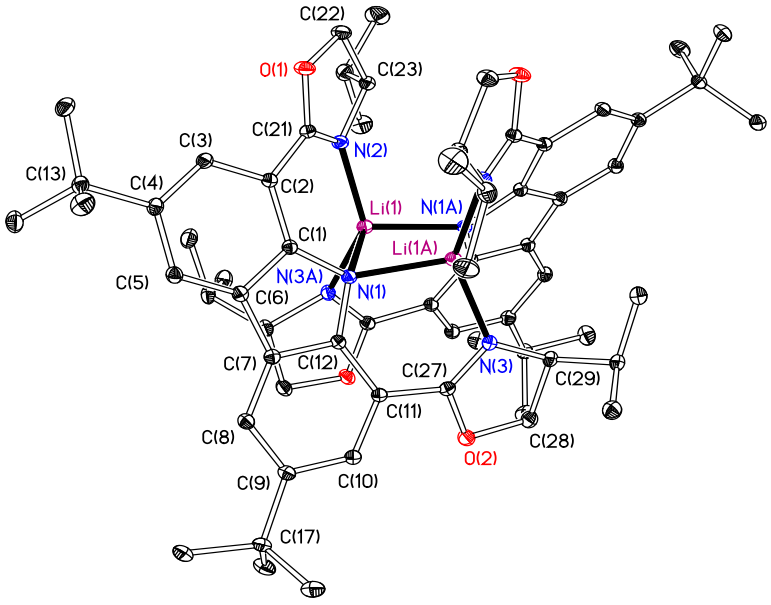


Figure 4.5. Displacement ellipsoid plot of (*S*,*S*)-Li(CzOx^{iPr}) (**(*S*,*S*)-33**) (20% probability level). H atoms and a pentane molecule of crystallisation omitted for clarity. Atoms carrying the suffix 'A' are related to their counterparts by the symmetry operator 1-x, 1-y, 1+z.

Table 4.2. Selected bond distances (Å) and angles (°) for (*S*,*S*)-Li(CzOx$^{i\text{Pr}}$) (**(*S*,*S*)-33**).

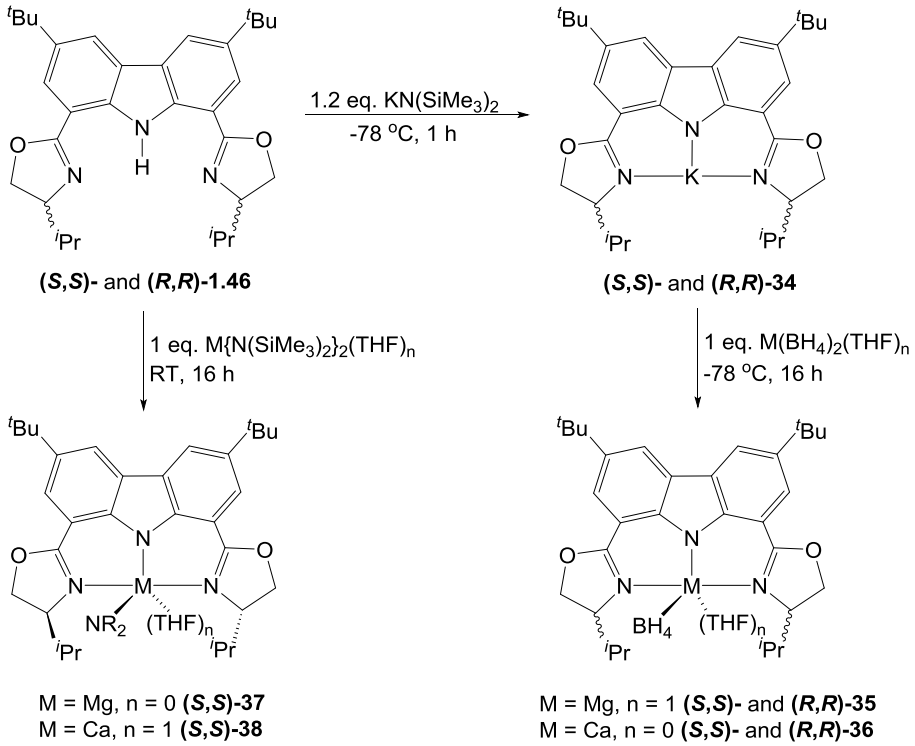
Li(1)-N(1)	2.151(3)	Li(1)-N(1A)	2.049(3)
Li(1)-N(2)	1.958(3)	Li(1A)-N(1A)	2.036(3)
Li(1A)-N(1)	2.178(3)	Li(1A)-N(2A)	1.969(3)
N(1A)-Li(1)-N(1)	110.82(13)	N(1A)-Li(1)-N(2)	108.59(14)
N(1)-Li(1)-N(2)	98.48(13)	N(1)-Li(2)-N(1A)	108.59(13)
N(1)-Li(2)-N(2A)	113.77(14)	N(1A)-Li(2)-N(2A)	97.03(12)

(*S*,*S*)-Li(CzOx$^{i\text{Pr}}$) (**(*S*,*S*)-33**) is dimeric in the solid state, with two four coordinate Li centres which coordinate to two N donors from each CzOx$^{i\text{Pr}}$ ligand, adopting a distorted tetrahedral geometry. The Li-N bond lengths of *ca*. 1.96-2.18 Å fall within the expected range of 1.93-2.21 Å.[41] Bond angles N(1)-Li(1)-N(2) and N(1A)-Li(2)-N(2A) are most distorted from the ideal tetrahedral bond angle (98.48(13) and 97.03(12)°, respectively). The oxazoline rings are rotated in order to allow the N donor to coordinate to either one of the Li atoms, resulting in a considerable deviation from planarity observed in **(*S*,*S*)-1.46**, with dihedral angles of 27.9° for C(1)-C(2)-C(21)-N(2) and 22.6° for C(12)-C(11)-C(27)-N(3).

4.3.2 Synthesis and characterisation of CzOx$^{i\text{Pr}}$-supported potassium, magnesium and calcium borohydride and amide complexes

The treatment of **(*S*,*S*)-** and **(*R*,*R*)-1.46** with 1.2 equivalents of KN(SiMe$_3$)$_2$ in THF afforded the potassiated salts, (*S*,*S*)- and (*R*,*R*)-K(CzOx$^{i\text{Pr}}$) (**(*S*,*S*)-** and **(*R*,*R*)-34**) as sparingly soluble yellow powders in 79 and 75% yield, respectively. Although **(*S*,*S*)-** and **(*R*,*R*)-34** were characterised with IR spectroscopy, mass spectrometry and elemental analysis, due to their extremely low solubilities, satisfactory ^{1}H or ^{13}C{^{1}H} NMR spectra could not be obtained. Scheme 4.2 details the synthesis of **(*S*,*S*)-** and **(*R*,*R*)-34** with the onwards reaction to synthesise (*S*,*S*)- and (*R*,*R*)-Mg(CzOx$^{i\text{Pr}}$)(BH$_4$)(THF) (**(*S*,*S*)-** and **(*R*,*R*)-35**) and (*S*,*S*)- and (*R*,*R*)-Ca(CzOx$^{i\text{Pr}}$)(BH$_4$) (**(*S*,*S*)-** and **(*R*,*R*)-36**). **(*S*,*S*)-** and **(*R*,*R*)-35** were obtained following the salt metathesis reaction of **(*S*,*S*)-** and **(*R*,*R*)-34** with 1 equivalent of Mg(BH$_4$)$_2$ in THF and were obtained in 43 and 42% yield, respectively, following purification and isolation. Analysis of the products in toluene-d_8 revealed there to be one molecule of

THF coordinated to the metal centre. The complexes were fully characterised by ^{1}H, ^{13}C{^{1}H} and ^{11}B NMR spectroscopy in THF-d_8, IR spectroscopy, mass spectrometry and elemental analysis. Unlike Mg(CzOx^{Me2})BH$_4$ (**7**), resonances corresponding to the hydrogen atoms of BH$_4$ were not observed in the ^{1}H NMR spectrum, despite observing a quintet at -38.0 ppm (^{1}J = 80-84 Hz) in the ^{11}B NMR spectrum. This is ascribed to "washing out" of the B-H coupling due to the quadrupolar nature of ^{11}B.[42]



Scheme 4.2. Synthesis of potassium, magnesium and calcium complexes **34**-**38** *via* protonolysis and salt metathesis reactions, R = SiMe$_3$.

(*S*,*S*)- and (*R*,*R*)-Ca(CzOx^{iPr})(BH$_4$) (**(*S*,*S*)-** and **(*R*,*R*)-36**) were obtained in a similar fashion: a salt metathesis reaction between **(*S*,*S*)-** and **(*R*,*R*)-34** and Ca(BH$_4$)$_2$(THF)$_2$ in THF afforded the products as yellow powders in 58 and 62% yield, respectively. Analysis of the ^{1}H NMR spectrum of a pyridine-d_5 solution of **(*S*,*S*)-** and **(*R*,*R*)-36** revealed there to be no coordinated THF molecules. Similarly to **(*S*,*S*)-** and **(*R*,*R*)-35**, resonances corresponding to the hydrogen atoms of BH$_4$ were not observed in the ^{1}H NMR spectrum, despite observing a quintet at -37.0 and -36.7 ppm (^{1}J = 82 Hz) in the ^{11}B NMR spectrum. The treatment of **(*S*,*S*)-34** with 1 equivalent of Sr(BH$_4$)$_2$(THF)$_2$ in THF at -78 °C followed by immediate solvent removal afforded a product in which there appeared no boron after analysis with ^{11}B NMR spectroscopy. It was strongly

suspected that this product was the homoleptic complex (*S*,*S*)-Sr(CzOx$^{i\text{Pr}}$)$_2$, therefore efforts were undertaken to independently synthesise and characterise (*S*,*S*)-Sr(CzOx$^{i\text{Pr}}$)$_2$ for comparison, *vide infra*.

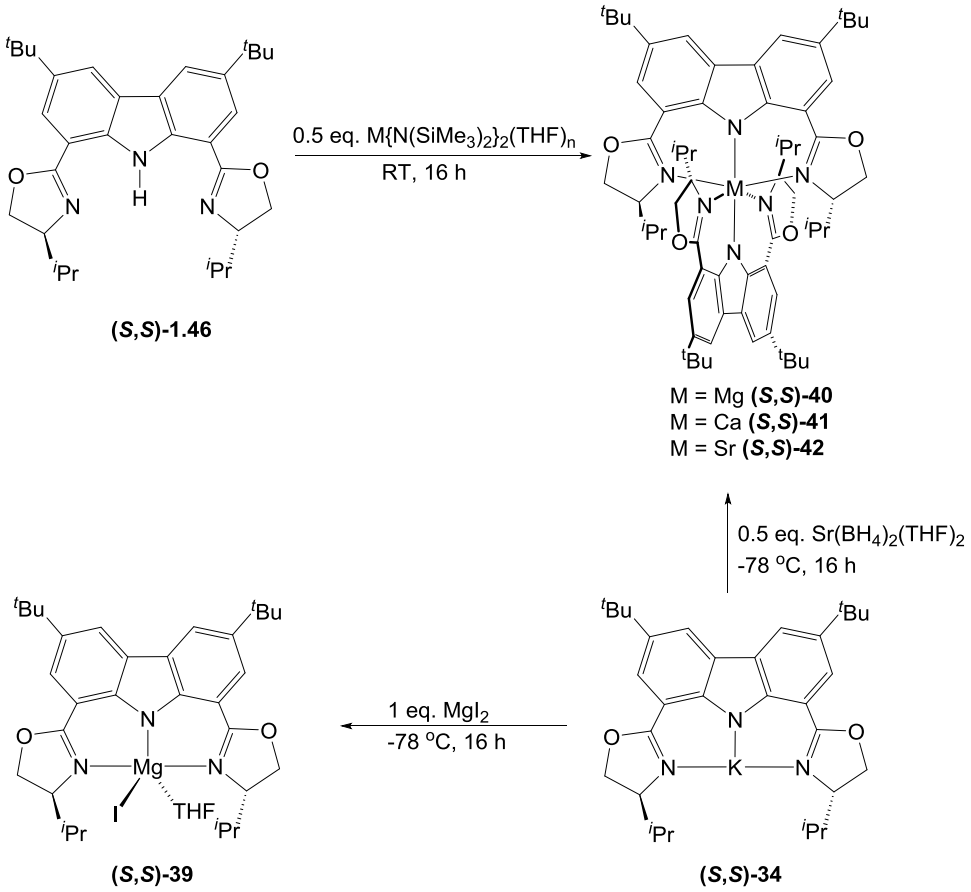
In order to gain further insight into the hapticities of the borohydride groups in (***S,S*)-** and **(*R,R*)-35** and **(*S,S*)-** and **(*R,R*)-36**, characterisation of the complexes with THF solution and solid state IR spectroscopy was conducted. The solid state spectrum recorded for **(*S,S*)-35** displayed a broad singlet at 2269 cm^{-1}, in a similar fashion to the alkaline earth complexes previously studied. In contrast, the solid state IR spectra of **(*R,R*)-35** and **(*S,S*)-** and **(*R,R*)-36** appeared as two broad singlets, instead of one. For **(*R,R*)-35**, a B–H$_t$ stretch was observed at 2390 cm^{-1}; however, the stretch corresponding to the B–H$_b$ doublet was only observed as a broad singlet at 2151 cm^{-1}, which may be tentatively assigned as tridentate. It has been postulated that the appearance of a broad singlet in the region of 2300-2200 cm^{-1} is caused by polymeric structures, or the presence of multiple bonding modes. The precise cause of the shift from a broad peak in the solid state IR spectrum of **(*S,S*)-35** to a tridentate configuration in **(*R,R*)-35** is not readily apparent at this stage. As expected, the spectra of **(*S,S*)-** and **(*R,R*)-36** were very similar: peaks at 2315 and 2313 cm^{-1} correspond to a B–H$_t$ stretch, whereas only broad singlets at 2280 and 2198 cm^{-1} were observed for the B–H$_b$ stretches. The failure to resolve clearly anticipated doublets with 50-80 cm^{-1} splitting for either the B–H$_t$ stretch between 2600-2400 cm^{-1}, corresponding to a κ^2-bound BH$_4$ ligand, or a doublet for the B–H$_b$ stretch between 2200-2100 cm^{-1}, corresponding to a κ^3-bound BH$_4$ ligand is suggestive of the occupation of multiple bonding configurations in the solid state. The THF solution IR spectra for both **(*S,S*)-** and **(*R,R*)-35** confirmed both complexes adopted tridentate borohydride configurations in solution, with B–H$_t$ stretches at 2394 and 2390 cm^{-1}, respectively, and B–H$_b$ doublets at 2242 and 2173 cm^{-1}, and 2255 and 2155cm^{-1}, respectively. Both THF solution IR spectra for **(*S,S*)-** and **(*R,R*)-36** confirmed the tridentate hapticity of the borohydride groups: singlets corresponding to B–H$_t$ stretches were observed at 2384 and 2383 cm^{-1}, respectively, and doublets corresponding to B–H$_b$ stretches were observed at 2251 and 2180, and 2252 and 2180 cm^{-1}, respectively.

(*S*,*S*)-Mg(CzOx$^{i\text{Pr}}$){N(SiMe$_3$)$_2$} (**(*S,S*)-37**) and **(*S,S*)-**Ca(CzOx$^{i\text{Pr}}$){N(SiMe$_3$)$_2$}(THF) (**(*S,S*)-38**) were synthesised as precursors to access the target alkoxide complexes

(Scheme 4.3) Both **(*S*,*S*)-37** and **(*S*,*S*)-38** were synthesised *via* the protonolysis of 1 equivalent of (*S*,*S*)-HCzOx$^{i\text{Pr}}$ with 1 equivalent of either Mg{N(SiMe$_3$)$_2$}$_2$ or Ca{N(SiMe$_3$)$_2$}$_2$(THF)$_2$ in toluene, followed by removal of the solvent *in vacuo*. The resultant products were washed with cold pentane to remove the side product HN(SiMe$_3$)$_2$; however, the contaminant could not be completely removed from the desired product, due to the high solubility of the target complexes in pentane and remained as an impurity of 13 and 19% by ^{1}H NMR spectroscopy for **(*S*,*S*)-37** and **(*S*,*S*)-38**, respectively. Although both **(*S*,*S*)-37** and **(*S*,*S*)-38** were fully characterised with ^{1}H NMR, ^{13}C{^{1}H} NMR, IR spectroscopy and mass spectrometry, elemental analyses confirming bulk purity could not be obtained for either complex. As it was postulated that HN(SiMe$_3$)$_2$ would not interfere with the onwards reaction of **(*S*,*S*)-37** and **(*S*,*S*)-38** with benzyl alcohol as a further equivalent is liberated during protonolysis, attempts to synthesise both (*S*,*S*)-Mg(CzOx$^{i\text{Pr}}$)(OBn) and (*S*,*S*)-Ca(CzOx$^{i\text{Pr}}$)(OBn) were undertaken following a similar synthetic protocol for the successful synthesis of Mg(CzOx$^{\text{Me}_2}$)(OBn) (**2**) and Ca(CzOx$^{\text{Me}_2}$)(OBn) (**10**). Toluene solutions of crude **(*S*,*S*)-37** and **(*S*,*S*)-38** cooled to -78 °C were treated with a toluene solution of benzyl alcohol, cooled to -10 °C. Following removal of the volatiles, the ^{1}H NMR spectrum of the resultant products confirmed the successful synthesis of both (*S*,*S*)-Mg(CzOx$^{i\text{Pr}}$)(OBn) and (*S*,*S*)-Ca(CzOx$^{i\text{Pr}}$)(OBn); however, attempts to isolate the complexes from protioligand and HN(SiMe$_3$)$_2$ contaminants in a viable yield for further studies were unsuccessful due to the target complexes' high solubility in pentane. Pure (*S*,*S*)-Mg(CzOx$^{i\text{Pr}}$)(OBn) was isolated in the extremely low yield of 9%, and pure (*S*,*S*)-Ca(CzOx$^{i\text{Pr}}$)(OBn) was isolated in less than 5% yield; in view of the low yields obtained, no further attempts were made to isolate the complexes for polymerisation studies.

(*S*,*S*)-34 was treated with 1 equivalent of MgI$_2$ in THF in order to synthesise the complex Mg(CzOx$^{i\text{Pr}}$)I(THF) (**(*S*,*S*)-39**): following isolation and purification, the product was obtained in 68% yield and fully characterised with ^{1}H and ^{13}C{^{1}H} NMR spectroscopy, IR spectroscopy, mass spectrometry and elemental analysis. **(*S*,*S*)-39** was treated with NaOBn and KOBn in order to generate (*S*,*S*)-Mg(CzOx$^{i\text{Pr}}$)(OBn); however, although (*S*,*S*)-Mg(CzOx$^{i\text{Pr}}$)(OBn) was successfully generated, the product was contaminated with the presence of protioligand, which is postulated to form as a

result of the presence of residual benzyl alcohol in KOBn. As it was not possible to isolate (*S*,*S*)-Mg(CzOx^{iPr})(OBn) in sufficiently high purity or quantity for polymerisation, efforts to synthesise the complex were discontinued.



Scheme 4.3. Synthesis of magnesium, calcium and strontium complexes **39**-**42** *via* protonolysis and salt metathesis reactions (M = Mg, n = 0; M = Ca, n = 2).

Considering the success observed in the controlled ROP of *rac*-LA with Mg(CzOx^{Me2})(Bu) (**3**), attempts were undertaken in order to synthesise (*S*,*S*)-Mg(CzOx^{iPr})(Bu): 1 equivalent of (*S*,*S*)-HCzOx^{iPr} was treated with a 1.0 M heptanes solution of $MgBu_2$ in toluene at -78 °C, followed by immediate removal of the solvent at -78 °C; however, no resonances corresponding to the Bu group were observed. For comparison, the homoleptic complex (*S*,*S*)-Mg(CzOx^{iPr})$_2$ (**(*S*,*S*)-40**) was independently synthesised from the reaction of 2 equivalents of (*S*,*S*)-HCzOx^{iPr} with Mg{N(SiMe$_3$)$_2$}$_2$ in toluene. The resultant product obtained in 36% yield was fully characterised by ^{1}H and ^{13}C{^{1}H} NMR spectroscopy, IR spectroscopy, mass spectrometry and elemental analysis; the ^{1}H NMR spectrum in C_6D_6 was found to be

identical to that of the product obtained in the attempted synthesis of Mg(CzOx^{iPr})(Bu). As it was not possible to synthesise Mg(CzOx^{iPr})(Bu) under kinetic control, all further efforts to isolate this complex were discontinued.

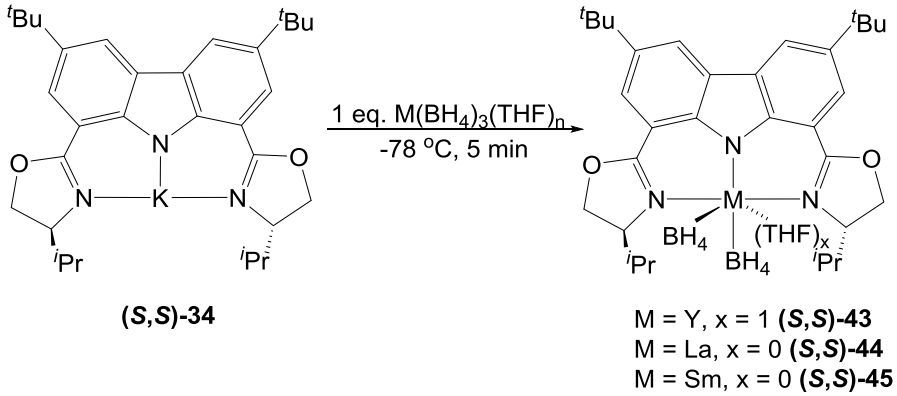
(*S*,*S*)-Ca(CzOx^{iPr})$_2$ (**(*S*,*S*)-41**) was synthesised 2 equivalents of (*S*,*S*)-HCzOx^{iPr} with Ca{N(SiMe$_3$)$_2$}$_2$(THF)$_2$ in toluene; the reaction had reached completion following 16 hours at room temperature, indicating that **(*S*,*S*)-41** is more readily formed than Ca(CzOx^{Me2})$_2$ (**11**), which required the application of heat and a 72 h reaction time. **(*S*,*S*)-41** was isolated in a similar yield of 68%, and fully characterised by ^{1}H and ^{13}C{^{1}H} NMR spectroscopy, IR spectroscopy, mass spectrometry and elemental analysis. Unlike **11**, **(*S*,*S*)-41** was not found to be air- or moisture-stable; however, it was significantly more soluble in non-donor solvents such as benzene, allowing for full characterisation in C_6D_6. The milder conditions required to isolate **(*S*,*S*)-41** successfully is perhaps indicative of the reduced steric hindrance associated with the CzOx^{iPr} ligand, in which one methyl group has been replaced with a hydrogen atom. This hypothesis is supported by the successful formation of **(*S*,*S*)-40**, whereas the CzOx^{Me2} analogue was not formed.

In order to verify whether the product obtained from the attempted synthesis of (*S*,*S*)-Sr(CzOx^{iPr})(BH$_4$) was the homoleptic complex, (*S*,*S*)-Sr(CzOx^{iPr})$_2$ was independently synthesised through the salt metathesis reaction of 2 equivalents of **(*S*,*S*)-34** and Sr(BH$_4$)$_2$(THF)$_2$ in THF at room temperature. Following isolation and purification, (*S*,*S*)-Sr(CzOx^{iPr})$_2$ (**(*S*,*S*)-42**) was obtained in 53% yield and fully characterised. Analysis of the ^{11}B NMR spectrum revealed there to be no boron environments in the complex, further supporting that the complex formed was the homoleptic. Comparison of the ^{1}H NMR spectra of the independently synthesised **(*S*,*S*)-42** with that of the product obtained from the attempted synthesis of (*S*,*S*)-Sr(CzOx^{iPr})(BH$_4$) revealed the spectra to be identical, confirming that the product obtained is **(*S*,*S*)-42**.

4.4 Synthesis and characterisation of CzOx^{iPr}-supported Group 3 and lanthanide complexes

Under close supervision by the author, L. Budden synthesised (*S*,*S*)-Y(CzOx^{iPr})(BH$_4$)$_2$(THF) (**(*S*,*S*)-43**) through the salt metathesis reaction of 1

equivalent of (*S*,*S*)-K(CzOx^{iPr}) (**(*S*,*S*)-34**) with 1 equivalent of Y$(BH_4)_3(THF)_2$, affording the product as a yellow powder in 50% yield (Scheme 4.4). Following this preliminary result, the series of chiral Group 3 and lanthanide catalysts was expanded to include the lanthanum and samarium analogues (*S*,*S*)-La(CzOx^{iPr})$(BH_4)_2$ (**(*S*,*S*)-44**) and (*S*,*S*)-Sm(CzOx^{iPr})$(BH_4)_2$ (**(*S*,*S*)-45**), which were synthesised *via* a similar method.



Scheme 4.4. Synthesis of yttrium, lanthanum and samarium complexes **(*S*,*S*)-43-(*S*,*S*)-45** *via* salt metathesis reactions with the appropriate precursor $M(BH_4)_3(THF)_n$ (M = Y, n = 2; M = Sm or La, n = 3).

In a similar fashion to previously synthesised supported lanthanide borohydride complexes, analysis of the ^{1}H NMR spectra for **(*S*,*S*)-43-(*S*,*S*)-45** displayed a broad singlet corresponding to the hydrogen atoms of the BH_4 group, as opposed to the expected quartet. Furthermore, analysis of the ^{11}B NMR spectra revealed apparent singlets corresponding to the BH_4 group; both observations are attributed to "washing out" of the $^1J_{B\text{-}H}$ coupling.

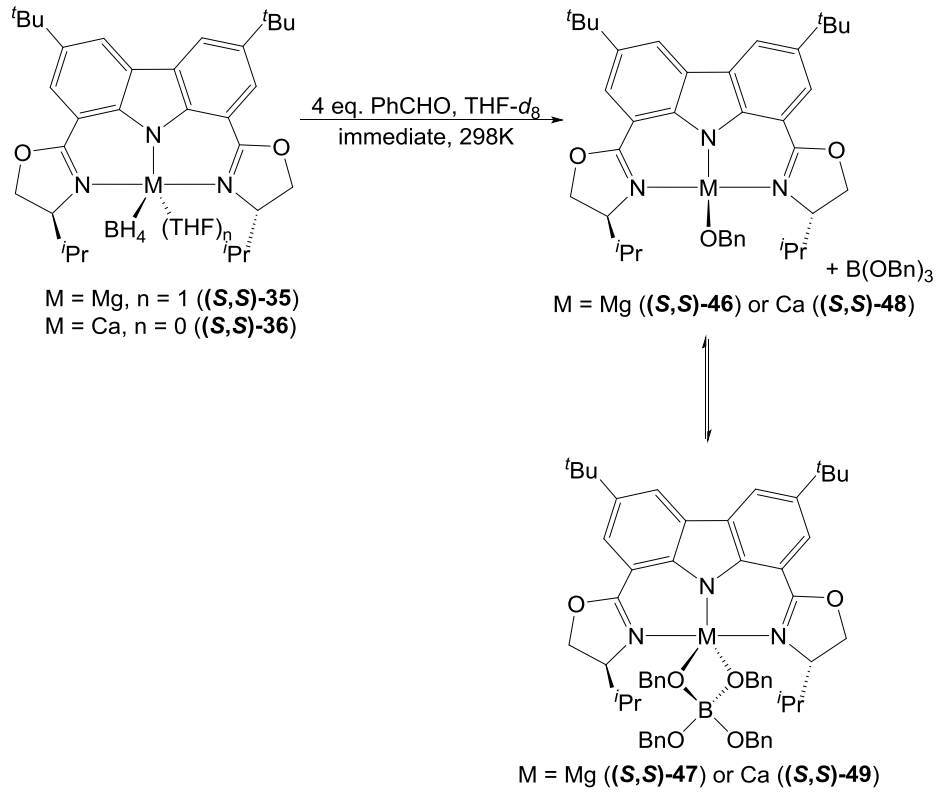
The bonding modes of the borohydride groups for complexes **(*S*,*S*)-43-(*S*,*S*)-45** were investigated with solid state and THF solution IR spectroscopy (Table 4.3). All complexes were readily identifiable as adopting a tridentate coordination mode both in the solid state as a Nujol mull and in a THF solution. The $\nu(B–H_t)$ stretching frequencies decrease as the ionic radius of the metal centre increases, such that Y > Sm > La. Furthermore, the splitting between the $\nu(B–H_t)$ and the $\nu(B–H_b)$ stretching frequencies decreases with increasing ionic radius, which may be a product of the decreasing covalency of the M-BH_4 bond.

Table 4.3. Solid state (Nujol mull) and solution (THF) ν(B–H) stretching frequencies (cm^{-1}) for complexes M(CzOx^{iPr})$(BH_4)_2(THF)_n$ (M = Y, n = 1 (**(*S*,*S*)-43**); M = La, n = 0 (**(*S*,*S*)-44**); or M = Sm, n = 0 (**(*S*,*S*)-45**)).

	(*S*,*S*)-43	**(*S*,*S*)-44**	**(*S*,*S*)-45**
Solid state			
$\nu(B–H_t)$	2499	2430	2443
$\nu(B–H_b)$	2224, 2174	2212, 2152	2211, 2157
Solution			
$\nu(B–H_t)$	2450	2420	2444
$\nu(B–H_b)$	2224, 2175	2238, 2173	2223, 2180

4.5 *In situ* generation of trialkyl borate esters as chain transfer agents

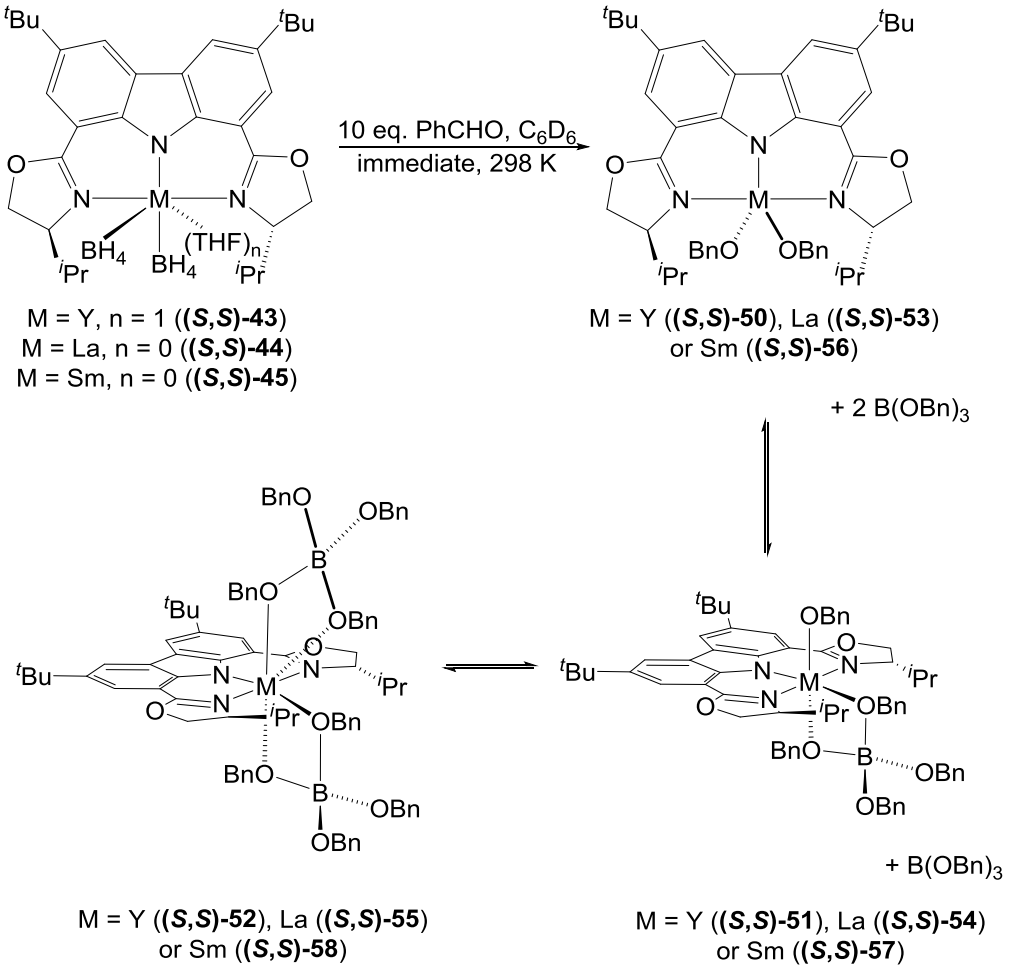
In a similar manner as the *in situ* generation of catalysts explored in Chapters 2 and 3, the treatment of (*S*,*S*)-Mg(CzOx^{iPr})(BH_4)(THF) (**(*S*,*S*)-35**) and (*S*,*S*)-Ca(CzOx^{iPr})(BH_4) (**(*S*,*S*)-36**) with 4.5 equivalents of benzaldehyde in THF-d_8 resulted in the immediate generation of the corresponding alkoxides, (*S*,*S*)-Mg(CzOx^{iPr})(OBn) (**(*S*,*S*)-46**) and (*S*,*S*)-Ca(CzOx^{iPr})(OBn) (**(*S*,*S*)-48**), with concurrent generation of $B(OBn)_3$ (Scheme 4.5). These complexes existed as the free species in which the $B(OBn)_3$ is uncoordinated to the metal centre, or as tetracoordinated adducts, (*S*,*S*)-Mg(CzOx^{iPr}){$B(OBn)_4$} (**(*S*,*S*)-47**) and (*S*,*S*)-Ca(CzOx^{iPr}){$B(OBn)_4$} (**(*S*,*S*)-49**). Again, the position of the equilibrium between the free species and the tetracoordinated adduct was dependent on metal size, with formation of the tetracoordinated adduct found to be more favourable when using a larger metal centre such as calcium.



Scheme 4.5. Transformation of complexes **(*S*,*S*)-35** to **(*S*,*S*)-46**, $B(OBn)_3$ and **(*S*,*S*)-47** , and **(*S*,*S*)-36** to **(*S*,*S*)-48**, $B(OBn)_3$ and **(*S*,*S*)-49** through the addition of 4.5 eq. PhCHO.

The addition of 10 equivalents of benzaldehyde to (*S*,*S*)-Y(CzOx^{iPr})$(BH_4)_2$(THF) (**(*S*,*S*)-43**), (*S*,*S*)-La(CzOx^{Me2})$(BH_4)_2$ (**(*S*,*S*)-44**) and (*S*,*S*)-Sm(CzOx^{iPr})$(BH_4)_2$ (**(*S*,*S*)-45**) resulted in the immediate generation of the corresponding alkoxides, (*S*,*S*)-Y(CzOx^{iPr})$(OBn)_2$ (**(*S*,*S*)-50**), (*S*,*S*)-La(CzOx^{Me2})$(OBn)_2$ (**(*S*,*S*)-53**) and (*S*,*S*)-Sm(CzOx^{iPr})$(OBn)_2$ (**(*S*,*S*)-56**) and 2 equivalents of $B(OBn)_3$. Analysis of the ^{11}B NMR spectra confirmed the evolution of uncoordinated $B(OBn)_3$, in addition to the formation of a species containing a tetracoordinated boron, most likely an adduct in which the $B(OBn)_3$ is coordinated to the metal centre. Following addition of 10 equivalents of benzaldehyde to (*S*,*S*)-Y(CzOx^{iPr})$(BH_4)_2$(THF) (**(*S*,*S*)-43**) two singlets were observed in the ^{11}B NMR spectrum: the resonance at 18.9 ppm corresponding to $B(OBn)_3$, and the resonance at 4.4 ppm corresponding to the mono(tetracoordinated) adduct (*S*,*S*)-Y(CzOx^{iPr})(OBn){$B(OBn)_4$} (**(*S*,*S*)-51**) (Scheme 4.6). A similar observation was made following addition of benzaldehyde to **(*S*,*S*)-44** and **(*S*,*S*)-45**. No resonances were observed corresponding to the bis(tetracoordinated) adducts

(*S*,*S*)-Y(CzOx^{iPr}){B(OBn)$_4$}$_2$ (**(*S*,*S*)-52**), (*S*,*S*)-La(CzOx^{iPr}){B(OBn)$_4$}$_2$ (**(*S*,*S*)-55**) or (*S*,*S*)-Sm(CzOx^{iPr}){B(OBn)$_4$}$_2$ (**(*S*,*S*)-58**) were observed at room temperature, which may be a result of steric hindrance reducing the favourability with which these complexes are formed.



Scheme 4.6. Transformation of complexes **(*S*,*S*)-43** to **(*S*,*S*)-50**, B(OBn)$_3$, **(*S*,*S*)-51** and **(*S*,*S*)-52**, **(*S*,*S*)-44** to **(*S*,*S*)-53**, B(OBn)$_3$, **(*S*,*S*)-54** and **(*S*,*S*)-55** and **(*S*,*S*)-45** to **(*S*,*S*)-56**, B(OBn)$_3$, **(*S*,*S*)-57** and **(*S*,*S*)-58** through the addition of 10 eq. PhCHO.

4.6 Polymerisation studies: ROP of *rac*-, *L*-, *D*- and *meso*-LA

Complexes (*S*,*S*)- and (*R*,*R*)-Mg(CzOx^{iPr})(BH$_4$)(THF) (**(*S*,*S*)-** and **(*R*,*R*)-35**), (*S*,*S*)-Ca(CzOx^{Me2})(BH$_4$) (**(*S*,*S*)-36**), (*S*,*S*)-Y(CzOx^{iPr})(BH$_4$)$_2$(THF) (**(*S*,*S*)-43**), (*S*,*S*)-La(CzOx^{Me2})(BH$_4$)$_2$ (**(*S*,*S*)-44**) and (*S*,*S*)-Sm(CzOx^{iPr})(BH$_4$)$_2$ (**(*S*,*S*)-45**) were evaluated as initiators for the ROP of lactide. These complexes were tested initially in the absence of any additives. *In situ* generated catalysts were synthesised following

the addition of the appropriate number of equivalents of benzaldehyde to a THF solution of the corresponding supported metal borohydride complex, and stirred for 5 min prior to the addition of lactide to ensure complete conversion. Polymerisation experiments were conducted in THF at room temperature, and under these conditions all complexes were found to be active. The polymerisation was followed by the collection of aliquots at regular time intervals, and the polymer samples were characterised by ^{1}H NMR spectroscopy, Gel Permeation Chromatography and MALDI-ToF MS. The results are summarised in Tables 4.4-4.7.

4.6.1 Polymerisation studies: ROP of *rac*-, *L*-, *D*- and *meso*-LA with Group 2 catalysts

A preliminary investigation into the stereocontrol of complex (*S*,*S*)-Mg(CzOx$^{i\text{Pr}}$)(BH$_4$)(THF) (**(*S*,*S*)-35**) was conducted in order to determine the impact of incorporating chiral centres in close proximity to the active site. In the presence of 100 equivalents of *rac*-LA, **(*S*,*S*)-35** was found to be considerably less active than its achiral counterpart Mg(CzOx^{Me2})(BH$_4$) (**7**), achieving 92% monomer conversion following 72 h compared to 88 % conversion after 120 min (Table 4.4, entry 1). The marked decrease in activity is attributed to the increased stability of the catalyst-monomer adduct following chelation of a lactide molecule to the vacant site at the magnesium, or stronger chelation of the growing polymeryl chain to the metal, caused by reduced steric hindrance. This hypothesis is supported by the relative ease with which the homoleptic complex, (*S*,*S*)-Mg(CzOx$^{i\text{Pr}}$)$_2$ (**(*S*,*S*)-40**) can be formed in comparison to the corresponding complex, Mg(CzOx^{Me2})$_2$, which could not be synthesised even under extremely forcing reaction conditions. Despite the apparent increase in steric bulk of the chiral CzOx$^{i\text{Pr}}$ ligand on one side of the oxazoline ring due to the isopropyl substituents, the reduction in steric bulk on the other side from a methyl substituent to a hydrogen atom may result in a more open metal centre, allowing for successful formation of **(*S*,*S*)-40**, and resulting in a stronger chelation of the lactide molecule or polymeryl chain to the metal.

Analysis with ^{1}H{^{1}H} NMR spectroscopy revealed a similar degree of heterotactic enrichment of the resultant polymer to that obtained from **7** (P_r = 0.88-0.81 *cf*. 0.82-0.84), indicating that there the introduction of chirality into the supporting ligand does

not result in a shift from chain end control, resulting in heterotactic enrichment, to enantiomorphic site control, which would result in isotactic enrichment. Considering the planarity of the supporting ligand and complexes, the chiral centres on the oxazoline rings may not be positioned in sufficiently close proximity to the incoming lactide molecule to result in the destabilisation of one catalyst-lactide adduct compared to another with opposing chirality, resulting in enantiomorphic site control.

Based on the successful results obtained in Chapters 2 and 3, in which the control of borohydride catalysts may be improved following their *in situ* transformation to an alkoxide initiators, **(*S*,*S*)-35** was treated with 4.5 equivalents of benzaldehyde prior to the addition of 100 equivalents of *rac*-LA to generate (*S*,*S*)-Mg(CzOx$^{i\text{Pr}}$)(OBn) (**(*S*,*S*)-46**) and $B(OBn)_3$. An additional experiment was conducted in which a further 1 equivalent of independently synthesised $B(OBn)_3$ was added following the generation of **(*S*,*S*)-46** and $B(OBn)_3$ in order to probe the role of the trialkyl borate ester during the polymerisation (Table 4.4, entries 2 and 3). The polymerisation of *rac*-LA with **(*S*,*S*)-46** and $B(OBn)_3$ was considerably more rapid than with **(*S*,*S*)-35** (93% monomer conversion after 0.75 h) whereas in the presence of a further equivalent of $B(OBn)_3$, the rate decreases substantially (88% monomer conversion after 48 h). The decrease in rate following this addition confirms that the borate ester adduct is not the active species during the polymerisation, and that **(*S*,*S*)-46** as the free species is the active catalyst. In addition, previous investigations have suggested that the formation of 1 equivalent of $B(OBn)_3$ results in decreased activity relative to the starting borohydride complex (Chapter 3), this does not occur here. Although the chiral supporting ligand results in a more open metal centre, this does not result in a sufficiently increased degree of formation of the inactive borate ester adduct in order to impact on the rate of polymerisation. Analysis of the polymer backbone with $^1H\{^1H\}$ NMR spectroscopy revealed a similar degree of heterotactic enrichment for **(*S*,*S*)-46** as for **(*S*,*S*)-35** ($P_r \approx 0.80$-0.86), confirming that the employment of a benzyl oxide initiating group does not impact the mechanism of stereocontrol during the polymerisation.

Table 4.4. Selected data for the polymerisation of *rac*-, *L*-, *D*- and *meso*-LA using (*S*,*S*)-Mg(CzOx$^{i\text{Pr}}$)(BH$_4$)(THF) (**(*S*,*S*)-35**) in THF.[a]

Entry	Catalyst	Monomer	Additive (eq.)	Conv.[b] %	Time (h)	M_n(obs)[c] (g mol^{-1})	M_n(calc)[d] (g mol^{-1})	M_w/M_n[c]	P_r[b]
1	**(*S*,*S*)-35**	*rac*	-	92	72	7,750	13,261	1.24	0.81-0.88
2	**(*S*,*S*)-35**	*rac*	PhCHO (4.5)	93	0.75	5,870	3,458	1.15	0.83-0.85
3	**(*S*,*S*)-35**	*rac*	PhCHO (4.5) + B(OBn)$_3$ (1)	88	48	2,780	1,920	1.16	0.80-0.86
4	**(*S*,*S*)-35**	*meso*	-	89	4	7,900	12,829	1.23	0.68-0.70
5	**(*S*,*S*)-35**	*meso*	PhCHO (4.5)	94	0.75	5,100	3,494	1.13	0.75-0.76
6	**(*S*,*S*)-35**	*L*	-	90	312	7,520	12,973	1.29	-
7	**(*S*,*S*)-35**	*L*	PhCHO (4.5)	95	120	5,280	3,530	1.09	-
8	**(*S*,*S*)-35**	*D*	-	89	384	8,000	12,829	1.27	-
9	**(*S*,*S*)-35**	*D*	PhCHO (4.5)	94	2	5,950	3,494	1.09	-

[a] Conditions: [LA]$_0$:[**(*S*,*S*)-35**]$_0$ = 100:1, 4 mL THF at 23 °C. [LA]$_0$ = 1.0 M. [b] Measured by ^{1}H NMR (CDCl$_3$) analyses. [c] Molecular weights (g mol^{-1}) determined from GPC using appropriate Mark-Houwink corrections. [d] Expected average M_n (g mol^{-1}) for stated number of chains per metal and stated % conversion: M_n (calc for entries 1, 4, 6 and 8) = (conversion (%) × 100 × 144.1) + 4.0; (calc for entries 2, 5, 7 and 9) = ¼(conversion (%) × 100 × 144.1) + 108.1; (calc for entry 3) = 1/7 (conversion (%) × 100 × 144.1) + 108.1.

Both in the presence and absence of benzaldehyde, the polymerisation of *rac*-LA with **(*S*,*S*)-35** resulted in a dependence on lactide concentration that was neither first- nor second-order; however, it appeared to observe a non-integer dependence intermediate between the two. This is consistent with previous observations in which a borate ester is present throughout the polymerisation which may coordinate to the metal centre, impacting the apparent rate constant. On the addition of a further equivalent of $B(OBn)_3$ to **(*S*,*S*)-46** and $B(OBn)_3$, the dependence on lactide concentration followed a non-integer order between second- and third-order. These results are indicative of a complex system of preequilibria which impact the dependence on lactide concentration, as described previously.

Of considerable importance was the molecular weight control exerted by **(*S*,*S*)-35**, and **(*S*,*S*)-46** with either one or two equivalents of $B(OBn)_3$ present (Figure 4.6). In each instance, the observed molecular weights did not agree well with those expected. With **(*S*,*S*)-35**, the observed molecular weights were found to be lower than expected assuming the growth of 1 polymer chain per metal centre. This is indicative of the presence of a borate ester species such as $B(LA\text{-}H)_3$ which acts as a chain transfer agent, and shifting the nature of the polymerisation from living to immortal. To confirm the evolution of a trialkyl borate ester species of the type $B(OR)_3$, such as $B(LA\text{-}H)_3$, a ^{1}H and ^{11}B NMR investigation was conducted into the behaviour of **(*S*,*S*)-35** in the presence of 10 equivalents of *rac*-LA. Following addition, several resonances were observed in the ^{11}B NMR spectrum, which are in the same region as previously tentatively assigned $B(LA\text{-}H)_3$ and $\{B(LA\text{-}H)_4\}$ species (21.0 and 6.0 ppm, respectively). Analysis of the ^{1}H NMR spectrum was limited due to broadening within the entire 4.0-6.0 ppm region preventing the polymer chain end-groups from being discerned. Although the mechanism of initiation with **(*S*,*S*)-35** has not been investigated with deuterium-labelling studies, these results suggest that the catalyst does undergo a similar mechanism of initiation to other borohydride initiators whose mechanisms have been well-studied, such as **7**. Furthermore, the increased rate of reaction upon generation of **(*S*,*S*)-46** with $B(OBn)_3$ compared to the starting borohydride initiator also serves to suggest that **(*S*,*S*)-35** follows the same initiation mechanism, in which $BH_3(THF)$ is liberated following the first hydride transfer forming an intermediate, (*S*,*S*)-Mg($CzOx^{iPr}$)(LA-H), concurrently with other catalytically inactive species which reduce the observed rate of polymerisation.

Analysis with MALDI-ToF MS of the polymer obtained from **(*S*,*S*)-35** confirmed the presence of both α,ω-dihydroxytelechelic and LA-H-terminated PLA.

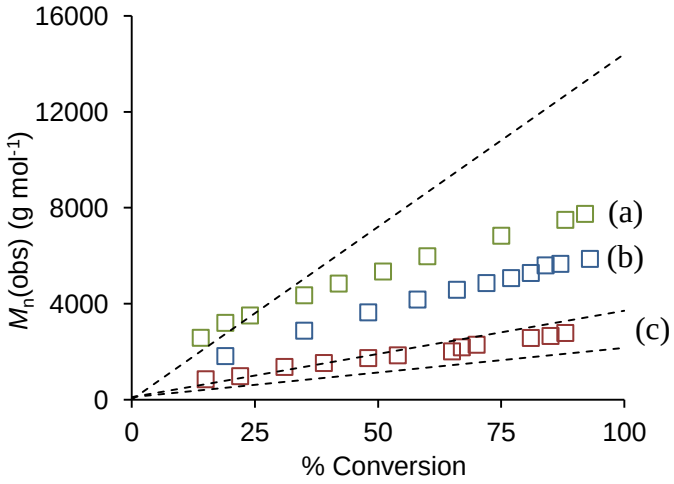


Figure 4.6. M_n(obs) (g mol^{-1}) *vs*. % conversion plot for the ROP of *rac*-LA using (*S*,*S*)-Mg(CzOx$^{i\text{Pr}}$)(BH$_4$)(THF) (**(*S*,*S*)-35**) and *in situ* generated (*S*,*S*)-Mg(CzOx$^{i\text{Pr}}$)(OBn) (**(*S*,*S*)-46**) and B(OBn)$_3$; the dashed lines are the M_n(calc) in each case. Conditions: 4 mL THF, 23 °C, [*rac*-LA]$_0$:[cat]$_0$:[B(OBn)$_3$]$_0$ = (a) 100:1:0; (b) 100:1:1; (c) 100:1:2; [*rac*-LA]$_0$ = 1.0 M. (a) **(*S*,*S*)-35** with no additives, expecting 1 chain per metal centre (green squares); (b) **(*S*,*S*)-46** and 1 eq. B(OBn)$_3$, expecting 4 chains per metal centre (blue squares); (c) **(*S*,*S*)-46** and 2 eq. B(OBn)$_3$, expecting 7 chains per metal centre (red squares).

The molecular weights obtained with **(*S*,*S*)-46** with either one or two equivalents of B(OBn)$_3$ were found to be consistently higher than anticipated, which is indicative of inefficient chain transfer. The agreement between M_n(obs) and M_n(calc) was improved in the presence of 2 equivalents of CTA than 1 equivalent, which may be due to the decreased rate of polymerisation caused by the coordination of the borate ester, leading to a decreased difference in the rate of chain transfer versus the rate of propagation (Figure 4.6). However, a plot of M_n(obs) *vs*. % conversion indicated a linear growth in molecular weights with a gradient of 25.6(7) g mol^{-1} (% conversion)$^{-1}$ (R^2 = 0.992), which remains higher than that expected for 7 chains per metal centre (20.6 g mol^{-1}), which indicates that k_{CT} remains greater than k_p. MALDI-ToF MS analysis of the PLA obtained from **(*S*,*S*)-46** confirmed the presence of polymer chains with the anticipated OBn end-groups, together with a low incidence of

transesterification, which is mirrored in the narrow PDIs observed (PDI ≈ 1.05-1.15) (Figure 4.7).

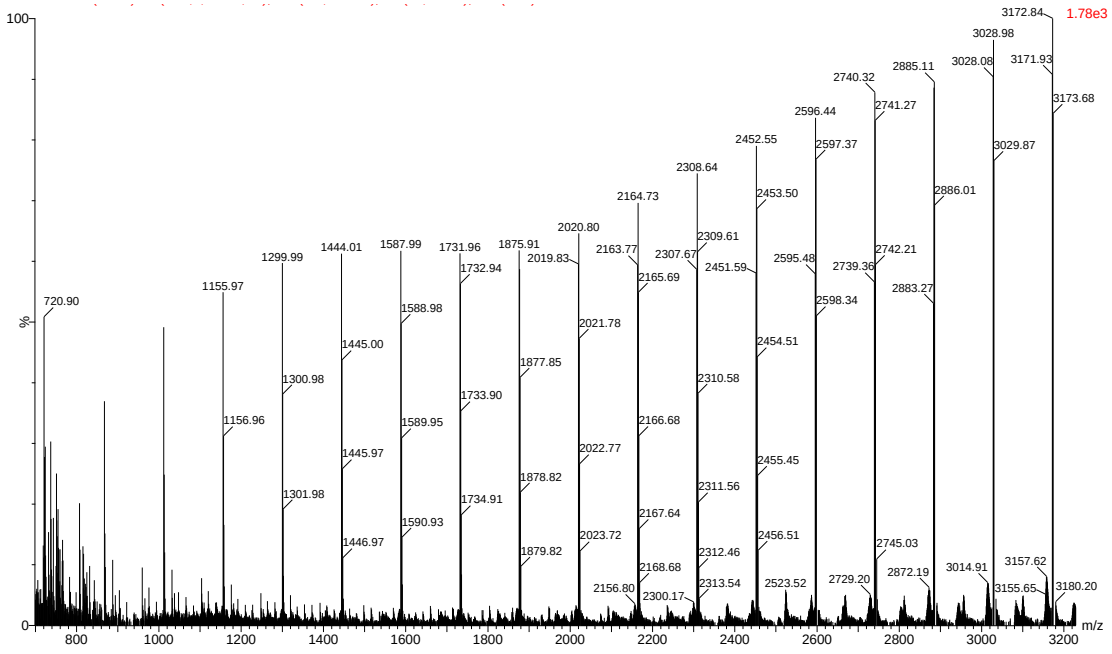


Figure 4.7. MALDI-ToF MS of PLA obtained from (*S*,*S*)-Mg(CzOx$^{i\text{Pr}}$)(OBn) (**(*S*,*S*)-46**) and B(OBn)$_3$. M_n by GPC analysis is 4,170 g mol^{-1}.

In the presence of various additives, **(*S*,*S*)-35** proved more active in the polymerisation of *meso*-LA than *rac*-LA; however, it was significantly less active than its achiral counterpart, **7**, which is similarly attributed to the reduced steric hindrance from the supporting ligand. In the absence of benzaldehyde, **(*S*,*S*)-35** achieved 89% monomer conversion after 4 h, observing a second-order dependence in lactide concentration (k_{obs} = 1.99(5) M^{-1} h^{-1}, R^2 = 0.996); whereas following the addition of 4.5 equivalents of benzaldehyde, **(*S*,*S*)-46** achieved 94% conversion after 0.75 h (Table 4.4, entries 4 and 5). Whilst the polymerisation of *meso*-LA with **(*S*,*S*)-35** is more rapid than the equivalent polymerisation of *rac*-LA, *in situ* generated **(*S*,*S*)-46** and B(OBn)$_3$ appeared to reach a similar degree of completion after an identical reaction time of 0.75 h. Unfortunately, as both experiments were neither clearly first- nor second-order, it was not possible to directly compare the apparent rate constants; however, after 5 min, **(*S*,*S*)-46** achieved 57% conversion of *meso*-LA to polymer, whereas after the same time period, only 35% *rac*-LA had been converted to polymer. The increased reactivity observed is attributable to the relative instability of the *meso*-LA monomer compared to *L*- or *D*-LA. Interestingly, the degree of

syndiotactic enrichment increased following the employment of the chiral supporting ligand (entry 4: P_r = 0.68-0.70; entry 5: P_r = 0.75-0.76). The formation of syndiotactically-enriched PLA from *meso*-LA arises due to the preference for the formation of *racemic* dyads instead of *meso* dyads, formed *via* a chain end control mechanism; however, in this instance the preference for enchainment *via racemic* dyads appears to have increased on introduction of a chiral environment, which may indicate a destructive effect of the ligand on exerting stereocontrol *via* an enantiomorphic site control mechanism.

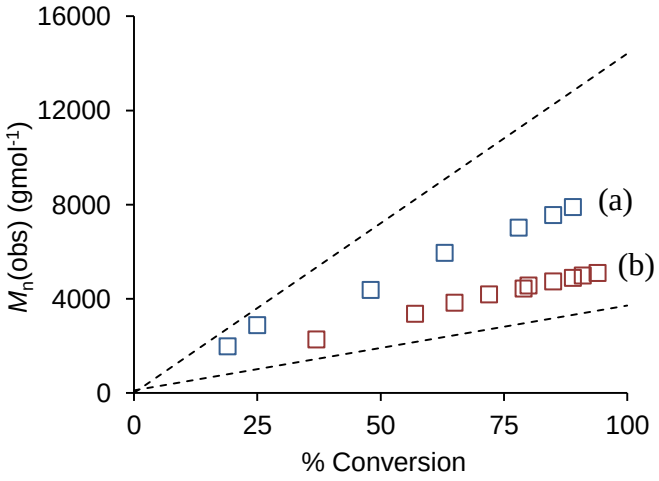


Figure 4.8. M_n(obs) (g mol^{-1}) *vs*. conversion plot for the ROP of *meso*-LA using (*S*,*S*)-Mg(CzOx$^{i\text{Pr}}$)(BH$_4$)(THF) (**(*S*,*S*)-35**) and *in situ* generated (*S*,*S*)-Mg(CzOx$^{i\text{Pr}}$)(OBn) (**(*S*,*S*)-46**) and 1 eq. B(OBn)$_3$; the dashed lines are the M_n(calc) in each case. Conditions: 4 mL THF, 23 °C, [*meso*-LA]$_0$:[cat]$_0$:[B(OBn)$_3$]$_0$ = (a) 100:1:0; (b) 100:1:1; [*meso*-LA]$_0$ = 1.0 M. (a) **(*S*,*S*)-35** with no additives, expecting 1 chain per metal centre (blue squares); (b) **(*S*,*S*)-46** and 1 eq. B(OBn)$_3$, expecting 4 chains per metal centre (red squares).

The molecular weight control was consistent with previous observations for the polymerisation of *rac*-LA with **(*S*,*S*)-35** (Figure 4.8). In the absence of any additives, the observed molecular weights were found to be lower than expected with a growth corresponding to approximately 2 chains per metal centre, which is highly suggestive of the presence of a borate ester such as B(LA-H)$_3$ acting as a CTA. The addition of 4.5 equivalents of benzaldehyde to generate *in situ* **(*S*,*S*)-46** and B(OBn)$_3$ resulted in the linear growth of molecular weights, corresponding to approximately 3 chains per

metal centre. The introduction of $B(OBn)_3$ appeared to suppress intermolecular transesterification, following analysis of the MALDI-ToF MS for both the polymerisation with **(*S*,*S*)-35** and **(*S*,*S*)-46** and $B(OBn)_3$, which is confirmed by the narrower PDIs observed (PDI ≈ 1.10-1.25 *cf.* PDI ≈ 1.10-1.15).

In order to understand the nature of the stereocontrol observed during the polymerisation of both *rac*- and *meso*-LA, **(*S*,*S*)-35** was treated with both *L*- and *D*-LA in the absence and presence of benzaldehyde (Table 4.4, entries 6-9). In the absence of benzaldehyde **(*S*,*S*)-35** exhibited low activity for the ROP of either *L*- or *D*-LA (90% *L*-LA polymerised after 312 h *vs.* 89% *D*-LA polymerised after 384 h) Although there is a slight increase in the activity of the catalyst in the presence of *L*-LA, due to the length of the polymerisation, this is attributed to the presence of small amounts of impurities whose impact on the polymerisation becomes significant over the long reaction time. Kinetic analysis of both experiments failed to assign the reaction as either first- or second-order dependence on [LA]; instead, an intermediary non-integer order was observed. However, following the conversion of **(*S*,*S*)-35** to **(*S*,*S*)-46** and one equivalent of $B(OBn)_3$, the catalysts showed a distinctive monomer preference when treated with either 100 equivalents of pure *L*- or *D*-LA, reaching 95% conversion of *L*-LA to PLLA after 120 h, compared to 94% conversion of *D*-LA to PDLA after 2 h. Despite the strong preference for the ROP of *D*-LA over *L*-LA, the rate of polymerisation remains slower than the rate of polymerisation of *rac*-LA, indicating that although the catalyst is capable of enacting a degree of enantiomorphic site control, enchainment *via racemic* dyads is still preferred. NMR investigations were conducted to probe the origin of the preference for the polymerisation of *D*-LA over *L*-LA with **(*S*,*S*)-46**. **(*S*,*S*)-46** was generated in situ and treated with 10 equivalents of either *D*- or *L*-LA. Although the ^{11}B NMR spectra were very similar forming resonances at 1.0 and 17.0 ppm, the ^{1}H NMR spectrum showed slightly different resonances corresponding to the end-groups of the polymer in the diagnostic region of 4.0-5.0 ppm (Figure 4.9). Although assignment of these resonances was not possible, they indicate the formation of different diastereotopic polymer environments during polymerisation. The relative stabilities of these diastereotopic environments may account for the observed monomer preference.

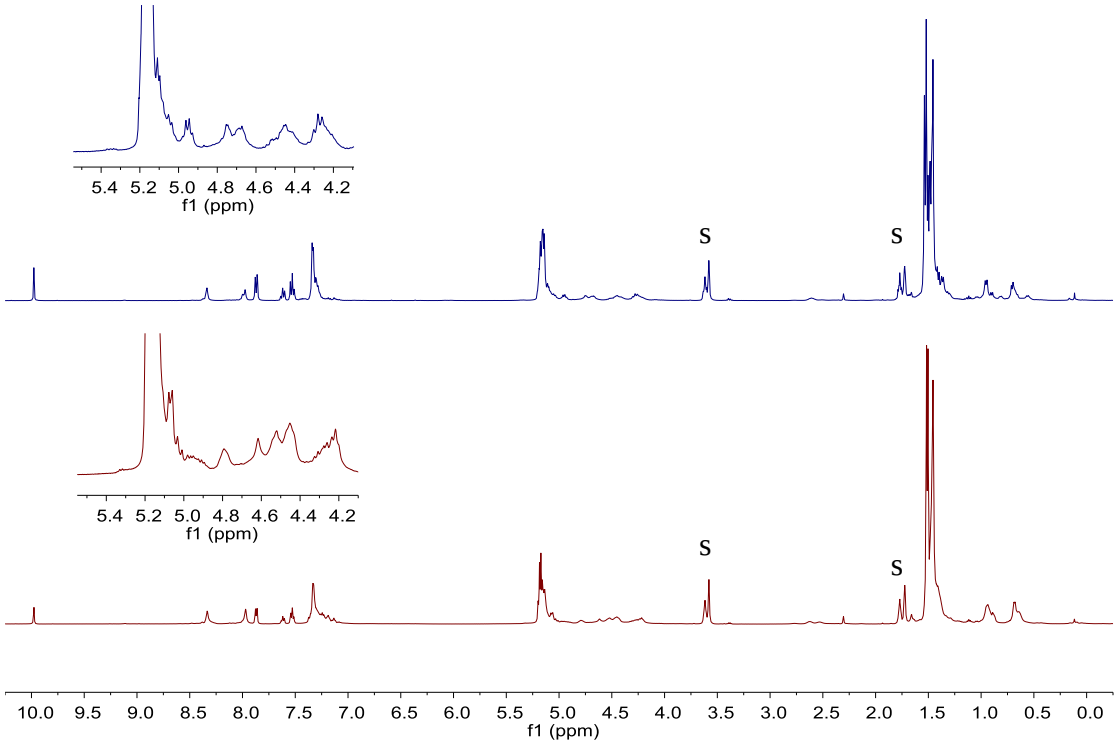


Figure 4.9. Overlay of ^{1}H NMR spectra (THF-d_8, 400.1 MHz, 298 K) of *in situ* generated (*S*,*S*)-Mg(CzOx$^{i\text{Pr}}$)(OBn) (**(*S*,*S*)-46**) with 1 eq. B(OBn)$_3$ and (a) 10 eq. *L*-LA (blue line) or (b) 10 eq. *D*-LA (red line). "s" denotes residual solvent signals.

The observed molecular weights for the polymerisation of both *L*- and *D*-LA with either **(*S*,*S*)-35** or **(*S*,*S*)-46** with 1 equivalent of B(OBn)$_3$ agreed with the previous trends observed with *rac*-LA. In the absence of benzaldehyde, **(*S*,*S*)-35** produced polymer with observed molecular weights consistent with the growth of two polymer chains per metal centre, whereas **(*S*,*S*)-46** resulted in the propagation of polymer consistent with approximately 3 chains per metal centre. The addition of benzaldehyde resulted in a narrowing of the polydispersities due to the immortal nature of the polymerisation (PDI ≈ 1.10-1.15), and analysis with MALDI-ToF MS confirmed the reduced incidence of transesterification when employing a CTA.[43]

As a control experiment in order to verify the monomer and enchainment preferences observed with **(*S*,*S*)-35** and **(*S*,*S*)-46**, an investigation into the catalytic behaviour of **(*R*,*R*)-35** and **(*R*,*R*)-46** in the ROP of *rac*-, *L*- and *D*-LA was performed. The results are summarised in Table 4.5.

Table 4.5. Selected data for the polymerisation of *rac*-, *L*- and *D*-LA using (*R*,*R*)-Mg(CzOx$^{i\text{Pr}}$)(BH$_4$)(THF) (**(*R*,*R*)-35**) and *rac*-Mg(CzOx$^{i\text{Pr}}$)(BH$_4$)(THF) (***rac*-35**) in THF.[a]

Entry	Catalyst	Monomer	Additive (eq.)	Conv.[b] %	Time (h)	M_n(obs)[c] (g mol^{-1})	M_n(calc)[d] (g mol^{-1})	M_w/M_n[c]	P_r[b]
1	**(*R*,*R*)-35**	*rac*	-	91	72	8,680	13,117	1.26	0.85-0.88
2	**(*R*,*R*)-35**	*rac*	PhCHO (4.5)	89	0.75	5,510	3,422	1.15	0.85-0.87
3	**(*R*,*R*)-35**	*L*	-	89	264	8,560	12,829	1.26	-
4	**(*R*,*R*)-35**	*L*	PhCHO (4.5)	93	2	5,700	3,458	1.09	-
5	**(*R*,*R*)-35**	*D*	-	90	336	7,930	12,973	1.26	-
6	**(*R*,*R*)-35**	*D*	PhCHO (4.5)	91	120	5,310	3,386	1.08	-
7	***rac*-35**	*rac*	-	88	24	9,870	12,829	1.32	0.87-0.90
8	***rac*-35**	*rac*	PhCHO (4.5)	91	0.75	7,300	3,386	1.19	0.87-0.88

[a] Conditions: [LA]$_0$:[initiator]$_0$ = 100:1, 4 mL THF at 23 °C. [LA]$_0$ = 1.0 M. [b] Measured by ^{1}H NMR ($CDCl_3$) analyses. [c] Molecular weights (g mol^{-1}) determined from GPC using appropriate Mark-Houwink corrections. [d] Expected average M_n (g mol^{-1}) for stated number of chains per metal and stated % conversion: M_n (calc for entries 1, 3, 5 and 7) = (conversion (%) × 100 × 144.1) + 4.0; (calc for entries 2, 4, 6 and 8) = ¼(conversion (%) × 100 × 144.1) + 108.1.

Gratifyingly, the results obtained from the ROP of *rac*-LA with **(*R*,*R*)-35** in the presence and absence of benzaldehyde mirrored those obtained with **(*S*,*S*)-35** (Table 4.5, entries 1 and 2). Although the rates of polymerisation of both *L*- and *D*-LA with **(*R*,*R*)-35** did not fully agree with the results obtained with **(*S*,*S*)-35**, this is similarly attributed to the presence of minor impurities in the sample whose effect becomes prominent over the lengthy duration of the polymerisation (Table 4.5, entries 3 and 4). Significantly, the rate of polymerisation of *D*-LA with the *in situ* generated **(*R*,*R*)-46** with one equivalent of $B(OBn)_3$ agreed with the rate of polymerisation of *L*-LA with **(*S*,*S*)-46** and $B(OBn)_3$, achieving 93% conversion following 2 h (Table 4.5, entry 5). The complementary polymerisation of *L*-LA with **(*R*,*R*)-46** and $B(OBn)_3$ similarly revealed close agreement with the results obtained from the ROP of *D*-LA with **(*S*,*S*)-46** and $B(OBn)_3$, which reached 91% monomer conversion following 120 h (Table 4.5, entry 6). Employment of a different diastereomeric form of the catalyst again results in a distinctive monomer preference; however, the preferred diastereomeric form of the monomer alternates from one form to another. In this instance, *L*-LA is polymerised at a faster rate than *D*-LA. Despite this monomer preference, enchainment *via racemic* dyads is again preferable to that *via meso* dyads, and as such the polymerisation of *rac*-LA results in the formation of highly heterotactically-enriched PLA (P_r = 0.85-0.87). In all instances, the observed molecular weights, molecular weight distributions and MALDI-ToF MS results were consistent with previous observations pertaining to polymer growth and immortal ROP.

The behaviour of the *racemic* form of the catalyst, *rac*-Mg($CzOx^{iPr}$)(BH_4)(THF) (***rac*-35**) was investigated in the presence of *rac*-LA (Table 4.5, entries 7 and 8). In the absence of any additives, ***rac*-35** was found to achieve 89% monomer conversion after 24 h: a marked increase in rate when compared to enantiomerically pure catalyst. $^1H\{^1H\}$ NMR spectroscopic analysis of the polymer backbone revealed the PLA to be slightly more heterotactically enriched than that obtained from the enantiomerically pure catalysts, **(*S*,*S*)-35** and **(*R*,*R*)-35** (P_r = 0.87-0.90). Kinetic analysis also revealed an unusual third-order dependence in lactide concentration (k_{obs} = 1.67(6) M^{-2} h^{-1}, R^2 = 0.991), which has been observed previously in the polymerisation of *rac*- and *L*-LA with Ca($CzOx^{Me2}$)(BH_4)$(THF)_2$ (**13**), but not with a magnesium system (Figure 4.10; top). As the rate of the polymerisation is significantly faster with the racemic catalyst than either enantiomeric form, it is postulated that the third-order lactide dependence

arises due to a cooperative mechanism between the two enantiomeric forms of the catalyst; however, at this stage the precise mechanism surrounding the polymerisation of *rac*-LA is unclear.

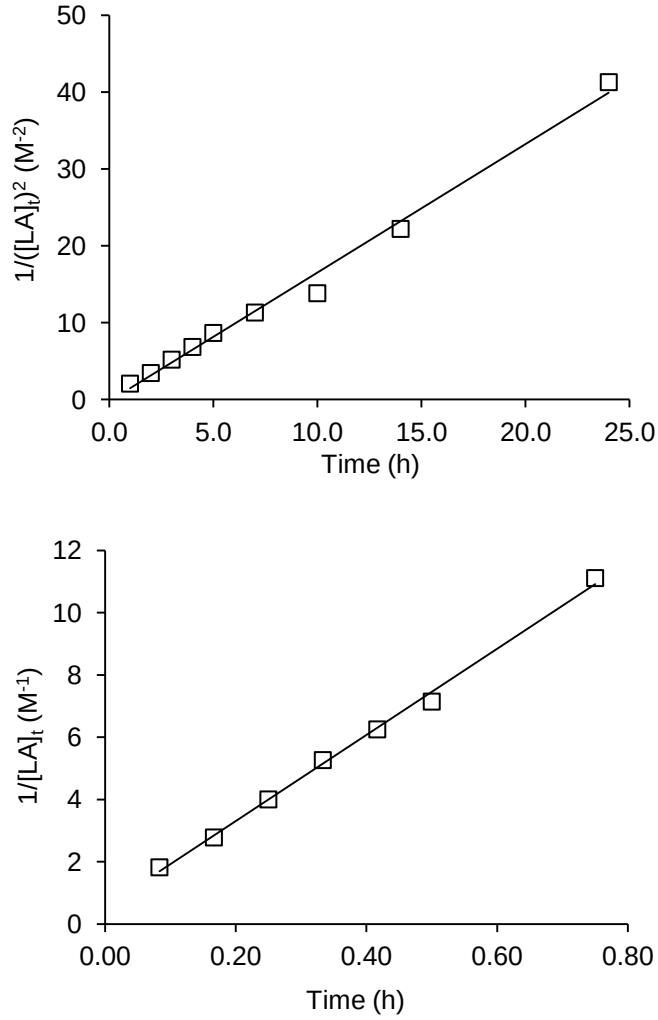


Figure 4.10. Top: data for the ROP of *rac*-LA with *rac*-Mg(CzOx$^{i\text{Pr}}$)(BH_4)(THF) (***rac*-35**); third-order plot of $1/([LA]_0)^2$ *vs.* time (k_{obs} = 1.67(6) M^{-2} h^{-1}, R^2 = 0.991). Bottom: data for the ROP of *rac*-LA with *rac*-Mg(CzOx$^{i\text{Pr}}$)(OBn) (***rac*-46**) and 1 eq. $B(OBn)_3$; second-order plot of $1/[LA]_0$ *vs.* time (k_{obs} = 13.8(3) M^{-1} h^{-1}, R^2 = 0.997).

***Rac*-35** was treated with 4.5 equivalents of benzaldehyde to generate *in situ* ***rac*-46** and one equivalent of $B(OBn)_3$, prior to treatment with 100 equivalents of *rac*-LA. ***Rac*-35** achieved 91% monomer conversion to polymer within 0.75 h: a similar timescale to the polymerisation with the enantiomerically pure catalysts. Most notably, the system observed an apparent second-order dependence in lactide concentration (k_{obs} = 13.8(3) M^{-1} h^{-1}, R^2 = 0.997), whereas neither **(*S*,*S*)-35** nor **(*R*,*R*)-**

35 could be assigned as having either a first- or second-order dependence on lactide concentration (Figure 4.10; bottom). The second-order dependency is similarly attributed to the presence of a trialkyl borate ester during polymerisation which results in the formation of complex preequilibria surrounding the ring-opening of the lactide molecule, giving rise to an observed rate which is second-order in lactide concentration. The degree of heterotactic enrichment was determined to similar to ***rac*-35**, with P_r = 0.87-0.88: higher than that obtained with the enantiomerically pure catalysts.

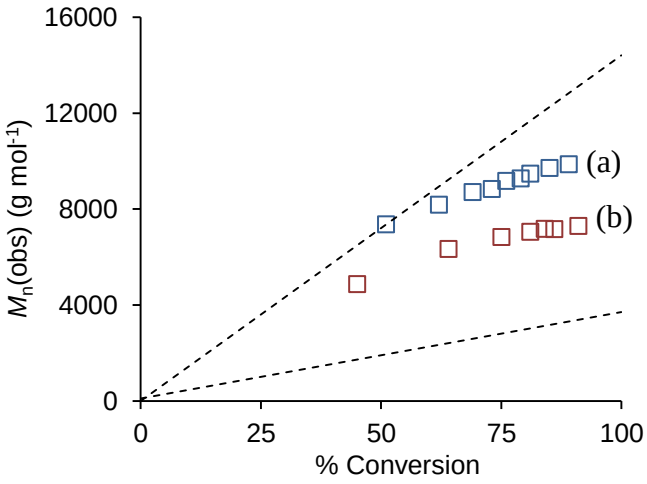


Figure 4.11. M_n(obs) (g mol^{-1}) *vs*. conversion plot for the ROP of *rac*-LA using *rac*-Mg(CzOx$^{i\text{Pr}}$)(BH$_4$)(THF) (***rac*-35**) and *rac*-Mg(CzOx$^{i\text{Pr}}$)(OBn) (***rac*-46**); the dashed lines are the M_n(calc) in each case. Conditions: 4 mL THF, 23 °C, [*rac*-LA]$_0$:[cat]$_0$:[B(OBn)$_3$]$_0$ = (a) 100:1:0; (b) 100:1:1; [*rac*-LA]$_0$ = 1.0 M. (a) ***rac*-35** with no additives, expecting 1 chain per metal centre (blue squares); (b) ***rac*-46** and 1 eq. B(OBn)$_3$, expecting 4 chains per metal centre (red squares).

For both ***rac*-35** and *in situ* generated ***rac*-46**, the molecular weight control was determined to be slightly poorer than that exerted by the enantiomerically pure forms of the catalyst (Figure 4.11). The molecular weight distributions obtained with either catalyst were marginally higher (PDI = *ca*. 1.25-1.30 for ***rac*-35**; *ca*. 1.10-1.20 for ***rac*-46** with B(OBn)$_3$); analysis with MALDI-ToF MS confirmed the presence of two distributions in each case, with peak envelopes of $\Delta m/z$ 72 g mol^{-1} between the two, which is indicative of transesterification. At this stage, it is not readily apparent why the use of the *racemic* form of the catalyst results in slightly poorer molecular weight control.

Following the results obtained with magnesium, the analogous calcium catalyst (*S*,*S*)-Ca(CzOx$^{i\text{Pr}}$)(BH$_4$) (**(*S*,*S*)-36**) was tested for its activity in the ROP of *rac*-, *L*-, *D*- and *meso*-LA; the results are summarised in Table 4.6. Upon the addition of 100 equivalents of *rac*-LA to a THF solution of **(*S*,*S*)-36**, a gel was formed almost instantaneously, which hindered sampling of the experiment (Table 4.6, entry 1). After 0.5 min, the catalyst had achieved 82% monomer conversion, which did not increase after 30 min; it is postulated that the immediate gel formation impeded adequate diffusion of the monomer, resulting in partial completion of the polymerisation. The extremely high activity observed precluded any kinetic investigations under these conditions. GPC analysis of the resultant polymer sample revealed moderate agreement with the observed and calculated molecular weights (M_n(obs) = 14,810 g mol^{-1} *cf.* M_n(calc) = 11,820 g mol^{-1}), with a broad PDI of 1.91, which suggests the rate of propagation exceeded the rate of initiation, resulting in poor molecular weight control. ^{1}H{^{1}H} NMR spectroscopy showed the polymer to have a slight heterotactic bias, with P_r = 0.61.

The addition of 4.5 equivalents of benzaldehyde to generate (*S*,*S*)-Ca(CzOx$^{i\text{Pr}}$)(OBn) (**(*S*,*S*)-48**) and 1 equivalent of B(OBn)$_3$ *in situ* prior to the addition of *rac*-LA resulted in decreased activity: the catalyst achieved 93% monomer conversion following 180 min. Kinetic analysis revealed the catalyst to observe a dependence in lactide which was intermediate between zero- and first-order, which is postulated to be a result of the presence of preequilibria surrounding the ring-opening step. Molecular weight control was found to be slightly more controlled: although M_n(obs) (6,180 g mol^{-1}) was found to be significantly higher than that expected based on M_n(calc) (3,458 g mol^{-1}), the PDI was slightly narrower over the course of the polymerisation (1.17-1.77). The higher than expected molecular weights is attributed to the faster rate of propagation versus the rate of chain transfer, resulting in the growth of fewer chains per metal centre than anticipated (Figure 4.12).

Table 4.6. Selected data for the polymerisation of *rac*-, *L*-, *D*- and *meso*-LA using (*S*,*S*)-Ca(CzOx$^{i\text{Pr}}$)(BH$_4$)(THF) (**(*S*,*S*)-36**) in THF.[a]

Entry	Catalyst	Monomer	Additive (eq.)	Conv.[b] %	Time (min)	M_n(obs)[c] (g mol^{-1})	M_n(calc)[d] (g mol^{-1})	M_w/M_n[c]	P_r[b]
1	**(*S*,*S*)-36**	*rac*	-	82	0.5	14,810	11,820	1.91	0.61
2	**(*S*,*S*)-36**	*rac*	PhCHO (4.5)	93	180	6,180	3,458	1.77	0.53-0.66
3	**(*S*,*S*)-36**	*L*	-	93	420	10,370	13,405	1.94	-
4	**(*S*,*S*)-36**	*L*	PhCHO (4.5)	92	180	6,600	3,422	1.35	-
5	**(*S*,*S*)-36**	*D*	-	92	1.5	16,330	13,261	2.23	-
6	**(*S*,*S*)-36**	*D*	PhCHO (4.5)	92	180	8,990	3,422	1.44	-
7	**(*S*,*S*)-36**	*meso*	-	91	2	12,590	13,117	1.62	0.63-0.66
8	**(*S*,*S*)-36**	*meso*	PhCHO (4.5)	92	25	6,530	3,530	1.34	0.53-0.57

[a] Conditions: [LA]$_0$:[**(*S*,*S*)-36**]$_0$ = 100:1, 4 mL THF at 23 °C. [LA]$_0$ = 1.0 M. [b] Measured by ^{1}H NMR ($CDCl_3$) analyses. [c] Molecular weights (g mol^{-1}) determined from GPC using appropriate Mark-Houwink corrections. [d] Expected average M_n (g mol^{-1}) for stated number of chains per metal and stated % conversion: M_n (calc for entries 1, 3, 5 and 7) = (conversion (%) × 100 × 144.1) + 4.0; (calc for entries 2, 4, 6 and 8) = ¼(conversion (%) × 100 × 144.1) + 108.1.

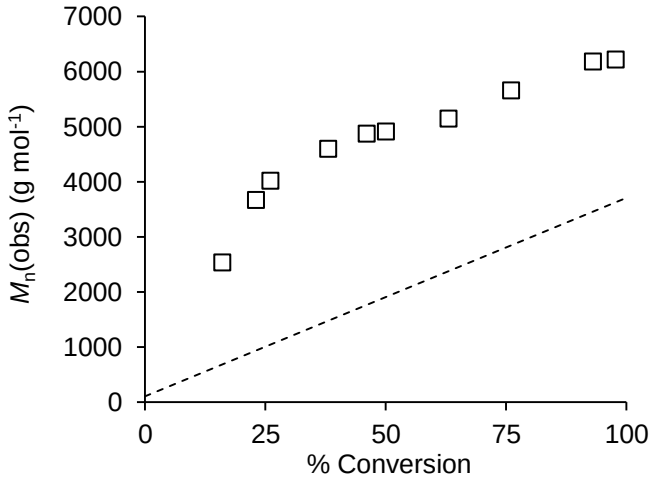


Figure 4.12. M_n(obs) (g mol^{-1}) *vs*. conversion plot for the ROP of *rac*-LA using *in situ* generated (*S*,*S*)-Ca(CzOx$^{i\text{Pr}}$)(OBn) (**(*S*,*S*)-48**) and 1 eq. B(OBn)$_3$; the dashed line represents M_n(calc), expecting 4 chains per metal centre. Conditions: 4 mL THF, 23 °C, [*rac*-LA]$_0$:[cat]$_0$:[B(OBn)$_3$]$_0$ = 100:1:1; [*rac*-LA]$_0$ = 1.0 M.

Complexes **(*S*,*S*)-36** and **(*S*,*S*)-48** were treated with *L*- and *D*-LA in order to probe the ability of the catalyst to exert enantiomorphic site control during the polymerisation (Table 4.6, entries 3-6). In the absence of any additives, **(*S*,*S*)-36** achieved 48% conversion *L*-LA to PLLA after 5 min and 93% conversion after 420 min, considerably slower than the ROP of *rac*-LA. Unfortunately, an investigation into the kinetic regime did not allow for any unambiguous classification of the dependence on lactide concentration. The first half-life of monomer consumption occurred following ~5 min; however, the second half-life was not achieved until ~240 min had elapsed. It is possible that after achieving 48% conversion, decomposition of the catalyst occurred, after which point remaining decomposition products which were active for the ROP of *L*-LA continued consuming the unreacted monomer until 93% conversion to PLLA was achieved after 420 min. GPC analysis of the polymer provides little insight: the growth appears to be non-linear with observed molecular weights generally lower than the molecular weights calculated assuming one chain per metal centre. Moreover, the PDIs are very broad, ranging from ~1.9 to 2.7. Analysis using MALDI-ToF MS following 15 min confirms the presence of two PLA distributions with a peak envelopes between the major and minor distribution of $\Delta m/z$ 72 g mol^{-1}, confirming the occurrence of transesterification. Both peak distributions indicated the polymer chains were terminated with the expected α,ω-dihydroxytelechelic and LA-H

end-groups; however, no polymer chains corresponding to an alternative end-group are observed. At this stage, the precise nature of any decomposition products which may be responsible for this decrease in rate remains unknown.

The polymerisation of *D*-LA with **(*S*,*S*)-36** proved more straightforward: 92% monomer conversion was achieved following 1.5 min, with almost immediate gel formation, indicating that the catalyst's activity towards the ROP of *D*-LA is higher than that for the ROP of *L*-LA. As previously observed in the magnesium analogue, the rate of polymerisation of *D*-LA to form purely isotactic PDLA remains slightly slower than the rate of polymerisation of *rac*-LA to form PLA with a heterotactic bias, which confirms that enchainment *via racemic* dyads is preferable to *meso* dyads. As the catalyst's activity towards the ROP of *D*-LA was extremely high, no kinetic information could be obtained under these conditions. The observed molecular weights were higher than expected assuming the growth of 1 chain per metal centre, indicating that the rate of propagation was higher than the rate of initiation. It is interesting to note that **(*S*,*S*)-36** displays a clear monomer preference in the absence of any additives, whereas **(*S*,*S*)-35** and **(*R*,*R*)-35** do not.

Conversely, the polymerisation of *L*- and *D*-LA with **(*S*,*S*)-48** and $B(OBn)_3$ were found to reach very similar degrees of monomer conversion within the same time period as the polymerisation of *rac*-LA (Table 4.6, entries 4 and 6). The catalyst achieved 92% monomer conversion within 180 min in the ROP of *L*- and *D*-LA, which is comparable to the achievement of 93% monomer conversion following 180 min in the ROP of *rac*-LA. Unfortunately, following kinetic analysis of the polymerisation of *L*-LA, the order in lactide could not be assigned clearly as either zero- or first-order; however, the polymerisation of *D*-LA was found to observe two distinct kinetic regimes during the polymerisation. The polymerisation maintained a first-order dependence in lactide concentration (k_{obs} = 1.48(6) h^{-1}, R^2 = 0.997); however after *ca*. 50% conversion, a notable decrease in rate was observed (k_{obs} = 0.66(1) h^{-1}, R^2 = 0.998). The origin of this shift in kinetic regime remains unclear at this stage. Although similar % conversions are achieved with **(*S*,*S*)-48** and $B(OBn)_3$ following the ROP of *rac*-, *L*- and *D*-LA after 180 min, more monomer is consumed within 30 min when **(*S*,*S*)-48** and $B(OBn)_3$ is treated with *D*-LA, than with *rac*- or *L*-LA. After 30 min, the complex achieves 57% conversion of *D*-LA into PDLA,

whereas only 33% *L*-LA is converted to PLLA and 38% *rac*-LA is converted to PLA, suggestive of a slight monomer preference in favour of *D*-LA. Similarly, despite the slight monomer preference during the polymerisation of the enantiomerically pure monomer feedstocks, the ROP of *rac*-LA results in the formation of heterotactically enriched PLA due to the comparative favourability of enchainment proceeding *via racemic* dyads.

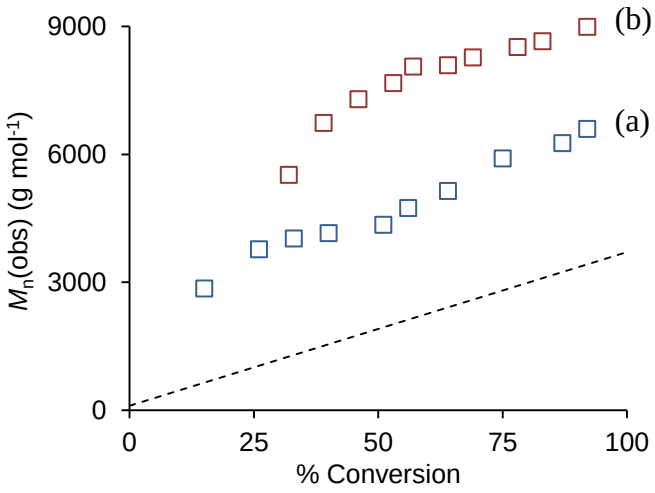


Figure 4.13. M_n(obs) (g mol^{-1}) *vs*. % conversion plot for the ROP of *L*- and *D*-LA using *in situ* generated (*S*,*S*)-Ca(CzOx$^{i\text{Pr}}$)(OBn) (**(*S*,*S*)-48**) and 1 eq. B(OBn)$_3$; the dashed line represents M_n(calc), expecting 4 chains per metal centre. Conditions: 4 mL THF, 23 °C, [LA]$_0$:[cat]$_0$:[B(OBn)$_3$]$_0$ = 100:1:1; [LA]$_0$ = 1.0 M. (a) *L*-LA (blue squares); (b) *D*-LA (red squares).

The observed molecular weights obtained from the polymerisation of *L*-LA were in closer agreement with those calculated for 4 polymer chains per metal centre than from the polymerisation of *D*-LA (Figure 4.13). At 92% conversion, M_n(obs) = 6,600 g mol^{-1} (M_n(calc) = 3,422g mol^{-1}) in the ROP of *L*-LA, whereas in the ROP of *D*-LA, M_n(obs) = 8,990 g mol^{-1} (M_n(calc) = 3,422g mol^{-1}), indicating that the rate of chain transfer is influenced by the stereochemistry of the growing polymer chain. The narrower molecular weight distribution of the resultant PLLA compared to the PDLA obtained confirms the greater efficiency of chain transfer during polymerisation (PDI = 1.35 *cf*. 1.44).

(*S*,*S*)-36 was found to be extremely active for the ROP of *meso*-LA, achieving 91% conversion following 2 min; in this instance no gel formation was observed, which

may have aided a homogeneous dispersion of monomer throughout the solution allowing a higher monomer conversion to be reached. Unfortunately, the polymerisation was too active to allow for kinetic analysis. Inspection of the observed molecular weights revealed the molecular weight increased rapidly at 65% conversion to 11,950 g mol^{-1} (M_n(calc) = 9,371 g mol^{-1}); however at 91% conversion, M_n(obs) was in close agreement with M_n(calc). This is attributed to a high incidence of transesterification resulting in a moderate molecular weight distribution (PDI = 1.62), which is confirmed by peak envelopes of $\Delta m/z$ 72 g mol^{-1} in the MALDI-ToF MS. On addition of 4.5 equivalents of benzaldehyde to generate *in situ* **(*S*,*S*)-48** and $B(OBn)_3$, the activity towards the ROP of *meso*-LA decreased such that 92% monomer conversion was achieved following 25 min. As with previously studied calcium catalysts within this series, this is attributed to the increased propensity for the borate ester to coordinate to the metal centre, resulting in a decrease in activity. The molecular weight control was found to be in line with previous observations for the ROP of other lactide monomers with **(*S*,*S*)-48**: the growth of the molecular weight followed a linear trend, but M_n(obs) was consistently higher than M_n(calc) throughout the run. The deviation from linearity in the latter stages of the polymerisation is attributed to the deleterious effects of transesterification resulting in broadening of the PDI (1.15-1.34). With both catalysts, the degree of syndiotactic enrichment was moderate, with slightly more stereocontrol offered with **(*S*,*S*)-36** instead of **(*S*,*S*)-48** (P_r = 0.63-0.66 *cf*. 0.53-0.57).

4.6.2 Polymerisation studies: ROP of *rac*-, *L*-, *D*- and *meso*-LA with Group 3 and lanthanide catalysts

Preliminary investigations into the behaviour of (*S*,*S*)-Y(CzOx$^{i\text{Pr}}$)$(BH_4)_2$(THF) (**(*S*,*S*)-43**) during the ROP of *rac*-, *L*- and *meso*-LA were conducted by L. Budden under the author's direct supervision (Table 4.7, entries 1, 2 and 4). **(*S*,*S*)-43** was treated with 100 equivalents of *rac*-LA and achieved 94% monomer conversion following 180 min. Unlike the ROP of *rac*-LA with its achiral counterpart **16**, **(*S*,*S*)-43** did not exhibit an induction period prior to polymerisation. Similarly to **16** in which the reaction was determined to be first-order in lactide concentration, (k_{obs} = 3.6(2) h^{-1}, R^2 = 0.991), **(*S*,*S*)-43** also observed a first-order dependence in lactide concentration; however, k_{obs} was significantly reduced at 1.01(3) h^{-1} (R^2 = 0.994).

Table 4.7. Selected data for the polymerisation of *rac*-, *L*-, *D*- and *meso*-LA using (*S*,*S*)-Y(CzOx$^{i\text{Pr}}$)(BH$_4$)$_2$(THF) (**(*S*,*S*)-43**), (*S*,*S*)-La(CzOx$^{i\text{Pr}}$)(BH$_4$)$_2$ (**(*S*,*S*)-44**) and (*S*,*S*)-Sm(CzOx$^{i\text{Pr}}$)(BH$_4$)$_2$ (**(*S*,*S*)-45**) in THF.[a]

Entry	Catalyst	Monomer	Additive (eq.)	Conv.[b] %	Time (min)	M_n(obs)[c] (g mol^{-1})	M_n(calc)[d] (g mol^{-1})	M_w/M_n[c]	P_r[b]
1	**(*S*,*S*)-43**[e]	*rac*	-	94	180	5,280	6,777	1.36	0.64-0.69
2	**(*S*,*S*)-43**[e]	*L*	-	92	45	7,030	6,634	1.42	-
3	**(*S*,*S*)-43**	*D*	-	93	90	8,040	6,705	1.43	-
4	**(*S*,*S*)-43**[e]	*meso*	-	92	135	5,550	6,634	1.44	0.40
5	**(*S*,*S*)-43**[e]	*rac*	PhCHO (10)	93	2	3,970	1,783	1.21	0.70-0.72
6	**(*S*,*S*)-44**	*rac*	-	90	120	7,110	6,489	1.59	0.55-0.58
7	**(*S*,*S*)-44**	*rac*	PhCHO (10)	91	10	4,730	1,747	1.46	0.55-0.58
8	**(*S*,*S*)-45**	*rac*	-	92	300	5,160	6,633	1.37	0.59-0.62
9	**(*S*,*S*)-45**	*rac*	PhCHO (10)	93	10	3,730	1,783	1.27	0.67-0.73

[a] Conditions: [LA]$_0$:[initiator]$_0$ = 100:1, 4 mL THF at 23 °C. [LA]$_0$ = 1.0 M. [b] Measured by ^{1}H NMR (CDCl$_3$) analyses. [c] Molecular weights (g mol^{-1}) determined from GPC using appropriate Mark-Houwink corrections. [d] Expected average M_n (g mol^{-1}) for stated number of chains per metal and stated % conversion: M_n (calc for entries 1-4, 6 and 8) = ½(conversion (%) × 100 × 144.1) + 4.0; (calc for entries 5, 7 and 9) = 1/8(conversion (%) × 100 × 144.1) + 108.1. [e] Performed by L. Budden.

The decrease in k_{obs} on employment of **(*S*,*S*)-43** is attributed to stronger chelation of the growing polymeryl chain caused by the reduced steric hindrance around the metal centre which reduces the activity. The chirality of **(*S*,*S*)-43** resulted in reduced heterotactic enrichment (P_r = 0.64-0.69), which may be a caused by an increase in enantiomorphic site control resulting in an increase in propensity for the formation of *meso* dyads and a resultant decrease in P_r. The increasing dominance of enantiomorphic site control is apparent from the reduced degree of heterotacticity from the PLA produced with **(*S*,*S*)-43** and *rac*-LA in comparison to that produced with **16**; however, it appears that it is not significant enough to result in the formation of isotactic PLA.

To investigate the origin of this decrease in P_r **(*S*,*S*)-43** was treated with 100 equivalents of *L*- and *D*-LA (Table 4.7, entries 2 and 3). Both experiments revealed a first-order dependence in lactide concentration: following an induction period of ~15 min during the ROP of *L*-LA, k_{obs} = 5.4(2) h^{-1} (R^2 = 0.995), and for the ROP of *D*-LA, k_{obs} = 1.84(3) h^{-1} (R^2 = 0.999) ($k_L/k_D \approx 3$). **(*S*,*S*)-43** exhibits a clear monomer preference in which *L*-LA polymerises more rapidly forming PLLA than *D*-LA polymerises to form PDLA, indicating that enchainment *via SS meso* dyads is preferential to enchainment *via RR meso* dyads. This is contrary to the results obtained with alkaline earth complexes such as **(*S*,*S*)-35** and **(*S*,*S*)-36**, in which the preferred monomer is *D*-LA indicating enchainment *via RR meso* dyads is more favourable. Interestingly, the observed rates for the ROP of either *D*- or *L*-LA are both faster than the k_{obs} for the ROP of *rac*-LA, despite the resultant polymer being heterotactically enriched. Previous reports by Mehrkhodavandi *et al.* have demonstrated the possibility of synthesising atactic PLA from enantiopure catalysts in which k_{obs} for the polymerisation of *rac*-LA is greater than k_{obs} for *D*-LA, but less than k_{obs} for *L*-LA;[44] however, in this instance, heterotactically enriched PLA is obtained from an enantiopure catalyst in which the k_{obs} for the polymerisation of either enantiopure *D*- or *L*-LA both exceed the k_{obs} for the polymerisation of *rac*-LA. In previous investigations into the monomer preference of other chiral catalysts including **(*S*,*S*)-** and **(*R*,*R*)-35** and **(*S*,*S*)-36**, both the rates of polymerisation of *D*- and *L*-LA to form isotactic PDLA and PLLA, respectively, have been slower than the rate of polymerisation of *rac*-LA, which is consistent with the formation of heterotactically enriched PLA. Although the rates of polymerisation of *D*- and *L*-LA

are both faster than the rate of polymerisation of *rac*-LA with **(*S*,*S*)-43**, they remain comparable, thus the k_D/k_L ratio may not be large enough in this instance to affect a monomer preference during the ROP of *rac*-LA to result in any isoselectivity. Moreover, although the polymerisation of an enantiomerically pure lactide feedstock is more rapid than the polymerisation of *rac*-LA, the propagating mechanism in the presence of both enantiomers may alter due to competing coordination of either monomer, which may result in *racemic* enchainment becoming more favourable.[44]

When treated with 100 equivalents of *meso*-LA, **(*S*,*S*)-43** achieved 92% conversion after 135 min (Table 4.7, entry 4). Kinetic analysis showed the reaction had neither a first- nor second-order dependence in lactide concentration; however, the polymerisation proceeded more rapidly than the corresponding polymerisation of *rac*-LA, as anticipated. Despite the increased rate of polymerisation in comparison to that of *rac*-LA, the rate was still slightly slower than that of either *D*- or *L*-LA. Furthermore, $^1H\{^1H\}$ NMR spectroscopy showed the resultant polymer to be slightly heterotactically enriched (P_r = 0.40), which may be indicative of the emerging dominance of enantiomorphic site control as opposed to chain end control. During the polymerisation of *meso*-LA, enchainment occurs preferentially *via meso* dyads, as opposed to *racemic* dyads. Although the polymerisation of *rac*-LA with **(*S*,*S*)-43** proceeds *via* chain end control, the polymerisation of *meso*-LA proceeds via enantiomorphic site control; the difference in polymerisation mechanisms for each polymerisation is tentatively assigned to the different enantiomeric forms of the monomer, which may affect the stability of the propagating species and therefore impacting on the relative rates of enchainment *via racemic* and *meso* dyads.

The observed molecular weights for the ROP of *rac*-, *L*-, *D*- and *meso*-LA with **(*S*,*S*)-43** were found to agree closely with the calculated molecular weights, in all cases corresponding to the propagation of approximately 2 polymer chains per metal centre. The observed molecular weights for the ROP of *rac*- and *meso*-LA were found to agree closely with those calculated, until ~50-75% monomer conversion, after which point the deleterious effects of transesterification became apparent, resulting in lower than expected molecular weights (Figure 4.14). In all instances, the polymer obtained had a similar molecular weight distribution, with PDI ≈ 1.35-1.45. Analysis with MALDI-ToF MS showed peak envelopes of $\Delta m/z$ 72 g mol^{-1}, confirming the presence

of transesterification. Furthermore, peaks at 1481-1482 g mol^{-1} and 1484 g mol^{-1} corresponded to the anticipated end-groups at the non-hydroxy polymer chain end of LA-H (calculated value 1481 g mol^{-1}) and C(H)MeCH$_2$OH (calculated value 1483 g mol^{-1}), respectively.

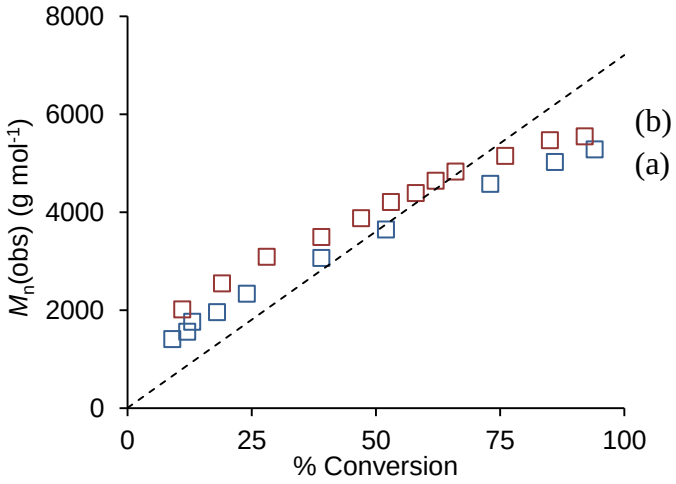


Figure 4.14. M_n(obs) (g mol^{-1}) *vs*. % conversion plot for the ROP of (a) *rac*-LA (blue squares) and (b) *meso*-LA (red squares) using (*S*,*S*)-Y(CzOx$^{i\text{Pr}}$)(BH$_4$)$_2$(THF) (**(*S*,*S*)-43**); the dashed line is M_n(calc) expecting 2 chains per metal centre. Conditions: 4 mL THF, 23 °C, [LA]$_0$:[cat]$_0$ = 100:1; [LA]$_0$ = 1.0 M.

The addition of 10 equivalents of benzaldehyde to **(*S*,*S*)-43** to generate *in situ* **(*S*,*S*)-50** and 2 equivalents of B(OBn)$_3$ resulted in an increase in rate observed during the ROP of *rac*-LA. **(*S*,*S*)-50** and 2 equivalents of B(OBn)$_3$ were highly active for the ROP of *rac*-LA, achieving 93% monomer conversion within 2 min (Table 4.7, entry 5). The polymerisation followed a first-order dependence in lactide concentration, with k_{obs} = 68(4) h^{-1} (R^2 = 0.994). This is considerably more rapid than the ROP of *rac*-LA with **(*S*,*S*)-43** in the absence of benzaldehyde to generate the corresponding alkoxide. This is attributed to incomplete transformation of complex **(*S*,*S*)-43** to a catalytically active species following the addition of lactide, resulting in a decrease in k_{obs} in a similar manner to **16** as discussed in Chapter 3. A similar degree of heterotactic enrichment was observed on addition of the benzaldehyde, with P_r = 0.70-0.72. This was slightly lower than the corresponding polymerisation of *rac*-LA with the achiral analogue, **24**, and 2 equivalents of B(OBn)$_3$ (P_r = 0.79-0.83). This is similarly attributed to the increasing prominence of enantiomorphic site control, resulting in an increased favourability of enchainment occurring *via meso* dyads and

therefore a decrease in the degree of heterotactic enrichment observed, as for the ROP of *rac*-LA with **(*S*,*S*)-43** in the absence of any additives. The molecular weight control was moderate, with M_n(obs) = 3,970 g mol^{-1} at 93% monomer conversion (M_n(calc) = 1,783 g mol^{-1}); however, gratifyingly, the molecular weight distribution was narrower, with PDI ≈ 1.20 throughout the polymerisation. Analysis with MALDI-ToF MS confirmed initiation proceeded *via* insertion of the lactide monomer into the Y–OBn bond, as the polymer chains were found to be terminated with an OBn end-group at the non-hydroxy chain end: a peak at 1587 g mol^{-1} corresponded to the fragment [HO-[LA]$_{10}$-OBn + K]$^+$ (calculated value = 1587 g mol^{-1}). Furthermore, the was minimal evidence of transesterification, with the presence of a secondary minor distribution with peak envelopes at 72 g mol^{-1}, which supports the narrow molecular weight distribution observed.

Following the results obtained with **(*S*,*S*)-43**, (*S*,*S*)-La(CzOx$^{i\text{Pr}}$)(BH$_4$)$_2$ (**(*S*,*S*)-44**) and (*S*,*S*)-Sm(CzOx$^{i\text{Pr}}$)(BH$_4$)$_2$ (**(*S*,*S*)-45**) were treated with 100 equivalents of *rac*-LA (Table 4.7, entries 6 and 8). **(*S*,*S*)-44** was found to be more active than **(*S*,*S*)-43**, achieving 90% monomer conversion following 120 min and observing a first-order dependence in lactide concentration (k_{obs} = 1.45(4) h^{-1}, R^2 = 0.995). However, despite having a larger ionic radius, **(*S*,*S*)-45** was found to be slightly less active than **(*S*,*S*)-43**, achieving 92% conversion following 300 min. Kinetic analysis revealed **(*S*,*S*)-45** also observed a first-order dependence in lactide concentration, with k_{obs} = 0.53(1) h^{-1} (R^2 = 0.997) (Figure 4.16; top). Both **(*S*,*S*)-44** and **(*S*,*S*)-45** produced polymer with good molecular weight control, with M_n(obs) in close agreement to the calculated molecular weights for the growth of two chains per metal centre (Figure 4.16; bottom). The polydispersities obtained were moderate, with the occurrence of transesterification confirmed through analysis of the PLA with MALDI-ToF MS.

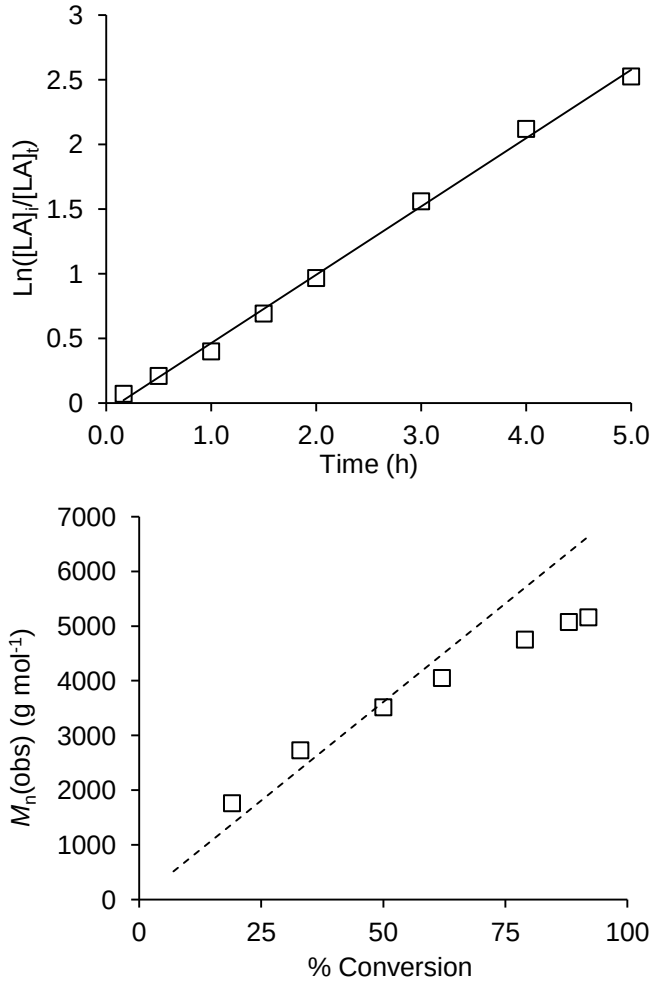


Figure 4.16. Top: data for the ROP of *rac*-LA with (*S*,*S*)-Sm(CzOx$^{i\text{Pr}}$)(BH$_4$)$_2$ (**(*S*,*S*)-45**); semi-logarithmic first-order plot of ln([LA]$_i$/[LA]$_t$) *vs*. time (k_{obs} = 0.53(1) h^{-1}, R^2 = 0.997). Bottom: M_n(obs) (g mol^{-1}) *vs*. % conversion plot for the ROP of *rac*-LA using (*S*,*S*)-Sm(CzOx$^{i\text{Pr}}$)(BH$_4$)$_2$ (**(*S*,*S*)-45**); the dashed line is M_n(calc) expecting 2 chains per metal centre. Conditions: 4 mL THF, 23 °C, [*rac*-LA]$_0$:[cat]$_0$ = 100:1; [*rac*-LA]$_0$ = 1.0 M.

The addition of 10 equivalents of benzaldehyde to generate (*S*,*S*)-La(CzOx^{Me_2})(OBn)$_2$ (**(*S*,*S*)-53**) and (*S*,*S*)-Sm(CzOx$^{i\text{Pr}}$)(OBn)$_2$ (**(*S*,*S*)-56**) and 2 equivalents of B(OBn)$_3$ resulted in an increase in the rate of reaction, with both catalysts achieving >90% conversion after 10 min (Table 4.7, entries 7 and 9). **(*S*,*S*)-53** and 2 equivalents of B(OBn)$_3$ achieved 91% conversion after 10 min, and kinetic analysis revealed the reaction to observe a second-order dependence in lactide concentration (k_{obs} = 59(2) M^{-1} h^{-1}, R^2 = 0.993). Similarly, **(*S*,*S*)-56** and 2 equivalents of B(OBn)$_3$ achieved 93% conversion after 10 min, with a second-order dependency in lactide concentration also

observed (k_{obs} = 82(1) M^{-1} h^{-1}, R^2 = 0.997, Figure 4.16). The distinct shift in kinetic regime observed is reminiscent of previous studies in which $B(OBn)_3$ is generated *in situ*, resulting in a second-order dependency in lactide concentration. Although the precise mechanism which results in a second-order dependency is still unknown, it is postulated that the borate ester has a role in effecting this shift.

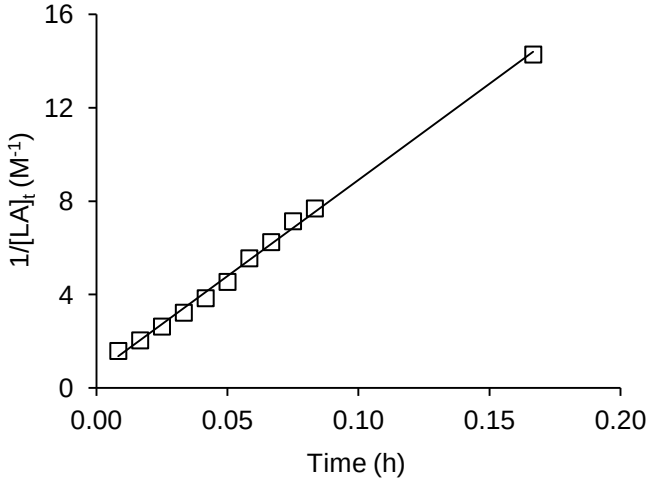


Figure 4.16. Data for the ROP of *rac*-LA with (*S*,*S*)-Sm(CzOx^{iPr})$(OBn)_2$ (**(*S*,*S*)-56**) and 2 eq. of $B(OBn)_3$; second-order plot of $1/[LA]_0$ *vs*. time (k_{obs} = 82(1) M^{-1} h^{-1}, R^2 = 0.997).

Whilst the observed molecular weights confirmed the immortal nature of the polymerisation with **(*S*,*S*)-53** and **(*S*,*S*)-56**, and 2 equivalents of $B(OBn)_3$, they were consistently higher than expected for the growth of 8 polymer chains per metal centre. The molecular weights grew linearly with conversion, and those obtained with **(*S*,*S*)-56** were found to be closer to the calculated molecular weights than with **(*S*,*S*)-53**, which is possibly due to the poorer control offered with a more reactive metal centre. However, the polydispersities were found to be slightly narrower when employing $B(OBn)_3$ as a CTA in comparison to the borohydride complexes. Analysis of the polymer chains with MALDI-ToF MS revealed the polymer chains to be terminated with OBn end-groups, as anticipated (Figure 4.17). In general, the PLA obtained from both **(*S*,*S*)-44** and **(*S*,*S*)-45** in the presence and absence of benzaldehyde was moderately heterotactically enriched ($P_r \approx$ 0.55-0.70): considerably lower than the heterotacticities reported with Sm(CzOx^{Me2})$(BH_4)_2$(THF) (**18**).

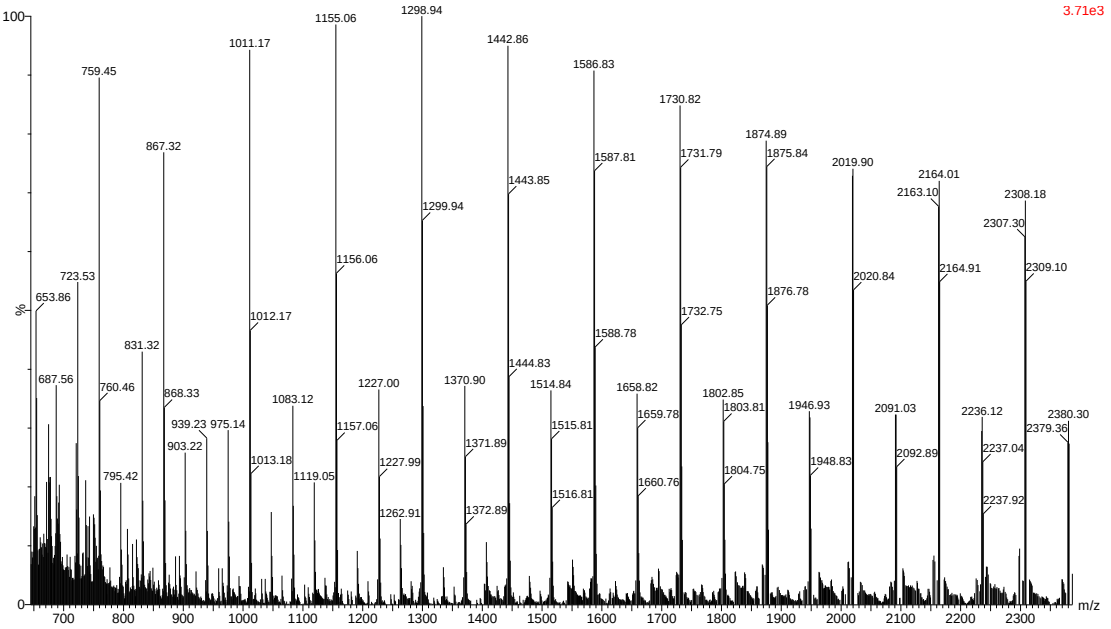


Figure 4.17. MALDI-ToF MS (GPC analysis: M_n(obs) = 3,080 g mol^{-1}) of PLA obtained from (*S*,*S*)-Sm(CzOx$^{i\text{Pr}}$)(OBn)$_2$ (**(*S*,*S*)-56**) and 2 eq. of B(OBn)$_3$.

4.7 Summary and conclusions

This Chapter has described the synthesis and characterisation of a series of CzOx$^{i\text{Pr}}$ -supported lithium, potassium, magnesium, calcium, strontium, yttrium, lanthanum and samarium complexes, complexes **(*S*,*S*)-33**-**44** and **(*R*,*R*)-34**-**35** their application as catalysts for the ROP of *rac*-, *L*-, *D*- and *meso*-lactide. Complexes **(*S*,*S*)-33**, **(*S*,*S*)-** and **(*R*,*R*)-34**, **(*S*,*S*)-37** and **(*S*,*S*)-38** were prepared in a good yield through protonolysis reactions between (*S*,*S*)- or (*R*,*R*)-HCzOx$^{i\text{Pr}}$ (**(*S*,*S*)-** or **(*R*,*R*)-1.46**) and the appropriate metal precursor; however, complexes **(*S*,*S*)-37** and **(*S*,*S*)-38** could not be isolated in high purity from the residual HN(SiMe$_3$)$_2$ contaminant due to high solubility of both complexes. Attempts to synthesise (*S*,*S*)-Mg(CzOx$^{i\text{Pr}}$)(OBn) or (*S*,*S*)-Ca(CzOx$^{i\text{Pr}}$)(OBn) in sufficient yield and purity for onwards polymerisation investigations were unsuccessful: although the complexes were successfully made following treatment of either **(*S*,*S*)-37** or **(*S*,*S*)-38** with benzyl alcohol, the complexes were obtained in extremely low yields of 5-10%. Homoleptic complexes **(*S*,*S*)-40** and **(*S*,*S*)-41** were readily accessed through the protonolysis of 2 equivalents of **(*S*,*S*)-1.46** and the appropriate metal precursor under mild conditions in moderate to good yields. Attempts to synthesise (*S*,*S*)-Mg(CzOx$^{i\text{Pr}}$)(Bu) were unsuccessful even under kinetic control and resulted in formation of the homoleptic complex **(*S*,*S*)-40**.

Complexes **(*S*,*S*)-** and **(*R*,*R*)-35**, **(*S*,*S*)-** and **(*R*,*R*)-36**, **(*S*,*S*)-39**, **(*S*,*S*)-43**, **(*S*,*S*)-44** and **(*S*,*S*)-45** were prepared through the salt metathesis of (*S*,*S*)- or (*R*,*R*)-K(CzOx$^{i\text{Pr}}$) (**(*S*,*S*)-** or **(*R*,*R*)-34**) and the appropriate metal precursor. The heteroleptic complex (*S*,*S*)-Sr(CzOx$^{i\text{Pr}}$)(BH$_4$) could not be obtained following treatment of **(*S*,*S*)-34** with Sr(BH$_4$)$_2$(THF)$_2$, instead resulting in the formation of the homoleptic complex **(*S*,*S*)-42**, which was independently synthesised from the reaction of **(*S*,*S*)-34** with Sr(BH$_4$)$_2$(THF)$_2$.

Complexes **(*S*,*S*)-** and **(*R*,*R*)-35**, **(*S*,*S*)-** and **(*R*,*R*)-36**, **(*S*,*S*)-44** and **(*S*,*S*)-45** were examined by IR spectroscopy in the solid state and in THF solution. In solid state, **(*S*,*S*)-35** revealed a highly unusual bonding mode which corresponded to either a polymeric configuration or indicated the presence of multiple bonding modes in the solid state, as observed with previously studied Group 2 borohydride complexes supported by the CzOx^{Me2} ligand. However, **(*R*,*R*)-35** revealed a κ^3-bound BH$_4$ ligand, although the difference observed in the IR spectra between the two enantiomers is not readily apparent at this stage. **(*S*,*S*)-** and **(*R*,*R*)-36** could not be resolved as either bidentate, or tridentate, which suggests the occupation of multiple bonding modes in the solid state. In THF solution, **(*S*,*S*)-** and **(*R*,*R*)-35** and **(*S*,*S*)-** and **(*R*,*R*)-36** occupied a tridentate borohydride configuration. The Group 3 and lanthanide analogues **(*S*,*S*)-43**, **(*S*,*S*)-44** and **(*S*,*S*)-45** were clearly identifiable tridentate in the solid state and in THF solution. The addition of benzaldehyde to complexes **(*S*,*S*)-35**, **(*S*,*S*)-36**, **(*S*,*S*)-44** and **(*S*,*S*)-45** resulted in the *in situ* transformation from the borohydride to the corresponding alkoxide with concurrent evolution of B(OBn)$_3$, which was confirmed using ^{1}H and ^{11}B NMR spectroscopy.

The ROP of *rac*-LA with **(*S*,*S*)-** and **(*R*,*R*)-35** did not result in an increase in isotactic enrichment compared to the achiral analogue **7** and were considerably less active, which may be a result of stronger chelation of the propagating lactide chain to the metal. The addition of benzaldehyde to either **(*S*,*S*)-** and **(*R*,*R*)-35** resulted in an increase in the rate of polymerisation, which is tentatively attributed to the circumvention of the formation of catalytically inactive species associated with the borohydride initiation mechanism as the starting borohydride is fully consumed prior to polymerisation. The addition of a further 1 equivalent of B(OBn)$_3$ to *in situ* generated **(*S*,*S*)-46** and B(OBn)$_3$ resulted in a decrease in the rate of polymerisation of

rac-LA, indicating that a tetracoordinated borate adduct is not the active species. The ROP of *meso*-LA with **(*S*,*S*)-35** both in the presence and absence of benzaldehyde was comparatively more rapid than for *rac*-LA; however, similar syndiotacticities to those obtained with **7** were observed. Neither **(*S*,*S*)-** nor **(*R*,*R*)-35** exhibited any preference for the ROP of either *D*- or *L*-LA in the absence of any additives. The ROP of *D*-LA with *in situ* generated **(*S*,*S*)-46** was considerably more rapid than the ROP of *L*-LA and a complementary preference for the ROP of *L*-LA with **(*R*,*R*)-46** was also observed, although the rate of polymerisation of *rac*-LA with both **(*S*,*S*)-** and **(*R*,*R*)-46** remained faster. Despite a demonstrable monomer preference is observed, this does not result in the formation of isotactic PLA from *rac*-LA, or heterotactic PLA from *meso*-LA, as enchainment preferentially occurs *via racemic* dyads. ***rac*-35** and ***rac*-46** generated in situ were more active for the ROP of *rac*-LA and afforded PLA with similar heterotactic enrichment to the enantiopure catalysts. In the absence of benzaldehyde, complexes **(*S*,*S*)-, (*R*,*R*)-** and ***rac*-35** produced polymer with low molecular weights and narrower polydispersities, which is ascribed to the formation of a trialkyl borate ester species, for instance $B(LA\text{-}H)_3$ during the borohydride initiation process, which acts as a chain transfer agent.

Although extremely active, the ROP of *rac*-LA and *D*-LA with **(*S*,*S*)-36** was poorly controlled, resulting in gel formation and broad polydispersities observed. Unlike the magnesium analogue, in the absence of benzaldehyde **(*S*,*S*)-36** exhibited a monomer preference, as the ROP of *L*-LA was considerably slower, but did not offer improved control. Despite this observed monomer preference, slightly heterotactically enriched PLA was obtained from the ROP of *rac*-LA, which is attributed to preferential enchainment *via racemic* dyads. The addition of benzaldehyde resulted in a decrease in rate for the ROP of *rac*- and *D*-LA, and an increased rate of the ROP of *L*-LA. A similar degree of monomer conversion was achieved in all cases after 3 h, indicating no monomer preference under these conditions. The ROP of *meso*-LA with **(*S*,*S*)-36** in the presence and absence of benzaldehyde resulted in the formation of slightly syndiotactically enriched PLA, which confirms the preference for the catalyst to propagate *via racemic* dyads.

The ROP of *rac*-LA with **(*S*,*S*)-43** was moderately active, although the heteroselectivity of the catalyst was lower in comparison to its achiral counterpart, **16**,

suggesting the enantiomorphic site control mechanism became more dominant, resulting in a decrease in P_r. The complex displayed a monomer preference in favour of *L*-LA during the ROP of either pure *D*- or *L*-LA, with $k_L/k_D \approx 3$; although the k_{obs} for the ROP of both *D*- or *L*-LA were slightly higher than that observed for *rac*-LA, the preference for enchainment via racemic dyads was more favourable when the complex was treated with both enantiomeric forms of the monomer. The ROP of *meso*-LA with **(*S*,*S*)-43** afforded slightly heterotactically enriched PLA, which is attributed to the dominance of the enantiomorphic site control mechanism in which enchainment occurs *via* meso dyads. The alternative mechanism observed may be a result of a difference in stability of the monomer feedstock, although at this stage the precise reason for this observation remains unclear. The addition of benzaldehyde to generate **(*S*,*S*)-50** and 2 equivalents of $B(OBn)_3$ *in situ* resulted in a similar degree of heteroselectivity observed as **(*S*,*S*)-43** in the absence of any additives. The ROP of *rac*-LA with **(*S*,*S*)-44** and **(*S*,*S*)-45** both in the absence and presence of benzaldehyde resulted in moderate degrees of molecular weight control and afforded moderately heterotactically enriched PLA ($P_r \approx 0.55 – 0.70$).

4.8 References for Chapter Four

1. N. Spassky, M. Wisniewski, C. Pluta and A. Le Borgne, *Macromol. Chem. Phys.*, 1996, **197**, 2627-2637.
2. T. M. Ovitt and G. W. Coates, *J. Polym. Sci., Part A: Polym. Chem.*, 2000, **38**, 4686-4692.
3. T. M. Ovitt and G. W. Coates, *J. Am. Chem. Soc.*, 2002, **124**, 1316-1326.
4. C. P. Radano, G. L. Baker and M. R. Smith, *J. Am. Chem. Soc.*, 2000, **122**, 1552-1553.
5. Z. Zhong, P. J. Dijkstra and J. Feijen, *Angew. Chem. Int. Ed.*, 2002, **41**, 4510-4513.
6. Z. Zhong, P. J. Dijkstra and J. Feijen, *J. Am. Chem. Soc.*, 2003, **125**, 11291-11298.
7. M. H. Chisholm, N. J. Patmore and Z. Zhou, *Chem. Commun.*, 2005, 127-129.
8. M. H. Chisholm, J. C. Gallucci, K. T. Quisenberry and Z. Zhou, *Inorg. Chem.*, 2008, **47**, 2613-2624.

9. N. Nomura, R. Ishii, M. Akakura and K. Aoi, *J. Am. Chem. Soc.*, 2002, **124**, 5938-5939.
10. Z. Tang, X. Chen, Y. Yang, X. Pang, J. Sun, X. Zhang and X. Jing, *J. Polym. Sci. A: Polym. Chem.*, 2004, **42**, 5974-5982.
11. Z. Tang, X. Chen, X. Pang, Y. Yang, X. Zhang and X. Jing, *Biomacromolecules*, 2004, **5**, 965-970.
12. N. Nomura, R. Ishii, Y. Yamamoto and T. Kondo, *Chem. Eur. J.*, 2007, **13**, 4433-4451.
13. R. Ishii, N. Nomura and T. Kondo, *Polym. J.*, 2004, **36**, 261-264.
14. P. L. Arnold, J.-C. Buffet, R. P. Blaudeck, S. Sujecki, A. J. Blake and C. Wilson, *Angew. Chem. Int. Ed.*, 2008, **120**, 6122-6125.
15. T. P. A. Cao, A. Buchard, X. F. Le Goff, A. Auffrant and C. K. Williams, *Inorg. Chem.*, 2012, **51**, 2157-2175.
16. C. Bakewell, T.-P.-A. Cao, X. F. Le Goff, N. J. Long, A. Auffrant and C. K. Williams, *Organometallics*, 2013, **32**, 1475-1483.
17. C. Bakewell, T. P. A. Cao, N. Long, X. F. Le Goff, A. Auffrant and C. K. Williams, *J. Am. Chem. Soc.*, 2012, **134**, 20577-20580.
18. C. Bakewell, A. J. P. White, N. J. Long and C. K. Williams, *Angew. Chem. Int. Ed.*, 2014, 9226-9230.
19. S. Song, H. Ma and Y. Yang, *Dalton Trans.*, 2013, **42**, 14200-14211.
20. D. C. Aluthge, B. O. Patrick and P. Mehrkhodavandi, *Chem. Commun.*, 2013, **49**, 4295-4297.
21. J.-C. Wu, B.-H. Huang, M.-L. Hsueh, S.-L. Lai and C.-C. Lin, *Polymer*, 2005, **46**, 9784-9792.
22. A. F. Douglas, B. O. Patrick and P. Mehrkhodavandi, *Angew. Chem. Int. Ed.*, 2008, **47**, 2290-2293.
23. I. Yu, A. Acosta-Ramirez and P. Mehrkhodavandi, *J. Am. Chem. Soc.*, 2012, **134**, 12758-12773.
24. J. Fang, I. Yu, P. Mehrkhodavandi and L. Maron, *Organometallics*, 2013, **32**, 6950-6956.
25. G. Labourdette, D. J. Lee, B. O. Patrick, M. B. Ezhova and P. Mehrkhodavandi, *Organometallics*, 2009, **28**, 1309-1319.
26. D. J. Darensbourg and O. Karroonnirun, *Inorg. Chem.*, 2010, **49**, 2360-2371.
27. L. Wang and H. Ma, *Macromolecules*, 2010, **43**, 6535-6537.

28. S. Song, X. Zhang, H. Ma and Y. Yang, *Dalton Trans.*, 2012, **41**, 3266-3277.
29. H. Wang, Y. Yang and H. Ma, *Macromolecules*, 2014, **47**, 7750-7764.
30. A. Otero, J. Fernández-Baeza, L. F. Sánchez-Barba, J. Tejeda, M. Honrado, A. Garcés, A. Lara-Sánchez and A. M. Rodríguez, *Organometallics*, 2012, **31**, 4191-4202.
31. M. Honrado, A. Otero, J. Fernandez-Baeza, L. F. Sanchez-Barba, A. Garces, A. Lara-Sanchez and A. M. Rodriguez, *Dalton Trans.*, 2014, **43**, 17090-17100.
32. M. Honrado, A. Otero, J. Fernández-Baeza, L. F. Sánchez-Barba, A. Lara-Sánchez, J. Tejeda, M. P. Carrión, J. Martínez-Ferrer, A. Garcés and A. M. Rodríguez, *Organometallics*, 2013, **32**, 3437-3440.
33. M. Honrado, A. Otero, J. Fernández-Baeza, L. F. Sánchez-Barba, A. Garcés, A. Lara-Sánchez and A. M. Rodríguez, *Organometallics*, 2014, **33**, 1859-1866.
34. F. Drouin, P. O. Oguadinma, T. J. J. Whitehorne, R. E. Prud'homme and F. Schaper, *Organometallics*, 2010, **29**, 2139-2147.
35. Y. Liu, M. Nishiura, Y. Wang and Z. Hou, *J. Am. Chem. Soc.*, 2006, **128**, 5592-5593.
36. V. C. Gibson, S. K. Spitzmesser, A. J. P. White and D. J. Williams, *Dalton Trans.*, 2003, 2718-2727.
37. J. Zou, D. J. Berg, D. Stuart, R. McDonald and B. Twamley, *Organometallics*, 2011, **30**, 4958-4967.
38. M. Durán-Galván, S. A. Worlikar and B. T. Connell, *Tetrahedron*, 2010, **66**, 7707-7719.
39. M. Klein, K. Krainz, I. N. Redwan, P. Dinér and M. Grøtli, *Molecules*, 2009, **14**, 5124.
40. S. D. Bennett, B. A. Core, M. P. Blake, S. J. A. Pope, P. Mountford and B. D. Ward, *Dalton Trans.*, 2014, **43**, 5871-5885.
41. D. A. Fletcher, R. F. McMeeking and D. Parkin, *J. Chem. Inf. Comput. Sci.*, 1996, **36**, 746.
42. T. J. Marks and J. R. Kolb, *Chem. Rev.*, 1977, **77**, 263.
43. N. Ajellal, J.-F. Carpentier, C. Guillaume, S. M. Guillaume, M. Helou, V. Poirier, Y. Sarazin and A. A. Trifonov, *Dalton Trans.*, 2010, **39**, 8363-8378.

44. I. Yu, A. Acosta-Ramírez and P. Mehrkhodavandi, *J. Am. Chem. Soc.*, 2012, **134**, 12758-12773.

Chapter Five

Experimental details and characterising data

5.1 General methods and instrumentation

All manipulations were carried out using standard Schlenk line or dry-box techniques under an atmosphere of argon or dinitrogen. Toluene, THF and diethyl ether (Et_2O) were predried over activated 4 Å molecular sieves prior to reflux over potassium (THF and toluene) or Na/K alloy (Et_2O) under dintrogen and distilled. Pentane, hexane and benzene were degassed by sparging with dinitrogen and dried by passing through a column of the appropriate drying agent.[1] Deuterated solvents were dried over potassium (C_6H_6 and THF-d_8), sodium (toluene-d_8) or P_2O_5 ($CDCl_3$ and CD_2Cl_2) at reflux, distilled under reduced pressure and stored under dinitrogen in Teflon valve ampoules. $CDCl_3$ was used as received for non-sensitive polymer samples.

Solution NMR samples were prepared in a dry-box in 5 mm Wilmad 507-PP tubes fitted with J. Young Teflon valves. ^{1}H, ^{2}H, ^{7}Li, $^{11}B\{^{1}H\}$, ^{11}B and $^{13}C\{^{1}H\}$ NMR spectra were recorded on Varian Mercury-VX 300, Varian Unity Plus 500, Bruker Avance III 500 or Bruker Avance III 400 spectrometers at ambient temperature unless stated otherwise. ^{1}H and $^{13}C\{^{1}H\}$ spectra were referenced internally to residual protio-solvent (^{1}H) or solvent (^{13}C) resonances, and are reported relative to tetramethylsilane (δ = 0 ppm). Assignments were confirmed using two dimensional ^{1}H-^{1}H and ^{13}C-^{1}H NMR correlation experiments. ^{11}B and $^{11}B\{^{1}H\}$ spectra were referenced externally to $BF_3.Et_2O$. ^{7}Li spectra were referenced externally to LiCl, D_2O, 9.7 M. IR spectra were recorded on a Thermo Scientific Nicolet iS5 FTIR spectrometer. Samples were prepared in a dry-box as Nujol mulls between NaCl plates or as a benzene or THF solution in a NaCl cell. Mass spectra were recorded by the departmental service of University of Oxford. Elemental analysis was carried out by the Elemental Analysis Service at the London Metropolitan University.

MALDI-ToF MS analysis was performed on a Waters MALDI micro equipped with a 337 nm nitrogen laser. An accelarting voltage of 25kV was applied. The polymer samples were dissolved in THF at a concentration of 1 mg mL^{-1}. The cationisation agent used was potassium trifluoroacetate (Fluka, > 99%) dissolved in THF at a concentration of 5 mg mL^{-1}. The matrix used was *trans*-2-[3-(4-*tert*-butylphenyl)-2-methy-2-propenylidene]malononitrile (DCTB) (Fluka) and was dissolved in THF at a concentration of 40 mg mL^{-1}. Solutions of matrix, salt and polymer were mixed in a volume ratio of 4:1:4, respectively. The mixed solution was hand-spotted on a

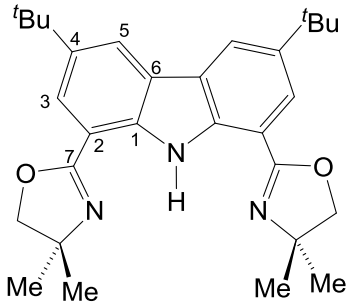
stainless steel MALDI target and left to dry. The spectra were recorded in refectron mode.

Polymer molecular weights (M_n, M_w) were determined by GPC using a Polymer Laboratories Plgel Mixed-D column (300 mm length, 7.5 mm diameter) and a Polymer Laboratories PL-GPC50 Plus instrument equipped with a refractive index detector. THF (HPLC grade, stabilised with BHT, 2.5 ppm) was used as an eluent at 30 °C with a flow rate of 1 mL^{-1} min. Samples were dissolved in THF (HPLC grade, stabilised with BHT, 2.5 ppm) at a concentration of 2.0 mg mL^{-1} and filtered before injection. Linear polystyrenes (Polymer Laboratories) were used as primary calibration standards, and Mark-Houwink corrections for poly(*rac*-LA) in THF were applied for the experimental samples (K = 17.4; α = 0.736).[2-4]

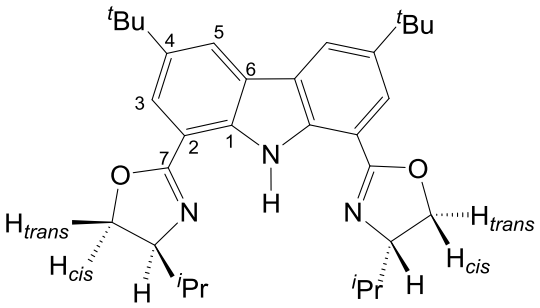
5.2 Literature preparations and reagent purification

$HCzOx^{Me_2}$,[5] (*S*,*S*)- and (*R*,*R*)-$HCzOx^{iPr}$,[5, 6] $Sr(BH_4)_2(THF)_2$,[7] $Ln(BH_4)_3(THF)_x$ (Ln = Y, x = 2; Sm, x = 3; or La, x = 3)[8, 9] $Mg\{N(SiMe_3)_2\}_2$[10] and $Ca\{N(SiMe_3)_2\}_2(THF)_2$[10] were prepared according to or adapted from literature procedures. $Li(CzOx^{Me_2})$ (**19**), $Y(CzOx^{Me_2})(BH_4)_2(THF)$ (**16**) and (*S*,*S*)-$Y(CzOx^{iPr})(BH_4)_2(THF)$ (**(*S*,*S*)-43**) were kindly provided by L. Budden. *Rac*- and *L*-LA was recrystallised twice from hot toluene solutions and dried *in vacuo*. The recrystallised material was then sublimed twice under reduced pressure. The purified *rac*- and *L*-LA was stored in a dry-box and used within a month of being sublimed. Crude *meso*-LA was provided by Uhde Inventa-Fisher which was purified by repeated recrystallisation from propan-2-ol at -30 °C, followed by recrystallisation from toluene and sublimed twice under reduced pressure. *D*-LA was provided by Purac and used as received. BnOH (anhydrous, Sigma Aldrich) and PhCHO (purified by redistilled, Sigma Aldrich) were degassed prior to use. $B(OMe)_3$ was dried over sodium at reflux overnight then distilled under reduced pressure. The purified liquid reagents were stored under argon in glass ampoules fitted with J. Young Teflon valve. Other commerially available reagents were used as received.

5.3 Ligand numbering system



HCzOx^{Me_2} (**1.45**)



(*S*,*S*)-HCzOx^{iPr} ((***S*,*S*)-1.46**)

5.4 Experimental details and characterising data for Chapter Two

Mg(CzOx^{Me_2}){N(SiMe$_3$)$_2$} (1). A stirred toluene solution (30 cm^3) of **1.45** (0.5 g, 1.06 mmol) was added dropwise to a stirred toluene solution (30 cm^3) of Mg{N(SiMe$_3$)$_2$}$_2$ (0.36 g, 1.06 mmol) and stirred for 16 h. The volatiles were removed *in vacuo* and the residue washed with pentane (15 cm^3) cooled to 0 °C to yield the final product as a yellow powder (0.51 g, 0.78 mmol, 73%). Diffraction-quality crystals were grown from a saturated toluene solution cooled to -30 °C. ^{1}H NMR (C_6D_6, 300.3 MHz, 295 K): δ 8.57 (2H, d, ^4J = 1.5 Hz, C_5–H), 8.41 (2H, d, ^4J = 1.5 Hz, C_3–H), 3.73 (2H, d, ^2J = 8.0 Hz, OCHHC(CH$_3$)$_2$), 3.38 (2H, d, ^2J = 8.0 Hz, OCHHC(CH$_3$)$_2$), 1.53 (6H, s, OCH$_2$C(CH$_3$)(CH$_3$)), 1.47 (18 H, s, C(CH$_3$)$_3$), 1.21 (6H, s, OCH$_2$C(CH$_3$)(CH$_3$)) and 0.12 (18 H, s, N(Si(CH$_3$)$_3$)$_2$) ppm. ^{13}C{^{1}H} NMR (C_6D_6, 75.5 MHz, 295 K): δ 168.9 (C_7), 150.0 (C_1), 139.6 (C_4), 127.3 (C_2) 123.8 (C_3), 122.9 (C_5), 109.0 (C_6), 79.2 (CH$_2$), 67.1 (C(CH$_3$)$_2$), 35.0 (C(CH$_3$)$_3$), 32.3 (C(CH$_3$)$_3$), 28.8 (OCH$_2$C(CH$_3$)(CH$_3$)), 27.9 (OCH$_2$C(CH$_3$)(CH$_3$)) and 7.2 (N(Si(CH$_3$)$_3$) ppm. IR (NaCl plates, Nujol mull, cm^{-1}): 1636 (w), 1598 (m), 1578 (s), 1308 (w), 1273 (s), 1251 (m), 1240 (m), 1188 (s), 1078 (m), 1016(m), 981 (s), 883 (m), 825 (m), 785 (w), 662 (w). EI-MS: *m/z* = 498 (100%). Anal. found (calcd. for $C_{36}H_{56}N_4O_2Si_2Mg$): C, 65.59 (65.78); H, 8.42 (8.59); N, 8.63 (8.52) %.

Mg(CzOx^{Me_2})(OBn) (2). A toluene solution (2 cm^3) of BnOH (0.089 g, 0.82 mmol) cooled to -10 °C was added dropwise with stirring to a toluene solution (80 cm^3) of **1.45** (0.574 g, 0.87 mmol) cooled to -78 °C over 1 h. The solution was gradually warmed to 25 °C over 5 h before the toluene was removed *in vacuo*. The residue was washed with pentane (10 cm^3) cooled to 0 °C to yield the final product as a yellow

powder (0.24 g, 0.40 mmol, 48%). ^{1}H NMR (THF-d_8, 400.1 MHz, 300 K): δ 8.33 (2H, br d, C_5–H), 8.10 (2H, br d, C_3–H), 7.45 (2H, app d, ^{3}J = 6.9 Hz, *meta*-OBn), 7.14 (2H, app t, ^{3}J = 6.7 Hz, *ortho*-OBn), 6.99 (1H app t, ^{3}J = 6.7 Hz, *para*-OBn), 5.34 (2H, s, CH_2Ph), 4.12 (4H, s, CH_2), 1.60 (12H, s, $(CH_3)_2$) and 1.47 (18H, s, $(CH_3)_3$) ppm. ^{13}C{^{1}H} NMR (THF-d_8, 100.6 MHz, 300 K): δ 166.1 (C_7), 151.8 (*ipso*-OBn), 149.2 (C_1), 137.5 (C_4), 127.7 (*meta*-OBn), 127.4 (*ortho*-OBn), 127.0 (C_2), 125.0 (*para*-OBn), 124.2 (C_3), 120.8 (C_5), 109.7 (C_6), 79.8 (CH_2), 69.4 ($C(CH_3)_2$), 68.6 (CH_2Ph), 34.9 ($C(CH_3)_3$), 32.3 ($C(CH_3)_3$) and 27.8 ($C(CH_3)_2$) ppm. IR (NaCl plates, Nujol mull, cm^{-1}): 1586 (w), 1269 (m), 1183 (w), 1072 (w), 1020 (w), 800 (w). EI-MS: *m/z* = 473 (85% [HCzOx^{Me_2}]$^{+}$), 458 (100). It was not possible to obtain an elemental analysis for **2**.

Mg(CzOx^{Me_2})(Bu) (3). A 1M heptanes solution of $MgBu_2$ (1.6 cm^3, 1.6 mmol) was added dropwise to a stirred toluene solution (30 cm^3) of **1.45** (0.5 g, 1.1 mmol) cooled to -78 °C. The solution was gradually warmed to 25 °C and stirred for 4 h. The solvent was removed *in vacuo* and the residue was washed with pentane (15 cm^3) cooled to 0 °C to yield the final product as a yellow powder (0.32 g, 0.58 mmol, 52%). Diffraction-quality crystals were grown from a saturated pentane solution. ^{1}H NMR (C_6D_6, 300.3 MHz, 293 K): δ 8.57 (2H, d, ^{4}J = 2.1 Hz, C_5–H), 8.39 (2H, d, ^{4}J = 2.1 Hz, C_3–H), 3.60 (4H, s, CH_2), 1.84-1.73 (2H, m, β-^{n}Bu), 1.49 (18H, s, $(CH_3)_3$), 1.47-1.42 (2H, m, γ-^{n}Bu), 1.22 (12H, br s, $(CH_3)_2$), 0.93 (3H, t, ^{3}J = 7.2 Hz $Mg(CH_2)_3CH_3$) and 0.06-0.01 (2H, m, α-^{n}Bu) ppm. ^{13}C{^{1}H} NMR (C_6D_6, 75.5 MHz, 293 K): δ 167.6 (C_7), 150.1 (C_1), 139.1 (C_4), 127.2 (C_2), 123.8 (C_3), 122.9 (C_5), 109.8 (C_6), 78.3 (CH_2), 66.4 ($C(CH_3)_2$), 35.0 ($C(CH_3)_3$), 32.7 (β-^{n}Bu), 32.4 ($C(CH_3)_3$), 31.9 (γ-^{n}Bu), 28.5 (($CH_3)_2$), 14.4 ($Mg(CH_2)_3CH_3$) and 13.3 (α-^{n}Bu) ppm. IR (NaCl plates, Nujol mull, cm^{-1}): 1636 (m), 1583 (s), 1340 (w), 1308 (m), 1270 (s), 1231 (m), 1183 (s), 1122 (w), 1095 (w), 1071 (s), 1013 (m), 880 (m), 784 (m), 632 (m). EI-MS: *m/z* = 496 (100% [Mg(CzOx^{Me_2})]$^{+}$). Anal. found (calcd. for $C_{34}H_{47}N_3O_2Mg$): C, 73.58 (73.70); H, 8.65 (8.55); N, 7.48 (7.58) %.

Zn(CzOx^{Me_2})(Et) (4). A 1.1M toluene solution of $ZnEt_2$ (1.1 cm^3, 1.16 mmol) was added dropwise to a stirred toluene solution (30 cm^3) of **1.45** (0.5 g, 1.06 mmol) cooled to -78 °C and the solution stirred for 16 h. The volatiles were removed *in vacuo* and the residue was washed with pentane (10 cm^3) cooled to 0 °C to yield the

final product as a yellow powder (0.29 g, 0.51 mmol, 48%). ^{1}H NMR (C_6D_6, 300.3 MHz, 293 K): δ 8.53 (2H, d, ^{4}J = 1.7 Hz, C_5–H), 8.36 (2H, d, ^{4}J = 1.7 Hz, C_3–H), 3.62 (4H, s, CH_2), 1.48 (18H, s, $(CH_3)_3$), 1.44 (3H, t, ^{3}J = 8.0 Hz, CH_2CH_3), 1.21 (12H, s, $(CH_3)_2$) and 0.52 (2H, q, ^{3}J = 8.0 Hz, CH_2CH_3) ppm. $^{13}C\{^{1}H\}$ NMR (C_6D_6, 75.5 MHz, 293 K): δ 165.7 (C_7), 149.3 (C_1), 139.2 (C_4), 126.6 (C_2), 123.5 (C_3), 122.5 (C_5), 109.0 (C_6), 78.1 (CH_2), 66.7 ($C(CH_3)_2$), 35.0 ($C(CH_3)_3$), 32.4 ($C(CH_3)_3$), 28.4 ($C(CH_3)_2$), 13.5 (CH_2CH_3) and 6.1 (CH_2CH_3) ppm. IR (NaCl plates, Nujol mull, cm^{-1}): 1635 (m), 1584 (s), 1308 (w), 1270 (s), 1231 (w), 1123 (w), 1072 (m), 1015 (m), 882 (m), 783 (w), 631 (w). EI-MS: *m/z* = 536 (55% $[Zn(CzOx^{Me2})]^{+}$), 57 (100 $[^{t}Bu]^{+}$). Anal. found (calcd. for $C_{32}H_{43}N_3O_2Zn$): C, 67.54 (67.78); H, 7.51 (7.64); N, 7.55 (7.41) %.

K(CzOx^{Me2}) (5). To a stirred solution of **1.45** (1 g, 2.1 mmol) in THF (20 cm^3) a stirred suspension of $KN(SiMe_3)_2$ (0.63 g, 3.2 mmol) in THF (20 cm^3) was added dropwise at -78 °C. The solution was gradually warmed to room temperature and stirred for 4 h before the volatiles were removed *in vacuo*. The residue washed with toluene (30 cm^3) followed by pentane (30 cm^3) and dried *in vacuo* to yield the final product as a yellow powder (0.74 g, 1.4 mmol, 74%). ^{1}H NMR (THF-d_8, 500.3 MHz, 298 K): δ 8.21 (2H, d, ^{4}J = 2.24 Hz, CH), 8.03 (2H, d, ^{4}J = 2.24 Hz, CH), 4.06 (4H, s, CH_2), 1.51 (12H, s, $C(CH_3)_2$) and 1.50 (18H, s, $C(CH_3)_3$) ppm. Due to poor solubility, a satisfactory $^{13}C\{^{1}H\}$ NMR spectrum could not be obtained for **5.** IR (NaCl plates, Nujol mull, cm^{-1}): 1637 (m), 1605 (m), 1542 (w), 1362 (m), 1267 (m), 1224 (w), 1173 (m), 1051 (m), 879 (w), 778 (w), 668 (w). EI-MS: *m/z* = 473 (95% $[HCzOx^{Me2}]^{+}$). Anal. found (calcd. for $C_{30}H_{38}KN_3O_2$): C, 70.26 (70.41); H, 7.61 (7.48); N, 8.10 (8.21) %.

Mg(CzOx^{Me2})I(THF)$_2$ (6). A 3M Et_2O solution of MeMgI (0.84 cm^3, 2.5 mmol) was added dropwise to a stirred Et_2O solution of **1.45** (1 g, 2.1 mmol) cooled to -78 °C. The resultant suspension was warmed to 25 °C and stirred for 1 h. The suspension was filtered and the residue redissolved in THF (30 cm^3). The volatiles were removed *in vacuo* to yield the final product as a yellow powder (1.23 g, 1.60 mmol, 76%). ^{1}H NMR (THF-d_8, 300.3 MHz, 293 K): δ 8.31 (2H, d, ^{4}J = 2.1 Hz, C_5–H), 8.15 (2H, d, ^{4}J = 2.1 Hz, C_3–H), 4.10 (4H, s, CH_2), 1.90 (12H, s, $(CH_3)_2$) and 1.42 (18H, s, $(CH_3)_3$) ppm. $^{13}C\{^{1}H\}$ NMR (THF-d_8, 75.5 MHz, 293 K): δ 166.8 (C_7), 148.2 (C_1), 138.0

($\underline{C}_4$), 127.4 ($\underline{C}_2$), 125.3 ($\underline{C}_3$), 121.1 ($\underline{C}_5$), 109.6 ($\underline{C}_6$), 81.2 ($\underline{C}H_2$), 70.3 ($\underline{C}(CH_3)_2$), 34.9 ($\underline{C}(CH_3)_3$), 32.3 ($C(\underline{C}H_3)_3$) and 29.0 ($(\underline{C}H_3)_2$) ppm. IR (NaCl plates, Nujol mull, cm^{-1}): 1634 (w), 1586 (m), 1566 (m), 1313 (w), 1267 (m), 1230 (w), 1182 (m), 1072 (m), 1028 (m), 882 (w), 801 (w). EI-MS: *m/z* = 623 (20% $[Mg(CzOx^{Me_2})I]^+$), 496 (100 $[Mg(CzOx^{Me_2})]^+$). Anal. found (calcd. for $C_{38}H_{54}N_3O_4IMg$): C, 59.21 (59.42); H, 7.18 (7.09); N, 5.47 (5.47) %.

Mg(CzOx^{Me_2})(BH$_4$) (7). A stirred THF suspension (30 cm^3) of **5** (0.5 g, 0.98 mmol) was added dropwise to a stirred THF suspension (30 cm^3) of magnesium borohydride (0.053 g, 0.98 mmol) cooled to -78 °C. The solution was gradually warmed to 25 °C and stirred for 16 h. The solvent was removed *in vacuo* and the product extracted into hot toluene (2 × 30 cm^3) and filtered. The volatiles were removed *in vacuo* and the residue washed with pentane (15 cm^3) to yield the final product as a yellow powder (0.35 g, 0.68 mmol, 69%). Diffraction-quality crystals were grown from slow diffusion of pentane into a dilute THF solution. ^{1}H NMR (THF-d_8, 300.3 MHz, 293 K): δ 8.35 (2H, d, ^4J = 1.9 Hz, C_5–$\underline{H}$), 8.10 (2H, d, ^4J = 1.9 Hz, C_3–$\underline{H}$), 4.14 (4H, s, ($C\underline{H}_2$)), 1.66 (12H, s, ($C\underline{H}_3)_2$), 1.46 (18H, s, ($C\underline{H}_3)_3$) and 0.79- -0.21(4H, br s, $B\underline{H}_4$) ppm. $^{13}C\{^1H\}$ NMR (THF-d_8, 75.5 MHz, 293 K:) δ 167.6 ($\underline{C}_7$), 148.9 ($\underline{C}_1$), 138.5 ($\underline{C}_4$), 127.3 ($\underline{C}_2$), 124.3 ($\underline{C}_3$), 121.5 ($\underline{C}_5$), 109.6 ($\underline{C}_6$), 79.2 ($\underline{C}H_2$), 69.5 ($\underline{C}(CH_3)_2$), 35.0 ($\underline{C}(CH_3)_3$), 32.3 ($C(\underline{C}H_3)_3$) and 27.0 ($(\underline{C}H_3)_2$) ppm. ^{11}B NMR (THF-d_8, 160 MHz, 300 K): -34.1 (br quintet, ^1J = 69.4 Hz, $\underline{B}H_4$) ppm. IR (NaCl plates, Nujol mull, cm^{-1}): 2250 (br s, B–H stretching), 1633 (s), 1580 (s), 1340 (w), 1309 (w), 1272 (m), 1124 (w), 1072 (m), 1029 (m), 977 (w), 965 (w), 880 (m), 817 (w). IR (NaCl cell, THF, ν(B−H), cm^{-1}): 2407 (s, B–H_t stretching), 2184 and 2126 (d, B–H_b stretching, 58 cm^{-1} splitting). IR (NaCl cell, benzene, ν(B−H), cm^{-1}): 2412 (s, B–H_t stretching), 2163 and 2105 (d, B–H_b stretching, 58 cm^{-1} splitting). EI-MS: *m/z* = 511 (10%, $[M]^+$), 458 (100). Anal. found (calcd. for $C_{30}H_{42}BN_3O_2Mg$): C, 70.24 (70.40); H, 8.16 (8.27); N, 8.15 (8.21) %.

Alternative synthesis of Mg(CzOx^{Me_2})(BH$_4$) (7). A stirred THF suspension (15 cm^3) of $NaBH_4$ (0.016g, 0.43 mmol) was added dropwise to a stirred THF solution (20 cm^3) of **6** (0.3, 0.43 mmol) at 25 °C and stirred for 2 h. The volatiles were removed *in vacuo* and the product extracted into toluene (30 cm^3). The toluene was removed *in vacuo* and the residue was washed with pentane (10 cm^3) at 0 °C before drying under

reduced pressure to yield the final product as a yellow powder (0.131 g, 0.26 mmol, 62%).

Mg(CzOx^{Me_2})(BD$_4$) (7-*d*$_4$). A stirred THF suspension (15 cm^3) of NaBD$_4$ (0.015 g, 0.36 mmol) was added dropwise to a stirred THF solution (20 cm^3) of **6** (0.25, 0.36 mmol) at 25 °C and stirred for 2 h. The volatiles were removed *in vacuo* and the product extracted into toluene (30 cm^3). The toluene was removed *in vacuo* and the residue was washed with pentane (10 cm^3) at 0 °C before drying under reduced pressure to yield the final product as a yellow powder (0.116 g, 0.22 mmol, 62%). ^{1}H NMR (THF-*d*$_8$, 400.1 MHz, 298 K): δ 8.35 (2H, br s, C$_5$–H), 8.10 (2H, br s, C$_3$–H), 4.14 (4H, s, (CH$_2$)), 1.69 (12H, s, (CH$_3$)$_2$) and 1.46 (18H, s, (CH$_3$)$_3$) ppm. ^{2}H NMR (THF, 76.7 MHz, 298 K): δ 0.60 (br s, BD$_4$) ppm. ^{13}C{^{1}H} NMR (THF-*d*$_8$, 100.6 MHz, 292 K): 167.4 (C$_7$), 148.8 (C$_1$), 138.4 (C$_4$), 127.3 (C$_2$), 124.4 (C$_3$), 121.4 (C$_5$), 109.6 (C$_6$), 79.4 (CH$_2$), 69.6 (C(CH$_3$)$_2$), 35.0 (C(CH$_3$)$_3$), 32.3 (C(CH$_3$)$_3$) and 27.2 ((CH$_3$)$_2$) ppm. ^{11}B NMR (THF-*d*$_8$, 128.4 MHz, 298 K) -35.3 (s, BD$_4$) ppm. IR (NaCl plates, Nujol mull, cm^{-1}): 1632 (w), 1595 (w), 1566 (br s), 1269 (m), 1186 (w), 1078 (w), 1016 (w), 886 (w), 802 (w). IR (NaCl cell, THF, ν(B−D), cm^{-1}): 1884 (s, B–D$_t$ stretching); ν_D/ν_H = 0.79, 1636 and 1597 (d, B–D$_b$ stretching, 39 cm^{-1} splitting); ν_D/ν_H = 0.76. EI-MS: *m*/*z* = 516 (10 %, [M]$^+$), 458 (70), 69 (100) %.

NMR tube scale synthesis of Mg(CzOx^{Me_2})(OBn) (2)/B(OBn)$_3$ and Mg(CzOx^{Me_2}){B(OBn)$_4$} (8). A THF-*d*$_8$ solution (0.5 cm^3) of Mg(CzOx^{Me_2})(BH$_4$) (**7**) (20 mg, 0.04 mmol) in an NMR tube equipped with a J. Young Teflon valve was treated with benzaldehyde (17.9 μL, 0.18 mmol) at RT. ^{1}H and ^{11}B NMR spectroscopy showed a mixture of **2**/B(OBn)$_3$ and **8**. The ^{1}H and ^{13}C{^{1}H} NMR gave a complex mixture of products. ^{11}B NMR (THF-*d*$_8$, 128.4 MHz, 298 K): δ 18.8 (s, B(OBn)$_3$) and 3.8 (s, B(OBn)$_4$) ppm.

NMR tube scale synthesis of Mg(CzOx^{Me_2})(OCHDPh) (2)/B(OCHDPh)$_3$ and Mg(CzOx^{Me_2}){B(OCHDPh)$_4$} (8-*d*$_4$). A THF-*d*$_8$ solution (0.5 cm^3) of Mg(CzOx^{Me_2})(BD$_4$) (**7-*d*$_4$**) (10 mg, 0.02 mmol) in an NMR tube equipped with a J. Young Teflon valve was treated with benzaldehyde (8.9 μL, 0.09 mmol) at RT. ^{1}H and ^{11}B NMR spectroscopy showed a mixture of **2-*d***/B(OCHDPh)$_3$ and **8-*d*$_4$**. The ^{1}H and ^{13}C{^{1}H} NMR gave a complex mixture of products. ^{2}H NMR (THF, 76.7 MHz,

298 K) δ 4.95 (s, B(OCH<u>D</u>Ph)$_3$) and 4.55 (br s, overlapping Mg(CzOx^{Me2})(OCH<u>D</u>Ph) and {B(OCH<u>D</u>Ph)$_4$}). ^{11}B NMR (THF-d_8, 160 MHz, 298 K): δ 18.8 (s, <u>B</u>(OCHDPh)$_3$) and 3.7 (s, <u>B</u>(OCHDPh)$_4$) ppm.

5.5 Experimental details and characterising data for Chapter Three

Ca(CzOx^{Me2}){N(SiMe$_3$)$_2$}$_2$(THF) (9). To a stirred solution of Ca{N(SiMe$_3$)$_2$}$_2$(THF)$_2$ (2.13 g, 4.2 mmol) in toluene (30 cm^3) a stirred solution of **1.45** (2.0 g, 4.2 mmol) in toluene (30 cm^3) was added dropwise and stirred for 16 h. The solvent was removed *in vacuo* and the product washed with pentane cooled to 0 °C (15 cm^3) to yield the final product as a yellow powder (2.1 g, 2.9 mmol, 68%). Diffraction-quality crystals were grown from a saturated THF solution. ^{1}H NMR (C_6D_6, 300.3 MHz, 293 K): δ 8.75 (2H, d, ^4J = 2.2 Hz, C$_3$-<u>H</u>), 8.66 (2H, d, ^4J = 2.2 Hz, C$_5$-<u>H</u>), 3.69 (4H, s, C<u>H</u>$_2$), 3.39 (4H, t, ^3J = 6.3 Hz, OC<u>H</u>$_2$CH$_2$), 1.51 (30H, br s, overlapping C(C<u>H</u>$_3$)$_2$ and C(C<u>H</u>$_3$)$_3$) 0.91 (4H, t, ^3J = 6.3 Hz, OCH$_2$C<u>H</u>$_2$) and 0.35 (18H, s, Si(C<u>H</u>$_3$)$_3$) ppm. ^{13}C{^{1}H} NMR (C_6D_6, 75.5 MHz, 293 K): δ 167.2 (<u>C</u>$_7$), 149.3 (<u>C</u>$_1$), 137.9 (<u>C</u>$_4$), 128.2 (<u>C</u>$_2$), 126.1 (<u>C</u>$_3$), 121.54 (<u>C</u>$_5$), 109.7 (<u>C</u>$_6$), 78.0 (<u>C</u>H$_2$), 69.4 (O<u>C</u>H$_2$CH$_2$), 68.4 (<u>C</u>(CH$_3$)$_2$), 34.7 (<u>C</u>(CH$_3$)$_3$), 32.3 (C(<u>C</u>H$_3$)$_3$), 29.0 (C(<u>C</u>H$_3$)$_2$), 24.9 (OCH$_2$<u>C</u>H$_2$) and 6.6 (Si(<u>C</u>H$_3$)$_3$) ppm. IR (NaCl plates, Nujol mull, cm^{-1}): 1634 (w), 1601 (m), 1542 (w), 1261 (m), 1170 (w), 1065 (w), 1022 (m), 819 (w), 668 (w). EI-MS: *m/z* = 512 (10% [Ca(CzOx^{Me2})]$^+$), 477 (95), 368 (100). Anal. found (calcd. for $C_{40}H_{64}N_4O_3Si_2Ca$): C, 64.26 (64.47); H, 8.56 (8.66); N, 7.46 (7.52) %.

Ca(CzOx^{Me2})(OBn) (10). Benzyl alcohol (42 µL, 0.4 mmol) was added dropwise to a stirred toluene solution (30 cm^3) of **9** (0.3 g, 0.4 mmol). The solution was stirred at room temperature for 1 h before the volatiles were removed *in vacuo*. The residue was washed with pentane (15 cm^3) cooled to 0 ºC and dried *in vacuo* to yield the final product as a yellow powder (0.093 g, 0.15 mmol, 38%). ^{1}H NMR (THF-d_8, 300.3 MHz, 293 K): δ 8.30 (2H, d, ^4J = 2.2 Hz, C$_5$–<u>H</u>), 8.13 (2H, d, ^4J = 2.2 Hz, C$_3$–<u>H</u>), 7.43 (2H, d, ^3J = 7.3 Hz, *ortho*-OBn), 7.17 (2H, app t, ^3J = 7.3 Hz, *meta*-OBn), 7.02 (1H, app t, ^3J = 7.3 Hz, *para*-OBn), 5.18 (2H, s, C<u>H</u>$_2$Ph), 4.12 (4H, s, C<u>H</u>$_2$), 1.64 (12H, s, (C<u>H</u>$_3$)$_2$) and 1.45 (18H, s, (C<u>H</u>$_3$)$_3$) ppm. ^{13}C{^{1}H} NMR (THF-d_8, 75.5 MHz, 293 K): δ 165.7 (<u>C</u>$_7$), 151.8 (*ipso*-OBn), 149.7 (<u>C</u>$_1$), 136.2 (<u>C</u>$_4$), 128.0 (*ortho*-OBn), 127.9 (<u>C</u>$_2$), 127.7 (*meta*-OBn), 125.3 (<u>C</u>$_3$), 125.1 (*para*-OBn), 120.7 (<u>C</u>$_5$), 110.2 (<u>C</u>$_6$), 78.7 (<u>C</u>H$_2$), 70.8 (<u>C</u>H$_2$Ph), 69.8 (<u>C</u>(CH$_3$)$_2$), 34.8 (<u>C</u>(CH$_3$)$_3$), 32.4 (C(<u>C</u>H$_3$)$_3$) and 28.3 (C(<u>C</u>H$_3$)$_2$)

ppm. IR (NaCl plates, Nujol mull, cm^{-1}): 1635 (m) 1598 (m), 1265 (m), 1227 (w), 1179 (s), 1122 (w), 1065 (s), 1026 (w), 878 (w), 780 (w). EI-MS: *m/z* = 477 (35%), 91 (95 [Bn^+]), 77 (100 [Ph^+]). Anal. found (calcd. for $C_{37}H_{45}N_3O_3Ca$): C, 71.57 (71.69); H, 7.41 (7.32); N, 6.70 (6.78) %.

$Ca(CzOx^{Me2})_2$ (11). A toluene solution (50 cm^3) of **1.45** (0.52 g, 1.09 mmol) was added dropwise with stirring to a toluene solution (50 cm^3) of $Ca\{N(SiMe_3)_2\}_2(THF)_2$ (0.25 g, 0.49 mmol) cooled to -78 °C. The solution was slowly warmed to room temperature and subsequently heated to 100 °C for 72 h. The precipitate was filtered, washed with pentane (15 cm^3) and dried *in vacuo* to yield the final product as an air- and moisture-stable yellow powder (0.31 g, 0.31 mmol, 28%). Diffraction-quality crystals were grown from slow evaporation of a dilute dichloromethane solution. ^{1}H NMR (CD_2Cl_2, 500.3 MHz, 298 K): δ 8.40 (2H, d, ^4J = 2.1 Hz, C_5–H), 8.19 (2H, d, ^4J = 2.1 Hz, C_3–H), 3.95 (4H, s, CH_2), 1.48 (18H, s, $C(CH_3)_3$) and 0.93 (12H, s, $C(CH_3)_2$) ppm. $^{13}C\{^1H\}$ NMR (CD_2Cl_2, 125.8 MHz, 298 K): δ 165.7 (C_7), 148.9 (C_1), 137.8 (C_4), 127.5 (C_2), 125.8 (C_3), 120.9 (C_5), 110.5 (C_6), 78.4 (CH_2), 69.0 ($C(CH_3)_2$), 34.8 ($C(CH_3)_3$), 32.2 ($C(CH_3)_3$) and 28.2 ($C(CH_3)_2$) ppm. IR (NaCl plates, Nujol mull, cm^{-1}): 1629 (m), 1602 (s), 1413 (w), 1302 (w), 1283 (w), 1256 (m), 1223 (w), 1167 (m), 1063 (m), 1029 (w), 883 (w), 776 (w), 668 (w). EI-MS: *m/z* = 985 (95% $[M]^+$), 473 (80 $[HCzOx^{Me2}]^+$), 458 (100), 386 (45). Anal. found (calcd. for $C_{60}H_{76}N_6O_4Ca$): C, 72.91 (73.13); H, 7.60 (7.77); N, 8.69 (8.53) %.

$Ca(CzOx^{Me2})I(THF)_2$ (12). CaI_2 (0.17 g, 0.59 mmol) was stirred in THF (30 cm^3) for 16 h, to which a stirred suspension of **5** (0.3 g, 0.59 mmol) in THF (30 cm^3) was added dropwise at room temperature and stirred for 16 h. The product was extracted into hot toluene (50 cm^3) and filtered. The volatiles were removed *in vacuo* to yield the final product as a yellow powder (0.32 g, 0.40 mmol, 69%). ^{1}H NMR (THF-d_8, 300.3 MHz, 293 K): δ 8.31 (2H, d, ^4J = 2.2 Hz, C_5–H), 8.17 (2H, d, ^4J = 2.2 Hz, C_3–H), 4.09 (4H, s, CH_2), 1.84 (12H, s, $C(CH_3)_2$) and 1.41 (18H, s, $C(CH_3)_3$) ppm. $^{13}C\{^1H\}$ NMR (THF-d_8, 75.5 MHz, 293 K): δ 166.8 (C_7), 148.8 (C_1), 137.3 (C_4), 127.8 (C_2), 126.1 (C_3), 121.1 (C_5), 110.0 (C_6) 79.9 (CH_2), 69.5 ($C(CH_3)_2$), 34.8 ($C(CH_3)_3$), 32.3 ($C(CH_3)_3$) and 29.1 ($C(CH_3)_2$) ppm. IR (NaCl plates, Nujol mull, cm^{-1}): 1634 (m), 1598 (s), 1542 (w), 1444 (w), 1305 (m), 1285 (m), 1257 (m), 1224 (m), 1167 (s), 1066 (s), 1033 (s), 887 (w), 860 (w). EI-MS: *m/z* = 512 (55%

[Ca(CzOx^{Me2})]$^+$). Anal. found (calcd. for $C_{38}H_{54}IN_3O_4Ca$): C, 58.37 (58.23); H, 6.87 (6.94); N, 5.43 (5.36) %.

Ca(CzOx^{Me2})(BH$_4$)(THF)$_2$ (13). To a stirred suspension of **5** (0.13 g, 0.26 mmol) in THF (30 cm^3) cooled to -78 ^{o}C, a stirred solution of $Ca(BH_4)_2(THF)_2$ (0.061 g, 0.29 mmol) in THF (30 cm^3) was added dropwise with stirring. The suspension was gradually warmed to room temperature and stirred for 16 h. The volatiles were removed *in vacuo* and the product extracted into hot toluene (50 cm^3). The toluene was removed *in vacuo* and product washed with pentane (20 cm^3) to yield the final product as an orange-yellow powder (0.11 g, 0.17 mmol, 61%). Diffraction-quality crystals were grown from a saturated THF solution. ^{1}H NMR (THF-d_8, 400.1 MHz, 298 K): δ 8.33 (2H, d, ^4J = 2.0 Hz, C_5–H), 8.21 (2H, d, ^4J = 2.0 Hz, C_3–H), 4.13 (4 H, s, CH_2), 1.73 (12 H, s, C(CH_3)$_2$), 1.46 (18 H, s, C(CH_3)$_3$) and 0.34 (4H, q, $^1J_{BH}$ = 82.5 Hz, BH_4) ppm. ^{13}C{^{1}H} NMR (THF-d_8, 100.4 MHz, 298 K): δ 166.8 (C_7), 148.9 (C_1), 137.0 (C_4), 127.8 (C_2), 126.0 (C_3), 121.0 (C_5), 110.2 (C_6), 79.2 (CH_2), 69.7 (C(CH$_3$)$_2$), 34.8 (C(CH$_3$)$_3$), 32.3 (C(CH$_3$)$_3$) and 28.3 (C(CH$_3$)$_2$) ppm. ^{11}B NMR (THF-d_8, 128.4 MHz, 298 K): -34.1 (quintet, $^1J_{BH}$ = 81.1 Hz. BH$_4$) ppm. IR (NaCl plates, Nujol mull, cm^{-1}): 2323 (weak shoulder), 2281 (br s, B–H stretching), 2212 (weak shoulder), 1634 (w), 1600 (s), 1540 (w), 1412 (w), 1303 (w), 1284 (w), 1261 (m), 1223 (w), 1158 (m), 1063 (m), 1035 (w), 884 (w), 802 (w), 776 (w), 668 (w). IR (NaCl cell, THF, ν(B−H), cm^{-1}): 2381 (br, B−H$_t$ stretching), 2258 (br shoulder, B−H$_t$ stretching), 2175 (br, B−H$_b$ stretching). EI-MS: *m/z* = 474 (80%), 368 (85), 71 (100 [THF$^+$]). Anal. found (calcd. for $C_{38}H_{58}BN_3O_4Ca$): C, 67.82 (67.94); H, 8.56 (8.70); N, 6.38 (6.26) %.

Ca(CzOx^{Me2})(BD$_4$)(THF)$_2$ (13-*d*$_4$). A stirred THF suspension (15 cm^3) of $NaBD_4$ (0.025 g, 0.59 mmol) was added dropwise to a stirred THF solution (20 cm^3) of **12** (0.466 g, 0.59 mmol) at 25 °C and stirred for 2 h. The volatiles were removed *in vacuo* and the product extracted into toluene (30 cm^3). The toluene was removed *in vacuo* and the residue was washed with pentane (10 cm^3) at 0 °C before drying under reduced pressure to yield the final product as a yellow powder (0.290 g, 0.43 mmol, 73%). ^{1}H NMR (THF-d_8, 400.1 MHz, 298 K): δ 8.34 (2H, ^4J = 1.6 Hz, C_5–H), 8.10 (2H, d, ^4J = 1.6 Hz, C_3–H), 4.13 (4H, s, (CH_2)), 1.88 (12H, s, (CH_3)$_2$) and 1.45 (18H, s, (CH_3)$_3$) ppm. ^{2}H NMR (THF, 76.7 MHz, 298 K): δ 0.23 (br s, BD$_4$) ppm. ^{13}C{^{1}H} NMR (THF-d_8, 100.4 MHz, 298 K): 166.8 (C_7), 148.8 (C_1), 137.3 (C_4), 127.8 (C_2),

126.1 (C$_3$), 121.1 (C$_5$), 110.0 (C$_6$), 79.9 (CH$_2$), 69.6 (C(CH$_3$)$_2$), 34.9 (C(CH$_3$)$_3$), 32.3 (C(CH$_3$)$_3$) and 29.2 ((CH$_3$)$_2$) ppm. ^{11}B NMR (THF-d_8, 128.4 MHz, 298 K): -36.5 (s, BD$_4$) ppm. IR (NaCl plates, Nujol mull, cm^{-1}): 1598 (s), 1258 (m), 1224 (w), 1168 (s), 1067 (m), 1036 (m), 881 (w), 820 (w), 775 (w). IR (NaCl cell, THF, ν(B−D), cm^{-1}): 1791 (br, B−D$_t$ stretching); ν_D/ν_H = 0.75, 1635 (br, B−D$_t$ stretching); ν_D/ν_H = 0.72, 1600 (br, B−D$_b$ stretching); ν_D/ν_H = 0.74. EI-MS: *m/z* = 458 (100%).

Sr(CzOx^{Me2})(BH$_4$)(THF)$_2$ (14). To a stirred solution of Sr(BH$_4$)$_2$(THF)$_2$ (0.15 g, 0.59 mmol) in THF (20 cm^3) a suspension of **5** (0.30 g, 0.59 mmol) in THF (20 cm^3) was added at -78 °C. The solvent was removed immediately under reduced pressure, and the product extracted into THF (10 cm^3) and filtered to yield the final product as a yellow powder. ^{1}H NMR (THF-d_8, 300.3 MHz, 293 K): δ 8.29 (2H, d, ^4J = 2.2 Hz, C$_5$–H), 8.16 (2H, d, ^4J = 2.2 Hz, C$_3$–H), 4.11 (4H, s, CH$_2$), 1.66 (12H, s, (CH$_3$)$_2$), 1.42 (18H, s, (CH$_3$)$_3$) and 0.34 (4H, q, ^1J = 79.0 Hz, BH$_4$) ppm. ^{13}C{^{1}H} NMR (THF-d_8, 75.5 MHz, 293 K): δ 166.6 (C$_7$), 149.4 (C$_1$), 136.7 (C$_4$), 128.1 (C$_2$), 126.1 (C$_3$), 120.8 (C$_5$), 110.4 (C$_6$), 78.8 (CH$_2$), 69.2 (C(CH$_3$)$_2$), 34.8 (C(CH$_3$)$_3$), 32.3 (C(CH$_3$)$_3$) and 28.3 (C(CH$_3$)$_2$) ppm. ^{11}B NMR (THF-d_8, 128.4 MHz, 298 K): δ -31.4 (q, $^1J_{BH}$ = 81.3 Hz, BH$_4$) ppm. IR (NaCl plates, Nujol mull, cm^{-1}): 2292 (br s, B–H stretching), 1633 (w), 1604 (s), 1443 (m), 1361 (w), 1300 (w), 1282 (m), 1222 (w), 1165 (s), 1061 (m), 882 (w), 774 (w). IR (NaCl cell, THF, ν(B−H), cm^{-1}): 2381 (br, B−H$_t$ stretching), 2249 and 2168 (b, B−H$_b$ stretching, 81 cm^{-1} splitting), 1634 (m), 1605 (s). EI-MS: *m/z* = 473 (80% [HCzOx^{Me2}]$^+$), 458 (100). Anal. found (calcd. for C$_{38}$H$_{58}$BN$_3$O$_4$Sr): C, 63.58 (63.45); H, 8.26 (8.13); N, 5.79 (5.84) %.

Sr(CzOx^{Me2})$_2$ (15). To a stirred suspension of **5** (0.30 g, 0.59 mmol) in THF (20 cm^3) a suspension of SrI$_2$ (0.10 g, 0.30 mmol) in THF (20 cm^3) was added dropwise at room temperature and stirred for 16 h. The solvent was removed *in vacuo* and the product extracted into dichloromethane (30 cm^3). The solvent was removed *in vacuo* to yield the final product as a yellow powder (0.12 g, 0.12 mmol, 41%). ^{1}H NMR (CD$_2$Cl$_2$, 300.3 MHz, 293 K): δ 8.40 (2H, d, ^4J = 2.1 Hz, C$_5$–H), 8.21 (2H, d, ^4J = 2.1 Hz, C$_3$–H), 4.00 (4H, s, CH$_2$), 1.49 (18H, s, (CH$_3$)$_3$) and 1.13 (12H, s, (CH$_3$)$_2$) ppm. ^{13}C{^{1}H} NMR (CD$_2$Cl$_2$, 75.5 MHz, 293 K): δ 166.0 (C$_7$), 149.3 (C$_1$), 137.5 (C$_4$), 128.0 (C$_2$), 126.3 (C$_3$), 121.1 (C$_5$), 110.4 (C$_6$), 78.3 (CH$_2$), 68.8 (C(CH$_3$)$_2$), 34.9 (C(CH$_3$)$_3$), 32.4 (C(CH$_3$)$_3$) and 28.9 (C(CH$_3$)$_2$) ppm. IR (NaCl plates, Nujol mull, cm$^-$

^{1}): 1632 (w), 1603 (s), 1299 (w), 1282 (w), 1260 (m), 1221 (w), 1160 (m), 1060 (m), 1025 (w), 802 (w). EI-MS: *m/z* = 473 (75% $[HCzOx^{Me2}]^{+}$), 458 (100). Anal. found (calcd. for $C_{60}H_{76}N_6O_4Sr$): C, 69.90 (69.77); H, 7.68 (7.42); N, 8.01 (8.14) %.

Y(CzOx^{Me2})(BD$_4$)$_2$(THF) (16-*d*$_8$). To a stirred suspension of **5** (0.22 g, 0.43 mmol) in THF (30 cm^3) cooled to -78 °C, a stirred solution of $Y(BD_4)_3(THF)_2$ (0.12 g, 0.43 mmol) in THF (30 cm^3) was added dropwise with stirring. The suspension was gradually warmed to room temperature and stirred for 5 min. The volatiles were removed *in vacuo* and the product extracted into toluene (50 cm^3). The toluene was removed *in vacuo* and product washed with pentane (20 cm^3) to yield the final product as an yellow powder (0.13 g, 0.21 mmol, 50%). ^{1}H NMR (THF-*d*$_8$, 400.1 MHz, 298 K): δ 8.54 (4H, app s, overlapping C_3–H and C_5–H), 3.46 (4H, s, CH_2),1.51 (12H, s, (CH_3)$_2$) and 1.46 (18H, s, (CH_3)$_3$) ppm.^{2}H NMR (C_6H_6, 76.7 MHz, 298 K): δ 1.58 (app. s, BD_4) ppm. ^{13}C{^{1}H} NMR (THF-*d*$_8$, 100.4 MHz, 298 K): δ 168.7 (C_7), 147.0 (C_1), 140.6 (C_4), 127.3 (C_2), 126.8 (C_3 or C_5), 122.4 (C_3 or C_5), 110.0 (C_6), 78.9 (CH_2), 69.8 (C(CH$_3$)$_2$), 34.7 (C(CH$_3$)$_3$), 32.1 (C(CH$_3$)$_3$) and 27.2 ((CH$_3$)$_2$) ppm. ^{11}B NMR (THF-*d*$_8$, 128.4 MHz, 298 K): δ -22.1 (s, BD_4) ppm. IR (NaCl plates, Nujol mull, cm^{-1}): 1859 (br), 1632 (w), 1585 (s), 1310 (w), 1290 (w), 1258 (m), 1176 (m), 1076 (m), 1035 (m), 813 (w). IR (NaCl cell, THF, ν(B−D), cm^{-1}): 1842 (br s, B−D_t stretching); ν_D/ν_H = 0.75, 1668 and 1587 (br d, B−D_t stretching, 81 cm^{-1} splitting); ν_D/ν_H = 0.75 and 0.73. EI-MS: *m/z* = 599 (20%, $[M]^{+}$), 580 (35, $[Y(CzOx^{Me2})(BD_4)]^{+}$), 458 (65), 375 (80), 57 (100).

La(CzOx^{Me2})(BH$_4$)$_2$(THF) (17). To a stirred suspension of **5** (0.30 g, 0.59 mmol) in THF (30 cm^3) cooled to -78 °C, a stirred solution of $La(BH_4)_3(THF)_3$ (0.22 g, 0.56 mmol) in THF (30 cm^3) was added dropwise with stirring. The suspension was gradually warmed to room temperature and stirred for 5 min. The volatiles were removed *in vacuo* and the product extracted into toluene (50 cm^3). The toluene was removed *in vacuo* and product washed with pentane (20 cm^3) to yield the final product as an yellow powder (0.21 g, 0.30 mmol, 53%). ^{1}H NMR (C_6D_6, 400.1 MHz, 298 K): δ 8.61 (2H, d, ^{4}J = 2.2 Hz, C_5–H), 8.59 (2H, d, ^{4}J = 2.2 Hz, C_3–H), 3.47 (4H, s, CH_2), 3.33 (4H, br t, ^{3}J = 6.0 Hz, OCH_2CH_2), 2.62-1.74 (8H, br m, BH_4), 1.54 (12H, s, C(CH_3)$_2$), 1.47 (18H, s, C(CH_3)$_3$) and 0.76 (4H, br t, ^{3}J = 6.0 Hz, OCH_2CH_2) ppm. ^{13}C{^{1}H} NMR (C_6D_6, 100.4 MHz, 298 K): δ 168.5 (C_7), 147.0 (C_1), 139.7 (C_4),

127.6 ($\underline{C}_2$), 127.3 ($\underline{C}_5$), 122.2 ($\underline{C}_3$), 110.2 ($\underline{C}_6$), 78.8 ($\underline{C}H_2$), 71.1 ($\underline{C}(CH_3)_2$), 68.8 ($O\underline{C}H_2CH_2$), 34.1 ($\underline{C}(CH_3)_3$), 32.1 ($C(\underline{C}H_3)_3$), 27.7 (($\underline{C}H_3)_2$) and 25.0 ($OCH_2\underline{C}H_2$) ppm. ^{11}B NMR (C_6D_6, 128.4 MHz, 298 K): δ -17.6 (br q, ^1J = 78.3, $\underline{B}H_4$) ppm. IR (NaCl plates, Nujol mull, cm^{-1}): 2427 (s, B-H_t stretching), 2220 and 2174 (d, B-H_b stretching, 46 cm^{-1} splitting), 1585 (s), 1363 (m), 1306 (w), 1286 (w), 1167 (s), 1072 (m), 885 (w), 772 (w). IR (NaCl cell, THF, ν(B−H), cm^{-1}): 2434 (s, B–H_t stretching), 2223 and 2171 (d, B–H_b stretching, 52 cm^{-1} splitting), 1632 (w), 1648 (w), 1590 (w). EI-MS: *m/z* = 498 (85%), 485 (95), 398 (100). Anal. found (calcd. for $C_{34}H_{54}B_2N_3O_3La$): C, 57.30 (57.25); H, 7.71 (7.63); N, 5.73 (5.89) %.

Sm(CzOx^{Me2})(BH$_4$)$_2$(THF) (18). To a stirred suspension of **5** (0.37 g, 0.72 mmol) in THF (30 cm^3) cooled to -78 °C, a stirred solution of $Sm(BH_4)_3(THF)_3$ (0.28 g, 0.69 mmol) in THF (30 cm^3) was added dropwise with stirring. The suspension was gradually warmed to room temperature and stirred for 5 min. The volatiles were removed *in vacuo* and the product extracted into toluene (50 cm^3). The toluene was removed *in vacuo* and product washed with pentane (20 cm^3) to yield the final product as a yellow powder (0.25 g, 0.36 mmol, 53%). ^{1}H NMR (C_6D_6, 400.1 MHz, 298 K): δ 8.71 (2H, app s, C_5–H), 8.53 (2H, app s, C_3–H), 3.63 (4H, app s, $OC\underline{H}_2CH_2$), 3.06 (4H, s, $C\underline{H}_2$), 1.52 (18H, s, $C(C\underline{H}_3)_3$), 1.02 (12H, s, $C(C\underline{H}_3)_2$), 0.84 (4H, app s, $OCH_2C\underline{H}_2$) and -4.21 (8H, br app s, $B\underline{H}_4$) ppm. ^{13}C{^{1}H} NMR (C_6D_6, 100.4 MHz, 298 K): δ 166.3 ($\underline{C}_7$), 150.0 ($\underline{C}_1$), 140.2 ($\underline{C}_4$), 127.5 ($\underline{C}_2$), 126.3 ($\underline{C}_7$), 122.5 ($\underline{C}_7$), 110.0 ($\underline{C}_6$), 77.0 ($\underline{C}H_2$), 72.3 ($\underline{C}(CH_3)_2$), 68.2 ($O\underline{C}H_2CH_2$), 34.9 ($\underline{C}(CH_3)_3$), 32.1 ($C(\underline{C}H_3)_3$), 27.1 ($OCH_2\underline{C}H_2$) and 24.9 (($\underline{C}H_3)_2$) ppm. ^{11}B NMR (C_6D_6, 128.4 MHz, 298 K): δ -26.3 (br app s, $\underline{B}H_4$) ppm. IR (NaCl plates, Nujol mull, cm^{-1}): 2444 (s, B-H_t stretching), 2215 and 2182 (s, B-H_b stretching, 33 cm^{-1} splitting), 1632 (w), 1585 (m), 1307 (m), 1257 (w), 1172 (m), 884 (w). IR (NaCl cell, THF, ν(B−H), cm^{-1}): 2444 (s, B–H_t stretching), 2230 and 2184 (d, B–H_b stretching, 46 cm^{-1} splitting) 1633 (m), 1591 (s). EI-MS: *m/z* = 513 (35%), 458 (40), 401 (100). Anal. found (calcd. for $C_{34}H_{54}B_2N_3O_3Sm$): C, 55.93 (56.34); H, 7.18 (7.51); N, 5.93 (5.80) %.

Y(BD$_4$)$_3$(THF)$_2$ (20). To a stirred THF suspension (50 cm^3) of YCl_3 (1.29 g, 6.61 mmol) a stirred THF suspension (50 cm^3) of $NaBD_4$ (0.97 g, 23.17 mmol) was added dropwise at 25 °C. The mixture was heated to 65 °C for 72 h, followed by removal of the solvent *in vacuo*. The product was extracted into benzene (3 × 50 cm^3) and

filtered. The solvent was removed *in vacuo* and the resultant oily residue was exposed to reduced pressure for 16 h to yield the product as a white powder (1.27 g, 4.40 mmol, 66%). ^{1}H NMR (C_6D_6, 400.1 MHz, 298 K): δ 3.78 (8H, br t, ^{3}J = 6.0 Hz, OC$\underline{H}_2$CH$_2$) and 1.10 (8H, br t, ^{3}J = 6.0 Hz, OCH$_2$C$\underline{H}_2$) ppm.^{2}H NMR (C_6H_6, 76.7 MHz, 298 K): δ 1.13 (app. br d, $^{2}J_{YD}$ = 15.5 Hz, B$\underline{D}_4$) ppm. ^{13}C{^{1}H} NMR (C_6D_6, 100.4 MHz, 298 K): δ 72.9 (O$\underline{C}$H$_2$CH$_2$) and 25.1 (OCH$_2\underline{C}$H$_2$) ppm. ^{11}B NMR (C_6D_6, 128.4 MHz, 298 K): δ -24.1 (s, $\underline{B}$D$_4$) ppm. IR (NaCl plates, Nujol mull, cm^{-1}): 2474 (w), 2184 (w), 1857 (s), 1626 (m), 1564 (m), 1455 (s), 1347 (w), 1299 (w), 1251 (w), 1178 (w), 1041 (w), 1008 (m), 834 (m), 669 (w). IR (NaCl cell, THF, ν(B−D), cm^{-1}): 1966 (s), 1811 (s), 1559 and 1398 (br, shoulder splitting 161 cm^{-1}). EI-MS: *m/z* = 71 (100 [THF-H]$^{+}$). Anal. found (calcd. for $C_8H_{16}D_{12}B_3O_2Y$): C, 33.08 (33.17); H, 13.83 (13.91) %.

NMR tube scale synthesis of Ca(CzOx^{Me2})(OBn) (10)/B(OBn)$_3$ and Ca(CzOx^{Me2}){B(OBn)$_4$} (21). A THF-d_8 solution (0.5 cm^3) of Ca(CzOx^{Me2})(BH$_4$)(THF)$_2$ (**13**) (20 mg, 0.03 mmol) in an NMR tube equipped with a J. Young Teflon valve was treated with benzaldehyde (13.6 μL, 0.13 mmol) at RT. ^{1}H and ^{11}B NMR spectroscopy showed a mixture of **10**/B(OBn)$_3$ and **21**. The ^{1}H and ^{13}C{^{1}H} NMR gave a complex mixture of products. ^{11}B NMR (THF-d_8, 128.4 MHz, 298 K): δ 18.8 (s, $\underline{B}$(OBn)$_3$) and 3.9 (s, $\underline{B}$(OBn)$_4$) ppm.

NMR tube scale synthesis of Sr(CzOx^{Me2})(OBn) (22)/B(OBn)$_3$ and Sr(CzOx^{Me2}){B(OBn)$_4$} (23). A THF-d_8 solution (0.5 cm^3) of Sr(CzOx^{Me2})(BH$_4$)(THF)$_2$ (**14**) (30 mg, 0.04 mmol) in an NMR tube equipped with a J. Young Teflon valve was treated with benzaldehyde (19.1 μL, 0.19 mmol) at RT. The ^{1}H and ^{13}C{^{1}H} NMR gave a complex mixture of products. ^{11}B NMR spectroscopy showed **23**. ^{11}B NMR (THF-d_8, 128.4 MHz, 298 K): δ 3.8 (s, $\underline{B}$(OBn)$_4$) ppm.

NMR tube scale synthesis of Y(CzOx^{Me2})(OBn)$_2$ (24)/2 B(OBn)$_3$, Y(CzOx^{Me2})(OBn){B(OBn)$_4$}/B(OBn)$_3$ (25) and Y(CzOx^{Me2}){B(OBn)$_4$}$_2$ (26). A C_6D_6 solution (0.5 cm^3) of Y(CzOx^{Me2})(BH$_4$)$_2$(THF) (**16**) (30 mg, 0.05 mmol) in an NMR tube equipped with a J. Young Teflon valve was treated with benzaldehyde (46.0 μL, 0.45 mmol) at RT. ^{1}H and ^{11}B NMR spectroscopy showed a mixture of

24/B(OBn)$_3$ and **25**. The ^{1}H and ^{13}C{^{1}H} NMR gave a complex mixture of products. ^{11}B NMR (C_6D_6, 128.4 MHz, 298 K) δ 18.9 (s, $\underline{B}$(OBn)$_3$) and 4.5 (s, (OBn){$\underline{B}$(OBn)$_4$}) ppm.

NMR tube scale synthesis of La(CzOx^{Me2})(OBn)$_2$ (27)/2 B(OBn)$_3$, La(CzOx^{Me2})(OBn){B(OBn)$_4$}/B(OBn)$_3$ (28) and La(CzOx^{Me2}){B(OBn)$_4$}$_2$ (29). A C_6D_6 solution (0.5 cm^3) of La(CzOx^{Me2})(BH$_4$)$_2$(THF) (**17**) (30 mg, 0.04 mmol) in an NMR tube equipped with a J. Young Teflon valve was treated with benzaldehyde (42.7 μL, 0.42 mmol) at RT. ^{1}H and ^{11}B NMR spectroscopy showed a mixture of **27**/B(OBn)$_3$ and **28**. The ^{1}H and ^{13}C{^{1}H} NMR gave a complex mixture of products. ^{11}B NMR (C_6D_6, 128.4 MHz, 298 K): δ 18.9 (s, $\underline{B}$(OBn)$_3$) and 4.3 (s, (OBn){$\underline{B}$(OBn)$_4$}) ppm.

NMR tube scale synthesis of Sm(CzOx^{Me2})(OBn)$_2$ (30)/2 B(OBn)$_3$, Sm(CzOx^{Me2})(OBn){B(OBn)$_4$}/B(OBn)$_3$ (31) and Sm(CzOx^{Me2}){B(OBn)$_4$}$_2$ (32). A C_6D_6 solution (0.5 cm^3) of Sm(CzOx^{Me2})(BH$_4$)$_2$(THF) (**18**) (30 mg, 0.04 mmol) in an NMR tube equipped with a J. Young Teflon valve was treated with benzaldehyde (42.0 μL, 0.41 mmol) at RT. ^{1}H and ^{11}B NMR spectroscopy showed a mixture of **30**/B(OBn)$_3$ and **31**. The ^{1}H and ^{13}C{^{1}H} NMR gave a complex mixture of products. ^{11}B NMR (C_6D_6, 128.4 MHz, 298 K): δ 18.9 (s, $\underline{B}$(OBn)$_3$) and 1.3 (s, (OBn){$\underline{B}$(OBn)$_4$}) ppm.

5.6 Experimental details and characterising data for Chapter Four

(*S*,*S*)-Li(CzOx^{iPr}) ((*S*,*S*)-33). To a stirred solution of **(*S*,*S*)-1.46** (0.20 g, 0.40 mmol) in THF (30 cm^3) cooled to -78 °C, a 1.6 M hexanes solution of ^{n}BuLi (0.27 cm^3, 0.44 mmol) was added dropwise with stirring. The solution was gradually warmed to room temperature and stirred for 1 h. The solvent was removed *in vacuo*. The crude product was washed with pentane (10 cm^3) and dried under reduced pressure to afford the product as a yellow powder (0.14 g, 0.28 mmol, 69%). Diffraction-quality crystals were grown from a saturated pentane solution. ^{1}H NMR (C_6D_6, 400.1 MHz, 298 K): δ 8.72 (2H, d, ^4J = 2.1 Hz, $\underline{C}_5$–$\underline{H}$), 8.43 (2H, d, ^4J = 2.1 Hz, C_3–$\underline{H}$), 4.25 (2H, app t, ^2J = 9.8 Hz, ^2J = 8.3 Hz, *cis*-C$\underline{H}_2$), 3.70 (2H, app t, ^2J = 8.3 Hz, *trans*-C$\underline{H}_2$), 3.24-3.16 (2H, m, C$\underline{H}$(CH(CH$_3$)$_2$)), 1.52 (18 H, s, (C$\underline{H}_3$)$_3$), 0.92-0.87 (2H, m, C$\underline{H}$(CH$_3$)$_2$), 0.25 (6H, d, ^3J = 6.7 Hz, CH(C$\underline{H}_3$)$_A$) and 0.15 (6H, d, ^3J = 6.7 Hz, CH(C$\underline{H}_3$)$_B$) ppm. ^{13}C{^{1}H}

NMR (C_6D_6, 100.6 MHz, 299 K): δ 167.2 ($\underline{C}_7$), 150.2 ($\underline{C}_1$), 137.6 ($\underline{C}_4$), 128.1 ($\underline{C}_2$), 123.7 ($\underline{C}_3$), 120.1 ($\underline{C}_5$), 112.9 ($\underline{C}_6$), 71.7 ($\underline{C}H(CH(CH_3)_2)$), 70.8 ($\underline{C}H_2$), 34.7 ($\underline{C}(CH_3)_3$), 33.0 ($C(\underline{C}H_3)_3$), 32.4 ($\underline{C}H(CH_3)_2$), 18.8 ($CH(\underline{C}H_3)_B$) and 17.4 ($CH(\underline{C}H_3)_A$) ppm. ^{7}Li NMR ($C_6D_6$, 155.5 MHz, 300 K): δ 4.0 (N–$\underline{Li}$) ppm. IR (NaCl plates, Nujol mull, cm^{-1}): 1642 (s), 1619 (w), 1362 (m), 1259 (m), 1178 (m), 1070 (w), 1027 (m), 800 (w). EI-MS: *m/z* = 507 (60% $[M]^+$), 492 (70), 458 (75), 207 (95), 75 (100). Anal. found (calcd. for $C_{32}H_{42}N_3O_2Li$): C, 75.55 (75.71); H, 8.48 (8.34); N, 8.36 (8.28) %.

(*S*,*S*)-K(CzOx$^{i\mathrm{Pr}}$) ((*S*,*S*)-34). To a stirred solution of **(*S*,*S*)-1.46** (1.00 g, 2.0 mmol) in THF (20 cm^3) a stirred suspension of $KN(SiMe_3)_2$ (0.50 g, 2.4 mmol) in THF (20 cm^3) was added dropwise at -78 ^oC. The suspension was gradually warmed to room temperature and stirred for 1 h. The volatiles were removed *in vacuo* and the residue washed with toluene (30 cm^3) followed by pentane (30 cm^3) to yield the final product as a yellow powder (0.85 g, 1.6 mmol, 79%). Due to poor solubility, a satisfactory ^1H or $^{13}C\{^1H\}$ NMR spectra could not be obtained for **(*S*,*S*)-34.** IR (NaCl plates, Nujol mull, cm^{-1}): 1631 (m), 1599 (s), 1361 (m), 1294 (m), 1261 (s), 1246 (m), 1207 (w), 1176 (s), 1068 (w), 1038 (m), 1006 (m). EI-MS: *m/z* = 501 (45% [(*S*,*S*)-HCzOx$^{i\mathrm{Pr}}$]$^+$), 458 (80), 207 (100). Anal. found (calcd. for $C_{32}H_{42}N_3O_2K$): C, 71.01 (71.20); H, 7.94 (7.84); N 7.64 (7.78) %.

(*R*,*R*)-K(CzOx$^{i\mathrm{Pr}}$) ((*R*,*R*)-34). To a stirred solution of **(*R*,*R*)-1.46** (1.00 g, 2.0 mmol) in THF (20 cm^3) a stirred suspension of $KN(SiMe_3)_2$ (0.50 g, 2.4 mmol) in THF (20 cm^3) was added dropwise at -78 ^oC. The suspension was gradually warmed to room temperature and stirred for 1 h. The volatiles were removed *in vacuo* and the residue washed with toluene (30 cm^3) followed by pentane (30 cm^3) to yield the final product as a yellow powder (0.81 g, 1.5 mmol, 75%). Due to poor solubility, a satisfactory ^1H or $^{13}C\{^1H\}$ NMR spectra could not be obtained for **(*R*,*R*)-34**. IR (NaCl plates, Nujol mull, cm^{-1}): 1603 (m), 1599 (s), 1293 (m), 1261 (m), 1207 (w), 1175 (m), 1068 (m), 1037 (m), 1005 (m), 930 (w), 884 (m), 836 (w), 777 (m), 632 (w). EI-MS: *m/z* = 508 (60%), 458 (100). Anal. found (calcd. for $C_{32}H_{42}N_3O_2K$): C, 71.04 (71.20); H, 7.98 (7.84); N 7.58 (7.78) %.

(*S*,*S*)-Mg(CzOx$^{i\mathrm{Pr}}$)(BH_4)(THF) ((*S*,*S*)-35). To a stirred solution of $Mg(BH_4)_2$ (0.30 g, 0.56 mmol) in THF (20 cm^3) a stirred suspension of **(*S*,*S*)-34** (0.045 g, 0.83 mmol) in THF (20 cm^3) was added dropwise at -78 ^oC. The suspension was gradually warmed

to room temperature and stirred for 4 h. The solvent was removed *in vacuo* and the product extracted into hot toluene (3 × 20 cm^3). The solvent was removed *in vacuo* and the product was washed with pentane (10 cm^3) at 0 °C to yield the final product as an orange-yellow powder (0.15 g, 0.24 mmol, 43%). ^{1}H NMR (THF-d_8, 300.3 MHz, 293 K): δ 8.35 (2H, d, ^4J = 2.0 Hz, C_5–H), 7.98 (2H, d, ^4J = 2.0 Hz, C_3–H), 4.99-4.86 (2H, m, CH(CH(CH_3)$_2$)), 4.52 (2H, dd, ^2J = 8.8 Hz, ^3J = 3.4 Hz, *trans*-CH_2), 4.28 (2H, app t, ^2J = 9.0 Hz, *cis*-CH_2), 2.62-2.48 (2H, m, CH(CH_3)$_2$), 1.42 (18H, s, (CH_3)$_3$), 0.95 (6H, d, ^3J = 7.0 Hz, CH(CH_3)$_A$) and 0.66 (6H, d, ^3J = 7.0 Hz, CH(CH_3)$_B$) ppm. Signals corresponding to BH_4 were not observed. ^{13}C{^{1}H} NMR (THF-d_8, 75.5 MHz, 293 K): δ 168.2 (C_7), 149.1 (C_1), 138.2 (C_4), 127.2 (C_2), 123.6 (C_3), 121.9 (C_5), 108.6 (C_6), 70.5 (CH(CH(CH_3)$_2$)), 66.9 (CH_2), 35.0 ($C(CH_3)_3$), 32.3 (C(CH_3)$_3$), 30.6 (CH(CH_3)$_2$), 19.3 (CH(CH_3)$_A$) and 14.1 (CH(CH_3)$_B$) ppm. ^{11}B NMR (THF-d_8, 128.4 MHz, 298 K): δ -38.0 (q, $^1J_{BH}$ = 80.0 Hz, BH_4) ppm. IR (NaCl plates, Nujol mull, cm^{-1}): 2269 (br s, B–H stretching), 1636 (w), 1594 (m), 1365 (m), 1316 (w), 1266 (s), 1214 (m), 1191 (m), 1126 (w), 1077 (m), 881 (w), 780 (w), 733 (w). IR (NaCl cell, THF, ν(B−H), cm^{-1}): 2394 (s, B–H_t stretching), 2242 and 2173 (d, B–H_b stretching, 69 cm^{-1} splitting), (s, B–H_b stretching). EI-MS: *m/z* = 524 (100%, [(*S*,*S*)-Mg(CzOx$^{i\text{Pr}}$)]$^+$). Anal. found (calcd. for $C_{36}H_{54}BN_3O_3Mg$): C, 70.49 (70.66); H, 8.96 (8.89); N, 7.05 (6.87) %.

(*R*,*R*)-Mg(CzOx$^{i\text{Pr}}$)(BH_4)(THF) ((*R*,*R*)-35). To a stirred solution of $Mg(BH_4)_2$ (0.30 g, 0.56 mmol) in THF (20 cm^3) a stirred suspension of **(*R*,*R*)-34** (0.045 g, 0.83 mmol) in THF (20 cm^3) was added dropwise at -78 °C. The suspension was gradually warmed to room temperature and stirred for 4 h. The solvent was removed *in vacuo* and the product extracted into hot toluene (3 × 20 cm^3). The solvent was removed *in vacuo* and the product was washed with pentane (10 cm^3) at 0 °C to yield the final product as an orange-yellow powder (0.14 g, 0.23 mmol, 42%). ^{1}H NMR (THF-d_8, 300.3 MHz, 293K): δ 8.38 (2H, d, ^4J = 2.0 Hz, C_5–H), 8.01 (2H, d, ^4J = 2.0 Hz, C_3–H), 4.95-4.89 (2H, m, CH(CH(CH_3)$_2$)), 4.55 (2H, dd, ^2J = 8.7 Hz, ^3J = 3.7 Hz, *trans*-CH_2), 4.31 (2H, app t, ^2J = 9.1 Hz, *cis*-CH_2), 2.59-2.54 (2H, m, (CH(CH_3)$_2$)),1.46 (18H, s, C(CH_3)$_3$), 0.98 (6H, d, ^3J = 7.1 Hz, CH(CH_3)$_A$) and 0.70 (6H, d, ^3J = 7.1 Hz, CH(CH_3)$_B$) ppm. Signals corresponding to BH_4 were not observed. ^{13}C{^{1}H} NMR (THF-d_8, 75.5 MHz, 298K): δ 168.2 (C_7), 149.1 (C_1), 138.2 (C_4), 127.2 (C_2), 123.6 (C_3), 121.9 (C_5), 108.6 (C_6), 70.5 (CH(CH(CH_3)$_2$)), 68.0 (CH_2), 35.0 ($C(CH_3)_3$), 32.3

(C(CH$_3$)$_3$), 30.6 (CH(CH$_3$)$_2$), 19.3 (CH(CH$_3$)$_A$) and 14.1 (CH(CH$_3$)$_B$) ppm. ^{11}B NMR (THF-d_8, 160 MHz, 298K): δ -38.0 (br q, $^1J_{BH}$ = 84.2 Hz, BH$_4$) ppm. IR (NaCl plates, Nujol mull, cm^{-1}): 2390 (br s, B–H stretching), 2151 (br s, B–H stretching), 1638 (m), 1597 (s), 1558 (w), 1319 (w), 1264 (m), 1213 (m), 1188 (m), 1074 (m), 1064 (w), 1011 (w), 956 (w), 882 (w), 781 (w). IR (NaCl cell, THF, ν(B−H), cm^{-1}): 2391 (s, B–H$_t$ stretching), 2255 and 2155 (d, B–H$_b$ stretching, 100 cm^{-1} splitting), 2155 (B–H$_b$ stretching). EI-MS: *m/z* = 539 (80%, [(*R*,*R*)-Mg(CzOx$^{i\text{Pr}}$)BH$_4$]$^+$), 524 (100 [(*R*,*R*)-Mg(CzOx$^{i\text{Pr}}$)]$^+$). Anal. found (calcd. for C$_{36}$H$_{54}$BN$_3$O$_3$Mg): C, 70.46 (70.66); H, 9.05 (8.89); N, 6.68 (6.87) %.

(*S*,*S*)-Ca(CzOx$^{i\text{Pr}}$)(BH$_4$) ((*S*,*S*)-36). To a stirred solution of Ca(BH$_4$)$_2$(THF)$_2$ (0.14 g, 0.67 mmol) in THF (20 cm^3) a stirred suspension of **(*S*,*S*)-34** (0.30 g, 0.56 mmol) in THF (20 cm^3) was added dropwise at -78 °C. The suspension was gradually warmed to room temperature and stirred for 4 h. The solvent was removed *in vacuo* and the product extracted into hot toluene (3 × 20 cm^3). The solvent was removed *in vacuo* and the product was washed with pentane (10 cm^3) at 0 °C to yield the final product as a yellow powder (0.18 g, 0.33 mmol, 58%). ^{1}H NMR (THF-d_8, 300.3 MHz, 293 K): δ 8.34 (2H, d, ^4J = 2.0 Hz, C$_5$–H), 8.08 (2H, d, ^4J = 2.0 Hz, C$_3$–H), 4.77-4.70 (2H, m, CH(CH(CH$_3$)$_2$)), 4.48 (2H, dd, ^2J = 8.8 Hz, ^3J = 4.5 Hz, *trans*-CH$_2$), 4.28 (2H, app t, ^2J = 9.2 Hz, *cis*-CH$_2$), 2.60-2.50 (2H, m, CH(CH$_3$)$_2$), 1.45 (18H, s, C(CH$_3$)$_3$), 0.99 (6H, d, ^3J = 7.0 Hz, CH(CH$_3$)$_A$) and 0.76 (6H, d, (6H, d, ^3J = 7.0 Hz, CH(CH$_3$)$_B$) ppm. Signals corresponding to BH$_4$ were not observed. ^{13}C{^{1}H} NMR (THF-d_8, 75.5 MHz, 293 K): δ 167.9 (C$_7$), 149.4 (C$_1$), 136.9 (C$_4$), 127.8 (C$_2$), 124.8 (C$_3$), 121.2 (C$_5$), 109.7 (C$_6$), 71.6 (CH(CH(CH$_3$)$_2$)), 66.6 (CH$_2$), 34.8 (C(CH$_3$)$_3$), 32.3 (C(CH$_3$)$_3$), 31.3 (CH(CH$_3$)$_2$), 19.4 (CH(CH$_3$)$_A$) and 14.3 (CH(CH$_3$)$_B$) ppm. ^{11}B NMR (THF-d_8, 160 MHz, 298 K): δ -37.0 (q, $^1J_{BH}$ = 82.2 Hz, BH$_4$) ppm. IR (NaCl plates, Nujol mull, cm^{-1}): 2315 (br s, B–H stretching), 2200 (br s, B–H stretching), 1633 (w), 1597 (m), 1303 (w), 1288 (w), 1261 (m), 1208 (w), 1178 (m), 1074 (m), 1015 (w), 884 (w), 777 (w). IR (NaCl cell, THF, ν(B−H), cm^{-1}): 2384 (s, B-H$_t$ stretching), 2251 and 2180 (d, B-H$_b$ stretching, 71 cm^{-1} splitting). EI-MS: *m/z* = 540 (35% [(*S*,*S*)-Ca(CzOx$^{i\text{Pr}}$)]$^+$), 501 (50 [(*S*,*S*)-HCzOx$^{i\text{Pr}}$]$^+$), 458 (100). Anal. found (calcd. for C$_{32}$H$_{46}$BN$_3$O$_2$Ca): C, 69.07 (69.17); H, 8.23 (8.35); N, 7.66 (7.56) %.

(*R*,*R*)-Ca(CzOx^{iPr})(BH$_4$) ((*R*,*R*)-36). To a stirred solution of $Ca(BH_4)_2(THF)_2$ (0.18 g, 0.83 mmol) in THF (20 cm^3) a stirred suspension of **(*R*,*R*)-34** (0.30 g, 0.56 mmol) in THF (20 cm^3) was added dropwise at -78 ^{o}C. The suspension was gradually warmed to room temperature and stirred for 4 h. The solvent was removed *in vacuo* and the product extracted into hot toluene (3 × 20 cm^3). The solvent was removed *in vacuo* and the product was washed with pentane (10 cm^3) at 0 °C to yield the final product as a yellow powder (0.19 g, 0.35 mmol, 62%). ^{1}H NMR (THF-d_8, 300.3 MHz, 293K): δ 8.34 (2H, d, ^4J = 2.0 Hz, C_5–H), 8.08 (2H, d, ^4J = 2.0 Hz, C_3–H), 4.76-4.70 (2H, m, CH(CH(CH$_3$)$_2$)), 4.48 (2H, dd, ^2J = 8.7 Hz, ^3J = 4.6 Hz, *trans*-CH$_2$), 4.28 (2H, dd , ^2J = 9.6 Hz, ^3J = 8.9 Hz, *cis*-CH$_2$), 2.60-2.50 (2H, m, CH(CH$_3$)$_2$), 1.45 (18H, s, C(CH$_3$)$_3$), 0.98 (6H, d, ^3J = 7.0 Hz, CH(CH$_3$)$_A$) and 0.76 (6H, d, (6H, d, ^3J = 7.0 Hz, CH(CH$_3$)$_B$) ppm. Signals corresponding to BH$_4$ were not observed. ^{13}C{^{1}H} NMR (THF-d_8, 75.5 MHz, 293K): δ 167.9 (C_7), 149.5 (C_1), 137.0 (C_4), 127.8 (C_2), 124.8 (C_3), 121.2 (C_5), 109.8 (C_6), 71.7 (CH(CH(CH$_3$)$_2$)), 66.7 (CH$_2$), 34.9 (C(CH$_3$)$_3$), 32.3 (C(CH$_3$)$_3$), 31.3 (CH(CH$_3$)$_2$), 19.4 (CH(CH$_3$)$_A$) and 14.3 (CH(CH$_3$)$_B$) ppm. ^{11}B NMR (THF-d_8, 160 MHz, 298K): δ -36.7 (q, $^1J_{BH}$ = 82.2 Hz, BH$_4$) ppm. IR (NaCl plates, Nujol mull, cm^{-1}): 2313 (br s, B–H stretching), 2198 (br s, B–H stretching), 1632 (m), 1597 (s), 1287 (w), 1261 (m), 1208 (w), 1178 (s), 1072 (s), 1009 (m), 955 (w), 883 (m), 778 (w), 734 (w), 633 (w). IR (NaCl cell, THF, ν(B−H), cm^{-1}): 2383 (s, B–H$_t$ stretching), 2252 and 2180 (d, B–H$_b$ stretching, 72 cm^{-1} splitting). EI-MS: *m/z* = 540 (35% [(*R*,*R*)-Ca(CzOx^{iPr})]$^+$), 505 (35), 368 (100). Anal. found (calcd. for $C_{32}H_{46}BN_3O_2Ca$): C, 69.07 (69.17); H, 8.42 (8.35); N, 7.50 (7.56) %.

(*S*,*S*)-Mg(CzOx^{iPr}){N(SiMe$_3$)$_2$} ((*S*,*S*)-37). To a stirred solution of $Mg\{N(SiMe_3)_2\}_2$ (0.21 g, 0.60 mmol) in toluene (30 cm^3) a stirred solution of **(*S*,*S*)-1.46** (0.30 g, 0.60 mmol) in toluene (30 cm^3) was added dropwise and stirred for 16 h. The solvent was removed *in vacuo* and the product washed with pentane cooled to 0 °C (15 cm^3) to yield the final product as a yellow powder (0.36 g, 0.52 mmol, 86%). ^{1}H NMR (C_6D_6, 400.1 MHz, 298 K): δ 8.58 (2H, d, ^4J = 1.4 Hz, C_5–H), 8.44 (2H, d, ^4J = 1.4 Hz, C_3–H), 4.41-4.35 (2H, m, CH(CH(CH$_3$)$_2$)), 4.06 (2H, dd, ^2J = 8.5 Hz, ^3J = 2.6 Hz, *trans*-CH$_2$), 3.84 (2H, app t, ^2J = 8.8 Hz, *cis*-CH$_2$), 2.50-2.37 (2H, m, (CH(CH$_3$)$_2$)), 1.44 (18H, s, (CH$_3$)$_3$), 0.77 (6H, d, ^3J = 6.9 Hz, CH(CH$_3$)$_A$), 0.70 (6H, d, ^3J = 6.9 Hz, CH(CH$_3$)$_B$) and 0.15 (18H, s, N(Si(CH$_3$)$_3$)$_2$) ppm. ^{13}C{^{1}H} NMR (C_6D_6, 100.4 MHz,

298 K): δ 169.7 ($\underline{C}_7$), 150.0 ($\underline{C}_1$), 139.5 ($\underline{C}_4$), 127.5 ($\underline{C}_2$), 123.9 ($\underline{C}_3$), 123.0 ($\underline{C}_5$), 108.3 ($\underline{C}_6$), 69.5 ($\underline{C}H(CH(CH_3)_2)$), 67.5 ($\underline{C}H_2$), 34.9 ($\underline{C}(CH_3)_3$), 32.3 ($C(\underline{C}H_3)_3$), 31.5 ($C\underline{H}(CH_3)_2$), 19.0 ($CH(\underline{C}H_3)_A$), 14.8 ($CH(\underline{C}H_3)_B$) and 6.1 ($N(Si(\underline{C}H_3)_3)_2$) ppm. IR (NaCl plates, Nujol mull, cm^{-1}): 1636 (m), 1578 (s), 1268 (m), 1239 (w), 1217 (w), 1191 (m), 1076 (m), 1013 (s), 882 (m), 823 (m), 785 (w). EI-MS: *m/z* = 501 (95% [(*S*,*S*)-HCzOx$^{i\text{Pr}}$]$^+$), 458 (100). It was not possible to obtain an elemental analysis for **(*S*,*S*)-37**.

(*S*,*S*)-Ca(CzOx$^{i\text{Pr}}$){N(SiMe$_3$)$_2$}(THF) ((*S*,*S*)-38). To a stirred solution of Ca{N(SiMe$_3$)$_2$}$_2$(THF)$_2$ (0.30 g, 0.60 mmol) in toluene (30 cm^3) a stirred solution of **(*S*,*S*)-1.46** (0.30 g, 0.60 mmol) in toluene (30 cm^3) was added dropwise and stirred for 16 h. The solvent was removed *in vacuo* and the product washed with pentane cooled to 0 °C (15 cm^3) to yield the final product as a yellow powder (0.25 g, 0.31 mmol, 54%). ^{1}H NMR (C_6D_6, 400.1 MHz, 299 K): δ 8.66 (2H, d, ^3J = 1.9 Hz,C_5–$\underline{H}$), 8.64 (2H, d, ^3J = 1.9 Hz, C_3–$\underline{H}$), 4.64 (2H, br s, C$\underline{H}$(CH(CH$_3$)$_2$)), 4.11 (2H, dd, ^2J = 8.8 Hz, ^3J = 4.3 Hz, *trans*-C$\underline{H}_2$), 3.96 (2H, app t, ^2J = 8.8 Hz, *cis*-C$\underline{H}_2$) 3.40 (8H, t, ^3J = 6.1 Hz, OC$\underline{H}_2$CH$_2$), 2.57 (2H, br s, C$\underline{H}$(CH$_3$)$_2$), 1.48 (18H, s, C(C$\underline{H}_3$)$_3$), 1.11 (8H, t, ^3J = 6.1 Hz, OCH$_2$C$\underline{H}_2$), 0.87 (6H, d, ^3J = 7.0 Hz, CH(C$\underline{H}_3$)$_A$) 0.70 (6H, d, ^3J = 7.0 Hz, CH(C$\underline{H}_3$)$_B$) and 0.35 (18H, s, N(Si(C$\underline{H}_3$)$_3$)$_2$). ^{13}C{^{1}H} NMR (C_6D_6, 100.4 MHz, 299 K): δ 168.6 ($\underline{C}_7$), 149.7 ($\underline{C}_1$), 137.9 ($\underline{C}_4$), 128.0 ($\underline{C}_2$, overlapping with solvent), 125.5 ($\underline{C}_3$), 121.8 ($\underline{C}_5$), 109.4 ($\underline{C}_6$), 70.8 (O$\underline{C}$H$_2$CH$_2$), 68.5 ($\underline{C}$H(CH(CH$_3$)$_2$)), 66.3 ($\underline{C}$H$_2$), 34.7 (C($\underline{C}$H$_3$)$_3$), 32.3 (C($\underline{C}$H$_3$)$_3$), 31.0 (C$\underline{H}$(CH$_3$)$_2$), 25.4 (OCH$_2$$\underline{C}H_2$), 19.5 (CH($\underline{C}H_3$)$_A$), 14.4 (CH($\underline{C}H_3$)$_B$) and 6.1 (N(Si($\underline{C}H_3$)$_3$)$_2$). IR (NaCl plates, Nujol mull, cm^{-1}): 1635 (w), 1601 (m), 1259 (m), 1175 (m), 1052 (m), 880 (w), 817 (m). EI-MS: *m/z* = 501 (95% [(*S*,*S*)-HCzOx$^{i\text{Pr}}$]$^+$), 458 (100). It was not possible to obtain an elemental analysis for **(*S*,*S*)-38**.

(*S*,*S*)-Mg(CzOx$^{i\text{Pr}}$)I(THF) ((*S*,*S*)-39). To a stirred suspension of MgI_2 (0.206 g, 0.74 mmol) in THF (30cm^3), a stirred suspension of **(*S*,*S*)-34** (0.40 g, 0.74 mmol) in THF (30 cm^3) was added at 0 °C. The suspension was gradually warmed to room temperature and stirred for 3 h. The THF was removed *in vacuo* and the product extracted into toluene (30 cm^3) and filtered. The volatiles were removed *in vacuo*, and the residue washed with pentane (10 cm^3) at 0 °C to yield the final product as a yellow powder (0.362 g, 0.50 mmol, 68%). ^{1}H NMR (C_6D_6, 400.1 MHz, 298 K): δ 8.67 (2H,

d, ^4J = 2.0 Hz, C_5–H), 8.48 (2H, d, ^4J = 2.0 Hz, C_3–H), 5.44-5.38 (2H, m, CH(CH(CH_3)$_2$)), 4.13 (2H, dd, ^2J = 8.7 Hz, ^3J = 3.3 Hz, *trans*-CH_2), 3.77 (2H, app t, ^2J = 9.0 Hz, *cis*-CH_2), 3.26 (4H, dt, ^2J = 22.8 Hz, ^3J = 7.2 Hz, OCH_2CH_2), 2.92 (2H, br t, J = 6.8 Hz, CH(CH_3)$_2$), 1.47 (18H, s, C(CH_3)$_3$), 0.92 (6H, d, J = 7.0 Hz, CH(CH_3)$_B$), 0.80 (4H, t, J = 5.9 Hz, OCH_2CH_2) and 0.62 (6H, d, J = 7.0 Hz, CH(CH_3)$_A$) ppm. $^{13}C\{^1H\}$ NMR (C_6D_6, 100.4 MHz, 298 K): δ 168.2 (C_7), 149.5 (C_1), 139.2 (C_4), 127.3 (C_2), 124.0 (C_3), 122.0 (C_5), 108.7 (C_6), 70.9 (CH(CH(CH_3)$_2$)), 69.3 (OCH_2CH_2), 66.5 (CH_2), 34.8 (C(CH_3)$_3$), 32.3 (C(CH_3)$_3$), 31.1 (CH(CH_3)$_2$), 24.6 (OCH_2CH_2), 19.0 (CH(CH_3)$_B$) and 13.8 (CH(CH_3)$_A$) ppm. IR (NaCl plates, Nujol mull, cm^{-1}): 1637 (w), 1595 (m), 1319 (w), 1263 (m), 1188 (m), 1075 (m), 1011 (w), 882 (w), 805 (w), 634 (w). EI-MS: *m/z* = 723 (5% [(*S*,*S*)-Mg(CzOx$^{i\text{Pr}}$)I(THF)]$^+$), 524 (80 [(*S*,*S*)-Mg(CzOx$^{i\text{Pr}}$)]$^+$), 497 (100). Anal. found (calcd. for $C_{36}H_{50}IN_3O_3Mg$): C 59.59, (59.72); H 7.06, (6.96); N 5.98, (5.80) %.

(*S*,*S*)-Mg(CzOx$^{i\text{Pr}}$)$_2$ ((*S*,*S*)-40). To a stirred solution of **(*S*,*S*)-1.46** (0.30 g, 0.60 mmol) in toluene (30 cm^3) a solution of Mg{N($SiMe_3$)$_2$}$_2$ (0.10 g, 0.30 mmol) in toluene (30 cm^3) was added dropwise at 25 °C. The solution was allowed to stir for 16 h before the volatiles were removed *in vacuo*. The residue was washed with pentane at 0 °C (30 cm^3) to yield the final product as a yellow-brown powder (0.11 g, 0.11 mmol, 36%). ^1H NMR (C_6D_6, 300.3 MHz, 293 K): δ 8.79 (2H, d, ^4J = 2.0 Hz, C_5–H), 8.49 (2H, d, ^4J = 2.0 Hz, C_3–H), 3.76-3.65 (4H, m, overlapping *trans*-CH_2 and CH(CH(CH_3)$_2$)), 3.26 (2H, app t, ^2J = 10.7 Hz, *cis*-CH_2), 1.60-1.53 (2H, m, CH(CH(CH_3)$_2$)), 1.49 (18H, s, C(CH_3)$_3$), 0.40 (6H, d, ^3J = 6.8 Hz, CH(CH_3)$_A$) and -0.21 (6H, d, ^3J = 6.8 Hz, CH(CH_3)$_B$) ppm. $^{13}C\{^1H\}$ NMR (C_6D_6, 75.5 MHz, 293 K): δ 166.8 (C_7), 150.3 (C_1), 137.8 (C_4), 127.4 (C_2), 123.6 (C_3), 121.3 (C_5), 109.4 (C_6), 70.6 (CH(CH(CH_3)$_2$)), 66.8 (CH_2), 34.8 (C(CH_3)$_3$), 32.4 (C(CH_3)$_3$), 30.3 (CH(CH_3)$_2$), 19.9 (CH(CH_3)$_B$) and 14.7 (CH(CH_3)$_A$) ppm. IR (NaCl plates, Nujol mull, cm^{-1}): 1637 (s), 1607 (s), 1363 (m), 1319 (w), 1261 (s), 1209 (m), 1183 (s), 1068 (s), 1005 (m), 973 (w), 954 (w), 882 (m), 782 (m), 634 (w). EI-MS: *m/z* = 1025 (10% [M]$^+$), 501 (80 [(*S*,*S*)-HCzOx$^{i\text{Pr}}$]$^+$), 458 (100). Anal. found (calcd. for $C_{64}H_{84}N_6O_4Mg$): C, 74.75 (74.94); H, 8.15 (8.25); N, 7.99 (8.19) %.

(*S*,*S*)-Ca(CzOx$^{i\text{Pr}}$)$_2$ ((*S*,*S*)-41). To a stirred solution of **(*S*,*S*)-1.46** (0.60 g, 1.19 mmol) in toluene (20 cm^3) a solution of Ca{N($SiMe_3$)$_2$}$_2$(THF)$_2$ (0.30 g, 0.59 mmol) in

toluene (20 cm^3) was added dropwise at 25 °C. The solution was stirred for 16 h and the volatiles removed *in vacuo*. The residue was washed with pentane at 0 °C (30 cm^3) to yield the final product as a yellow powder (0.42 g, 0.40 mmol, 68%). ^{1}H NMR (C_6D_6, 300.3 MHz, 293 K): δ 8.77 (2H, d, ^4J = 2.0 Hz, C_5–H), 8.63 (2H, d, ^4J = 2.0 Hz, C_3–H), 4.06-3.96 (2H, m, CH(CH(CH_3)$_2$)), 3.74 (2H, dd, ^2J = 8.8 Hz, ^3J = 5.7 Hz, *trans*-CH_2), 3.58 (2H, app t, ^2J = 9.4 Hz, *cis*-CH_2), 1.77-1.64 (2H, m, (CH(CH_3)$_2$)), 1.50 (18H, s, C(CH_3)$_3$), 0.44 (6H, d, ^3J = 6.8 Hz, CH(CH_3)$_A$) and 0.03 (6H, d, ^3J = 6.8 Hz, CH(CH_3)$_B$) ppm. ^{13}C{^{1}H} NMR (C_6D_6, 75.5 MHz, 293 K): δ 167.5 (C_7), 150.3 (C_1), 137.4 (C_4), 127.9 (C_2), 125.2 (C_3), 121.6 (C_5), 109.9 (C_6), 71.0 (CH(CH(CH_3)$_2$)), 67.2 (CH_2), 34.7 (C(CH_3)$_3$), 32.4 (C(CH_3)$_3$), 31.5 (CH(CH_3)$_2$), 19.0 (CH(CH_3)$_B$) and 15.6 (CH(CH_3)$_A$) ppm. IR (NaCl plates, Nujol mull, cm^{-1}): 1634 (s), 1605 (s), 1361 (w), 1280 (m), 1258 (m), 1205 (m), 1173 (s), 1065 (w), 1003 (w), 882 (w), 801 (m). EI-MS: *m/z* = 1040 (60% $[M]^+$), 502 (65), 57 (100 $[^tBu]^+$). Anal. found (calcd. for $C_{64}H_{84}N_6O_4Ca$): C, 73.65 (73.81); H, 8.29 (8.13); N, 7.91 (8.07) %.

(*S*,*S*)-Sr(CzOx^{iPr})$_2$ ((*S*,*S*)-42). To a stirred THF solution (20 cm^3) of $Sr(BH_4)_2(THF)_2$ (0.145 g, 0.56 mmol) a THF suspension (30 cm^3) of **(*S*,*S*)-34** (0.30 g, 0.56 mmol) was added at 25 °C and stirred for 16 h. The volatiles were removed *in vacuo* and the product extracted into toluene (30 cm^3) and filtered. The residue was washed with pentane (10 cm^3) at 0 °C to yield the final product as a yellow powder (0.32 g, 0.30 mmol, 53%). ^{1}H NMR (C_6D_6, 400.1 MHz, 298 K): δ 8.76 (2H, d, ^4J = 2.1 Hz, C_5–H), 8.68 (2H, d, ^4J = 2.1 Hz, C_3–H), 4.08-4.02 (2H, m, CH(CH(CH_3)$_2$)), 3.74 (2H, app s, *cis*- or *trans*-CH_2), 3.73-3.71 (2H, m, *cis*- or *trans*-CH_2), 1.71-1.65 (2H, m, (CH(CH_3)$_2$)), 1.51 (18 H, s, C(CH_3)$_3$), 0.48 (6H, d, ^3J = 6.9 Hz, CH(CH_3)$_A$) and 0.23 (6H, d, ^3J = 6.9 Hz, CH(CH_3)$_B$) ppm. ^{13}C{^{1}H} NMR (C_6D_6, 100.4 MHz, 298 K): δ 168.0 (C_7), 150.4 (C_1), 137.1 (C_4), 128.4 (C_2), 125.9 (C_3), 121.5 (C_5), 110.1 (C_6), 71.6 (CH(CH(CH_3)$_2$)), 67.6 (CH_2), 34.7 (C(CH_3)$_3$), 32.4 (C(CH_3)$_3$), 32.1 (CH(CH_3)$_2$), 18.7 (CH(CH_3)$_B$) and 16.6 (CH(CH_3)$_A$) ppm. IR (NaCl plates, Nujol mull, cm^{-1}): 1634 (m), 1604 (s), 1362 (w), 1280 (w), 1259 (m), 1239 (w), 1170 (s), 1066 (m). EI-MS: *m/z* = 1088 (70% $[M]^+$), 501 (75 $[(S,S)$-H– CzOx$^{iPr}]^+$), 458 (100). Anal. found (calcd. for $C_{64}H_{84}N_6O_4Sr$): C, 70.35 (70.59); H, 7.60 (7.77); N, 7.58 (7.72) %.

(*S*,*S*)-La(CzOx^{iPr})(BH$_4$)$_2$ ((*S*,*S*)-44). To a stirred suspension of **(*S*,*S*)-34** (0.31 g, 0.57 mmol) in THF (30 cm^3) cooled to -78 °C, a stirred solution of $La(BH_4)_3(THF)_3$ (0.22

g, 0.55 mmol) in THF (30 cm^3) was added dropwise with stirring. The suspension was gradually warmed to room temperature and stirred for 5 min. The volatiles were removed *in vacuo* and the product extracted into toluene (50 cm^3). The toluene was removed *in vacuo* and product washed with pentane (20 cm^3) to yield the final product as a yellow powder (0.21 g, 0.31 mmol, 57%). ^{1}H NMR (C_6D_6, 400.1 MHz, 298 K): δ 8.52 (2H, app s, C_5–H), 8.43 (2H, app s, C_3–H), 4.68 (2H, br app s, CH(CH(CH_3)$_2$), 3.94 (2H, br dd, ^2J = 8.3 Hz, ^3J = 3.6 Hz, *trans*-CH_2), 3.72 (2H, br t, ^2J = 8.3 Hz, *cis*-CH_2), 2.59 (2H, br app s, CH(CH_3)$_2$), 2.41-1.66 (8H, br m, BH_4), 1.41 (18H, s, C(CH_3)$_3$), 0.68 (6H, d, ^3J = 6.5 Hz, CH(CH_3)$_A$) and 0.68 (6H, d, ^3J = 6.5 Hz, CH(CH_3)$_B$) ppm. ^{13}C{^{1}H} NMR (C_6D_6, 100.4 MHz, 298 K): δ 169.6 (C_7), 147.7 (C_1), 140.0 (C_4), 127.5 (C_2), 125.9 (C_3), 122.4 (C_5), 109.8 (C_6), 71.4 (CH(CH(CH_3)$_2$)), 67.5 (CH_2), 34.7 (C(CH_3)$_3$), 32.1 (C(CH_3)$_3$), 31.7 (CH(CH_3)$_2$), 19.2 (CH(CH_3)$_A$) and 14.3 (CH(CH_3)$_B$) ppm. ^{11}B NMR (C_6D_6, 128.4 MHz, 298 K): δ -18.9 (br app s, BH_4) ppm. IR (NaCl plates, Nujol mull, cm^{-1}): 2430 (s, B-H_t stretching), 2212 and 2152 (d, B-H_b stretching, splitting 60 cm^{-1}),1633 (w), 1595 (s), 1260 (w), 1173 (m), 1075 (m). IR (NaCl cell, THF, ν(B−H), cm^{-1}): 2420 (s, B-H_t stretching), 2238 and 2173 (d, B-H_b stretching, splitting 101 cm^{-1}), 1648 (m), 1599 (w). EI-MS: *m/z* = 501 (65%, [(*S*,*S*)-HCzOx$^{i\mathrm{Pr}}$]$^+$), 470 (90), 415 (100). Anal. found (calcd. for $C_{32}H_{50}B_2N_3O_2La$): C, 57.63 (57.43); H, 7.66 (7.53); N, 6.35 (6.28) %.

(*S*,*S*)-Sm(CzOx$^{i\mathrm{Pr}}$)(BH_4)$_2$ ((*S*,*S*)-45). To a stirred suspension of **(*S*,*S*)-34** (0.35 g, 0.65 mmol) in THF (30 cm^3) cooled to -78 °C, a stirred solution of $Sm(BH_4)_3(THF)_3$ (0.25 g, 0.62 mmol) in THF (30 cm^3) was added dropwise with stirring. The suspension was gradually warmed to room temperature and stirred for 5 min. The volatiles were removed *in vacuo* and the product extracted into toluene (50 cm^3). The toluene was removed *in vacuo* and product washed with pentane (20 cm^3) to yield the final product as an yellow powder (0.29 g, 0.42 mmol, 64%). ^{1}H NMR (C_6D_6, 400.1 MHz, 298 K): δ 8.95 (2H, br app s, C_5–H), 8.69 (2H, br app s, C_3–H), 4.25 (2H, br app s, CH(CH(CH_3)$_2$), 3.71 (2H, br app d, *cis*- or *trans*-CH_2), 3.52 (2H, br app t, *cis*- or *trans*-CH_2), 1.56 (18H, br s, C(CH_3)$_3$), 0.89 (2H, br app s, CH(CH_3)$_2$), 0.48 (6H, br app s, CH(CH_3)$_A$), -0.15 (6H, br app s, CH(CH_3)$_B$) and -5.71 (8H, br app s, BH_4) ppm. ^{13}C{^{1}H} NMR (C_6D_6, 100.4 MHz, 298 K): δ 168.5 (C_7), 152.5 (C_1), 140.7 (C_4), 127.3 (C_2), 126.8 (C_3), 123.3 (C_5), 110.4 (C_6), 72.1 (CH(CH(CH_3)$_2$)), 66.1 (CH_2), 35.0 (C(CH_3)$_3$), 32.2 (C(CH_3)$_3$), 30.5 (CH(CH_3)$_2$), 18.9 (CH(CH_3)$_A$) and 13.0

($CH(\underline{C}H_3)_B$) ppm. ^{11}B NMR (C_6D_6, 128.4 MHz, 298 K): δ -29.6 (br app s, $\underline{B}H_4$) ppm. IR (NaCl plates, Nujol mull, cm^{-1}): 2443 (s, B–H_t stretching), 2211 and 2157 (br d, B–H_b stretching, splitting 54 cm^{-1}), 1633 (w), 1594 (s), 1364 (w), 1285 (w), 1258 (m), 1178 (s), 1076 (m). IR (NaCl cell, THF, ν(B−H), cm^{-1}): 2444 (s, B–H_t stretching), 2223 and 2180 (br d, B–H_b stretching, splitting 43 cm^{-1}), 1634 (s), 1597 (s). EI-MS: *m/z* = 667 (45%, [(*S*,*S*)-Sm($CzOx^{iPr}$)(BH_4)]$^+$), 652 (95), 415 (100). Anal. found (calcd. for $C_{32}H_{50}B_2N_3O_2Sm$): C, 56.23 (56.46); H, 7.53 (7.40); N, 6.03 (6.17) %.

NMR tube scale synthesis of (*S*,*S*)-Mg($CzOx^{iPr}$)(OBn) ((*S*,*S*)-46)/$B(OBn)_3$ and (*S*,*S*)-Mg($CzOx^{iPr}$){$B(OBn)_4$} ((*S*,*S*)-47). A THF-d_8 solution (0.5 cm^3) of (*S*,*S*)-Mg($CzOx^{iPr}$)(BH_4)(THF) (**(*S*,*S*)-35**) (30 mg, 0.05 mmol) in an NMR tube equipped with a J. Young Teflon valve was treated with benzaldehyde (22.4 μL, 0.22 mmol) at RT. ^1H and ^{11}B NMR spectroscopy showed a mixture of **(*S*,*S*)-46**/$B(OBn)_3$ and **(*S*,*S*)-47**. The ^1H and $^{13}C\{^1H\}$ NMR gave a complex mixture of products. ^{11}B NMR (THF-d_8, 128.4 MHz, 298 K): δ 18.8 (s, $\underline{B}(OBn)_3$) and 3.7 (s, $\underline{B}(OBn)_4$) ppm.

NMR tube scale synthesis of (*S*,*S*)-Ca($CzOx^{iPr}$)(OBn) ((*S*,*S*)-48)/$B(OBn)_3$ and (*S*,*S*)-Ca($CzOx^{iPr}$){$B(OBn)_4$} ((*S*,*S*)-49). A THF-d_8 solution (0.5 cm^3) of (*S*,*S*)-Ca($CzOx^{iPr}$)(BH_4) (**(*S*,*S*)-36**) (30 mg, 0.05 mmol) in an NMR tube equipped with a J. Young Teflon valve was treated with benzaldehyde (24.7 μL, 0.24 mmol) at RT. ^1H and ^{11}B NMR spectroscopy showed a mixture of **(*S*,*S*)-48**/$B(OBn)_3$ and **(*S*,*S*)-49**. The ^1H and $^{13}C\{^1H\}$ NMR gave a complex mixture of products. ^{11}B NMR (THF-d_8, 128.4 MHz, 298 K): δ 18.8 (s, $\underline{B}(OBn)_3$) and 3.7 (s, $\underline{B}(OBn)_4$) ppm.

NMR tube scale synthesis of (*S*,*S*)-Y($CzOx^{iPr}$)$(OBn)_2$ ((*S*,*S*)-50)/2 $B(OBn)_3$, (*S*,*S*)-Y($CzOx^{iPr}$)(OBn){$B(OBn)_4$}/$B(OBn)_3$ ((*S*,*S*)-51) and (*S*,*S*)-Y($CzOx^{iPr}$){$B(OBn)_4$}$_2$ ((*S*,*S*)-52). A C_6D_6 solution (0.5 cm^3) of (*S*,*S*)-Y($CzOx^{iPr}$)$(BH_4)_2$(THF) (**(*S*,*S*)-43**) (30 mg, 0.04 mmol) in an NMR tube equipped with a J. Young Teflon valve was treated with benzaldehyde (44.1 μL, 0.43 mmol) at RT. ^1H and ^{11}B NMR spectroscopy showed a mixture of **(*S*,*S*)-50**/$B(OBn)_3$ and **(*S*,*S*)-51**. The ^1H and $^{13}C\{^1H\}$ NMR gave a complex mixture of products. ^{11}B NMR (C_6D_6, 128.4 MHz, 298 K): δ 18.9 (s, $\underline{B}(OBn)_3$) and 4.4 (s, (OBn){$\underline{B}(OBn)_4$}) ppm.

NMR tube scale synthesis of (*S*,*S*)-La(CzOx^{iPr})(OBn)$_2$ ((*S*,*S*)-53)/2 B(OBn)$_3$, (*S*,*S*)-La(CzOx^{iPr})(OBn){B(OBn)$_4$}/B(OBn)$_3$ ((*S*,*S*)-54) and (*S*,*S*)-La(CzOx^{iPr}){B(OBn)$_4$}$_2$ ((*S*,*S*)-55). A C_6D_6 solution (0.5 cm^3) of (*S*,*S*)-La(CzOx^{iPr})(BH$_4$)$_2$ (**(*S*,*S*)-44**) (30 mg, 0.04 mmol) in an NMR tube equipped with a J. Young Teflon valve was treated with benzaldehyde (45.5 μL, 0.45 mmol) at RT. ^{1}H and ^{11}B NMR spectroscopy showed a mixture of **(*S*,*S*)-53**/2 B(OBn)$_3$ and **(*S*,*S*)-54**. The ^{1}H and ^{13}C{^{1}H} NMR gave a complex mixture of products. ^{11}B NMR (C_6D_6, 128.4 MHz, 298 K): δ 18.8 (s, B(OBn)$_3$) and 4.2 (s, (OBn){B(OBn)$_4$}) ppm.

NMR tube scale synthesis of (*S*,*S*)-Sm(CzOx^{iPr})(OBn)$_2$ ((*S*,*S*)-56)/2 B(OBn)$_3$, (*S*,*S*)-Sm(CzOx^{iPr})(OBn){B(OBn)$_4$}/B(OBn)$_3$ ((*S*,*S*)-57) and (*S*,*S*)-Sm(CzOx^{iPr}){B(OBn)$_4$}$_2$ ((*S*,*S*)-58). A C_6D_6 solution (0.5 cm^3) of (*S*,*S*)-Sm(CzOx^{iPr})(BH$_4$)$_2$ (**(*S*,*S*)-45**) (30 mg, 0.04 mmol) in an NMR tube equipped with a J. Young Teflon valve was treated with benzaldehyde (44.8 μL, 0.44 mmol) at RT. ^{1}H and ^{11}B NMR spectroscopy showed a mixture of **(*S*,*S*)-56**/B(OBn)$_3$ and **(*S*,*S*)-57**. The ^{1}H and ^{13}C{^{1}H} NMR gave a complex mixture of products. ^{11}B NMR (C_6D_6, 128.4 MHz, 298 K): δ 18.7 (s, B(OBn)$_3$) and 6.7 (s, (OBn){B(OBn)$_4$}) ppm.

5.7 Polymerisation procedures

General procedure for the polymerisation of *rac*-, *L*-, *D*- and *meso*-LA (without additives). In a dry box, a solution of lactide (0.576 g, 4 mmol) in THF (2 cm^3, at 60 °C or RT) was added rapidly in one portion to a stirred THF solution (2 cm^3, at 60 °C or RT) of catalyst (0.04 mmol). [LA]$_0$:[initiator]$_0$ = 100:1. Aliquots (approx. 0.1 cm^3) were taken at appropriate time intervals and quenched outside the dry box with wet THF (1 cm^3) or inside the dry box with degassed, wet THF (1 cm^3). The volatiles were evaporated to dryness to give PLA. The monomer to polymer % conversion was determined using ^{1}H NMR ($CDCl_3$), and measured by integration of the CHMe resonances of the unreacted monomer and PLA. Aliquots were recovered for GPC and MALDI-ToF MS analyses. The polymerisation experiments were performed twice.

General procedure for the polymerisation of *rac*-, *L*-, *D*- and *meso*-LA (with additives). In a dry box, a solution of lactide (0.576 g, 4 mmol) in THF (2 cm^3, at 60 °C or RT) was added rapidly in one portion to a 5 min stirred THF solution (2 cm^3, at

60 °C or RT) of catalyst (0.04 mmol) and additive. $[LA]_0$:$[initiator]_0$:$[additive]_0$ = 100:1:1, unless otherwise specified. Aliquots (approx. 0.1 cm^3) were taken at appropriate time intervals and quenched outside the dry box with wet THF (1 cm^3) or inside the dry box with degassed, wet THF (1 cm^3). The volatiles were evaporated to dryness to give PLA. The monomer to polymer % conversion was determined using ^1H NMR ($CDCl_3$), and measured by integration of the C<u>H</u>Me resonances of the unreacted monomer and PLA. Aliquots were recovered for GPC and MALDI-ToF MS analyses. The polymerisation experiments were performed twice.

5.8 X-ray data collection and processing parameters

Crystals were mounted on glass fibres using perfluoropolyether oil and cooled rapidly in a stream of cold dinitrogen using an Oxford Cryosystems Cryostream unit. Diffraction data were measured using an Enraf-Nonius KappaCCD diffractometer or Agilent Technologies Supernova diffractometer using Mo-κα or Cu-κα, respectively. As appropriate, absorption and decay corrections were applied to the data and equivalent reflections merged.[11, 12] The structures were solved using SIR92[13] or Superflip[14] and further refinements and all other crystallographic calculations were performed using the CRYSTALS program suite.[15] Other details of the structure solution and refinements are given in the CD Appendix.

5.9 References for Chapter Five

1. A. B. Pangborn, M. A. Giardello, R. H. Grubbs, R. K. Rosen and F. J. Timmers, *Organometallics*, 1996, **15**, 1518-1520.
2. A. Rudin and H. L. W. Hoegy, *J. Polym. Sci. A: Polym. Chem.*, 1972, **10**, 217-235.
3. I. Barakat, P. Dubois, R. Jérôme and P. Teyssié, *J. Polym. Sci. A: Polym. Chem.*, 1993, **31**, 505-514.
4. J. R. Dorgan, J. Janzen, D. M. Knauss, S. B. Hait, B. R. Limoges and M. H. Hutchinson, *J. Polym. Sci. B: Polym. Phys.*, 2005, **43**, 3100-3111.
5. J. Zou, D. J. Berg, D. Stuart, R. McDonald and B. Twamley, *Organometallics*, 2011, **30**, 4958-4967.
6. M. Durán-Galván, S. A. Worlikar and B. T. Connell, *Tetrahedron*, 2010, **66**, 7707-7719.

7. M. Bremer, H. Nöth, M. Thomann and M. Schmidt, *Chem. Ber.*, 1995, **128**, 455-460.
8. U. Mirsaidov, I. B. Shaimuradov and M. Khikmakov, *Russ. J. Inorg. Chem.*, 1986, **5**, 753.
9. S. M. Cendrowski-Guillaume, G. Le Gland, M. Nierlich and M. Ephritikhine, *Organometallics*, 2000, **19**, 5654-5660.
10. Y. Sarazin, R. H. Howard, D. L. Hughes, S. M. Humphrey and M. Bochmann, *Dalton Trans.*, 2006, 340-350.
11. Z. Otwinowski and W. Minor, *Processing of X-ray Diffraction Data Collected in Oscillation Mode*, Academic Press, New York, 1997.
12. Agilent Technologies, 2011, Oxford.
13. A. Altomare, G. Cascarano, C. Giacovazzo, A. Guagliardi, M. C. Burla, G. Polidori and M. Camalli, *J. Appl. Crystallogr.*, 1994, **27**, 435-435.
14. L. Palatinus and G. Chapuis, *J. Appl. Crystallogr.*, 2007, **40**, 786-790.
15. P. W. Betteridge, J. R. Carruthers, R. I. Cooper, K. Prout and D. J. Watkin, *J. Appl. Crystallogr.*, 2003, **36**, 1487.

Appendix

A1. ROESY NMR spectrum of Mg(CzOx^{Me_2}){N(SiMe$_3$)$_2$}$_2$ (1)

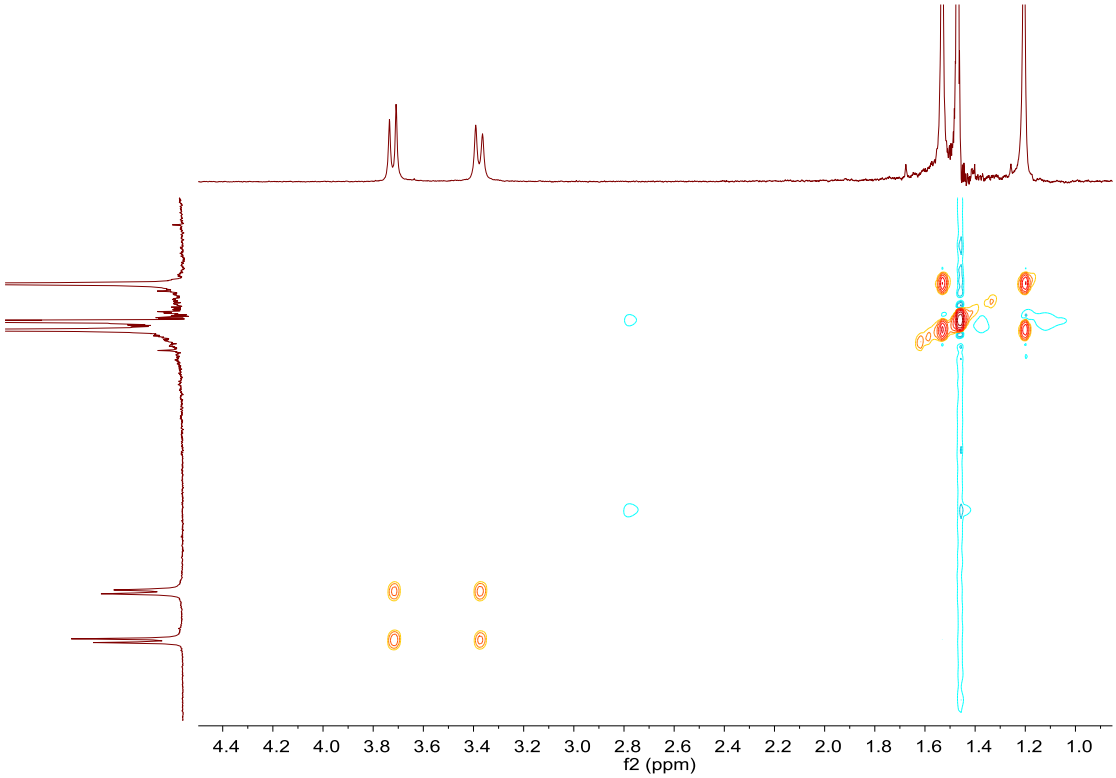


Figure A1.1. ROESY NMR spectrum (C_6D_6, 499.9 MHz, 298 K) of Mg(CzOx^{Me_2}){N(SiMe$_3$)$_2$}$_2$ (**1**).

A2. ROP of LA with CzOx^{Me_2}-supported magnesium and zinc initiators

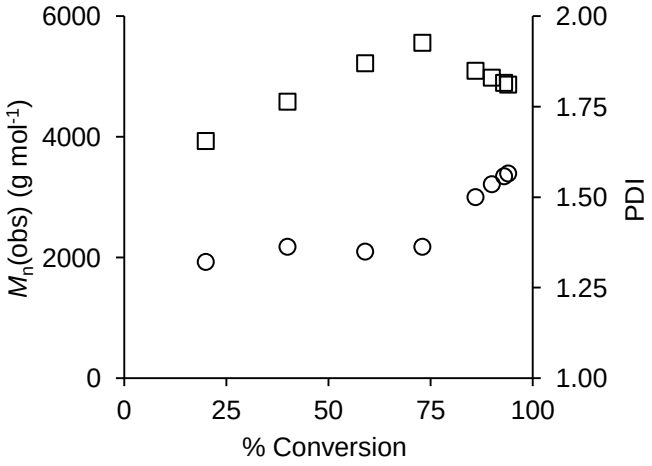


Figure A2.1. M_n(obs) (g mol)$^{-1}$ *vs*. % conversion plot (squares) and PDI *vs*. % conversion plot (circles) for the ROP of *rac*-LA using Mg(CzOx^{Me_2}){N(SiMe$_3$)$_2$}$_2$ (**1**).

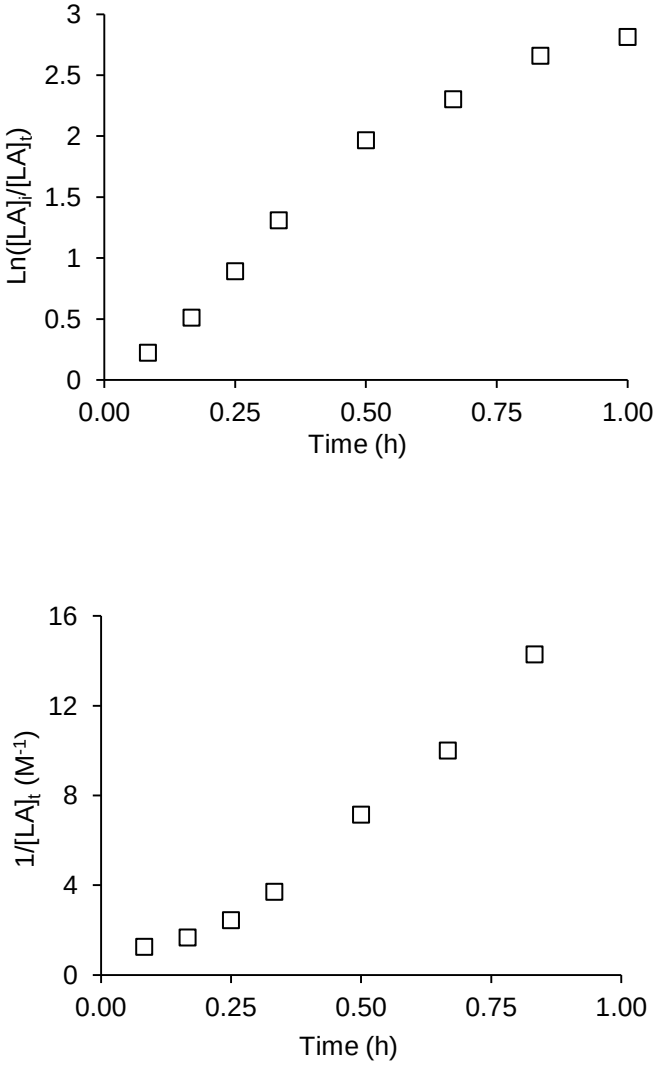


Figure A2.2. Data for the ROP of *rac*-LA using $Mg(CzOx^{Me_2})\{N(SiMe_3)_2\}_2$ (**1**) with 1 eq. $B(OBn)_3$. Top: first-order plot of $\ln[LA]_i/[LA]_t$ *vs*. time. Bottom: second-order plot of $1/[LA]_t$ *vs*. time.

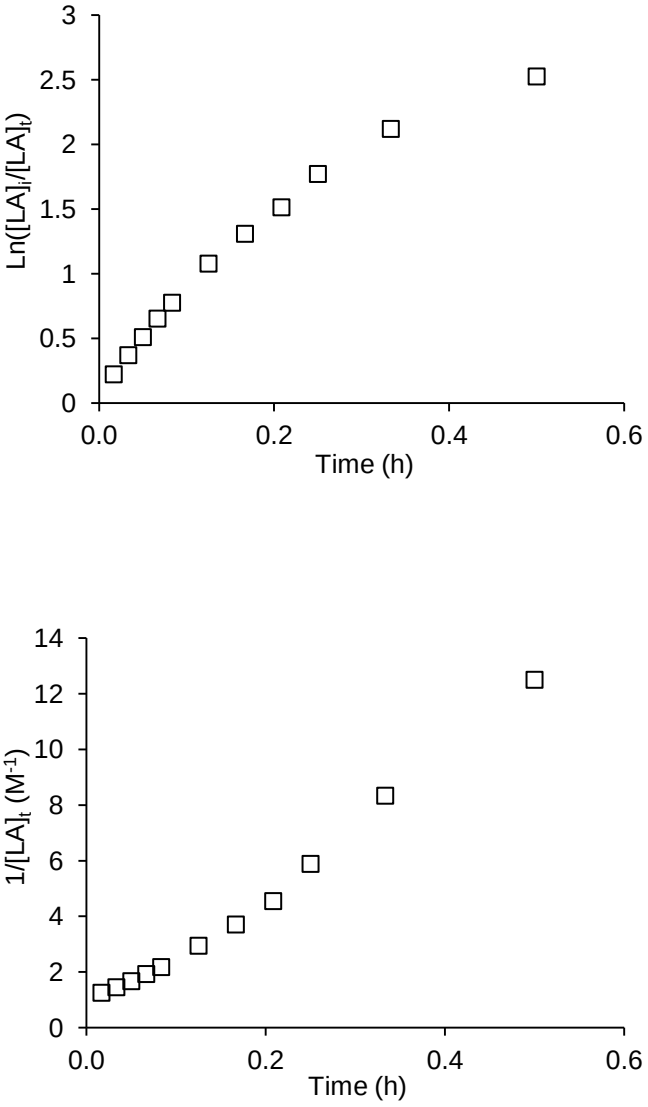


Figure A2.3. Data for the ROP of *rac*-LA using Mg(CzOx^{Me2})(OBn) (**2**) with 1 eq. B(OBn)$_3$. Top: first-order plot of ln[LA]$_i$/[LA]$_t$ *vs*. time. Bottom: second-order plot of 1/[LA]$_t$ *vs*. time.

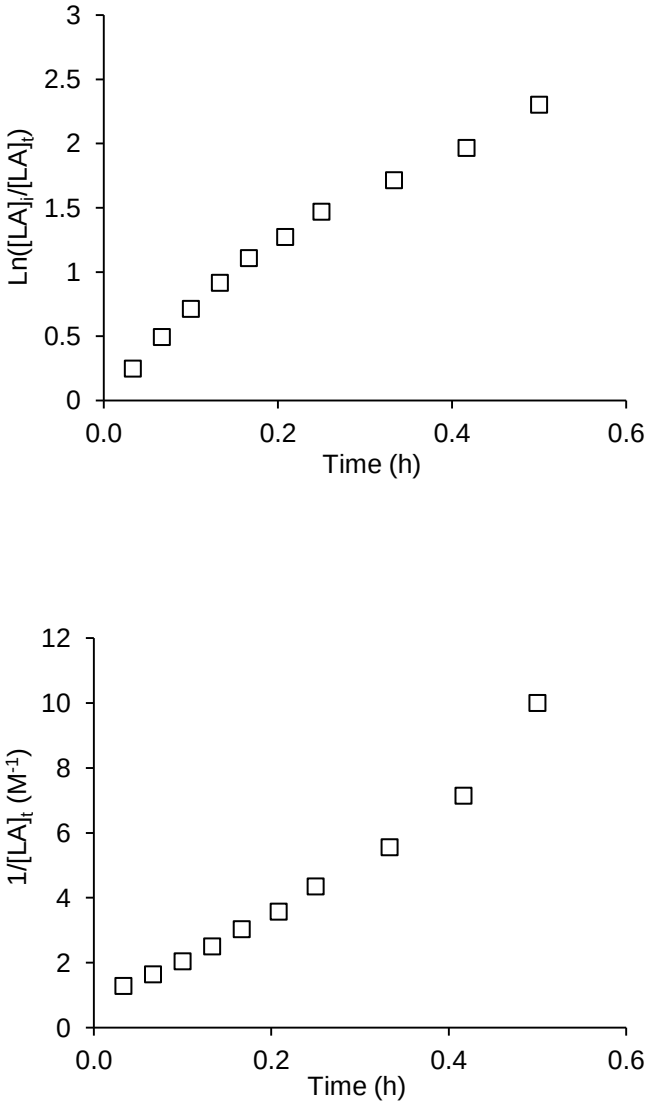


Figure A2.4. Data for the ROP of *rac*-LA using Mg(CzOx^{Me2})(BH_4) (**7**) with 4.5 eq. PhCHO. Top: first-order plot of $\ln[LA]_i/[LA]_t$ *vs*. time. Bottom: second-order plot of $1/[LA]_t$ *vs*. time.

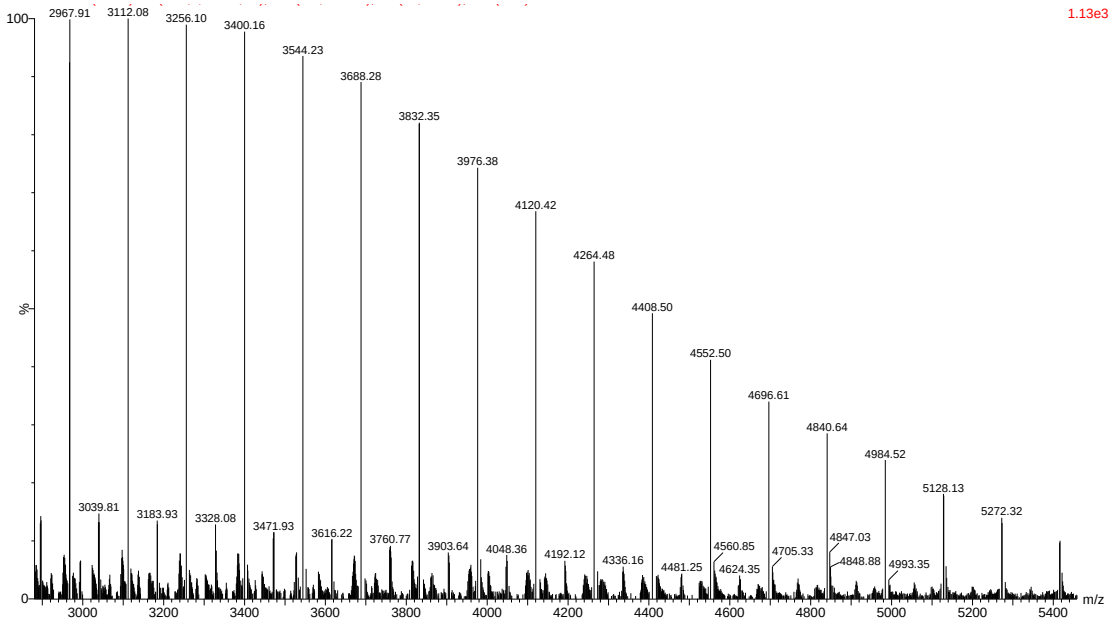


Figure A2.5. MALDI-ToF MS of PLA synthesised from Zn(CzOx^{Me_2})(Et) (**4**). Peak at 3,400 g mol^{-1} corresponds to [H-[LA]$_{20}$-CzOx^{Me_2}-K]$^+$ (calculated value = 3,395 g mol^{-1}).

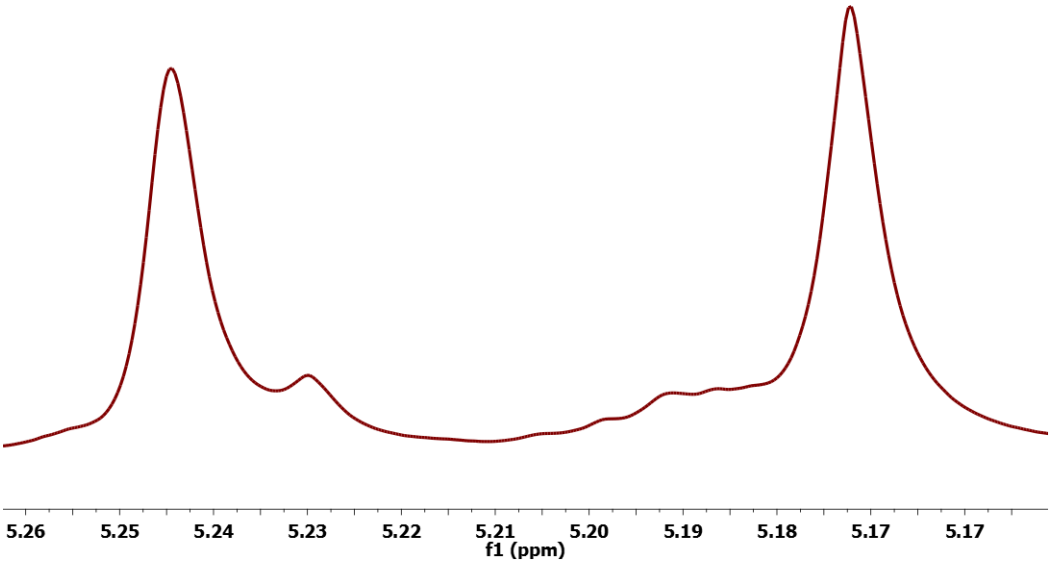


Figure A2.6. ^{1}H{^{1}H} NMR spectrum ($CDCl_3$, 499.9 MHz, 298 K) of PLA synthesised from Mg(CzOx^{Me_2})(BH_4) (**7**) and *rac*-LA.

A.3. Characterisation spectrum for $Y(BD_4)_3(THF)_2$ (20)

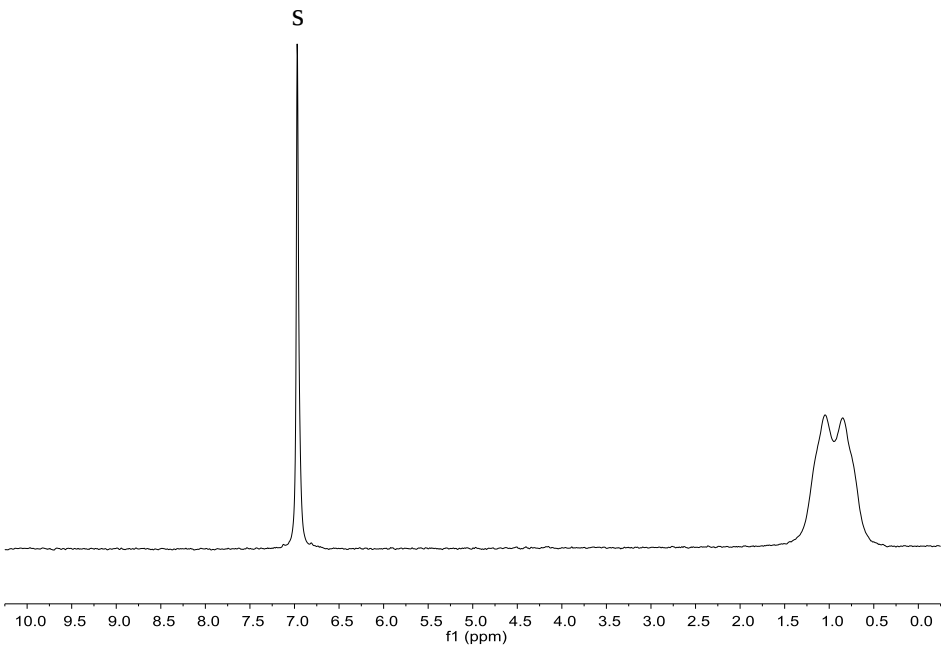


Figure A3.1. ^2H NMR spectrum (C_6H_6, 76.7 MHz, 298 K) of $Y(BD_4)_3(THF)_2$ (**20**). "s" denotes the residual solvent signal.

A.4. ROP of LA with $CzOx^{Me_2}$-supported calcium, lanthanum and samarium initiators

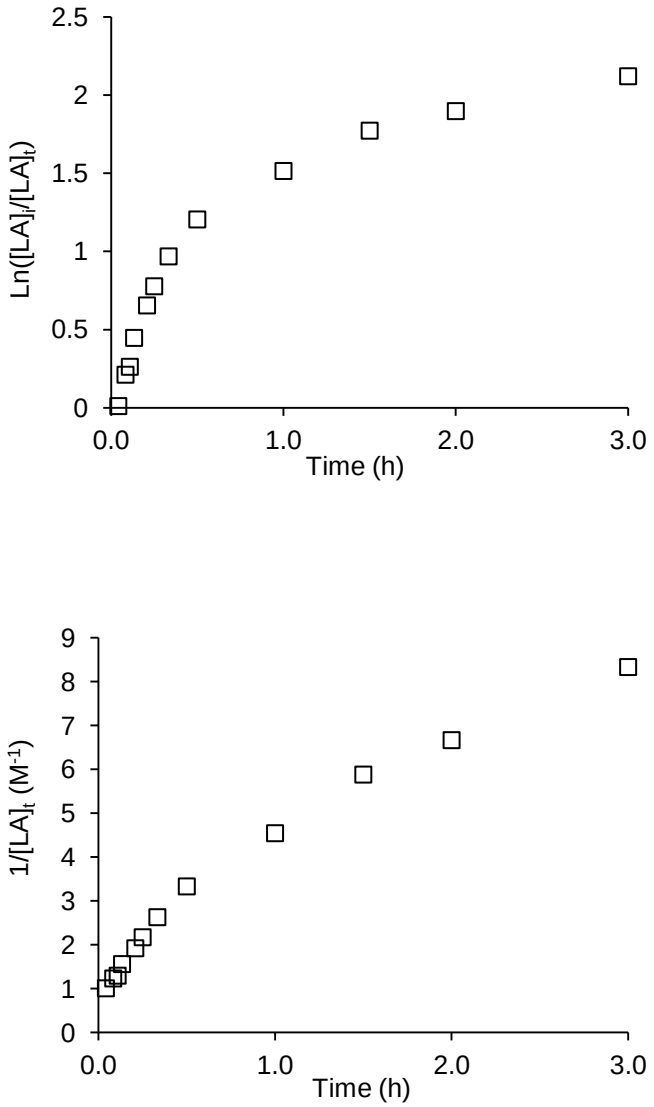


Figure A4.1. Data for the ROP of *rac*-LA using $Ca(CzOx^{Me_2})(BH_4)(THF)_2$ (**13**). Top: first-order plot of $\ln[LA]_i/[LA]_t$ *vs*. time. Bottom: second-order plot of $1/[LA]_t$ *vs*. time.

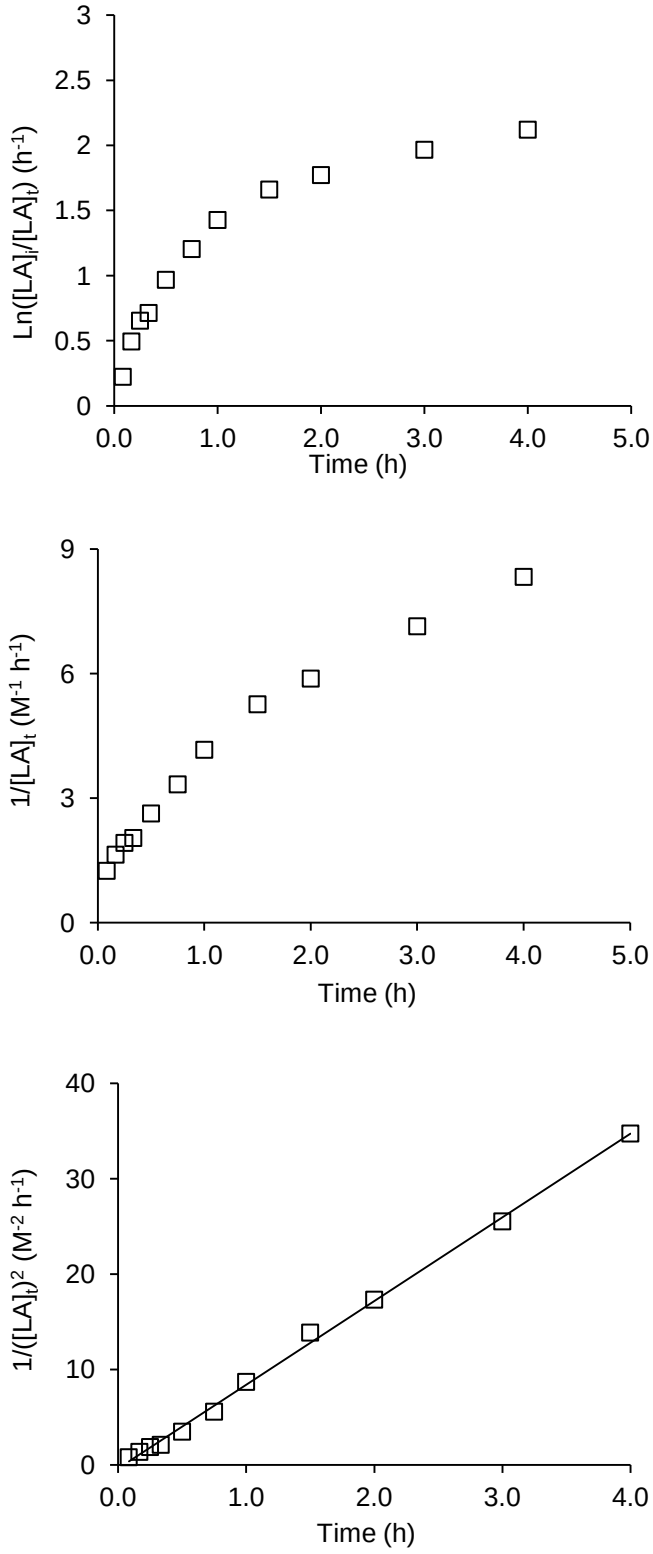


Figure A4.2. Data for the ROP of *L*-LA using Ca(CzOx^{Me_2})(BH$_4$)(THF)$_2$ (**13**). Top: first-order plot of ln[LA]$_i$/[LA]$_t$ *vs*. time. Middle: second-order plot of 1/[LA]$_t$ *vs*. time. Bottom: third-order plot of 1/([LA]$_t$)^2 *vs*. time (k_{obs} = 8.8(1) M^{-2} h^{-1}, R^2 = 0.998).

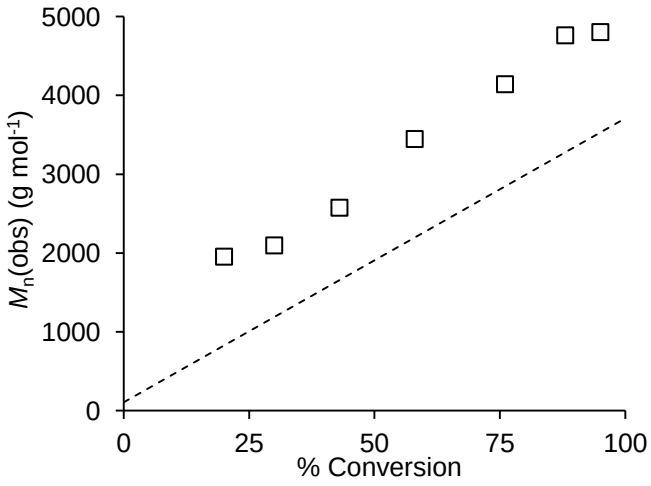


Figure A4.3. M_n(obs) *vs*. % conversion for the ROP of *L*-LA using Ca(CzOx^{Me_2})(BH$_4$)(THF)$_2$ (**13**) with 4.5 eq. PhCHO. ROP of *L*-LA; the dashed line is the M_n(calc) corresponding to 4 chains per metal centre.

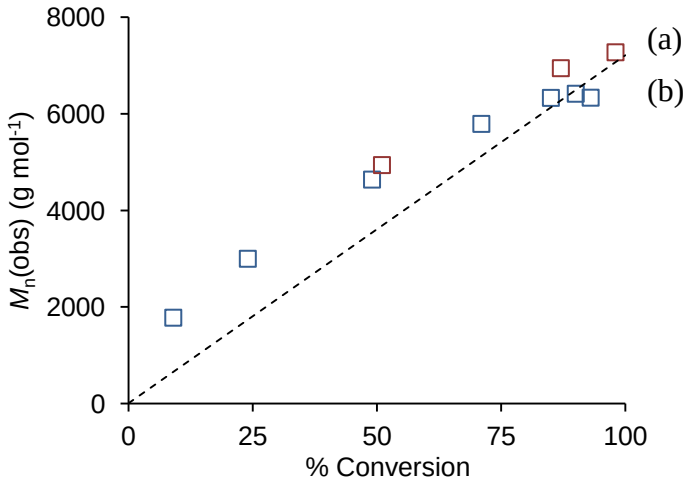


Figure A4.4. M_n(obs) *vs*. % conversion for the ROP of *rac*-LA using (a) La(CzOx^{Me_2})(BH$_4$)(THF)$_2$ (**17**) (red squares) and (b) Sm(CzOx^{Me_2})(BH$_4$)(THF)$_2$ (**18**) (blue squares); the dashed line is the M_n(calc) in each case corresponding to 2 chains per metal centre.

A.5. ROP of LA with CzOx^{iPr}-supported magnesium, calcium and yttrium initiators

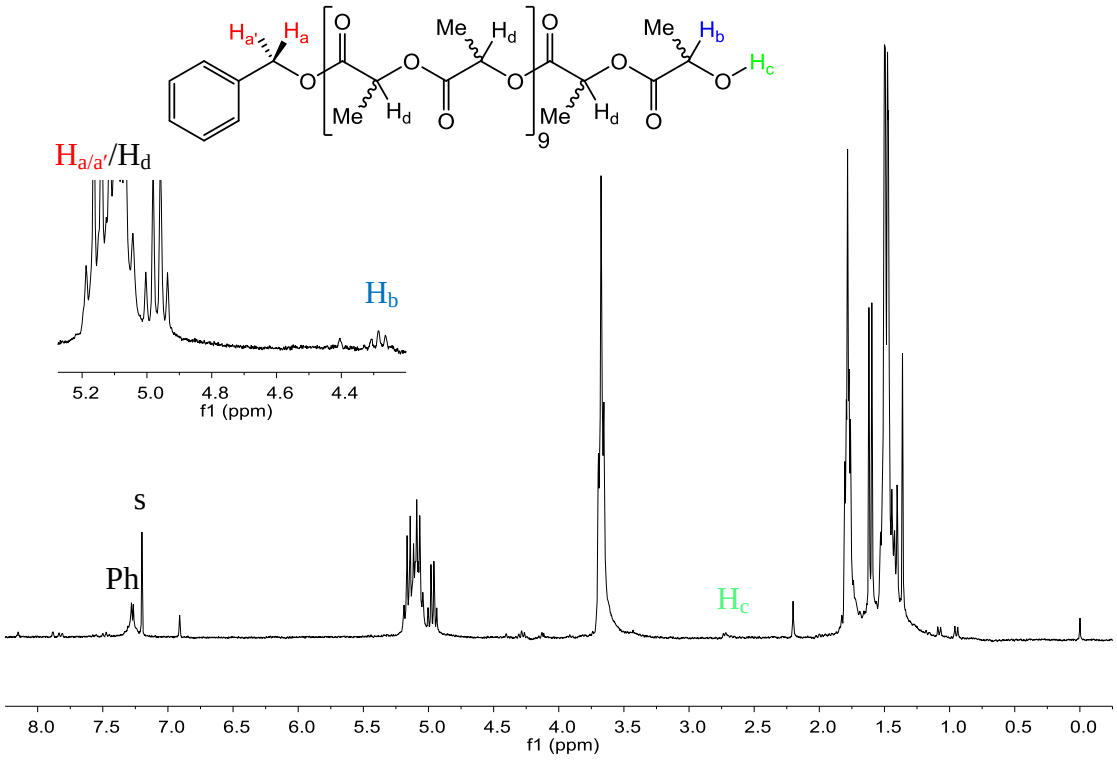


Figure A5.1. ^{1}H NMR ($CDCl_3$, 300.3 MHz, 298 K) spectrum of PLA synthesised from *in situ* generated (*S*,*S*)-Mg(CzOx^{iPr})(OBn) (**(*S*,*S*)-46**) and 2 eq. $B(OBn)_3$. "s" denotes residual solvent signals. M_n by GPC analysis was 2,570 g mol^{-1}.

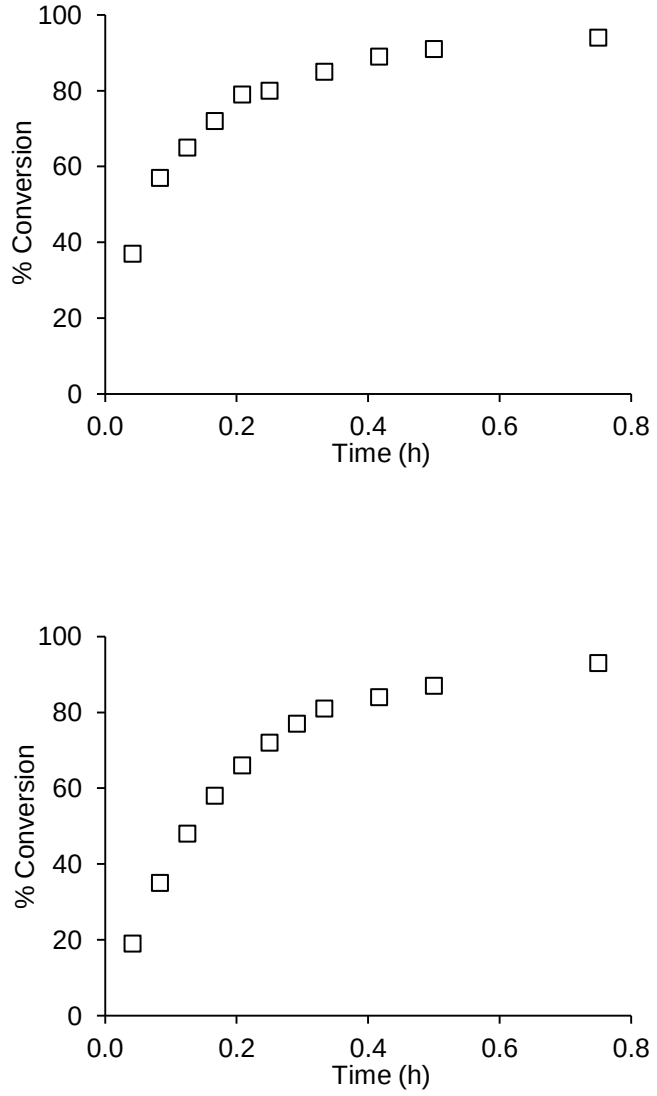


Figure A5.2. Top: % Conversion vs. time (h) for the ROP of *meso*-LA with (*S*,*S*)-Mg(CzOx$^{i\text{Pr}}$)(BH$_4$)(THF) (**(*S*,*S*)-35**) and 4.5 eq. PhCHO. Bottom: % Conversion vs. time (h) for the ROP of *rac*-LA with (*S*,*S*)-Mg(CzOx$^{i\text{Pr}}$)(BH$_4$)(THF) (**(*S*,*S*)-35**) and 4.5 eq. PhCHO.

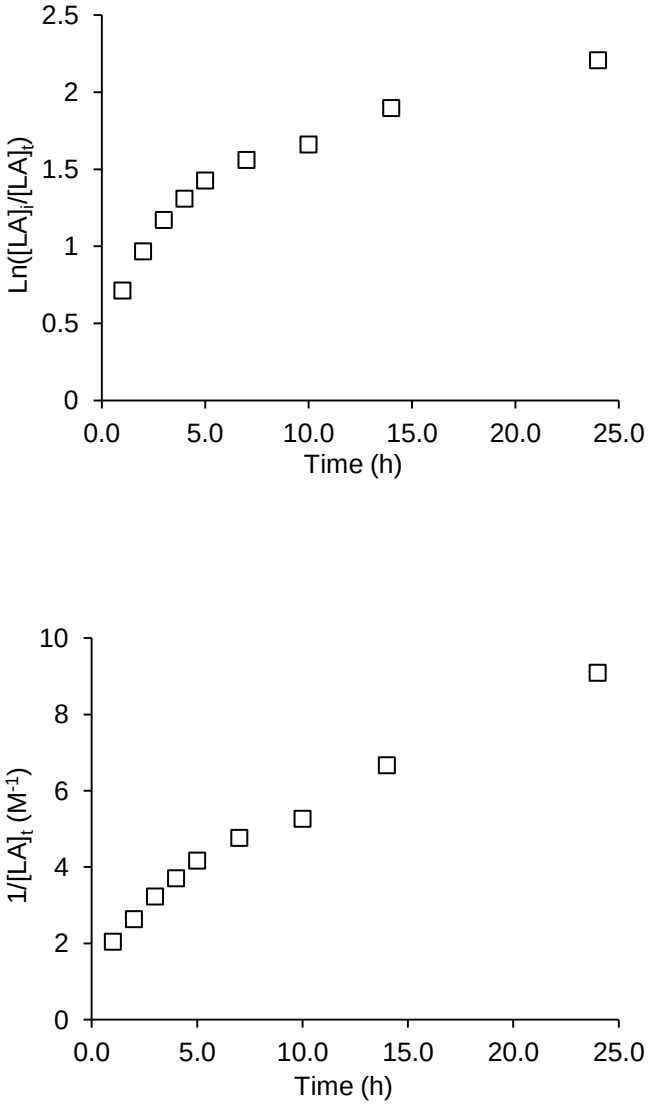


Figure A5.3. Data for the ROP of *rac*-LA using *rac*-Mg(CzOx$^{i\text{Pr}}$)(BH$_4$)(THF) (***rac*-35**). Top: first-order plot of ln[LA]$_i$/[LA]$_t$ *vs*. time. Bottom: second-order plot of 1/[LA]$_t$ *vs*. time.

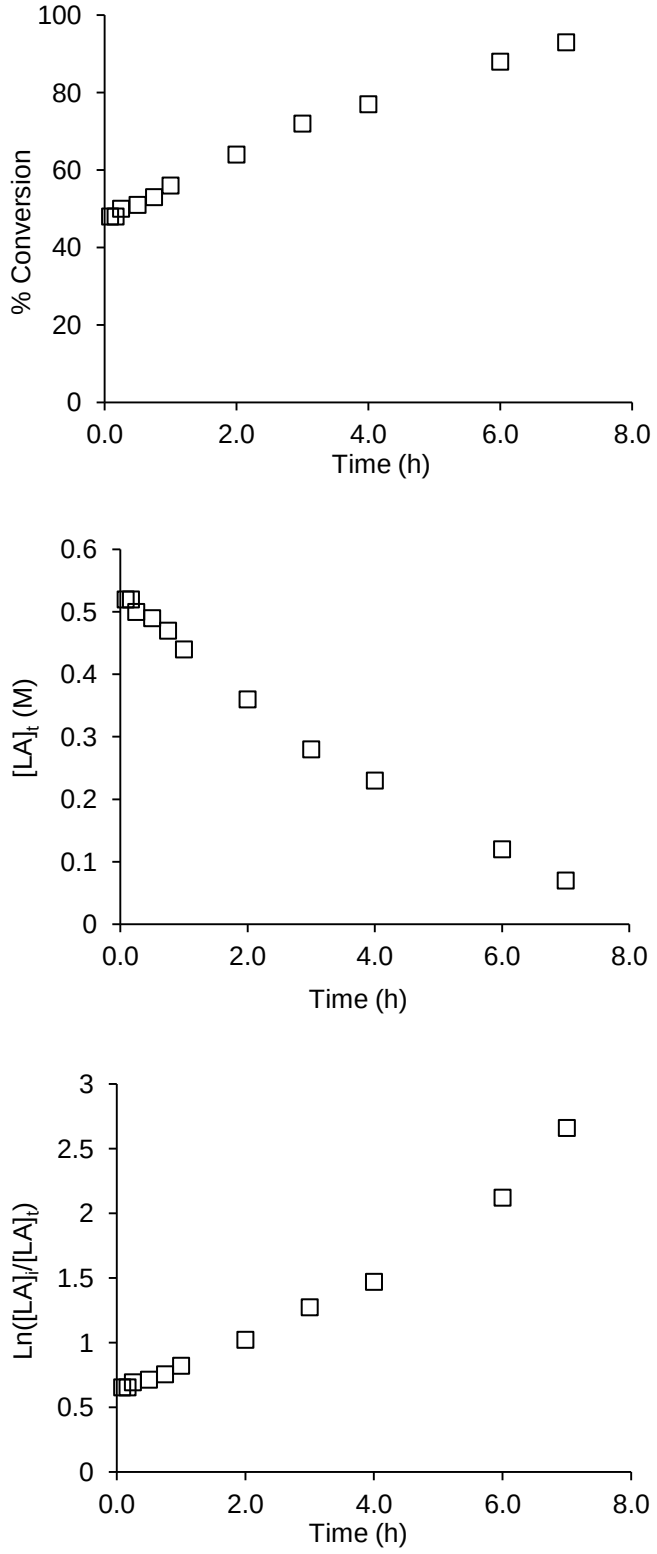


Figure A5.4. Top: % Conversion vs. time for the ROP of *meso*-LA with (*S*,*S*)-Mg(CzOx$^{i\text{Pr}}$)(BH$_4$)(THF) (**(*S*,*S*)-35**) and 4.5 eq. PhCHO. Middle: zero-order plot of $[LA]_t$ *vs*. time. Bottom: first-order plot of $1/[LA]_t$ *vs*. $\ln[LA]_i/[LA]_t$ *vs*. time.

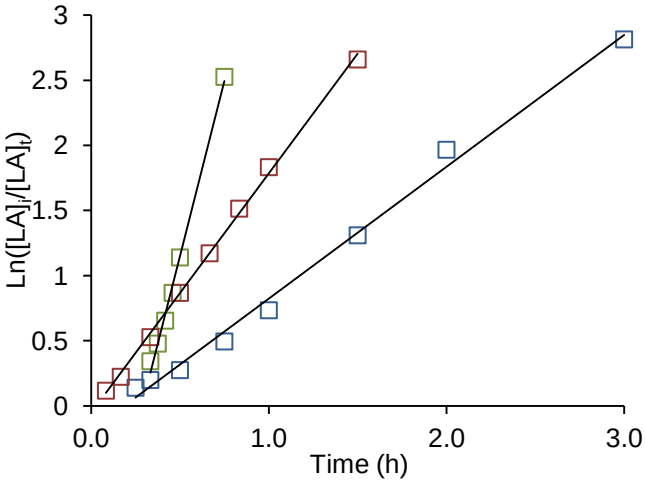


Figure A5.5. Data for the ROP of *rac*-, *D*- and *L*-LA with (*S*,*S*)-Y(CzOx$^{i\text{Pr}}$)(BH$_4$)$_2$(THF) (**(*S*,*S*)-43**). Semi-logarithmic plot of ln[LA]$_i$/[LA]$_t$ *vs*. time. (a) ROP of *rac*-LA: k_{obs} = 1.01(3) h^{-1}, R^2 = 0.994 (blue squares). (b) ROP of *L*-LA: k_{obs} = 5.4(2) h^{-1}, R^2 = 0.995 (red squares). (c) ROP of *D*-LA: k_{obs} = 1.84(3) h^{-1}, R^2 = 0.999 (green squares).

A6. Kinetic profiles of initiators $CzOx^{Me_2}$- and $CzOx^{iPr}$-supported Group 2, Group 3, lanthanide and zinc complexes for the ROP of LA

A6.1. Summary of k_{obs} for $CzOx^{Me_2}$-supported magnesium and zinc initiators for the ROP of *rac*-, *L*- and *meso*-LA.[a]

Entry	Catalyst	Monomer	Additive (eq.)	Conv.[b] %	Time (min)	k_{obs}[b]
1	$Mg(CzOx^{Me_2})(OBn)$ (**2**)	*L*-LA	-	95	60	2.91(9) h^{-1}
2	$Mg(CzOx^{Me_2})(OBn)$ (**2**)	*L*-LA	$B(OBn)_3$ (1)	94	60	16.0(6) M^{-1} h^{-1}
3	$Mg(CzOx^{Me_2})\{N(SiMe_3)_2\}$ (**1**)	*rac*-LA	-	93	60	3.67(8) h^{-1}
4	$Mg(CzOx^{Me_2})\{N(SiMe_3)_2\}$ (**1**)	*rac*-LA	$B(OBn)_3$ (1)	93	50	[d]
5	$Mg(CzOx^{Me_2})(OBn)$ (**2**)	*rac*-LA	-	93	30	6.8(1) h^{-1}
6	$Mg(CzOx^{Me_2})(OBn)$ (**2**)	*rac*-LA	$B(OBn)_3$ (1)	92	30	[d]
7	$Mg(CzOx^{Me_2})(OBn)$ (**2**)	*rac*-LA	$B(OBn)_3$ (3)	93	90	9.2(3) M^{-1} h^{-1}
8	$Mg(CzOx^{Me_2})(OBn)$ (**2**)	*rac*-LA	$B(OBn)_3$ (1) + PhCHO (0.5)	91	30	21.7(4) M^{-1} h^{-1}
9	$Mg(CzOx^{Me_2})(Bu)$ (**3**)	*rac*-LA	-	93	30	7.5(4) h^{-1}
10	$Zn(CzOx^{Me_2})(Et)$ (**4**)	*rac*-LA	-	90	1,560	[d]
11	$Mg(CzOx^{Me_2})(BH_4)$ (**7**)	*rac*-LA	-	88	120	3.91(8) M^{-1} h^{-1}
12	$Mg(CzOx^{Me_2})(BD_4)$ (**7-*d*$_4$**)[c]	*rac*-LA	-	88	2,880	0.179(6) M^{-1} h^{-1}
13	$Mg(CzOx^{Me_2})(BH_4)$ (**7**)	*rac*-LA	$B(OMe)_3$ (1)	92	180	4.0(1) M^{-1} h^{-1}
14	$Mg(CzOx^{Me_2})(BH_4)$ (**7**)	*rac*-LA	$B(OBn)_3$ (1)	92	240	2.24(3) M^{-1}
15	$Mg(CzOx^{Me_2})(BH_4)$ (**7**)	*rac*-LA	PhCHO (4.5)	90	30	[d]
16	$Mg(CzOx^{Me_2})(BH_4)$ (**7**)	*rac*-LA	PhCHO (8)	90	45	11.8(3) M^{-1} h^{-1}
17	$Mg(CzOx^{Me_2})(BH_4)$ (**7**)	*meso*-LA	-	93	40	4.2(2) h^{-1}
18	$Mg(CzOx^{Me_2})(BH_4)$ (**7**)	*meso*-LA	PhCHO (4.5)	92	10	[d]

[a] Conditions: [*rac*-LA]$_0$:[initiator]$_0$ = 100:1, 4 mL THF at 23 °C. [*rac*-LA]$_0$ = 1.0 M. [b] Measured by ^{1}H NMR ($CDCl_3$) analyses. [c] Conditions: [*rac*-LA]$_0$:[initiator]$_0$ = 100:1, 4 mL THF at 60 °C. [*rac*-LA]$_0$ = 1.0 M. [d] k_{obs} not determined.

A6.2. Summary of k_{obs} for CzOx^{Me_2}-supported calcium and strontium initiators for the ROP of *rac*-, *L*- and *meso*-LA.[a]

Entry	Catalyst	Monomer	Additive (eq.)	Conv.[b] %	Time (min)	k_{obs}[b]
1	Ca(CzOx^{Me_2}){N(SiMe$_3$)$_2$}(THF) (**9**)	*rac*	-	91	15	40.8(4) M^{-1} h^{-1}
2	Ca(CzOx^{Me_2})(OBn) (**10**)	*rac*	-	93	3.5	44(1) h^{-1}
3	Ca(CzOx^{Me_2})(OBn) (**10**)	*rac*	B(OBn)$_3$ (1)	90	50	14.3(3) M^{-1} h^{-1}
4	Ca(CzOx^{Me_2})(BH$_4$)(THF)$_2$ (**13**)	*rac*	-	88	180	11.6(1) M^{-2} h^{-1}
5	Ca(CzOx^{Me_2})(BH$_4$)(THF)$_2$ (**13**)	*rac*	B(OBn)$_3$ (1)	90	1,440	[c]
6	Ca(CzOx^{Me_2})(BH$_4$)(THF)$_2$ (**13**)	*rac*	PhCHO (4.5)	93	360	-0.142(6) M h^{-1}
7	Ca(CzOx^{Me_2})(BH$_4$)(THF)$_2$ (**13**)	*rac*	PhCHO (8)	88	360	-0.115(3) M h^{-1}
8	Ca(CzOx^{Me_2})(BH$_4$)(THF)$_2$ (**13**)	*L*	-	88	240	8.8(1) M^{-2} h^{-1}
9	Ca(CzOx^{Me_2})(BH$_4$)(THF)$_2$ (**13**)	*L*	PhCHO (4.5)	95	420	-0.134(6) M h^{-1}
10	Ca(CzOx^{Me_2})(BH$_4$)(THF)$_2$ (**13**)	*meso*	-	97	5	50(2) h^{-1}
11	Ca(CzOx^{Me_2})(BH$_4$)(THF)$_2$ (**13**)	*meso*	PhCHO (4.5)	89	5	86(2) M^{-1} h^{-1}
12	Sr(CzOx^{Me_2})(BH$_4$)(THF)$_2$ (**14**)	*rac*	-	91	2	[c]
13	Sr(CzOx^{Me_2})(BH$_4$)(THF)$_2$ (**14**)	*rac*	PhCHO (4.5)	92	300	0.58(2) h^{-1}

[a] Conditions: [*rac*-LA]$_0$:[initiator]$_0$ = 100:1, 4 mL THF at 23 °C. [*rac*-LA]$_0$ = 1.0 M. [b] Measured by ^{1}H NMR (CDCl$_3$) analyses. [c] k_{obs} not determined.

A6.3. Summary of k_{obs} for CzOx^{Me_2}-supported yttrium, lanthanum and samarium initiators for the ROP of *rac*- and *meso*-LA.[a]

Entry	Catalyst	Monomer	Additive (eq.)	Conv.[b] %	Time (min)	k_{obs}[b]
1	Y(CzOx^{Me_2})(BH$_4$)$_2$(THF) (**16**)	*rac*	-	94	50	3.6(2) h^{-1}
2	Y(CzOx^{Me_2})(BH$_4$)$_2$(THF) (**16**)	*rac*	B(OBn)$_3$ (2)	93	45	6.4(2) h^{-1}
3	Y(CzOx^{Me_2})(BH$_4$)$_2$(THF) (**16**)	*rac*	B(OMe)$_3$ (2)	91	45	5.7(1) h^{-1}
4	Y(CzOx^{Me_2})(BH$_4$)$_2$(THF) (**16**)	*rac*	PhCHO (10)	90	3	[c]
5	Y(CzOx^{Me_2})(BH$_4$)$_2$(THF) (**16**)	*meso*	-	92	10	25.4(8) h^{-1}
6	Y(CzOx^{Me_2})(BH$_4$)$_2$(THF) (**16**)	*meso*	PhCHO (10)	93	1	[c]
7	La(CzOx^{Me_2})(BH$_4$)$_2$(THF) (**17**)	*rac*	-	98	1.5	[c]
8	La(CzOx^{Me_2})(BH$_4$)$_2$(THF) (**17**)	*rac*	PhCHO (10)	96	1.5	[c]
9	Sm(CzOx^{Me_2})(BH$_4$)$_2$(THF) (**18**)	*rac*	-	93	3.5	60(3) h^{-1}
10	Sm(CzOx^{Me_2})(BH$_4$)$_2$(THF) (**18**)	*rac*	PhCHO (10)	96	0.5	[c]

[a] Conditions: [*rac*-LA]$_0$:[initiator]$_0$ = 100:1, 4 mL THF at 23 °C. [*rac*-LA]$_0$ = 1.0 M. [b] Measured by ^{1}H NMR (CDCl$_3$) analyses. [c] k_{obs} not determined.

A6.4. Summary of k_{obs} for CzOx^{iPr}-supported magnesium initiators for the ROP of *rac*-, *L*-, *D*- and *meso*-LA.[a]

Entry	Catalyst	Monomer	Additive (eq.)	Conv.[b] %	Time (min)	k_{obs}[b]
1	(*S*,*S*)-Mg(CzOx^{iPr})(BH$_4$)(THF) (**(*S*,*S*)-35**)	*rac*	-	92	72	[c]
2	(*S*,*S*)-Mg(CzOx^{iPr})(BH$_4$)(THF) (**(*S*,*S*)-35**)	*rac*	PhCHO (4.5)	93	0.75	[c]
3	(*S*,*S*)-Mg(CzOx^{iPr})(BH$_4$)(THF) (**(*S*,*S*)-35**)	*rac*	PhCHO (4.5) + B(OBn)$_3$ (1)	88	48	[c]
4	(*S*,*S*)-Mg(CzOx^{iPr})(BH$_4$)(THF) (**(*S*,*S*)-35**)	*meso*	-	89	4	1.99(5) M^{-1} h^{-1}
5	(*S*,*S*)-Mg(CzOx^{iPr})(BH$_4$)(THF) (**(*S*,*S*)-35**)	*meso*	PhCHO (4.5)	94	0.75	[c]
6	(*S*,*S*)-Mg(CzOx^{iPr})(BH$_4$)(THF) (**(*S*,*S*)-35**)	*L*	-	90	312	[c]
7	(*S*,*S*)-Mg(CzOx^{iPr})(BH$_4$)(THF) (**(*S*,*S*)-35**)	*L*	PhCHO (4.5)	95	120	[c]
8	(*S*,*S*)-Mg(CzOx^{iPr})(BH$_4$)(THF) (**(*S*,*S*)-35**)	*D*	-	89	384	[c]
9	(*S*,*S*)-Mg(CzOx^{iPr})(BH$_4$)(THF) (**(*S*,*S*)-35**)	*D*	PhCHO (4.5)	94	2	[c]
10	(*R*,*R*)-Mg(CzOx^{iPr})(BH$_4$)(THF) (**(*R*,*R*)-35**)	*rac*	-	91	72	[c]
11	(*R*,*R*)-Mg(CzOx^{iPr})(BH$_4$)(THF) (**(*R*,*R*)-35**)	*rac*	PhCHO (4.5)	89	0.75	[c]
12	(*R*,*R*)-Mg(CzOx^{iPr})(BH$_4$)(THF) (**(*R*,*R*)-35**)	*L*	-	89	264	[c]
13	(*R*,*R*)-Mg(CzOx^{iPr})(BH$_4$)(THF) (**(*R*,*R*)-35**)	*L*	PhCHO (4.5)	93	2	[c]
14	(*R*,*R*)-Mg(CzOx^{iPr})(BH$_4$)(THF) (**(*R*,*R*)-35**)	*D*	-	90	336	[c]
15	(*R*,*R*)-Mg(CzOx^{iPr})(BH$_4$)(THF) (**(*R*,*R*)-35**)	*D*	PhCHO (4.5)	91	120	[c]
16	(*rac*)-Mg(CzOx^{iPr})(BH$_4$)(THF) (**(*rac*)-35**)	*rac*	-	88	24	1.67(6) M^{-2} h^{-1}
17	(*rac*)-Mg(CzOx^{iPr})(BH$_4$)(THF) (**(*rac*)-35**)	*rac*	PhCHO (4.5)	91	0.75	13.8(3) M^{-1} h^{-1}

[a] Conditions: [*rac*-LA]$_0$:[initiator]$_0$ = 100:1, 4 mL THF at 23 °C. [*rac*-LA]$_0$ = 1.0 M. [b] Measured by ^{1}H NMR (CDCl$_3$) analyses. [c] k_{obs} not determined.

A6.4. Summary of k_{obs} for CzOx^{iPr}-supported calcium, yttrium, lanthanum and samarium initiators for the ROP of *rac*-, *L*-, *D*- and *meso*-LA.[a]

Entry	Catalyst	Monomer	Additive (eq.)	Conv.[b] %	Time	k_{obs}[b]
1	(*S*,*S*)-Ca(CzOx^{iPr})(BH$_4$)(THF) (**(*S*,*S*)-36**)	*rac*	-	82	0.5	[c]
2	(*S*,*S*)-Ca(CzOx^{iPr})(BH$_4$)(THF) (**(*S*,*S*)-36**)	*rac*	PhCHO (4.5)	93	180	[c]
3	(*S*,*S*)-Ca(CzOx^{iPr})(BH$_4$)(THF) (**(*S*,*S*)-36**)	*L*	-	93	420	[c]
4	(*S*,*S*)-Ca(CzOx^{iPr})(BH$_4$)(THF) (**(*S*,*S*)-36**)	*L*	PhCHO (4.5)	92	180	[c]
5	(*S*,*S*)-Ca(CzOx^{iPr})(BH$_4$)(THF) (**(*S*,*S*)-36**)	*D*	-	92	1.5	[c]
6	(*S*,*S*)-Ca(CzOx^{iPr})(BH$_4$)(THF) (**(*S*,*S*)-36**)	*D*	PhCHO (4.5)	92	180	1.48(6) h^{-1}[d]
7	(*S*,*S*)-Ca(CzOx^{iPr})(BH$_4$)(THF) (**(*S*,*S*)-36**)	*meso*	-	91	2	[c]
8	(*S*,*S*)-Ca(CzOx^{iPr})(BH$_4$)(THF) (**(*S*,*S*)-36**)	*meso*	PhCHO (4.5)	92	25	[c]
9	(*S*,*S*)-Y(CzOx^{iPr})(BH$_4$)$_2$(THF) (**(*S*,*S*)-43**)	*rac*	-	94	180	1.01(3) h^{-1}
10	(*S*,*S*)-Y(CzOx^{iPr})(BH$_4$)$_2$(THF) (**(*S*,*S*)-43**)	*L*	-	92	45	5.4(2) h^{-1}
11	(*S*,*S*)-Y(CzOx^{iPr})(BH$_4$)$_2$(THF) (**(*S*,*S*)-43**)	*D*	-	93	90	1.84(3) h^{-1}
12	(*S*,*S*)-Y(CzOx^{iPr})(BH$_4$)$_2$(THF) (**(*S*,*S*)-43**)	*meso*	-	92	135	[c]
13	(*S*,*S*)-Y(CzOx^{iPr})(BH$_4$)$_2$(THF) (**(*S*,*S*)-43**)	*rac*	PhCHO (10)	93	2	68(4) h^{-1}
14	(*S*,*S*)-La(CzOx^{iPr})(BH$_4$)$_2$ (**(*S*,*S*)-44**)	*rac*	-	90	120	1.45(4) h^{-1}
15	(*S*,*S*)-La(CzOx^{iPr})(BH$_4$)$_2$ (**(*S*,*S*)-44**)	*rac*	PhCHO (10)	91	10	59(2) M^{-1} h^{-1}
16	(*S*,*S*)-Sm(CzOx^{iPr})(BH$_4$)$_2$ (**(*S*,*S*)-45**)	*rac*	-	92	300	0.53(1) h^{-1}
17	(*S*,*S*)-Sm(CzOx^{iPr})(BH$_4$)$_2$ (**(*S*,*S*)-45**)	*rac*	PhCHO (10)	93	10	82(1) M^{-1} h^{-1}

[a] Conditions: [*rac*-LA]$_0$:[initiator]$_0$ = 100:1, 4 mL THF at 23 °C. [*rac*-LA]$_0$ = 1.0 M. [b] Measured by ^{1}H NMR (CDCl$_3$) analyses. [c] k_{obs} not determined. [d] Before *ca*. 50% conversion, k_{obs} = 1.48(6) h^{-1}; after *ca*. 50% conversion, k_{obs} = 0.66(1) h^{-1}.